21ST INTERNATIONAL CONFERENCE ON THE **PHYSICS** OF **ESTUARIES** AND **COASTAL SEAS** **(PECS 2024)**

September 23-27, 2024
Bordeaux (France)

BOOK OF ABSTRACTS

Organized by
Aldo Sottolichio – University of Bordeaux, France
Lauren Ross – University of Maine, USA
Florent Grasso – Ifremer, France

The idea behind PECS

PECS (Physics of Estuaries and Coastal Seas) is an independent organization whose sole purpose is to organize the PECS biennial conferences. The objectives of these conferences are to:

- promote exchange of information on recent developments in physics of estuaries and coastal seas;
- stimulate cooperation between coastal engineers and coastal oceanographers, and
- to provide a forum for graduate students and young scientists and engineers where they feel comfortable to interact with experienced scientists.

Emphasis is on the results of field and laboratory measurements, and theoretical and numerical analysis, with the aim of better understanding the underlying physical processes. Other relevant topics are also acceptable. This conference series emphasizes informal exchanges in a collegial environment. All sessions are plenary and attendance is limited to one hundred and fifty participants.

History of PECS

by Prof. J. van de Kreeke (1935-2023), co-founder of PECS conferences

During the 1950s and '60s, coastal engineers and coastal oceanographers focused on different problems with regard to estuaries. Coastal engineering problems related mostly to stability of tidal inlets, land reclamation and the closure of estuaries and bays for storm surge protection. Solving these problems required knowledge of tides and tidal currents. In contrast, coastal oceanographers tended to concentrate on tidal mean properties including salinity, stratification, gravitational circulation. While coastal engineers derived their tools from hydraulics, coastal oceanographers relied on geophysical fluid dynamics.

In the seventies the coastal engineers started to face different types of problems relating mostly to water quality. Because water quality is largely determined by tidal mean motions, the coastal engineers began to seek help from coastal oceanographers. As a result of this the coastal oceanographers detected an interest in their work that had been absent in the community of blue water oceanographers.

The logical place for the two disciplines to meet and exchange ideas seemed to be the biennial International Conference on Coastal Engineering (ICCE). Unfortunately, the forum of the ICCE became increasingly focused on the nearshore, relegating estuarine problems to the status of stepchild. It was at the ICCE of 1976 that a small group of coastal engineers and coastal oceanographers realised that their interests would be better served by a specialty conference focusing on the physics of estuaries. The idea was to have this conference at the same venue and either directly preceding or following the ICCE. This idea ultimately was abandoned because it was difficult to find host institutions in some of the places where the ICCE was held.

With the intent of focusing on estuaries, the first conference was organised in September 1978 in Hamburg. The second conference did not take place until 1984 in Miami. Since 1984 conferences have been held every two years. With the inclusion of physics of coastal seas in 1990, the conference series became known as PECS. A complete list of the conferences, chairpersons and host institutions is given below.

PECS has a Steering Committee consisting of the chairpersons of the previous meetings. The Committee ensures that future conferences adhere to the above-mentioned objectives. The board also selects the venue of future conferences. Organising a conference and publishing conference papers is the sole responsibility of the local organising committee.

List of past conferences

- 1978 Hamburg, Germany - organised by Jürgen Sündermann, University of Hamburg, Institute for Oceanography. Proceedings: Mathematical Modeling of Estuarine Physics, Eds.: J. Sündermann and K. P. Holz, Lecture Notes on Coastal and Estuarine Studies, Springer-Verlag.
- 1984 Miami, Florida, USA - organised by Jacobus van de Kreeke, University of Miami, Rosenstiel School of Marine and Atmospheric Science. Proceedings: Physics of Shallow Estuaries and Bays, Ed.: J. van de Kreeke, Lecture Notes on Coastal and Estuarine Studies, Springer-Verlag.
- 1986 Qingdao, China - organised by Huatong Wang, Ocean University of Qingdao. Proceedings: Physics of Shallow Seas, Eds: Huatong Wang, Jinyong Wang and Hua Day, China Ocean Press.
- 1988 Monterey, California, USA - organised by Ralph Cheng, U.S. Geological Survey. Proceedings: Residual Currents and Long-term Transport, Ed.: R.T.Cheng, Coastal and Estuarine Studies, Springer-Verlag.
- 1990 Gregynog, Wales, UK - organised by David Prandle, Proudman Oceanographic Laboratory, Bidston Observatory. Proceedings: Dynamics and Exchanges in Estuaries and the Coastal Zone, Ed.: D. Prandle, Coastal and Estuarine Studies, American Geophysical Union.
- 1992 Margaret River, Australia - organised by Charitha Pattiaratchi, University of Western Australia. Proceedings: Mixing in Estuaries and Coastal Seas, Ed.: Ch. Pattiaratchi, Coastal and Estuarine Studies, American Geophysical Union.
- 1994 Woods Hole, Massachusetts, USA - organised by David Aubrey, Woods Hole Oceanographic Institution. Proceedings: Buoyancy Effects on Coastal an Estuarine Dynamics, Eds.: D.G. Aubrey and C.T. Friedrichs, Coastal and Estuarine Studies, American Geophysical Union. Sediment Transport and Buoyancy in Estuaries, Ed.: D.G. Aubrey, Journal of Coastal Research, Special Issue No. 25, 1997.
- 1996 The Hague, The Netherlands - organised by Job Dronkers, National Institute for Coastal and Marine Management. Proceedings: Physics of Estuaries and Coastal Seas, Eds.: J. Dronkers and M.B.A.M. Scheffers, A.A. Balkema Publishers.
- 1998 Matsuyama, Japan - organised by Tetsuo Yanagi, Ehime University. Proceedings: Interactions between Estuaries, Coastal Seas and Shelf Seas, Ed.: T. Yanagi, Terra Scientific Publishing Company, Tokyo.
- 2000 Norfolk, Virginia, USA - organised by Carl Friedrichs, College of William and Mary, Virginia Institute of Marine Science and Arnoldo Valle-Levinson, Old Dominion University, Center for Coastal Physical Oceanography. Proceedings: Special issues of Continental Shelf Research - 2002, 22(11-13) and 22(18-19), Eds.: C.T. Friedrichs and A. Valle-Levinson.
- 2002 Hamburg, Germany - jointly organised by Hans Burchard, Institute for Oceanography of the University of Hamburg, and Iris Grabemann and Jens Kappenberg, GKSS Research Centre, Geesthacht, Germany. Proceedings: Special issue of Ocean Dynamics - 2003, 53(3), Eds.: H. Burchard, I. Grabemann and J. Kappenberg.
- 2004 Mérida, Yucatán, México - organised by Paulo Salles, Institute of Engineering, National Autonomous University of Mexico. Proceedings: Special issues of Ocean Dynamics - 2005, 55(5-6) and 2006, 56(3-4), Eds.: P. Salles and A.J. Souza.
- 2006 Astoria, Oregon, USA - organised by David Jay, Civil and Environmental Engineering Department, Portland State University, Oregon. Proceedings: Special issue of Continental Shelf Research - 2009, 29(1), Eds: P. MacCready and D.A. Jay.
- 2008 Liverpool, England, UK - organised by Alejandro Souza, Proudman Oceanographic Laboratory, Liverpool. Proceedings: Special issue of Ocean Dynamics.
- 2010 Colombo, Sri Lanka - organised by Charitha Pattiaratchi, The University of Western Australia. Proceedings: Special issue of Ocean Dynamics.
- 2012 New York City, New York, USA - organised by Robert Chant, Institute of Marine and Coastal Sciences, Rutgers University, and Rockwell Geyer, Woods Hole Oceanographic Institution. Proceedings: Special issue of Ocean Dynamics.
- 2014 Porto de Galhinas, Pernambuco State, Brazil - organised by Carlos Augusto Schettini, Coastal Hydrodynamics Laboratory, Department of Oceanography, Center of Geosciences & Engineering, Federal University of Pernambuco. Proceedings: Special issue of Ocean Dynamics.
- 2016 Scheveningen, The Netherlands - Organized by Henk Schuttelaars and Tjerk Zitman, Delft University of Technology and Mick Van Der Wegen UNESCO-IHE. Proceedings: Special Issue of Ocean Dynamics
- 2018 Galveston, Texas - Organized by Rob Hetland, Texas A&M University and Julie Pietrzak, Delft University of Technology. Proceedings: Special Issue of Journal of Geophysical Research: Oceans
- 2020 Virtual PECS Seminar Series https://www.io-warnemuende.de/v-pecs.html . Organized by Hans Burchard and the Steering Committee
- 2022 Shanghai, China & Perth, Austrailia - Organized by He Qing, East China Normal University & Charitha Pattiaratchi, University of Western Australia. Proceedings: Special Issue of Journal of Geophysical Research: Oceans

PECS Steering Committee

- Jürgen Sündermann (University of Hamburg, Institute for Oceanography, Germny)
- Jacobus van de Kreeke (†) (University of Miami, Rosenstiel School of Marine and Atmospheric Science, USA)
- Huatong Wang (Ocean University of Qingdao, China)
- Ralph Cheng (U.S. Geological Survey, USA)
- David Prandle (Proudman Oceanographic Laboratory, Bidston Observatory, USA)
- Charitha Pattiaratchi (University of Western Australia), **chair**
- David Aubrey (Woods Hole Oceanographic Institution, USA)
- Job Dronkers (National Institute for Coastal and Marine Management, The Netherlands)
- Tetsuo Yanagi (Ehime University, Japan)
- Carl Friedrichs (College of William and Mary, Virginia Institute of Marine Science, USA)
- Arnoldo Valle-Levinson (University of Florida, Gainesville, USA)
- Hans Burchard (Leibniz Institute for Baltic Sea Research Warnemünde, Germany)
- Iris Grabemann (GKSS Research Centre, Geesthacht, Germany)
- Jens Kappenberg (GKSS Research Centre, Geesthacht, Germany)
- Paulo Salles (Laboratorio Nacional de Resiliencia Costera, UNAM, Sisal, Mexico)
- David Jay (Civil and Environmental Engineering Department, Portland State University, Oregon, USA)
- Alejandro Souza (CINESTAV Mérida, Mexico)
- Robert Chant (Institute of Marine and Coastal Sciences, Rutgers University, USA)
- Rockwell Geyer (Woods Hole Oceanographic Institution, USA)
- Carlos Augusto Schettini (Universidade Federal do Rio Grande - FURG, Brazil)
- Henk Schuttelaars (Institute of Applied Mathematics, Delft University of Technology, The Netharlands)
- Mick van der Wegen (UNESCO-IHE, The Netherlands)
- Tjerk Zitman (Department of Hydraulic Engineering, Delft University of Technology, The Netherlands)
- Rob Hetland (Texas A&M University, USA)
- Julie Pietrzak (Delft University of Technology, The Netherlands)
- He Qing (East China Normal University, China)

Organizing Committee for the 21st PECS conference

- Aldo Sottolichio - University of Bordeaux, France
- Lauren Ross - University of Maine, USA
- Florent Grasso - Ifremer, DYNECO/DHYSED, France

Topics of the 21st PECS conference

- Tidal, subtidal and wave dynamics in estuaries
- Salt dynamics and stratification
- Sediment transport
- Channel and tidal flat dynamics
- Barrier coasts, lagoons and tidal inlets
- River-coast interaction
- Shelf sea dynamics
- Anthropogenic pressures and impacts
- Estuaries under climate change

Acknowledgments

We acknowledge all the sponsors and the volunteers for making this conference possible. We are especially grateful to Taylor Bailey, Marine Barré, Betty John Kaimathuruthy, Edwin Nagy, Arnaud Le Pevedic, Elias Pinilla, Cristian Rojas, Jun Zheng, the Maine College of Engineering and Computing, the University of Maine Civil and Environmental Engineering Department, the EPOC CNRS laboratory, and UBevent.

Sponsors

Région Nouvelle-Aquitaine

DeepBlue Technology

NORTEK

RBR

Office de tourisme et des congrès de Bordeaux Métropole

This project has received financial support from the French government within the frame of France 2030

Réseau de recherche Risques et Vulnérabilité pour l'Adaptation et la Gestion du littoral en Nouvelle-Aquitaine

NKE Instrumentation

The Marine Turbulence Experts

AUV with Confidence

Maine College of Engineering and Computing
U. Maine Civil and Env. Eng. Dep.

EPOC CNRS laboratory

Bordeaux, France
(Organizing institution)

Maine, USA
(Organizing institution)

Centre de Bretagne, France
(Organizing institution)

Table of content

Preliminary results of the Lowest Astronomical Tide (LAT) Reference Surface in the Belgian part of the North Sea

Abdollahi S. [1], Verstraeten J. [2], Vanlede J. [3], Verbeurgt J. [4], Gurdebeke P. [2], and De Wulf A. [1]

Keywords: LAT, reference surface, hydrodynamic, North Sea.

Abstract

This study presents an update on the ongoing research project conducted by the Flemish agency for Maritime Services – Coastal Department, aimed at enhancing navigation safety in the Belgian part of the North Sea through the revision of the Lowest Astronomical Tide (LAT) reference surface.

The Belgian coastal waters of the North Sea present a dynamic environment for studying tidal dynamics and their implications. This research aims to conduct a comprehensive harmonic analysis of tidal constituents at three strategically located tide gauge stations along the Belgian coast: Nieuwpoort, Ostend, and Zeebrugge.

A comprehensive dataset of harmonic constituent data for these stations have been compiled. Through harmonic analysis techniques, tidal constituents are being extracted to understand the complex tidal behavior of the North Sea. Using the extracted tidal constituents, LAT values are being meticulously calculated for each of the designated stations. This process involves robust mathematical algorithms and careful consideration of local environmental factors affecting tidal patterns.

The Tide Gauge stations in Belgium play a crucial role in monitoring coastal tidal dynamics. Tidal analysis of the extensive dataset spanning from 2000 to 2022 with a step of 5 minutes offers valuable insights into long-term tidal behavior. In this analysis, we leverage the UTide Python package, a powerful tool designed for harmonic analysis of time series data. As a sample, the observed and reconstructed water level and the corresponding misfit for the Newport tide gauge station (NPT) have been shown in Fig.1. The Root Mean Square Deviation (RMSD) has been computed, yielding a value of 0.3. The amplitudes, phases, and their corresponding uncertainties for the top 10 constituents have been calculated and are presented in Table 1, sorted by descending amplitude.

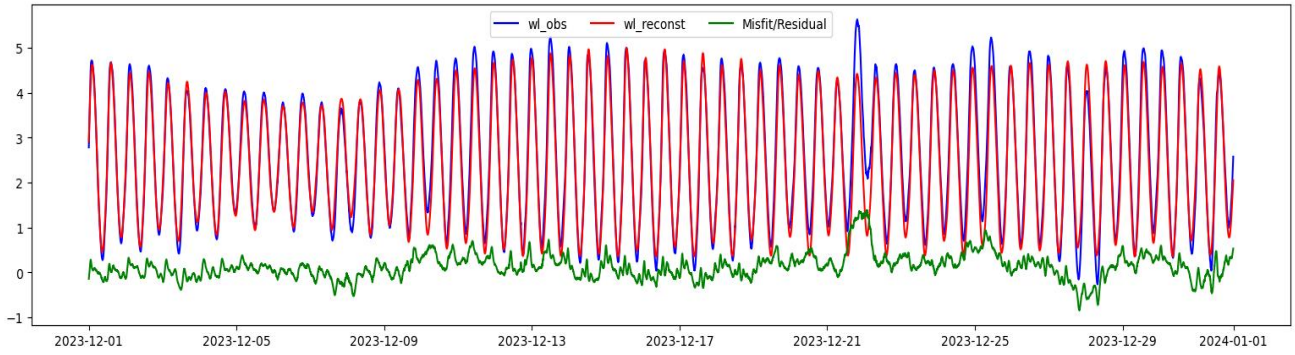

Figure 1. Comparison of observed and reconstructed water levels in NPT station with RMSD of 0.3.

Research goals

In the next stages, we'll combine the hydrodynamic and gravimetric geoid models to refine our LAT determination. Our goal is to provide an improved LAT reference surface for the Belgian North Sea, enhancing navigation safety and accuracy in the area.

[1] Department of Geography, Ghent University, BE-9000 Ghent, Belgium, Somayeh.abdollahi@ugent.be, alain.dewulf@ugent.be
[2] Agentschap Maritieme Dienstverlening & Kust, BE-8400 Ostend, Belgium, johan.verstraeten@mow.vlaanderen.be, pieter.gurdebeke@mow.vlaanderen.be
[3] Flanders Hydraulics, BE-2140 Antwerp, Belgium, joris.vanlede@mow.vlaanderen.be
[4] National Geographic Institute, BE-1000 Brussels, Belgium, jeffrey.verbeurgt@ngi.be

Table 1: The first 10 constituents sorted by descending amplitude (A), along with their respective phases (g) and uncertainties (A_ci and g_ci) for Newport tide gauge station.

Name	A	A_ci	g	g_ci
M2	1.93178	0.00607	0.53966	0.17991
S2	0.56890	0.00607	54.1608	0.61099
N2	0.33106	0.00607	336.33	1.049798
K2	0.16359	0.00607	52.75323	2.124622
L2	0.15605	0.00607	9.292952	2.227442
M4	0.13951	0.004316	308.4894	1.772361
MU2	0.10531	0.006066	103.1659	3.301266
NU2	0.090653	0.006067	334.1575	3.834067
MS4	0.085649	0.004316	9.204863	2.886764
O1	0.0804914	0.003553	164.1088	2.530487

Funding

This research was funded by the Coastal Division, Agency for Maritime and Coastal Services (MDK), Flemish Ministry of Mobility and Public Works, under project No. 221.195, "Creation and validation of: geodetic and tidal datums, acquisition tools at sea and in the intertidal zone".

Acknowledgments

The data from the Belgian wave gauges were provided by the Agency for Maritime and Coastal Services (MDK) (https://meetnetvlaamsebanken.be/, accessed on 31 December 2023). The authors are thankful to MDK for their continued support in this study. The authors thank the reviewers for their comments that helped to improve the quality of this paper.

References

Rochlin, I. and Morris, J.T. (2017) Regulation of salt marsh mosquito populations by the 18.6-yr lunar-nodal cycle. Ecology, 98: 2059-2068. https://doi.org/10.1002/ecy.1861. https://doi.org/10.1002/ecy.1861.

Doodson, A. T. (1921) The harmonic development of the tide-generating potential. Proceedings of the Royal Society of London. Series A, Containing Papers of a Mathematical and Physical Character 100: 305–329. https://doi.org/10.1098/rspa.1921.0088.

Codiga, D.L., 2011. Unified Tidal Analysis and Prediction Using the UTide Matlab Functions. Technical Report 2011-01. Graduate School of Oceanography, University of Rhode Island, Narragansett, RI. 59pp. ftp://www.po.gso.uri.edu/pub/downloads/codiga/pubs/2011Codiga-UTide-Report.pdf

Intra-tidal variability of the hydrodynamics in a salt-wedge estuary

Álvarez-Silva Ó. [1], Cardona Y. [2], and Valle-Levinson A. [3]

Keywords: estuaries, salt-wedge, momentum-balance, tidal variability.

Abstract

This study describes the intra-tidal variability of the circulation, stratification, and relative dominance of the momentum terms in the hydrodynamics of a salt-wedge estuary. The case study is the Magdalena River Estuary, located on the Caribbean coast of Colombia. The Magdalena River is the largest source of freshwater, sediments, nutrients, and pollutants in the Caribbean Sea, with regional impacts on coastal and ocean ecosystems. The average discharge of this river is approximately 7000 m^3/s, with mean monthly variability between 4000 m^3/s and 10000 m^3/s. The tidal regime is mixed with diurnal predominance; it is microtidal with a maximum tidal range of 0.5 m. Geomorphologically, the estuary is restricted to one channel with laterally fixed margins, forming a nearly prismatic estuary (Restrepo, 2020). For discharges above 5000 m^3/s, freshwater is present all along the river channel down to its connection with the ocean, and mixing processes take place at the outer river plume. On the other hand, for lower discharges, a persistent salt-wedge intrudes throughout a distance that is inversely proportional to the river flow (Arévalo, 2022).

To conduct this study, field measurements of ADCP and CTD profiles were taken along two transverse sections during a low discharge condition of 3000 m^3/s (95% of exceedance probability), under the presence of an extensive salt-wedge. The measurement transects were located at 2.4 km and 3.4 km upstream of the transition with the ocean. Measurements in both sections were taken nearly simultaneously eleven times along a tidal cycle of 25 hours. Along-channel profiles of salinity were also taken from the mouth to the salt-wedge front during high and low water levels. The measurements were complemented by water level gauges located upstream and downstream of the transverse sections, at 8.2 km and 1.6 km landward of the transition with the ocean, respectively.

Current velocity data were pre-processed for quality control. North-East components of the velocity were rotated to the principal axis. CTD data were processed to determine the water density using TEOS-10 routines. The mean along-channel velocity and density profiles were extracted for both sections and for the eleven measuring times from transverse averaging of velocity and density fields. The degree of stratification and its temporal variability were analyzed from the vertical and temporal variability of Buoyancy Frequency (N^2) and Richardson Number (Ri). To determine the key forcers of hydrodynamics, we assessed the temporal variability of local acceleration, along-channel advective acceleration, and barotropic and baroclinic pressure gradients using finite differences. The residual acceleration was associated with Reynolds' stress divergence following the methodology described by Nijs, Pietrzak, and Winterwerp (2011). This assessment allowed estimates of the vertical variability of the eddy viscosity as the ratio between the Reynolds' stress and the shear, as described by Geyer, Trowbridge, and Bowen (2000).

The along-estuary salinity transects show that the salt-wedge front, represented by the 5g/kg isohaline, advanced about 2 km upstream during high water level in comparison to low water level, indicating that although the estuary has a micro-tidal regime, the tide indeed influences the salinity intrusion extent in the short term (<1 day). According to the data of the two transverse sections, the estuary remains strongly stratified, as indicated by $N^2 > 0.1$ and $Log_{10}(4*Ri) > 0$, throughout the tidal cycle. Stratification is concentrated at a narrow pycnocline in the mid-water column, with a homogeneous freshwater mass above the pycnocline and a homogeneous seawater mass below the pycnocline, forming a stable three-layer density profile. Stratification was found to be slightly higher during flood than during ebb, evidenced by lower values of N^2 and a thicker pycnocline during ebb tides. This behavior is opposite to the classical definition of tidal straining (Simpson 1990) and could be attributed to the large shear in the water profile (that overcomes stratification and generates mixing) when the barotropic pressure gradient -mainly controlled by the river discharge- is enhanced by the ebb tide.

The analysis of the momentum equation terms led to identifying the role of advective acceleration in the observed hydrodynamics patterns. In the upper freshwater layer, the local acceleration is dominant in the variability of the velocity profile. The dominance of this term is generated by the along-channel tilting of the pycnocline, which is shallower seaward, shrinking the freshwater layer toward the surface and accelerating the upper-layer flow seaward. This effect is exacerbated during high water levels, when the pycnocline is higher in the water column, reducing the freshwater layer's thickness. Meanwhile, in the pycnocline layer, the advective acceleration reveals a landward jet generated by the longitudinal density gradient generated again by the upstream pycnocline's deepening (Geyer, Farmer, 1989). Finally, in the deeper seawater layer, the balance between the opposing barotropic and baroclinic pressure gradients determines the magnitude of the inland flow

[1] Universidad del Norte, Barranquilla-Colombia, oalvarezs@uninorte.edu.co
[2] Universidad Nacional de Colombia – Sede Medellín, ymcardon@unal.edu.co
[3] University of Florida, arnoldo@ufl.edu.

The estimated eddy viscosity profiles show a reduction of the viscosity in the pycnocline layer, showing a decoupling of the pycnocline from the upper and lower mixed layers. This decoupling generates a slippery boundary above the pycnocline that allows flow acceleration in the interface between the upper layer and the pycnocline, which is evidenced by the persistent presence of a local outflow maximum in the velocity profiles. This decoupling of the three layers can also be observed in the diverse patterns of the overtides in the velocity throughout the water column.

References

Arevalo, F. M., Álvarez-Silva, Ó., Caceres-Euse, A., Cardona, Y. (2022). Mixing mechanisms at the strongly-stratified Magdalena River's estuary and plume. Estuarine, Coastal and Shelf Science, 277(September). https://doi.org/10.1016/j.ecss.2022.108077

de Nijs, M. A. J., Pietrzak, J. D., Winterwerp, J. C. (2011). Advection of the salt wedge and evolution of the internal flow structure in the rotterdam waterway. Journal of Physical Oceanography, 41(1), 3–27. https://doi.org/10.1175/2010JPO4228.1

Geyer, W. R., & Farmer, D. M. (1989). Tidal-induced variation of the dynamics of a salt wedge estuary. Journal of Physical Oceanography, 19(3), 55.

Geyer, W. R., Trowbridge, J. H., & Bowen, M. M. (2000). The dynamics of a partially mixed estuary. Journal of Physical Oceanography, 30(8), 2035–2048. https://doi.org/10.1175/1520-0485(2000)030<2035:TDOAPM>2.0.CO;2

Restrepo, J. C., Orejarena-Rondón, A., Consuegra, C., Pérez, J., Llinas, H., Otero, L., Álvarez-Silva, O. (2020). Siltation on a highly regulated estuarine system: The Magdalena River mouth case (Northwestern South America). Estuarine, Coastal and Shelf Science, 245(September). https://doi.org/10.1016/j.ecss.2020.107020

Simpson, J. H., Brown, J., Matthews, J., & Allen, G. (1990). Tidal straining, density currents, and stirring in the control of estuarine stratification. Estuaries, 13(2), 125–132. https://doi.org/10.2307/1351581

Along-channel exchange flow structure in a seasonally inverse low-inflow estuary

Anidjar N., Giddings S.N., Brasseale E., Rodriguez A., and Wu X.

Keywords: Low-inflow, total exchange flow, subtidal circulation, inverse estuary

Abstract

Along-channel structure and characterization of the time varying exchange flow of estuaries are understudied (Geyer & MacCready 2014). Low-inflow estuaries are also understudied, despite their global distribution. Changes to precipitation patterns and higher temperatures in in arid and semi-arid regions motivate increased investigation into the structure of, and transitions between, classical and inverse circulation in existing and emerging low-inflow estuaries (Largier 2023). Building on previous work in San Diego Bay by Largier et al. (1997), and the developments of the total exchange flow (TEF) framework by Macready et al. (2011 & 2021) and Lorenz et al. (2020), this study decomposes the exchange flow across 14 cross sections along San Diego Bay, using a dual coordinate salinity and temperature TEF analysis. The goals of this study are to 1) examine the temporal variability in the along-channel exchange flow, with an emphasis on the seasonal shifts from classical estuarine dynamics to inverse dynamics and 2) identify the spatiotemporal boundaries of the competing estuarine regimes (thermally driven or salinity driven). Ultimately, we aim to link this knowledge of TEF to residence times critical to ecosystem dynamics.

San Diego Bay and the surrounding coastal region were simulated over three separate yearly periods (2017- 2019) using the Coupled Ocean-Atmosphere-Wave-Sediment Transport (COAWST) model system (Warner et al..,2010 and Kumar et al., 2012) as described by Wu et al. (2020). Cross sections were extracted with a 1.5km along channel spacing, from the estuary mouth to the back of the bay (Figure 1). Fluxes of salinity and temperature through each cross section were calculated in salinity and temperature coordinates and then sub-tidally filtered based on Godin et al. (1981). These fluxes were then summed over an entire year or a season to produce exchange profiles in salinity, temperature, and density coordinates. Profiles from all the cross sections were then synthesized to examine the along- channel exchange structure.

We found seasonal variation in the spatial extent and magnitude of classical- and inverse-circulation regimes in San Diego Bay (Figure 2). The spatial boundaries between these circulation cells were identified using the density difference between the mean outflowing density and mean inflowing density at each time step (Figure 2). The contour at zero (black line in Figure 2) indicates where the flow switches from classical to inverse. Whether these shifts to inverse flow were due to hypothermal or hypersaline conditions was determined using the ratio of terms in the linear equation of state: the relative contributions of salinity and temperature on changes to inflowing and outflowing density difference at each cross section. This ratio was then compared to the along-channel salinity and temperature distributions, to verify the relationship between transitions in the exchange flow and the along-channel gradient of properties.

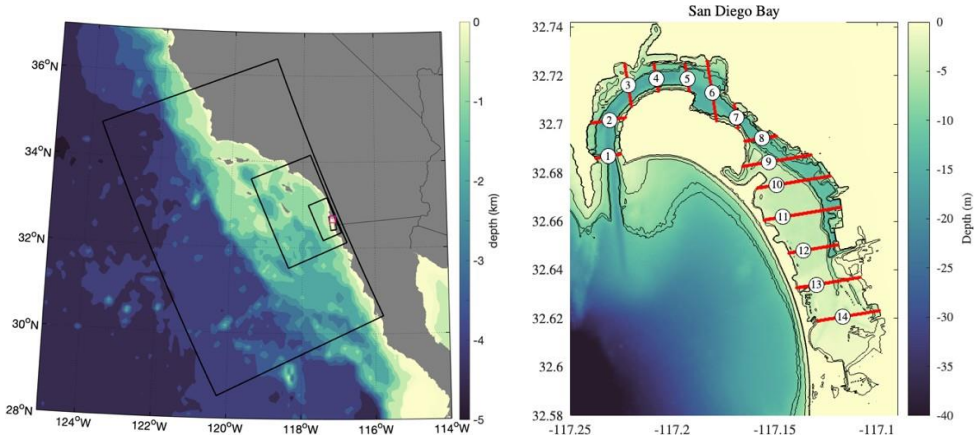

Figure 1: Regional map and zoom in of San Diego Bay with bathymetry. The regional map (left) includes nested grids (black) and the zoom-in region on the finest nest shown on the right (pink). San Diego Bay (right) contours are shown in black at 11,10,5,1, and 0 meters depth. Red lines indicate extracted cross-sections, with their corresponding indices from 1 (mouth) to 14 (back bay).

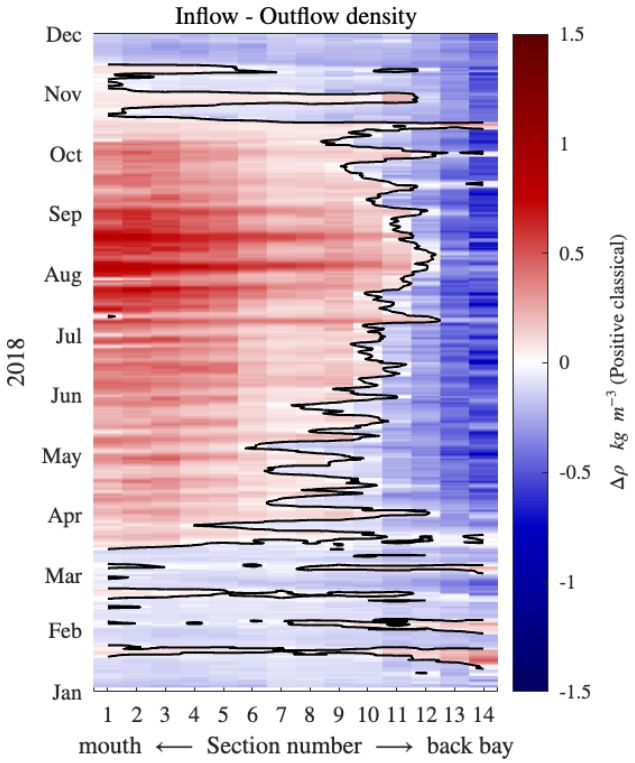

Figure 2: 1-year long time series (y axis) of density difference between mean inflowing and outflowing density across each cross- section from the estuary mouth (1, left) to the estuary interior (14, right). Positive values in red indicate that the flow is classical (i.e., surface buoyant outflow and bottom dense inflow), while negative values in blue indicate inverse estuarine circulation. The black contour shows where the flow transitions (no difference in density).

References

Geyer, W. R., & MacCready, P. (2014). The Estuarine Circulation. *Annual Review of Fluid Mechanics*, *46*(1), 175–197. https://doi.org/10.1146/annurev-fluid-010313-141302

Godin, G., Candela, J., & de la Paz-Vela, R. (1981). On the feasibility of detecting net transports in and out of Georgia strait with an array of current meters. *Atmosphere-Ocean*, *19*(2), 148–157. https://doi.org/10.1080/07055900.1981.9649106

Kumar, N., Voulgaris, G., Warner, J. C., & Olabarrieta, M. (2012). Implementation of the vortex force formalism in the coupled ocean-atmosphere-wave-sediment transport (COAWST) modeling system for inner shelf and surf zone applications. *Ocean Modelling*, *47*, 65–95. https://doi.org/10.1016/j.ocemod.2012.01.003

Largier, J. L., Hollibaugh, J. T., & Smith, S. V. (1997). Seasonally Hypersaline Estuaries in Mediterranean- climate Regions. *Estuarine, Coastal and Shelf Science*, *45*(6), 789–797. https://doi.org/10.1006/ecss.1997.0279

MacCready, P., McCabe, R. M., Siedlecki, S. A., Lorenz, M., Giddings, S. N., Bos, J., Albertson, S., Banas, N. S., & Garnier, S. (2021). Estuarine Circulation, Mixing, and Residence Times in the Salish Sea. *Journal of Geophysical Research: Oceans*, *126*(2), e2020JC016738. https://doi.org/10.1029/2020JC016738

MacCready, P. (2011). Calculating Estuarine Exchange Flow Using Isohaline Coordinates*. *Journal of Physical Oceanography*, *41*(6), 1116–1124. https://doi.org/10.1175/2011JPO4517.1

Warner, J. C., Armstrong, B., He, R., & Zambon, J. B. (2010). Development of a Coupled Ocean– Atmosphere–Wave–Sediment Transport (COAWST) Modeling System. *Ocean Modelling*, *35*(3), 230–244. https://doi.org/10.1016/j.ocemod.2010.07.010

Wu, X., Feddersen, F., Giddings, S. N., Kumar, N., & Gopalakrishnan, G. (2020). Mechanisms of Mid- to Outer-Shelf Transport of Shoreline-Released Tracers. *Journal of Physical Oceanography*, *50*(7), 1813–1837. https://doi.org/10.1175/JPO-D-19-0225.1

On the effects of SPM composition on the inherent acoustic and optical particle properties of the SPM

Baeye M. [1], Fettweis M. [2], and Verney R. [3]

Keywords: mixed sediments, flocculation, turbidity, SPM, sensor sensitivity, in-situ water sampling.

Abstract

From high-resolution in-situ time series of calibrated optical and acoustic instruments, robust relationships that can be applied to SPM (suspended particulate matter) concentrations were aimed at as part of refining the SPM - POM (particulate organic matter) model (see Fettweis et al., 2022) for the North Sea and the English Channel. In 10 stations located along nearshore to offshore transects in the Belgian coastal zone, Seine Bay, German Bight and Thames plume have been sampled in spring and winter 2023 during a tidal cycle. The presence of mixed sediments in the seabed and/or strong currents and wave conditions may cause sandy material or particle with other erosion characteristics to be resuspended up to the detection volumes of acoustic and optical sensors (see e.g. Baeye et al., 2011). Sand grains do not contain mineral attached POM and the presence of them lowers the POM content of the SPM and thus increases the uncertainty of the SPM-POM model. The presence of mixed sediments in suspension influences also the acoustic and optical inherent particle properties and thus the SPM concentration derived from sensors (see e.g. Fettweis et al., 2019). If not considered, the SPM concentration output of optical and acoustic sensors will over- or underestimate the SPM concentration and thus also the derived POM proxies.

In Fig. 1, the relationship between the ADCP echo intensity and SPM concentration (following the method of Kim et al. 2004) when including all the stations yields a positive linear relationship. Although, when focusing on the different stations separately most of the slopes are somewhat weaker compared to the general one. This is likely due to the presence of mixed sediments (solid grains, flocs and phytoplankton) that are triggering the acoustic signal differently than the optical one.

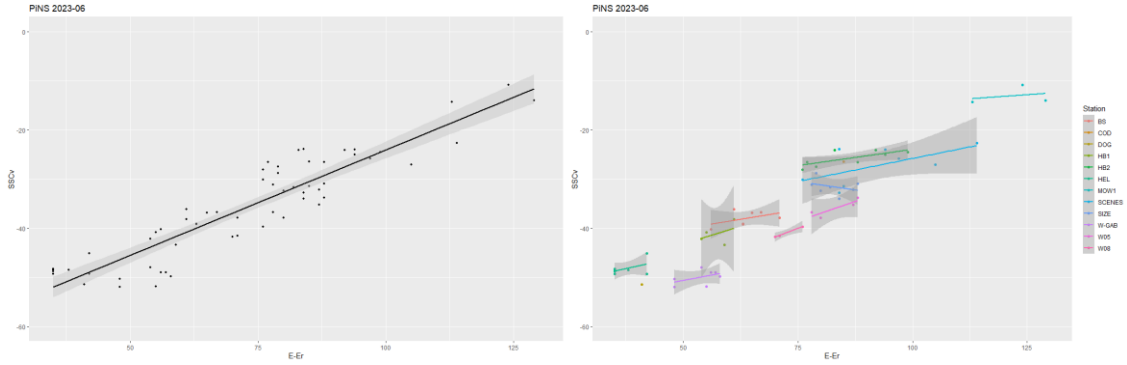

Figure 1 Left, relationship between SPM concentration (from filtration) and associated hull-mounted ADCP backscatter; right, station-based color-coded relationships between SPM concentration and ADCP echo intensity.

Concentration of SPM is recorded by the ADCP as shown for station Sizewell (southern coast of Suffolk, UK) in Fig.2, the corresponding current speed illustrates that the SPM is transported by a combination of advective process and locally re-suspended seafloor sediment.

[1] Institute of Natural Sciences, Brussels, Belgium.
[2] Institut Français de Recherche pour l'Exploitation de la Mer, France.

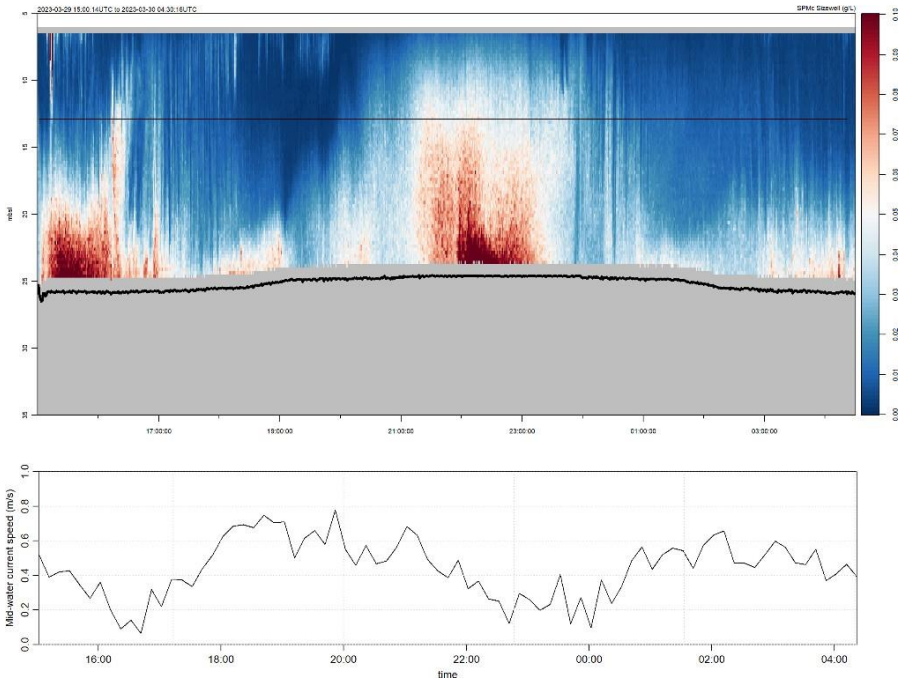

Figure 2 Top, Example of the ADCP-derived SPM concentration at station Sizewell; bottom, the water current speed during a full tidal- cycle.

Station-averaged LISST-100 particle size distributions (PSD) show differences (Fig.3), likely due to biologically dominated aggregated SPM in the offshore stations. The latter are predominately characterized by PSDs with larger particle sizes, resulting also in larger scaling factors between turbidity and SPM mass concentration (Fig 3, right).

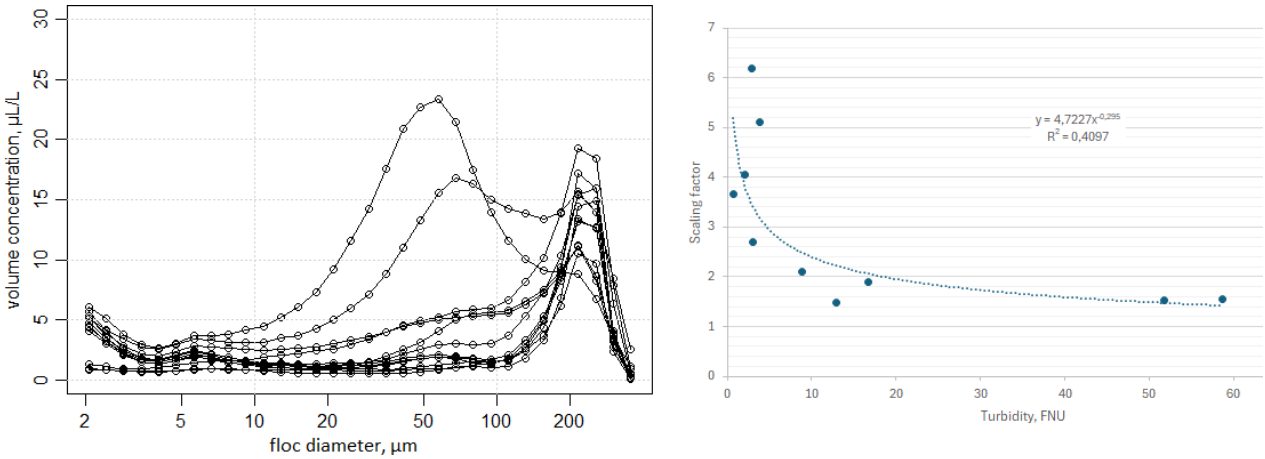

Figure 3 Left, LISST-100 averaged particle size distributions per station, and right, the scaling factor between FNU and the SPM concentration from filtration for each station.

References

Baeye M, Fettweis M, Voulgaris G, Van Lancker V. 2011. Sediment mobility in response to tidal and wind-driven flows along the Belgian inner shelf, southern North Sea. Ocean Dynamics 61, 611-622.

Fettweis M, Riethmüller R, Verney R, Becker M, Backers J, Baeye M, et al. 2019. Uncertainties associated with in situ long-term observations of suspended particulate matter concentration using optical and acoustic sensors. Progress in Oceanography 178, 102162.

Fettweis, Michael & Schartau, Markus & Desmit, Xavier & Lee, Byung Joon & Terseleer, Nathan & Van der Zande, Dimitry & Parmentier, Koen & Riethmüller, Rolf. (2022). Organic Matter Composition of Biomineral Flocs and Its Influence on Suspended Particulate Matter Dynamics Along a Nearshore to Offshore Transect. Journal of Geophysical Research: Biogeosciences. 127.

Kim Y H, Gutierrez B, Nelson T, Dumars A, Maza M, Perales H, Voulgaris G. 2004. Using the acoustic Doppler current profiler (ADCP) to estimate suspended sediment concentration Technical Report. CPSD #04-01

Interannual Exchange Flow Variability in a Morphologically Complex Estuary with Low Freshwater Input

Bailey T. [1], Ross L. [1], Rojas C. [1], and Smith C. [2,3]

Keywords: Total exchange flow, interannual variability in freshwater input, morphologically complex estuary

Abstract

Knowledge of circulation and material transport patterns in estuaries is essential for informed decision-making related to management of coastal water quality issues, like harmful algal blooms (HABs) and bacterial pollution, and for ensuring the sustainability of resources derived from estuaries and the communities that depend on them. Variability in freshwater input to estuaries has been found to impact circulation, having implications for the transport of suspended materials like HABs. Prediction of the ecological response of coastal areas to forecasted changes in precipitation patterns first requires an understanding of how freshwater input influences estuarine circulation and exchange flows. Although estuarine exchange flow has been well-studied in estuaries of simplified geometry, with relatively large freshwater inputs, it is not as well understood for complex systems with networks of streams and channels (MacCready et al., 2021), particularly under conditions of low freshwater inflows.

The goal of this research is to understand how interannual variations in freshwater input to a morphologically complex coastal bay can influence exchange with the outer ocean and between connected embayments. Two questions are posed to achieve this goal: 1) What is the tidal influence on exchange flow in a morphologically complex bay with low rates of freshwater input? 2) What is the influence from interannual variations in freshwater input on exchange flow? To address these questions, we investigate the exchange flow of Frenchman Bay, Maine, a macrotidal estuary system located within the Gulf of Maine with numerous channels, islands, and bathymetric complexities that influence tidal flows (Figure 1a). The total exchange flow (TEF) method is used to compute exchange to account for tidal variations in the salt flux due to mechanisms like tidal pumping (MacCready, 2011). The TEF framework uses an isohaline coordinate system to quantify transport in salinity bins, ranging from the minimum to the maximum salinity over a chosen transect or volume. By integrating over layers of positive and negative transport, the TEF bulk values (volume inflow, Q_{in}, and volume outflow, Q_{out}) and the respective salinities (S_{in} and S_{out}) are determined (Lorenz et al. 2018; Lemagie et al. 2022).

We use three-dimensional numerical model simulations from an unstructured Telemac3D model of Frenchman Bay to compute TEF. Simulations of a 'dry' year (2016) and comparatively 'wet' year (2021) are performed to quantify and compare the exchange flow in the bay under varying freshwater conditions. The TEF is calculated across two cross-sectional transects. One is located upstream where Frenchman Bay is connected to Blue Hill Bay (Figure 1b) by a narrow inlet, which constricts the exchange between the bays (hereon the Trenton transect). The second transect is located across the middle of the Bay (hereon the Frenchman Bay transect), separating Upper Frenchman Bay from Lower Frenchman Bay (Figure 1a).

Total exchange flow was estimated based on the methodology of Lemangie et al. (2022) for numerical data from an unstructured model domain, and the dividing salinity method of Lorenz et al. (2018) was used to compute the TEF bulk values. A profile of the time-averaged exchange flow and the TEF bulk values were computed over a ~14 day spring-neap period during early October of 2016 and 2021 for both the Trenton (Figure 1c) and the Frenchman Bay transects (Figure 1d). The dashed lines in Figure 1c and 1d denote the dividing salinities used to determine the transport layers (Lorenz et al. 2018). At the Trenton transect (Figure 1c), inflow (Q_{in}, positive) denotes transport into Blue Hill Bay, and outflow (Q_{out}, negative) denotes flow into Frenchman Bay. On the Blue Hill Bay side of the inlet, the Union River (Figure 1a), a major freshwater source to the study area, generates lower salinities. Flow into Frenchman Bay through the inlet occurs over a broader range of salinity classes during ebb tide as a result (not shown). Well-mixed water of higher salinities flows from Frenchman Bay into Blue Hill Bay during flood tide conditions (not shown). Over the spring-neap period in early October, the outflowing transport was greater in 2016 compared to 2021 (Figure 1c), indicating a greater contribution of freshwater input to Frenchman Bay. Both the S_{in} and S_{out} are lower in 2021 compared to 2016 due to the influence of higher rates of freshwater input on both sides of the inlet in 2021. The volume transport also spans a wider range of salinity classes, indicating less well-mixed conditions in 2021.

[1] University of Maine, Department of Civil and Environmental Engineering
[2] University of Maine, School of Earth and Climate Sciences
[3] Senator George J. Mitchell Center for Sustainability Solutions.

For the Frenchman Bay transect (Figure 1d), inflow (Q_{in}, positive) denotes flow into Upper Frenchman Bay, and outflow (Q_{out}, negative) denotes flow into Lower Frenchman Bay. Multiple estuaries contribute freshwater to the Upper Frenchman Bay; however the combined total discharge is relatively low compared to freshwater sources offshore (less than ~50 m^3/s on average). Freshwater input from larger rivers upcoast of Frenchman Bay in the northeastern Gulf of Maine, including the Saint John River (~1,000 m^3/s; not shown), can reduce the salinity of inflowing waters. During neap tide, the range of inflowing and outflowing salinities is reduced compared to spring tide (not shown). The outcomes suggest stronger spring tides promote the intrusion of saltier offshore waters into the bay, possibly expanding the salinity range and enhancing exchange. The magnitude of the exchange flow averaged over the spring-neap cycle in early October was greater in 2016 compared to 2021, with greater inflow at higher salinities (Figure 1d). Higher exchange flow in 2016 is consistent with greater ΔS (0.29 PSU) compared to ΔS in 2021 (0.17 PSU), as enhanced density differences increase exchange. However, inflowing salinities in 2016 were higher compared to 2021, suggesting a reduction in freshwater input from the offshore currents that carry in waters at lower salinities from freshwater sources along the northeast coast of Maine.

An increase in exchange flow was observed at the ocean boundary of Frenchman Bay due to inflowing waters of higher salt concentrations from offshore in 2016. This enhanced exchange may have been a factor contributing to the appearance of a regionally novel species of harmful algal bloom, *Pseudo-nitzschia*, in Frenchman Bay in late September-October of 2016. The blooms that likely originated offshore in the Gulf of Maine (Clark et al. 2021) were advected into Frenchman Bay, forcing closures of economic activities like shellfish harvesting and aquaculture. This study highlights the role of offshore variations in salinity on exchange flow in an estuary with low freshwater input, and the implications of these dynamics for material transport in regions with complex morphology like Frenchman Bay. This is an important step toward understanding the connectivity between regions like Frenchman Bay and the Gulf of Maine, and how that connectivity might influence water quality conditions and harmful algal blooms under future climate change scenarios.

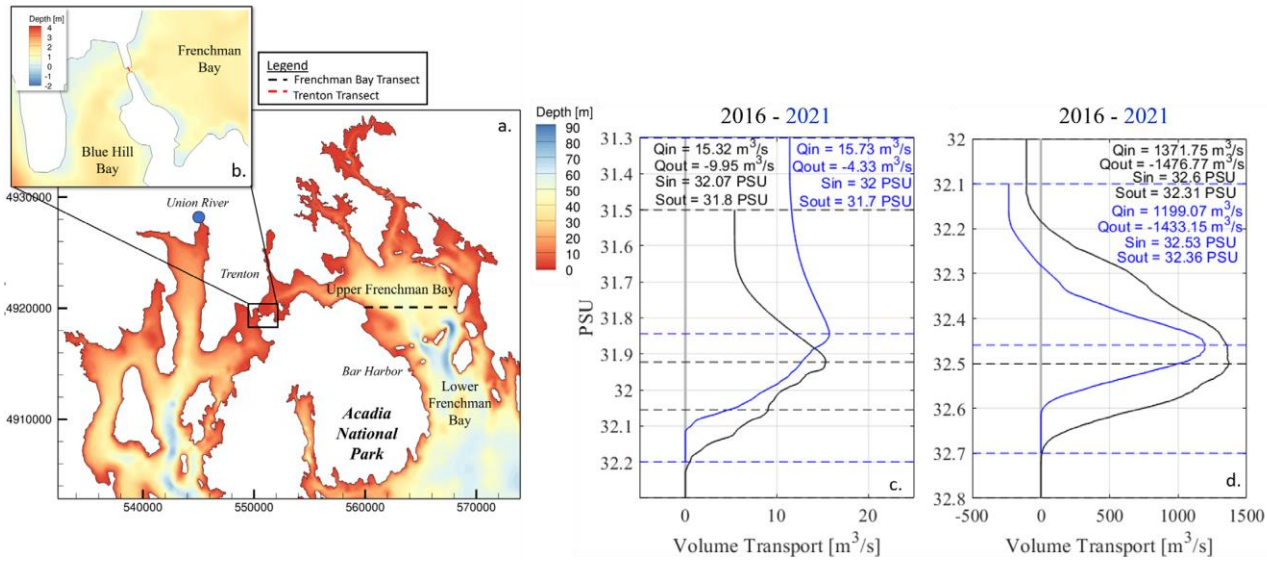

Figure 1. a) Study region of Frenchman Bay, Maine, depicting the location of the bay transect. b) Zoom in on the upstream inlet that separates Frenchman Bay from Blue Hill Bay. c) Time-averaged volume transport (Q) over a spring-neap cycle in October of 2016 (black line) and 2021 (blue line) for the Trenton transect. TEF bulk values are shown for 2016 (black) and 2021 (blue). d) Same as c) but for the Frenchman Bay transect.

References

Clark, S., Hubbard, K. A., McGillicuddy Jr, D. J., Ralston, D. K., Shankar, S. (2021). Investigating Pseudo-nitzschia australis introduction to the Gulf of Maine with observations and models. *Continental shelf research*, 228, 104493.

Lemagie, E. P., Giddings, S. N., MacCready, P., Seaton, C.,Wu, X. (2022). Measuring estuarine total exchange flow from discrete observations. *Journal of Geophysical Research: Oceans*, 127(10), e2022JC018960.

Lorenz, M., Klingbeil, K., Burchard, H. (2020). Numerical study of the exchange flow of the Persian Gulf using an extended total exchange flow analysis framework. *Journal of Geophysical Research: Oceans*, 125(2), e2019JC015527.

MacCready, P. (2011). Calculating estuarine exchange flow using isohaline coordinates. *Journal of Physical Oceanography*, 41(6), 1116-1124.

MacCready, P., McCabe, R. M., Siedlecki, S. A., Lorenz, M., Giddings, S. N., Bos, J., Albertson, S., Banas, N.S., Garnier, S. (2021). Estuarine circulation, mixing, and residence times in the Salish Sea. *Journal of Geophysical Research: Oceans*, 126(2), e2020JC016738.

Turbulent mixing in a salt-wedge microtidal estuary

Barros D. [1], Bailey T. [2], Ross L. [2], and Schettini C.A.F. [1]

Keywords: vertical eddy viscosity, turbulent mixing, microtidal estuary, funnel-shaped, salt wedge.

Abstract

Turbulence plays a key role in the dynamics and in the mixing of water properties and processes, such as bio-geochemistry inherent to estuaries, including the dispersion of salt, sediments, and pollutants as well as the vertical and horizontal distribution of plankton (Peters 1999, Geyer et al. 2000, Simpson & Sharphels, 2012). Mixing arises through momentum exchanges as the flow interacts with the bottom (Peters 1999, Geyer et al. 2000, Collignon & Stacey 2013). Research on turbulence and mixing in estuaries has traditionally centered around partially mixed, meso-tidal systems (Peters 1997, Collignon & Stacey 2013, Huguenard et al. 2015) or macrotidal estuaries (Allen et al. 1980, Giddings et al. 2011, Ross et al. 2019). Consequently, these studies have emphasized the impact of tides on turbulence and mixing.

The micro-tidal estuary in which this study took place, the Patos Lagoon in southern Brazil, is the biggest choked lagoon in the world (Kjerfve, 1986) and is primarily forced by wind and river discharge (Fernandes et al. 2005; Moller et al. 1996). Coastal lagoons generally have a well-mixed salt distribution pattern, however, the Patos Lagoon varies from well-mixed to highly stratified depending on river flow and wind conditions (Hartmann & Schettini 1991, Moller & Castaing 1999). In addition, the inlet of the lagoon was altered in 2010 to include converging jetties extending up to 700 m offshore of the lagoon mouth. A study by Yuk & Aoki, 2007 found that topographic changes, such as the narrowing of an inlet of a semi-enclosed bay, can lead to the intensification of currents, which increased vertical mixing. The enhanced current velocities were not only due to the alterations in topography, but also from the subsequent changes in bathymetry resulting from the construction of the jetties. There have been many studies on the Patos Lagoon, yet most have been based on the hydrodynamics before the addition of the convergent jetties (Marques et al. 2010, Marques et al. 2011). The handful of studies on the hydrodynamics of the lagoon after 2010 investigated freshwater discharge, wind effect and water level (Barros et al. 2014, Oliveira et al. 2019, Tavora et al. 2019, Antonio et al. 2020), with a primary emphasis on sediment dynamics (Silva et al. 2015, Lisboa et al. 2015). The along-channel variation in the current structure and mixing regime have remained uninvestigated topics, particularly in the inlet of the lagoon, despite their influence on sediment transport and estuary water quality.

In this study, high-resolution observations of temperature, salinity, velocity, and turbulent dissipation were collected in a longitudinal gradient to quantify the spatial variability in the circulation structure and mixing. Data were collected at three distinct transect positions along the channel and parameters such as the Richardson number, vertical eddy viscosity, and mixing efficiency were calculated from these transects. The survey was performed at the inlet zone and a micro-structure profiler (MicroCTD) was used to collect data and estimate dissipation rates of turbulence kinetic energy. An Acoustic Doppler Current Profiler (ADCP) was also used to collect horizontal flow velocities to calculate current speed and vertical shear.

Results showed that despite the short interval between the collection of data from each transect and their proximity (less than 9 km apart), mixing was enhanced or suppressed by different forces. The driving mechanisms ranged from channel curvature and differential advection (Valle-Levinson, 2010) to bottom stresses and the shear of the pycnocline on the salt wedge. Also, the funnel-shaped channel accelerated the current toward the constriction, although the expected increase in mixing was rebutted due to the effect of stratification. The comparison between the transects and the investigation of the different mechanisms promoting mixing in each will contribute to a better understanding of the hydrodynamics in the Patos Lagoon as well as salt wedge, microtidal estuaries found worldwide.

[1] Laboratory of Physical Oceanography of Coasts and Estuaries / Federal University of Rio Grande (LOCostE / FURG), Rio Grande, RS, Brazil; debor@furg.br

[2] Department of Civil and Environmental Engineering, University of Maine, Orono, ME, USA; lauren.ross1@maine.edu

References

Allen, G. P., Salomon, J. C., Bassoullet, P., Du Penhoat, Y., & de Grandpré, C. (1980). Effects of tides on mixing and suspended sediment transport in macrotidal estuaries. Sedimentary Geology, 26(1-3), 69–90. doi:10.1016/0037-0738(80)90006-8

António, M., Fernandes, E., Muelbert, J. (2020) Impact of jetty configuration changes on the hydrodynamics of the subtropical patos lagoon estuary, Brazil. Water (Switzerland), 1-27, 12(11). doi: 10.3390/w12113197

Barros, G., Marques, W., Kirinus, E. (2014) Influence of the Freshwater Discharge on the Hydrodynamics of Patos Lagoon, Brazil. *International Journal of Geosciences*, **5**, 925-942. doi: 10.4236/ijg.2014.59080.

Collignon, A., Stacey, M. (2013). Turbulence dynamics at the shoal-channel interface in a partially stratified estuary. Journal of Physical Oceanography,43, 970–989

Fernandes, E., Dyer, K., Moller, O. (2005) Spatial Gradients in the Flow of Southern Patos Lagoon, *Journal of Coastal Research* 2005(214), 759-769, (1 July 2005). doi:10.2112/006-NIS.1

Geyer, R. W., Trowbridge, J. H., & Bowen, M. M. (2000). The dynamics of a partially mixed estuary. Journal of Physical Oceanography,30, 2035–2048

Giddings, S. N., Fong, D. A., & Monismith, S. G. (2011). Role of straining and advection in the intratidal evolution of stratification, vertical mixing, and longitudinal dispersion of a shallow, macrotidal, salt wedge estuary. Journal of Geophysical Research,116, C03003. doi: 10.1029/2010JC006482

Hartmann, C. & Schettini, C. (1991) Aspectos Hidrológicos Na Desembocadura Da Laguna Dos Patos, Rs. Revista Brasileira de Geociências, 371-377, 21(4), doi: 10.25249/0375-7536.1991371377

Huguenard, K.D.; Valle-Levinson, A., Li, M.; Chant, R.J.; Souza, A.J. (2015). Linkage between lateral circulation and near-surface vertical mixing in a coastal plain estuary. *Journal of Geophysical Research: Oceans*, 120, 4048-4067. doi: 10.1002/2014JC010679

Kjerfve, B., Magill, E.K.E. (1986) Comparative oceanography of coastal lagoons. In Estuarine Variability; Wolfe, D.A., Ed.; Academimc Press: New Yourk, NY, USA, pp.63-81

Lisboa, P.V., Fernandes, E.H. (2015) Anthropogenic influence on the sedimentary dynamics of a sand spit bar, PatosLagoon Estuary, RS, Brazil.J. Integr. Coast. Zone Manag.15, 35–46

Marques, W.C., Fernandes, E.H.L., Moller, O.O. (2010) Straining and advection contributions to the mixing process of the Patos Lagoon coastal plume, Brazil.J. Geophys. Res. 115, C06019

Marques, W.C., Fernandes, E.H.L., Rocha, L.A.O. (2011) Straining and advection contributions to the mixing process in the Patos Lagoon estuary, Brazil.J. Geophys. Res.115, C03016.

Moller Jr, O. O., and Castaing, P. (1999), Hydrographical Characteristics of the Estuarine Area of Patos Lagoon (30°S, Brazil), In Estuaries ofSouth America, edited by Perillo G.M.E., Piccolo M.C., Pino-Quivira M. Environmental Science. Springer, Berlin, Heidelberg. doi:10.1007/978-3-642-60131-6_5

Oliveira, H., Fernandes, E., Möller, O., Jr., García-Rodríguez, F. (2019) Relationships between Wind Effect, Hydrodynamics and Water Level in the World's Largest Coastal Lagoonal System. *Water11*, 2209. doi:10.3390/w11112209

Peters, H. (1997), Observations of stratified turbulent mixing in an estuary: Neap-to-spring variations during high river flow,Estuarine Coastal Shelf Sci., 45, 69–88.

Peters, H. (1999). Spatial and temporal variability of turbulent mixing in an estuary. Journal of Marine Research,57, 805–84 Ross, L., Huguenard, K. D., Sottolichio, A. (2019). Intratidal and fortnightly variability of vertical mixing in a macrotidal estuary: The Gironde.Journal of geophysical research: Oceans,124, 2641–2659.https://doi.org/10.1029/2018JC014456

Silva, P., Lisboa, P., Fernandes, E. (2015) Changes on the fine sediment dynamics after the Port of Rio Grande expansion. Advances in Geosciences, 123-127, 39. doi: 10.5194/adgeo-39-123-2015

Simpson, J. & Sharphels, J. (2012) Introduction to the Physical and Biological Oceanography of Shelf Seas. Cambridge University Press. 4.3 -4.4

Tavora, J., Fernandes, E.H.L., Thomas, A.C., Weatherbee, R., Schettini, C.A. F. (2019): The influence of river discharge and wind on PatosLagoon, Brazil, Suspended Particulate Matter, International Journal of Remote Sensing, doi:10.1080/01431161.2019.1569279

Valle-Levinson, A. (2010) Contemporary Issues in Estuarine Physics. Cambridge University Press. pp. 112-124

Yuk, J.H.; Aoki, S. (2007) Impact of Jetty construction on the current and Ecological Systems in the Estuary with a Narrow Inlet.J. Coast. Res., 784–788

A Local Eddy Viscosity Parameterization for Estuarine Exchange Flow

Basdurak N.B. [1,2], Burchard H. [2], and Schuttelaars H.M. [3]

Keywords: estuaries, tidal and wind mixing, wind entrainment, boundary layers, exchange flow.

Abstract

Structure and intensity of estuarine exchange flow depend significantly on the eddy viscosity A_v profile which is dynamically linked to various forces (e.g., gravitational, tidal, wind-driven). The impact of winds on the exchange flow is complex due to its direct (local and remote changes in shear and density stratification) and indirect (modifications to A_v profiles) contributions (see Basdurak et al., 2021). This study aims (i) to include wind entrainment effects in the tidally averaged A_v parameterization (Fig. 1); (ii) to develop an analytical one-dimensional model for the wind driven exchange flow by using this novel parameterization and assess the tidally averaged dynamics over a relevant physical parameter-space, subdomains of which have not yet been explored numerically. This one-dimensional model is based on a balance between frictional forces and pressure gradient, calibrated with a tidally-resolving one-dimensional water-column model with second-moment closure. Structure and intensity of the resulting exchange flow profiles are analyzed with respect to three dimensionless parameters (the unsteadiness of boundary layer mixing *Un*, scaled-directional wind stress *W*, and horizontal stratification *Si*). While down-estuarine winds enhance the gravitational circulation, up-estuarine winds result in either a two-layer inverted circulation opposing the gravitational circulation, or a three-layer flow (favored by relatively strong *Si*, weak *W*, and moderate *Un*) that is up-estuarine at the surface with classical two-layer circulation underneath. Relative thicknesses of surface and bottom boundary layers affect both the intensity and the inflection depth of the exchange flow layers. Up-estuarine winds with $W \gtrsim 0.5$ yield unstable stratification and reduce the exchange flow intensity with increasing *W* (see Basdurak et al., 2023).

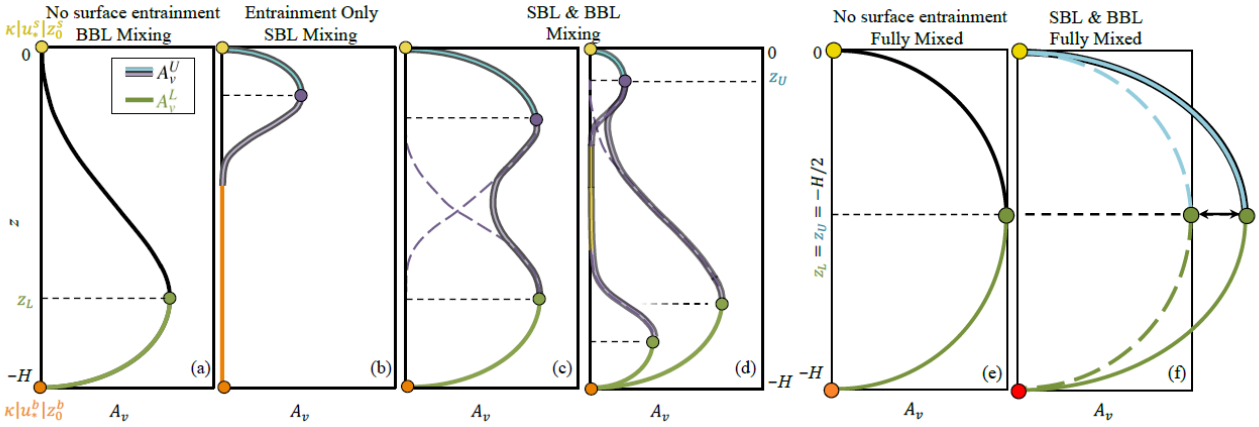

Figure. 1 A sketch of tidally averaged eddy viscosity profiles under stratified conditions: (a) only bottom boundary layer BBL mixing, (b) only surface boundary layer SBL mixing, and (c, d) both BBL and SBL mixing. Critical depths are marked by circles, e.g., yellow/orange circles are associated with surface/bottom friction velocities u_* and roughness lengths z_0 (κ is the van Kármán constant). The upper layer A_v^U is formulated as a single layer or two layers (without or with wind entrainment). (e, f) Fully mixed conditions without and with surface entrainment. Red circle in (f) denotes $\kappa(|u_*^s| + |u_*^s|)\, z_0^b/2$ in case of an unstable stratification (solid line). Green line denotes the BBL; black line denotes the upper layer without SBL; blue and purple lines denote the surface and interfacial layers, respectively.

References

Basdurak, N. B., Burchard, H., & Schuttelaars, H. M. (2021). A local eddy viscosity parameterization for wind-driven estuarine exchange flow. Part I: Stratification dependence. Progress in Oceanography, 193, 102548.

Basdurak, N. B., Burchard, H., & Schuttelaars, H. M. (2023). A local eddy viscosity parameterization for wind-driven estuarine exchange flow, Part II: Entrainment. Progress in Oceanography, 219, 103166.

[1] Institute of Marine Sciences, Middle East Technical University, Erdemli 33731, Türkiye
[2] Leibniz Institute for Baltic Sea Research Warnemünde, Seestr. 15, D-18119, Rostock, Germany
[3] Delft Institute of Applied Mathematics, Delft University of Technology, Delft, Netherlands

Salt fluxes and salt intrusion in the Weser estuary, North Sea

Becker M. [1], Zorndt A. [2], Kösters F. [2], and Winter C. [1]

Keywords: salt intrusion, salt fluxes, partially mixed estuaries, dispersion, surge discharge interaction

Abstract

This study investigates salt flux mechanisms and the dynamics of the salt intrusion of the Weser estuary. The Weser was subject to several measures of river engineering during the last century. River deepening caused an increase of the tidal range, now exceeding 4 m at the city of Bremen. The salt intrusion increased by 2.5 km, as shown by the recent study of Kolb et al. (2022). However, information on mixing, stratification, and on the estuarine transport processes, which are affected by these long-term changes, is sparse. We analyze salt fluxes based on one year of numerical model results. The simulation period includes a period of constantly low discharge, a period of slightly elevated and more variable discharge, and one discharge peak. The time series also includes two characteristic storm surges. We determine the contributions to the subtidal salt flux (Fischer 1976) at 16 cross-sections, distributed in steps of 5 km along the channel. This extent covers the dynamic range of the location of the brackish zone.

On first sight, the down-gradient salt flux is often controlled by tidal pumping, which mostly exceeds the contribution due to the estuarine exchange flow (steady shear dispersion). While this is the case for the low discharge period, the exchange flow contribution eventually exceeds the tidal pumping flux, at least at certain along-channel locations and during times of increased discharge and stratification. In general, the governing salt flux mechanisms are highly variable throughout the hydrological year, as expected for a partially mixed estuary (Geyer et al. 2000). They also depend on the salt intrusion itself. As the brackish zone is advected downstream during the discharge peak, stratification increases and the exchange flow contribution exceeds the tidal pumping flux in the outer Weser (Figure 1). Tidal pumping is increased during spring tide, in line with changes of the tidal velocity asymmetry. Alternatingly, the exchange flow contribution is slightly increased during neap tides, in response to changes of stratification. As to the combined effect, the salt intrusion varies insignificantly along the neap-spring cycle, on average. On shorter timescales, surge-induced upstream-directed barotropic fluxes contribute substantially to the salt intrusion. We then use these results to identify hotspots of dispersion and to analyze the internal structure of the brackish zone, as the locations of isohalines vary in terms of their distance to the maximum along-channel salinity gradient. Since the salt intrusion did not reach an equilibrium during low discharge conditions, we have a closer look at the salt flux mechanisms further upstream, in the channelized part of the estuary.

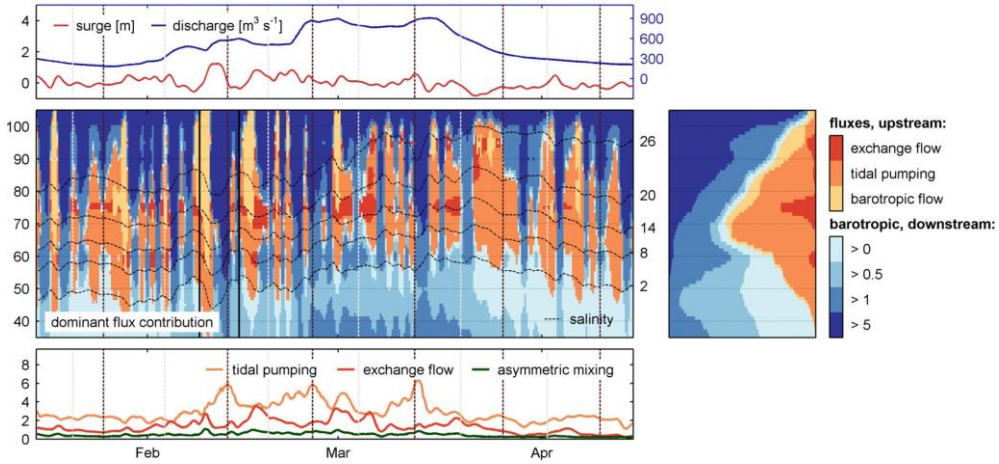

Figure 1: Flux contributions during the discharge peak. The second panel shows the along channel distribution (river km) of the dominant contribution to the salt flux. Fluxes in the lower panel are averaged between the locations of isohaline 2 and 26. Light grey and black dashed vertical lines indicate neap and spring tides, respectively.

References

Fischer, H. B. (1976), Mixing and Dispersion in Estuaries, Annual Review of Fluid Mechanics, 8(1), 107-133.

Geyer, W. R., J. H. Trowbridge, and M. M. Bowen (2000), The Dynamics of a Partially Mixed Estuary, Journal of Physical Oceanography, 30(8), 2035-2048.

Kolb, P., A. Zorndt, H. Burchard, U. Gräwe, and F. Kösters (2022), Modelling the impact of anthropogenic measures on saltwater intrusion in the Weser estuary, Ocean Sci., 18(6), 1725-1739

[1] Institute of Geosciences, Christian-Albrechts-Universität, Kiel, Germany. marius.becker@ifg.uni-kiel.de
[2] Federal Waterways Engineering and Research Institute, Hamburg, Germany

Human Footprint on Tides Dominates Water Levels in Estuaries and Tidal Rivers around the Globe

Beemster J.G.W. [1], Talke S.A. [2], van Maren B. [3], and Hoitink T.J.F. [4]

Keywords: tidal hydrodynamics, land reclamation, deepening, tidal amplification

Abstract

Estuaries and tidal rivers represent critical coastal ecosystems, profoundly influenced by human activities over centuries. Anthropogenic interventions such as land reclamation and channel deepening have transformed these environments, altering estuarine hydrodynamics and water level patterns. Understanding the complex interplay between human alterations and natural tidal dynamics is essential for assessing the resilience of coastal regions in the face of rising sea levels and changing climatic conditions. This study investigates the impact of human interventions on tidal hydrodynamics in 18 estuaries scattered around the globe. By recovering, digitizing, collecting and examining historical data of estuarine geometry and tidal patterns, we unravel centennial-scale changes of estuarine tidal dynamics and discuss the extent to which human activities have influenced tidal amplitudes, water level extremes, and the spatial distribution of this influence. The objective of this study is to evaluate the effects of human interventions on tidal hydrodynamics in 18 estuaries around the world. We conducted a comprehensive analysis of historical data spanning multiple decades to centuries, focusing on estuarine geometry, tidal amplitudes, and water level extremes. Our methodology involved collating and analysing long-term hydrodynamic and geometric data from each estuary. Next, we determined characteristic geometric (e.g. average channel depth, intertidal area) and hydrodynamic (e.g. max tidal range, mean annual discharge) variables over time to understand how changes in geometry affect hydrodynamic behavior. By integrating historical insights with contemporary data, we aim to understand the complex dynamics governing the interaction between human activities and natural tidal processes. Preliminary analysis reveals significant alterations in tidal hydrodynamics across the 18 estuaries studied. Human interventions, particularly channel deepening, land reclamation and barrier construction, have led to widespread changes in tidal amplitudes and water levels (Fig 1). Our results indicate a general trend of tidal amplification, with the most pronounced effects observed in the landward reaches of estuaries, generally exceeding rates of sea level rise. The spatial distribution of tidal effects suggests a complex interplay between estuarine geometry and human alterations, with narrow funnel-shaped estuaries exhibiting heightened sensitivity to anthropogenic interventions. These findings underscore the pervasive influence of human activities on estuarine hydrodynamics and highlight the need for adaptive estuarine management strategies in the face of changing environmental conditions.

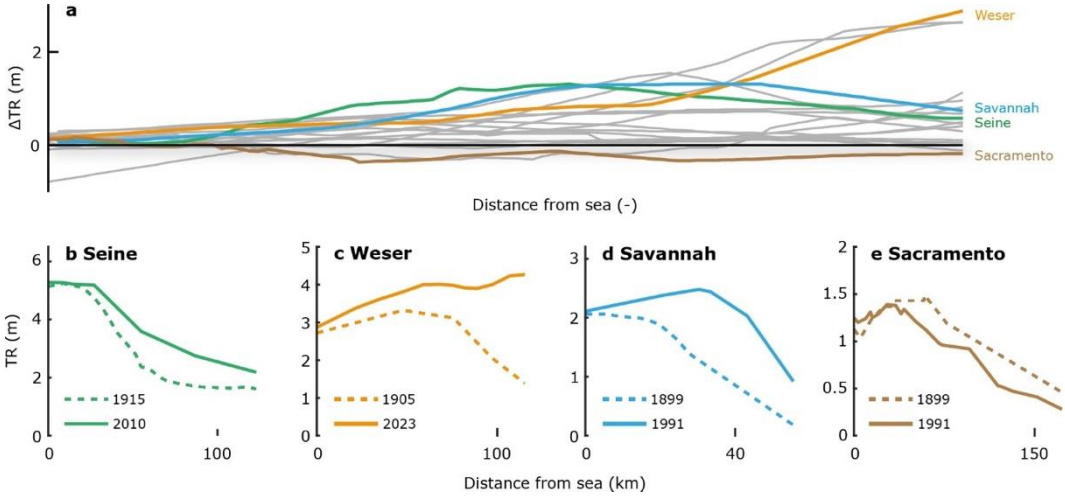

Figure 1. Changes of the tidal range in the eighteen estuaries. a. Along channel changes of the tidal range for the 18 estuaries included in our study, the distance to the sea is normalized by the distance to the most landward observation, along channel profiles of the tidal range in b. the Seine in 1915 and 2010, c. the Weser in 1905 and 2023, d. the Savannah in 1899 and 1992, and e. the Sacramento in 1899 and 1992.

[1] Hydrology and Environmental Hydraulics Group, Department of Environmental Sciences, Wageningen University & Research, Wageningen, The Netherlands; joris.beemster@wur.nl
[2] Department of Civil and Environmental Engineering, California Polytechnic State University, San Luis Obispo, CA, USA; stalke@calpoly.edu
[3] Faculty of Civil Engineering and Geosciences, Delft University and Technology, Delft, The Netherlands; Deltares, Marine and Coastal Systems Unit, Boussinesqweg 1, Delft, The Netherlands; bas.vanmaren@deltares.nl
[4] Hydrology and Environmental Hydraulics Group, Department of Environmental Sciences, Wageningen University & Research, Wageningen, The Netherlands; ton.hoitink@wur.nl

Effects of turbid and liquid plumes in modulating the Western Black Sea ROFI: a modelling study

Bellafiore D. [1], Shamsnia S.H. [2], Van Gils J. [3], Loos S. [4], Fach B. [5], Sadighrad E. [6], Bajo M. [7], and Ferrarin C. [8]

Keywords: plumes, finite element modeling, Wave-current interaction, ROFI, sediment transport.

Abstract

This study provides a comprehensive numerical study of the effects of waves, and wave-current interaction on the river plume hydrodynamics and sediment dispersal along the western coast of the Black Sea, with a focus on the Danube Delta area. The modeling study has been carried out using a novel model chain, from catchment to sea covering the Western Black Sea. It comprises a 3D finite element model of the coastal area including the last portions of the rivers and coastal bodies, is forced laterally with outputs of a catchment model developed by Deltares on 11 river catchments around the Black Sea, and forced at the open sea boundaries by a 3D Black Sea model implemented by METU (Sadighrad et al., 2021). In the coastal domain the coupled SHYFEM-WWIII models, with the Sedtrans05 module (embedded in SHYFEM) activated (Umgiesser et al., 2014). The model was applied in the past in the Black Sea area (Bajo et al., 2014, Dinu et al., 2011). It has been successfully applied to study 3D baroclinic cross-scale lake-river-estuary-plume-shelf- ocean circulation (Umgiesser et al., 2004, Umgiesser et al. 2014). The model chains is suited for investigating the land- sea interaction and the effects of water and sediment loads from rivers in the coastal area, since the catchment model provides water and sediment loads and the coastal model reproduces 3D circulation, wave-current interaction and suspended sediment transport.

An unstructured grid was produced (24694 nodes, 43864 elements) covering the Western Black Sea from the Turkish coast North of the Bosphorus Strait up to Crimea. The grid includes four river inputs (Figure 1).

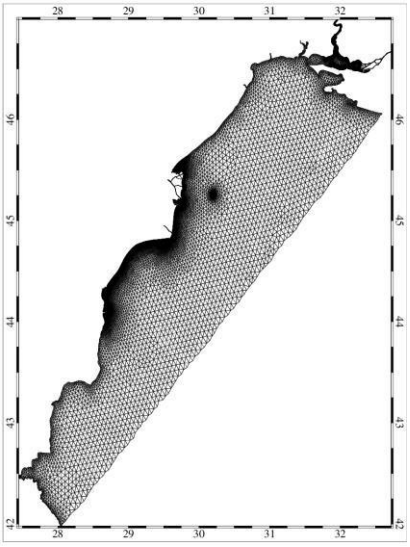

Figure 1: Model Domain, Western Black Sea finite element grid.

The boundary forcings include the river forcings (discharges), sediment loads, and temperature from the rivers computed by the catchment model developed by Deltares, together with the open sea boundary conditions from NEMO (METU run).

[1] CNR-ISMAR, Institute of Marine Sciences, National Research Council, Venice, Italy. debora.bellafiore@cnr.it.
[2] Institute of Marine Sciences, National Research Council, Venice, Italy. seyedhadi.shamsnia@ve.ismar.cnr.it, hadikntuci@gmail.com
[3] Deltares, Delft, The Netherlands. jos.vangils@deltares.nl.
[4] Deltares, Delft, The Netherlands. sibren.loos@deltares.nl
[5] Middle East Technical University, Turkey. bfach@ims.metu.edu.tr
[6] Middle East Technical University, Turkey. ehsan@ims.metu.edu.tr
[7] CNR-ISMAR, Institute of Marine Sciences, National Research Council, Venice, Italy. marco.bajo@cnr.it.
[8] CNR-ISMAR, Institute of Marine Sciences, National Research Council, Venice, Italy. christian.ferrarin@cnr.it.

The simulation protocol includes circulation runs and wave-current coupled runs modelling both with atmospheric forcing and river/sediment inputs to disentangle the relative effect of waves of haline and turbid plumes and extension of ROFI. Model results were valudated through comparison with satellite products (Fig. 2).

The study describes the plumes dynamics, the variability of salinity and SSC patterns along the year, inferring on the effect of the main drivers (wind, river water and solid discharge, waves) evaluating specific events and the relative effect of circulation and waves, as well as the river discharge and sediment load in modulating the ROFI (Region of Freshwater Influence) and the turbid plumes.

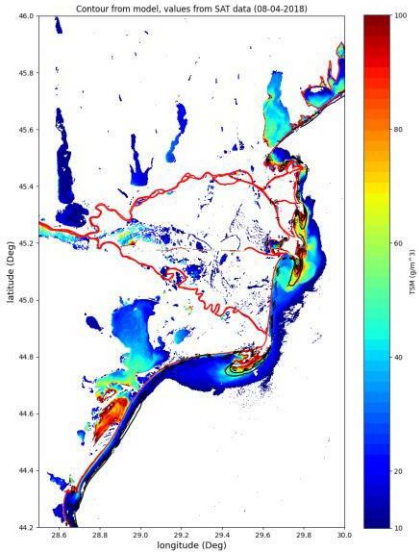

Figure 2: SSC model validation: Derived TSM, in colour, for the day 8th of April 2018 10UTC. Modelled SSC is represented through isolines.

The model chain, thanks to the improved outputs from the catchment model and the open sea boundary conditions provides good results and evidence the importance not only of a good representation of the domain, but the central role of lateral forcingins, as well as a full set of information on the liquid and solid loads from rivers, to reproduce the coastal dynamics of the Western Black Sea. This model chain is a first step which can be further improved either for specific process study implementations of for broader operational uses to support coastal management.

References

Bajo, M., Ferrarin, C., Dinu, I., Umgiesser, G., & Stanica, A. (2014). The water circulation near the Danube Delta and the Romanian coast modelled with finite elements. Continental Shelf Research, 78, 62-74. https://doi.org/10.1016/j.csr.2014.02.006

Dinu, I., M. Bajo, G. Umgiesser and A. Stanica 2011. Influence of wind and freshwater on the current circulation along the Romanian Black Sea coast. Geo-Eco-Marina, Vol. 17/2011, 13-26.

Umgiesser G, Melaku Canu D, Cucco A, Solidoro C (2004) A finite element model for the Venice Lagoon. Development, set up, calibration and validation. J Marine Syst 51:123–145

Umgiesser, G., Ferrarin, C., Cucco, A., De Pascalis, F., Bellafiore, D., Ghezzo, M., & Bajo, M. (2014). Comparative hydrodynamics of 10 Mediterranean lagoons by means of numerical modeling. Journal of Geophysical Research: Oceans, 119(4), 2212-2226.

Sadighrad, E.; Fach, B.A.; Arkin, S.S.; Salihoğlu, B.; Hüsrevoğlu, Y.S. (2021) Mesoscale Eddies in the Black Sea: Characteristics and Kinematic Properties in a High-Resolution Ocean Model. J. Mar. Syst., 223, 103613, doi:10.1016/j.jmarsys.2021.103613

Tidally Driven Stokes Transport in a Multi-inlet lagoon

Benton C. [1] and Chant B. [2]

Keywords: physics, estuaries, stokes transport, residual circulation, multi-inlet, lagoon.

Abstract

Multi-inlet lagoons are not characterized well by the classic estuary momentum balance between a depth dependent pressure gradient and a vertical stress divergence. Furthermore, recent studies have shown that these bays are flushed primarily by tidally driven residual flows, this contrasts with earlier studies that suggested that flushing was driven by synoptic atmospheric forcing Vieira, M. E., and R. Chant (1993). Instead, we hypothesize that circulation in these systems is driven by a landward tidally driven Stokes transport though the inlets. Stokes transport at the inlets will drive a sea-level set up in the bay, or superelevation, which results in a Eulerian seaward flow. Because these systems have multiple inlets, a difference in Stokes transport between inlets will result in a super-elevation gradient across the bay and ultimately may lead to a through-flow circulation. We investigate tidally driven Stokes transport as a mechanism contributing to the residual circulation in Barnegat Bay, New Jersey, Defne, Z., and N. K. Ganju (2015). To do this we collected data from moorings in Barnegat Bay's primary inlets, Barnegat Inlet (BI) in the north and Little Egg Inlet (LEI) in the south, figure1. Shipboard Surveys and ROMS will help us better understand the lateral structure in the channels and circulation within the bay. Understanding tidal residual circulation in these systems is important because they may contribute to effective flushing in the form of through-flow circulation.

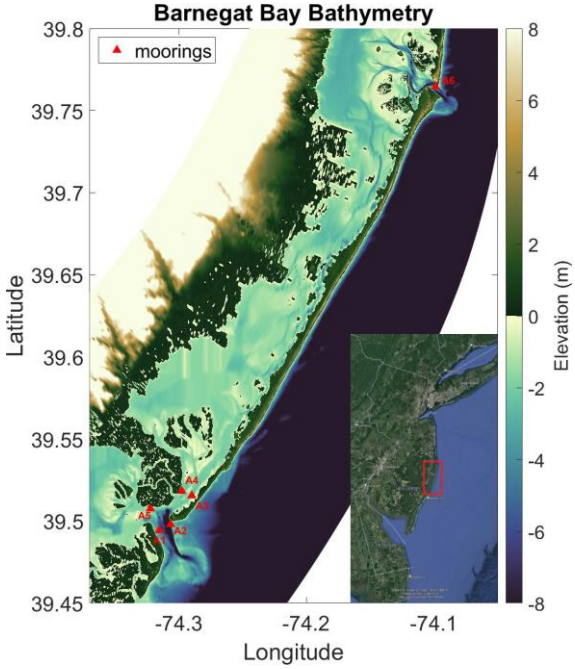

Figure 1. Map of Barnegat Bay, NJ. Colorbar indicates bathymetry from ROMs model grid. Mooring locations are denoted with red triangles. Moorings A1-A5 are located in Little Egg Inlet and A6 is located in Barnegat Inlet.

Lagoons are shallow, well mixed estuaries often located behind barrier islands. It is common for them to have multiple inlets. Some well-known examples include Great South Bay in New York, Pamlico Sound in North Carolina, and Lagos Bay in Nigeria. Tides are strongly attenuated in these systems; however, recent studies have shown tidal residual circulation to play an important role in their circulation, Hinrichs, C., et al. (2018) & Defne, Z., and N. K. Ganju (2015). The barrier islands and inlets in these systems are morphologically dynamic and changes in inlet morphology have a first order impact on circulation and residence times in these systems. Work done in Great South Bay highlights this. Great South Bay consisted of four inlets until hurricane Sandy caused a breach in the barrier island in 2012. This breach resulted in a new inlet (ironically named 'old inlet') which was much smaller than the existing four. Even with the transport of "old inlet" being an order of magnitude smaller than the other inlets, the tidal residual circulation within Great South Bay increased four-fold, Hinrichs, C., et al. (2018). Another study done for Barnegat Bay New Jersey found a small but persistent residual transport through the bay, Defne, Z., and N. K. Ganju (2015). These lagoonal systems have mixing timescales of weeks to months, which means synoptic atmospheric forcing, with timescales of 3-5 days, are ineffective at flushing them. However, the persistent residual transports can have a significant effect on flushing.

[1] Rutgers University, cody.benton@marine.rutgers.edu
[2] Rutgers University, chant@marine.rutgers.edu

We have collected data from two, six-week mooring deployments during 2023 (with a 3rd deployment currently underway). The moorings consist of upward looking ADCPs and surface and bottom CT sensors. Estimates of Stokes, Eulerian and total transport have been made with the moored data. Results confirm that Stokes transport is persistently landward at the inlets and fluctuates over the spring neap tidal cycle, figure 2. The Stokes transport is smaller than the Eulerian but is a non-negligible component of the total transport. Of particular interest is how inlet morphology effects both Stokes and Eulerian mean residual transport. Stokes transport is influenced by tidal current amplitude, tidal range, channel width and the phase between tidal currents and sea level, where the largest Stokes transport occurs when the phase difference is zero. All of these are influenced by both inlet morphology and dynamics of the back bays. BI (mooring A6) experiences a more in-phase tidal current and tidal amplitude, which make it more conducive to Stokes transport, however the width of LEI (mooring A1 & A2) means it experiences a higher Stokes transport even though the phase difference through this inlet is not as conducive for Stokes transport. Shipboard surveys and modelling studies will also be used to resolve the lateral variability in transport across the inlets and characterize the link between transport in the inlets and circulation in the interior lagoon.

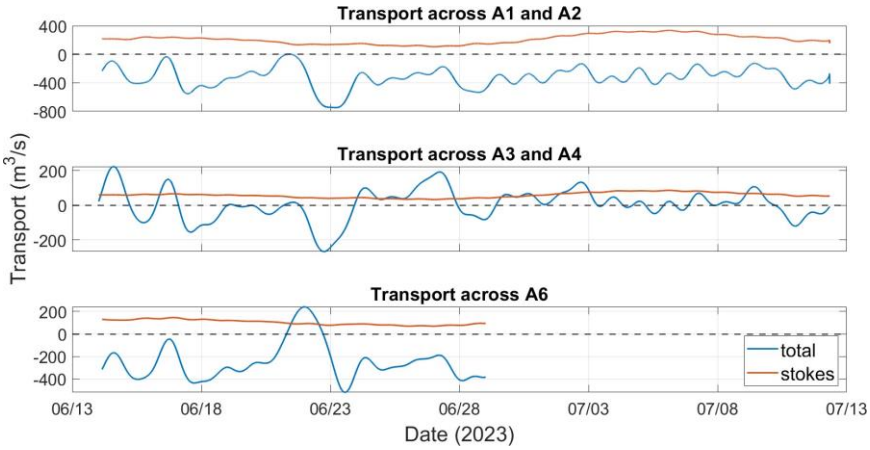

Figure 2 Mooring estimates for Stokes transport and total transport across several mooring lines. A1 and A2 correspond to LEI, A6 is BI. The southern terminus of the bay is represented by the A3 and A4 line. Total transport is Stokes + Eulerian.

To date we have conducted several shipboard tidal-cycle surveys across the mooring lines and several more are plannied in the coming months. These surveys consist of CTD casts and ADCP observations. Early results show that while these systems show very little vertical variability, they exibit significant lateral variability. Even more challenging is capturing the dynamics in shallow regions such as tidal flats where we suspect a significant landward transport occurs. This is because tidal flows are highly rectified over regions that become dry at low tide, when currents are generally ebbing. To adress this our most recent deployment consists of several shallow water current meters on the tidal flats between moorings. We anticipate the data from these moorings to be useful when analysing the model results, which is the next step for understanding how tidally driven Stokes transport effects circulation in these mutli-inlet systems.

References

Defne, Z. and N. K. Ganju (2015). "Quantifying the residence time and flushing characteristics of a shallow, back-barrier estuary: Application of hydrodynamic and particle tracking models." Estuaries and Coasts 38: 1719-173

Hinrichs, C., et al. (2018). "Great South Bay after Sandy: Changes in circulation and flushing due to new inlet." Estuaries and Coasts 41: 2172-2190.

Vieira, M. E. and R. Chant (1993). "On the contribution of subtidal volume fluxes to algal blooms in Long Island estuaries." Estuarine, Coastal and Shelf Science 36(1): 15-29.

The relative importance of density-driven and tidal advective salt transport in partially mixed estuaries

Biemond B. [1], de Swart H.E. [1], and Dijkstra H.A. [1]

Keywords: salt intrusion mechanisms, estuaries, idealized modelling.

Abstract

Salt intrusion in estuaries threatens coastal freshwater supplies. This threat is expected to become worse in the context of climate change, as this will cause an increase in sea level and a decrease in freshwater discharge into estuaries (Lee et al., 2024). To quantify the dependence of salt intrusion on environmental conditions, it is necessary to gain fundamental understanding about the salt transport processes involved, this being the focus of this study.

From observations it is known that the most important contributions to the landward salt transport in partially mixed estuaries are density-driven and tidal advective transport (Díez-Minguito et al, 2013, Aristizábal and Chant, 2015). To gain fundamental knowledge about these different types of transport, idealized models are a helpful tool. The idealized models of Hansen and Rattray (1966) and Chatwin (1976) deal with the properties of density-driven salt transport but exclude tidal transport. Tidal advective transport is studied by McCarthy (1993) and Wei et al. (2016), but these models do not contain density-driven transport. Therefore, the interaction of these two processes cannot be studied using available models in literature.

The aim of this study is to find expressions for the relative importance of density-driven and tidal advective salt transport in estuaries. For this, we extend existing width-averaged models, by constructing a set of semi-analytical equations which solve for density-driven and tidal transport simultaneously. The existing models which only consider density-driven or tidal transport follow from specific assumptions on this set of equations.

The model solves the width-averaged momentum equations and continuity equation for hydrodynamics, coupled to an advection-diffusion equation for salt. These equations are simplified using harmonic decomposition and scaling analysis. As a case study, the Guadalquivir estuary is used, which is selected based on the availability of observations of salinity and discharge (Navarro et al., 2011, 2012).

The cross-sectionally and tidally averaged salt transport T in the estuary is decomposed following Lerczak et al. (2006):

$$T = T_Q + T_E + T_T + T_D, \tag{1}$$

in which TQ represent advective transport with the subtidal depth-averaged flow, TE is advective transport due to density-driven flow, TT is advective transport due to tidal flow, and TD is horizontal diffusion.

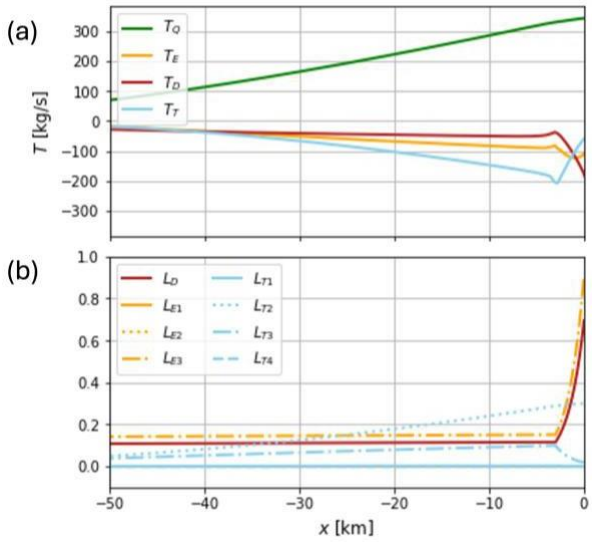

Figure 1. (a) Modelled salt transport processes in the Guadalquivir estuary under low discharge conditions versus x, where x = 0 is the estuary mouth. (b) As (a), but for the terms (length scale ratios) in Eq. 2.

[1] Institute for Marine and Atmospheric research Utrecht, w.t.biemond@uu.nl .

The different contributions to the modelled salt transport in the Guadalquivir for low discharge conditions are shown in Fig. 1a. It is visible that in most of the estuary, tidal transport is dominant, in agreement with Díez-Minguito et al. (2013), but density-driven transport and horizontal diffusion are non-negligible. Close to the estuary mouth, where the width increases, the relative contribution of tidal transport decreases.

To be able to determine the relative importance of the different salt transport processes without the need of a numerical model, analytical expressions for the transport processes derived from the semi-analytical model are inserted in Eq. 1, and the equation is written in a non-dimensional form, which yields

$$\Sigma = \left(\frac{L_{E3}}{L_{sc}}\right)^3 \left(\frac{\partial \Sigma}{\partial \lambda}\right)^3 + \left(\left(\frac{L_{E1}}{L_{sc}}\right)^2 + \left(\frac{L_{T2}}{L_{sc}}\right)^2 + \left(\frac{L_{T4}}{L_{sc}}\right)^2\right)\left(\frac{\partial \Sigma}{\partial \lambda}\right)^2 + \left(\frac{L_{E1}}{L_{sc}} + \frac{L_{T1}}{L_{sc}} + \frac{L_{T3}}{L_{sc}} + \frac{L_D}{L_{sc}}\right)\left(\frac{\partial \Sigma}{\partial \lambda}\right), \quad (2)$$

where Σ is the dimensionless salinity and λ dimensionless along-channel distance. The interpretation of the first four length scales is in MacCready (2004); in short, LD is the length scale associated with salt intrusion due to horizontal diffusion, LE1 quantifies effects of the shear of the river flow, LE2 represents effects of the interaction of the shear of the river flow with density-driven flow, and LE3 describes the salt intrusion due to density-driven flow. The new length scales LT1 to LT4 quantify the effects of tidal advective transport.

The terms in Eq. 2 as a function of along-channel coordinate are shown in Fig. 1b. It is visible that the same ratio between the different processes is present in these terms as in the transport balance. This indicates that these length scales are a suitable tool to determine the relative importance of salt transport processes in estuaries, which has the advantage with respect to other methods that the length scales can be calculated analytically.

To demonstrate the scope of this method, we will show results for multiple estuaries and environmental conditions.

References

Aristizábal, M. F., & Chant, R. J. (2015). An observational study of salt fluxes in Delaware Bay. Journal of Geophysical Research: Oceans, 120 (4), 2751-2768. https://doi.org/10.1002/2014JC010680

Chatwin, P. (1976). Some remarks on the maintenance of the salinity distribution in estuaries. Estuarine and Coastal Marine Science, 4(5),555–566. https://doi.org/10.1016/0302-3524(76)90030-X

Díez-Minguito, M., Contreras, E., Polo, M., & Losada, M. (2013). Spatio-temporal distribution, along-channel transport, and post-riverflood recovery of salinity in the Guadalquivir Estuary (SW Spain). Journal of Geophysical Research: Oceans, 118, 2267– 2278. https://doi.org/10.1002/jgrc.20172

Hansen, D. V., & Rattray, M. (1966). New dimensions in estuary classification 1. Limnology & Oceanography, 11(3), 319–326. https://doi.org/10.4319/lo.1966.11.3.0319

Lee, J., Biemond, B., de Swart, H.E., Dijkstra, H.A. (2024) Increasing risks of extreme salt intrusion events across European estuaries in a warming climate. Communications Earth Environment 5, 60. https://doi.org/10.1038/s43247-024-01225-w

Lerczak, J. A., Geyer, W. R., & Chant, R. J. (2006). Mechanisms driving the time-dependent salt flux in a partially stratified estuary. Journal of Physical Oceanography, 36 (12), 2296 - 2311. https://doi.org/10.1175/JPO2959.1

McCarthy, R. K. (1993). Residual currents in tidally dominated, well-mixed estuaries. Tellus A: Dynamic Meteorology and Oceanography, 45 (4), 325-340. https://doi.org/10.3402/tellusa.v45i4.14896

MacCready, P. (2004). Toward a unified theory of tidally-averaged estuarine salinity structure. Estuaries, 27(4), 561–570. https://doi.org/10.1007/BF02907644

Navarro, G., Gutiérrez, F. J., Díez-Minguito, M., Losada, M. A., & Ruiz, J. (2011). Temporal and spatial variability in the Guadalquivir Estuary: A challenge for real-time telemetry. Ocean Dynamics, 61(6), 753–765. https://doi.org/10.1007/s10236-011- 0379-6

Navarro, G., Huertas, I. E., Costas, E., Flecha, S., Díez-Minguito, M., Caballero, I., et al. (2012). Use of a real-time remote monitoring network (RTRM) to characterize the Guadalquivir Estuary (Spain). Sensors, 12(2), 1398–1421. https://doi.org/10.3390/s120201398

Wei, X., Schramkowski, G. P., & Schuttelaars, H. M. (2016). Salt dynamics in well-mixed estuaries: Importance of advection by tides. Journal of Physical Oceanography, 46 (5), 1457-1475. https://doi.org/10.1175/JPO-D-15-0045.1

Water flux quantification in a subtropical estuarine lagoon complex through numerical modeling

Birocchi P. [1], Dottori M. [2], Fabre-Lima L. [3], de Godoi Rezende Costa C. [4], Sasaki Dalton K. [5], and Chant R.J. [6]

Keywords: water flux, estuaries, hydrodynamic model, river discharge, extreme events, climate change.

Abstract

Understanding the response of the river flow and estuarine hydrodynamics to future climate change is essential to managing water resources and stress on living organisms under these changing conditions (Yang et al., 2015). Our scientific inquiry seeks to understand how water flux varies under different physical conditions within the main channel of a subtropical estuarine-lagoon complex. We focused on the river discharge variability caused by rainfall changes between present climatological values and future climate change scenarios for the period of 2089-2100 (Almazroui et al., 2021). In addition, we investigate present conditions under the influence of two storm tides and atmospheric blocking events in changing the water flux. The water flux calculation in an estuary is important to comprehend its hydrodynamics and the transport of particles and substances in this system. To calculate it for a subtropical estuarine lagoon complex system, we implemented and validated the Estuarine and Coastal Ocean Model (ECOM) for the Cananéia-Iguape estuary, in Brazil, and we found skill values of 0.80-0.94, 0.57-0.84, and 0.93 for salinity, currents, and total sea level, respectively. Then the water fluxes were calculated in different scenarios, including storm tide and atmospheric blocking events, and present and climate change scenarios SSP126 and SSP585 (from the Intergovernmental Panel on Climate Change – IPCC) considering the river discharge variability due to rainfall fluctuations (Almazroui et al., 2021). We calculated the cross-section water flux in the estuarine channel for all scenarios in three different sections: in the northern and southern inlets, and at the Valo Grande channel (VGC) (the main freshwater tributary) considering the Stokes drift in tides. As we expected, the water flux was higher (lower) during stronger (weaker) river discharge flows, mainly during June SSP585 and the storm tide of August 2016 (September SSP585 and atmospheric blocking) scenarios (Fig. 1). The highest water fluxes were detected during the storm tide of August 2016 with anomalous values of 485.54 $m^3.s^{-1}$, -255.37 $m^3.s^{-1}$ (negative because it is flowing southward and out of the estuary), and 668.95 $m^3.s^{-1}$ for the northern, and southern inlets, and at VGC, respectively (Fig. 1). There is an increase in water fluxes during the spring tide in comparison to the neap tide of approximately of 7%, 5%, and 1%, in the northern inlet, southern inlet and VGC, respectively, which is statistically significant for some scenarios, mainly at the VGC. The ebb tidal fluxes (with a mean value of 163.10 $m^3.s^{-1}$) are significantly (p-value<0.05) stronger than the flood tidal fluxes (with a mean value of 123.94 $m^3.s^{-1}$) by 24% considering all scenarios. Both inlets presented faster ebb periods, with mean values of 6.14 and 5.98 hours, in comparison to the flood periods of 6.25 and 6.41 hours, respectively, while the VGC cross section presented longer ebb tides than flood tides, with mean durations of 7.76 hours and 4.66 hours, respectively, due to the strong influence of the continental runoff. Considering all scenarios, the water flux is transported dominantly through the northern inlet of the estuary with approximately 68.3% ±4.3% and 29.1%±2.4% flowing through the southern inlet of the total mean water flux transport (100%) (Fig. 2). We were able to classify the estuary as hypersynchronous, detecting an increase of approximately 0.2 m in the tidal amplitude landward, between its two (northern and southern) inlets with the highest tidal amplitude region, of approximately 0.8 m, in the main channel.

[1]Oceanographic Institute, University of São Paulo, Brazil. paula.birocchi@usp.br
[2] Oceanographic Institute, University of São Paulo, Brazil. mdottori@usp.br
[3]Oceanographic Institute, University of São Paulo, Brazil and now at the University of Massachussets Dartmouth, USA. ldelima@umassd.edu
[4]Oceanographic Institute, University of São Paulo, Brazil and now at MetOcean New Zealand. carine.costa@alumni.usp.br
[5]Oceanographic Institute, University of São Paulo, Brazil and now at the Northeastern University, USA. d.sasaki@northeastern.edu
[6]Rutgers University, USA. chant@marine.rutgers.edu

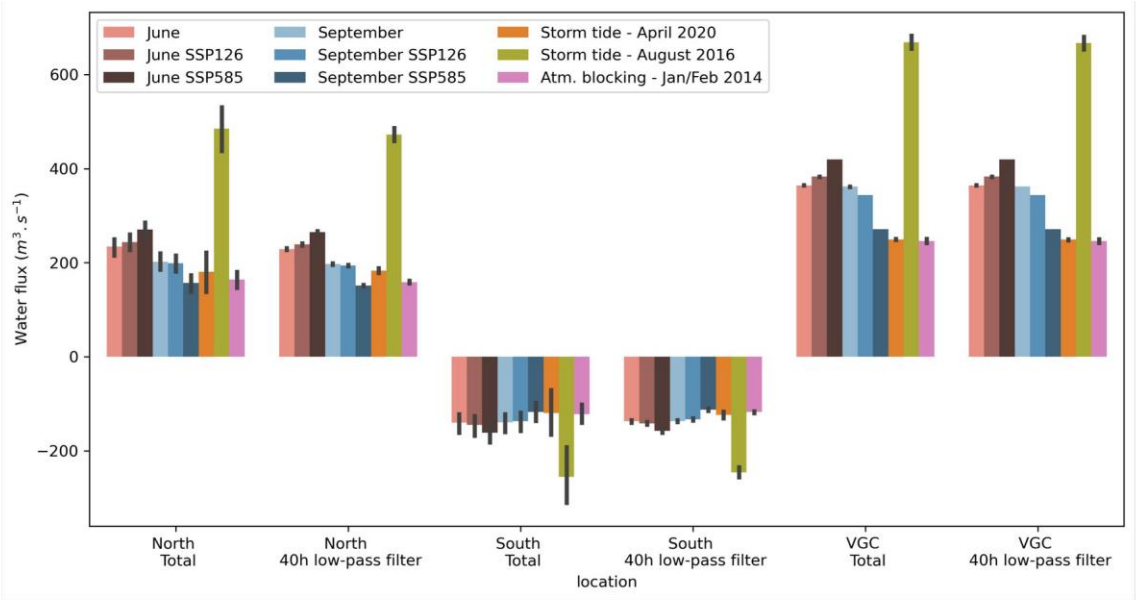

Significant differences (p-value < 0.05):

		North		South		VGC	
		Total	**40h filtered**	**Total**	**40h filtered**	**Total**	**40h filtered**
June	<-> June SSP126	0.40	0.00	0.75	0.03	0.00	0.00
June SSP126	<-> June SSP585	0.03	0.00	0.26	0.00	0.00	0.00
June	<-> June SSP585	0.00	0.00	0.15	0.00	0.00	0.00
September	<-> September SSP126	0.80	0.00	0.85	0.05	0.00	0.00
September SSP126	<-> September SSP585	0.00	0.00	0.14	0.00	0.00	0.00
September	<-> Setember SSP585	0.00	0.00	0.09	0.00	0.00	0.00
Storm tide April 2020	<-> Atm. Blocking	0.39	0.00	0.90	0.00	0.34	0.43
Storm tide August 2016	<-> Atm. Blocking	0.00	0.00	0.00	0.00	0.00	0.00

Figure 1. Mean water flux (in $m^3.s^{-1}$) for each one of the scenarios, including climatological June and September under present, SSP126 and SSP585 conditions, and, two different storm tide events (in August 2016 and April 2020) and one atmospheric blocking event from 13th January to 14th February 2014. The table below the figure shows the p-values comparing the present with the climate change scenarios, and the storm tides with the atmospheric blocking. There were significant differences for the majority of the comparisons, mainly for the low-pass filtered (40h) water fluxes.

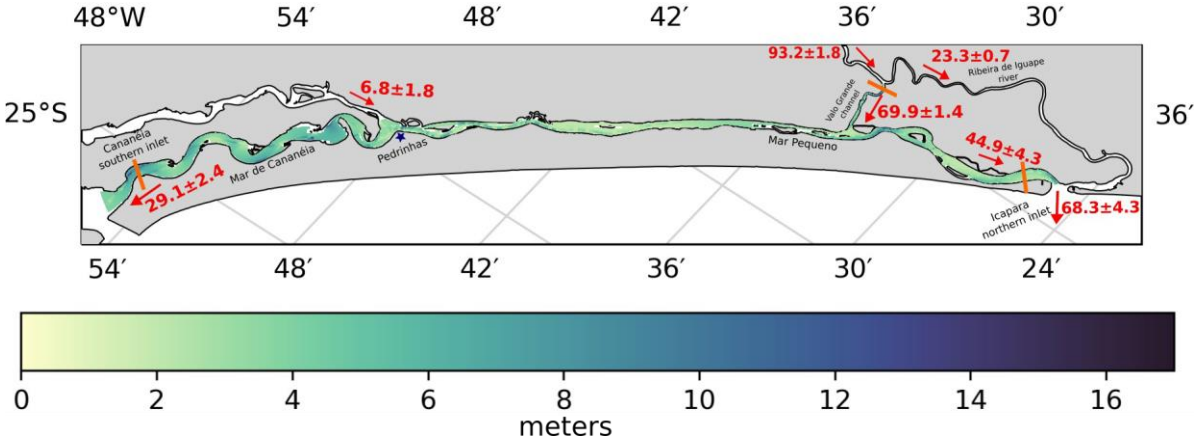

Figure 2. The Cananéia-Iguape estuary and its bathymetry (in meters). The numbers in red correspond to the percentage of water flux transported in each estuarine channel in this system and their standard deviations. The orange lines show the three locations for the cross sections where we calculated the water fluxes at the Cananéia southern inlet, Valo Grande Channel (VGC), and Icapara northern inlet.

References

Almazroui, M., Ashfaq, M., Islam, M. N., Rashid, I. U., Kamil, S., Abid, M. A., and Sylla, M. B. (2021). Assessment of CMIP6 performance and projected temperature and precipitation changes over South America. *Earth Systems and Environment*, *5*(2), 155- 183.

Yang, Z., Wang, T., Voisin, N., & Copping, A. (2015). Estuarine response to river flow and sea-level rise under future climate change and human development. *Estuarine, Coastal and Shelf Science*, *156*, 19-30.

Characteristics of flow and turbulence over estuarine dunes under reversing tidal flows

Bobiles K. [1,2], Carstensen C. [3], Miramontes E. [1,2], and Lefebvre A. [1]

Keywords: estuarine bedforms, flow, turbulence, boundary layer flow, flume experiments

Abstract

Under the action of river, tidal, wind-driven and other currents, sediments can be mobilised and frequently form rhythmic wavy features, collectively known as bedforms. Due to the high availability of sand and strong hydrodynamics, bedforms are particularly abundant in the lower reaches of rivers, and in coastal tidal environments, where they develop into large fields of underwater dunes with a complex morphology. A detailed study and characterisation of the flow over these dune fields is important for many fundamental and engineering applications such as sediment transport modelling, channel management or submarine cable burial. Bedforms also have a dominant influence on the bottom frictional properties and turbulence generation and are indicative of sediment transport pathways.

Flow patterns and dynamics above angle-of-repose (30°) asymmetric dunes, typically found in laboratory flumes and small rivers, are well known (Best, 2005; Venditti, 2013). Over such dunes, the flow separates at the crest creating a flow separation zone over the steep lee side and a turbulent wake develops from the crest that dissipates downstream. Dunes in large rivers are mainly low- to intermediate-angle dunes (mean lee side ca. 5-20°) with their steepest slope located close to the trough (Cisneros et al., 2020). Flow over such dunes is less well known, but it has been observed that flow separation is inexistent or intermittent and only little turbulence is generated (Kostaschuk and Villard, 1996; Kwoll et al., 2016).

Dunes that form in estuaries and tidal rivers are also low- to intermediate-angle dunes having a mean lee slope between 5° and 20° (Dalrymple and Rhodes, 1995; Lefebvre et al., 2021). Unlike river bedforms, estuarine bedforms generally have a sharp pointed crest with its steepest slope located close to the crest (Aliotta and Perillo, 1987; Lefebvre et al., 2021). It is not clear yet how much flow properties vary between high-angle flat-crested dunes and low-angle sharp-crested dunes. Particularly, it is unknown whether a permanent or an intermittent flow separation would develop over some segments of the lee side. Moreover, the relation between reversing tidal flow and natural estuarine morphology is not yet well understood. A detailed consideration of the morphology including three-dimensional features of low- to intermediate-angle dunes is necessary to characterise in detail the hydrodynamics and, consequently, the resulting flow resistance and sediment movement over such low-angle bedforms.

In this study, laboratory flume experiments are conducted to measure the mean flow and turbulence properties over fixed representative estuarine dunes with varying morphology. Based on the results, a detailed description of velocity and turbulence over large-scale low-angle sharp-crested bedforms will be provided, which can help in better understand and model flows in estuaries and coastal seas.

The experiments are conducted at the large flume facility of BAW (Federal Waterways Engineering and Research Institute), Hamburg. The facility is a recirculating flume consisting of two straight sections connected at their respective ends by a semi-circular segment to form a closed recirculating channel. The total length of the flume is 220 m with a straight channel section having a length of 70 m, a width of 1.5 m and a maximum water depth of approximately 1.3 m. A maximum flow velocity of around 1 m/s can be generated in two opposite directions through an underground pump. Previous experiments performed by Carstensen and Holzwarth (2023) demonstrated the potential of high-resolution measurements over a large-scale estuarine dune in this laboratory flume setup. Three sets of experiments are planned with modelled shapes resembling that of the estuarine dunes observed in the Weser Estuary, Germany (Lefebvre et al., 2021) scaled down by a factor of 10. The three modelled dune shapes are described as steep asymmetric, low-angle asymmetric and low-angle symmetric, respectively (Figure 1). For each experiment, a set of 10 prototype two-dimensional fixed concrete dunes are installed. The three prototypes each have different geometries and slope angles, with the position of the maximum lee side slope near the crest. The water depth, dune overall length and height are kept constant for all the experimental cases and only the dune profile is changed to allow comparison of the results between the experiments. Importantly, measurements are conducted for each setup with flow in each direction. This allows to characterise for the first-time flow properties over representative estuarine dunes in a tidal-like setting, with measurements of (steady) reversing flow over symmetric and asymmetric dunes.

[1] MARUM – Center for Marine Environmental Sciences, University of Bremen, Bremen, Germany, kbobiles@marum.de.
[2] Faculty of Geosciences, University of Bremen, Bremen, Germany
[3] Federal Waterways Engineering and Research Institute (BAW), Hamburg, Germany

Instantaneous flow velocities are measured for each experiment using a sideward-looking Acoustic Doppler Velocimeter (ADV), Nortek Vectrino. Data are collected at the centerline of the flume over the 5th dune where the flow is expected to be fully adapted to the bedform field. The high-resolution horizontal (u, v) and vertical (w) velocities are used to identify the presence and size of the (permanent or intermittent) flow separation zone and the shear layer. The turbulent kinetic energy is used to characterise the size and intensity of the turbulent wake.

Based on these results, a detailed characterisation of flow and turbulence structures over low- to intermediate-angle sharp crested estuarine bedforms will be provided and will allow to better understand the mutual interaction between bedforms, hydrodynamics and sediment transport in a tidally dominated environment.

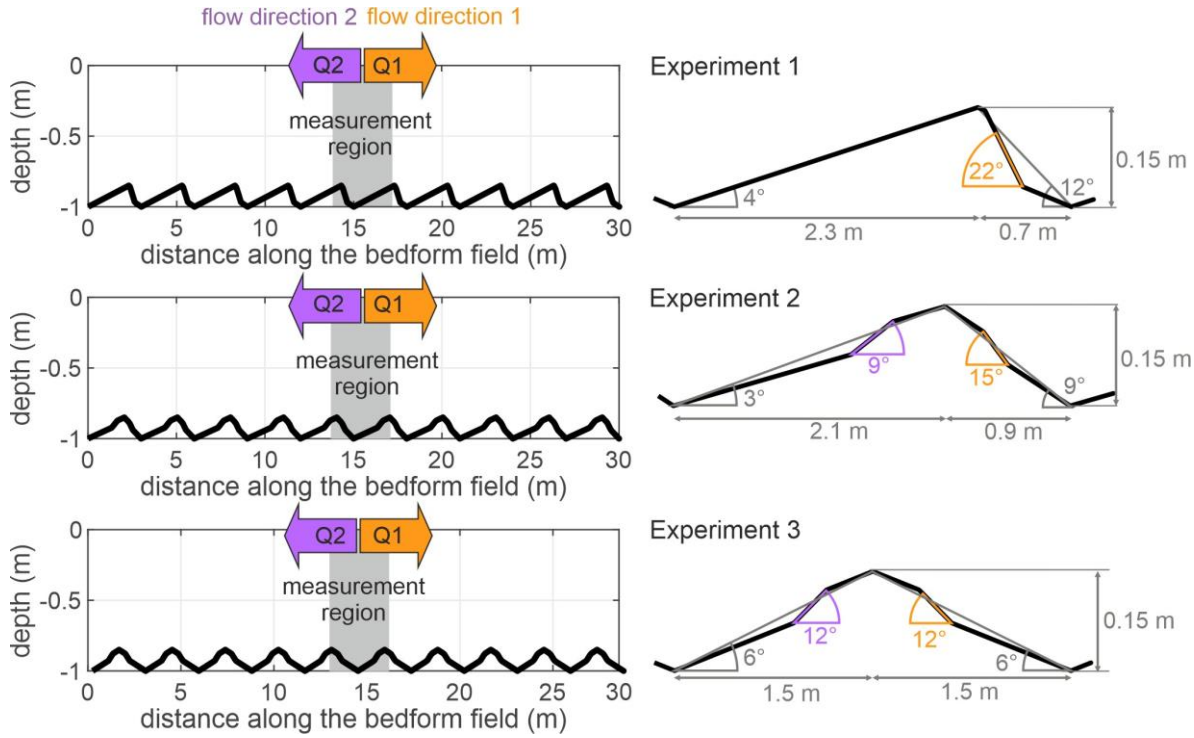

Figure 1. Setup and design of the flume experiments

References

Aliotta, S. & Perillo, G.M.E., 1987. A sand wave field in the entrance to Bahia Blanca Estuary, Argentina. *Marine Geology*, 76, 1-14.

Best, J. 2005. The fluid dynamics of river dunes: A review and some future research directions. *Journal of Sedimentary Research*, 110, 20.

Carstensen, C. & Holzwarth, I., 2023. Flow and Turbulence over an Estuarine Dune – Large-Scale Flume Experiments. *Die Küste, 93 - Online First.*

Cisneros, J., Best, J., Van Dijk, T., De Almeida, R.P., Amsler, M., Boldt, J., Freitas, B., Galeazzi, C., Huizinga, R., Ianniruberto, M., Ma, H.B., Nittrouer. J.A., Oberg, K., Orfeo, O., Parsons, D., Szupiany, R., Wang, P., Zhang, Y.F., 2020. Dunes in the world's big rivers are characterized by low-angle lee-side slopes and a complex shape. *Nature Geoscience*, 13, 156-162.

Dalrymple, R.W. & Rhodes, R.N., 1995. *Estuarine dunes and bars. In: Perillo, G.M.E (ed) Geomorphology and Sedimentology of Estuaries. Developments in Sedimentology*, Elsevier.

Kwoll, E., Venditti, J.G., Bradley, R.W., Winter, C., 2016. Flow structure and resistance over subaqueous high- and low-angle dunes. *Journal of Geophysical Research: Earth Surface*, 121, 545-564.

Kostaschuk, R. & Villard, P., 1996. Flow and sediment transport over large subaqueous dunes: Fraser River, Canada. *Sedimentology*, 43, 849-863.

Lefebvre, A., Herrling, G., Becker, M., Zorndt, A., Krämer, K., Winter, C., 2021. Morphology of estuarine bedforms, Weser Estuary, Germany. *Earth Surface Processes and Landforms*.

Venditti, J.G., 2013. *Bedforms in sand-bedded rivers. In: Shrodder, J. & Wohl, E. (eds) Treatise on Geomorphology*, San Diego, CA: Academic Press, 137-162.

Intertidal vegetation altering estuarine currents and implications for salt intrusion

Bootsma J. [1], Borsje B.W. [2], van der Wal D. [3], and Hulscher S.J.M.H. [4]

Keywords: estuaries, vegetated intertidal area, managed realignment sites, currents, salt intrusion

Abstract

Vegetation is commonly present in estuarine intertidal areas, and the distribution of plant species is depending on environmental conditions, such as salinity level. In turn, some of these vegetation species are known to act as ecosystem engineers by modulating their environment, affecting estuarine currents and habitat for other species. The ecosystem engineering capacity is linked to biophysical vegetation traits, such as plant stiffness and height (Bouma et al., 2013). Since environmental conditions are dynamic over space and time, so is the vegetation, including a changing vegetation extent, shifts in species distribution and hence the biophysical traits of the vegetation community. It may be expected that this would subsequently result in a spatiotemporally varying ecosystem engineering capacity of intertidal areas, both fringing and mid-channel flats, influencing hydrodynamics and salt intrusion. The aim of this paper is to determine the magnitude, extent and variability of the impact of intertidal vegetation on currents and explore the implications for salt intrusion. Vegetation dynamics are studied through a combination of available vegetation maps and remote sensing techniques. Subsequently, a process-based hydrodynamic model, Delft3D-FM, is utilized to study the hydrodynamic impact of intertidal vegetation, including spatial and temporal variation. The study area is the Scheldt estuary on the Dutch-Belgian border, covering the Western Scheldt in the Netherlands and the Sea Scheldt in Belgium. The Scheldt is a macrotidal, well-mixed estuary, with a mean tidal range of 3.8 m, amplifying to 5.2 m 100 km upstream. Tidal influence reaches to the sluices of Gent, 160 km from the mouth (Stark et al., 2017). The estuary consists of a multi- channel system with ebb and flood channels separated by intertidal flats.

Vegetation maps were established by Rijkswaterstaat, the Dutch national water authority, for the Western Scheldt and by INBO, the Belgian institute for nature and forest, for the Sea Scheldt. A combination of false-color aerial imagery with in-situ field measurements was used to derive these vegetation maps. This resulted in a complete overview of intertidal vegetation in the Scheldt estuary with a frequency of ca. 6 years, spanning the period 1998-2016. These maps are used to study the variation in marsh extent and species distribution. Next to this, Landsat satellite imagery is processed in Google Earth Engine (GEE). By combining the NDVI (Normalized Difference Vegetation Index) with a NDWI (Normalized Difference Water Index), a classification in marsh, mudflat and water is derived using a method previously set up by Laengner et al. (2019). Besides, the NDVI is used as a proxy for vegetation density in combination with a range of density per vegetation species from the literature, to obtain a value for the number of stems per square meter of soil. Other vegetation characteristics, including height, stem diameter and drag coefficient, were also obtained from the literature. These vegetation characteristics were implemented in a hydrodynamic model for the species: common cordgrass (*Salicornia europeana*), common glasswort (*Spartina anglica*), saltmarsh bulrush (*Scirpus maritimus*), sea aster (*Aster tripolium*), sea couch (*Elytrigia atherica*), common reed (*Phragmites australis*), and willows (*Salix alba*). These seven species are common in the Scheldt estuary and contribute to most of the coverage of the vegetated intertidal flats.

The hydrodynamic model adopted here is the depth-averaged Delft3D-FM NeVla model, already developed, calibrated and validated by Deltares using a 2013 hindcast (Tiessen et al., 2016). The original model did not include vegetation on intertidal flats and included a spatially varying bed roughness. For our study, the model is set up for three scenarios, i.e., with (i) a spatially uniform bed roughness (no vegetation scenario), (ii) monospecific vegetation and (iii) multi-species vegetation, respectively. The impact of vegetation on estuarine currents is studied for a period of calm weather conditions in May 2013 and a period of storm conditions in December 2013. For the monospecific vegetation scenario, it is assumed that the same species is present for all vegetated areas in the estuary. Vegetation characteristics for this were derived from Vuik et al. (2016) who performed field measurements on two marshes in the Western Scheldt, mainly covered by common glasswort (*Spartina anglica*) and saltmarsh bulrush (*Scirpus maritimus*). These consist of a mean vegetation height of 25 cm, mean stem diameter of 5 mm and mean stem density of 1000 stems/m2. A comparison is made between a 2016 and a 1993 vegetation distribution and bathymetry, to study the temporal variation in hydrodynamic impact by changes in vegetation distribution. The largest change in vegetation extent is present between these years, thus the difference in hydrodynamic impact is expected to be maximal.

An increase in total marsh extent is observed for the Scheldt estuary over the period 1998-2016. On a vegetation community level, there is no clear increase in extent, except for common reed (*Phragmites australis*), showing a constant upward trend. The mid-channel flats (Hooge Platen and Plaat van Walsoorden) are most pronounced in marsh establishment, going from an almost bare flats to extensive vegetation coverage over the years.

[1] University of Twente, the Netherlands, jesse.bootsma@utwente.nl
[2] University of Twente, the Netherlands, b.w.borsje@utwente.nl
[3] University of Twente and Royal Netherlands Institute for Sea Research (NIOZ), the Netherlands, d.vanderwal@utwente.nl
[4] University of Twente, the Netherlands, s.j.m.h.hulscher@utwente.nl

When modelling themonospecific vegetation scenario and comparing this with a bare flat scenario, a local impact on water levels is observed whereas on currents a wider impact can be seen (Figure 1). On the vegetated marshes, flow reduction (in blue) is seen, whereas flow enhancement (in red) is present in some tidal creeks on the marsh. Besides, a phase difference between water levels and flow velocities is observed between the mono-specific and no vegetation scenario, with the water levels on the marshes being delayed, most likely due to flow resistance by the vegetation. Next to this single moment in time (around high tide) the impact on water levels and currents is studied throughout the rest of the tidal cycle. Furthermore, multi-species vegetation and a different year (therefore a different vegetation extent and species distribution) are compared.

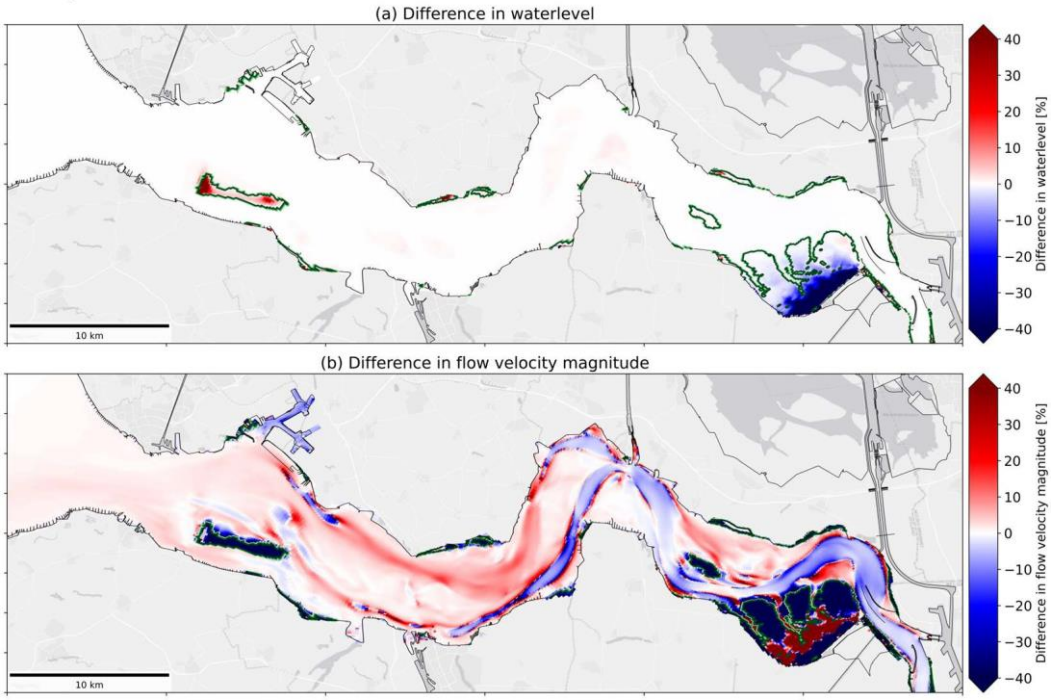

*Figure 1: Relative difference in (a) water level and (b) flow velocity magnitude, on a single moment in time around high tide during storm conditions, comparing a monospecific vegetation scenario with a bare flat scenario ((vegetated-unvegetated)/unvegetated)*100). Vegetated areas are displayed by the green contour line.*

Next to the impact on currents, changes in salt intrusion in the estuary under influence of intertidal area will be studied. From fringing and mid-channel flats this may be induced by increased friction due to vegetation presence. Furthermore, the restoration of intertidal area through managed realignment is expected to alter salt intrusion in the estuary through the effect on the tidal prism (Hendrickx et al., 2023). We will study this impact by adding managed realignment sites in the hydrodynamic model to the present-day situation of the Scheldt estuary.

References

Bouma, T. J., Temmerman, S., van Duren, L. A., Martini, E., Vandenbruwaene, W., Callaghan, D. P., Balke, T., Biermans, G., Klaassen, P. C., van Steeg, P., Dekker, F., van de Koppel, J., de Vries, M. B., & Herman, P. M. J. (2013). Organism traits determine the strength of scale-dependent bio-geomorphic feedbacks: A flume study on three intertidal plant species. *Geomorphology*, *180– 181*, 57–65. https://doi.org/10.1016/j.geomorph.2012.09.005

Hendrickx, G. G., Kranenburg, W. M., Antolínez, J. A. A., Huismans, Y., Aarninkhof, S. G. J., & Herman, P. M. J. (2023). Sensitivity of salt intrusion to estuary-scale changes: A systematic modelling study towards nature-based mitigation measures. *Estuarine, Coastal and Shelf Science*, *295*(April), 108564. https://doi.org/10.1016/j.ecss.2023.108564

Laengner, M. L., Siteur, K., & van der Wal, D. (2019). Trends in the seaward extent of saltmarshes across Europe from long- term satellite data. *Remote Sensing*, *11*(14), 1–25. https://doi.org/10.3390/rs11141653

Stark, J., Smolders, S., Meire, P., & Temmerman, S. (2017). Impact of intertidal area characteristics on estuarine tidal hydrodynamics: A modelling study for the Scheldt Estuary. Estuarine, Coastal and Shelf Science, 198, 138–155. https://doi.org/10.1016/j.ecss.2017.09.004

Tiessen, M.C.H., Vroom, J. & van der Werf, J.J., (2016), Ontwikkeling van het Delft3D FM NeVla model voor het Schelde estuarium (*in Dutch*), Deltares

Vuik, V., Jonkman, S. N., Borsje, B. W., & Suzuki, T. (2016). Nature-based flood protection: The efficiency of vegetated foreshores for reducing wave loads on coastal dikes. *Coastal Engineering*, *116*, 42–56. https://doi.org/10.1016/j.coastaleng.2016.06.001

Larval dispersion dynamics in a macrotidal estuary: coupled role of larval behaviour and hydrodynamic processes

Bouyssou R. [1], Jalón-Rojas I. [2], Arevalo E. [3], Cabral H. [4], Huybrechts N. [5], Fernandes E.H. [6], and Lepage M. [7]

Keywords: transport, larvae, Selective Tidal Stream Transport, modelling, Gironde estuary.

Abstract

Estuaries are essential nursery habitats for the early life stages of marine and estuarine fish species. The migration of larvae from their spawning locations to estuarine nursery grounds is a critical aspect of fish life cycles, recruitment, and population dynamics, intricately tied to hydrodynamics and physical processes governing transport within estuarine environments (Arevalo, 2023). However, larvae can adjust their dynamical behavior as they develop, indicating a complex interplay between biological and physical factors often overlooked in dispersal studies (Pineda and Reyns, 2018). Understanding the transport mechanism of larvae within these complex environments is therefore challenging but essential for effective management and conservation efforts.

In this study, we investigate the dynamics of larval dispersion and colonization within the macrotidal Gironde estuary (SW France), focusing on the influence of hydrodynamic processes and larval behavior. The Gironde estuary, renowned for its ecological significance and non-linear flow offers a compelling setting for investigating larval dynamics. For this purpose, 24 scenarios representing four environmental conditions typical of larval spawning periods, three larval behaviors, and two ecological guilds were simulated using the TELEMAC-GAIA hydro-sedimentary model (Huybrecht et al., 2022) and the TrackMPD Lagrangian particle-tracking model (Jalón-Rojas et al., 2019). The models were validated from both Eulerian and Lagrangian perspectives, demonstrating excellent agreement with observations. Strategic releases of larvae were conducted at typical spawning sites for marine-estuarine opportunist and estuarine resident guilds, enabling the analysis of trajectories through probability density maps, source-to-sink matrix, and retention maps in relation to environmental and hydrodynamic conditions. Three distinct larval behaviors — passive drifting and two variations of Selective Tidal Stream Transport (STST, Jager, 1999) — were reproduced to assess their impact on dispersion patterns:

Passive drifting involves larvae solely influenced by hydrodynamics, remaining neutrally buoyant.

In STST-Forced Vertical Position behavior, larvae exhibit high vertical migration capacity, settling at the bottom during ebb and moving through the water column neutrally buoyant during flood.

STST-Settling Behavior entails larvae settling or resuspending based on their density and prevailing hydrodynamic conditions.

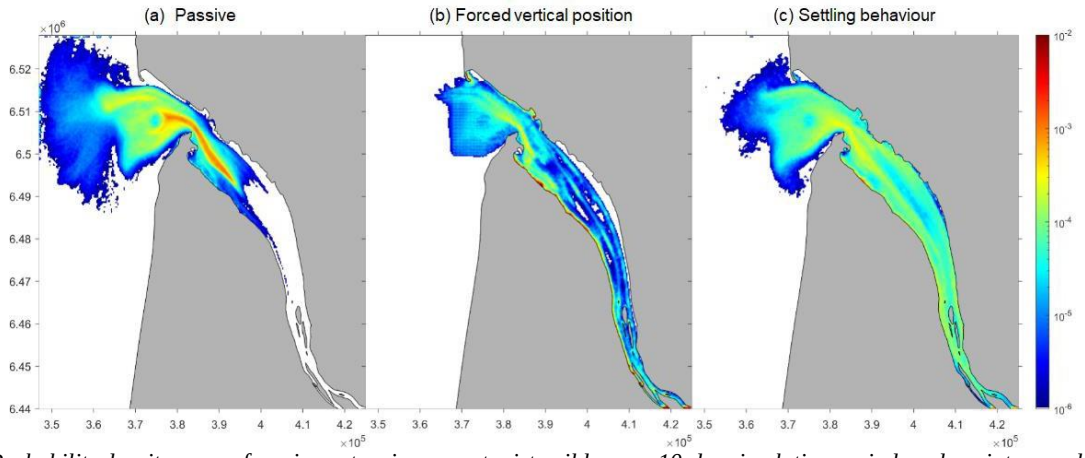

Figure 1. Probability density maps of marine-estuarine opportunist guild over a 10-day simulation period, under winter conditions, and employing different larval behaviors: (a) passive drifting, (b) forced vertical positioning, and (c) settling behavior. The particle distributions (colorbar) are normalized regarding the total number of released particles.

[1] INRAE, UR EABX, F-33612 Cestas, France. remibouyssou@orange.fr
[2] Univ. Bordeaux, CNRS, Bordeaux INP, EPOC, UMR 5805, F-33600 Pessac, France. isabel.jalon-rojas@u-bordeaux.fr
[3] AZTI, Marine Research, Basque Research and Technology Alliance (BRTA), Txatxarramendi Ugartea z/g, Sukarrieta, 48395 Spain. earevalo@azti.es
[4] INRAE, UR EABX, F-33612 Cestas, France. henrique.cabral@inrae.fr
[5] CEREMA, Margny-lès-Compiègne, France. nicolas.huybrechts@cerema.fr
[6] Instituto de Oceanografia, Universidade Federal do Rio Grande, Rio Grande, RS, 96203-900, Brazil. fernandes.elisa@gmail.com
[7] INRAE, UR EABX, F-33612 Cestas, France. mario.lepage@inrae.fr

Results reveal highly contrasting dispersion patterns for the three different behaviors, evident in both marine-estuarine opportunist and resident guilds across all environmental conditions. For example, under typical winter conditions, marine- associated larvae tended to remain around the mouth when considering passive drifting behavior, while exhibiting colonization of the upper estuary with both STST-related behaviors (Fig. 1). Larvae adopting STST-Forced Vertical Position behavior showed higher concentrations near the left bank, with colonization proving more challenging on the right bank (Fig. 1.b). Conversely, larvae with STST-Settling behavior displayed a more uniform distribution across the estuary, with two main entry routes observed through the channel and in proximity to the right bank (Fig. 1.c). These dispersion trends remained quite consistent across various environmental conditions during different spawning periods, albeit with quantifiable differences. For example, larvae exhibiting STST behaviors demonstrated higher rates of upper- reach colonization during spring-to-neap tides compared to neap-to-spring tides under similar river flow conditions. These findings will be discussed in the context of estuarine hydrodynamics and physical processes. The retention regions identified in the right banks for STST-Forced Vertical Position (Fig. 1.b), for example, could be associated with areas characterized by eddy-like structures and comparatively lower current velocities. The transport patterns of larvae with STST-Settling behavior are notably influenced by tidal pumping and lateral convergence zones in the mid-reaches of the estuary.

References

Arevalo, E., Cabral, H.N., Villeneuve, B., Possémé, C., Lepage, M. (2023). Fish larvae dynamics in temperate estuaries: A review on processes, patterns and factors that determine recruitment. Fish and Fisheries, 24(3), 466-487.

Huybrechts, N., Tassi, P., Klein, F. (2022). Three-Dimensional Sediment Transport Modeling of the Gironde Estuary. In Advances in Hydroinformatics: Models for Complex and Global Water Issues—Practices and Expectations, 753-771.

Jager, Z. (1999). Selective tidal stream transport of flounder larvae. Estuarine, Coastal and Shelf Science, 49, 347– 362.

Jalón-Rojas, I., Wang, X.H., Fredj, E. (2019). A 3D numerical model to Track Marine Plastic Debris (TrackMPD): Sensitivity of microplastic trajectories and fates to particle dynamical properties and physical processes, Marine Pollution Bulletin, 141, 256-272. DOI: 10.1016/j.marpolbul.2019.02.052.

Pineda, J. and Reyns, N. (2018) Larval transport in the coastal zone: biological and physical processes. In. Evolutionary Ecology of Marine Invertebrate Larvae. Edited by Tyler J. Carrier, Adam M. Reitzel, and Andreas Heyland: Oxford University Press.DOI: 10.1093/oso/9780198786962.003.0011

Effects of sills on estuarine exchange flow mechanism, residence times, and mixing

Broatch E. [1] and MacCready P. [1]

Keywords: sill, estuaries, idealized model, salt flux, residence time, exchange flow, tidal pumping, mixing, salinity variance

Abstract

We seek to characterize the effects of sills on estuarine circulation patterns. Sills are common in fjords, where they are often formed by the terminal moraines of glaciers or resistant areas of hard bedrock. These sills restrict exchange between basins and with the open ocean, particularly in the bottom waters. By using idealized numerical estuary models, we are able to vary the length, width and height of the sill in a way that would not be possible in an observational or realistic modeling study. An ensemble of models with a range of sill geometry parameters is created using ROMS, with bathymetry loosely based on Puget Sound.

The idealized model output is used to conduct particle tracking experiments and estimate residence times for the estuary. We characterize the estuarine exchange flow across the sill using the Total Exchange Flow (TEF) method as well as the standard salt flux decomposition. The mixing in various regions of the estuary is calculated from salinity variance budgets. We will examine the results of these analyses for the model ensemble to understand how the geometry of sills impacts residence times and mixing throughout the estuary and whether gravitational circulation or tidal pumping dominates as the primary mechanism for the exchange flow.

[1] University of Washington, correspondence to: ebroatch@uw.edu

The estuarine exchange flow intensity and the diahaline mixing gradient are interrelated

Burchard H. [1], Klingbeil K. [1], Lange X. [1], Li X. [1], Lorenz M. [1], MacCready P. [2], and Reese L. [1]

Keywords: diahaline turbulent mixing, estuarine circulation, isohaline framework

Abstract

Exchange flow with inflow of saline water from the ocean side and outflow of brackish water towards the ocean is one of the major characteristics of estuaries with excess freshwater discharge. The intensity of estuarine circulation is known to be connected to the characteristics of salinity mixing inside the estuary, where mixing is here conveniently defined as the destruction of salinity variance within an estuarine volume. In the present study, we derive a new relation that shows how the time-averaged estuarine exchange flow and the mixing inside the estuary determine each other. The result is a direct quantitative relation between the inflow volume at a fixed transect across the estuary and the gradient of the diahaline mixing inside the estuary with respect to salinity, taken at the isohaline surface dividing inflow and outflow at the transect. The relation is derived by integrating the dependence of the entrainment velocity on the local mixing gradient (with respect to salinity) over the part of the dividing salinity isohaline that is inside the transect. Once having recognised the relevance of the diahaline mixing distribution inside the estuary, we show for two example estuaries how this mixing is distributed in space. Those estuaries include the meso-tidal Elbe estuary and the non-tidal Warnow estuary, both situated in Northern Germany. While the Elbe estuary shows a classical estuarine circulation with only one dividing salinity and inflow at high salinities and outflow at low salinities, the Warnow estuary has two different inflows, one at high salinity (during upwelling) and one at low salinity (during downwelling), separated by an outflow at intermediate salinities. With this, we show where and due to which processes estuarine exchange flow is generated by mixing inside these two different types of estuaries.

1 Leibniz Institute for Baltic Sea Research Warnemünde, Germany
2 School of Oceanography, University of Washington, Seattle, USA

The role of rain on suspended sediment fluxes in small Estuaries and Tidal Inlets

Burgess H. [1], Dale J. [2], and Hartless R. [3]

Keywords: Sediment Movement, Small Estuaries, Rain, Climate Change, Intertidal Processes

Abstract

With climate change and the realisation of the importance of the myriad of roles that sediment plays in the near shore eco-system, it is imperative globally that we are better informed of the role that small estuaries and tidal inlets have on the coastal sediment dynamics.

The Southdowns and the Weald, which form the hinterland of the south coast of England, are drained by numerous highly engineered small estuaries and tidal inlets. This coastal area is macro-tidal, and the timing and balance of the tides combined with the highly variable freshwater input have a significant impact on suspended sediment fluxes within and through these systems.

This presentation looks at the analyses of one of the south coast tidal inlet systems, where freshwater input is controlled by tidal gates. This hydraulic control has enabled us to sepa- rate the three input sources of sediment (runoff erosion of intertidal sediment, marine input and terrestrial input) and understand their pathway through the system. From this, a model has been produced which allows us to understand the suspended sediment mechanisms in other small estuarine systems including those where freshwater input is not controlled.

[1] University of Brighton (UoB) – Cockcroft Building, Lewes Road, Brighton, BN2 4GJ, United Kingdom

[2] University of Reading (UOR) – Whiteknights, PO Box 217, READING, Berkshire, RG6 6AH, United Kingdom

[3] Environment Agency - National Water Quality Instrumentation Service (EA NWQIS) – Caversham Lakes, Henley Road, Reading, RG4 9RA, United Kingdom

Far-field transport and mixing of episodic storm runoff plumes

Byrne S. [1], Giddings S.N. [2], Merrifield M. [3], Spydell M. [4], Simpson A., Horner-Devine A. [6], and O'Reilly W. [7]

Keywords: river plume, precipitation, transport, mixing.

Abstract

Freshwater enters the ocean as discharge from land, serving an important role in both hydrological and biogeochemical cycles (Syed et al. 2010). The interaction of less-dense freshwater and the saltier, denser coastal ocean forms horizontally advecting plumes (Horner-Devine et al. 2015). Plumes can contain a suite of land-based and estuary-modified particles, sediment, debris, and pollutants (Reeves et al. 2004, Aguilera et al. 2019). Thus, understanding plume behavior is critical for assessing health risks to beachgoers and coastal ecosystems.

Buoyant plumes from small-discharge systems are poorly understood. Low inflow estuaries create freshwater plumes on every ebb tide that dissipate on the following flood tide (Horner-Devine et al. 2015). The tidal pulsing of plumes is interrupted in two main ways: the estuary mouth closes and plumes no longer form, or a large outflow event overrides the system and produces a relatively large plume regardless of tidal phase. Precipitation flooding into a low-inflow system can do the latter by increasing discharge from O($1m^3/s$) up to O($100m^3/s$) generating an episodic plume larger in freshwater volume than a tidally pulsed plume, but still very small compared to well-studied larger discharge plumes.

Previous work by Warrick et al. (2007) has shown that, once in the far-field where river discharge momentum is negligible, southern California storm runoff plumes follow the direction of wind-forcing. Winds typically blow southward and opposite the expected direction from Coriolis forcing during and after peak discharge times. Hence, southern California episodic plumes tend to propagate southward.

This study investigates the far-field river plume transport from the low-inflow Los Peñasquitos lagoon in San Diego over three winter months (Dec. 2022 – Feb. 2023). Observations were collected as part of the NSF-funded experiment "Plumes in Nearshore Conditions" or PiNC led by PIs Sarah N. Giddings (SIO) and Alexander Horner-Devine (UW). In-situ data features five moorings located at the 8m isobath, one mooring inside the estuary, and one mooring at the 30m isobath directly offshore of the mouth (see Figure 1a). Measurements include surface and bottom salinity and temperature, vertical velocity profiles, and wave height and direction.

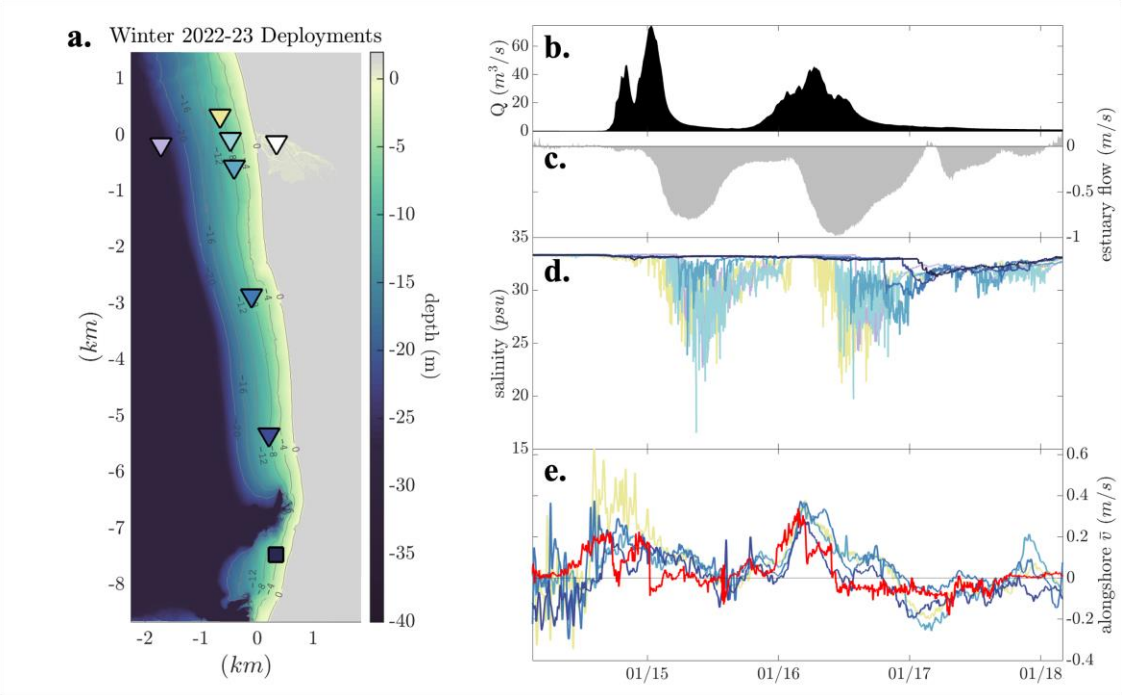

[1] Scripps Institution of Oceanography, s2byrne@ucsd.edu
[2] Scripps Institution of Oceanography, sgiddings@ucsd.edu
[3] Scripps Institution of Oceanography, mamerrifield@ucsd.edu
[4] Scripps Institution of Oceanography, mspydell@ucsd.edu
[5] US Army Corps of Engineers, ajoysimpson@gmail.com
[6] University of Washington, arhd@uw.edu
[7] Scripps Institution of Oceanography, woreilly@ucsd.edu

Figure 1: a. Map of data collection locations during the winter of 2022-2023 off the coast of La Jolla in San Diego, CA. Coordinate (x=0, y=0) is the estuary mouth. Triangles denote moorings that have both CTDs and ADCPs, the square denotes the Scripps Pier with CTD data only. b. Los Peñasquitos streamflow recorded upstream, c. along-channel depth-averaged estuary flow (recorded at the white triangle location), d. near-surface salinity from each mooring, and e. depth-averaged alongshore flow (red line represents wind-driven component of the flow) displayed for plumes 2 and 3. Line colors in d. and e. correspond to the mooring marker fill colors from panel a. to show location.

During the study period, three instances occur where tidal pulsing is disrupted by larger outflow; these events are chronologically dubbed plumes 1, 2, and 3. Figure 1 shows mooring data from plumes 2 and 3 that occur sequentially in January of 2023. Upstream discharge increased from near 0m3/s to 75m3/s and 45m3/s for plumes 2 and 3 respectively (Figure 1b). Along-channel estuary flow responded with strong outflow after peak discharge (Figure 1c). Plume 1 traveled southward and did not feature a large initial cross-shore extent. Plume 2 traveled northward and farther offshore. Under low wind conditions, plume 2 traveled offshore more quickly. Plume 3 traveled southward and featured a larger initial cross-shore extent. The dynamics moderating the initial cross-shore extent of these plumes is investigated in this analysis, with specific quantification of wave and wind impacts presented.

Momentum budgets of the inner-shelf moorings show an alongshore balance of wind and bottom stress during the storm events, and negligible contribution from rotational forces. This differs from far-field transport of large plume systems which is commonly dominated by buoyancy, Ekman wind dynamics, and geostrophy (Horner-Devine et al. 2015). There is strong coherence in the depth-averaged alongshore flow (Figure 1e) across the inner-shelf, implying the forcings act on a scale greater than 8km. Assuming a surface to bottom stress balance, the component of alongshore flow that is driven by alongshore winds ($v$wind) is quantified by $v_{wind} = \left(\sqrt{\left\{\left(\frac{\rho_{air}}{\rho_{ocean}}\right) * \left(\frac{C_{10}}{C_{Da}}\right)\right\}} * \mathrm{V}\right)$ (Whitney and Garvine 2005)

where C_{10} and C_{Da} are the air-sea and sea-seabed drag coefficients respectively; ρ_{air} and ρ_{ocean} are the air and ocean density; and V is the alongshore wind velocity. The values of v_{wind} for plumes 2 and 3 are shown with the red line in Figure 1e overlain on the measured depth-average alongshore currents. The wind-induced velocity leads the observed velocity by ~3 hours and correlates relatively well during these events, except some periods where the observed velocity exceeds that predicted by the winds. This suggests that the inner-shelf alongshore flow direction is predominantly driven by alongshore winds and the plume is transported in this direction in the far-field, as Warrick et al. predicts. However, as plume 2 shows, this direction is not always southward, particularly when there are back-to-back storm events. Moreover, to more accurately reconstruct the magnitude of observed alongshore flow, additional consideration likely needs to be given to the buoyancy driven component. Using mooring observations, an assessment of the buoyancy-driven/ baroclinic components of the flow during plumes will be quantified.

An observable loss of freshwater occurs in plumes 1 and 3 that travel southward between moorings (see Figure 1d during plume 3). This is consistent with advection, diffusion, and mixing of the freshwater as the plume propagates. Estimates of diffusion rates of the buoyant waters are presented in this analysis. Additionally, time and length scale estimates for how far these plumes propagated in the far-field are calculated. These quantities are relevant for understanding the scope of where and when the potentially polluted plume waters could impact beachgoers and inner-shelf ecosystems.

References

Aguilera, R., Gershunov, A., & Benmarhnia, T. (2019). Atmospheric rivers impact California's coastal water quality via extreme precipitation. Science of the total environment, 671, 488-494.

Horner-Devine, A. R., Hetland, R. D., & MacDonald, D. G. (2015). Mixing and transport in coastal river plumes. Annual Review of Fluid Mechanics, 47, 569-594.

Reeves, R. L., Grant, S. B., Mrse, R. D., Copil Oancea, C. M., Sanders, B. F., & Boehm, A. B. (2004). Scaling and management of fecal indicator bacteria in runoff from a coastal urban watershed in southern California. Environmental science & technology, 38(9), 2637-2648.

Syed, T. H., Famiglietti, J. S., Chambers, D. P., Willis, J. K., & Hilburn, K. (2010). Satellite-based global-ocean mass balance estimates of interannual variability and emerging trends in continental freshwater discharge. Proceedings of the National Academy of Sciences, 107(42), 17916-17921.

Warrick, J.A., DiGiacomo, P.M., Weisberg, S.B., Nezlin, N.P., Mengel, M., Jones, B.H., Ohlmann, J.C., Washburn, L., Terrill, E.J. and Farnsworth, K.L. (2007). River plume patterns and dynamics within the Southern California Bight. Continental Shelf Research, 27(19), 2427-2448.

Whitney, M. M., & Garvine, R. W. (2005). Wind influence on a coastal buoyant outflow. Journal of Geophysical Research: Oceans, 110(C3).

Tide-discharge interactions and detiding of SWOT altimetric observations in the Gironde estuary

Caubet L. [1], Lyard F. [2], Ayoub N. [3], Jan G. [4], Chevrier R. [5], and Penney J. [6]

Keywords: tide-discharge interactions, estuary hydrodynamics, rating curves, unsteady tides, Gironde

Abstract

Estuaries form the last sections of rivers before reaching the ocean which are both governed by the river flow dynamics and subjected to ocean forcing, especially tides. The study of their complex dynamics is motivated by environmental and socio-economic related issues, as estuaries combine special ecosystems to be protected and highly urbanized shores. The new satellite altimetric mission SWOT, with its two wide swaths and collection of data over both on the ocean and continental waters, is expected to provide a new view of the estuarine dynamics. However, the SWOT mission has just started and there is still a long way to go before the data can be routinely exploited for estuarine studies. The first step indeed is to compare the SWOT water elevations with some reference elevations in order to 1/ evaluate at first order the consistency of SWOT data with ancillary data and background knowledge, 2/ characterize the measurements errors. A good understanding of the SWOT data content will also imply to separate tidal signals from other possible dynamical signals, which requires an accurate tide prediction. However, one of the major difficulties in depicting the global estuarine dynamics is the representation of the tides that propagate from the mouth to upper river sections where tidal attenuation occurs, due to an increasing bottom friction as well as the bed slope rise. In addition, the typical quasi-sinusoidal signal of ocean tides at the mouth is affected by the non-linear processes, the constrained geometry of the estuary and environmental parameters, mainly the river discharge. These constraints result in an increasingly asymmetrical (e.g., Allen et al., 1980) and unsteady upstream signal, the non-stationarity being due to the modulation by time discharge variations and, to a lesser extent by possible surge events in the coastal ocean or in the downstream estuary (e.g., Hointink and Jay, 2016; Zhang et al., 2018; Jan et al., 2021). The classical tide prediction method, i.e. the harmonic method, is therefore no longer fully reliable in such systems. In this work, we aim at characterizing those possibly large tide-discharge interactions, responsible for unsteady estuarine tides. Most earlier investigations have addressed this point by using numerical simulations, wavelet analysis or adapting the standard harmonic analysis (e.g., Matte et al., 2013; Guo et al., 2015). We propose an empirical method, based on rating curve linking river discharge and tidal range, that can be then used to improve our tidal predictions. The Gironde estuary is a convenient study area because it is well-monitored with a dense network of tide gauges and river discharge gauging stations upstream the tidal limit on the Garonne and Dordogne rivers along with the Isle tributary.

The first and main part of this presentation is dedicated to the rating curve method. In a second part, we will present first results comparing SWOT sea surface elevation with ancillary data. The rating curves are calculated for each year of the period 2017-2022 and are representative of the dynamics at a given tide gauge station. The analysis reveals two distinct interaction regimes between the upper estuary and the lower estuary. In the upper estuary, the rating curves clearly depict an attenuation of tidal range when river discharge increases, possibly because of bottom friction enhancement. The root mean square error (RMSE) between observed tidal range and parameterized tidal range is of the order of tens centimeters (whereas tidal range variations are of the order of a few meters) which is an indicator of the great overall performances (accuracy, robustness) of our approach. In the lower estuary, tides are much less impacted by the river discharge with variations of tens of cm. Moreover, the river discharge does not interact with tides the same way as in the upper part, as we no longer observed the highest tidal range for the smallest discharge. Yet, there is a strong Spearman correlation between tides and the river discharge that suggests that tidal range fluctuations can largely be attributed to variations in the discharge. Nonetheless, we should keep in mind that other processes, especially coastal processes like storm surges may modulate tidal amplitude in the lower part of the estuary. Finally, despite strong interannual variability in hydrological conditions, the parametric curves appeared to be robust over time, especially in the upper estuary. Therefore, in addition to their contribution to the improvement of the prediction of the unsteady estuarine tide, they have a potential interest for poorly monitored estuaries for assessing either the tidal range or the river discharge in the absence of one of the two quantities. As the rating curve is a steady characteristic of the local hydrodynamic properties, it also can serve to validate numerical configurations. This presentation is complementary to the one of Lyard et al. (this meeting) which addresses the detiding issue over tidal river systems using a modeling approach with data assimilation.

[1] LEGOS laboratory, CNRS/UPS/CNES/IRD, lucie.caubet@univ-tlse3.fr
[2] LEGOS laboratory, CNRS/UPS/CNES/IRD, florent.lyard@univ-tlse3.fr.
[3] LEGOS laboratory, CNRS/UPS/CNES/IRD, nadia.ayoub@univ-tlse3.fr
[4] EODYN, gwenaele.jan@eodyn.com (Shom, now at eOdyn)
[5] CLS, rchevrier@groupcls.com
[6] Fisheries and Oceans Canada, penney@dfo-mpo.gc.ca

References

Allen,G.P., Salomon, J.C., Bassoullet, P., Du Penhoat, Y., de Grandpré, C., (1980). Effects of tides on mixing and suspended sediment transport in macrotidal estuaries. Sediment. Geol. 26, 69–90. https://doi.org/10.1016/0037-0738(80)90006-8

Guo, L., van der Wegen, M., Jay, D.A., Matte, P., Wang, Z.B., Roelvink, D., He, Q., (2015). River-tide dynamics: Exploration of nonstationary and nonlinear tidal behavior in the Yangtze River estuary. J. Geophys. Res. Oceans 120, 3499–3521. https://doi.org/10.1002/2014JC010491

Hoitink, A.J.F., Jay, D.A., (2016). Tidal river dynamics: Implications for deltas. Rev. Geophys. 54, 240–272. https://doi.org/10.1002/2015RG000507

Jan, G., Lyard, F., Allain, D., Tchilibou, M., Penney, J., (2021). Tide in Gironde estuary in: 9th EuroGOOS International Conference, Advances in Operational Oceanography: Expanding Europe´s Observing and Forecasting Capacity. Shom and Ifremer and EuroiGOOS AISBL, Brest, France.

Matte, P., Jay, D.A., Zaron, E.D., (2013). Adaptation of Classical Tidal Harmonic Analysis to Nonstationary Tides, with Application to River Tides. J. Atmospheric Ocean. Technol. 30, 569–589. https://doi.org/10.1175/JTECH-D-12-00016.1

Zhang, F., Sun, J., Lin, B., Huang, G., (2018). Seasonal hydrodynamic interactions between tidal waves and river flows in the Yangtze Estuary. J. Mar. Syst. 186, 17–28. https://doi.org/10.1016/j.jmarsys.2018.05.005

Tidally Driven Circulation in a Multiple Inlet lagoon System

Chant R. [1], Pfeiffer-Herbert A. [2], Lerczak J. [3], Ertle N. [2], Benton C. [1], and Wilkin J. [1]

Abstract

Barrier island systems comprise 10% of the world's coastlines and nearly the entirety of the US east and Gulf Coasts. Behind these barrier islands are coastal lagoons that are generally shallow and connected to the ocean through tidal inlets. Most of these lagoon systems have multiple inlets connecting them to the coastal ocean allowing a net and persistent throughflow. Large lagoonal systems, such as Great South Bay along Long Island New York, Barnegat Bay New Jersey and Pamlico Sound North Carolina, act as low pass filters where tidal variability is strongly attenuated while lower-frequency wind-driven and other coastal processes that drive subtidal sea level variability pass into these systems relatively unattenuated. The dominance of wind-forced sea-level variability in these systems has led to the idea that their flushing is controlled by wind-driven subtidal motions (Wong and Wilson, 1984; Vieria and Chant 1993).

However, more recent studies have documented the importance of tidally-driven residual motion in driving a net transport and flushing of these lagoonal systems. In a modeling study of Barnegat Bay, Defne and Ganju [2015] found that a tidally- averaged rectified flow was the dominant process that flushed the bay and that 75% of the mean circulation in the bay was driven by tidal rectification. Hinrichs et al. [2018] found that tidally-driven residual circulation in Great South Bay increased four-fold after the opening of a relatively small new inlet in 2012 following Hurricane Sandy.

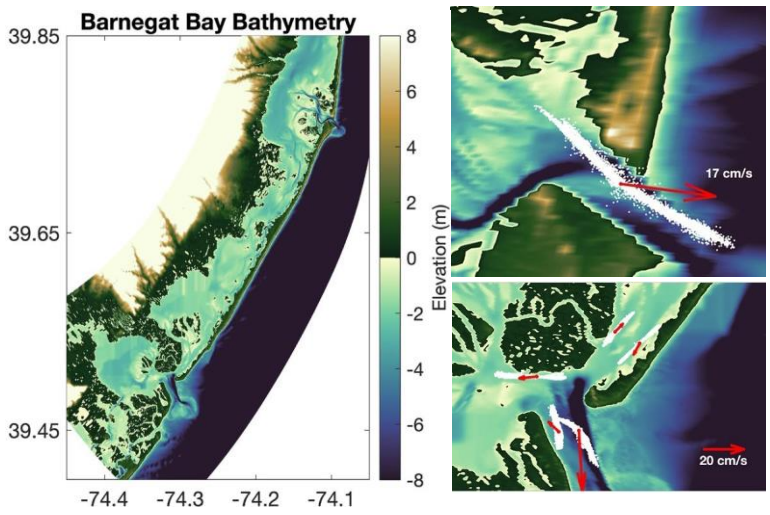

Figure 1. Model domain and Bathymetry of the Great Bay/Little Egg Harbor/Barnegat Bay system (left panel) Right panel shows hourly depth averaged currents (white dots) and record mean depth averaged Eulerian mean flows (red arrows) from Barnegat inlet (upper right) and Little Egg Inlet (lower right)

To investigate the dynamics driving circulation through these inlets we are currently conducting ship board and moored observations as well as numerical modeling of the Little Egg Harbor/Barnegat Bay lagoonal system which is located along the New Jersey, USA coast. We are focusing our efforts on the geomorphologically active Little Egg inlet to the south, and the highly engineered Barnegat Inlet to the north (Figure 1). Our overarching aim is to understand how realistic inlet morphology and processes, such as channels and shoals, trapping by coves, effects of buoyancy, finite amplitude tides and friction inside lagoons influence residual circulation in multiple inlets lagoon systems. Particular emphasis is focusing on processes that influence the phase relationship between currents and sea-level at the inlets and the resultant Stokes transport, the superelevation in the lagoon, the net transport through the inlets (Eulerian + Stokes), and the net transport and residence time within the lagoon. Our work is also exploring the role of local and remote meteorological forcing in modifying lagoon circulation, particularly how it influences tidally-driven Stokes and Eulerian transports and contrast its relative importance on driving exchange.

[1] Rutgers University
[2] Stockton University
[3] Oregon State University

Results to date have confirmed that both inlets drive a mean Stokes landward transport and have a seaward Eulerian mean transport (Fig 1) and both the Stokes transport and Eulerian mean flows are strongly modulated by the spring Neap cycle. Complex Empirical Orthogonal Function Analysis (EOF) performed on the depth averaged Eulerian currents found that 84 percent of the variance was found in the first two modes and both were highly correlated with tidal amplitude. Wind forcing decomposed into directions that were correlated and uncorrelated with local sealevel were also coherent with the EOF modal time series but with lower correlations that of tidal amplitude. The EOF modes are laterally sheared both at the inlet and in the Bay and net transport through the inlet is dominated by flows in the deep channel. The spring/neap variability augments the mean flow during spring tides and competes with the mean flow during neap tides Details of these flow, and thus the flushing, are probably dependent on channel morphology and will change in response to inlet engineering and in systems that undergo rapid geomorphological change.

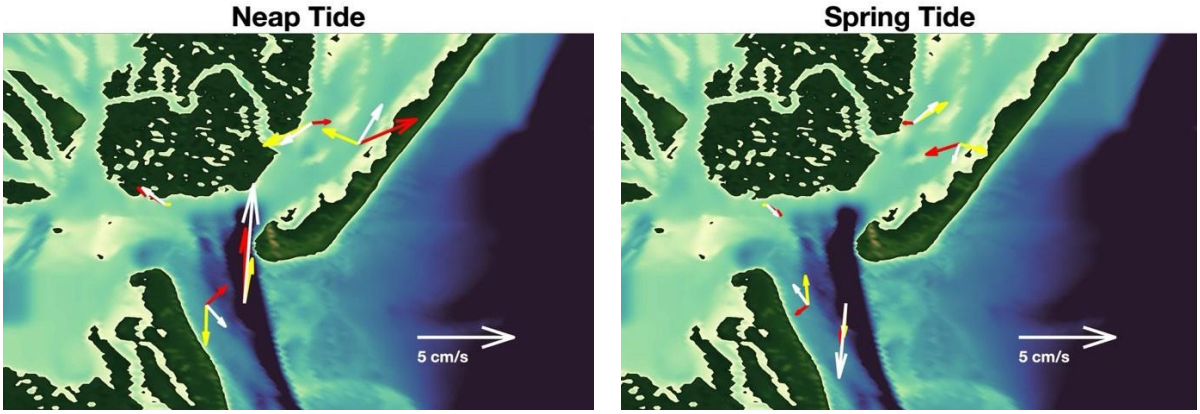

Figure 2. Mode 1 (red), Mode 2(yellow) and their sum (white) during spring (upper) and neap tidal conditions.

References

Defne, Z. and N. K. Ganju (2015). "Quantifying the residence time and flushing characteristics of a shallow, back-barrier estuary:Application of hydrodynamic and particle tracking models." Estuaries and Coasts 38: 1719-173

Hinrichs, C., et al. (2018). "Great South Bay after Sandy: Changes in circulation and flushing due to new inlet." Estuaries and Coasts 41: 2172-2190.

Vieira, M. E. and R. Chant (1993). "On the contribution of subtidal volume fluxes to algal blooms in Long Island estuaries." Estuarine, Coastal and Shelf Science 36(1): 15-29.

Wong, K.-C. and R. E. Wilson (1984). "Observations of low-frequency variability in Great South Bay and relations to atmospheric forcing." Journal of Physical Oceanography 14(12): 1893-1900

3D modelling sediment dynamics in the hyper turbid upper Ems-Dollard estuary

Chen W. [1], Staneva J. [1], Jacob B. [1], and Badewien T. [2]

Keywords: sediment, induced stratification, fluid mud, suspended sediment, SCHISM

Abstract

The increasing likelihood of extreme natural hazards in coastal areas, driven by global climate change, enhances the need for coastal risk prediction. The Ems-Dollard estuary in the southern North Sea is characterized by the interplay between meso-tidal and buoyancy forcing and intensive natural/human-induced changes. Its ecosystem suffers from enhanced flooding and hyper-turbidity. This study applies the SCHISM 3D unstructured-grid framework, which couples coastal hydro-, sediment-, and wave-dynamics, and simulates the fine sediment trapping and transport in the Ems-Dollard system. The model exhibits its capability in qualitatively resolving the development of hyper-turbid conditions, variation between fully mixed and mud-induced periodic stratification, as well as sediment transport processes in the upper Ems estuary zone. The model agrees with the E(ms)Do(llard)M(easurements)'18 field measurements. Further, a series of scenarios are designed to investigate the response of sediment dynamics to different river discharges, significant wave height, sediment supply. Various tide-related sediment transport mechanisms in the Ems-Dollard Estuary are addressed. With the major focus on sediment dynamics, this study is subject to extensive human use of the estuarine resource, a natural-based solution for coastal protection, which represents a crossing point of different interests and the concerns of the European H2020 Green Deal REST-COAST project.

[1] Department of Hydrodynamics and Data Assimilation, Institute of Coastal Systems-Analysis and Modelling, Helmholtz-Zentrum Hereon – Germany
[2] Institute for Chemistry and Biology of the Marine Environment, University of Oldenburg – Germany

How do extreme conditions impact salinity intrusion in Delaware Bay?

Cook S.E. [1], Warner J.C. [1], and Russel K.L. [2]

Keywords: estuaries, numerical modelling, salinity intrusion

Abstract

Climate change, population growth and sea level rise have put increased pressure on coastal environments such as the Delaware Bay River Basin, which provides water resources for approximately 13 million people, or roughly 4% of the US population. Management of the salt front (~0.5 PSU) location is used as a measure to limit salt intrusion and protect drinking water and industrial intakes. This work is focused on understanding how river discharge and bathymetric features affect salinity intrusion within the Delaware Bay estuary. We employ the COAWST (Warner et. al. 2010) numerical modeling system to perform simulations that include river discharge; tidal and subtidal low frequency signals forced at the mouth of the estuary; and local winds to drive bulk atmospheric forcings. The model was run for a drought year (2016) and a wet year (2019) to investigate the role of variable hydrodynamic conditions on the location of the salt front. Model results show good agreement to NOAA and USGS observed time series of water level and salinity and represent seasonal patterns of the observed daily salt front location (Preucil and Reavy, 2020). The location of the salt front depends primarily upon the river discharge (Fig. 1), however as discharge wanes in the summer months, bathymetric features, subtidal water levels and winds become more important. In some cases, these processes can move the daily average salt front over 1 mile a day, and at other times bathymetric sill-like features suppress movement of the salt front and delay the intrusion event. Understanding relative importance of the driving mechanisms that determine the position of the salt front can aid in better water resource management in the region, especially during periods of drought.

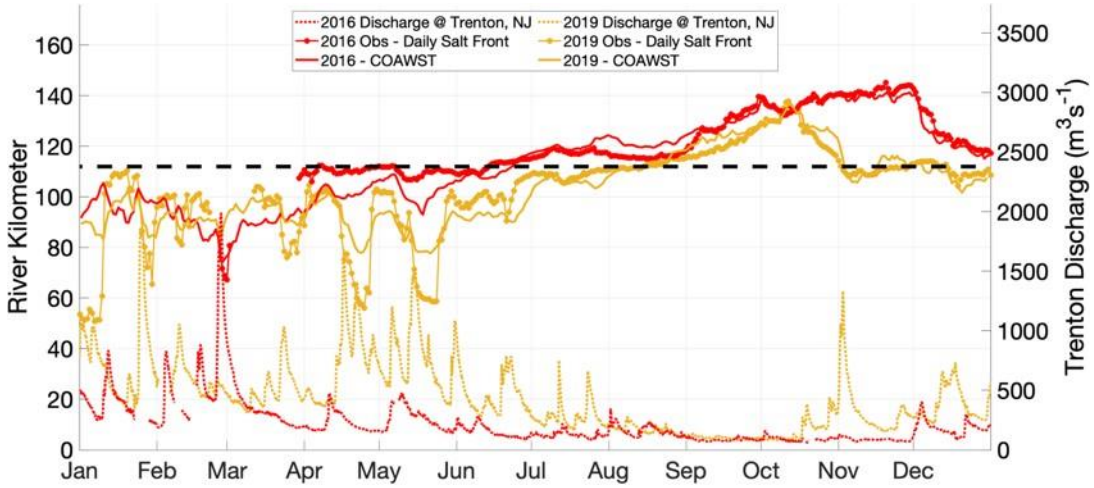

Figure 1. Modeled (solid lines) and observation-based (filled in circles) salt front locations for 2016 (red) and 2019 (yellow), and observed discharge at Trenton NJ (dashed lines). Black dashed line indicates a bathymetric control point at river kilometer 112.

References

Preucil, A. and Reavy, K. *Description and data sources for the Flow Management Snapshot.* 2020, February 10. Delaware River Basin Commission Hydrology Report. https://drbc.maps.arcgis.com/home/index.html.

Warner, J. C., Armstrong, B., He, R., & Zambon, J. B. (2010). Development of a Coupled Ocean-Atmosphere-Wave-Sediment Transport (COAWST) Modeling System. *Ocean Modelling*, *35*(3), 230–244.

[1] U.S. Geologic Survey, Woods Hole, MA, 02543, USA
[2] U.S. Geologic Survey, Reston, VA, 20192, USA E-mail: secook@usgs.gov

The characteristics of the tide over the Amazon estuary: evolution in future sea level rise scenarios

Coulet P. [1,2], Durand F. [1,2], Testut L. [3], Fassoni-Andrade A. [2,1], Khan J. [1], Guedes Santos L. [4], Toublanc F. [1], and Medeiros Moreira F. [5,6]

Keywords: Amazon, tide, sea level rise, modulation, modeling, Atlantic.

Abstract

The Amazon River outflows its freshwater to the western equatorial Atlantic Ocean through a macrotidal terminal delta. This delta is one of the longest and widest on Earth. More than 4 million people are settled there (IBGE, 2010), among which one third live under consistent exposure to the coastal flooding hazard (Mansur et al., 2016). This already alarming situation is bound to deteriorate further, under the ongoing sea level rise (SLR). The SLR is going to perturbate the hydrodynamics of the delta through two mechanisms. On one side, it will have a direct impact on the mean sea level at the coast and on the other side, it will modulate the characteristics of the ocean tide entering the delta. These two phenomena jointly are prone to impact the dynamics of coastal flooding in the delta. Indeed, the tide is the dominant factor of water level extremes across the delta; in this very shallow water region, the tidal amplitude is likely to be modulated by the long-term trend of water level, as is the case in other deltaic and estuarine regions worldwide (Talke and Jay, 2020; Khan et al., 2020).

In the present study, we investigate the sensitivity of the tide to SLR in the Amazon estuary based on a hydrodynamic numerical modeling approach. Our model consists of a 2DH configuration of the SCHISM model, implemented at high resolution over the whole Amazon River - delta - Atlantic Ocean hydraulic continuum. We conducted a reference simulation of the model, extensively validated against all available in situ and remotely-sensed tidal datasets over the study area. Our model was found to reproduce satisfactorily the dominant tidal constituents as well as their seasonal variability, with a typical error of order 10 cm.

We then assessed the sensitivity of the simulated tide to a range of SLR scenarios, varying from +0.5m to +2.5m with regards to the current sea level. It was found that the Amazon delta exhibits a regionally-varying pattern of tidal modulation. In the Northern Channel, M2 amplitude was found to moderately increase as sea level rises, with a typical amplitude increase amounting to 3% of the SLR. In the Southern Channel, in contrast, M2 amplitude gets augmented by up to 10% of the SLR. Further to the South-East, at the mouths of Pará, M2 amplitude moderately decays with SLR. These contrasted responses will obviously translate into different impacts in the long-term trends of high tide water level. Our results imply that a differentiated, localized perspective is required in any attempt to anticipate the future impacts of SLR over a region with such a complex geometry as the Amazon delta.

References

IBGE. Instituto Brasileiro de Geografia e Estatıstica (Brazilian Institute of Geography and Statistics) (2010). Data from demographic census 2010. Census online: http://www.ibge.gov.br

Khan, M.J.U., Durand, F., Testut, L., Krien, Y., Islam, A.K.M.S (2020) Sea level rise inducing tidal modulation along the coasts of Bengal delta. Cont. Shelf Res. 211, 104289. doi: 10.1016/j.csr.2020.104289

Mansur, A.V., Brondízio, E.S, Roy, S., Hetrick, S., Vogt, N.D., Newton, A. (2016) An assessment of urban vulnerability in the Amazon Delta and Estuary: a multi-criterion index of flood exposure, socio-economic conditions and infrastructure. Sustain Sci 11: 625–643. doi: 10.1007/s11625-016-0355-7

Talke, S.A., Jay, D.A. (2020). Changing tides: the role of natural and anthropogenic factors. Annual Review of Marine Science 12 (1), 121–151. https://doi.org/ 10.1146/annurev-marine-010419-010727.

[1] LEGOS, Université Toulouse, IRD, CNRS, CNES, UPS, Toulouse, France, paul.coulet@legos.obs-mip.fr
[2] University of Brasília (UnB), Institute of Geosciences, Brasília, Brazil
[3] LIENSs UMR 7266, CNRS- La Rochelle University, 17000 La Rochelle, France
[4] CPRM, Serviço Geológico do Brasil, Avenida Doutor Freitas, 3645, Marco, Belém, Brazil [5]CPRM, Serviço Geológico do Brasil, Avenida Pasteur, 404, Urca, Rio de Janeiro, Brazil [6]GET, CNRS/CNES/IRD/UPS, 31400 Toulouse, France

Storm driven subtidal flows at the confluence of two estuaries

Cyr N. [1] and Huguenard K. [2]

Keywords: subtidal flows, estuaries, stratification, storms, material transport

Abstract

Subtidal flows drive long term material transport, dictating the exchange of sediments, pollutants, and particulate organic matter within estuarine systems. Subtidal flows can be modulated by external forcings, such as river discharge and wind. When driven by density gradients, subtidal flows generally follow a vertically sheared pattern, with inflow of dense water along the bottom and outflow of lighter water along the surface. This pattern can be modified by tides, wind, and bathymetric forcing. Glacially carved, complex estuaries often feature the confluence of two systems that are likely to interact under given forcing regimes. This work aims to understand how storm events featuring enhanced precipitation and wind modulate subtidal flow at the confluence of two estuaries. A field campaign occurred at the convergence of East Penobscot Bay with the Bagaduce River in Maine, USA. The Bagaduce River is a shallow, low inflow system that connects to the deeper, partially stratified East Penobscot Bay, both of which experience mesotidal forcing. Field observations were collected during the stormy season from December 2022 to February 2023. A series of bottom-mounted Acoustic Doppler Current Profilers were co-located with vertically oriented Conductivity Temperature Depth sensors along the channel-shoal transition. Preliminary results reveal a vertically sheared two-layer structure with inflow on the bottom and outflow at the surface during periods of low discharge- consistent with gravitational exchange. Subtidal flow patterns reverse during the highest discharge events that coincide with stormy periods, where outflow occurs at the bottom and inflow at the surface. During these reverse circulation events, stratification from East Penobscot Bay is advected into the Bagaduce River on the flood tide, yielding a pattern opposite from strain induced periodic stratification where floods are more stratified than ebbs. These results suggest that a deeper, more stratified system can control material exchange at an adjoining system when storm conditions increase river discharge and enhance tidal currents.

1 University of Maine, nicolas.cyr@maine.edu

2 University of Maine, kimberly.huguenard@maine.edu

Physical processes shaping low-oxygen events in a highly flushed coral atoll lagoon

Davis K.A. [1], Merrigan S. [2], Fu K.-H. [3], and Pawlak G. [4]

Keywords: coral reef, hypoxia, tides, ocean-lagoon exchange, oxygen

Abstract

In the coastal ocean, reported low-oxygen and even hypoxic ([O2] < 2 mg L-1) events have increased exponentially since the 1960s and are associated with fish kills, sea grass die offs, coral bleaching events, and dead-zones (Altieri et al., 2017; Gilbert et al. 2010, Zhang et al. 2010). In most coastal systems, hypoxia is induced through eutrophication, long residence times, and lack of ventilation to the atmosphere (Fennel and Testa, 2019). Here, we investigate the processes driving observed low-oxygen events in the Dongsha Atoll lagoon, a coral atoll in the South China Sea. The lagoon has been shown to be a highly-flushed body of water (full lagoon residence times of 2-3 days) and is remote without significant anthropogenic nutrient inputs. Observations from a field campaign in summer 2019 are used to construct a bottom water mass budget in Dongsha Atoll lagoon in order to understand the physical processes governing residence time and renewal of the bottom waters. Deep water renewal events, which typically transport dense, higher oxygen water to depth, have been primarily observed in fjords, but a recent study observed this mechanism in a tropical embayment (Adelson et al., 2022). Results show frequent bottom water renewal events driven by tidally modulated advective processes through the lagoon channels and over the reef flat. Though bottom water renewal events are usually a mechanism for refreshing oxygen levels in stratified systems, the water advected into Dongsha Atoll lagoon from the reef flat can, at times, be hypoxic. The water flowing off of the reef flat into the Dongsha Atoll lagoon is intermittently oxygen deficient, due to seasonal phase-alignments between the primarily diurnal tidal flow and biological respiration on the reef. During the study period, Summer 2019, the flood phase of the tide, which drives flow of cooler offshore water across the reef flat from the ocean to the lagoon, occurred at night when strong biological respiration draws down oxygen on the shallow reef flat. These cooler, low oxygen waters sink to the bottom of the stratified lagoon waters, creating a pool of isolated low-oxygen water. These observations point to a unique physical-biological mechanism for creating low-oxygen environments in tropical waters.

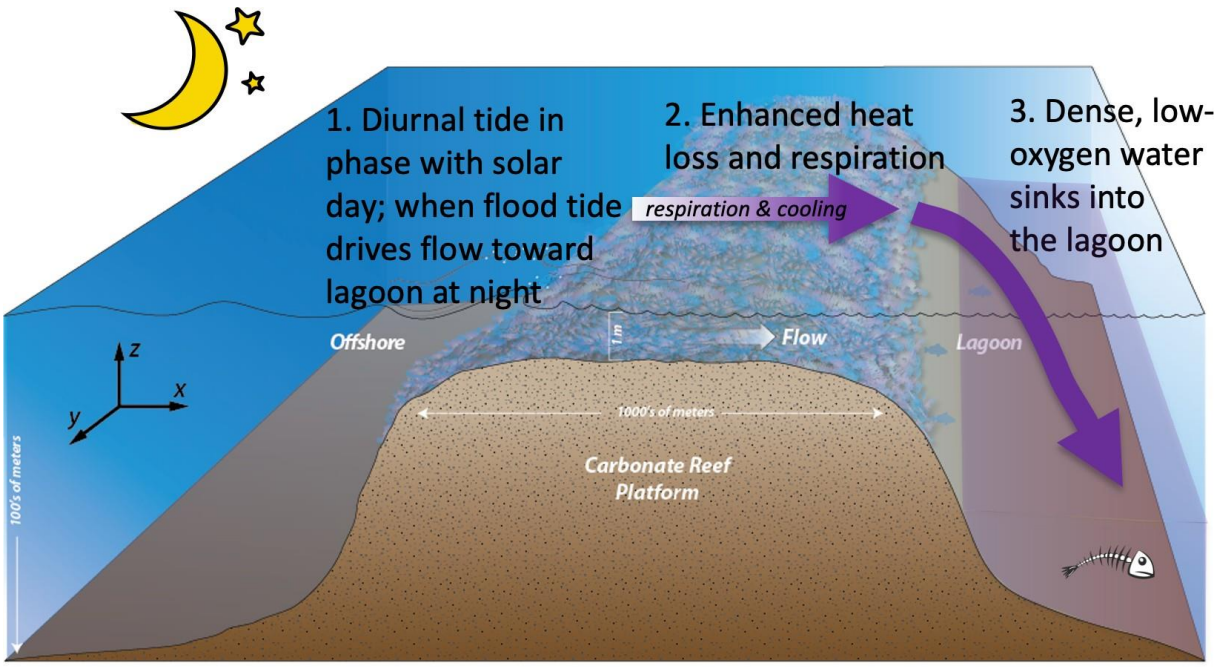

Figure 1. Schematic illustrating the mechanism for generation of dense, low-oxygen water on a reef flat and transport into the bottom of a lagoon.

[1] Stanford University, Oceans, Stanford, CA, USA; kristen.davis@stanford.edu
[2] University of California, Irvine, Civil & Environmental Engineering, Irvine, CA, USA; smerriga@uci.edu
[3] National Academy of Marine Research, Taiwan; ke.hsien.fu@gmail.com
[4] University of California, San Diego, Mechanical & Aerospace Engineering, La Jolla, CA, USA; epawlak@ucsd.edu

References

Adelson, A.E., Altieri, A.H., Boza, X., Collin, R., Davis, K.A., Gaul, A., Giddings, S.N., Reed, V. and Pawlak, G. (2022) Seasonal hypoxia and temperature inversions in a tropical bay. *Limnology and Oceanography*, 67 (10), 2174–2189.

Altieri, A. H., S. B. Harrison, J. Seemann, R. Collin, R. J. Diaz, and N. Knowlton, (2017) Tropical dead zones and mass mortalities on coral reefs. *Proceedings of the National Academy of Sciences*,114 (14), 3660–3665.

Fennel, K., and J. M. Testa, 2019: Biogeochemical controls on coastal hypoxia. *Annual Review of Marine Science*, 11, 105–130.

Gilbert, D., N. 416 N. Rabalais, R. J. Diaz, and J. Zhang, (2010) Evidence for greater oxygen decline rates in the coastal ocean than in the open ocean. *Biogeosciences*, 7 (7), 2283–2296.

Zhang, J., Gilbert, D., Gooday, A.J., Levin, L., Naqvi, S.W.A., Middelburg, J.J., Scranton, M., Ekau, W., Pena, A., Dewitte, B. and Oguz, T., (2010) Natural and human-induced hypoxia and consequences for coastal areas: synthesis and future development. *Biogeosciences*, *7*(5), 1443-1467.

Sediment trapping in estuaries

Defontaine S. [1], Dijkstra Y.M. [2], and Grasso F. [3]

Keywords: sediment transport, estuaries, estuarine turbidity maxima, transport capacity, sediment trapping regimes

Abstract

Motivation

Convergent transport of suspended sediment is responsible for generating areas of sediment accumulation named Estuarine Turbidity Maxima (ETM). ETMs are common features of tidal estuaries worldwide; however, ETM characteristics (location, concentration, extension) largely differ among estuaries and within the same estuary depending on external forcing. So far, understanding of ETM generation has been mainly gained through study cases (Uncles et al., 2002). Although very instructive, such insights are difficult to extend further. A comprehensive understanding of processes involved in the convergence of sediment in estuaries for various estuary types under a wide range of forcing conditions is still lacking. The aim of this study is then to provide a broad-based understanding of ETM dynamics and to suggest a parameter space to classify estuaries in terms of trapping capacity. Two primary questions had to be answered:

1) Which transport processes are responsible for ETM generation for various combinations of estuarine parameters?
2) How estuarine parameters influence the position and the sediment concentration of the ETM?

Material and methods

The idealized width-averaged modelling framework iFlow v3.0 has been chosen to study the dependence of sediment transport processes on estuarine parameters in simple domains (Dijkstra et al., 2017). Due to the large number of transport processes that may be involved in ETM generation, this study will focus on a simplified configuration with a limited number of parameters and processes. In our first set of 3168 simulations, the estuary was represented by a straight rectangular channel, where width and depth are held constant. In a second phase, simulations consisting of an estuary with a constant rectangular cross-section and a sloping bed were used to analyze the influence of bed slope on the sediment transport processes and to help expanding results towards reality. Four input parameters have been selected to systematically vary throughout the simulations: the length of the estuary, the bed friction, the river discharge and the tidal amplitude.

Results

The first set of model experiments has permitted to identify three sediment trapping regimes (named after the dominant sediment import mechanism): the Baroclinic Regime, the Sediment advection regime and the Dispersive Regime (Fig.1). These regimes are extreme cases and simulated ETM are mostly generated by a combination of two or more regimes. The baroclinic regime is defined as a balance between sediment import by the gravitational circulation and sediment export by the river flow. This regime dominates in low friction setups for short and long estuaries, except for long estuaries strongly tidally forced. Under this regime, the ETM is moderately to strongly concentrated and may be associated with bottom fluid mud. The ETM location mostly depends on the river flow and the bottom friction coefficient. The sediment advection regime is governed by the convergence of sediment import due to spatial settling lag and sediment export due to internally-generated tidal asymmetry. This regime dominates in strongly tidally forced estuaries and/or long estuaries. Under this regime, the ETM is generally generated in the upper part of the estuary with a low to moderate concentration. The dispersive regime is driven by a balance between sediment import due to background dispersion and export by river-induced flushing. Under this regime, sediment is dispersed along the estuary until the convergent point and a maximum of sediment availability on the bed is reached at this location. In the water column, the maximum of suspended sediment concentration is reached at the entrance of the estuary with the concentration imposed at this boundary. This regime dominates in estuaries characterized by strong bottom friction.

The second set of model experiments has revealed that the presence of a slopping bed induces a fourth dominant trapping regime: the internally-generated tidal asymmetry regime. This regime dominates in long estuaries characterized by low to moderate bottom friction. Under this regime, the ETM is generally generated in the upper part of the estuary with a moderate to high concentration. The slopping bed has a little impact on the trapping regimes for short estuaries, whereas it strongly affects transport processes in long estuaries. The relative importance of the sediment advection regime is reduced and superseded by the baroclinic and internally-generated tidal asymmetry regimes for low to moderate mixing conditions.

[1] Ifremer – DYNECO/DHYSED, Centre de Bretagne, CS 10070, 29280 Plouzané, France, sophie.defontaine@cerema.fr
[2] Delft Institute of Applied Mathematics, Delft University of Technology, Delft, The Netherlands, y.m.dijkstra@tudelft.nl
[3] Ifremer – DYNECO/DHYSED, Centre de Bretagne, CS 10070, 29280 Plouzané, France, florent.grasso@ifremer.fr

Discussion

Despite most of the major processes contributing to sediment trapping are resolved in this study, some physical processes have been neglected for sake of simplicity. Among these processes are the sediment transport induced by temporally or spatially varying eddy viscosity such as tidal straining or stratification-induced turbulence damping, turbidity gradient induced circulation, flocculation and lateral correlations. Such processes may have a significant contribution to the SSC distribution along the estuary and could be included in future work to help extend our results toward more realistic estuaries. The channel model presented in this study should be looked as a starting point for including more complex processes. It is not supposed to be predictive but rather give insights on physical processes involved in sediment trapping in estuaries.

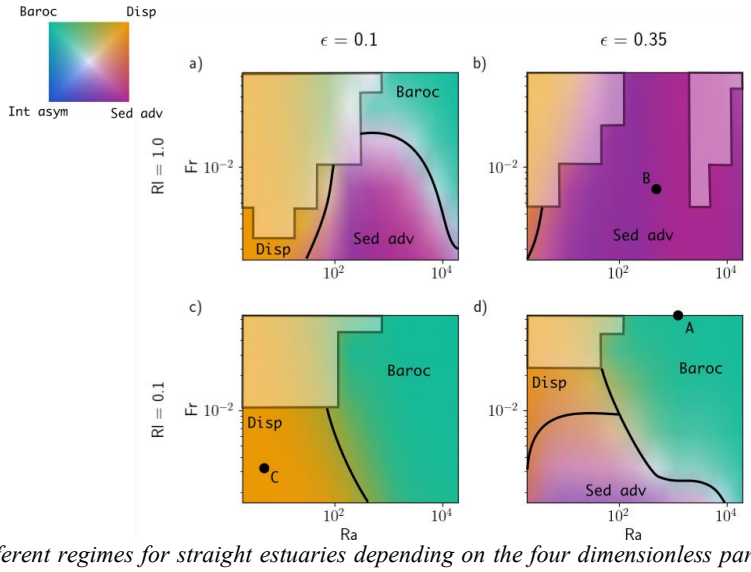

Figure1 Mapping of the different regimes for straight estuaries depending on the four dimensionless parameters F r, Ra, ε and Rl. Each panel corresponds to constant values of ε (i.e. dimensionless amplitude of tide) and Rl (i.e. dimensionless length of the estuary), whereas interior axes of each panel show varying values of Ra (changing with the inverse of Av) and Fr (varying with values of Q). Shaded areas show simulations where the sediment export capacity overcomes the sediment import capacity all along the estuary, impeding the formation of an ETM.

Acknowledgement

This work has been supported by the CATURE project (OFB-MIE).

References

Chernetsky, A.S., Schuttelaars, H.M., Talke, S.A. (2010). The effect of tidal asymmetry and temporal settling lag on sediment trapping in tidal estuaries. Ocean Dynamics 60, 1219–1241.

Dijkstra, Y.M., Brouwer, R.L., Schuttelaars, H.M., Schramkowski, G.P., 2017. The iflow modelling framework v2. 4: A modular idealized process-based model for flow and transport in estuaries. Geoscientific Model Development 10, 2691–2713.

Dijkstra, Y.M., Schuttelaars, H.M., Schramkowski, G.P., Brouwer, R.L. (2019). Modeling the transition to high sediment concentrations as a response to channel deepening in the ems river estuary. Journal of Geophysical Research: Oceans 124, 1578–1594.

Uncles, R., Stephens, J., Smith, R., 2002. The dependence of estuarine turbidity on tidal intrusion length, tidal range and residence time. Continental shelf research 22, 1835–1856.

Tide-surge interactions in an estuary: a case study in south-west Long Island Sound

de Vos M. [1], Onat Y. [1], and O'Donnell J. [1, 2]

Keywords: tide, surge, estuary.

Abstract

Coastal flooding due to the combination of astronomic tide and storm surge is a well-known hazard for the communities of Long Island Sound in the north-east United States (Liu et al., 2020, 2021). Associated socio-economic impacts are often significant due to the high (and increasing) population and infrastructure density along the shore (Poudel et al., 2023). Ongoing intensification of these impacts is likely, due to rising sea levels and increasingly frequent and severe extreme events associated with climate change (e.g. Kirshen et al., 2008; O'Donnell, 2019; Spanger-Siegfried et al., 2014).

Given this vulnerability, resilient infrastructure design and management policy require a robust understanding of the expected flood extent for a given total water level (TWL), which is the sum of the contributions from the astronomic tide (AT) and meteorologically driven, non-tidal residual (NTR). One common approach assumes that AT and NTR elevations are independent (Idier et al., 2012), and, consequently, that the NTR resulting from a given meteorological condition could occur at any phase of the tide (Williams et al., 2016). Worst-case-scenario TWL can be inferred by summing the NTR and highest-astronomic tidal elevations, or by considering the distribution of skew-surge, which is the difference between the maximum TWL and the elevation within a tidal cycle (irrespective of whether they coincide or not).

Whilst the independence of AT and NTR has been demonstrated in some places (Williams et al., 2016), numerous studies have shown the interaction between them to be important in others. More recently, Arns et al. (2020) showed that neglecting tide-surge interactions (TSI) in extreme-value analysis may result in underestimations of extreme TWL of up to 70 cm globally, and Costa et al. (2023) found TSI of up to 27 cm around coastal New Zealand. In a study domain more similar to ours, Idier et al. (2012) determined TSI of up to 74 cm (half the maximum storm surge) in the eastern English Channel. This suggests that extreme value analyses underpinning town-scale risk assessments should include local analysis of TSI for design purposes.

We present preliminary findings from an investigation into TSI near the coastal town of Stamford, Connecticut, in south-western Lond Island Sound. A depth-integrated configuration of the ADvanced CIRCulation (ADCIRC, version 55) model (Luettich & Westerink, 2004) on an unstructured mesh is utilized. Three simulations which differ in their boundary forcing are run; a control member, forced by TWL (i.e. tide and surge), and two members forced at their boundaries by NTR and AT only, respectively. Each three-member experiment was performed for 4 historical storms: two tropical cyclones and two extratropical cyclones. Total water levels, tides and surges which develop with and without dynamical interaction are then compared to each other to determine the magnitude of the TSI. Results indicate that TSI can cause instantaneous differences in surge and tide of up to 31 and 27 cm respectively in key nearshore areas. These instantaneous differences are mainly induced by a slight phase shift of the tide, though tidal and surge amplitudes are also modulated in some cases (and to a lesser extent). Since differences are mainly due to phase shifts, the instantaneous surge and tide differences do not necessarily produce concomitantly high differences in TWL (and, by extension, flood risk), and may dampen each other. In the most severe case, neglecting TSI caused a very slight modulation of the tide (instantaneous difference of 1.4 cm) and an overestimation of the surge (instantaneous difference of 33.4 cm), which together produced an overestimation of the TWL of 12.1 cm (Figure 1). Since this difference occurred near low water, the impact would have been minor. Further work is required to determine whether such differences could manifest at high water, thereby posing a risk of underestimating maximum TWL during a storm.

[1]Connecticut Institute for Resilience & Climate Adaptation, University of Connecticut: marc.devos@uconn.edu, yaprak.onat@uconn.edu, james.odonnell@uconn.edu
[2] University of Connecticut Department of Marine Sciences

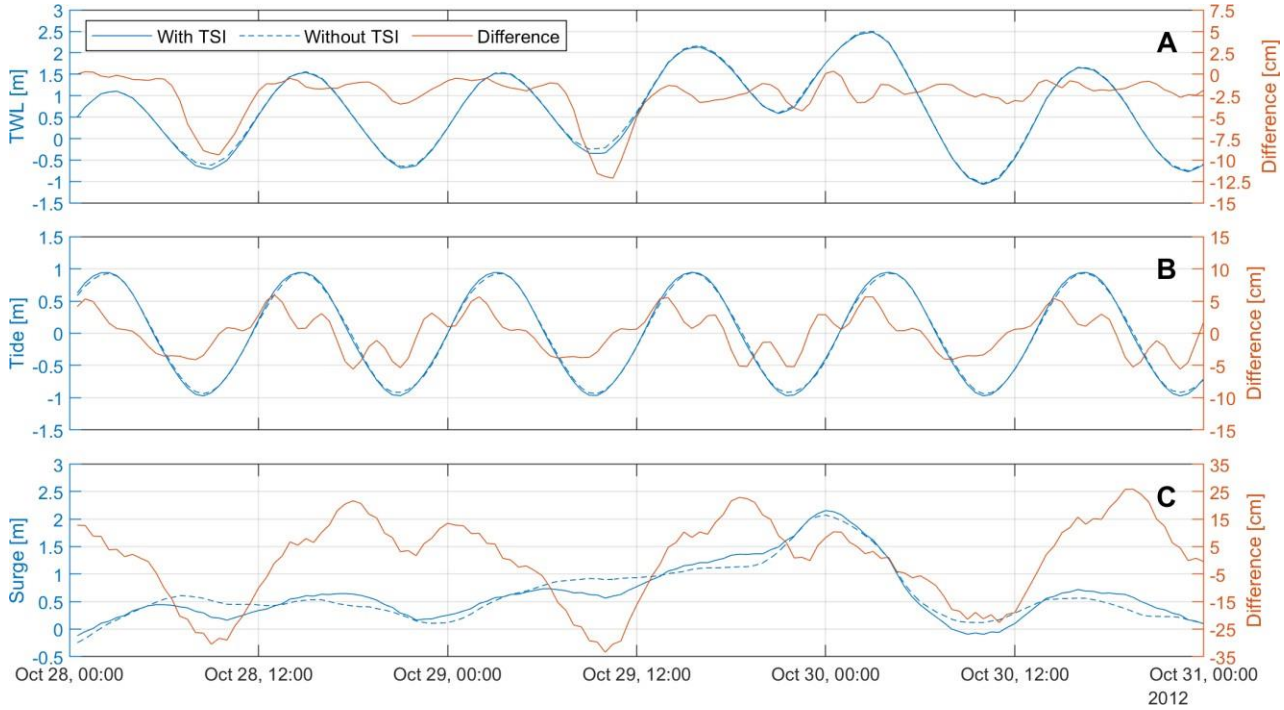

Figure 1. Total water level (A), tide (B) and surge (C) during Hurricane Sandy for a point near West Beach in Stamford. Blue curves show magnitudes and orange curves show the differences between them due to tide-surge interactions.

References

Arns, A., Wahl, T., Wolff, C., Vafeidis, A. T., Haigh, I. D., Woodworth, P., Niehüser, S., & Jensen, J. (2020). Non-linear interaction modulates global extreme sea levels, coastal flood exposure, and impacts. *Nature Communications*, *11*(1). https://doi.org/10.1038/s41467-020-15752-5

Costa, W., Bryan, K. R., Stephens, S. A., & Coco, G. (2023). A regional analysis of tide-surge interactions during extreme water levels in complex coastal systems of Aotearoa New Zealand. *Frontiers in Marine Science*, *10*. https://doi.org/10.3389/fmars.2023.1170756

Idier, D., Dumas, F., & Muller, H. (2012). Tide-surge interaction in the English Channel. *Natural Hazards and Earth System Science*, *12*(12), 3709–3718. https://doi.org/10.5194/nhess-12-3709-2012

Kirshen, P., Watson, C., Douglas, E., Gontz, A., Lee, J., & Tian, Y. (2008). Coastal flooding in the Northeastern United States due to climate change. *Mitigation and Adaptation Strategies for Global Change*, *13*(5–6), 437–451. https://doi.org/10.1007/s11027- 007-9130-5

Liu, C., Jia, Y., Onat, Y., Cifuentes-Lorenzen, A., Ilia, A., McCardell, G., Fake, T., & O'Donnell, J. (2020). Estimating the annual exceedance probability of water levels and wave heights from high resolution coupled wave-circulation models in long island sound. *Journal of Marine Science and Engineering*, *8*(8). https://doi.org/10.3390/JMSE8070475

Liu, C., Onat, Y., Jia, Y., & O'Donnell, J. (2021). Modeling nearshore dynamics of extreme storms in complex environments of Connecticut. *Coastal Engineering*, *168*. https://doi.org/10.1016/j.coastaleng.2021.103950

Luettich, R., & Westerink, J. (2004). *Formulation and Numerical Implementation of the 2D/3D ADCIRC Finite Element Model Version 44.XX*. https://www.researchgate.net/profile/Richard-Luettich-Jr/publication/240474926_Formulation_and_Numerical_Implementation_of_the_2D3D_ADCIRC_Finite_Element_Model_Version _44XX/links/55eedbc008aef559dc4449fb/Formulation-and-Numerical-Implementation-of-the-2D-3D-ADCIRC-Finite-Element- Model-Version-44XX.pdf

O'Donnell, J. (2019). *Sea Level Rise in Connecticut Final Report*. https://circa.media.uconn.edu/wp-content/uploads/sites/1618/2019/10/Sea-Level-Rise-Connecticut-Final-Report-Feb-2019.pdf

Poudel, S., Caridad, C., Elliott, R., & Knighton, J. (2023). Housing market dynamics of the post-Sandy Hudson estuary, Long Island Sound, and New Jersey coastline are explained by NFIP participation. *Environmental Research Letters*, *18*(9). https://doi.org/10.1088/1748-9326/acea38

Spanger-Siegfried, E., Fitzpatrick, M., & Dahl, K. (2014). *Encroaching Tides How Sea Level Rise and Tidal Flooding Threaten U.S. East and Gulf Coast Communities over the Next 30 Years*. www.ucsusa.org

Williams, J., Horsburgh, K. J., Williams, J. A., & Proctor, R. N. F. (2016). Tide and skew surge independence : New insights for flood risk. *Geophysical Research Letters*, *43*, 6410–6417. https://doi.org/10.1002/2016GL069522.

Tidal salt transport regimes. Uncovering the importance of ESCO in estuaries mixed to stratified

Dijkstra Y.M. [1]

Keywords: salt intrusion, transport processes, stratification, SIPS, ESCO, classification.

Abstract

The transport of salt in estuaries is governed by various tidal and subtidal processes that depend on the geometry, flow and salinity in a complex and nonlinear way. As a result, different processes are important in different estuaries. In order to understand how salt intrusion in any particular estuary changes with climate change and human interventions, it is important to understand which processes are dominant and how these may change in the future.

One of the processes that is thought to be essential in many estuaries is related to tidal variations in stratification, or strain-induced periodic stratification (SIPS, Simpson et al (1990)). SIPS has been shown to contribute to an important exchange flow contribution caused by eddy viscosity-shear covariance (ESCO, Dijkstra et al (2017). The empirical classification by Geyer & MacCready (2014) hypothesises that SIPS-related processes are dominant in many partially stratified estuaries all around the world. However, this suggestion has not been verified by means of a physics-based model. Recent work by Dijkstra et al (2022) started to investigate which salt transport processes are important for which estuaries based on a width-averaged physics-based model. This has resulted in the identification of 7 estuarine regimes. However, the work so far has not included SIPS-related processes.

In this contribution, the importance of SIPS-related processes is investigated in over 40,000 different estuarine configurations, representing different depth, roughness, tide and river discharge. Hence, this represents estuarine conditions ranging from well-mixed to salt wedge. The model used for this study is a width-averaged physics-based model that dynamically resolves the water motion and salinity. The effects of tidal variations in stratification on turbulence are accounted for, so that the model also resolves ESCO.

As a new finding, preliminary results indicate that ESCO has a dominant role in tide-dependent salt wedge estuaries. Whereas such estuaries are usually described by means of the dynamics during different tidal stages, this finding can offer a different interpretation of the dynamics in terms of subtidal effects of tidal correlations. As other estuarine types are interpreted this way, this helps to unify the way we understand estuaries. Also, the identification of the dominant processes helps to understand how salt intrusion and stratification change with essential variables such as depth and discharge.

Fig. 1 shows an example of a model result for a tide-dependent salt wedge, showing salinity during four stages of the tide (top row) and the six most dominant transport contributions (bottom row). The transport contributions are described in terms of subtidal interactions (TM0) and tidal correlations (TM1), following by the two processes that cause variations in velocity and salinity. Results show similar magnitudes of processes related to gravitational circulation (gc), momentum advection (adv) and ESCO.

During the presentation, the importance of ESCO for various types of estuaries is discussed as well as the implications this has on our understanding of salt intrusion in these estuaries.

[1] Delft Institute of Applied Mathematics, Delft university of Technology. y.m.dijkstra@tudelft.nl

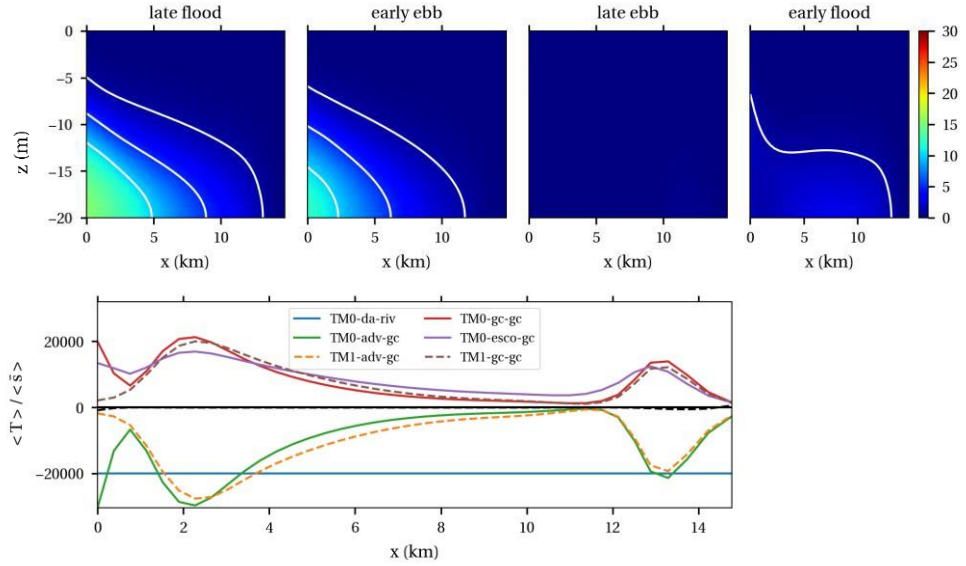

Figure 1. Model results for one case with large ESCO contribution (with dimensionless parameters Ra: 5640, Fr: 0.5, StRa: 1278, Ft:0.35, see Dijkstra et al (2022)). Top: salinity in psu in along-channel (x) and vertical (z) direction during various stages of the tide. Bottom: transport processes decomposition relative to the subtidal depth-averaged salinity. The purple line indicates ESCO- related processes (see main text for explanation).

References

Dijkstra, Y. M., Schuttelaars, H. M., & Burchard, H. (2017). Generation of exchange flows in estuaries by tidal and gravitational eddy viscosity-shear covariance (ESCO). Journal of Geophysical Research: Oceans, 122, 4217–4237. https://doi.org/10.1002/2016JC012379

Dijkstra, Y. M., Schuttelaars, H. M., & Kranenburg, W. M. (2022). Salt transport regimes caused by tidal and subtidal processes in narrow estuaries. Journal of Geophysical Research: Oceans, 127, e2021JC018391. https://doi.org/10.1029/2021JC018391

Geyer, W. R., and MacCready, P. (2014), The estuarine circulation, Annu. Rev. Fluid Mech., 46, 175–197, doi:10.1146/annurev- fluid-010313-141302.

Simpson, J. H., Brown, J., Matthews, J., and Allen G. (1990), Tidal straining, density currents, and stirring in the control of estuarine stratification, Estuaries, 13, 125–132, doi:10.2307/1351581.

3D numerical model of fine sediment transport and morphodynamics to analyse the seasonal variations of bed evolution in a macrotidal estuary

Do T.K-A. [1,2], Huybrechts N. [1,2], Jalón-Rojas I. [3], Sottolichio A. [4], Tassi P. [4], and Klein F. [5]

Keywords: 3D modeling, sediment transport, settling velocity, Gironde estuary, bed evolution

Abstract

A three-dimensional (3D) numerical model of the Gironde estuary has been implemented in the openTELEMAC system (Hervouet., 2000) to analyse the indirect effects of maritime navigation and port activities on the estuarine environment. The Gironde Estuary, as observed in most estuaries worldwide, pose challenges for morphodynamic modeling due to complex hydrodynamics and complex sediment processes involving diverse sediment types, both cohesive and non- cohesive. The 3D model developed in this work couples the TELEMAC-3D module (hydrodynamics, based on the solution of the Navier-Stokes equation), with the sediment transport and bed evolution module GAIA (Tassi et al. 2023) and TOMAWAC module to account for wave effects. The model has been validated using in situ data collected in 2018 from the mouth to the central estuary (km81, Fig 1) including water level and vertical profiles of current velocities, suspended sediment concentrations (SSC) and salinity over the water column. This contribution aims to further analyse the model ability to simulate seasonal variation in: (1) the hydro sedimentary dynamics in the Garonne tidal river, which exhibits large differences between summer and winter and (2) the bed morphodynamic, focusing on key parameters shaping morphodynamics including erosion, consolidation effects, mud sliding, settling velocities. The advection-diffusion equation is used to model the transport of cohesive material, with the bed structure discretized with 10 layers. Consolidation of deposited mud is addressed using a multilayer approach with mass transfer coefficients calibrated using experimental data from Van (2012). A sensitivity test with different settling velocity formulas is conducted, prioritizing using the Soulsby et al.(2013), van Leussen (1994), Le Hir et al. (2000) and Defontaine et al. (2023) formulas. Different 300-day simulations are performed from winter to fall to assess the ability of the model to track the migration of the turbidity maximum zone (Jalón-Rojas, et al., 2015) and the associated mud deposit. Then, the impact of dredging and dumping operations carried out in the navigation channel is also taken into account through a coupling with the NESTOR module of the openTELEMAC system. The morphodynamic model is compared with bimensual bathymetric surveys performed by the port authorities along the navigation channel.

The results (Fig 1) indicated significant variability in the evolution of the mud thickness, influenced by the settling velocity, the initial fluid mud setup, and the wave effects. Simulations using the Soulsby et al.(2013) formula showed limited mud evolution in the central part, while those using the van Leussen (1994) and Le Hir et al. (2000) formula exhibited more variability, suggesting a higher mud layer in the lower and central estuary. Analysis of the influence of initial mud setup and wave effects using the van Leussen formula revealed enhanced mud development in the central estuary, likely due to increased currents. This work is important to optimize port operations and better understand their impact on the surrounding environment, particularly regarding new technologies on water injection dredging. The model will also help to improve the knowledge of the current and future behavior of the Gironde estuary. It will also be part of an open-source digital twin aiming at testing scenarios and improving operations of the Port of Bordeaux.

[1] Cerema REM-RHITME Research Team, Margny Les Compiegne, France: thi-kim-anh.do@cerema.fr; nicolas.huybrechts@cerema.fr.
[2] UNIROUEN, UNICANE, CNRS, UMR 6143, Continental and Coastal Morphodynamics, M2C, Normandy University, France
[3] UMR 5805 EPOC, CNRS, OASU, University of Bordeaux, 33615 Pessac, France; isabel.jalon-rojas@u-bordeaux.fr; aldo.sottolichio@u-bordeaux.fr
[4] Electricité de France Research & Development (EDF R&D), National Hydraulics and Environment Laboratory (LNHE), Chatou, France, pablo.tassi@edf.fr.
[5] Grand Port Maritime de Bordeaux, Bordeaux, France, F-Klein@bordeaux-port.fr

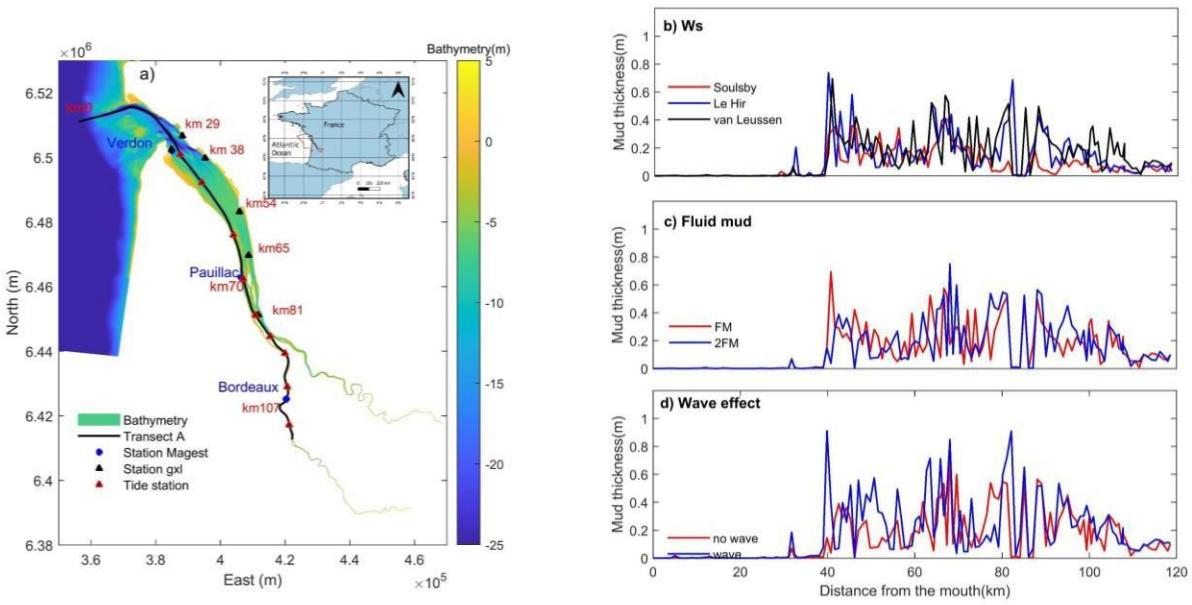

Figure 1. (Left) Location of Gironde estuary including location of in situ data for validation (surface situ measurement (the blue circle), near bottom measurement (the black triangle) and tide station (the red triangle); (Right) The influence of model parameters on mud development was extracted along channel navigation (Transect A in left panel).

References

Defontaine, S., Jalon-Rojas, I., Sottolichio, A., Gratiot, N., & Legout, C. (2023). Settling dynamics of cohesive sediments in a highly turbid tidal river. Marine Geology, 457, 106995.

Jalón-Rojas, I., Schmidt, S., & Sottolichio, A. (2015). Turbidity in the fluvial Gironde Estuary (southwest France) based on 10- year continuous monitoring: sensitivity to hydrological conditions. Hydrology and Earth System Sciences, 19(6), 2805-2819.

Hervouet, J. M. (2000). TELEMAC modelling system: an overview. Hydrological processes, 14(13), 2209-2210.

Le Hir, P., Bassoullet, P., & Jestin, H. (2000). Application of the continuous modeling concept to simulate high-concentration suspended sediment in a macrotidal estuary. In Proceedings in Marine Science (Vol. 3, pp. 229-247). Elsevier.

Leussen, V. (1994). Estuarine macroflocs and their role in fine-grained sediment transport. Ph. D. Thesis, University of Utrecht.

Soulsby, R. L., Manning, A. J., Spearman, J., & Whitehouse, R. J. S. (2013). Settling velocity and mass settling flux of flocculated estuarine sediments. Marine Geology, 339, 1-12.

Tassi, P., Benson, T., Delinares, M., Fontaine, J., Huybrechts, N., Kopmann, R., ... & Walther, R. (2023). GAIA-a unified framework for sediment transport and bed evolution in rivers, coastal seas and transitional waters in the TELEMAC-MASCARET modelling system. Environmental Modelling & Software, 159, 105544.

Van, L. A. (2012). Numerical modelling of sand-mud mixtures settling and transport processes: application to morphodynamic of the Gironde estuary (France) (Doctoral dissertation, Université Paris-Est).

Lagrangian transport time scales in a coastal system of intertidal basins

Duran-Matute M. [1], Fajardo-Urbina J.M. [1], Giesbergen M. [1], Clercx H.J.H. [1], Gräwe U. [2], and Gerkema T. [3]

Keywords: Lagrangian transport time scales, residence time, depth-averaged and 3D models, coastal systems.

Abstract

Introduction

Transport time scales (TTS) in estuaries quantify the flushing of the system and are relevant quantities that help to monitor their local and system-wide functioning. In coastal ecosystems that display complex geometry and bathymetry, like in systems of intertidal basins, TTS can exhibit strong anisotropic response to different forcing mechanisms like winds (Duran-Matute et al., 2014; Fajardo-Urbina et al., 2023). To capture well this spatiotemporal variability, Lagrangian transport time scales (LTTS), such as the residence and exposure times, are commonly employed (Monsen et al., 2002). They are also used as a proxy to understand ecological processes like eutrophication (Schwichtenberg et al., 2017) and as a first order estimation of the capacity of a system to expel pollutants (Pawlowicz et al., 2019). In recent years, numerous studies on LTTS have been performed using three-dimensional (3D) hydrodynamic models. These studies showed notable variations in the vertical structure of the LTTS, which were related to the presence of estuarine circulation (Du and Sheng 2016, Hewageegana et al. 2023). Thus, employing 3D numerical models that account for these circulation patterns is imperative for accurately determining LTTS in estuaries. However, for coastal systems in which the forcing can exhibit daily, seasonal and interannual scales, long-term simulations spanning several decades are necessary to understand the potential response of the LTTS to such temporal variations. The enormous amount of data required to perform LTTS based on 3D currents for regions that require simulations with high spatiotemporal resolution, motivate studies to use depth-averaged currents for understanding long-term variations (Fajardo-Urbina et al., 2023). Here, we elucidate and quantify the differences on the LTTS when using particles advected by 3D or depth-averaged currents. The analysis is made in the Dutch Wadden Sea (DWS): an estuarine system of intertidal basins of high ecological relevance, but the results can be extended to other systems with similar dynamics. Due to computational constraints when using high-resolution 3D currents, we focus on years with different forcing conditions, which were selected from a Lagrangian simulation spanning 36 years (1980-2015) based on depth-averaged currents (Fajardo-Urbina et al., 2023). To understand better the effects of depth-averaged currents and currents with vertical dependence on the LTTS, we also performed simulations with the idealized single-inlet width-averaged estuarine model of Dijkstra and Schuttelaars (2021).

Results

Maps of the residence time per season between 1994 to 1996 computed from depth-averaged (Figure 1, left column) and 3D (Figure 1, right column) currents are shown in Figure 1. To map the residence time from 3D currents in a 2D plane, the 3D structure of the residence time is averaged in the vertical. In autumn 1994 and winter 1995, characterized by prevailing strong southwesterly winds, depth-averaged currents generally yield slightly higher residence times in most of the domain, but the main spatial patterns are similar for both cases. This suggest that vertical effects are less pronounced during such events due to wind-induced mixing and predominant horizontal advection. During spring, summer and autumn of 1995 and winter of 1996, when both the number and magnitude of wind events were lower compared to the previous two seasons, the results display larger residence times for depth-averaged than 3D currents, particularly pronounced in the western DWS. During these conditions, less vertical mixing due to the weak or lack of winds, a more stratified water column together with a more pronounced estuarine circulation, and larger probability of inhomogeneous velocity profiles, lead to LTTS driven by depth-averaged currents that do not represent well these 3D effects. From a system-wide perspective similar results are obtained (Figure 2). During periods with strong southwesterly winds, mainly related to autumn-winter, similar values for the system-wide residence time are found for both cases. During periods with weak winds, mainly occurring during spring-summer, the residence time computed from depth- averaged currents overestimates the values from 3D currents up to 5-10 days, which is mainly evident in the western DWS (Figure 2). This was also the case for anomalous stormy seasons, like in autumn-winter of 1996, a famous period in the North Sea region due to low temperature records and lack of strong southwesterly wind. We found that during weak-wind periods, the difference in the residence is positively correlated to the freshwater discharge. However, despite these observed differences, the temporal variability of the system-wide residence time in the DWS seems to be well captured when using depth-averaged currents, i.e., larger residence time during weak wind conditions and smaller values during strong winds are observed when using either 3D or depth-averaged currents, which is consistent with the long- term depth-averaged simulation of Fajardo-Urbina et al. (2023).

[1]Eindhoven University of Technology, Netherlands, m.duran.matute@tue.nl, j.fajardo.urbina@tue.nl, m.t.a.giesbergen@student.tue.nl, h.j.h.clercx@tue.nl.
[2] Leibniz Institute for Baltic Sea Research, Rostock, Germany, ulf.graewe@io-warnemuende.de.
[3] NIOZ Royal Netherlands Institute for Sea Research, Yerseke, Netherlands, theo.gerkema@nioz.nl.

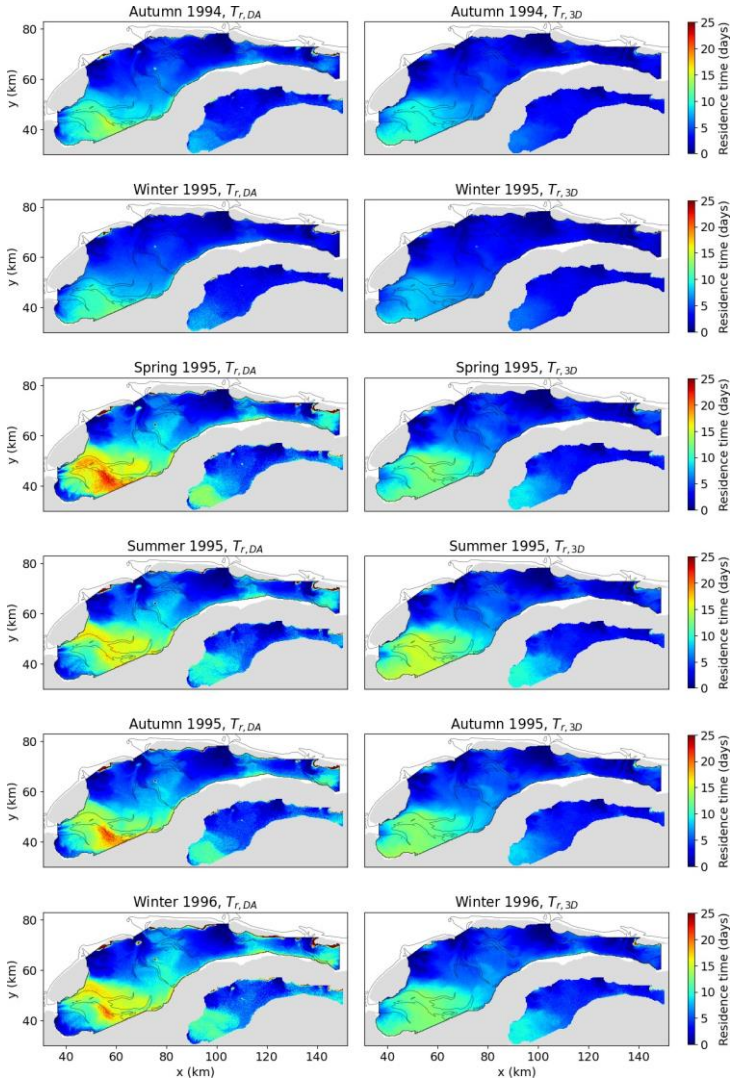

Figure 1. Spatial distribution of the residence time and standard deviation (inset) per season for depth-averaged currents ($T_{r,DA}$, left column) and 3D currents ($T_{r,3D}$, right column).

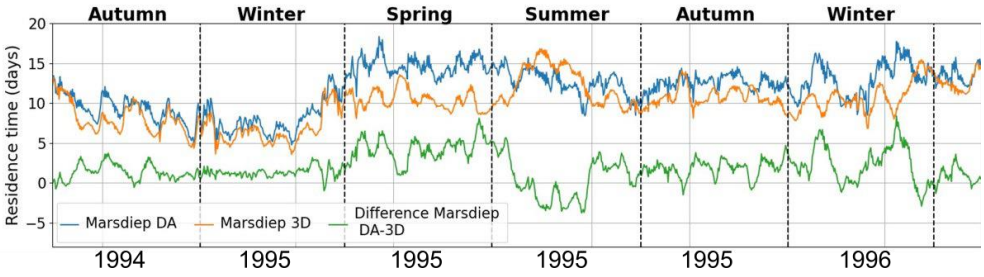

Figure 2. Time series of the spatial average residence time for the Marsdiep basin (western DWS), for depth-averaged DA, 3D currents, and their difference.

References

Dijkstra, Y. M., & Schuttelaars, H. M. (2021). A unifying approach to subtidal salt intrusion modeling in tidal estuaries. Journal of Physical Oceanography, 51(1), 147-167, https://doi.org/10.1175/JPO-D-20-0006.1.

Du, J., & Shen, J (2016). Water residence time in chesapeake bay for 1980–2012. Journal of Marine Systems, 164, 2016, https://doi.org/10.1016/j.jmarsys.2016.08.011.

Duran-Matute, M., Gerkema, T., De Boer, G., Nauw, J., Gräwe, U. (2014). Residual circulation and freshwater transport in the Dutch Wadden Sea: a numerical modelling study. Ocean Science 10, 611–632, https://doi.org/10.5194/os-10-611-2014.

Fajardo-Urbina, J. M., Arts, G., Gräwe, U., Clercx, H. J., Gerkema, T., Duran-Matute, M. (2023). Atmospherically Driven Seasonal and Interannual Variability in the Lagrangian Transport Time Scales of a Multiple-Inlet Coastal System. Journal of Geophysical Research: Oceans, 128(6), e2022JC019522, https://doi.org/10.1029/2022JC019522.

Hewageegana, V. H., Olabarrieta, M., & Gonzalez-Ondina, J. M. (2023). Main Physical Processes Affecting the Residence Times of a Micro-Tidal Estuary. Journal of Marine Science and Engineering, 11(7), 1333., https://doi.org/10.3390/jmse11071333.

Monsen, N. E., Cloern, J. E., Lucas, L. V., & Monismith, S. G. (2002). A comment on the use of flushing time, residence time, and age as transport time scales. Limnology & Oceanography, 47(5), 1545–1553. https://doi.org/10.4319/lo.2002.47.5.1545.

Pawlowicz, R., Hannah, C., & Rosenberger, A. (2019). Lagrangian observations of estuarine residence times, dispersion, and trapping in the Salish Sea. Estuarine. Coastal and Shelf Science, 225, 106246. https://doi.org/10.1016/j.ecss.2019.106246

Schwichtenberg, F., Callies, U., & van Beusekom, J. E. (2017). Residence times in shallow waters help explain regional differences in Wadden Sea eutrophication. Geo-Marine Letters, 37(2), 171–177. https://doi.org/10.1007/s00367-016-0482-2

Storm Surge Amplification by Basin Shape, the Case of Extratropical Typhoon Merbok in Western Alaska

Dykstra S.L. [1], Talke S.A. [2], Jay D.A. [3], Lobo M. [4], Innocenti S. [5], and Matte P. [5]

Keywords: storm surge, flooding, convergence, partial reflection, non-stationary tides, parameter space.

Abstract

Observed wind gusts exceeded 33 m s-1 in the Bering Sea on September 16, 2022 as Extratropical Typhoon Merbok produced a 1 to 2-day surge that flooded >4,000 km of the Western Alaska coastline. A still water level of 4.7 m NAVD88 was measured in Unalakleet, AK, 4.5 times the predicted tidal range of 0.84 m. In this presentation, we investigate the role that coastal morphology and bathymetry has in amplifying tides and the storm surge. To investigate the effects of basin shapes on storm surge, water levels at 24 stations were detided with a new tide wavelet tool, CWT_multi (Lobo et al., 2024), and compared to longwave theory using a nondimensional friction-convergence parameter space. Results show the surge height increased into Norton Sound (resonant at the diurnal frequency) and decreased into Bristol Bay, which is resonant at a shorter semidiurnal frequency. Landward funneling occurs at the Kuskokwim River; in a landward direction, over ~180km to Bethel, the ~2-day surge amplified by 1.3 while O1, K1, and M2 attenuated by 0.43, 0.34, and 0.23, respectively. These results indicate that the bays and estuaries of western Alaska have frequency dependent relationships that control both tidal long-waves and storm surge and suggests that non-linear frictional interaction is occurring between tides and surge waves. In the non-dimensional parameter space, the storm surge and tidal waves represent different regimes where partial reflections from convergence are relatively strong or weak, respectively, compared to friction. The positive interference from the reflected waves and transmitted waves are greater for the longer period storm surges than the tides. Findings suggest that, due to local geometry effects, flood exposure for common ~1-day storm surges are greater for communities with predominantly diurnal tides than communities with semidiurnal tides.

References

Lobo, M, Jay, D. A., Innocenti, S., Talke, S. A., Dykstra, S., Matte P. (2023). Implementing Super-Resolution of Non-Stationary Tides with Wavelets: An Introduction to CWT_Multi, submitted to *Journal of Atmospheric and Oceanic Technology*. (code available from https://github.com/mjclobo/CWT_Multi)

[1] College of Fisheries and Ocean Science, University of Alaska Fairbanks, Fairbanks, Alaska
[2] Department of Civil & Environmental Engineering, Cal State Polytechnic University at San Luis Obispo
[3] Department of Civil & Environmental Engineering, Portland State University, Portland, OR USA
[4] Princeton University, Atmospheric and Oceanic Sciences Program, Princeton, New Jersey
[5] Environment and Climate Change Canada, Meteorological Research Division, Québec City, Québec, Canada

Characterizing impacts of river discharge on the Alabama shelf during unprecedented 2019 openings of the Bonnet Carré Spillway in the northern Gulf of Mexico

Dzwonkowski B. [1,2], Puzhankara A. [1,2], Lehrter J. [1,2], Liu Z. [1,2], Lockridge G. [2,3], and Rao D.R.M. [1,2]

Keywords: region of freshwater influence, circulation, stratification, dissolved oxygen, Gulf of Mexico.

Abstract

Large-scale management responses to short-term weather phenomena are rare events whose impacts can be difficult to quantify. The coupling of weather events and management responses can have compounding effects that are not well understood and can be a cause for significant concern when assessing issues associated with disaster risk and coastal resiliency (Zscheischler et al. 2020). In spring and summer of 2019, the Mississippi River (4th largest river in the world) experienced intense flood conditions which required the diversion of freshwater through the Bonnet Carré Spillway to reduce inland flooding risks. This led to unprecedented, repeated openings of the Bonnet Carré Spillway altering the typical flow of river water into the northern Gulf of Mexico, potentially impacting natural modes of variability in Mississippi Bight, a shallow, stratified coastal sea. In addition to the magnitude of the two diversions, the timing coincided with the typical spring flooding in the local river systems and the seasonal shift in wind forcing driving circulation from the west (fall/winter) to east (spring/summer). These local changes in river discharge and wind may amplify the impacts of the spillway opening over the shelf (Fig 1).

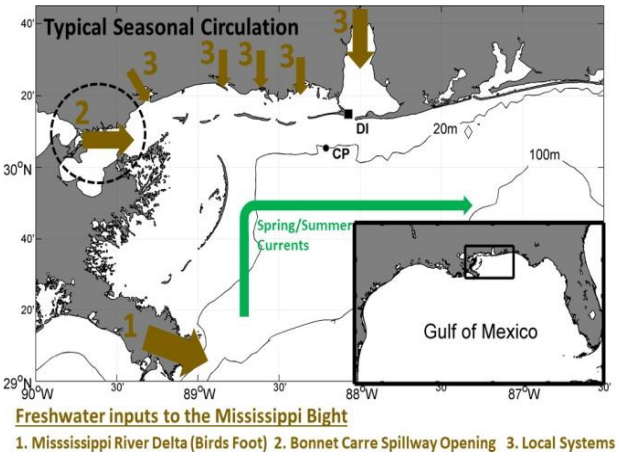

Fig. 1 Conceptual diagram of system forcings and circulation in the Mississippi Bight during the summer season including river discharge (brown arrows) and upwelling-favorable winds (gray arrow). The summer circulation (green arrow) favors the advective of river discharge from western sources, like the MS River, into the region.

Inset shows the study region in the context of the broader Gulf of Mexico (Lower right box). Location of the long-term mooring site (CP, black circle) and Dauphin Island Sea Lab (DI, black square).

Amplifying buoyancy inputs during the natural flooding period of the hydrological cycle has the potential to drive shifts in the hydrographic conditions over the shelf, and in turn modify large- scale circulation, heat budget dynamics, and water quality. This in turns can alter the expected risk assessments for a range of coastal hazards (e.g., exposure to red tides, hypoxia, hurricane intensification). The repeated openings of the Bonnet Carré Spillway in the northern Gulf of Mexico, represents an opportunity to determine whether the compounding impacts of a freshwater diversion in conjunction with the natural flooding cycle can change the fundamental characteristics of a coastal system. More specifically, the overarching objective is to determine whether a large-scale river diversion during a specific time period in the natural hydrological cycle will result in extreme hydrographic conditions which in turn will affect water quality. To address this objective, a combination of in situ data from a long-term mooring site and from shelf hydrographic surveys were used to characterize variability in the physical and dissolved oxygen conditions so that the Bonnet Carre Spillway opening can be placed in context with typical shelf conditions. In addition, the dissolved oxygen dynamics and their relationship to physical processes were investigated during the summer of 2019. The investigation of a 5-year (2019-2023) time series of hourly bottom dissolved oxygen (DO) concentration revealed significant interannual variability, including extensive hypoxia in 2019 as well as hypoxic ornear-hypoxic conditions in subsequent years (Fig. 2). To begin understanding patterns in these data, ensemble statistics over a calendar year were produced. The ensemble mean and standard deviation showed clear seasonal patterns. During the late fall through winter, there were high mean values, typically at or near saturation, and low variance. In contrast, spring through early fall showed lower mean values and higher variance. Further exploration of the monthly frequency of hypoxia or near-hypoxia conditions showed a larger difference between the summer of 2019 and other years. Hypoxia and near-hypoxia conditions were common throughout the summer of 2019, while years 2020-2023 had a reduced frequency and showed a peak in September.

[1] Stokes School of Marine and Environmental Sciences, University of South Alabama (briandz@disl.org)
[2] Dauphin Island Sea Lab, Dauphin Island, AL, United States 36528
[3] U.S. Naval Research Laboratory, Stennis Space Center, Mississippi,39529

Focusing on the 2019, extensive areas of hypoxia on the shelf were observed throughout the summer study period with high variability in both space and time. Patterns in the along and across-shelf bottom dissolved oxygen spatial structure were apparent in the data. In the along-shelf direction, dissolved oxygen tended to decrease from east to west. The across-shelf pattern was more complex with mid-shelf minimum between~12-25 m. Furthermore, timeseries of bottom DO from June through September were correlated with changes in bottom temperature (Fig. 3), revealing a significant connection to upwelling/downwelling events and the presence or absence of hypoxia on the inner to mid-shelf.

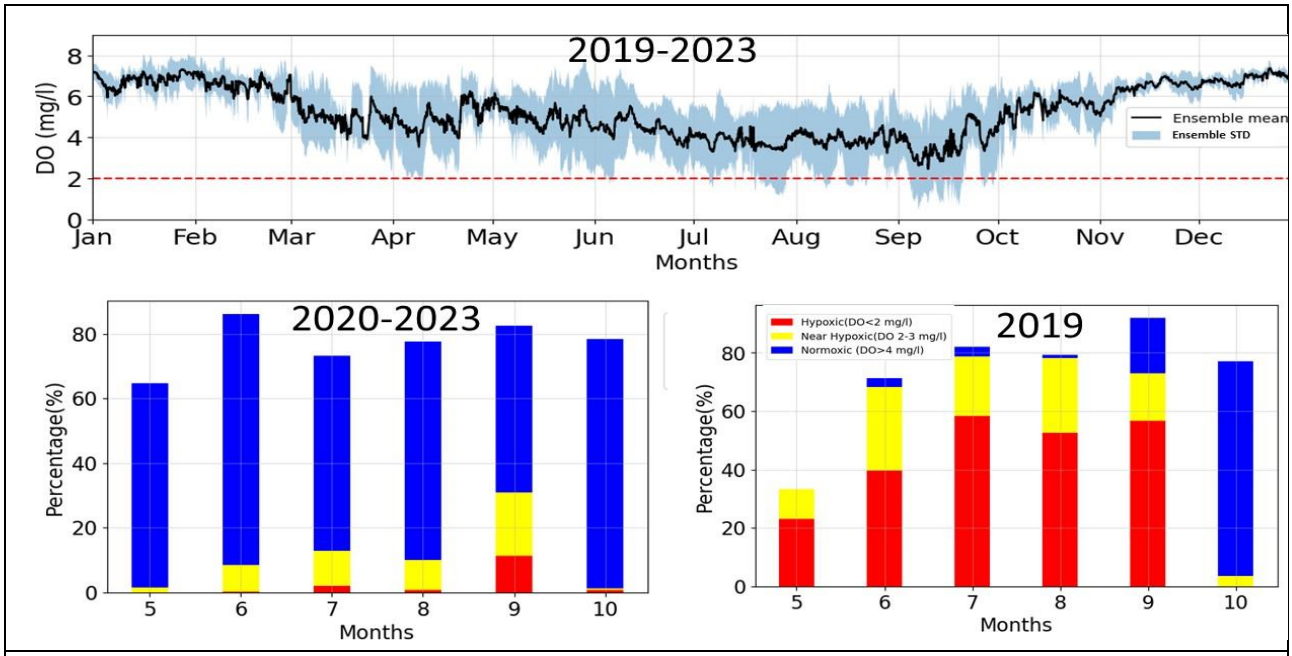

Fig. 2 Ensemble statistics of bottom dissolved oxygen from the CP/FOCAL mooring from May 2019 to October 2023(Top). Percent occurrence of hypoxic(red), near-hypoxic(yellow), and norm-oxic (blue) conditions at the CP/FOCAL mooring during summer for 2020-2023 (Bottom Left) and 2019 (Bottom Right)

Identifying the direct impacts of the Bonnet Carré Spillway requires more robust exploration of the physical data as well as experiments with a regional numerical model. At this point, 2019 clearly stands out as a summer with excessive hypoxia in this region of the shelf. Interestingly, September emerged as a critical month for hypoxic conditions with the highest percentage, highlighting the importance of considering periods beyond summer for water quality management. Further investigation will focus on the impact of a storm event during July of 2019 as well as combining the survey data with the time series data to conduct an oxygen budget at the mooring site. The results of this study are expected to facilitate the development of more effective mitigation and adaptation strategies in response to impacts of current and predicted changes from river inflow into coastal oceans.

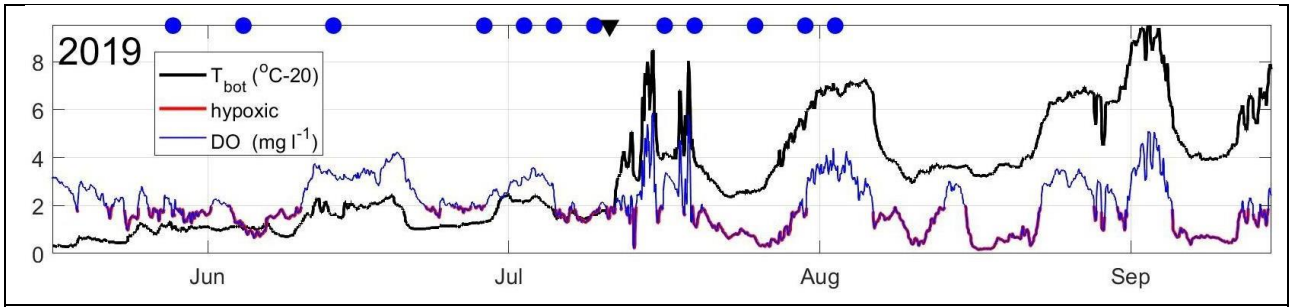

Fig. 3 Time series of bottom dissolved oxygen and temperature from the FOCAL/CP mooring during the summer of 2019. Note that 20 °C has been removed from the water temperature so that the variability in both time series can be more easily compared. Circles (Triangle) at the top of the plot indicate dates of CTD surveys (passage of T.S. Barry). Red highlighting on the dissolvedoxygen time series indicate periods of hypoxia.

References

Zscheischler, J., Westra, S., Van Den Hurk, B.J., Seneviratne, S.I., Ward, P.J., Pitman, A., AghaKouchak, A., Bresch, D.N., Leonard, M., Wahl, T. and Zhang, X., 2018. Future climate risk from compound events. *Nature Climate Change*, *8*(6), pp.469-477.

High-Resolution Simulations of the Freshwater Plume Dynamics in Simplified Domains

Escauriaza C. [1,2], Contreras M. [1], Williams M.E. [1,2], and Fringer O. [2]

Keywords: river plume, numerical simulations, turbulence, three-dimensional models.

Abstract

Small glacial river plumes are important features in the dynamics of the Patagonian fjords. They can generate high-frequency internal waves, produce a horizontal advection of freshwater near the coast, and vertical entrainment and mixing near the water surface. However, the multiple physical processes governing the interactions of turbulence in the water column at different scales are not well understood, including the importance of fundamental forcings that influence the plume dynamics, such as the interactions with the coastal morphology, discharge variations by glacial melting, tidal amplitudes, Earth's rotation, and wind.

To study the basic dynamics of these plumes, in this investigation we perform numerical simulations at different scales. First, we carry out large-eddy simulations (LES) (Barros and Escauriaza, 2024), to resolve the dynamics of freshwater plumes based on the experimental work of Yuan and Horner-Devine (2013, 2017). We analyze the non-dimensional parameters that characterize the structure of the plume and study the development and evolution of turbulent coherent structures, quantifying the vertical density fluxes and effects on mixing. From the LES results we provide additional insights on the potential mechanisms of internal wave formation and transport processes.

To observe these processes at larger scales, we also incorporate basic field data to reproduce the propagation of internal waves in an idealized geometry, considering dimensions based on a field site, to represent the basic river-fjord interactions and internal wave motions. We perform simulations in SUNTANS (Fringer et al., 2006), solving the 3D nonhydrostatic Reynolds-averaged Navier-Stokes equations, using the Boussinesq approximation. The interaction mechanisms of the plume with the fjord are captured along with the wave reflection on the steep bathymetry and trapping for multiple tidal cycles (Figure 1).

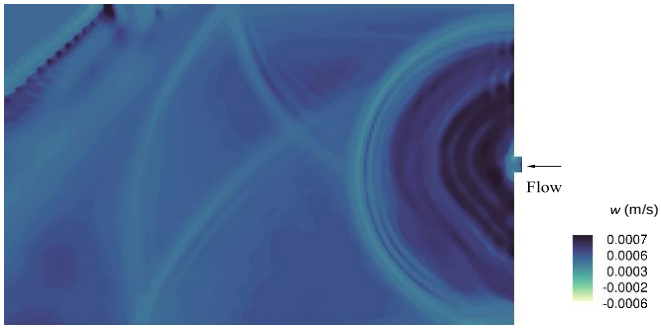

Figure 1. Instantaneous image of vertical velocity contours near the surface showing the generation of internal waves, reflection and trapping in an idealized fjord geometry after multiple tidal cycles using SUNTANS.

This work has been supported by the project "Stratified Coastal Dynamics of Internal Waves and Glacial River Plume Interactions", funded by U.S. Office of Naval Research Global Grant N62909-23-1-2004.

References

Barros, M., & Escauriaza, C. (2024). Lagrangian and Eulerian perspectives of turbulent transport mechanisms in a lateral cavity.
Journal of Fluid Mechanics.

Fringer, O. B., Gerritsen, M., & Street, R. L. (2006). An unstructured-grid, finite-volume, nonhydrostatic, parallel coastal ocean simulator. Ocean modelling, 14(3-4), 139-173.

Yuan, Y., & Horner-Devine, A. R. (2013). Laboratory investigation of the impact of lateral spreading on buoyancy flux in a river plume. Journal of Physical Oceanography, 43(12), 2588-2610.

Yuan, Y., & Horner-Devine, A. R. (2017). Experimental investigation of large-scale vortices in a freely spreading gravity current. Physics of Fluids, 29(10).

[1] Hydraulic and Environmental Engineering. Pontificia Universidad Católica de Chile. Email: cescauri@uc.cl
[2] Civil & Environmental Engineering. Stanford University.

Particle patch dynamics and its use for fast transport prediction in coastal systems

Fajardo-Urbina J.M. [1], Duran-Matute M. [1], Clercx H.J.H. [1], Gräwe U. [2], Gerkema T. [3], Georgievska S. [4], Liu Y. [4], and Grootes M.W. [4]

Keywords: advection, dispersion, chaotic stirring, particle patches, surrogate modeling, deep learning, coastal systems.

Abstract

Introduction

In tidal coastal areas, rapid water exchange and hence dispersal of material occurs due to a mechanism known as chaotic stirring or advection. This is a consequence of Lagrangian chaos in deterministic time-dependent 2D or 3D flows (Aref et al., 2017), like the flows in coastal regions where currents are induced by the interaction of the coastal geometry and the bottom topography with the tides (Ridderinkhof and Zimmerman, 1992; Orre et al, 2006). In coastal environments, the wind-driven circulation can also promote transport of material over large distances (Cucco and Umgiesse, 2006), and induce transport time scales with variability at daily, seasonal, and interannual scales (Duran-Matute et al., 2014; Fajardo-Urbina et al., 2023). In the present work, we study the transport of particle patches in a multiple-inlet estuarine system: the Dutch Wadden Sea. Here, we define a particle patch as a cloud of passive particles, which can either follow only the currents or the currents with diffusion added to the trajectories, with the latter case to approximate better an advection-diffusion tracer equation. Initially, we aim to establish a connection between the forcing and the variability of the displacement and dispersal of the particle patches. Our second aim is to develop a deep learning surrogate method to predict the transport of these patches, which can potentially be extended to track, for example, micro-plastics, oil, or larvae. This last aim is motivated by the need of fast, cost-effective and accurate forecasting solutions.

Method

We performed a realistic 3D hydrodynamic simulation between 1980-2015 using the General Estuarine Transport Model (see Fajardo-Urbina et al. 2023 for details). From this simulation, we use depth-averaged and 3D currents to feed a Lagrangian model to track particle patches released at every grid cell of our domain. The transport of these patches is then simplified by computing their advective and dispersive components at the end of a tidal period ~12.42 h (as originally proposed by Ridderinkhof and Zimmerman, 1990). Advection represents the displacement of the center of mass and dispersion the spread of the patch given by the covariance matrix of the particle positions. Both quantities are determined for each tidal cycle spanning the duration of the simulations. For our second aim, we perform three different experiments (prediction, reconstruction, and benchmark). As a proof-of-concept these experiments are only based on simulations using depth-averaged currents. The prediction experiment contains two steps. First, we train a deep learning model to predict advection and dispersion after one tidal period. Then, we propose a simplified Lagrangian model based on these statistics to predict the transport of particle patches for times larger than a tidal period. The reconstruction experiment skips the use of machine learning, and instead, it feeds the actual advection and dispersion to the simplified Lagrangian model. This experiment allows us to show that our simplified model works well, and to determine what can be achieved if a perfect prediction of advection and dispersion is obtained. Finally, the benchmark experiment uses a Lagrangian model driven by currents to track particle patches (the ground truth).

Results

Maps of advection and dispersion based on depth-averaged currents for two cases with distinct wind conditions (weak and strong winds from the southwesterly quadrant) are shown in Figure 1. Advection reveals mostly features at the scale of the basin (Figure 1a,c), whereas dispersion shows the predominance of localized structures covering mostly the regions around the inlets and with strong bathymetric gradients (Figure 1b,d). These regions of large dispersion with filamentary composition reveals the localized nature of chaotic stirring. A strong correlation is found between the wind and the system-wide (spatial average) norm of advection. This correlation is observed both on the temporal scale of events (i.e., storms), and on a seasonal scale due to the seasonality of the wind forcing, which is stronger during autumn and winter. On the other hand, the spring-neap tidal cycle governs the system-wide dispersion. However, an enhancement in dispersion is observed during a few storms (Figure 1d). The results based on 3D currents are similar to those obtained with the vertically averaged fields. The main difference is that the dispersion of particles is enhanced when using the 3D currents due to the more intrinsic chaotic nature of 3D flows (Aref, 2017).

[1] Eindhoven University of Technology, Netherlands, j.fajardo.urbina@tue.nl, m.duran.matute@tue.nl, h.j.h.clercx@tue.nl.
[2] Leibniz Institute for Baltic Sea Research, Rostock, Germany, ulf.graewe@io-warnemuende.de.
[3] NIOZ Royal Netherlands Institute for Sea Research, Yerseke, Netherlands, theo.gerkema@nioz.nl.
[4]Netherlands eScience Center, Amsterdam, Netherlands, s.georgievska@esciencecenter.nl, y.liu@esciencecenter.nl, m.grootes@esciencecenter.nl.

For our second aim, the prediction and reconstruction experiments show that the evolution of a particle patch, during a windy period, follows quite well the results from the benchmark (Figure 2). This patch is clearly advected towards the northeast due to strong southwesterly winds. Dispersion also takes place, but advection is quite dominant in the transport of the patch. Good predictability is also found for other periods, like during weak wind conditions when chaotic stirring is more dominant. Notably, our approach eliminates the need for currents during predictions, and our simplified Lagrangian model achieves speeds one to two orders of magnitude faster than state-of-the-art alternatives. Thus, our surrogate model can potentially be used as an auxiliary fast tool for predicting the transport of substances in coastal areas.

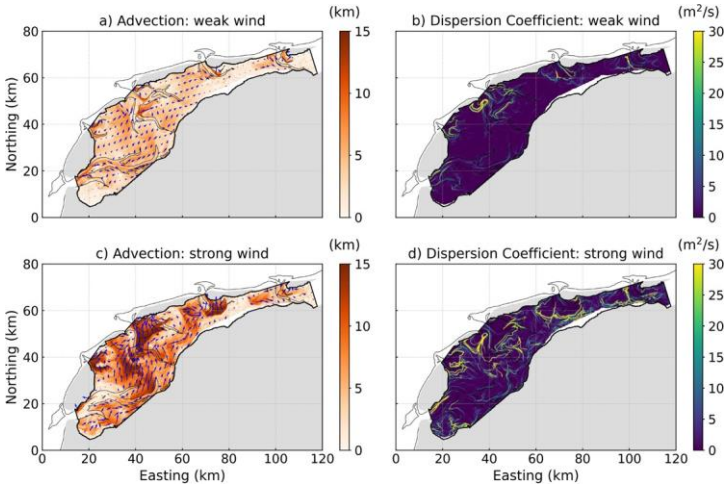

Figure 1. (a) Advection and (b) dispersion coefficient during weak winds, and the same quantities for (c) and (d) but during a strong wind event.

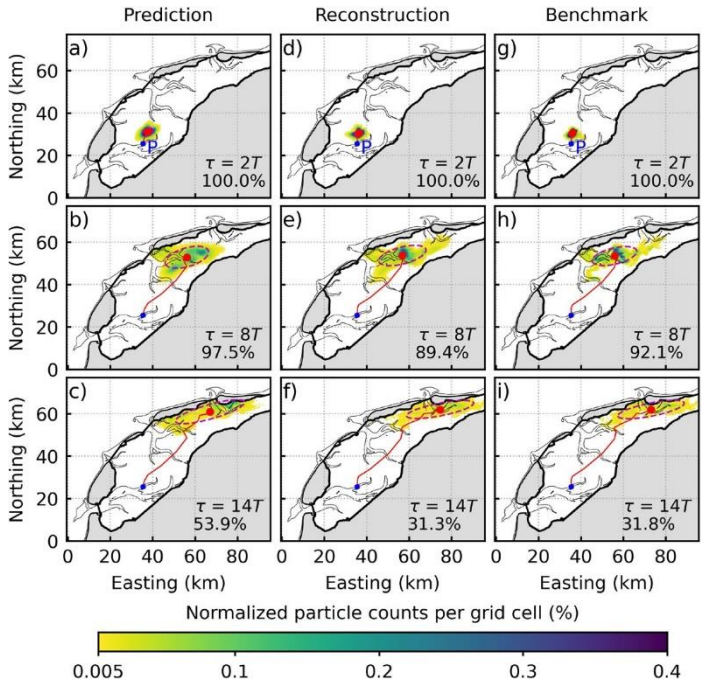

Figure 2. Normalized particle counts per grid cell for different elapsed times τ during strong winds for the prediction experiment (a)-(c), reconstruction experiment (d)-(f), and benchmark experiment (g)-(h). The initial position of the patch is indicated with the letter P; the trajectory of the center of mass is indicated with a red line; and the dispersion ellipse is drawn with a dashed line. The percentage (below the time τ) represents the current number of particles in the system.

References

Aref, H., Blake, J. R., Budišić, M., Cardoso, S. S., Cartwright, J. H., Clercx, H. J., ... & Tuval, I. (2017). Frontiers of chaotic advection. Reviews of Modern Physics, 89(2), 025007, https://doi.org/10.1103/RevModPhys.89.025007.

Cucco, A., Umgiesser, G., 2006. Modeling the venice lagoon residence time. Ecological modelling 193, 34–51, https://doi.org/10.1016/j.ecolmodel.2005.07.043.

Duran-Matute, M., Gerkema, T., De Boer, G., Nauw, J., Gräwe, U., 2014. Residual circulation and freshwater transport in the Dutch Wadden Sea: a numerical modelling study. Ocean Science 10, 611–632, https://doi.org/10.5194/os-10-611-2014.

Fajardo-Urbina, J. M., Arts, G., Gräwe, U., Clercx, H. J., Gerkema, T., Duran-Matute, M. (2023). Atmospherically Driven Seasonal and Interannual Variability in the Lagrangian Transport Time Scales of a Multiple-Inlet Coastal System. Journal of Geophysical Research: Oceans, 128(6), e2022JC019522, https://doi.org/10.1029/2022JC019522.

Orre, S., Gjevik, B., LaCasce, J. H. (2006). Characterizing chaotic dispersion in a coastal tidal model. Continental Shelf Research, 26(12-13), 1360-1374, https://doi.org/10.1016/j.csr.2005.11.015.

Ridderinkhof, H., Zimmerman, J. T. F. (1992). Chaotic stirring in a tidal system. Science, 258(5085), 1107-1111, DOI: 10.1126/science.258.5085.1107.

Influence of seawater intrusion on the residual circulation at the Guadiana Estuary

Garel E. [1], Khosravi M. [1], and Valle-Levinson A. [2]

Keywords: residual flow drivers, densimetric tidal Froude number, ADCP observations.

Abstract

The residual circulation in estuaries should result from the competition between barotropic (tidally driven) and baroclinic (density-driven) forcing. In most estuaries, however, the dominant forcing is baroclinic. At these settings, the residual flow is modulated by tidal forcing but generally maintains a persistent direction and lateral distribution.

However, recent observations at various (less described) systems suggest a switching of the residual flow driver at fortnightly time scales (Garel and Ferreira, 2013; Ross et al., 2017; Valle-Levinson and Schettini, 2016; Tenorio-Fernandez et al., 2019). The present study addresses the dynamics of such variability based on ADCP observations at the Guadiana Estuary (South Portugal).

The Guadiana is a long (80 km), narrow (700 m at maximum at the mouth) and relatively shallow (5 m mean depth) estuary with low freshwater inputs (about 10 m^3/s, year-round). The tide in the area is semi-diurnal, with a large variation in amplitude (from 0.4 m to 1.6 m) due to a relatively strong S2 component.

ADCP data were collected in summer 2023 along two cross-channel transects, one near the mouth and one 20 km upstream. At each transect, 3 ADCPs were moored at the seabed (at deep, intermediate and shallow water depths) from July 14 to September 21. These records were completed by tidal-cycle surveys of 24 h performed simultaneously at both transects (using 2 boats), at neap (July 27) and spring (August 03) tides. Residual along-channel velocities were obtained from low-pass filtering (moored data) and least square fits to tidal harmonics (tidal cycle data). The transverse structure of the residual flow at the two transects was then determined and compared to theoretical expectations.

Furthermore, the temporal variabililty of the subtidal circulation was characterized based on Empirical Orthogonal Functions (EOFs) applied to the concatenated moored data.

The transverse structure of along-channel residual flows varies between a vertically sheared 2-layer exchange flow at neap tide and laterally sheared vertically homogeneous outflows or inflows at spring tide (Figure 1).

Comparisons with predictions from analytical solutions suggest a switch between baroclinicity being the dominant forcing at neap to tidal forcing at spring. In support, the EOF analysis of the moored time series indicates distinct trends for the main residual flow variability when the tidal velocity amplitude is weaker or larger than a threshold (0.6 m/s in this case). To evaluate the forcing variability, both temporally (between neap and spring tides) and spatially (between both transects), the ratio of the barotropic and baroclinic forcings was computed as the densimetric tidal Froude number. The fortnightly variability of the horizontal salinity gradient between the two transects was derived from previous measurements collected under similar low river discharge conditions. In general, the Froude number depicts a fortnightly modulation between tidally and density-driven flows, which is concordant with observations of the lateral flow structures. Yet, barotropic processes are strongest near the mouth than upstream, resulting in transition periods when the residual circulation has a distinct driver at both transects. The temporal variability of the drivers relates to fluctuations of the horizontal density gradient between neap and spring tide, induced by differences in the seawater intrusion length along the channel. At spring tide, seawater salinity (about 35 PSU) is observed at more than 10 km upstream from the mouth. As a result, the horizontal density gradient is negligible at the lower estuary and the tidal forcing dominates. At neap tide, seawater hardly intrudes the estuary, resulting in a horizontal density gradient that dominates over tidal forcing.

Overall, this study challenges the typical view of residual flow drivers in estuaries, generally assumed to be baroclinic. It reports that, at some settings, the dominance of barotropic and baroclinic forcing may alternate between neap and spring tide, but also, and this is a new finding, along the system. At the Guadiana estuary, the switch in residual flow drivers is mainly produced by the large difference in seawater intrusion (hence horizontal density gradient) along the lower estuary at neap and spring tides. Ongoing work aims at exploring further the dynamics of drivers' variability at the Guadiana, and at generalizing the results to other estuaries.

[1] CIMA/ARNET, Universidade do Algarve, Faro, Portugal
[2] Civil and Coastal Engineering Department, University of Florida, Gainesville, USA.

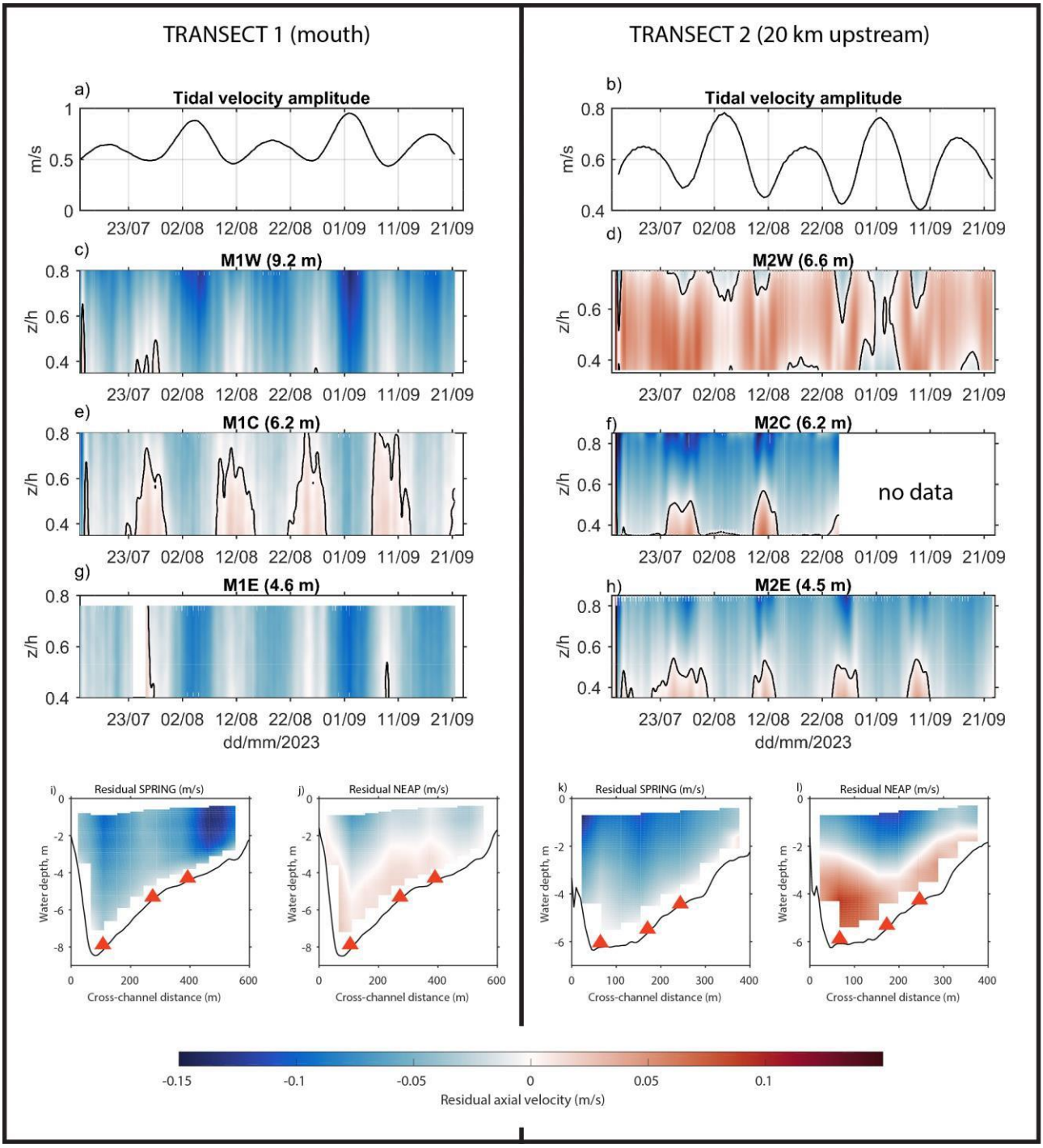

Figure 1. Residual along-channel flows (m/s, positive upstream) at Transect 1 (left panel) and Transect 2 (right panel). a,b: tidal velocity amplitude at the mouth; c-h: subtidal flows at deep (M1W, M2W), intermediate (M1C, M2C) and shallow (M1E, M2E) water depths; i, l: residual flows across the channel at spring (i, k) and neap (j, l) tides, with indication of the approximate location of the ADCP moorings (red triangles).

References

Ross, L., A. Valle-Levinson, A. Sottolichio, and N. Huybrechts (2017), Lateral variability of subtidal flow at the mid-reaches of a macrotidal estuary, J. Geophys. Res. Oceans, 122, 7651–7673, doi:10.1002/2016JC012504.

Valle-Levinson, A., Schettini, C.A.F. (2016). Fortnightly switching of residual flow drivers in a tropical semiarid estuary. Estuarine Coastal and Shelf Science. 169, 46-55.

Tenorio-Fernandez, L., Zavala-Hidalgo, J., Olvera-Prado, E.R. (2019). Seasonal variations of river and tidal flow interactions in a tropical estuarine system. Continental Shelf Research. 188, 103965.

Garel, E., Ferreira, Ó. (2013). Fortnightly Changes in Water Transport Direction Across the Mouth of a Narrow Estuary. Estuaries and coasts. 36(2), 286-299.

Estuarine Sand Dunes Decrease Salt Intrusion by Increased Vertical Advective Mixing

Geerts S.J. [1], van der Sande W.M. [2], Hulscher S.J.M.H. [3], Geurts B.J. [4], and Roos P.C. [5]

Keywords: salt intrusion, estuarine sand dunes, vertical transport, process-based modelling.

Abstract

Estuarine salt intrusion is a phenomenon that arises when saline water infiltrates the estuarine system, potentially leading to a shortage of freshwater. This can have significant implications for drinking water extraction, industry, agriculture and environmental stability. The amount of vertical mixing and freshwater river flushing are key predictors of the amount of salt intrusion, which both decrease salt intrusion when enhanced (Geyer & MacCready, 2014). Estuarine sand dunes are a type of bedform with heights in the order of meters and wavelengths of tens to hundreds of meters, and are found in several river mouth estuaries (e.g. Berne et al., 1993 and Zorndt et al., 2011). Due to an increase in large-scale turbulence (Bradley et al. 2013), tide-averaged circulation cells (Hulscher & Dohmen-Janssen, 2005) and resonant internal waves (Pietrzak et al., 1990), these bedforms potentially increase the net vertical transport and, as such, decrease salt intrusion. In this study, we aim to understand the influence of estuarine sand dunes on salt intrusion and investigate determine the influence of dune geometry on salt transport dynamics on an estuarine scale.

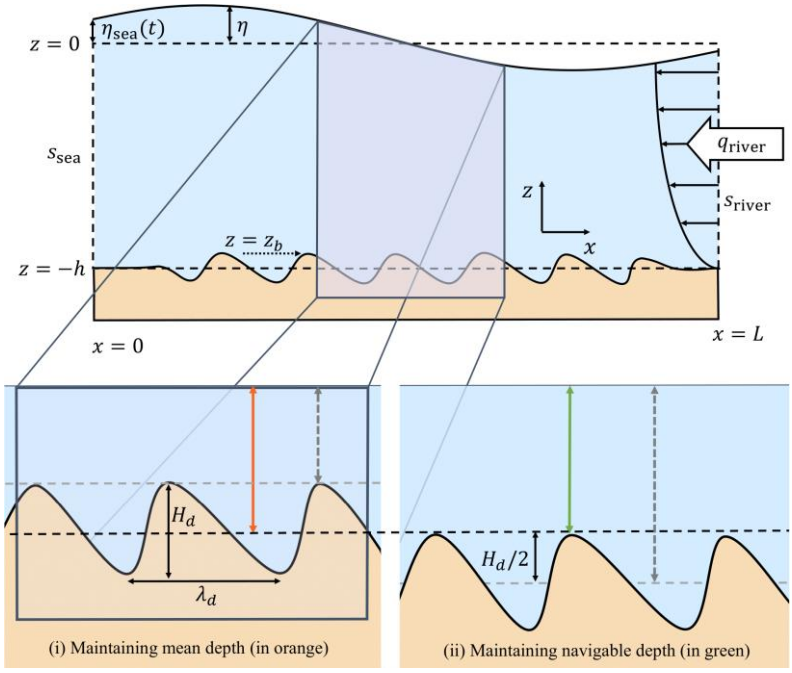

Figure 1: Top: Model setup and geometry, with inflowing width-averaged river discharge q_{river} =1.5 m^2/s of salinity $s_{river} = 0$ ppt at the riverine boundary $x = L$. Free surface elevation $\eta_{sea}(t)$ that consists of an M2 tide with amplitude 1 m at the seaward boundary $x = 0$. Inflowing water has salinity $s_{sea} = 35$ ppt. Bottom: Dune geometry with indicated dune height H_d and dune length λ_d. Two types of dune geometry configurations are shown relative to reference level $z = -h$. Type (i) maintains mean depth and decreases navigability with height $H_d/2$ for increasing dune height H_d. Type (ii) maintains navigability and increases mean water depth with $H_d/2$ for increasing dune height H_d. These changing depths are indicated by the grey arrow.

Estuarine sand dunes can be schematised as 2DV bedforms, and the main transport mechanisms occur in the same directions. Therefore, we develop an idealised morphostatic model with 2DV geometry that explicitly implements sand dunes (Figure 1). This model is implemented and solved in Delft3D-FLOW. The geometry allows us to study the effect of vertical flow behaviour without possible interaction with other estuarine-scale processes. Model settings are based on the Rotterdam Waterway, the Netherlands, during summertime conditions, when salt intrusion is most detrimental. A mean initial water depth is h = 15 m and estuary length L = 50 km (over which the tidal flow decays) are used. The model effectively captures most of the flow and transport dynamics representative of field measurements of the Rotterdam Waterway (de Nijs et al, 2011). Its characteristics are similar to other modelling studies (Dijkstra et al., 2022).

[1] Water Engineering and Management, University of Twente, the Netherlands, s.j.geerts@utwente.nl
[2] Water Engineering and Management, University of Twente, the Netherlands, w.m.vandersande@utwente.nl
[3] Water Engineering and Management, University of Twente, the Netherlands, s.j.m.h.hulscher@utwente.nl
[4] Mathematics of Multiscale Modelling and Simulation, University of Twente, the Netherlands, b.j.geurts@utwente.nl
[5] Water Engineering and Management, University of Twente, the Netherlands, p.c.roos@utwente.nl

We focus on two dune types relative to the reference level $z = -h$, both visualised in Figure 1. We vary the dune characteristics (such as dune height Hd, dune length λd and asymmetry) while (i) maintaining the mean water depth, and

(ii) maintaining the navigable depth. Consequently, we determine the salt intrusion length; the tide-averaged distance

from the seaward end where the maximum concentration over the water column equals 1 ppt. Furthermore, we quantify all horizontal and vertical transport processes such that the dominant processes can be determined.

The dominant horizontal transport mechanisms and stratification remain relatively similar across all model runs. The presence of estuarine sand dunes changes the salt intrusion length. (i) An increase in dune height and a decrease in dune length reduces the salt intrusion length significantly (Figure 2a), which is correlated to an increase in vertical advective transport (Figure 2c). In this model, the influence of dune asymmetry on salt intrusion is negligible (not shown) which likely originates from the hydrostatic assumption. (ii) Small dunes that increase the mean depth increase the salt intrusion, by a similar mechanism as channel deepening (Figure 2b). With increasing dune height Hd, salt intrusion is significantly decreased, which follows the trend of type (i). A decrease in salt intrusion length is accompanied by an increase in mean vertical advective transport, changes in dispersive transport are negligible.

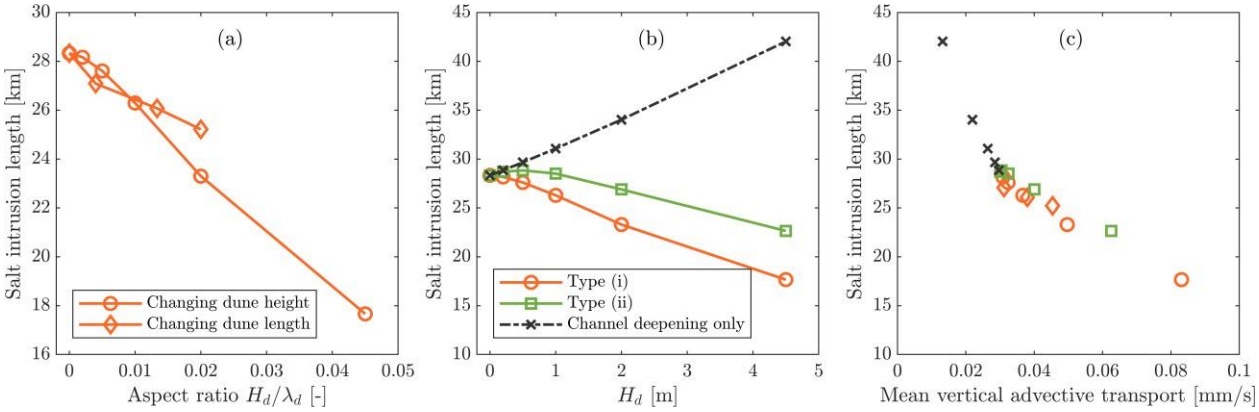

Figure 2: (a) Influence of dune aspect ratio on the salt intrusion length for dunes that maintain mean depth (type (i)). (b) Influence of changing dune height, comparing type (i) with type (ii). The influence of an equivalent channel deepening of depth change $H_d/2$ is also shown. (c) Relation of mean amount of vertical advective transport in the region of significant salinity and the salt intrusion length across all model runs with equal markers as in panels (a) and (b).

This research shows that estuarine sand dunes need to be taken into account when predicting the salt intrusion length with numerical models. Changes in dune geometry significantly impacts the salt intrusion length, with dune height being the most influential factor. Dredging practices – either by replacing sediment from the troughs into the crest, or by removing sediment – leads to reduced vertical transport and increased salt intrusion as local topography is removed. Furthermore, this research demonstrates the potential of new efficient dredging strategies, that retain these bedforms and maintain navigability. Steep and high sand dunes can counteract the adverse effects of channel deepening. Overall, as a naturally-existing bedform, estuarine sand dunes can likely be used as a nature-based solution to mitigate salt intrusion.

References

Berne, S., Castaing, P., Le Drezen, E., & Lericolais, G. (1993). Morphology, internal structure, and reversal of asymmetry of large subtidal dunes in the entrance to Gironde Estuary (France). Journal of Sedimentary Research, 63 (5), 780-793.

Bradley, R. W., Venditti, J. G., Kostaschuk, R. A., Church, M., Hendershot, M., & Allison, M. A. (2013). Flow and sediment suspension events over low-angle dunes: Fraser estuary, Canada. Journal of geophysical research: Earth surface, 118 (3), 1693–1709.

de Nijs, M.A.J., Winterwerp, J.C., & Pietrzak, J.D. (2010). The effects of the internal flow structure on SPM entrapment in the Rotterdam waterway. Journal of Physical Oceanography, 40 (11), 2357–2380.

Dijkstra, Y.M., Schuttelaars, H.M., & Kranenburg, W.M. (2022). Salt transport regimes caused by tidal and subtidal processes in narrow estuaries. Journal of Geophysical Research: Oceans, 127.

Geyer, W.R., & MacCready, P. (2014). The estuarine circulation. Annual review of fluid mechanics, 46,175–197.

Hulscher, S. J. M. H., & Dohmen-Janssen, C. M. (2005). Introduction to special section on marine sand wave and river dune dynamics. Journal of Geophysical Research: Earth Surface, 110 (F4).

Pietrzak, J. D., Kranenburg, C., & Abraham, G. (1990). Resonant internal waves in fluid flow. Nature, 344 (6269), 844–847. Zorndt, A.C., Wurpts, A., & Schlurmann, T. (2011). The influence of hydrodynamic boundary conditions on characteristics, migration, and associated sand transport of sand dunes in a tidal environment: A long-term study of the Elbe estuary. Ocean Dynamics, 61, 1629–1644.

Exploring the Coastal Protection Potential and Resilience of Mangrove Forests in Grand-Pierre Bay, Haiti using Remote Sensing and Hydrodynamic Modeling

Georges A.E.S [1], Stacey M.T. [2], and Ramsewak D. [3]

Keywords: Estuarine and Coastal Dynamics, Estuaries under Climate Change, Mangroves, Remote Sensing, Storm Surges, Haiti, the Caribbean

Abstract

Coastal areas and estuaries worldwide are increasingly facing vulnerability due to the impacts of climate change. This is particularly true in the Caribbean, as the Small Island Developing States (SIDS) in the region are becoming increasingly vulnerable to rising sea levels and increased hurricane activity (Murakami et al., 2020). These changes lead to more frequent storm surges in the regions and potential worsening of their effects on coastal communities therein. As the cost-prohibitive nature of built protective infrastructure, such as seawalls and floodwalls, keeps them out of reach of SIDS, nature-based/landform solutions such as the mangrove forests native to the region may act as an alternative or adapted pathway to coastal resilience. Mangrove trees, which are prevalent in the intertidal zones of the tropics, possess complex and dense root systems, which, at a tree/local scale, have been shown to increase turbulence levels and reduce velocity fields near the bed. (Maza et al., 2017) When scaled up to the forest, the aggregated drag created by the roots serves to attenuate storm surges and dissipate surface waves. In a storm surge event, mangroves choke the flow going through the forest, reducing water transport, velocities, and water levels within and behind the forest. (Montgomery et al., 2019) (Chen et al., 2021). Additionally, mangroves exhibit sediment accretion properties as a byproduct of the velocity reduction. When combined with sediment accretion, mangroves' elevation building property due to the slow decomposing nature of their roots may in some instances help them keep pace with future sea-level rise. These properties make mangrove forests promising natural barriers against storm surges, and in certain cases, against sea-level rise, making them potential "climate change attenuators" that can be strategically used for coastal defense. However, despite their undeniable importance as both rich habitat and coastal defense structures, mangrove forests in the Caribbean are under stress by human activities and may be increasingly vulnerable to rapid sea-level rise and extreme weather events (Lagomasino et al., 2021; Duke et al., 2017; Saintilan et al., 2020). This means that the potential of mangroves as effective natural infrastructure hinges then on their resilience against climate change and their conservation.

This research aims to investigate the potential of mangrove forests as critical parts of adaptation pathways for Caribbean islands. To assess the future protection provided by mangroves as well as their vulnerability to climate change in the region, we conduct the hydrodynamic modeling of the Grand-Pierre Bay mangrove forest in Haiti under different storm surges, sea-level rise, and forest cover scenarios. The Baie de Grand-Pierre (Grand-Pierre Bay) mangrove forest (Fig. 1) is the largest extent of mangrove forest in Haiti and is situated in the largest estuary system of the country. It is situated south of Gonaives, the 3rd most populated city in Haiti, and serves as a buffer to parts of the Artibonite Valley coastline. We model this system due not only to its size but also its strategic location close to some of the largest population and economic zones of Haiti.

As a preliminary step, we conducted the land classification and detection of mangroves in Grand-Pierre Bay using imagery from PlanetLab's RapidEye satellite, deriving high-resolution maps of mangrove cover at the site. With its' 5-meter pixel resolution, this satellite lets us distinguish smaller-scale forest cover compared to other satellites such as Landsat (30-meter resolution). Using the satellite's 5 bands (Red, Green, Blue, Red Edge and Near-Infrared), indices such as the Normalized Difference Vegetation Index (NDVI) and Normalized Difference Water Index (NDWI), and the Histogram-based Gradient Boosting Classifier (HGB), a supervised learning method, we classify our satellite images into the following categories: water, mangrove, mud flat, intertidal zones, crops, and urban cover. Classifying images between 2010 and 2020 yields a library of mapped mangrove cover for our site, which can be used not only for looking at the forest evolution within that period but also for parameterizing and modeling different mangrove cover scenarios. The covers derived from our remote sensing workflow are parameterized as a bottom friction coefficient in the ADCIRC hydrodynamic model based on vegetation health and density. Estimating bottom friction coefficients in a storm surge model based on land cover is an effective way of simulating vegetation effects on storm surge flooding (Zhang et al., 2012) and this method has been used to simulate storm surge interactions with other wetlands. Developed by Luettich and Westerlink, 1991, ADCIRC (ADvanced CIRCulation model) is a numerical model extensively used for simulating hydrodynamics in coastal regions and is primarily used for reproducing storm surges and tides. The model runs explore different variables such as mangrove cover (using current and different historic covers as derived from remote sensing), river outflows, and mean sea levels, based on IPCC projections for different global warming scenarios, and storm surge scenarios.

[1] University of California, Berkeley, alexandre_georges@berkeley.edu
[2] University of California, Berkeley, mstacey@berkeley.edu
[3] University of Trinidad and Tobago, deanesh.ramsewak@utt.edu.tt

These simulations, running on 3-year timescales, quantify the spatial and temporal variability of salinity and inundation in the mangrove forest under forcing from sea-level rise, to help determine which sections of the forest are most vulnerable to diebacks due to environmental stressors. Additionally, shorter simulations of various surge events will be used to evaluate the coastal protection provided in different scenarios. Together, these two simulations allow us to evaluate: 1) how the Grand-Pierre mangrove forest contributes to shoreline protection and, 2) the resilience of the forest itself under climate-change forcing.

Figure 1. The Grand-Pierre is located on the Western coast of Haiti, in the Gulf of Gonave. Planet Basemaps [January to April 2023], Image ©2023, Planet Labs PBC.

References

Hiroyuki Murakami, Thomas L. Delworth, William F. Cooke, Ming Zhao, Baoqiang Xiang, and Pang-Chi Hsu. Detected climatic change in global distribution of tropical cyclones. Proceedings of the National Academy of Sciences, 117(20):10706–10714, May 2020. doi: 10.1073/pnas.1922500117. URL https://www.pnas.org/doi/10.1073/pnas.1922500117. Publisher: Proceedings of the National Academy of Sciences.

Maria Maza, Katherine Adler, Diogo Ramos, Adrian Mikhail Garcia, and Heidi Nepf. Velocity and Drag Evolution From the Leading Edge of a Model Mangrove Forest. Prof. Nepf via Elizabeth Soergel, November 2017. ISSN 2169-9291. URL https://dspace.mit.edu/handle/1721.1/119430. Accepted: 2018-12-04T19:54:28Z Publisher: American Geophysical Union (AGU).

J. M. Montgomery, K. R. Bryan, J. C. Mullarney, and E. M. Horstman. attenuation of Storm Surges by Coastal Mangroves. URL At Geophysical Research Letters, 46(5):2680–2689, 2019. ISSN 1944-8007. doi: 10.1029/2018GL081636. URL https://onlinelibrary.wiley.com/doi/abs/10.1029/2018GL081636.

Qiang Chen, Yuepeng Li, David M. Kelly, Keqi Zhang, Brian Zachry, and Jamie Rhome. Improved modeling of the role of mangroves in storm surge attenuation. Estuarine, Coastal and Shelf Science, 260:107515, October 2021. ISSN 0272-7714. doi: 10.1016/j.ecss.2021.107515. URL https://www.sciencedirect.com/science/article/pii/S0272771421003668.

David Lagomasino, Temilola Fatoyinbo, Edward Castaˇ neda-Moya, Bruce D. Cook, Paul M. Montesano, Christopher S. R. Neigh, Lawrence A. Corp, Lesley E. Ott, Selena Chavez, and Douglas C. Morton. Storm surge and ponding explain mangrove dieback in southwest Florida following Hurricane Irma. Nat Commun, 12(1):4003, June 2021. ISSN 2041-1723. doi: 10.1038/s41467 021-24253-y. URL https://www.nature.com/articles/s41467-021-24253-y. Number: 1 Publisher: Nature Publishing Group.

Norman C. Duke, John M. Kovacs, Anthony D. Griffiths, Luke Preece, Duncan J. E. Hill, Penny van Oosterzee, Jock Mackenzie, Hailey S. Morning, and Damien Burrows. Large-scale dieback of mangroves in Australia's Gulf of Carpentaria: a severe ecosystem response, coincidental with an unusually extreme weather event. Mar. Freshwater Res., 68(10):1816–1829, March 2017. ISSN 1448- 6059. doi: 10.1071/MF16322. URL https://www.publish.csiro.au/mf/MF16322. Publisher: CSIRO PUBLISHING.

Keqi Zhang, Huiqing Liu, Yuepeng Li, Hongzhou Xu, Jian Shen, Jamie Rhome, and Thomas J. Smith. The role of mangroves in attenuating storm surges. Estuarine, Coastal and Shelf Science, 102-103:11–23, May 2012. ISSN 0272-7714. doi: 10.1016/j.ecss.2012.02.021. URL https://www.sciencedirect.com/science/article/pii/S0272771412000674

Salinity variance and mixing processes in the Rhine-Meuse Delta under drought conditions

Geraeds M. [1], Pietrzak J.D. [2], Verlaan M. [3], and Katsman C.A. [4]

Keywords: drought, salt wedge, river plume, tidal plume fronts, salinity variance.

Abstract

Deltas are complex and dynamic coastal ecosystems that are particularly sensitive to environmental changes, especially in the context of climate change. The vulnerability of deltaic environments to drought events is further increased by a combination of climatic and anthropogenic factors. Changing precipitation patterns, coupled with rising temperatures, contribute to prolonged periods of water scarcity and increased evapotranspiration rates, all the while water demands increase (KNMI, 2023). This combination can lead to increased salt intrusion, which may impact both the availability and quality of freshwater resources and the estuarine ecosystem. Yet, the impact of droughts on estuaries is not well understood. Therefore, this study investigates one of the most notable droughts in recent years, the severe 2022 European drought. We explicitly examine its effects on salt intrusion in the Rhine-Meuse Delta (RMD).

The RMD is a highly branched and engineered delta with a multitude of islands, gates, weirs, and barriers. The Rhine River's only natural open connection to the North Sea is the Rotterdam Waterway. The Rotterdam Waterway is an example of a dynamic strongly forced salt wedge estuary (De Nijs et al., 2010), which has been significantly altered by humans for shipping and harbour activities. The outflow of the Rhine River through the Rotterdam Waterway forms the strongly stratified Rhine River plume (De Boer et al., 2006; Rijnsburger, et al., 2021). Besides this natural connection, the estuary is also connected to the sea through the Haringvliet gates, a row of seventeen gates that together form a storm surge barrier. This storm surge barrier is opened during ebb tides, but can also be completely shut as a measure to decrease salt intrusion during droughts.

Although previous studies have looked at the estuary and the plume separately, they together form a coupled system that is not well understood. The geometric complexity of the system also obscures insight into the overall governing salt transport processes. In this work, we therefore look at the overall coupled-coast delta system but also zoom in on its sub-systems, to get the most complete picture of the system's response as a whole.

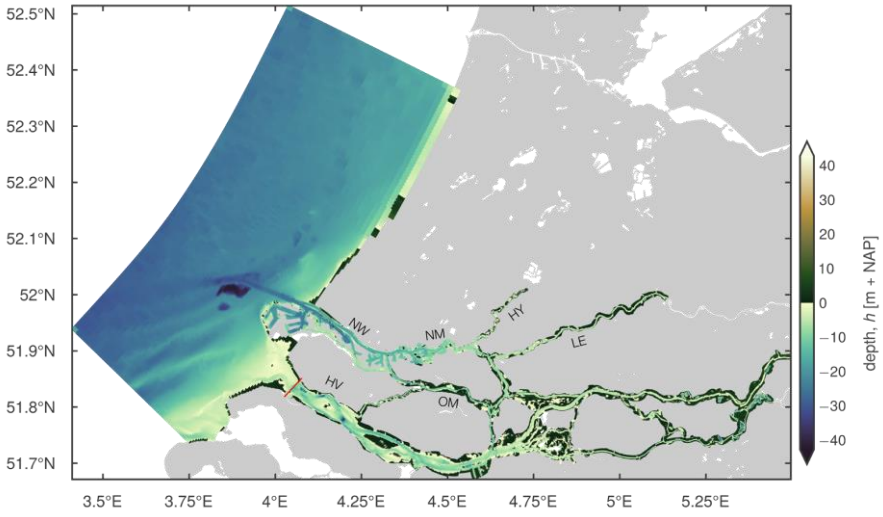

Figure 1: Overview of RMD model bathymetry and domain. The Main branches are indicated with abbreviations: New Waterway (NW), New Meuse (NM), Old Meuse (OM), Hollandse IJssel (HY), Lek (LE), and Haringvliet (HV). The red line indicates the location of the Haringvliet gates.

To be able to look at the entire system in detail, we use an unstructured 3D coupled coast-delta model implemented in D-FLOW Flexible Mesh (see Figure 1). The model extends 40 kilometers offshore as well as 70 kilometers alongshore, while also extending 100 kilometers inland. Its resolution varies throughout the domain, with the highest resolution in the estuary and the lowest resolution in the far-field region of the plume. The ocean boundary conditions are obtained from a nested simulation of the Dutch Continental Shelf Model (DCSM), which covers the entire North Sea. Boundary conditions on the river side are obtained from measurements. Meteorological conditions, such as the boundary conditions for the heat flux model, are obtained from the high-resolution HARMONIE weather model.

[1] Delft University of Technology, M.E.G.Geraeds@tudelft.nl
[2] Delft University of Technology, J.D.Pietrzak@tudelft.nl
[3] Deltares, Martin.Verlaan@deltares.nl; Delft University of Technology, M.Verlaan@tudelft.nl
[4] Delft University of Technology, C.A.Katsman@tudelft.nl

We investigate the tidal plume fronts and their response throughout the drought and couple this to the changing dynamics in the estuary. The dominant processes in different parts of the coupled coast-delta system are determined by applying a salinity variance analysis following Li et al. (2018) to our model results, from which we obtain spatial patterns of stratification, straining, and mixing. We highlight different dynamic zones in the estuary and look at how the dynamics in these zones change throughout the drought. To determine the relative importance of lateral, along-channel, and vertical contributions for the processes following from the salinity variance analysis, we additionally determine the terms in a simplified along-channel momentum balance.

Throughout the drought, the frequency and intensity of the tidal plume fronts change. As the tidal plume fronts retreat, we observe a changing salt wedge structure in different parts of the estuary. We find that different branches of the estuary have contrasting responses to the drought, as the timing of maximum salt intrusion in the Old Meuse branch is markedly different from the timing of maximum salt intrusion in the New Meuse. Through a dissemination of the along-channel momentum balance, we find that in the Rotterdam Waterway and the New Meuse the subtidal baroclinic pressure gradient and along-channel advection term together compete with the barotropic pressure gradient. In contrast, the along-channel advection term competes against the baroclinic pressure gradient in the Old Meuse. Interestingly, the vertical advection term is dominant in the Old Meuse branch. This dominance suggests that bathymetric features contribute to local mixing, altering the strength of the salt wedge and influencing the timing of maximum salt intrusion in the branch.

Our findings emphasize the connection between the river plume dynamics and the estuarine response of the different branches in the RMD, while also highlighting the dissimilarities in their respective responses.

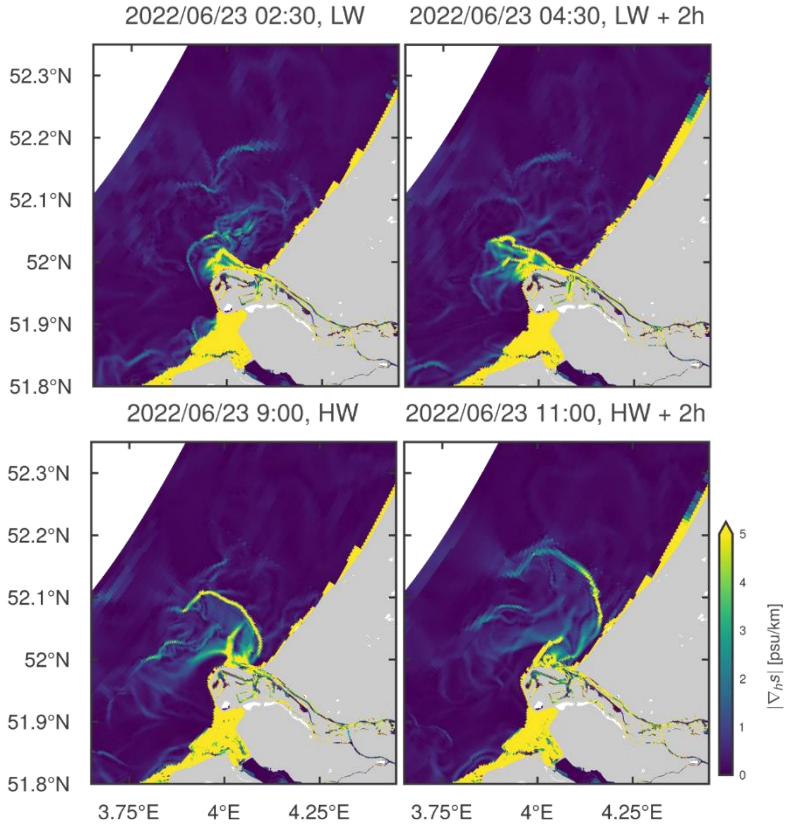

Figure 2: Plan view of the absolute value of the horizontal salinity gradient in the Rhine region of freshwater influence and part of the Rhine-Meuse Delta in the beginning of the drought period.

References

De Boer, G., Pietrzak, J., & Winterwerp, J. (2006). On the vertical structure of the Rhine region of freshwater influence. Ocean Dynamics, 56(3-4), 198-216.

De Nijs, M. A., Pietrzak, J., & Winterwerp, J. (2010). Advection of the Salt Wedge and Evolution of the Internal Flow Structure in the Rotterdam Waterway. Journal of Physical Oceanography, 41(1), 3-27.

Koninklijk Nederlands Meteorologisch Instituut (KNMI). (2023). KNMI'23-klimaatscenario's voor. De Bilt: KNMI-Publicatie 23-03.

Li, X., Geyer, W. R., Zhu, J., & Wu, H. (2018). The transformation of salinity variance: A new approach to quantifying the influence of straining and mixing on estuarine stratification. Journal of Physical Oceanography, 48(3), 607-623.

Rijnsburger, S., Flores, R. P., Julie, D. P., Horner-Devine, A. R., Souza, J. A., & Zijl, F. (2021). The Evolution of Plume Fronts in the Rhine Region of Freshwater Influence. Journal of Geophysical Research: Oceans, 126(7), 1-28.

Mixing Hot-Spots in a Partially Mixed Estuary

Geyer R. [1] and Scully M. [1]

Keywords: mixing, strain, baroclinicity

Abstract

The James River is the ”classic” partially mixed estuary, being selected by Pritchard to provide the first description of the balance between along-estuary mixing and estuarine exchange flow. Pritchard did not have many data points to verify his depiction of the estuary as a region of relatively uniform along-estuary salinity gradient and along-estuary mixing. Seventy-two years later, our measurements and models tell us that neither the salinity gradient nor the intensity of mixing is uniform.

A high-resolution, finite-difference simulation of the James River estuary using the Regional Ocean Modeling System (ROMS) was used to examine the spatial and temporal distribution of mixing in the James River during moderate river discharge, when the estuary exhibits partially mixed conditions. Mixing was quantified based on the destruction of salinity variance. Similar results are obtained by considering the distribution of turbulent buoyancy flux, but the destruction of variance is a more precise measure of mixing, and it has been recently shown to be closely linked to the along-estuary variation of exchange flow.

This study revealed that the strongest mixing in the James River occurs at the mouth of the estuary during the middle to late ebb tide, in association with the lift-off front, where the low-salinity estuarine water rises and buoyantly spreads over the saltier water of Chesapeake Bay. A similar lift-off front occurs behind a pronounced constriction within the estuary, making a smaller but significant contribution to mixing. Two other important mixing zones were identified. During the flood tide, significant mixing occurs in association with a tidal intrusion front that occurs at the same constriction just mentioned. An extensive but not particularly intensive zone of mixing occurs in the upper estuary during the mid-ebb, where stratified boundary-layer mixing is supported by the destruction of stratification that is created by both local ebb-tide straining and lateral straining during preceeding flood tide.

The most intense mixing occurs as a result of baroclinic strain-the shear and strain that re- sult from localized regions of intensified along-estuary (and sometimes cross-estuary) salinity gradient. The strain acting on the horizontal salinity gradient increases the stratification. But in the hydraulically supercritical conditions that occur in the lift-off zones, the square of the shear increases more rapidly than the stratification (as measured by the buoyancy frequency squared), causing the gradient Richardson number (Ri) to go below its critical value of 0.25, initiating mixing. The ”marginal instability” regime ensues, in which Ri ˜0.25 and an approximate balance is maintained between straining and mixing. This baroclinically driven mixing regime explains three of the four important mixing zones in the James River, including the two lift-off zones and the tidal intrusion front. The intensity of these localized mixing zones are explained by the nonlinear dependence of mixing on the horizontal salinity gradient, which is highly heterogeneous, in stark contrast to the assumptions in Prichard’s classic formulation for partially-mixed estuaries.

[1]Woods Hole Oceanographic Institution (WHOI) – 266 Woods Hole Rd Woods Hole, MA 02543, United States, rgeyer@whoi.edu

Reconstructing water levels during flooding in the Seine estuary using machine learning methods

Gilbert R. [1], Turki I. [1], David P.-Y. [2], and Laignel B. [1]

Keywords: machine learning, flooding, risks, forecasting

Abstract

With the global context of climate change, most of researchers claim that the water level variability and the increase of extreme events are considered significant hazards for several low-lying coastal and estuarine communities (Nicholls et al. 2011). Hence, many efforts have been devoted to better understand the natural processes driving the multi-scale variability of the hydrodynamics with the aim for producing a more accurate estimation of their fluctuations and ensuring reliable coastal risk assessments. This challenge serves as the basis for implementing an appropriate adaptation strategy for estimating extreme water levels and mapping compound floods, which is crucial to reduce the disastrous risks of the flooding in the different context of coasts, estuaries and rivers.

In estuarine contexts, controlled by the combined effects of different continental and marine drivers, the compound flooding events are frequently produced and cause severe con- sequences. For such systems, the main approach used considers the predominance of high- energy storms, extreme discharge and wave-induced events responsible for flooding. The effects of hydrological forces on superficial flooding is neglected.

This research aims at investigating the dynamics of extreme water levels, induced by cascading flooding risks in a river-tide environment, with the objective to reconstruct extreme water levels at different timescales between 1990 and 2019. The studied case, the estuary of Seine, is considered an excellent natural laboratory to analyze river-surge interaction because of its time-varying flow and the available water-level records provided by tide gauges along the estuary.

This context is controlled by different drivers that are produced cascading since they are induced by the same climate forcing. For example, the combined effects of low atmospheric pressure and strong winds associated with synoptic-scale storms can induce storm surges along the coast (Turki et al., 2023).

The physical drivers, including the effects of tides (non-stationary tidal signal), hydrological (discharge), meteorological (precipitation, wind, temperature, evapotranspiration), marine (swell, tide), and hydrogeological (groundwater levels) forcings, have been extracted from ERA-5 models and in situ observations. They have been used as stochastic variables within an integrated comprehensive range of environmental datasets through the development of an innovative AI-based approach. The different events have been modelled by the application of advanced supervised machine learning techniques were implemented, featuring gradient boosting and XGBoost, at five key tide gauge stations.

The results obtained highlight good accuracy in predicting water levels, with a margin of error of 20–30 cm during training phases and 30–40 cm during flooding periods. This ac- curacy is more pronounced down the estuary. Tides considered as the predominant factor and accounting for more than 90% of the estuary's hydrodynamic dynamics, contribute to a range of between 2–7% of the reconstructed signal. Other parameters, such as meteorological and hydrogeological conditions, although in the minority, play an essential supporting role in the flood dynamics.

This research offers a new perspective on the underlying mechanisms of flooding in the Seine estuary, by integrating a variety of parameters that were previously neglected or difficult to incorporate into models. This finding demonstrates the crucial role of non-stationary tides for monitoring estuarine flooding. It highlights as well the accuracy of machine learning techniques for assessing the hydrodynamics of tide-river environments.

References

Nicholls, R.J., Wong, P.P., Burkett, V., Codignotto, J., Hay, J., McLean, R., Ragoonaden, S., Woodroffe, C.D., Abuodha, P.A.O., Arblaster, J., 2007. Coastal Systems and Low-Lying Areas.

E.I. Turki, J. Deloffre, N. Lecoq, R. Gilbert, E.T. Mendoza, B. Laignel, E. Salameh, A.D. Gutierrez Barcelo, M. Fournier, N. Massei. Multi-timescale dynamics of extreme river flood and storm surge interactions in relation with large-scale atmospheric circulation: Case of the Seine estuary, Estuarine, Coastal and Shelf Science, Volume 287, 2023, 108349, ISSN 0272–7714, https://doi.org/10.1016/j.ecss.2023.108349.

[1] Morphodynamique Continentale et Côtière (M2C) – Université de Caen Normandie, Institut National des Sciences de l'Univers, Université de Rouen Normandie, Centre National de la Recherche Scientifique – 24 rue des Tilleuls 14000 Caen, France

[2] Bureau de Recherches Géologiques et Minières (BRGM) – France

The South Atlantic Central Water intrusion process in the São Sebastião Channel

Gnamah M. [1] and Dottori M. [1]

Keywords: São Sebastião Channel, hydrodynamics, SACW intrusion, numerical modeling, ROMS

Abstract

The São Sebastião Channel hydrodynamics (SSC) is dominated by the local wind stress. During winter, the thermohaline vertical structure is quasi homogeneous and during summer, the South Atlantic Central Water (SACW) enters the SSC, creating a stratified vertical profile. The process and mechanism of the SACW intrusion in the channel are relatively well known. During persistent upwelling favorable wind events, especially in the summer and spring, the SACW intrusion can be observed at the bottom of the channel Coelho (1997). According to Castro (1998) and Dottori et al. (2015), the intrusion of the SACW at the bot- tom occurs by the south entrance of SSC. This study aims to explore the favorable periods of the intrusion, in response to the remote wind stress and the tracking mechanism of SACW intrusion. To achieve this, we used historical in-situ temperature time series (recorded every 0.5 hour from 2009 to 2019) at the surface (at 3.5 m) and near the bottom channel (Figure 1), and winds from ERA5 reanalysis (25 km of resolution) of the northern part of SBB (Cabo Frio and surrounding areas) in order to estimate the wind impulse, combined with a serie of simulations based on the ROMS model in order to consolidate the statistical analyzes. High vertical temperature gradients in the channel are associated with the arrival of SACW (temperature colder than 18 ºC) in summer (December-February). Strong values of temperature gradient are associated with weak values of local (SSC) wind magnitude, while they are strongly associated with remote (Cabo Frio) wind magnitude (Figure 2). This reveals that remote wind plays an important role in temperature change in the SSC. We observed various negative trends of the remote along-shore winds impulse, that testifies the favorable upwelling winds event in the northern part of the SBB. During the summer, high lag-correlation coefficients (0.93 and 0.75) between the remote along-shore wind impulse and the channel near bottom temperature was found, respectively for lag -7 and -14 days (Figure 3). Low correlation coefficients (0.07 and -0.12) were found for positive lag, respectively for 7 and 14 days. The high correlation indicates clearly that the SSC near bottom temperature changes in summer are related to the northern upwelling winds system that occurred one or two weeks in advance.

The ROMS model was adapted to the SBB on a 3km resolution grid, in order to simulate the temperature changes in the SSC during the months of July and December that represent winter and summer respectively, for each year from 2010 to 2020. Initial and boundary conditions were set using climatology characteristic of winter and summer for all the simulations and a daily wind stress (from ERA5 wind products) was provided as atmospheric forcing at the sea surface boundaries. The model response showed no SACW upwelling in Cabo Frio and a bottom thermal structure almost homogeneous along the coastal region, associated with temperature values between 20 and 21 C in July (Figure 4). In December the simulation showed cold water about 15 C in Cabo Frio and the whole continental shelf. The simulation indicates that along-shore wind stress favors the Cabo Frio SACW upwelling and controls upwelled water flowing southwestward (Figure 5). Additionally, cold water can be observed reaching the SSC bottom. During the summer period, SACW flows southward from Cabo Frio and intrudes toward the bottom channel, due to along-shore wind intensification. During winter, this flow of SACW weakens, going northward, keeping the SSC temperature structure almost homogeneous at the surface and bottom.

[1]Instituto Oceanográfico da Universidade de São Paulo (IO-USP) – Praça do Oceanográfico, 191 - Cidade Universitária CEP 05508-120 - São Paulo (SP) - Brasil, Brazil. mgnamah@usp.br

Morphodynamic variability of the Somme Bay from seasonal to pluriannual scale in response to hydrodynamic forcings

Goulas T. [1, 2], Le Bot S. [2], Deloffre J. [2], Huybrechts N. [1, 3], Turki I. [2], Froideval L. [4], Conessa C. [4], Monfort O. [5], and Salameh E. [2]

Keywords: estuary morphodynamics, hydrodynamic forcings, LiDAR, pluriannual variability, Somme Bay

Abstract

Bays and estuaries are transitional environments between the open sea and the coast, enabling large exchanges of sedimentary material. In the English Channel, these environments experience infilling of their intertidal zones with marine sands combined with erosion of their tidal delta fronts (Verger, 2005; Tessier et al., 2012; Latapy, 2020; Grenard-Grand et al., 2021). Polderization (Bastide, 2011) and climate change-induced evolution of forcings (like tidal range, sea level, and storm intensity) may increase these processes (Van Vliet-Lanoë et al., 2014) leading to significant changes in land use (fisheries, navigation…).

The Somme Bay is an example of an infilling environment (Verger, 2005; Michel et al., 2017) relatively unaffected by human activity, mainly confined to the inner bay (Bastide, 2011). This bay is a very dynamic environment under the combined action of strong tidal current (macrotidal regime) and swell climates. Sediments in the bay correspond to fine marine sands coming from the subtidal sedimentary supply and sandy-muddy mixtures in restricted sheltered areas (Dupont, 1981; Anthony, 2000; Anthony & Héquette, 2007; Ferret et al., 2010; Michel et al., 2017). While the bay is generally infilling, temporary erosion occurs in some sectors (Michel, 2016).

This study aims to enhance understanding of the spatio-temporal variability of the bay's morphodynamics in response to hydrodynamic forcings on a seasonal to pluriannual scale. Airborne LiDAR topographic data provide spatial information on intertidal topography at biennial to 2-year time-intervals for the last decade (11 datasets between 2011 and 2020). In addition, hydro-marine-meteorological data (tides, winds, waves, storms, etc.) extracted from a DELFT3DFM model (Solano et al., 2024) are used to characterize the hydrodynamic regime across inter-survey periods. Spatial and temporal variability of the morphodynamic evolution is analyzed. The recent infilling of the bay is quantified: volumetric sediment budgets are computed for the entire bay (within the derived Digital Terrain Models limits from the LiDAR data in the intertidal zone) at each inter-survey period from seasonal to pluriannual scale. For the whole surveyed period (from 2011 to 2020), the mean elevation of the bay has increased of more than 20 cm. Most inter-survey periods between 2011 and 2020 (8 out of 10) show general accretion, with budgets varying between 0.7 $cm.year^{-1}$ and 12 $cm.year^{-1}$ at the bay scale.

At more local scales, variation trends are observed, particularly in the external intertidal part of the bay: volumetric variation is higher in the lowest/external intertidal parts compared to the highest/internal already mostly infilled parts. In the external part (Fig. 1), with sediment budgets computed for a resolution of 100 m × 100 m, some sectors display a systematic accretion or erosion pattern, while others show variable evolution trends.

Morphological evolutions are confronted with hydrodynamic, marine and meteorological forcings (including storms) for each specific period through correlation analysis, in order to identify the forcing key-parameters that govern the morphodynamic evolution of the bay at a pluriannual scale. Finally, this paper focuses on morphological evolutions at 'intermediate time scales' that are relatively unexplored in the literature, which is much more abundant on 'short-term/process' scales (i.e. tidal range, swell) or 'long-term' scales (i.e. century to geological scale).

[1] Cerema REM, RHITME Research Team, Margny Les Compiègne, F 60280 FRANCE, tatiana.goulas@cerema.fr, nicolas.huybrechts@cerema.fr

[2] Univ Rouen Normandie, Université Caen Normandie, CNRS, Normandie Univ, M2C UMR6143, F-76000 Rouen, France, tatiana.goulas@univ-rouen.fr, sophie.lebot@univ-rouen.fr, julien.deloffre@univ-rouen.fr, imen.turki@univ-rouen.fr, edward.salameh@univ-rouen.fr

[3] Univ Rouen Normandie, Université Caen Normandie, CNRS, Normandie Univ, M2C UMR6143, F-60280 Margny Les Compiègne, France, nicolas.huybrechts@cerema.fr

[4] Univ Caen Normandie, Université Rouen Normandie, CNRS, Normandie Univ, M2C UMR6143, F-14000 Caen, France, laurent.froideval@unicaen.fr, christophe.conessa@unicaen.fr

[5] Université de Caen Normandie-CREC, Luc-sur-Mer, France, olivier.monfort@unicaen.fr

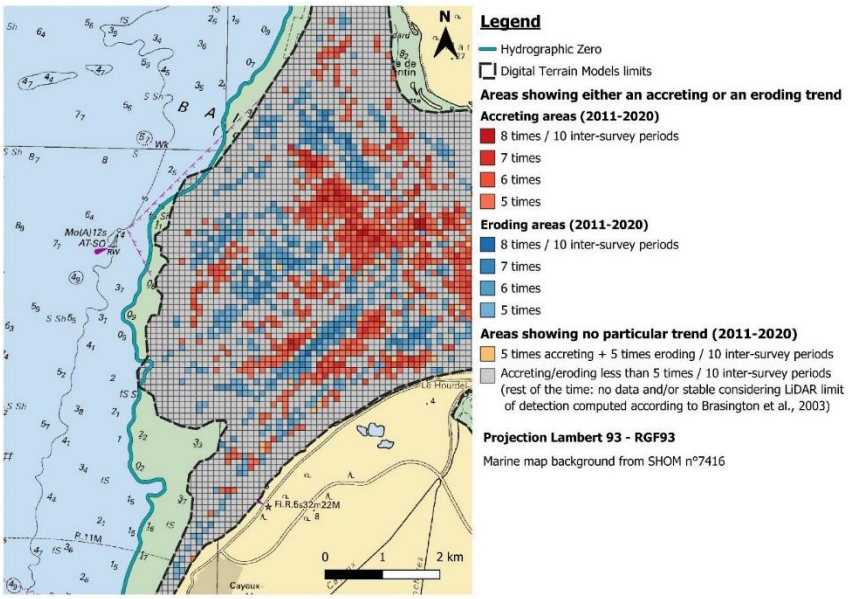

Fig. 1: Accreting and eroding areas (with a 100×100 m resolution) in the external intertidal part of Somme Bay for inter-survey (LiDAR) periods from 2011 to 2020

References

Anthony, E.J. (2000) Marine sand supply and Holocene coastal sedimentation in northern France between the Somme estuary and Belgium. SP 175, 87–97, https://doi.org/10.1144/GSL.SP.2000.175.01.08

Anthony, E.J., Héquette, A. (2007) The grain-size characterisation of coastal sand from the Somme estuary to Belgium: Sediment sorting processes and mixing in a tide- and storm-dominated setting. Sedimentary Geology 202, 369–382, https://doi.org/10.1016/j.sedgeo.2007.03.022

Bastide, J. (2011) Morphodynamique et enjeux d'aménagement des franges littorales d'un estuaire macrotidal tempéré : la Baie de Somme, Picardie, France. Thèse de doctorat, Université du Littoral Côte d'Opale, 303 p.

Brasington, J., Langham, J., Rumsby, B. (2003) Methodological sensitivity of morphometric estimates of coarse fluvial sediment transport. Geomorphology, 53(3-4), 299-316.

Dupont, J.-P. (1981) Relations entre bios et phénomènes sédimentaires intertidaux : le modèle de la Baie de Somme. Thèse de doctorat, Université de Rouen, 309 p.

Ferret, Y., Le Bot, S., Tessier, B., Garlan, T., Lafite, R. (2010) Migration and internal architecture of marine dunes in the eastern English Channel over 14 and 56 year intervals: the influence of tides and decennial storms. Earth Surface Processes and Landforms 35, 1480–1493, https://doi.org/10.1002/esp.2051

Grenard-Grand, E., Tessier, B., Le Bot, S., Ponsolle, J. (2021) Analyse de l'évolution des dynamiques et des stocks sédimentaires subtidaux depuis le XIXème siècle au large des côtes de Normandie (NW France). 27e édition de la Réunion des Sciences de la Terre, 1st-5th November 2021, Lyon, France

Latapy, A. (2020) Influence des modifications morphologiques de l'avant-côte sur l'hydrodynamisme et l'évolution du littoral des Hauts-de-France depuis le XIXe siècle. Thèse de doctorat, Université du Littoral Côte d'Opale, 217 p.

Michel, C. (2016) Morphodynamique et transferts sédimentaires au sein d'une baie mégatidale en comblement (Baie de Somme, Manche Est). Stratégie multi-échelles spatio-temporelles. Thèse de doctorat, Université de Rouen, 325 p.

Michel, C., Le Bot, S., Druine, F., Costa, S., Levoy, F., Dubrulle-Brunaud, C., Lafite, R. (2017) Stages of sedimentary infilling in a hypertidal bay using a combination of sedimentological, morphological and dynamic criteria (Bay of Somme, France). Journal of Maps 13, 858–865, https://doi.org/10.1080/17445647.2017.1389663

Solano, C. L., Turki, E. I., Mendoza, E. T., Barceló, A.D.G., Migaud, A., Laignel, B., Lafite, R. (2024) An integrated wave modelling framework for classifying extreme events in the English Channel and on the Normandy coasts. Natural Hazards, https://doi.org/10.21203/rs.3.rs-3369989/v1

Tessier, B., Billeaud, I., Sorrel, P., Delsinne, N., Lesueur, P. (2012) Infilling stratigraphy of macrotidal tide-dominated estuaries. Controlling mechanisms: Sea-level fluctuations, bedrock morphology, sediment supply and climate changes (The examples of the Seine estuary and the Mont-Saint-Michel Bay, English Channel, NW France). Sedimentary Geology 279, 62–73, https://doi.org/10.1016/j.sedgeo.2011.02.003

Van Vliet-Lanoë, B., Penaud, A., Hénaff, A., Delacourt, C., Fernane, A., Goslin, J., Hallégouët, B., Le Cornec, E. (2014) Middle- to late-Holocene storminess in Brittany (NW France): Part II – The chronology of events and climate forcing. The Holocene 24, 434- 453, https://doi.org/10.1177/0959683613519688

Verger, F. (2005) Marais et estuaires du littoral français. Paris, Belin, 300 p., ISBN 2-7011-3339-4

A simple method for estimating potential turbidity maximum in NW European tidal estuaries

Grasso F. [1], Bismuth E. [1], Burchard H. [2], Defontaine S. [1,3], Dijkstra Y. [4], Geyer W.R. [5], Kösters F. [6], Lafite R. [7], Reese L. [2], Schuttelaars H. [4], Sottolichio A. [8], Van Kessel T. [9], Vanlede J. [10], Van Maren B. [9,11,12], Verney R. [1], Walther R. [13], and Zorndt A. [6]

Keywords: estuary, sediment dynamics, suspended particulate matter, in-situ observation, numerical modeling.

Abstract

Large amounts of suspended particulate matter (SPM) are observed in tidal estuaries, increasing water turbidity and impacting estuarine ecosystems. However, the SPM concentrations strongly vary between estuaries, ranging from a few mg/l to tens of g/l at the surface, implying specific management strategies. Mechanisms driving estuarine turbidity maxima (ETM) formation are now relatively well understood (Allen et al., 1980; Burchard et al., 2018) and ETM responses to environmental conditions are well characterized (Sommerfield & Wong, 2011). However, a realistic description of estuarine sediment dynamics currently requires extensive in-situ observations (Jalón-Rojas et al., 2016) and validated numerical modeling (Van Maren & Cronin, 2016). Such time-consuming and costly approaches limit their use for estuary stakeholders.

The overarching goal of this study is to predict the maximum SPM concentration expected within an estuary based on a limited number of environmental parameters. For practical use, these parameters have to be easily accessible to estuary stakeholders (i.e., tidal range, river discharge, estuary morphology). To reach this objective, this work relies on the analysis of in-situ measurements and validated numerical simulations in seven meso- to macro-tidal NW European estuaries (Elbe, Weser, Scheldt, Seine, Loire, Gironde, and Ems; Fig. 1). These estuaries present contrasted forcing, in terms of tidal range, river discharge, and estuary morphology (Fig. 1). It results in maximum SPM concentrations at the surface ranging from 0.4 to 6 g/l. This one-year-long high-frequency (every 30 minutes) dataset provides the opportunity to investigate estuarine physics for a wide range of configurations and to go beyond site-specific analyses.

The definition of appropriate estuary boundaries is essential to properly compare the different systems. Using the limit of tidal influence up-estuary and the maximum of the horizontal salinity gradient seaward provides a relevant frame for characterizing estuarine physical functioning. Computed within this range, the fresh-water Froude number (Fr) and the mixing number (M), characterizing river and tidal energies, respectively (Geyer & MacCready, 2014), are more consistent for inter-estuary comparisons. Measurements and simulations corroborate that maximum SPM concentrations occur at specific locations of the Fr-M diagram. In addition, using easily accessible estuary parameters (i.e., tidal range and river discharge at the mouth, estuary depth and width), a simplified Frs-Ms diagram proves to be relevant as well for characterizing measured SPM concentrations at the surface (Fig. 2).

The obtained Frs-Ms-SPMmax parameter space still needs to be completed with worldwide observations, especially within areas where SPM concentration is likely to decrease due to strong mixing conditions (i.e., large Ms). Nonetheless, it already provides an interesting tool for predicting the expected turbidity maximum within estuaries and the potential trajectories resulting from human-induced and natural changes (e.g., estuary deepening and narrowing, low river discharge decreasing).

[1] Ifremer – DYNECO/DHYSED, Centre de Bretagne, CS10070, F-29280 Plouzané, France. florent.grasso@ifremer.fr
[2] Department of Physical Oceanography and Instrumentation, Leibniz Institute for Baltic Sea Research Warnemünde, D-18119 Rostock, Germany.
[3] Now at Cerema REM, RHITME Research Team, Margny Les Compiègne, France.
[4] Delft Institute of Applied Mathematics, Delft University of Technology, NL-2628 CD Delft, The Netherlands.
[5] Department of Applied Ocean Physics and Engineering, Woods Hole Oceanographic Institution, Woods Hole, Massachusetts 02543, USA.
[6] Federal Waterways Engineering and Research Institute, BAW, 22559, Hamburg, Germany.
[7] Normandie Univ, UNIROUEN, UNICAEN, CNRS, M2C, 76000 Rouen, France.
[8] Université de Bordeaux, CNRS, Bordeaux INP, EPOC, UMR 5805, Pessac, France
[9] Deltares, Department of Marine and Coastal Systems, P.O. Box 177, 2600 MH, Delft, The Netherlands.
[10] Flanders Hydraulics Research, Berchemlei 115, B-2140, Antwerp, Belgium.
[11] Delft University of Technology, Faculty of Civil Engineering and Geosciences, Department of Hydraulic Engineering, P.O. Box 5048, 2600GA, Delft, The Netherlands.
[12] State Key Laboratory of Estuarine and Coastal Research, East China Normal University, Shanghai, 200241, China.
[13] Artelia, 6 rue de Lorraine, 38130, Echirolles, France.

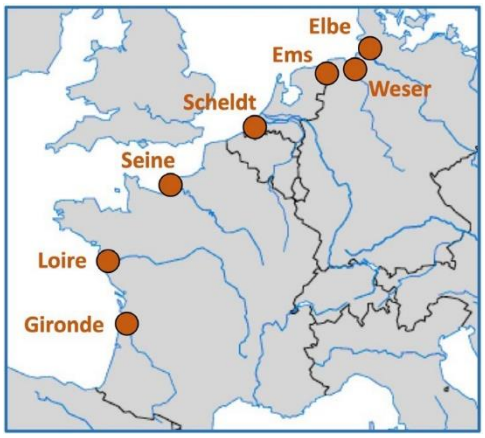

	Length (km)	Relative length (L_e/L_t)	Mean tidal range (m)	Mean river discharge (m^3/s)	SPM_{surf} conc. (p_{95}, g/l)
Elbe (2013)	122	1.3	2.8	1074	0.5
Weser (2016)	64	0.8	2.7	270	0.5
Scheldt (2006)	102	1.4	3.8	99	0.4
Seine (2016)	152	1.9	5.4	602	1.1
Loire (2018)	82	1.2	3.5	872	2.9
Gironde (2015)	116	1.8	3.3	619	5.1
Ems (2005)	32	0.6	3.1	71	6.1

Figure 1. (Left) NW European estuaries investigated in this study. (Right) Synthesis of the yearly-averaged conditions observed in the seven estuaries. The relative length is the ratio of the estuary length (L_e) over the tidal length (L_t). The measured SPM concentration is expressed as the yearly 95th percentile.

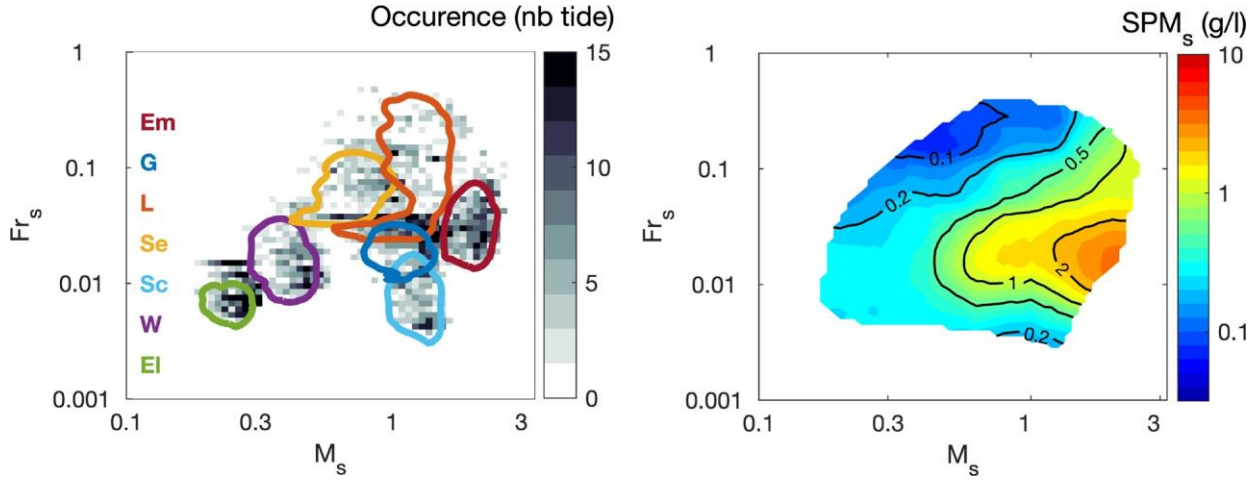

Figure 2. (Left) Mean conditions observed for the seven estuaries within the frame of the simplified Fr_s-M_s diagram (Elbe 'El', Weser 'W', Scheldt 'Sc', Seine 'Se', Loire 'L', Gironde 'G', and Ems 'Em'). (Right) Tide-averaged SPM concentration at the surface (SPM_s) measured at the highest-turbidity station for each estuary, interpolated in the frame of the simplified Fr_s-M_s diagram. Black contours represent SPM_s concentration levels.

References

Allen, G. P., Salomon, J. C., Bassoullet, P., Du Penhoat, Y., & De Grandpre, C. (1980). Effects of tides on mixing and suspended sediment transport in macrotidal estuaries. Sedimentary Geology, 26(1-3), 69-90.

Burchard, H., Schuttelaars, H. M., & Ralston, D. K. (2018). Sediment trapping in estuaries. Annual review of marine science, 10, 371-395.

Geyer, W. R., & MacCready, P. (2014). The estuarine circulation. Annual review of fluid mechanics, 46, 175-197.

Grasso, F., Verney, R., Le Hir, P., Thouvenin, B., Schulz, E., Kervella, Y., ... & Garnier, V. (2018). Suspended sediment dynamics in the macrotidal Seine Estuary (France): 1. Numerical modeling of turbidity maximum dynamics. Journal of Geophysical Research: Oceans, 123(1), 558-577.

Jalón-Rojas, I., Schmidt, S., Sottolichio, A., & Bertier, C. (2016). Tracking the turbidity maximum zone in the Loire Estuary (France) based on a long-term, high-resolution and high-frequency monitoring network. Continental Shelf Research, 117, 1-11.

Sommerfield, C. K., & Wong, K. C. (2011). Mechanisms of sediment flux and turbidity maintenance in the Delaware Estuary. Journal of Geophysical Research: Oceans, 116(C1).

Van Maren, D. S., & Cronin, K. (2016). Uncertainty in complex three-dimensional sediment transport models: equifinality in a model application of the Ems Estuary, the Netherlands. Ocean Dynamics, 66, 1665-1679.

Taming turbulence closure in tidally driven simulations of coastal oceans and estuaries

Harcourt R.R. [1], Mickett J.B., and Prakash K.R. [2]

Keywords: Turbulence parameterization, numerical stability, open channel, tidal forcing, coastal ocean, estuaries.

Abstract

Simulations of the coastal shelf ocean of Washington (WA) State from LiveOcean, and operational model (MacCready et al., 2021), based upon the Regional Ocean Modeling System (ROMS), were compared with observations of thermohaline stratification layers responsible for a widespread prevalence of mid-frequency (1-10 KHz) subsurface acoustic ducts observed over the outer shelf and the continental slope in July-August 2022. These layered variations of sound speed were observed throughout the WA coastal ocean between 100 m mid-shelf depths and the continental shelf break near 200 m and sampled intensively with the Shallow Water Integrated Mapping System (SWIMS; Klymak and Gregg, 2001) towed body platform. Cycling between surface and bottom boundaries, SWIMS recorded high-resolution rapid transects of temperature, salinity and dissolved oxygen, during a wide-ranging coastal shelf and slope survey, and continuously along a cross-shelf transmission line during two weeks of acoustic propagation measurements over the outer shelf, set within an instrumented mooring array and extensive archived regional ocean observatory data.

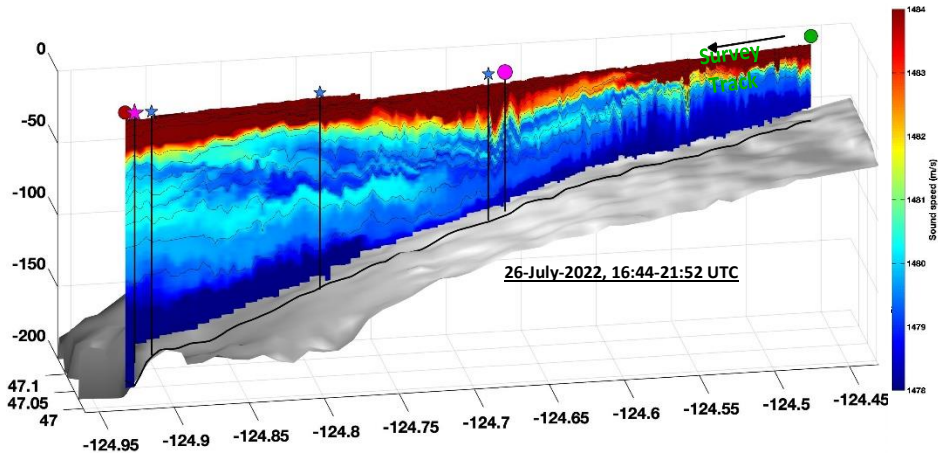

Figure 1. SWIMS sound speed section along acoustic line survey track (between magenta circles), through ocean moorings OM-W, OM-C and OM-E (blue stars), with the track for this section starting further inshore (green). The subsurface acoustic ducts are characterized by the mid-depth layers of local sound speed minima, creating waveguides for propagation of acoustic energy.

A great benefit of interdisciplinary collaborations is that requirements of the counterparties can set a higher bar of performance for each discipline to adopt as a goal. In this case, a nearly complete absence of the observed layered thermohaline structure of the subsurface acoustic ducts throughout the LiveOcean operational model was traced first to ocean lateral forcing at open boundaries using the formatted netCDF output distribution from the Hybrid Coordinate Ocean Model (HYCOM; Chassignet et al., , 2007), a product in widespread use wherein vertical resolution of such features can be negatively impacted by interpolation to standard geopotential (z-gridded) levels from the model's native hybrid coordinate system. Replacing this ocean forcing at the lateral open boundaries, and reinitializing as well, with higher vertical resolution GLORYS12 global operational and reanalysis products, based on the NEMO ocean model and distributed by Copernicus Marine (Lellouche et al., 2021), successfully populated the slope and offshore portions of LiveOcean with resolved acoustic ducts. However, poor model skill in prediction of layered structures over the outer shelf persisted in LiveOcean, accompanied by significantly low model values of both stratification and shear in the lower half of the water column over the outer shelf. These shortcomings in predicting outer shelf dynamics and tracer profiles were traced to excessive vertical mixing due to a high default setting for minimum turbulent kinetic energy (TKE) in the selected k-ε second moment turbulence closure parameterization. This k-ε parameterization for vertical eddy viscosity and diffusivity employs prognostic equations for TKE ('k') and dissipation (ε and an algebraic solution to Reynolds covariance equations linearized in second moments by 'Weak-equilibrium' closure assumptions, attributable in part to Canuto et al. (2001) and couched in the Generic Length Scale (GLS) framework of Umlauf and Burchard (2003). It is one of three options commonly available in the open distributions of ROMS, where the two other choices are the 'Quasi-equilibrium' version (Kantha and Clayson, 1994) of the Mellor-Yamada second moment closure, and the non-local first moment closure of K-Profile Parametrization (KPP; Large et al.., 1994).

[1] harcourt@uw.edu
[2] Applied Physics Laboratory, University of Washington

In some sense, both Mellor-Yamada and KPP give shorter shrift to the greater mathematical articulation of physically complex turbulence dynamics that is pursued within the formulation of the local, Weak-equilibrium k-ε closure. A default minimum TKE value setting of $k > 7.6 \times 10^{-6} m^2/s^2$ in ROMS traces through the General Ocean Turbulence Model (GOTM; Burchard *et al*., 1999) to model-data comparisons between measurements of tidally-driven ε in the Irish Sea and a column model implementation of the k-ε closure to parameterize vertical mixing (Burchard *et al*., 1998) where the addition of this floor on TKE levels is used to match observed mid-depth dissipation levels and attributed to unresolved internal wave forcing.

In three-dimensional regional ocean models that span from estuaries and inland seas out to deep ocean lateral boundaries through the coastal ocean, the pernicious effects of excessive vertical mixing in the weaker deep stratification stemming from this high default for minimum TKE is not unknown, at least within the 'grey literature' of periodic re-discovery within the ROMS modelling community (Scully, 2011; Pringle, 2017; Cherian, 2020). However, the straightforward prescription to drastically reduce the floor on TKE to a level below $O(10^{-9}\ m^2/s^2)$ was found to immediately render LiveOcean numerically unstable when the tidal forcing critically relevant to simulating the inland Salish Sea and Puget Sound was retained, even at greatly reduced and operationally impractical timesteps. While neither KPP nor Mellor-Yamada parameterization options suffer from either the excessive deep mixing in weak stratification or such problematic instability of tidally driven open channel flows, a modification of constraints in the k-ε turbulence parameterization was sought, based upon possibly blind faith in the prospective benefits to modelling stratified turbulence with the more modern, higher order closure. A simple and effective solution was obtained by replacing the minimum TKE constraint with a minimum dissipation level directly constraining mid-depth predictions of ε that originally motivated the TKE minimum. This constraint on ε is always physically justified in coastal and estuarine circulation models, irrespective of the level of internal wave forcing potentially unresolved in a high-resolution regional model.

The new approach to directly constraining the dynamic ε equation predictions in the Weak-equilibrium k-ε closure is examined in both 3D and column model implementations, along with the implications for other choices of turbulence length scale or frequency for the second prognostic equation within the unifying GLS formalism. The question set aside by this new constraint, of how to represent the impact of unresolved internal waves on turbulent mixing is restated as an unresolved source of shear and strain impacting both the linearized algebraic closure and the dynamic equations for TKE and dissipation. Reframing the problem in these terms charts a self-consistent approach to including important internal wave forcing, at least some of which remains unresolved in regional ocean models, either because it is absent from larger scale model forcing at the boundaries, or because the grid puts the waves or their generation beyond possible resolution.

References

Burchard, H., Bolding, K., Villarreal, M. R. (1999) GOTM – a general ocean turbulence model. Theory, applications and test cases, Tech. Rep. EUR 18745 EN, European Commission.

Burchard, H., Petersen, O., Rippeth, T. P., (1998) Comparing the performance of the Mellor-Yamada and the κ-ε two-equation turbulence models, *J. Geophys. Res.*, 103(C5), 10543–10554. doi:10.1029/98JC00261.

Canuto, V. M., Howard, A., Cheng, Y., Dubovikov, M. S. (2001) Ocean Turbulence. Part I: One-point closure model.
Momentum and heat vertical diffusivities. *J. Phys. Oceanogr*, 31, 1413–1426.

Chassignet, E. P., et al. (2007) The HYCOM (hybrid coordinate ocean model) data assimilative system *J. Mar. Syst*., 65, 60-83. Cherian, D. (2020) Living with ROMS. *Public Communication*: https://cherian.net/static/living-with-roms.pdf. Updated April 20,2020.

Klymak, J. M., Gregg, M. C. (2001) The three-dimensional nature of flow near a sill. J. Geophys. Res., 106C, 22295–22311.

Large, W. G., McWilliams, J.C., Doney, S.C. (1994). Oceanic vertical mixing: a review and a model with nonlocal boundary layer parameterization. *Rev. Geophys*., 32:363–403.

Lellouche, J.-M., et al., (2021) The Copernicus Global 1/12° Oceanic and Sea Ice GLORYS12 Reanalysis. *Front. Earth Sci*.9:698876.

MacCready, P. et al., (2021) Estuarine circulation, mixing, and residence times in the Salish Sea. *J. Geophys. Res. Oceans* 126: e2020JC016738.

Pringle, J. (2017) "Re: excess mixing in k-epsilon GLS mixing; bug or misconfigu" Post #8 by jpringle to *ROMS/TOMS Ocean Modeling Discussion:* https://www.myroms.org/forum/viewtopic.php?t=4789

Scully, M. (2011) "Re: Changing AKT_BAK values has no effect on model results." *Public Communication*. Post #6 by scully_ROMS to *ROMS/TOMS Ocean Modeling Discussion:* www.myroms.org/forum/viewtopic.php?t=2310

Umlauf, L., Burchard, H. (2003) A generic length-scale equation for geophysical turbulence models. J. Mar. Res. 61, (2) 235– 265.

Storms & tides: studying their effect on salt intrusion in rivers using a 2D model

Harper R. [1], Dijkstra Y. [1], and Schuttelaars H. [1]

Abstract

Storms can intensify saltwater intrusion in rivers, threatening freshwater ecosystems and water supplies. This study aims to investigate the sensitivity of salt intrusion in estuaries with various geometric and forcing conditions to storm surges, high winds and river discharge changes. To this end, we construct and use a 2DV model applied to idealised estuaries. In the expected results it is hoped that key conditions that increase salt levels in rivers will be identified, providing general insights for improving understanding of potential extreme salt intrusion events.

[1] Delft Institute of Applied Mathematics (DIAM), Delft University of Technology

HF Radar observations of flow curvature-enhanced upwelling at the entrance to the South Australian Gulfs

Hetzel Y. [1], Pattiaratchi C. [2], and Cosoli S. [3]

Keywords: Upwelling, topographic influences, HF Radar, surface currents

Abstract

Eastern boundaries of ocean basins are generally characterised by upwelling that influences coastal bays, gulfs, and estuaries. Australia's western and southern coasts do not experience the same intense and persistent upwelling as the Benguela, Canary, Humbolt, or California current systems due to anomalous boundary flow. However, seasonal and episodic upwelling events are important contributors to the ecological health of coastal ocean and embayments (Largier, 2020). Low rainfall and river input means that nutrient inputs to coastal regions along Australia's southern and western coasts are generally low and upwelling at the entrances to these bays likely plays an important role. The dominant mechanism along major upwelling coasts is alongshore winds driving offshore Ekman transport that results in upwelling of colder water along the coast regardless of coastal topography. However, where conditions are less favourable for wind-driven upwelling, the influence of along-shelf topographic variations on currents and winds becomes significant (Alaee et al., 2007; Largier, 2020). Where currents encounter rapid changes in the coastline such as occurs near a headland or island, flow divergence and centrifugal forces drive secondary flows that can induce or enhance upwelling (Alaee et al., 2007; Geyer, 1993).

During January 2024, stronger than normal winds induced upwelling and anomalous cooling along South Australia and northwest of Australia (Figure 1a) due to the El Niño event. In South Australia (Figure 1b), flow curvature and upwelling were observed at distinct locations across the entrance to the Gulfs (Figure 2).

Understanding the mechanisms driving upwelling requires oceanographic observations both high temporal and spatial resolution. The Australian Integrated Marine Observation System (IMOS) Ocean Radar facility has been collecting hourly maps of surface currents around Australia since 2007, with more than 10 years of hourly surface current data available at the entrance to South Australia Gulfs. This study used these HF Radar and satellite data to investigate flow curvature as a mechanism to induce or enhance upwelling in the study region.

The South Australian Gulfs are known as the testbed used by Lennon et al. (1987) to characterise inverse estuaries due to the high evaporation rates and strong density gradients with unique 'dodge' tides within the gulfs that strongly modulate the strength of tidal currents and mixing on a fortnightly basis. The Gulfs represent an important commercial fishery for prawns, fish, and aquaculture including Bluefin tuna raised in the entrance to Spencer Gulf. The HF Radar domain covers the entrance to Spencer Gulf and Gulf St. Vincent between Cape Wiles and Kangaroo Island over depths of 80 m out past the edge of the continental shelf, which narrows to 40 kilometres to the west of Kangaroo Island. The HF Radar is the German WellEn RAdar (WERA) system operating with linear antennae arrays at Cape Wiles and Cape Spencer (Figure 2a).

Around 19 January 2024 strong southeasterly winds drove along-shelf currents toward the northwest that were curved toward the right as they encountered western end of Kangaroo Island and to a lesser extent as they passed Cape Wiles further north (Figure 2a). Each of these regions where flow was observed to curve toward the land was associated with enhanced local cooling (Figure 2a) and chlorophyll production (Figure 2b). When currents reversed a week later (not shown), flow curvature in the opposite direction occurred along Kangaroo Island and near Cape Wiles and Cape Spencer, but at a smaller scale with weaker and more localised influences on SST and chlorophyll. This talk will explore these and other events in more detail to assess interactions of winds and currents with topographic features in order to better understand the dynamics of periodic upwelling along Australian coasts.

[1] yasha.hetzel@uwa.edu.au, School of Civil, Environmental and Mining Engineering and the UWA Oceans Institute, The University of Western Australia

[2] chari.pattiaratchi @uwa.edu.au, School of Civil, Environmental and Mining Engineering and the UWA Oceans Institute, The University of Western Australia

[3] simone.cosoli @uwa.edu.au, School of Civil, Environmental and Mining Engineering and the UWA Oceans Institute, The University of Western Australia

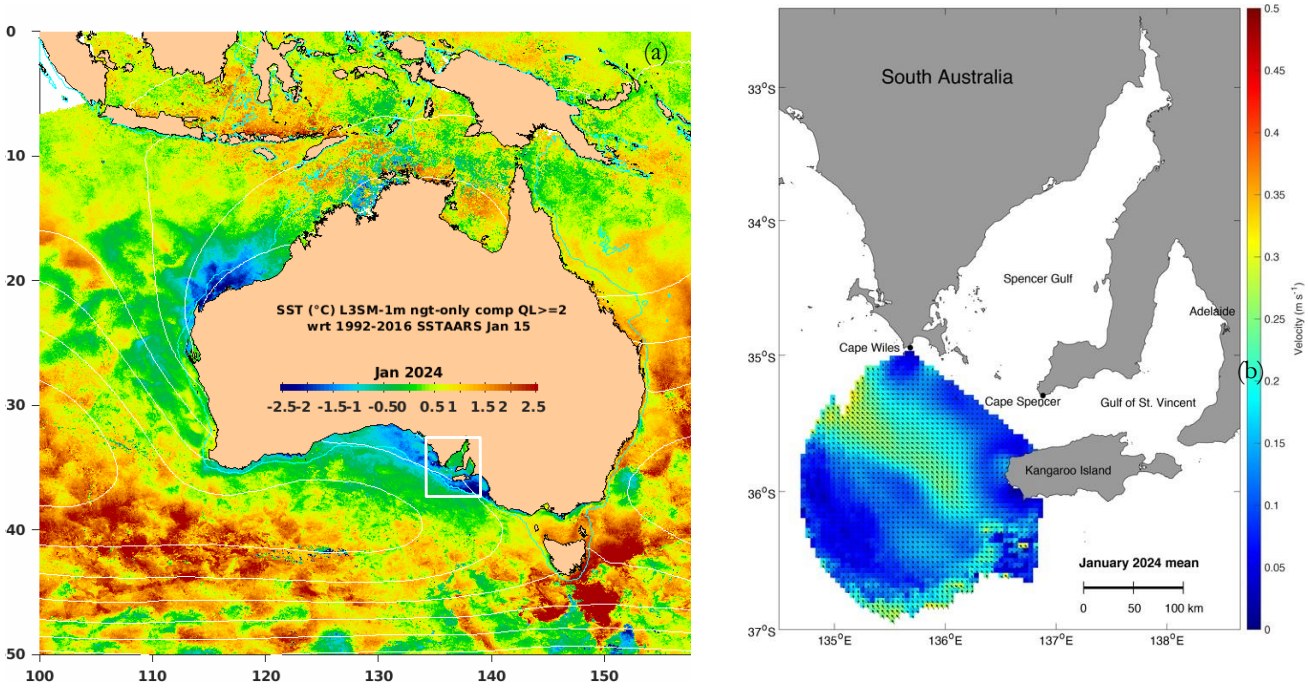

Figure 1 – (a) Sea Surface Temperature (SST) anomaly for January 2024 showing enhanced upwelling and colder water in South and Western Australia due to strong winds; (b) South Australian Gulf study region showing HF Radar domain and monthly mean surface currents for January 2024 at the entrance to the gulfs.

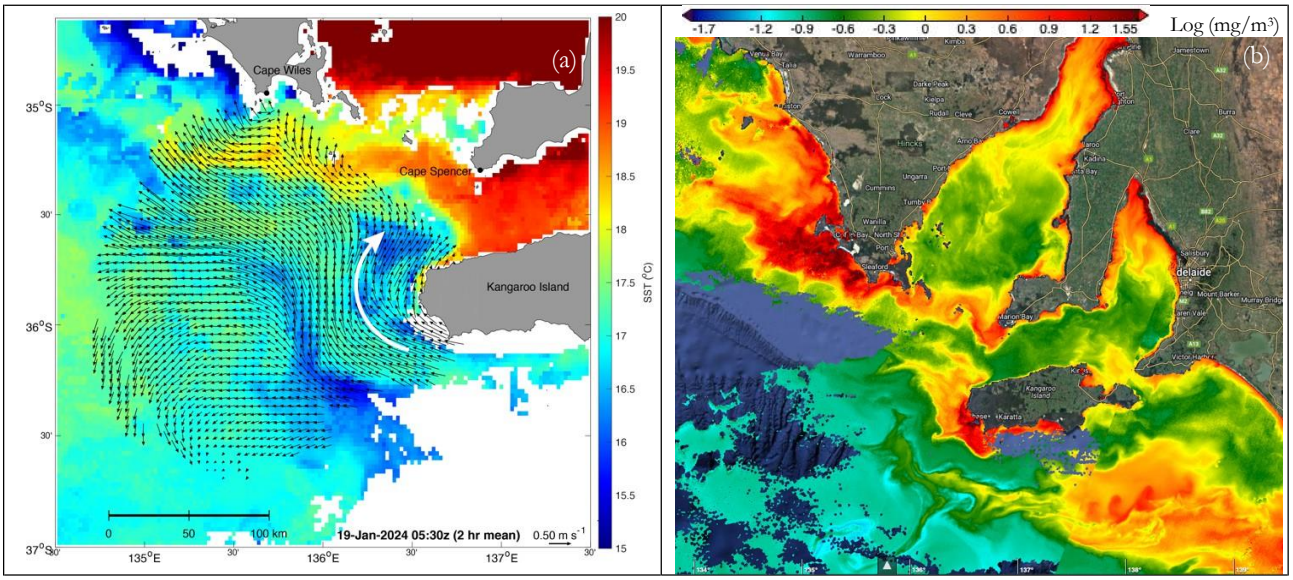

Figure 2 – (a) HF Radar 2-hour mean of surface currents showing flow curvature around Kangaroo Island overlaid on satellite sea surface temperature (SST); and, (b) Sentinel-3 image of surface chlorophyll concentrations at the entrance to the South Australian Gulfs for nearest cloud-free image, 22 January 2024, showing upwelled areas with high chlorophyll concentrations off of Kangaroo Island, Cape Spencer, and Cape Wiles.

References

Alaee, M. J., Pattiaratchi, C., & Ivey, G. (2007). Numerical simulation of the summer wake of Rottnest Island, Western Australia. *Dynamics of Atmospheres and Oceans*, *43*(3), 171-198. https://doi.org/https://doi.org/10.1016/j.dynatmoce.2007.01.001

Geyer, W. R. (1993). Three-dimensional tidal flow around headlands. *Journal of Geophysical Research: Oceans*, *98*(C1), 955-966. https://doi.org/https://doi.org/10.1029/92JC02270

Largier, J. L. (2020). Upwelling Bays: How Coastal Upwelling Controls Circulation, Habitat, and Productivity in Bays. *Annual Review of Marine Science*, *12*(1), 415-447. https://doi.org/10.1146/annurev-marine-010419-011020

Lennon, G. W., Bowers, D. G., Nunes, R. A., Scott, B. D., Ali, M., Boyle, J., Cai, W. J., Herzfeld, M., Johansson, G.,Nield, S., Petrusevics, P., Stephenson, P., Suskin, A. A., & Wijffels, S. E. A. (1987). Gravity Currents And The Release Of Salt From An Inverse Estuary. *Nature*, *327*(6124), 695-697. https://doi.org/citeulike-article- id:6014315

Physical drivers of near shore hypoxia in the western Baltic Sea and consequences for fish stock

Holtermann P. [1], Nauman M. [2], Bukowski C. [3], Haase S. [4], Thiele O. [5], Mohrholz V. [6], and Krumme U. [7]

Keywords: turbulent mixing, physical transport, coastal seas, anoxia, hypoxia, fish stock.

Abstract

Coastal hypoxia is a global and growing threat to the health of coastal marine systems (Breitburg et al. 2018). Since the middle of the last century the deep water of the the Baltic Sea is almost permanently anoxic (Carstensen et al. 2014). The causes and consequences of the anoxia have been studied since then by a manifold of scientists (for example Wulff et al. 1990; Conley et al. 2002; Neumann et al. 2017; Holtermann et al. 2020 and references therein).

In contrast to the anoxia in the deep water of the Baltic Sea, near coastal hypoxia, which is defined here as hypoxic water in depths shallower than 20 m, has not been extensively observed in the Baltic Sea but for roughly a decade several signs point to the direction of an increase of coastal hypoxia (Conley et al. 2011; Lennartz et al. 2014; Piehl et al. 2022). To increase our understanding of the relevance, spatial-, timescales and strength of coastal hypoxia we have setup up a coastal long term observatory in the western Baltic Sea near the town Boltenhagen, an area used as well by commercial and recreational fishers. The observatory measured water velocities, temperature and bottom oxygen concentration along a slope between 5 and 25 m water depth using moored temperature and oxygen sensors in combination with an acoustic current meter. The moorings are accompanied by regularly sampling cruises along the same slope using standard CTD measurements as well as measurements with a velocity shear microstructure probe. Measurements started in Jul. 2021 and are continuing (Naumann et al. in prep.). The most surprising results of the measurements are short term hypoxic events even in the shallowest parts of the sampling area. See Fig. 1A for an overview of a one year record in 10 m depth and Fig. 1B for a detailed zoom of a hypoxic event during Aug. 2022. These events can be shorter than half a day, having oxygen concentrations low enough to be lethal for higher organisms. Such short term events are hard to resolve with a regular monitoring program and require a different monitoring regime, for example a continuous sampling with moored sensors. An investigation of the relevant processes show that the hypoxic events are generated by a combination of coastal upwelling of deep hypoxic water, local turbulent mixing, oxygen consumption processes and lateral transport. Our analysis shows that a major factor for the coastal hypoxia is the oxygen concentration of the deep water in the western Baltic Sea, that is itself highly variable over the course of a year. The contribution of the different processes to coastal hypoxia is discussed.

We found that one of the drivers of the hypoxic events is the increased stratification by the thermocline during the summer months. The thermocline reduces the vertical transport of oxygen and fosters the risk for hypoxia. In addition it reduces the size of usable habitat for fish. For example cod avoid temperatures above 15°C (Freitas et al. 2016) and requires oxygen concentrations well above 30% saturation (Claireaux and Dutil 1992). During the summer months, with the warm upper water above the thermocline, large areas of the western Baltic are unhabitable by cod. We show that additionally to the warm surface waters, within the observation location, which has been a fishing ground for cod, almost 50% of the time of the year, the watercolumn has extremely unfavourable abiotic conditions for cod. This is by a combination of the warm surface water with the local hypoxia, which is both lethal to fish and caused by the physical processes discussed above. The fish become heckled by heat and anoxia, see also Fig. 2 for a schematic representation of the processes. The lack of continuous habitat use may be a major stressor to cod (Receveur et al. 2022) and other fish species. Moreover, local up- and downwelling events could lead to increased natural mortality in cod, thus possibly providing a link to the missing recovery of the western Baltic cod stock despite historically low fishing pressure. While the presented measurement are a local study, they are nevertheless shedding light on the potentially strong negative effects of hypoxia and a warming climate on shallow non-tidal estuarine ecosystems. They do serve as well as the basis for a subsequent study that will extrapolate these processes to the western Baltic Sea using high resolution numerical modeling.

[1] Leibniz Institute for Baltic Sea Research, Warnemünde, peter.holtermann@io-warnemuende.de
[2] Leibniz Institute for Baltic Sea Research, Warnemünde, michael.naumann@io-warnemuende.de
[3] Thünen Institute of Baltic Sea Fisheries, carl.bukowski@thuenen.de
[4] Thünen Institute of Baltic Sea Fisheries, stefanie.haase@thuenen.de
[5] University of Rostock, oliver.thiele@uni-rostock.de
[6] Leibniz Institute for Baltic Sea Research, Warnemünde, volker.mohrholz@io-warnemuende.de
Thünen Institute of Baltic Sea Fisheries , uwe.krumme@thuenen.de

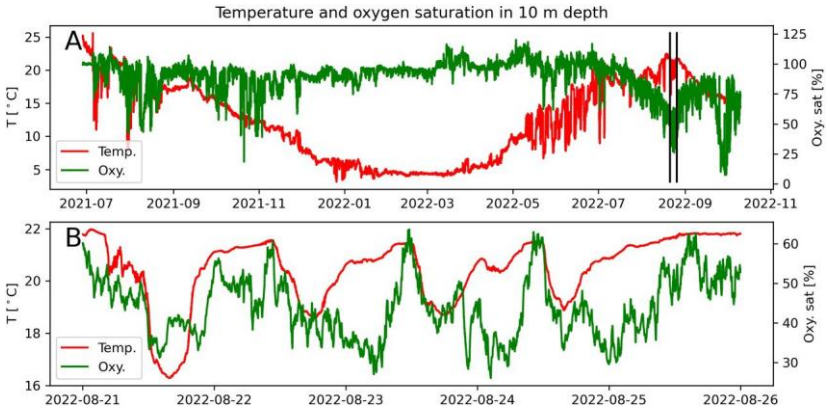

Figure 1: Temperature and oxygen saturation at the Boltenhagen observatory, western Baltic Sea, in 10 m water depth (0.5 m above the seafloor). Temperature in red, oxygen in green. Black lines in A depict a zoom of panel B.

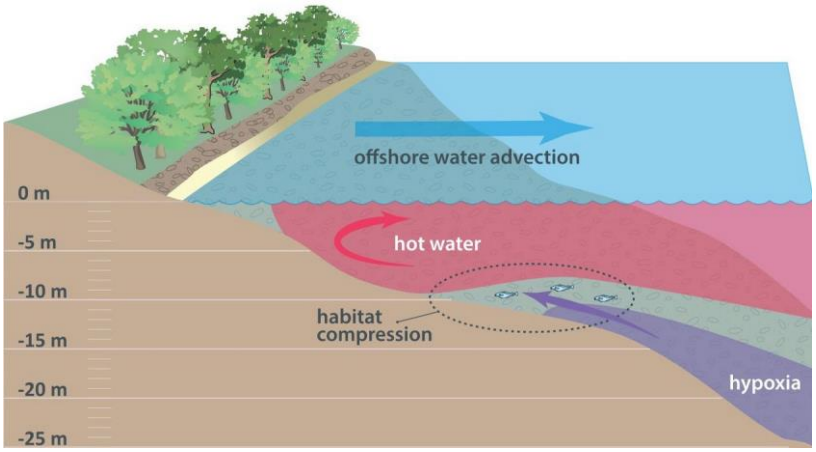

Figure 2: Sketch of the habitat compression of a cod population due to a thermocline in the upper watercolumn and hypoxia near the seafloor. These effects can be generated or amplified by local water mass transport mechanisms as, for example, upwelling.

References

Breitburg, D., L. A. Levin, A. Oschlies, and others. 2018. Declining oxygen in the global ocean and coastal waters. Science 359: eaam7240. doi:10.1126/science.aam7240

Carstensen, J., J. H. Andersen, B. G. Gustafsson, and D. J. Conley. 2014. Deoxygenation of the Baltic Sea during the last century. Proc. Natl. Acad. Sci. 201323156. doi:10.1073/pnas.1323156111

Claireaux, G., and J.-D. Dutil. 1992. Physiological Response of the Atlantic Cod (Gadus Morhua) to Hypoxia at Various Environmental Salinities. J. Exp. Biol. 163: 97–118. doi:10.1242/jeb.163.1.97

Conley, D. J., J. Carstensen, J. Aigars, and others. 2011. Hypoxia Is Increasing in the Coastal Zone of the Baltic Sea. Environ. Sci. Technol. 45: 6777–6783. doi:10.1021/es201212r

Conley, D. J., C. Humborg, L. Rahm, O. P. Savchuk, and F. Wulff. 2002. Hypoxia in the Baltic Sea and Basin-Scale Changes in Phosphorus Biogeochemistry. Environ. Sci. Technol. 36: 5315–5320. doi:10.1021/es025763w

Freitas, C., E. M. Olsen, H. Knutsen, J. Albretsen, and E. Moland. 2016. Temperature-associated habitat selection in a cold- water marine fish. J. Anim. Ecol. 85: 628–637. doi:10.1111/1365-2656.12458

Holtermann, P., R. Prien, M. Naumann, and L. Umlauf. 2020. Interleaving of oxygenized intrusions into the Baltic Sea redoxcline. Limnol. Oceanogr. 65: 482–503. doi:10.1002/lno.11317

Lennartz, S. T., A. Lehmann, J. Herrford, F. Malien, H.-P. Hansen, H. Biester, and H. W. Bange. 2014. Long-term trends at the Boknis Eck time series station (Baltic Sea), 1957–2013: does climate change counteract the decline in eutrophication? Biogeosciences 11: 6323–6339. doi:10.5194/bg-11-6323-2014

Naumann, M., P. Holtermann, C. Bukowski, S. Haase, V. Mohrholz, O. Thiele, and U. Krumme. in prep. Seasonal coastal hypoxia in the western Baltic Sea – A: testcase for high resolution timeseries measurements for quantification of dynamics in duration, effected volumes and areas.

Neumann, T., H. Radtke, and T. Seifert. 2017. On the importance of Major Baltic Inflows for oxygenation of the central Baltic Sea. J. Geophys. Res. Oceans. doi:10.1002/2016JC01252

Piehl, S., R. Friedland, B. Heyden, W. Leujak, T. Neumann, and G. Schernewski. 2022. Modeling of Water Quality Indicators in the Western Baltic Sea: Seasonal Oxygen Deficiency. Environ. Model. Assess. doi:10.1007/s10666-022-09866-x

Receveur, A., M. Bleil, S. Funk, S. Stötera, U. Gräwe, M. Naumann, C. Dutheil, and U. Krumme. 2022. Western Baltic cod in distress: decline in energy reserves since 1977. ICES J. Mar. Sci. 79: 1187–1201. doi:10.1093/icesjms/fsac042

Wulff, F., A. Stigebrandt, and L. Rahm. 1990. Nutrient Dynamics of the Baltic Sea. Ambio 19: 126–133.

Diagnosing the drivers of cross-shore freshwater flux through the surf zone

Horner-Devine A. [1], Giddings S. [2], Lou Y. [3], Simpson A. [4], Derakhti M. [5], Flores R. [6], Williams M. [7], Kastner S. [8], Thomson J. [9], Spydell M. [10], Byrne S. [11], and Rodriguez A. [12]

Keywords: physics, river plume, surf zone, waves

Abstract

Freshwater carried to the coastal ocean by rivers typically carries sediment, nutrients and pollutants that can impact the coastal ecosystem. In small systems, discharge often occurs on short timescales associated with storm events that carry high concentrations of terrestrial material from the watershed. At the coast, wave action has been observed to trap freshwater discharge in the surf zone, increasing the residence time of water-borne pollutants and other material nearshore. While transport and mixing processes in large-scale river systems, which are unaffected by surf zone processes, have been studied for decades (Horner-Devine *et al*., 2015), the processes that mix, retain and transport freshwater from small rivers discharging into the surf zone is not well understood. This research seeks to understand the following questions: 1) under what conditions is river water trapped in the surf zone instead of being discharged directly to the inner shelf? 2) can these conditions be generalized and applied across a range of sites? 3) what are the primary processes responsible for the cross-shelf exchange of freshwater that is initially trapped in the surf zone? The present research addresses these questions using data from field campaigns in three different coastal river systems and compared with idealized numerical modelling results.

Prior idealized numerical modelling showed that trapping of freshwater in the surf zone depends on offshore wave height (Hs) and river discharge (Q); trapping occurs preferentially for higher values of wave height and lower values of discharge (Rodriguez et al., 2018). This work concluded that the trapping was a result of the competition between the radiation stress gradient and river momentum. In a separate modelling and observational study, Wong et al. (2013) showed that the wave angle was also important to the fate of coastal discharge; as waves deviate from shore-normal, alongshore currents in the surf zone deflect the discharge jet, causing it to be trapped in the surf zone. They develop a dimensionless ratio that compares the cross-shore length scale imposed by the alongshore current (L_a) with the surf zone width (L_{sz}). They show that their field observations from San Pedro Creek CA are consistent with the trapping limit suggested by this ratio. Using drifter-based field observations in the Quinault River WA, Kastner *et al*. (2019) found that an alternative ratio, (L_{nf}/L_{sz}) provided a reasonable prediction for trapping of the plume. Here, L_{nf} is the nearfield length scale, which characterizes the momentum of the river discharge. They also observed escapes during low discharge periods, when wave breaking was interrupted offshore of the river mouth due to a channel. This latter case occurred when the channel length L_c exceeded L_{sz}. More recently, Lou *et al* (in prep), using a numerical model of an idealized plume, found that the alongshore plume extent and the volume of freshwater trapped in the surf zone scaled with L_{nf}/L_{sz}.

In the present work, we compile 112 field observations of plume fate from three river systems to address the three questions listed above. For each of the field observations we have obtained corresponding independent parameters that influence the fate of freshwater in the surf zone: H_s, Q, wave direction, tidal elevation and phase, and discharge velocity. The compiled data set also includes an assessment of whether or not the plume was trapped in the surf zone. This assessment was based on: 34 drifter tracks from the Quinault River WA (Kastner et al., 2019), 72 high resolution satellite images from the Maipo River, Chile (Flores *et al*., 2022; Moreno, 2023) and six dye releases from Los Peñasquitos Lagoon, CA. The dye releases at the mouth of Los Peñasquitos Lagoon (LPL) took place in January - February 2023 as part of the Plumes in Nearshore Conditions (PiNC) project led by S. Giddings and A. Horner-Devine. This experiment included moorings, drifters, hyperspectral and RGB drone imaging and jetski transects. For the current work we focus on the six dye releases that occurred on 1/20/2023, 2/1/2023 and 2/2/2023. Two dye releases were conducted per day, early and late in the ebb tide. Please see descriptions of the Quinault data in Kastner et al., (2019) and Maipo River data in Flores *et al*., (2022) and Moreno, (2023).

[1] University of Washington, arhd@uw.edu
[2] Scripps Institution of Oceanography, UCSD, sgiddings@ucsd.edu
[3] University of Washington, yzlou@uw.edu
[4] US Army Corps of Engineers, ajoysimpson@gmail.com
[5] University of Washington, mderakhti@apl.uw.edu
[6] Universidad Technica Federico Santa Maria, raul.flores@usm.cl
[7] Pontificia Universidad Católica de Chile, mwilliams@bio.puc.cl
[8] Western Washington University, kastnes@wwu.edu
[9] University of Washington, jthomson@apl.washington.edu
[10] Scripps Institution of Oceanography, UCSD, mspydell@ucsd.edu [11]Scripps Institution of Oceanography, UCSD, s2byrne@ucsd.edu
[12] Jet Propulsion Laboratory, Caltech, angelica.rodriguez@jpl.nasa.gov

Figure 1 shows a preliminary result, in which all 112 observations from the three study systems are plotted on the L_{nf}/L_{sz} and L_c/L_{sz} regime plot proposed by Kastner *et al*., (2019). As predicted, escapes (traps) tend to occur for higher (lower) values of L_{nf}/L_{sz}. However, there are many exceptions, and the predictive skill of this approach is relatively low.

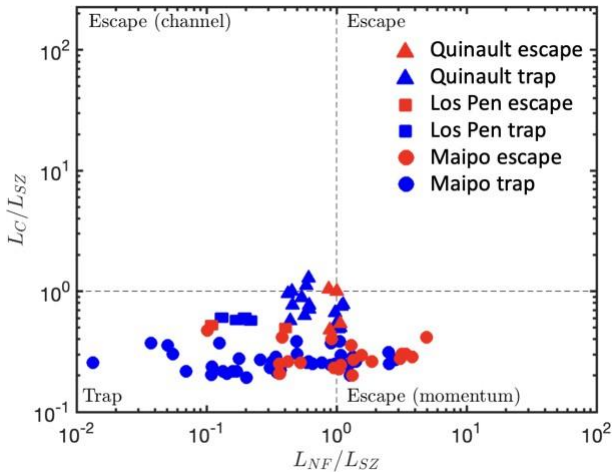

Figure 1: Regime plot of plume fate based on observations from the Quinault River WA, Los Peñasquitos Lagoon, CA and the Maipo River, Chile.

While the L_{nf}/L_{sz} scaling successfully explains the variability with Q and Hs in an idealized model (Lou *et al*., (in prep), it is clear in Figure 1 that there is much more variability in natural systems. This work will evaluate whether this variability can be characterized to improve our ability to predict the fate of freshwater in the surf zone. In addition, we will evaluate the conditions that activate secondary transport pathways such as rip currents, which are observed often in the LPL and Maipo River observations.

References

Flores, R., M. E. Williams, A. R. Horner-Devine. (2022) River plume modulation by infragravity wave forcing. Geophysical Research Letters 49, e2021GL097467

Horner-Devine, A. R., R.D. Hetland and D.G. MacDonald, (2015). Transport and mixing in coastal river plumes. Annual Review of Fluid Mechanics 47:569–94.

Kastner, S. E., Horner-Devine, A. R., Thomson, J. M. (2019). A conceptual model of a river plume in the surf zone. Journal of Geophysical Research: Oceans, 124, 8060–8078. https://doi.org/10.1029/2019JC015510.

Moreno, F.I.(2023). Caracterización de la interacción de la plume del Río Maipo con la zona de rompiente de oleaje mediante análisis de imágenes satelitales. Honors thesis. Universidad Technica Federico Santa Maria.

Rodriguez, A. R., Giddings, S. N., Kumar, N. (2018). Impacts of nearshore wave-current interaction on transport and mixing of small-scale buoyant plumes. Geophysical Research Letters, 45, 8379–8389. https://doi.org/10.1029/2018GL078328.

Wong, S. H. C., Monismith, S. G., Boehm, A. B. (2013). Simple estimate of entrainment rate of pollutants from a coastal discharge into the surf zone. Environmental Science and Technology, 47(20), 11,554–11,561. https://doi.org/10.1021/es402492f.

The role of storm winds and river discharge in modulating overtides in a well-mixed reach of an estuary

Huguenard K. [1,2] and Lakmali E. [2]

Keywords: tide, surge, river interaction, tidal distortion, subtidal flows

Abstract

Storm surge and river discharge cause tidal distortion by modulating superharmonics in long, shallow estuaries. Sixth- and eighth- diurnal overtides can be exacerbated during storm events, and their amplitudes can exceed water levels driven by storm surge alone. The exact mechanism responsible for the tidal distortion, such as currents induced by wind, storm surge, or river discharge, isn't well understood. This work aims to discern how storm events enhance overtides in the Penobscot River, which is an estuary that features moderate tidal distortion and tide-surge-river interactions. Field observations were collected from August to November 2023, where two moored Acoustic Doppler Current Profilers (ADCPs) collected profiles current velocities at two locations- one near a partially removed dam and one farther downstream. These observations were complemented by eight pressure sensors measuring water levels along the river in order to understand spatial patterns of storm influenced currents and water levels. A rare storm event, Hurricane Lee, skirted the coast of Maine, inducing significant offshore wind and increased precipitation. The storm effects can be considered in two phases, where the first phase features the initial passage of the storm with strong winds (15 m/s), low barometric pressure and a slight increase in precipitation on September 15th. The second phase occurs after winds have calmed, yet the river discharge continues to increase, peaking approximately 4 days after the storm passage at Q > 1000 m3/s. The storm influenced spatial differences in the water levels during both phases, where the D2 tidal species amplitude reduced upstream, and D6 and D8 oscillations were identified during both storm phases. Offshore wind during phase 1 did not markedly affect D2 tidal currents, but it did modulate D6 and D8 tidal currents. Conversely, elevated river discharge during phase 2 did enhance D2 currents, in addition to D4, D6 and D8 currents. A measure of tidal distortion can be assessed by comparing the relative amplitudes of overtide velocities with that of the principal tide. During the initial passage of the storm where winds and river discharge acted in concert, tidal distortion was enhanced and dominated at the D8 superharmonic, with D6/D2 = 1.09 and D8/D2 = 1.34, compared to D6/D2 and D8/D2 = 1 during non-storm conditions. During phase 2, where river discharge was the primary external forcing, tidal distortion was diminished under increasing mean flows, where D6/D2 = 0.9 and D8/D2 = 0.78. The storm also promoted a shift in subtidal flow direction from predominantly landward, induced by flood dominant tidal distortion, to seaward during the duration of the storm effects. These results indicate that external forcing by wind and river discharge can modulate overtides during extreme conditions, and the amplitudes of overtide velocities exceed that of the principal tide under the action of wind. This suggests that storm events may play a role in the local resuspension and seaward export of sediment during extreme events.

[1] Associate Professor – Civil and Environmental Engineering 313 Boardman Hall University of Maine, United States
[2] University of Maine – University of Maine, Orono, Maine 04469, United States

Temperature variability scales at the Río de la Plata estuary and its maritime front

Jackson M. [1], Fossati M. [2], Mateus M. [3], and Pinto L. [4]

Keywords: estuaries, temperature, Río de la Plata, in situ data, numerical modelling.

Abstract

The Rio de la Plata is an estuary, located between Uruguay and Argentina that discharges into the Atlantic Ocean (Figure 1). It has relevant features such as high fluvial discharges from Parana and Uruguay rivers (second highest basin in South America), micro-tidal astronomical tides and relevant meteorological tide, and strong effect from the atmospheric forcing such as winds and pressures at the surface. This combined with its particular geometry, lead to very complex hydrodynamic conditions.

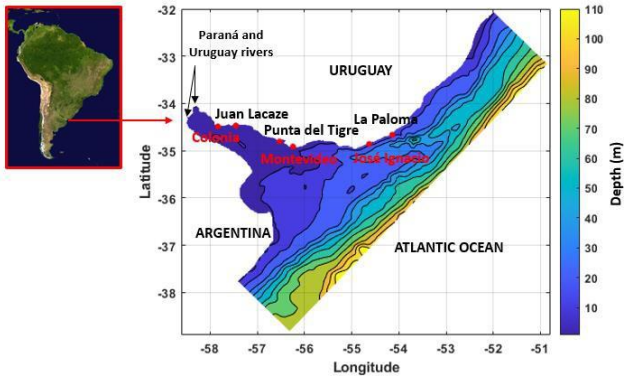

Figure 1- Río de la Plata estuary location. Red dots indicate some of the stations with temperature in situ data.

Over the years, much progress has been made in the knowledge of the estuary regarding variables such as sea level, currents, waves and salinity, both through measurements analysis (e.g. Mosquera & Pedocchi, 2019) and the implementation of 2D (e.g. Santoro et al, 2017) and 3D (e.g. Jackson *et al*, 2021) numerical models. Despite the importance of improve research regarding temperature dynamics as a means to manage water quality issues in the Uruguayan coasts, there are no specific local studies describing the dynamics of temperature and its dependence on the different processes involved and the estuarie forcings. However, in recent years, efforts have been made through research projects and others that managed to leave a large data base of historical measurements (e.g. Simionato et al, 2011). Neverthless, these data present several measurement frequencies and was made in different periods, which does not allow a complete understanding of the processes and variability scales of water temperature.

Thus, the objective of the present work is to improve knowledge of the estuary by applying a numerical model to resolve temperature. In particular, the 3D baroclinic hydrodynamic numerical model MOHID (Mateus and Neves 2019) is applied, which solves the flow governing equations using the finite element approach, with the hydrostatic and boussinesq approximations.

In addition, in order to obtain a model that could be used as a temperature prediction tool, we work with global forecast models as forcing to the local model. Through what is observed in the measured data, we look forward to analyze which processes related to temperature are explain by measurements, as well as which scales of variation are related to the different forcing of the estuary.

Figure 1 shows several of the measurement stations where temperature in situ data are available. On the other hand, as an example, figure 2 shows measurements along year 2019 corresponding to the stations Juan Lacaze, Punta del Tigre and Jose Ignacio (figure 1), one located closer to the rivers discharge, one in the estuary intermediate zone and another on the Atlantic Ocean. An annual scale variation is clearly observed in all stations corresponding to high temperatures in the summer months and low temperatures in the winter months.

The MOHID numerical model has been successfully implemented in the estuary of the Río de la Plata in previous works, modelling variables such as sea level, currents (Alonso et al, 2017) and salinity (Jackson et al, 2021). Regarding temperature, the model has been used in other estuary with good results (De Pablo et al 2019).

[1] IMFIA, Facultad de Ingeniería, Universidad de la República de Uruguay, mjackson@fing.edu.uy.
[2] IMFIA, Facultad de Ingeniería, Universidad de la República de Uruguay, mfossati@fing.edu.uy.
[3] MARETEC, Instituto Superior Técnico, Universidad de Lisboa, marcos.mateus@tecnico.ulisboa.pt
[4] MARETEC, Instituto Superior Técnico, Universidad de Lisboa, ligia.pinto@tecnico.ulisboa.pt

By modeling scenarios from less to more forcings, we seek to analyze the influence of the different forcing on temperature dynamics. In order to correctly model the temperature, all forcings considered includes:

- Freshwater fluvial discharges with continental water temperature.
- Astronomical and meteorological tide from open ocean boundary.
- Temperature and salinity from open ocean boundary.
- Winds and pressures at sea surface.
- Air temperature, relative humidity, clouds and radiation at the sea surface.

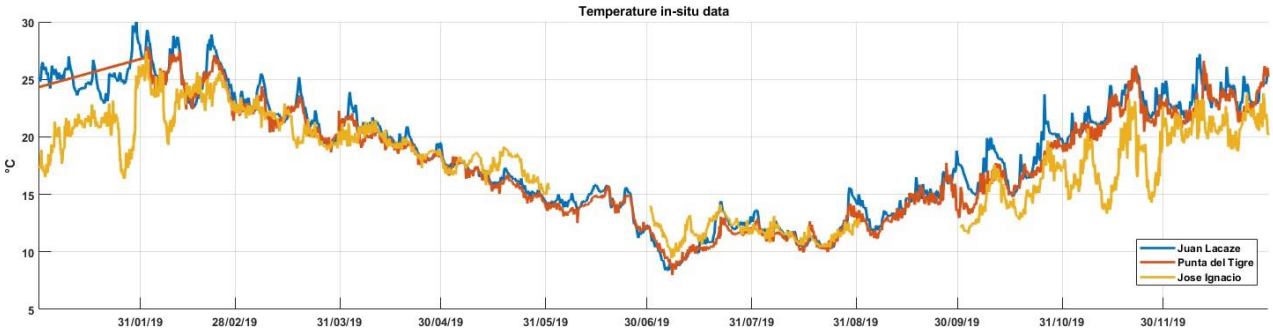

Figure 2- Surface water temperature mesured data in Juan Lacaze, Punta del Tigre and José Ignacio stations for 2019.

The domain used for the simulations arises from previous work (e.g. Alonso et al 2017) and comprises the Río de la Plata and the Atlantic Ocean continental shelf. The grid is structured in longitude-latitude with a resolution of 0.1°x0.1° and sigma layers vertical discretization. A sensitivity analysis of the domain, spatial and vertical discretization is being carried out. Data from NOAA-NCEP RTOFS-HYCOM model, combined with FES2014 is used as ocean boundary forcing for sea levels, while those used as atmospheric forcings are from NOAA GFS with 1/4° spatial resolution. Mean fluvial discharges based on historical series are used as the fluvial boundary.

	Vertical discretization	**Ocean boundary**	**Discharges**	**Surface**
Sim 1	10 sigma	AT, MT	Annual mean with T	W, P
Sim 2	10 sigma	AT, MT, T and S	Annual mean with T	W, P
Sim 3	10 sigma	AT, MT, T and S	Annual mean with T	W, P, Air T, RH
Sim 4	20 sigma	AT, MT, T and S	Annual mean with T	W, P, Air T, RH

Table 1-Simulation details. AT: astronomical tide; MT: meteorological tide; T: temperature; S: salinity; W: wind; P: pressure; RH: relatuve humidity

Figure 3 shows as an example the annual temperature series in Montevideo (Figure 1) obtained as results of the model with different forcings according to table 1. Radiation in these cases is calculated by the model at surface level and cloudiness is not considered. It is mainly observed that the annual cycle observed in the measurements analyzed along the estuary is only captured by including the air temperature and relative humidity forcing. This way, we continue analyzing the dependence of different scales and processes with the forcings, as well as the effect of the simulation characteristics.

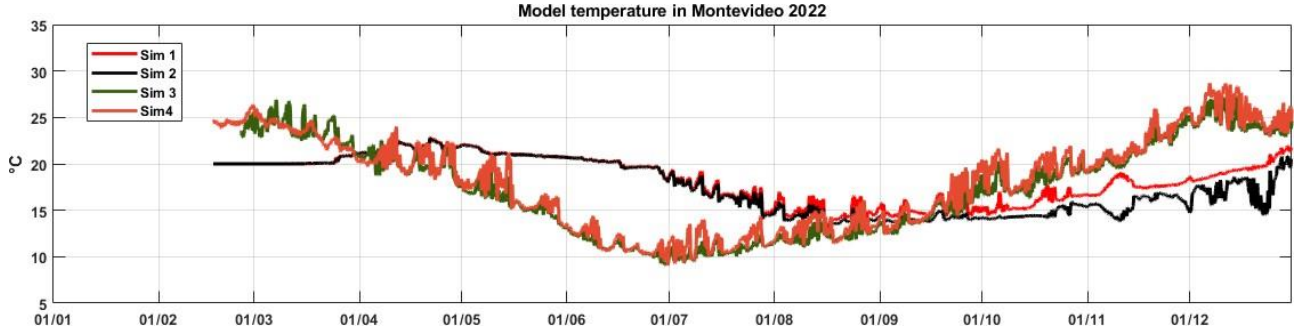

Figure 3-Model temperature from simulations according to table 1.

References

Alonso, R., Jackson, M., Santoro, P., Fossati, M., Solari, S., (2017). Wave and tidal energy resource assessment in Uruguayan shelf seas. Renewable Energy, 114A, 18-31.

De Pablo, H., Sobrinho, J., Garcia, M., Campuzano, F., Juliano, M., Neves, R. (2019). Validation of the 3D-MOHID Hydrodynamic Model for the Tagus Coastal Area. Water, 11, 1713.

Jackson, M.; Sienra, G.; Santoro, P.; Fossati, M. (2021). Temporal and Spatial Variability Scales of Salinity at a Large Microtidal Estuary. J. Mar. Sci. Eng, 9, 860. https://doi.org/10.3390/jmse9080860.

Mateus M. and Neves R. (eds.) (2013). Ocean modelling for coastal management – Case studies with MOHID. IST Press. Mosquera, R., Pedochi, F. (2019). Salinity estimation from Acoustic Doppler Velocimeter measurments. Continental Shelf Research, 180, 59-62.

Santoro, P., Fossati, M., Tassi, T., Huybrechts, N., Pham Van Bang, D., Piedra-Cueva, I., (2017). A coupled wave–current– sediment transport model for an estuarine system: Application to the Río de la Plata and Montevideo Bay. Applied Mathematical Modelling, 52, 107-130.

Simionato, C., Moreira, D., Piedra Cueva, I., Fossati, M. (2011). Proyecto FREPLATA – FFEM Modelado numérico y mediciones in-situ y remotas de las transferencias de sedimentos finos a través del Río de la Plata. Parte A : adquisicíon de datos.

Rheological properties of cohesive sediments from Gironde estuary and their impact on the erosion threshold

Jarny S. [1], Gomit G. [2], Gelmi L. [3], and Thomas L. [4]

Keywords: rheology, cohesive sediments, erosion threshold.

Abstract

The accumulation of cohesive sediments is one of the most prominent issues in many tidal estuaries, as it has major implications on estuarine morphodynamics and on water quality and dredging strategies to support harbour activities. The work presented here focuses on the Gironde estuary, and more specifically on the Cadillac site located 40 km upstream of Bordeaux where sediments were taken.

The first step was to characterise the physical properties of these materials by means of a granulometric analysis and rheological tests. Granulometric analysis (Mastersizer 3000, Malvern) is used to ensure the homogeneity of the sediments taken during the various campaigns. These reworked materials are then studied from a rheological point of view (HR2, TA Instruments) in order to identify in particular their yield stress for setting in motion (Yang et al. [1]). After testing several methods of determining yield stresses, using stress ramps, oscillations and flow curves, our choice fell on flow tests which were carried out in a coaxial disc geometry in order to define the corresponding rheogram (Fig.1a). The Hershel-Bulkley behaviour law is then applied to the down curve to identify the yield stress. Once the protocol has been established, the effect of concentration is measured by diluting the sediments taken and the concentration is measured a posteriori by weighing the samples before and after drying. In this way, the law governing the evolution of yield stress as a function of concentration can be established (Fig.1b). A power law can be applied, providing a good model of the observed behaviour.

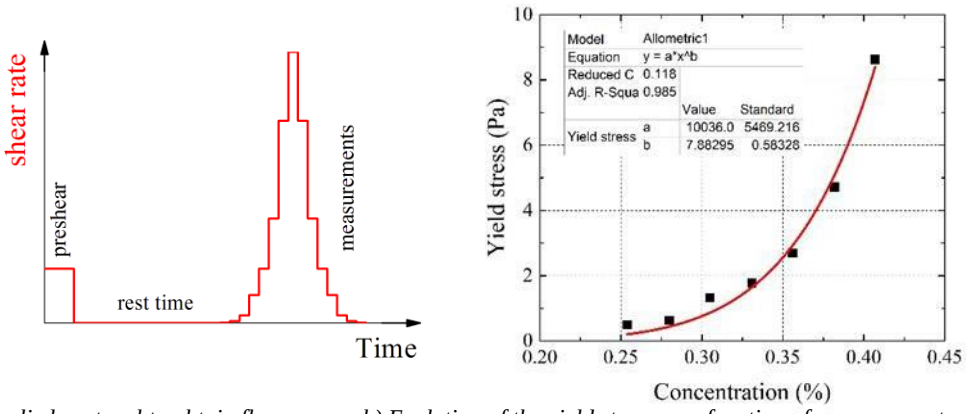

Figure 1. a) Applied protocol to obtain flow curves. b) Evolution of the yield stress as a function of mass concentration of sediment.

Erosion tests were then carried out in a laboratory channel. The sediments were placed in the space left free between two ramps placed at the bottom of the channel (Fig. 2a). Initially, the threshold stress for setting the various samples in motion was established by gradually increasing the flow rate in the channel for a given height of water. The flow rate at which movement starts to occur on the sediment surface is noted (Fig. 2b). This flow rate is then translated into parietal stress on the bottom using PIV calibration on a rigid surface. In a previous study to qualify the channel (Nihlat [2]), PIV velocity field measurements were carried out in the developed boundary layer. Analysis of the velocity profiles using the closer-chart method made it possible to trace the parietal stresses on the bottom of the channel (in this study, the sediments were replaced by a rigid PMMA block). It is assumed that the friction stress on the rigid bottom is equal to the minimum stress required to set the sediment in motion. These tests are repeated for different sediment concentrations. In this way, the thresholds for erosion initiation are related to the rheological yield stress of the sediments.

[1] Prime Institute, CNRS-University of Poitiers-ISAE ENSMA, Poitiers, FRANCE, sebastien.jarny@univ-poitiers.fr
[2] Prime Institute, CNRS-University of Poitiers-ISAE ENSMA, Poitiers, FRANCE, guillaume.gomit@univ-poitiers.fr
[3] Prime Institute, CNRS-University of Poitiers-ISAE ENSMA, Poitiers, FRANCE, lisagelmi@gmail.com
[4] Prime Institute, CNRS-University of Poitiers-ISAE ENSMA, Poitiers, FRANCE, lionel.thomas@univ-poitiers.fr

Hydropower peaking in the Lower Columbia River Estuary: capturing transient tidal processes using "super-resolution"

Jay D.A. [1], Lobo M. [2], Talke S.A. [3], Dykstra S.L. [4], Innocenti S. [5], and Matte P. [5]

Keywords: river-estuary, tidal river, non-stationary tides, tidal analysis methods.

Abstract

Introduction

Here, we attempt to define the physics of a transient, quasi-tidal phenomenon—hydropower peaking from a reservoir at the head of a tidal river, the Lower Columbia River Estuary (LCRE)—and to inquire how to best capture a process that challenges time-frequency resolution limits set by the Heisenberg Uncertainty Principle. Demand for hydropower exhibits diel (period 24 hr) and weekly (W7D) cycles, both of which vary seasonally. A diel cycle in water level (WL) has the same period as minor tidal constituent S1, whose origin is usually mostly radiational (e.g., from diel sea breeze). S1 is difficult to capture in a short tidal analysis window, because it is sandwiched between two of the three largest diurnal (D1) constituents, P1 and K1, from which it differs by only ±1 cy/yr. The S1 and W7D waves propagate and damp seaward from Bonneville Dam (at Rkm 233), but are detectable to the head of the estuary, 87 km from the ocean (Jay et al., 2016). Accordingly, average S1 amplitude () increases from about 10-20 mm in the estuary to >80 mm below the dam (Fig. 1). Also, as they propagate, the S1 and W7D waves are subject to nonlinear friction, creating many overtides; e.g., at N2 (approximately =O1+S1), S2 (=2×S1) and 3.5 d (AKA W3.5D=2×W7D). Accordingly, the time-average ratio increases by ~3.5× from the Rkm 29 to Rkm 232, and grows modestly (Fig. 1).

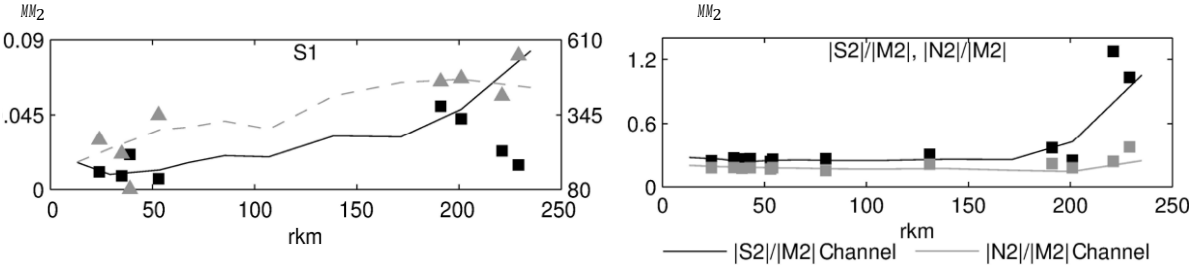

Figure 1: Harmonic analysis results (1-year window) for channel stations (continuous curves) and floodplain stations (symbols): left, average amplitudes in m (black) and phases (gray) of S_1; and right, constituent ratios as a function of rkm (from Jay et al.*, 2016).*

The above statistics are annual averages obtained by harmonic analysis (HA). However, when salmon spawn below the dam, what matters for survival of the eggs is the magnitude of the WL fluctuations (largely driven by power peaking) during a spawning period of 1-2 weeks. Accordingly we need to derive time-variable estimates of tidal species properties (e.g., $|DD1|$ to $|DD4|$, |W3.5D|, and |W7D| and their corresponding phases), but also of transient constituent values like $|PP1|$, $|SS1|$, and $|KK1|$ (and other constituents), needed to quantify the role of power peaking in WL fluctuations. Moreover, a sizeable

$SS1$wave provides an opportunity to look at tidal dynamics, by looking for fluctuations in constituents like N2, R2 (=$SS1$+$KK1$),

S2 (=S1+S1 or $PP1$+$KK1$) and T2 (=$SS1$+$PP1$). While S2 is a large constituent, R2 and T2 are small and only □1 cy/yr from S2. The Heisenberg Principle (and its cousin the Rayleigh Criterion) suggest that a window approaching 1 yr is needed to estimate R2 and T2; clearly, we need to cheat efficiently on Heisenberg Principle to capture transient variations.

Method

How to proceed? We employ here a new continuous wavelet transform (CWT) tidal analysis code written in Matlab, CWT_Multi (available from https://github.com/mjclobo/CWT_Multi; Lobo et al., 2024) that implements the Munk-Hasselman idea of super-resolution beyond the limits of the Rayleigh criterion, based on the background noise level of the data (Munk and Hasselman, 1964).

[1] Department of Civil & Environmental Engineering, Portland State University, Portland, OR USA

[2] Princeton University, Atmospheric and Oceanic Sciences Program, Princeton, New Jersey

[3] Department of Civil & Environmental Engineering, Cal State Polytechnic University at San Luis Obispo

[4] College of Fisheries and Ocean Science, University of Alaska Fairbanks, Fairbanks, Alaska

[5] Environment and Climate Change Canada, Meteorological Research Division, Québec City, Québec, Canada

It provides tidal species estimates on times scales of a few days and estimates for selected constituent groups (the 3-4

largest in the D_1 to D_4 species, e.g., N_2, M_2 and S_2) with fortnightly filters (weekly time scale=half the filter length). This is possible despite the strong overlap of the constituent filters, because wavelet convolution is linear and the response functions of the filters are known. Obtaining estimates for smaller constituents requires another step – we define a new form of tidal inference ("Dynamic Inference" or DynIn) that uses constituent ratios defined with 6-mo filters (time scale = 3 mo) to separate constituents like P_1, S_1 and in the constituent group, and T_2, S_2, R_2, and K_2 in the S_2 constituent group. No user-defined constituent ratios are needed. DynIn assumes that the constituent ratios found with the 6-mo filters are stable over the several month time scale of the filter – this is not entirely true for power peaking, but results suggest that the assumption is good enough. CWT_Multi also provides SNR estimates, confidence limits, and a novel constituent selection criterion, with the standard error defined by either a Residual Spectrum or a Moving-Block method, the latter per Innocenti et al. (2022).

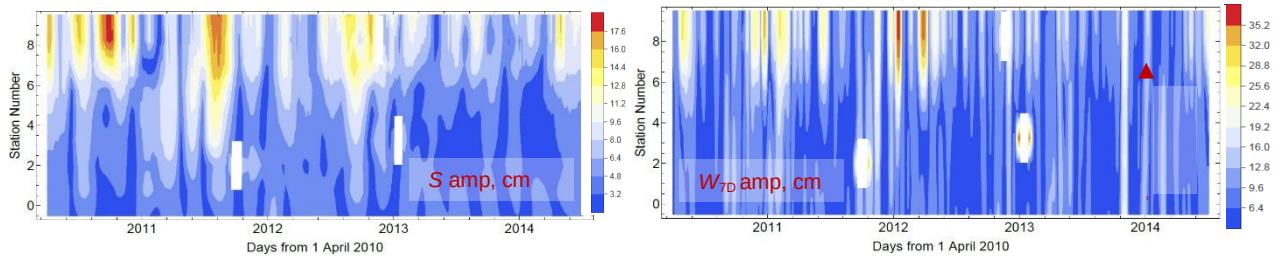

Fig. 2: A time-space view of S_1 (left) and W_{7D} (right) amplitude in the LCRE over a 3.5 yr period. Station 1 is at Rkm-29, Station 9 at Rkm 232, determined by CWT_Multi. Amplitudes larger than ~20 mm have SNR >2.

Results

We show the time time-space dependent variability of S_1 and W_{7D} in Figure 2. Obviously, both are highly variable, and have their greatest amplitude upriver. Both also penetrate to Station 1 (Rkm-29) at times, though there is also weekly variability entering from the ocean, strongest in winter. $|W_{7D}|$ can reach 0.35m while $|S_1|$ can be as large 0.17m near the dam, with amplitudes 30-60% that large at stations 7 and 8, of significance to navigation in Portland Harbor. We can also compare outputs at the fortnightly level (after DynIn) with those from the seasonal filters (Figure 3). While we expect the fortnightly filters to show additional detail, large deviations might indicate that the DynIn process was unstable; fortunately, the DynIm results seem stable, and $|S_1|$ is consistently larger than $|P_1|$. Finally, it is useful to examine small constituents like T_2 using an admittance (γ); i.e., a complex ratio of T_2 at upriver stations to its value at Rkm-29. (Fig. 4). Clearly, $|T_2|$ is much elevated upriver, suggestive of nonlinear effects.

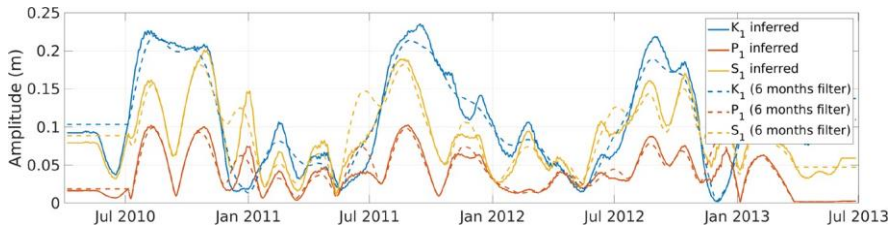

Fig. 3: Amplitudes for the K1 constituent group (K1, S1 and P1) at Rkm-171.5 found using DynIm (solid lines) and from the 6-mo filters (dotted); end effects are evident in the first and last 3 mo. The strong annual cycle stems from the damping effects of river flow.

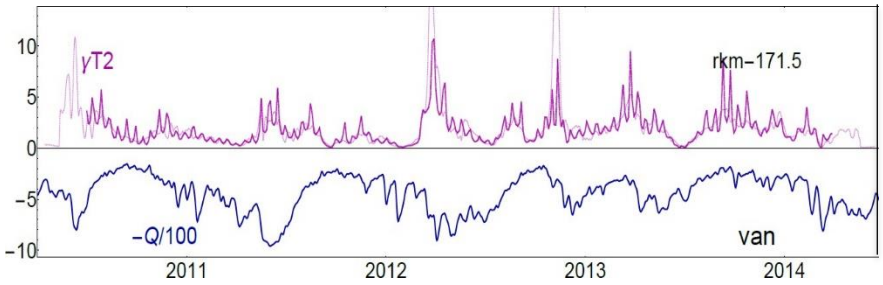

Fig. 4: Admittance amplitude $|\gamma_{T2}|$ (unitless) at Rkm 171.5; the solid line has been smoothed for clarity.

Conclusions and caveats

The preliminary results shown here are encouraging—the S_1 and W_{7D} results are statistically robust and represent seaward propagation of waves from Bonneville Dam most of the way to the ocean. Other results are less clear. Yes, $|T_2|$ is elevated upriver, but we cannot conclude that we are observing nonlinear generation, absent a careful examination of the frequency structure of the river flow input at the dam. Also, it may be hard to disentangle the marine N_2 from the nonlinear component generated near the dam, and R_2 results are not very satisfactory. On the other hand, we are also not at end of the road w.r.t. methods—adjustment of filter lengths, and/or use of Gabor filters rather than Kaiser filters in some or all of the filter banks may improve results.

References

Innocenti, S.,Matte, P., Fortin, V., Bernier, N. (2022) Analytical and residual bootstrap methods for parameter uncertainty assessment in tidal analysis with temporally correlated noise. *J. Atmos. Oceanic Technol.*, **39**, 1457–1481, doi.org/10.1175/JTECH- D-21-0060.1.

Jay, D. A., Leffler, K., Diefenderfer, H., Borde, A. (2014) Tidal-fluvial and estuarine processes in the Lower Columbia River: I: along-channel water level variations, Pacific Ocean to Bonneville Dam, *Estuaries and Coasts*, DOI 10.1007/s12237-014-9819-0.

Lobo, M, Jay, D. A., Innocenti, S., Talke, S. A., Dykstra, S., Matte, P. (2023). Implementing Super-Resolution of Non-Stationary Tides with Wavelets: An Introduction to CWT_Multi, submitted to *Journal of Atmospheric and Oceanic Technology*.

Munk, W., Hasselmann, K. (1964) Super-resolution of tides. *Studies on Oceanogr.*, Collection of papers dedicated to Koji Hidaka, Seattle, WA, 339–344.

Understanding three-dimensional subtidal salt transport processes in estuaries

Jongbloed H. [1,2], Schuttelaars H.M. [2], Dijkstra Y.M. [2], and Hoitink A.J.F. [1]

Keywords: 3D idealized modelling, salt transport processes, gravitational circulation, averaging

Abstract

Estuarine environments worldwide are subject to rapid development as a result of direct and indirect effects of human activity as well as natural processes. Amidst these changing conditions, surface water salt intrusion is on average expected to increase in the coming decades, threatening but also being enhanced by drinking water extraction, irrigation and industry (Hoitink et al., 2020). In addition, in estuaries worldwide large-scale system interventions are implemented, such as large-scale deepening for shipping purposes.

In order to understand estuarine dynamics on long timescales or after large-scale interventions, knowledge of dominant salt transport processes is crucial. The study of dominant processes leads to the notion of idealized estuarine salt transport modelling, in which one aims to include only dominant terms in the momentum and salinity advection-dispersion equations. Currently, salt transport processes are mainly understood in terms of width-averaged processes, e.g. through idealized models of Hansen and Rattray (1965), MacCready (2004), and Dijkstra et al. (2021). However, it is known that in estuaries dominated by gravitational circulation, estuarine depth plays a very sensitive role in governing salt transport and intrusion. Since many estuaries exhibit considerable lateral depth variation, the goal of this contribution is to study how the traditional 2DV salt transport processes, dominant balances and resulting transport regimes respond to such lateral variation, which may even be a dominant contributing factor to longitudinal salt intrusion. In a broader sense, we want to systematically extend current understanding in terms of width-averaged salt transport processes to three dimensions, so we may start to understand the role of e.g. estuarine bathymetry and geometry on salt intrusion.

We present a three-dimensional subtidal model for water motion and salinity in partially stratified estuaries, extending the width-averaged approaches of Hansen & Rattray (1965) and MacCready (2004) to general 3D geometries. The model is nonlinear, and the equations are solved using analytical techniques and the Python-accessible FEM-package NGSolve (Schöberl, 2014). Despite its nonlinear nature, a clear interpretation of different transport terms and mechanisms is possible, as a decomposition of the transport terms can be defined unambiguously. This way, to quantify the effect of laterally varying bathymetry on salt transport processes and salt intrusion, we are able to semi- analytically derive a width-averaged effective depth parametrization that follows directly from the analysis of the transport equations.

As a first result, we demonstrate that in single channel systems, lateral depth variations may directly cause a first-order increase in salt intrusion, keeping other parameters (i.e. width-averaged depth and thus cross-sectional area) unchanged More specifically, in single-channel estuaries dominated by gravitational circulation, it is well-known that the importing mechanism scales as H8, where H is the width-averaged depth of the estuary. We demonstrate that this large sensitivity carries over to the 3D salt transport equations as $\underline{H8}$, where the power 8 is inside the lateral averaging operator ( ). Since $\underline{H8} \geq H\ 8$, this results in a considerably larger effective width-averaged depth and a significantly increased salt intrusion for estuaries showing lateral depth variations (Figure 1).

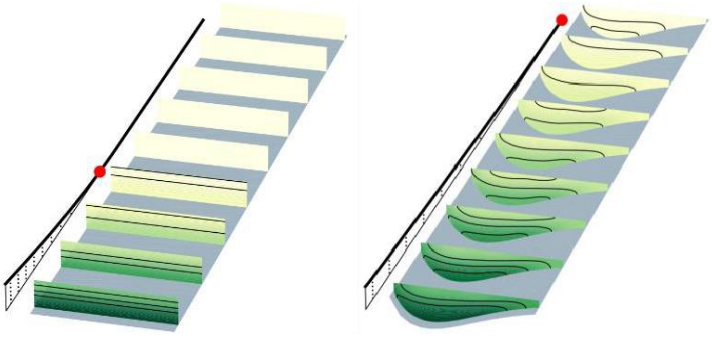

Figure 1: Comparison of salinity distribution (green) in an flat-bottom estuary (left) and a laterally variable-bottom estuary (right). The more than twofold increase in salt intrusion (red dot) is well explained by a semi- analytically derived effective depth.

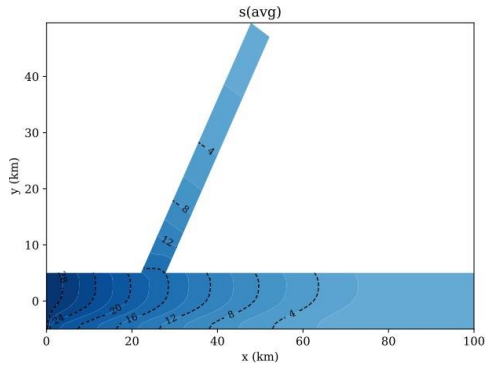

Figure 2: Salinity distribution in an estuary with a tributary (top view). Blue contours denote salinity levels. With the 3D model, we are able to study and decompose salt transport mechanisms at channel junctions to study the influence of e.g. bed discordance.

Secondly, we quantify the influence of bed variations in branched estuaries in which a width-averaged interpretation is challenging, and demonstrate that bed variations impact the horizontal distribution and transport processes of salinity again significantly in case of estuaries dominated by gravitational circulation (Figure 2).

We conclude by examining the role and sensitivity of the chosen turbulence closure and eddy diffusivity in the model, in particular a horizonal eddy diffusivity tensor parametrizing tidal dispersion.

In short, using a newly developed 3D idealized model, we demonstrate that lateral variability in parameters (e.g. bathymetry and geometry) induce additional transport terms and mechanisms that would in 2DV or 1D models have to be parametrized. These mechanisms may become significant and even dominant in systems of large lateral variability, and we are able to study and quantify their impact on longitudinal salt transport and resulting salt intrusion semi-analytically.

References

Hansen, D. V., Rattray, M. (1965). Gravitational circulation in straits and estuaries. Journal of Marine Research, 23(2), 104–122.

Schöberl, J. (2014). C++11 Implementation of Finite Elements in NGSolve.

MacCready, P. (2004). Toward a unified theory of tidally-averaged estuarine salinity structure. Estuaries, 27(4), 561–570. https://doi.org/10.1007/BF02907644

Hoitink, A. J. F., Nittrouer, J. A., Passalacqua, P., Shaw, J. B., Langendoen, E. J., Huismans, Y.,van Maren, D. S. (2020). Resilience of River Deltas in the Anthropocene. Journal of Geophysical Research: Earth Surface, 125(3), 1–24. https://doi.org/10.1029/2019JF005201

Dijkstra, Y. M., Schuttelaars, H. M. (2021). A Unifying Approach to Subtidal Salt Intrusion Modeling in Tidal Estuaries. Journal of Physical Oceanography, 51(1), 147–167. https://doi.org/10.1175/jpo-d-20-0006.1

Influence of estuarine physical processes in the transport of microplastics: a modelling study in the Gironde estuary

Kaimathuruthy B.J. [1], Jalon-Rojas I. [2], Sous D. [3,4], and Huybrechts N. [5,6]

Keywords: transport processes, microplastic dynamics, fronts, turbulence, Estuarine MicroPlastic Maxima.

Abstract

Estuaries play a crucial role in the transport, stock, and transfer of matter at the land-sea interface, including emerging pollutants such as microplastics. Microplastics are defined as minute plastic particles ranging in size from 0.1µm to 5mm whose production and discharge into marine systems have increased dramatically over the last decades. Once within the estuaries, they undergo different transport processes influenced by hydrodynamics, the particle's physical properties including density, shape, and size, as well as interaction with sediments or microorganisms (Jalón-Rojas et al., 2024). Understanding the dynamics of microplastics in estuarine environments is crucial for identifying plastic sinks, quantifying the plastic export to the ocean, evaluating environmental and socio-economic risks, and implementing effective mitigation programs. However, this can be very challenging due to the vast diversity of plastic particles, numerous sources of plastic pollution and the complex hydrodynamics of estuarine environments. In this context, advanced numerical models are have emerged as valuable tools for exploring and predicting microplastic transport.

The Gironde estuary (SW France) is a macrotidal estuary renowned for its significant trapping of suspended particulate matter (Jalón-Rojas et al., 2015). The complexities of microplastic transport in this estuary are notably linked to energetic tidal currents, strong turbulence, and hyper-turbid conditions. Understanding and predicting microplastic transport trends and accumulation requires a comprehensive investigation of the influence of diverse physical processes. In particular, the main objective of this study is to assess the significance of various physical processes that may be relevant to the microplastic dynamics in an estuarine environment including vertical turbulence, water density patterns, beaching, refloating, and bottom resuspension, as well as to explore the transport mechanisms governing their trapping. For this purpose, we simulated and compared 36 scenarios using the TrackMPD Lagrangian particle tracking model (Jalón-Rojas et al., 2019) coupled with the TELEMAC3D hydrodynamic model (Huybrechts et al., 2022), both well-validated from Lagrangian and Eulerian perspectives, respectively. Each scenario was characterized by specific physical process (e.g. turbulence, water density, beaching, and resuspension conditions), particle behavior (floating/sinking, different critical shear stress), release configuration, and hydrological conditions. In light of the potential sources of microplastics in the estuary, two release scenarios were examined: one involving release only at a single point near Bordeaux city, and the other one, releasing particles throughout the estuary at different locations. Simulations were performed during the summer and spring seasons to identify the impact of river discharge on the underlying transport mechanisms.

The simulated particle trajectories and density distributions suggest a limited influence of the spatio-temporal variability of vertical turbulence on floating particles. However, a notable impact is observed for settling particles underscoring the significance of vertical turbulence in particle resuspension and transport within the estuary. The time-space varying water density shows a relatively low impact on the transport patterns of both floating and settling microplastics, probably related to the well-mixed nature of the estuary and the stronger influence of turbulent processes, which can mitigate the effect of changes in the particle buoyancy. Noticeably, the process of beaching-refloating emerges as a crucial factor, leading to an increased residence time of floating particles within the upper estuary.

Our numerical simulations also emphasize the seasonal variability of microplastic transport patterns in the estuary and the mechanisms inducing particle trapping. The heightened river discharge during the spring season plays a pivotal role in mobilizing a large chunk of floating particles that eventually end up in the open sea (Fig 1.b). Notably, floating particles form elongated lines in the middle estuary, aligning with convergent currents at the onset of each ebb period (Fig. 1.b). Concurrently, the settling particles exhibit persistence within the estuary throughout both the summer and spring seasons. During the summer season, the denser microplastics tend to be trapped within the upper estuary by tidal pumping, aligned with the previously identified estuarine turbidity maxima (Fig. 1.c). In a flood-dominated estuary like Gironde, the peak current velocity and associated vertical turbulence during the mid-flood period increase the resuspension rate of microplastics compared to the ebb phase, leading to residual upstream transport and the formation of an Estuarine MicroPlastic Maxima.

[1] Univ. Bordeaux, CNRS, Bordeaux INP, EPOC, UMR 5805, F-33600 Pessac, France. betty-john.kaimathuruthy@u-bordeaux.fr
[2] Univ. Bordeaux, CNRS, Bordeaux INP, EPOC, UMR 5805, F-33600 Pessac, France. isabel.jalon-rojas@u-bordeaux.fr
[3] Université de Toulon - MIO, France. damien.sous@mio.osupytheas.fr
[4] Université de Pau et des Pays de l'Adour - SIAME, France
[5] CEREMA, RHITME Research Team, Margny-lès-Compiègne, France. nicolas.huybrechts@cerema.fr
[6] UNIROUEN, UNICAEN, CNRS, UMR 6143, Continental and Coastal Morphodynamics, M2C, Normandy University

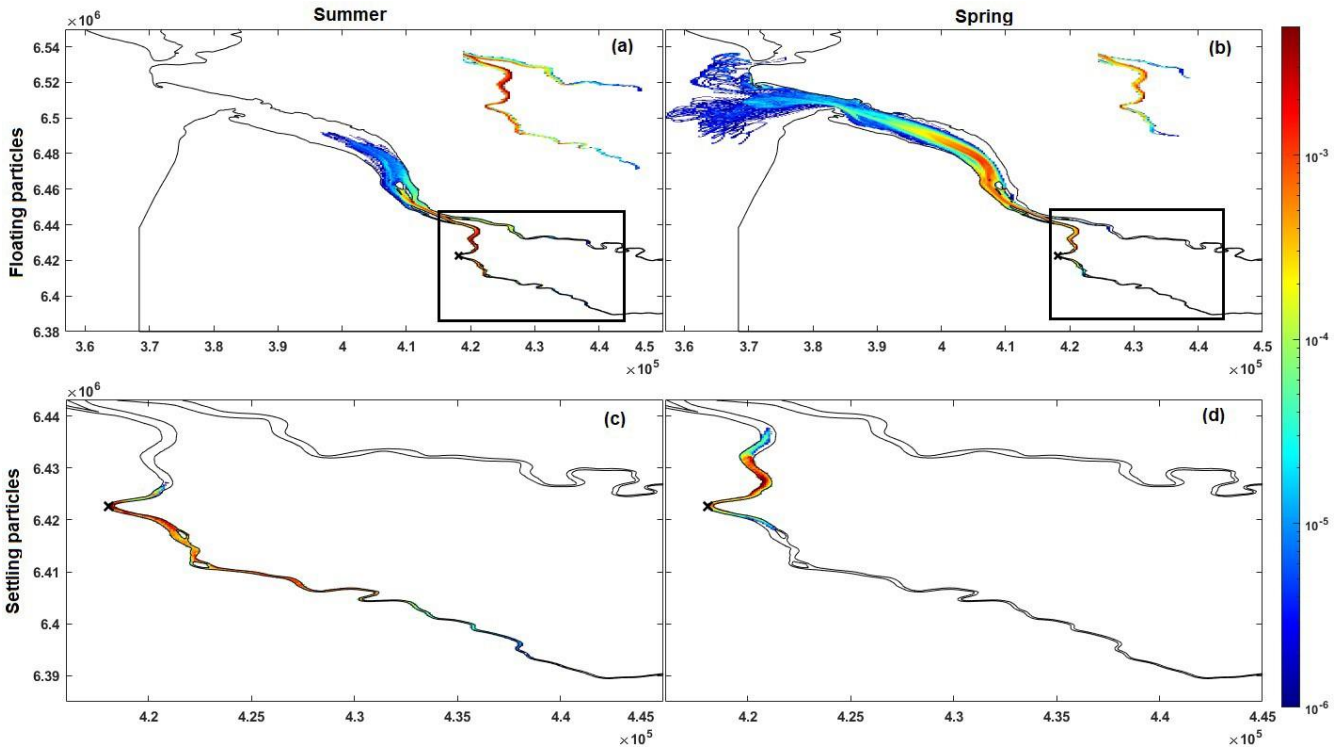

Figure 1. Probability density maps under Summer (a and c) and Spring (b and d) conditions, for the floating (a and b) and settling (c and d) particles. Black cross indicates the particle release point. The colorbar represents the normalized particle distribution.

References

Jalón-Rojas, I., Defontaine, S., Bermúdez, M., Díez-Minguito, M. (2024). Transport of microplastic debris in estuaries. Reference Module in Earth Systems and Environmental Sciences: Treatise of estuarine and coastal science, 2.

Huybrechts, N., Tassi, P., Klein, F. (2022). Three-Dimensional Sediment Transport Modeling of the Gironde Estuary. In Advances in Hydroinformatics: Models for Complex and Global Water Issues—Practices and Expectations, 753-771.

Jalón-Rojas, I., Wang, X.H., Fredj, E. (2019). A 3D numerical model to Track Marine Plastic Debris (TrackMPD): Sensitivity of microplastic trajectories and fates to particle dynamical properties and physical processes, Marine Pollution Bulletin, 141, 256-272. DOI: 10.1016/j.marpolbul.2019.02.052.

Jalón-Rojas, I., Schmidt, S., & Sottolichio, A. (2015). Turbidity in the fluvial Gironde Estuary (SW France) based on 10 year continuous monitoring: sensitivity to hydrological conditions. Hydrology & Earth System Sciences Discussions, *12*(3).

Physical Processes in Clam Gardens

Kastner S. [1], Heffernan M. [1], Cason C. [1], Greiner C. [2], and Hatch M. [1]

Abstract

For at least 3500 years, the Indigenous people of the Pacific Northwest and Southeast Alaska have improved shellfish access and productivity through the use of clam gardens, low rock walls across embayments that extend the intertidal zone and create favorable conditions for clam growth (Augustine and Dearden, 2014, Lepofsky et al., 2017, Smith et al., 2019, Lepofsky et al., 2021). Clam gardens have been constructed and managed for millenia to replicate ideal natural growing conditions for a variety of bivalves, including weak velocities that facilitate larval settling and warming of the water (Groesbeck et al., 2014, Deur et al., 2015, Roegner, 2000). In the Pacific

Northwest, clam gardens have become an important component of Indigenous resurgence as communities restore existing gardens and build new ones. The first of these new clam gardens was built in 2021 by the Swinomish Indian Tribal Community (SITC) on Kiket Island, WA. In partnership with SITC, we are conducting the first study to investigate the physical processes that result in increased bivalve productivity in clam gardensand the hypothesis that low velocities contribute to high clam growth rates in clam gardens by creating growth-favorable conditions.

Specifically, slow flow in the gardens may lead to high residence times, increased temperatures, and be favorable for larval recruitment in the clam garden (Groesbeck et al., 2014).

As an intertidal features, the SITC clam garden experiences a variety of physical forcing over the course of both the semidiurnal and neap-spring tidal cycles. As the clam garden is in a low wave energy environment, at high tidal stage, the surf zone is onshore of the garden wall, leading circulation at the wall to be primarily influenced by forcing from the wind and local estuarine dynamics. As the tidal stage decreases, the surf zone edge and waterline migrate offshore, exposing some of the garden bed to the air and the garden wall to breaking waves. When the tidal range is large, the entire garden is be exposed at low tide. As the tidal stage increases from its minimum, this progression reverses, and the garden is resubmerged. Throughout the tidal cycle described here, the mechanisms that determine flow characteristics and water properties in the clam garden change, potentially altering the residence time of the clam garden.

We will present observations from a two week field campaign at the SITC clam garden to characterize the clam garden hydrodynamics and residence time. The garden wall is roughly 0.5m high, and extends 50m alongshore. Instruments deployed will include Acoustic doppler current profilers (ADCPs), acoustic doppler velocimeters (ADVs), and conductivity, temperature, and depth (CTD) sensors on either side of the clam garden wall and at a nearby beach with no garden wall, as well as an alongshore array of pressure sensors within the clam garden to assess water level variability. RTK GPS surveys will be conducted at low water each day to assess bathymetric variability and to allow the calculation of a clam garden volume budget. We will use this budget to assess the relative importance of cross-shore and alongshore velocities to flushing the clam garden, and how these processes may change in response to tidal, wind, and wave forcing, in turn altering the garden residence time.

References

Skye Augustine and Philip Dearden. Changing paradigms in marine and coastal conservation: A case study of clam gardens in the southern gulf islands, canada. Canadian Geographies / Les géographies canadiennes, 58(3):305–314, 2014. doi: https://doi.org/10.1111/cag.12084.

Dana Lepofsky, Chelsey Geralda Armstrong, Spencer Greening, Julia Jackley, Jennifer Carpenter, Brenda Guernsey, Darcy Mathews, and Nancy J. Turner. Historical ecology of cultural keystone places of the northwest coast. American Anthropologist, 119(3):448–463, 2017. doi: https://doi.org/10.1111/aman.12893.

Dana Lepofsky, Ginevra Toniello, Jacob Earnshaw, Christine Roberts, LouisWilson, Kirsten Rowell, and Keith Holmes. Ancient anthropogenic clam gardens of the northwest coast expand clam habitat. Ecosystems, 24:248–260, 2021. doi: https://doi.org/10.1007/s10021-020-00515-6.

Nicole F. Smith, Dana Lepofsky, Ginevra Toniello, Keith Holmes, Louie Wilson, Christina M. Neudorf, and Christine Roberts. 3500 years of shellfish mariculture on the northwest coast of north america. PLOS ONE, 14(2):1–18, 02 2019. doi: 10.1371/journal.pone.0211194.

[1] Western Washington University, Department of Environmental Science, kastnes@wwu.edu

[2] Swinomish Indian Tribal Community, Fisheries Department

Amy S. Groesbeck, Kirsten Rowell, Dana Lepofsky, and Anne K. Salomon. Ancient clam gardens increased shellfish production: Adaptive strategies from the past can inform food security today. PLOS ONE, 9(3):1–13, 03 2014. doi: 10.1371/journal.pone.0091235.

Douglas Deur, Adam Dick, Kim Recalma-Clutesi, and Nancy J. Turner. Kwakwaka'wakw "clam gardens". Human Ecology, 43:201–212, 2015. doi: https://doi.org/10.1007/s10745-015-9743-3.

Curtis Roegner. Transport of molluscan larvae through a shallow estuary. Journal of Plankton Research, 22(9):1779–1800, 09 2000. ISSN 0142-7873. doi: https://doi.org/10.1093/plankt/22.9.1779.

Can the Internal Tidal Froude Number determine the dominant residual flow driver in estuaries?

Khosravi M. [1], Garel E. [1], Fortunato A. [2], Lopez-Ruiz A. [3], and Valle-Levinson A. [4]

Keywords: residual flow drivers, internal tidal Froude number, numerical simulations.

Abstract

Recent observations from subtropical, semi-arid, and temperate estuaries indicate that the drivers of residual flow, such as horizontal density gradients and tidal stresses, can vary on a fortnightly or seasonal time scale (Reyes- Hernández and Valle-Levinson, 2013; Valle-Levinson and Schettini, 2016; Valle-Levinson et al., 2000). Despite few observations, it has been suggested that the dominant driver of the residual circulation can be locally characterized by a non-dimensional Internal Tidal Froude Number (Fr0). Fr0 is derived from scaling the tidal stresses to the baroclinic pressure gradient terms in the tidally averaged momentum equation, under the assumption that the tidal excursion length equals the salinity intrusion length (Valle-Levinson and Schettini, 2016), although this restriction can be relaxed (Valle-Levinson, 2021).

This study aimed at investigating the applicability of Fr0 in identifying the spatiotemporal switches in dominant residual flow drivers in narrow estuaries. This aim was pursued with a 3D process-oriented numerical model. The hydrodynamic model, Delft3D (Lesser et al., 2004), simulated a 80 km semi-closed channel with a Gaussian-shaped cross-section of 1 km. A series of 20 six-month runs explored the effects of depth, river discharge, and M2 tidal amplitude on the lateral structure of residual flows. Based on these experiments, a neap-spring cycle experiment was conducted using a depth of 10 m and a river discharge of 50 m3/s, reproducing varying transverse residual flow distributions. To evaluate the applicability of Fr0 in representing the changes of the residual flow drivers, the ratio R=log10(tidal stresses / baroclinic pressure gradient), derived from the momentum terms of the model, was compared against Fr0. The tidal excursion was obtained from the semi-diurnal period and the local tidal velocity amplitude, while distinct salinity intrusion length scales were tested.

The fortnightly experiment showed variable lateral residual flow structures (see for example the residual bottom flow in Figure 1a, b) related to a laterally sheared flow at spring tide and a vertically sheared flow at neap tide. These distinct patterns correspond the lateral flow structures described theoretically for barotropic and baroclinic circulations, respectively. Near the mouth, R indicated a fortnightly switching in dominance between tidal stresses and baroclinic pressure gradient, over both the thalweg and shoals (Figure 1c, d). In this presented experiment, the tidal excursion (about 14 km) was significantly different from the salinity intrusion (about 30 km). Considering these lengths, Fr0 failed to diagnose the dominance of the baroclinic forcing at neap (the flow is always barotropic). A similar result is obtained when the salinity intrusion is considered as equal to the tidal excursion at each grid point. Further analyses show that smaller salinity intrusion length scales (of the order of 1 km or less) improve the prediction capability of Fr0, particularly over the thalweg. For example, Fr0 is similar to R at the mouth considering a salinity length scale of 300 m (Figure 1e, f).

Overall, these preliminary results indicate that Fr0 is sensible to the salinity intrusion length scale. For the simulated conditions, Fr0 failed to predict the residual flow driver when scaled by the total salinity intrusion length or when taken as equal to the tidal excursion. Ongoing work is investigating the range of application of Fr0 in function of the scaling, position along the channel and external forcing (particularly, the river discharge).

[1] CIMA/ARNET, Universidade do Algarve, Faro, Portugal
[2] LNEC – Laboratório Nacional de Engenharia Civil, Avenida do Brasil 101, 1700-066 Lisboa, Portugal
[3] Departamento de Ingeniería Aeroespacial y Mecánica de Fluidos, Universidad de Sevilla, Camino de los Descubrimientos s/n, 41092, Seville, Spain
[4] Civil and Coastal Engineering Department, University of Florida, Gainesville, USA

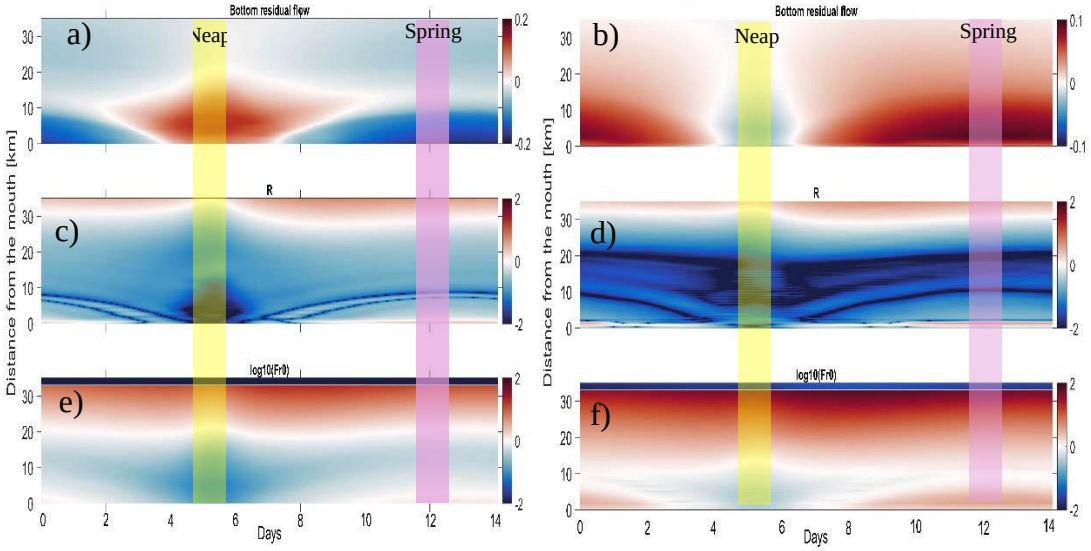

Figure 1. Results of the simulations over a fortnightly cycle: bottom residual flow (m/s, positive landward) at the thalweg (a) and shoals (b), R (positive: barotropic driver dominates) at the thalweg (c) and shoals (d), and tidal Froude number (positive: barotropic driver dominates) at the thalweg (e) and shoals (f).

References

Lesser, G. R., J. v. Roelvink, J. T. M. van Kester, and G. Stelling (2004), Development and validation of a three-dimensional morphological model, Coastal engineering, 51(8-9), 883-915.

Reyes-Hernández, C., and A. Valle-Levinson (2013), Fortnightly variations of the lateral structure of flow and hydrography at the Chesapeake Bay entrance, Continental Shelf Research, 52, 46-61.

Valle-Levinson, A. (2021), Dynamics-based classification of semienclosed basins, Regional Studies in Marine Science, 46, 101866, doi: https://doi.org/10.1016/j.rsma.2021.101866.

Valle-Levinson, A., and C. A. Schettini (2016), Fortnightly switching of residual flow drivers in a tropical semiarid estuary, Estuarine, Coastal and Shelf Science, 169, 46-55.

Valle-Levinson, A., Wong, K. C., & Lwiza, K. M. (2000). Fortnightly variability in the transverse dynamics of a coastal plain estuary. Journal of Geophysical Research: Oceans, 105(C2), 3413-3424.

Periodic Stratification and Tidal Dynamics in the German Bight Region of Freshwater Influence

Kopte R. [1], Becker M. [1], Holtermann P. [2], and Winter C. [1]

Keywords: ROFI, tidal ellipses, stratification, ADCP, lander, river plume.

Abstract

In a Region of Freshwater Influence (ROFI), the state of stratification is determined by the competing effects of stratifying processes like lateral freshwater input and mixing by tides, winds, and waves. Alternating mixed and stratified conditions on intra-tidal time scales are considered to be controlled by strain-induced periodic stratification (SIPS, Simpson et al., 1990). The oscillating vertical shear of the tidal currents interacts with the horizontal density gradient maintained by the lateral freshwater input, periodically stratifying and mixing the water column. Tidal ellipses respond to the density straining, which is reflected in modifications of the vertical velocity structure. For different ROFIs characterized by SIPS conditions, it was shown that the stratified period of the tidal cycle is associated with a counter-rotation of the tidal current ellipses (e.g. Palmer, 2010; Verspecht et al., 2010; Souza and Simpson, 1996; Visser et al., 1994). The counter-rotation is the result of a separation in an upper and lower layer by the temporary pycnocline, which decouples the upper layer from the influence of bed friction (Simpson and Souza, 1995).

The German Bight ROFI is located in the Southeast of the European North Sea. The region is strongly affected both by freshwater inflow of the rivers Elbe and Weser and tidal wave propagation, communicating the signal of the North Atlantic autonomous tides. In this study, the characteristics of the tidal velocity profile and their relation to stratification are investigated based on high-resolution current and hydrographic data collected at four locations (Kopte et al., 2022). The measurements were conducted during field campaigns in August 2016 and May 2018 with each deployment covering two to three tidal cycles. The time series of the tidal velocity profiles consistently show tidal asymmetries with higher flood than ebb velocities near the surface and counter-clockwise rotation of the velocity trajectories at depth (Figure 1a, b). Near the surface, phase-locked periodic changes in the sense of rotation within the tidal cycle are observed during episodes when the water column is stratified (Figure 1a). Counter-rotation is initiated after a sudden decoupling developing from the surface downward with subsequent rapid development of stratification and velocity shear (Figure 1c). The observed decoupling is triggered by advection of the plume-induced lateral surface density gradient by weakly sheared ebb currents toward the study site. The observed dynamics are qualitatively compared to the well-studied Rhine ROFI and Liverpool Bay. The two regimes differ in terms of the phasing of the occurrence of counter-rotation and associated straining relative to the tidal motion. In the Rhine ROFI, maximum stratification and therefore the occurrence of counter-rotation is reached around high water (Souza and Simpson, 1996; Visser et al., 1994), whereas in Liverpool Bay it is observed during low water (Fisher et al., 2002; Palmer, 2010; Verspecht et al., 2010). According to Fisher et al. (2002), these differences in the phasing are explained by the characteristics of the tidal wave. The tide in the Rhine ROFI is dominated by a coast-parallel Kelvin wave interacting with a coast-normal horizontal density gradient. In contrast, the tide in Liverpool Bay is a standing wave, where the major tidal axis is directed parallel to the lateral density gradient. The tide in the German Bight ROFI is a hybrid of progressive and standing wave. The orientation of the horizontal density gradient in principle allows for interaction with both the major and minor axes of the tidal flow. However, since the standing wave dominates in the German Bight, the observed dynamics are more similar to the Liverpool Bay than to the Rhine ROFI, with maximum stratification and the onset of counter-rotation occurring shortly after low water.

During a follow-up field campaign, six similar data sets were acquired within a 2-week period in March 2022. The measurement locations were arranged parallel to the orientation of the plume-induced lateral density gradient across the Helgoland Mud Area, close to the 2016 and 2018 deployment sites. These data will help to understand whether the SIPS-induced periodic counter-rotation is spatially confined to a band extending along the main density front of the plume, as hypothesized in Kopte et al. (2022).

[1] Institute of Geosciences, Christian-Albrechts-Universität, Kiel, Germany. robert.kopte@ifg.uni-kiel.de, marius.becker@ifg.uni-kiel.de, christian.winter@ifg.uni-kiel.de

[2] Leibniz Institute for Baltic Research Warnemünde (IOW), Rostock, Germany, peter.holtermann@io-warnemuende.de

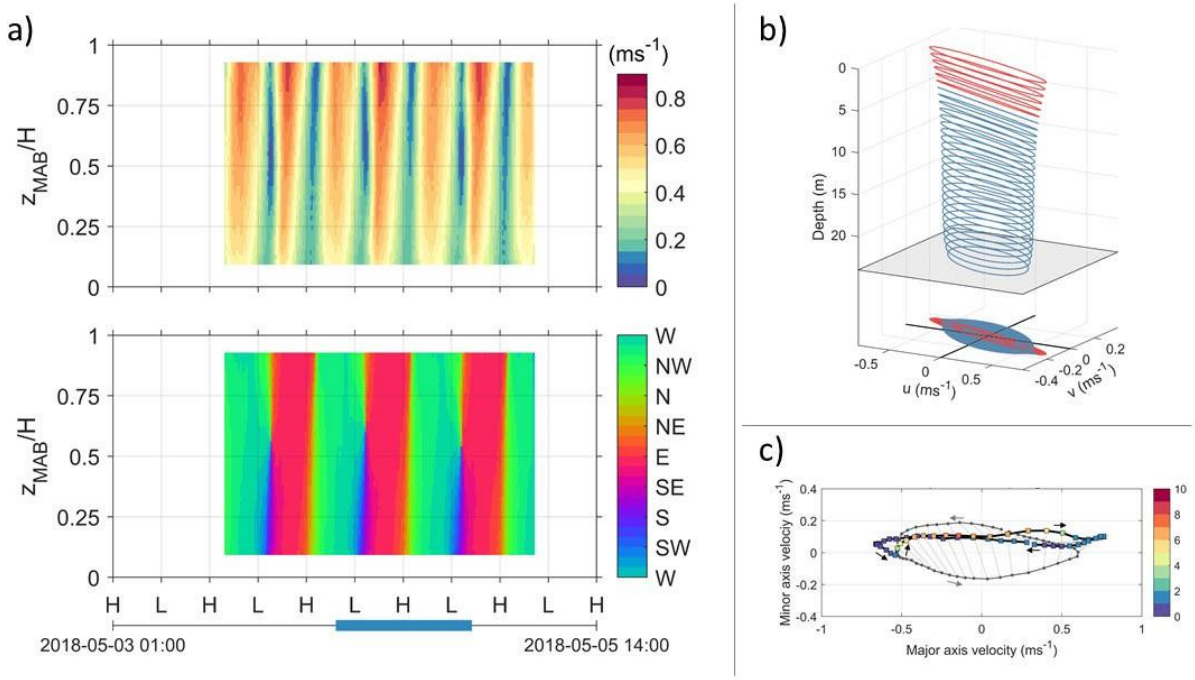

Figure 1: Observed tidal dynamics at deployment site NOAHC in May 2018. a) current velocity (m s^{-1}, top) and direction (bottom). b) Vertical structure of M2 tidal current ellipses. Red ellipses indicate clockwise rotation, blue lines indicate anti-clockwise rotation. Axis u refers to velocity in east-west direction, while v refers to velocity in north-south direction. c) Trajectories of tidal current depth-averaged for the upper layer (top-most 8 m, black line) and lower layer (lowest 8 m, grey line). Coloured squares show the potential energy anomaly (PEA, J m^{-3}). Black and grey arrows indicate the direction of upper and lower tidal trajectories, respectively. Light grey lines show the direction and strength of velocity shear between upper and lower layers at each point of the tidal cycle.

References

Fisher, N. R., Simpson, J. H., & Howarth, M. J. (2002). Turbulent dissipation in the Rhine ROFI forced by tidal flow and wind stress. Journal of Sea Research, 48(4), 249–258. DOI: 10.1016/S1385-1101(02)00194-6

Kopte, R., Becker, M., Holtermann, P., Winter, C. (2022). Tides, Stratification, and Counter Rotation: The German Bight ROFI in Comparison to Other Regions of Freshwater Influence. Journal of Geophysical Research: Oceans, 127, e2021JC018236, DOI: 10.1029/2021JC018236.

Palmer, M. R. (2010). The modification of current ellipses by stratification in the Liverpool Bay ROFI. Ocean Dynamics, 60(2), 219–226. DOI: 10.1007/s10236-009-0246-x.

Simpson, J. H., Brown, J., Matthews, J., Allen, G. (1990). Tidal straining, density currents, and stirring in the control of estuarine stratification. Estuaries, 13(2), 125. DOI: 10.2307/1351581.

Simpson, J. H., & Souza, A. J. (1995). Semidiurnal switching of stratification in the region of freshwater influence of the Rhine. Journal of Geophysical Research, 100(C4), 7037. DOI: 10.1029/95JC00067

Souza, A. J., & Simpson, J. H. (1996). Interaction between mean water column stability and tidal shear in the production of semidiurnal switching of stratification in the Rhine ROFI. In D. G. Aubrey & C. T. Friedrichs (Eds.), Buoyancy effects on coastal and estuarine dynamics. American Geophysical Union (AGU). DOI: 10.1029/ce053p0083

Verspecht, F., Simpson, J. H., & Rippeth, T. P. (2010). Semidiurnal tidal ellipse variability in a region of freshwater influence. Geophysical Research Letters, 37(18). DOI: 10.1029/2010GL044470.

Visser, A., Souza, A., Hessner, K., & Simpson, J. (1994). The effect of stratification on tidal current profiles in a region of freshwater influence. Oceanologica Acta, 17, 369–381.

Future Needs in Estuarine Physical Processes Research from a Hydraulic Engineering Perspective

Kösters F. [1], Lepper R. [1], Zorndt A. [1], and Wehr D. [1]

Keywords: research strategy, sediment transport modelling, sediment dynamics, climate change

Abstract

Introduction

The PECS community offers a unique opportunity to present and discuss recent scientific findings to gain and share knowledge of physical processes in estuaries and coasts. This exchange has contributed to transfer analysis methods and process descriptions were between research groups worldwide. Examples that have influenced our work were tidal straining effects or salt flux decomposition methods. However, a coordinated discussion on mutual future research directions is somewhat neglected. Due to limited resources in terms of human work force and money, a joint effort would be beneficial to advance research even further. As a starting point, the German Federal Waterways Engineering and Research Institute's (BAW) perspective is de-scribed here. BAW is currently in the process of updating its research program for a new 5-year period. Main topics are the adaption to climate change, sustainable sediment management, nature-based solutions in coastal engineering, and the interaction of ships and waterways. This abstract focuses on the adaption to climate change and sustainable sediment management. It is hopefully likely that this view can be transferred to other governmental organizations and there-fore represents a more general perspective.

Recent studies and future needs

- Sediment transport

Uncles (2002) stated in his review on recent studies and future needs in estuarine research that our understanding of fine sediment dynamics needs to be improved. In the field of sediment transport progress has been made, e.g., by a description of trapping mechanisms (Burchard et al. 2018). However, sediment transport modelling still suffers from a lack of sound physical process descriptions or at least the validated transfer into numerical models. Instead, many empirical formulations are still used which necessarily depend on regional settings and are therefore of limited use in estuarine applications. This imposes limitations if modelers consider cross-scale sediment transport models, e.g., from local dredging operations in connection with the large-scale sediment transport patterns. Uncles (2002) gave sediment transport properties such as settling velocity and the effects of flocculation as topics of future research. Progress can be seen here but a general description of settling velocity still seems far away. One drawback here is certainly the low availability of techniques for measuring in-situ settling velocity for operational use. The same uncertainty applies to the exchange processes between sea-bed and water column. Erosion rates of sediments depend on the sediment composition of the bed, i.e. sand-mud inter-action (Colina Alonso et al., 2023), and the degree of consolidation. Again, these processes cannot yet be described sufficiently well in cross-scale numerical models. Finally, the impact of biology such as macrofauna on sediment transport has made first steps (Nasermoaddeli et al. 2017) but has somehow come to a standstill.

- Climate change

The scientific assessment of climate change has produced and still produces numerous studies and authorities had the chance to develop adaption measures. What is needed today in coastal engineering is most often more of a site-specific recommendation than basic research. Due to the uncertainty of the effects of climate change, e.g., the exact increase in mean sea level over time, authorities follow a step wise plan. For the German coast this has led to coastal defence structures (dikes) which are designed for a medium increase in mean sea level but can easily be adapted to higher rates of sea-level increase. What is missing in climate change impact studies, are sound descriptions of long-lasting effects due to the interaction of hydrodynamics and sediment transport. The Wadden Sea and its tidal flats will certainly change with climate change (Wachler et al. 2020) and sensitivity studies have shown the resulting impact of hydrodynamics (Lepper et al. 2024). It is at least questionable to which extent reliable projections of future bathymetric evolution can be made. To refine existing estimates, new (data-based) techniques and improved descriptions of sediment transport mechanisms in numerical models are needed. Moreover, regional studies need to consider the effect of adaption measures in order to optimize them. Here we need to improve our understanding of the interaction of large-scale flow and hydraulic structures, e.g., storm surge barriers, which will be necessary more frequently in the future.

[1] Federal Waterways Engineering and Research Institute (BAW), Frank.Koesters@baw.de

References

Colina Alonso, A., van Maren, D. S., van Weerdenburg, R. J. A., Huismans, Y., & Wang, Z. B. (2023). Morphodynamic modeling of tidal basins: The role of sand-mud interaction. Journal of Geophysi-cal Research: Earth Surface, 128, e2023JF007391. https://doi.org/10.1029/2023JF007391

Burchard, Hans; Schuttelaars, Henk M.; Ralston, David K. (2018): Sediment Trapping in Estuaries. In: Annu. Rev. Marine. Sci. 10, S. 371–395. DOI: 10.1146/annurev-marine-010816-060535.

Lepper, Robert; Jänicke, Leon; Hache, Ingo; Jordan, Christian; Kösters, Frank (2024): Exploring the Tidal Response to Bathymetry Evolution and Present-Day Sea Level Rise in a Channel-Shoal Environment. Submitted to Ocean Science DOI: https://doi.org/10.5194/egusphere-2024-283

Nasermoaddeli, M. H.; Lemmen, C.; Stigge, G.; Kerimoglu, O.; Burchard, H.; Klingbeil, K. et al. (2017): A model study on the large-scale effect of macrofauna on the suspended sediment con-centration in a shallow shelf sea. In: Estuarine, Coastal and Shelf Science. DOI: 10.1016/j.ecss.2017.11.002.

Uncles, R. J. (2002): Estuarine Physical Processes Research: Some Recent Studies and Progress. In: Estuarine, Coastal and Shelf Science 55 (6), S. 829–856. DOI: 10.1006/ecss.2002.1032.

Wachler, Benno; Seiffert, Rita; Rasquin, Caroline; Kösters, Frank (2020): Tidal response to sea level rise and bathymetric changes in the German Wadden Sea. In: Ocean Dynamics 70 (8), S. 1033–1052. DOI: 10.1007/s10236-020-01383-3.

Mechanisms behind circulation, mixing and salt transport in a former estuary after reintroducing limited seawater inflow

Kranenburg W.M. [1], Bom S. [2], van Leeuwen B. [3], and Tiessen M.C.H. [4]

Keywords: estuaries, mixing dynamics, wind-driven currents, salinity, stratification, pycnocline tilting, 3D-modelling.

Abstract

We study the dynamics behind circulation, mixing and salt transport in the Haringvliet, a former estuary in the Rhine-Meuse Delta. This estuary was closed-off in 1970 with floodgates blocking seawater inflow and regulating freshwater outflow. A limited seawater inflow was reintroduced into this system in 2018, to enhance fish migration. As the incoming saltwater may threaten freshwater intake from the basin, the dispersion of salt through the system needs to be carefully managed. This invokes the question how the salt spreads through the system under various circumstances, by what mechanisms this is determined, and how this spreading may be influenced by control measures.

In an earlier observational study (Kranenburg et al, 2023), we established the importance of wind-driven upwind currents in former tidal channels for the salt transport in the Haringvliet. To further study the dynamics, we now developed a high-resolution 3D numerical model, using the unstructured hydrostatic modelling software DFlow-FM. The model has a horizontal grid with typical cell side lengths of 60 m and a combination of z- and σ-layers in the vertical with a typical thickness of only 0.125 m. The model results show - in accordance with the observational data - that the incoming saltwater reaches the deeper parts of the system, induces a strong stratification, and is only flushed out of the system after multiple events of large outward floodgate discharges. When the gates are closed during low river discharge and salt is still present in the system, wind becomes the dominant forcing of mixing and transport. For axial winds, the model results show a considerable horizontal circulation, with downwind currents over the shallow parts and significant upwind currents over the deep parts of the system. Analysis of the dynamics confirms our earlier interpretation of the observations that this circulation is explained by the fact that in the deeper parts the wind stress influence is too small to balance the set-up induced pressure gradient (in line with Csanady, 1975; and Fischer, 1976). The upwind currents in the former tidal channels are an important mechanism for inland transport of salt after upward mixing, and increased salinity values are found at landward locations for seaward wind.

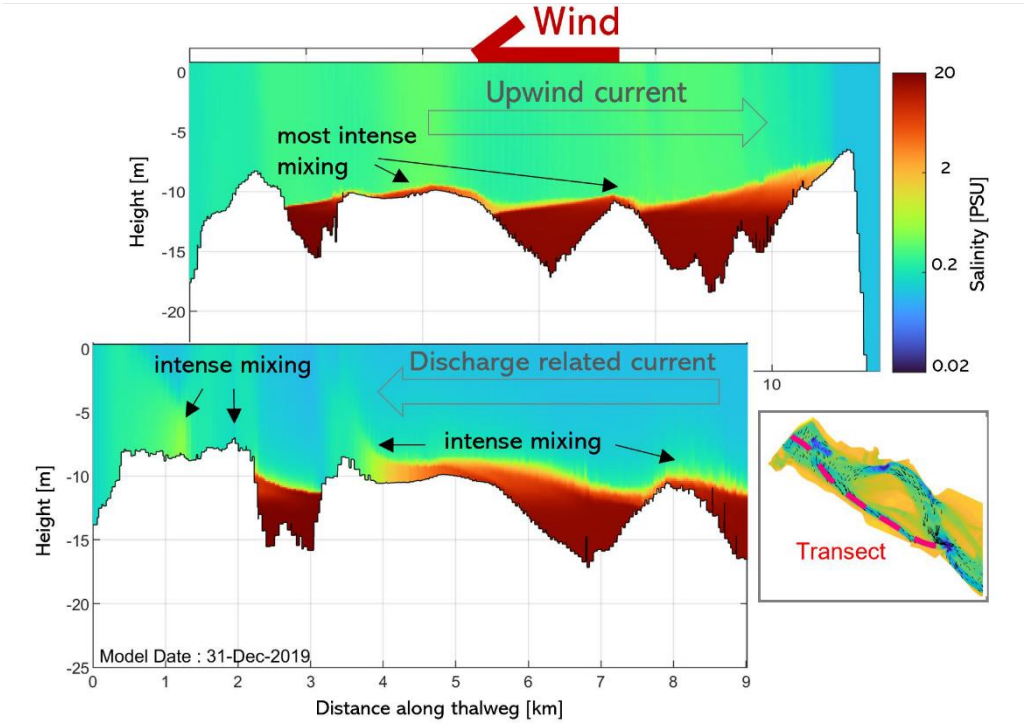

Figure 1: Salinity (log-scale) as function of height and distance along the thalweg for a situation with wind-driven horizontal circulation (top) and with a discharge related seaward flow (bottom), both showing most intense mixing where the saltwater reaches shallower areas due to interface tilting.

[1] Delft University of Technology and Deltares, Delft, The Netherlands; w.m.kranenburg@tudelft.nl
[2] Svašek Hydraulics, Rotterdam, The Netherlands; bom@svasek.nl
[3] Svašek Hydraulics, Rotterdam, The Netherlands; leeuwen@svasek.nl
[4] Deltares, Delft, The Netherlands; meinard.tiessen@deltares.nl.

The next question is then: what mechanism(s) is/are responsible for the upward mixing? We found that for the situation with closed gates, the shear due to the wind-induced currents was generally not strong enough to induce interfacial mixing directly above the deep parts. Mixing mostly occurs when, due to tilting of the pycnocline, saltwater reaches less deep areas, where it is subsequently more easily entrained by the current (see figure 1). Also in the presence of discharge related currents, the strongest mixing takes place after transport of the high-salinity water to shallower areas. We will discuss a further analysis of this 'mixing pathway' in our presentation.

Finally, with scenario analyses, we investigated the changes in the circulation, mixing and underlying dynamics for changing wind conditions and discharge situations. In this way, we determined for what rates of seawater inflow and outward floodgate discharges dynamic equilibria can be reached in which the incoming salt mass equals the mass flushed out during the subsequent ebb – and how this depends on the salinity of the inflowing water, the level of the density interface and flushing velocities.

Around the world, estuaries have been partially or completely closed-off from the sea as prevention against flooding, and the number of closed-off estuaries may increase with rising sea levels. At the same time, there is a trend to reintroduce seawater inflow into enclosed systems for ecosystem improvement. Against this background, studying the dynamics of this former estuary after reintroducing seawater inflow has a much wider relevance.

References

Kranenburg, W.M., Tiessen, M.C.H., Blaas, M., Van Veen, N.P. 2023. Circulation, stratification and salt dispersion in a former estuary after reintroducing seawater inflow; Estuarine, Coastal and Shelf Science, Volume 282, https://doi.org/10.1016/j.ecss.2023.108221.

Csanady, G.T., 1975. Hydrodynamics of large lakes. Annu. Rev. Fluid Mech. 7, 357–386. Fischer, H.B., 1976. Mixing and dispersion in estuaries. Annu. Rev. Fluid Mech. 8, 107–133

Lateral transport controls the tidally averaged gravitationally driven estuarine circulation: Tidal mixing effects

Kukulka T. [1] and Chant R.J. [2]

Keywords: physics, estuaries, estuarine circulation, exchange flow, density driven flow.

Abstract

In classic models of the tidally averaged gravitationally driven estuarine circulation, denser salty oceanic water moves up the estuary near the bottom while less dense riverine water flows towards the ocean near the surface. Traditionally, it is assumed that the associated pressure gradient forces and salt advection are balanced by vertical mixing. This study, however, demonstrates that lateral (across the estuary width) transport processes are essential for maintaining the estuarine circulation. This is because for realistic estuarine bathymetry, the depth-integrated salt transport up the estuary is enhanced in the deeper estuary channel. A closed salt budget then requires the lateral transport of this excess salt in the deeper channel towards the estuarine flanks. To understand how such lateral transport affects the estuarine salt and momentum balances, we devise an idealized model with explicit lateral transport focusing on tidally-averaged lateral mixing effects. Solutions for the along-estuary velocity and salinity are non-dimensionalized to depend only on one single non-dimensional parameter, referred to as Fischer number, which describes the relative importance of lateral to vertical tidal mixing. For relatively strong lateral tidal mixing (greater Fischer number), salinity and velocity variations are predominantly vertical. For relatively weak lateral tidal mixing (smaller Fischer number), salinity and velocity variations are predominantly lateral. Overall, lateral transport greatly affects the estuarine circulation and controls the estuarine salinity intrusion length, which is demonstrated to scale inversely with Fischer number.

[1] University of Delaware, kukulka@udel.edu
[2] Rutgers University, chant@marine.rutgers.edu

Seasonal and Synodic Longitudinal Distribution of Water Properties in São José Bay, Maranhão, Brazil

Lago L.C.O. [1] and Schettini C.A.F. [1]

Keywords: Estuaries; longitudinal distribution; seasonal variations; synodic variations.

Abstract

Estuaries serve as critical transitional zones between continents and oceans, spanning diverse coastal regions worldwide and subject to varying climates and tidal patterns (Fairbridge, 1980; Nichols & Biggs, 1985; Perillo, 1995; Dyer, 1997; Miranda et al., 2002). These environments foster remarkable productivity while remaining highly sensitive to hydrological, meteorological, and oceanographic influences. Despite their significant geomorphological, oceanographic, and sedimentological diversity, they share common characteristics (Nichols & Biggs, 1985). São José do Ribamar Bay, located on the coast of Maranhão, exemplifies such complexity as a macrotidal environment with dynamic hydrodynamics. The significance of São José de Ribamar Bay, situated in Maranhão, Brazil, lies in its ecological and socioeconomic importance as an estuarine ecosystem. This study aims to explore the longitudinal distribution of water properties within this region, with a specific focus on zonal and synodic variations. Understanding the dynamic nature of these properties is crucial for the sustainable management of natural resources and the preservation of coastal ecosystems. Thus, this research offers a meticulous analysis of the spatiotemporal variations in the physical and chemical attributes of water in São José de Ribamar Bay, providing invaluable insights into the environmental processes shaping this vital Brazilian estuary. Our investigation delves into the longitudinal distribution of water properties – salinity, temperature, and turbidity – across São José Bay throughout both wet and dry seasons, particularly during spring and neap tides. Four comprehensive surveys were conducted, covering São José Bay (~40 km), the connecting channel (~20 km), and the lower section of São Marcos Bay (~5 km). Leveraging a CTD sensor and a turbidity meter, we captured vertical water property profiles at 2 km intervals. Conductivity and temperature measurements obtained via the CTD were transformed into salinity using the Practical Salinity Scale-1978 (UNESCO, 1981). In addition to direct measurements, advanced data analysis techniques were employed, including tide forecasts to account for tidal influences and complex demodulation and Hilbert transform to extract detailed temporal variations in water properties. Despite the expansive study area hindering a quasi-synoptic snapshot of variable distributions, notable variations were observed between spring/neap tides and more pronounced disparities between wet and dry periods. Our findings illuminate the dynamic interplay between tides and seasonal fluctuations within the studied estuarine system, shedding light on the intricate relationship between water properties and environmental factors. Recognizing the influence of climatic factors on the management and conservation of coastal ecosystems is paramount (MARQUES et al., 2020). This research deepens our comprehension of coastal dynamics, offering insights with direct implications for estuarine management and conservation endeavors.

References

Fairbridge, R.W. 1980. The estuary: its definition and geodynamic cycle. In: E. Olausson & I. Cato (eds.). Chemistry and Biogeochemistry of Estuaries. New York: Wiley and Sons. 1-35p.

Nichols, M.M.; Biggs, R.B. 1985. Estuaries. In: R.A. Davis (ed.). Coastal Sedimentary Environments. Berlin: Springer-Verlag. 77-186p.

Dam remnant effects on tidal hydrodynamics in a mesotidal estuary

Lakmali E. [1] and Huguenard K. [1]

Keywords: Estuary, dam remnants, tidal harmonics, distortion.

Abstract

The general behaviour of an estuary is dependent on both natural phenomenon and anthropogenic activities like dams or bridges. These human interventions can alter the tidal range, tidal wave propagation, stratification, sediment transport and pollutant dispersion through an estuarine system. This study investigates the impact of a partially removed dam on tidal dynamics at a heavily engineered stretch of the Penobscot River estuary. The dam remnants located about 43km upstream from the Penobscot bay, where in the dynamic region of the flood limit. This partially removed dam creates a sudden change of the reiver bathymetry acting as a hump making an obstruction to the landward tidal flow. The analysis combines

field observations of water levels upstream and downstream of the dam remnants from August to November 2023, and (2) a calibrated and validated DELFT3D numerical of the Penobscot River estuary. The analysis focuses on the dam remnant's effect on the amplitudes of tidal harmonics during typical river flow conditions and during high river discharge conditions. According to the measured data, the tidal energy is still evident in the upstream of the dam remnants. Principal lunar tidal constituent M2 and shallow water overtide constituents (M4, M6 and M8) were examined to understand there behaviour individually in upstream and downstream of the dam remnants. In addition to individual harmonic constituents D2, D4, D6 and D8 tidal species bands were examined, and asymmetric ratios (D4/D2 and D6/D2) were computed. The dam remnants promoted a decrease in the amplitude of M_2 from 1.6284 m to 1.0080 m, a 38% reduction, while the amplitude of M4 increased from 0.1597 m to 0.2410 m, demonstrating a 51% increase. M8 increased from 0.0331 m to 0.0480 m (44%) while M6 was nearly constant with only a 4% reduction. The amplitude decay of the dominant constituent M2 evident the energy dissipation due to frictional effect from the dam remnants. However not all the energy is dissipated due to frictional effect, and some is transferred to higher order harmonic M4 through the nonlinear interaction and frictional effect that create tidal asymmetry. The nonlinear tidal distortion, assessed using the D4/D2 ratio, increased from 0.1788 to 0.3553 which is nearly a 100% increase. The D6/D2 ratio also increased from 0.2262 to 0.3142 (39%) across the dam remnants. These numbers suggest that the dam remnants locally enhance tidal distortion. During high river discharge conditions, subtidal water levels are enhanced upstream of the dam, suggesting the dam remnants act as obstacle to river flow, causing an increase in mean water levels. These observations reveal that partially removed dams can alter tidal behaviour, increase tidal distortion, and affect mean flows. Numerical modelling will be used to analyse the magnitude and phase differences of the tidal currents in the vicinity of the dam remnants, how it makes impact on net sediment transport in the system and to assess the role of reflection in reducing the principal tide.

[1] Department of Civil and Environmental Engineering, University of Maine, Orono, ME, USA.

Modeling the impact of wastewater discharge on oxygen in Puget Sound

Leeson A. [1], Mascarenas D. [2], Horner-Devine A.R. [3], MacCready P. [4], Roberts B. [5], and Brett M.T. [6]

Keywords: Puget Sound, numerical modeling, oxygen, hypoxia, nutrients, wastewater.

Abstract

Puget Sound is a fjord-like estuary in the Salish Sea with a large population that includes the Seattle metropolitan area. Several inlets in Puget Sound experience seasonal hypoxia which degrades water quality and occasionally results in fish kills (Newton et al., 2007). One suspected driver of low dissolved oxygen (DO) is excess nitrogen discharged from wastewater treatment plant (WWTP) outfalls (Khangaonkar et al., 2018; Ahmed et al., 2021). However, WWTP nutrients currently account foronly~2% of the dissolved inorganic nitrogen (DIN) supplied to the region, whereas ocean upwelling contributes ~95% (Figure 1). Complex physical processes such as energetic tidal mixing, estuarine circulation, and deep water intrusions also play a role in the region's oxygen dynamics (Ebbesmeyer et al., 1988; Geyer & Cannon, 1982). Furthermore, it is difficult to identify the dominant factors contributing to low DO because Puget Sound's hypoxic inlets are sparsely sampled (Mascarenas et al., 2024). Thus, numerical models are critical tools for building a mechanistic understanding of Puget Sound hypoxia.

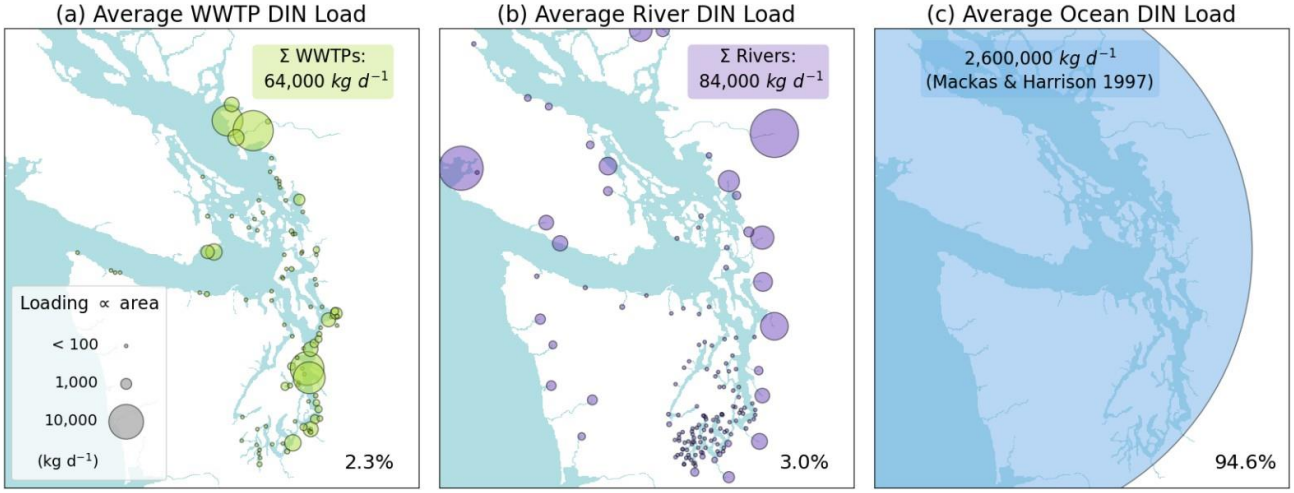

Figure 1. Major sources of dissolved inorganic nitrogen (DIN) loading to the Salish Sea. Each circle corresponds to an individual source, and circle area is proportional to DIN loading. The percentage value in the bottom right corner of each panel denotes the percent contribution of DIN from each source type. We use river and WWTP loading data from Washington State Department of Ecology (2020).

Our research goal is to understand the physical and biogeochemical processes contributing to Puget Sound's hypoxia, and to quantify the sensitivity of Puget Sound's DO concentrations to WWTP discharge. We explore these topics using LiveOcean (MacCready et al., 2021), a realistic ROMS model coupled to a NPZD+O (nutrients, phytoplankton, zooplankton, detritus, plus oxygen) biogeochemistry module (Shchepetkin & McWilliams, 2005; Davis et al., 2014). To this model, we have added 99 WWTPs and 179 rivers. Figures 1a and 1b show the locations and loadingof these WWTPs and rivers. We use this model to compare a hindcast scenario with existing levels of DIN in WWTP effluent (anthropogenic) to a scenario with zero DIN in WWTP effluent (natural). Results from this modeling study in 2013 suggest that WWTP loading alters bloom dynamics and slightly decreases bottom DO concentration. In Puget Sound Main Basin (Figure 2d), WWTP loading introduces ~10% more DIN to the water column. These excess nutrients delay the onset of the spring bloom by two weeks (see surface chlorophyll in Figures 2a and 2b), but also intensify summer blooms during June and July (Figure 2c). By mid-June, the anthropogenic run has a consistently lower bottom DO concentration, deviating from the natural run by only ~0.1 mg/L. Notably, this DO deficit fluctuates with a step-like pattern at a monthly frequency (Figure 2c). This step-like signature is consistent with known deep water intrusion events observed over Admiralty Sill at the mouth of Puget Sound every other neap tide (Deppe et al., 2018). These intrusion events tend to drive anthropogenic DO concentrations back towards their natural values.

[1] University of Washington, auroral@uw.edu
[2] University of Washington, dakotamm@uw.edu
[3] University of Washington, arhd@uw.edu
[4] University of Washington, pmacc@uw.edu
[5] University of Washington, bedaro@uw.edu
[6] University of Washington, mtbrett@uw.edu

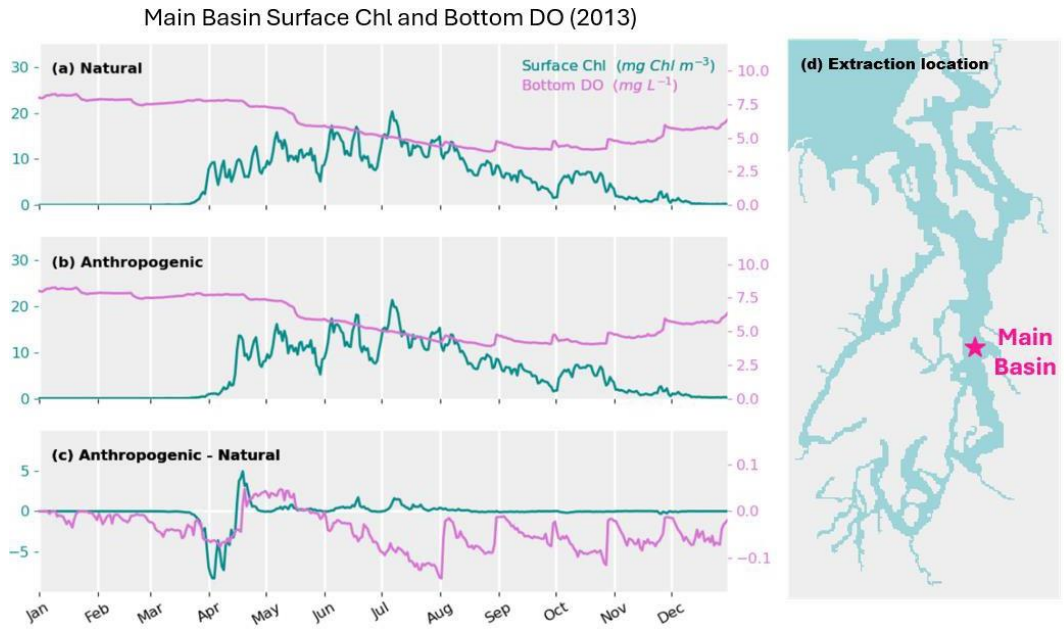

Figure 2. Modelled surface chlorophyll and bottom DO time series in Puget Sound Main Basin for the year 2013. (a) Time series from the natural test case. (b) Time series from the anthropogenic test case. (c) The anthropogenic time series minus the natural time series. (d) Puget Sound Main Basin location from which we extracted time series results.

Through continued comparison of the anthropogenic and natural scenarios, we hope to understand how and why WWTP loading influences DO throughout Puget Sound. By identifying the dominant drivers and processes leading to hypoxia, we can ultimately help inform nutrient management decisions in the future.

References

Ahmed, A., Gala, J., Mohamedali, T., Figueroa-Kaminsky, C., & McCarthy, S. (2021). Technical Memorandum: Puget Sound Nutrient Source Reduction Project Phase II - Optimization Scenarios (Year 1). https://www.ezview.wa.gov/DesktopDefault.aspx?alias=1962&pageid=37106.

Davis, K. A., Banas, N. S., Giddings, S. N., Siedlecki, S. A., MacCready, P., Lessard, E. J., ... & Hickey, B. M. (2014). Estuary - enhanced upwelling of marine nutrients fuels coastal productivity in the US Pacific Northwest . *Journal of Geophysical Research: Oceans*, 119(12), 8778-8799.

Deppe, R. W., Thomson, J., Polagye, B., & Krembs, C. (2018). Predicting deep water intrusions to Puget Sound, WA (USA), and the seasonal modulation of dissolved oxygen. Estuaries and coasts, 41, 114 -127.

Ebbesmeyer, C., Word, J. Q., & Barnes, C. A. (1988). Puget Sound: A fjord system homogenized with water recycled over sills by tidal mixing (pp. 17-29). CRC Press.

Geyer, W. R., & Cannon, G. A. (1982). Sill processes related to deep water renewal in a fjord. *Journal of Geophysical Research: Oceans*, 87(C10), 7985-7996.

Khangaonkar, T., Nugraha, A., Xu, W., Long, W., Bianucci, L., Ahmed, A., Mohamedali, T., & Pelletier, G. (2018). Analysis of hypoxia and sensitivity to nutrient pollution in Salish Sea. Journal of Geophysical Research: Oceans, 123(7), 4735 -4761.

MacCready, P., McCabe, R. M., Siedlecki, S. A., Lorenz, M., Giddings, S. N., Bos, J., ... & Garnier, S. (2021). Estuarine circulation, mixing, and residence times in the Salish Sea. *Journal of Geophysical Research: Oceans*, 126(2), e2020JC016738.

Mackas, D. L., & Harrison, P. J. (1997). Nitrogenous nutrient sources and sinks in the Juan de Fuca Strait/Strait of Georgia/ Puget Sound estuarine system: assessing the potential for eutrophication. *Estuarine, Coastal and Shelf Science*, 44(1), 1-21.

Mascarenas, D., Leeson, A., Roberts, B., Horner-Devine, A. R., MacCready, P., Brett, M. T. (2024), Toward Salish Sea Dissolved Oxygen Trends and Drivers, Abstract (CP44B-1928) presented at OSM24, 18–23 Feb.

Newton, J., Bassin, C., Devol, A., Kawase, M., Ruef, W., Warner, M., ... & Rose, R. (2007, March). Hypoxia in Hood Canal: An overview of status and contributing factors. In *Proceedings of the 2007 Georgia Basin Puget Sound Research Conference* . Olympia: Puget Sound Action Team.

Shchepetkin, A. F., & McWilliams, J. C. (2005). The regional oceanic modeling system (ROMS): a split-explicit, free-surface, topography-following-coordinate oceanic model. *Ocean modelling*, 9(4), 347-404. Washington State Department of Ecology. (2020). *Daily Time series* (Oct. 2020 version) [Data set of nutrient concentrations and discharge for rivers and point sources] https://fortress.wa.gov/ecy/ezshare/EAP/SalishSea/SalishSeaModelBoundingScenarios.html

An experimental testbed for environmental stratified turbulence and mixing: the Stratified Inclined Duct

Lefauve A. [1]

Keywords: laboratory experiment, exchange flow, density stratification, shear instability, stratified turbulence, mixing.

Abstract

We discuss a relatively recent laboratory experiment, the Stratified Inclined Duct (SID) (see figure 1a), that sustains a buoyancy-driven exchange flow and allows to accurately control and measure sheared stratified turbulence and mixing. Coastal flows, and particularly estuaries, experience very high levels of turbulent kinetic energy dissipation and mixing, which have first-order impacts on their circulation, salinity levels and stratification, chemistry and biology. This stratified turbulence and mixing involves an extraordinarily large range of eddies and lengthscales, from the forcing scale of 1-10 m to the μm scale at which molecular diffusion irreversibly mix the active scalar (typically salinity) and other passive scalars (e.g. nutrients, dissolved gases). The environmental fluid dynamics community recognises that efforts are still needed to improve our understanding of multi-scale turbulent mixing processes, which is necessary to improve their subgrid-scale parameterisation in large-scale circulation models (Dauxois et al. 2021). To complement idealised numerical studies, laboratory studies such as the SID have a key role to play in this community effort as they allow real (i.e. not overly idealised) turbulence to be generated and sustained in a parameter regime approaching that relevant to environmental flows. This paper will argue that SID can serve as a versatile and fruitful testbed for studying the physics and parameterisation of turbulent mixing processes in estuaries and coastal seas, in the hope to stimulate collaborations with physical oceanographers and turbulence modellers.

First, we present the SID setup, first introduced in Meyer & Linden (2014), whose latest version consists of two large (400 litres) reservoirs containing salt solutions at densities $\rho_0 \pm \Delta\rho/2$ connected by a long rectangular duct of height O(10 cm). The long-lasting exchange within the duct has a Reynolds number Re = O(10^3-10^4). Importantly, the apparatus can be tilted at a small angle θ, which energises the flow and increases turbulent dissipation levels, due to hydraulic control.

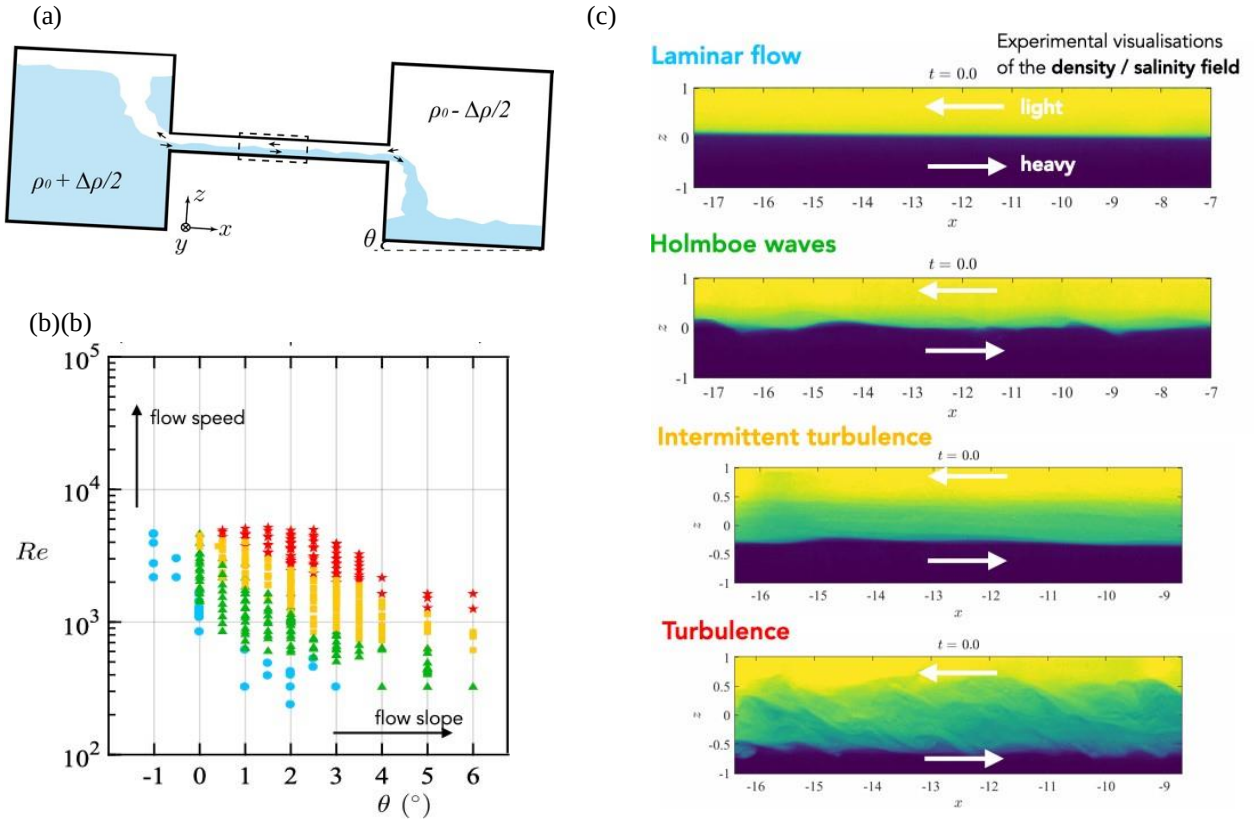

Figure 1: (a) Schematic of the SID setup; (b) typical regime diagram; (c) illustration of the regimes with laser induced fluorescence.

[1] Department of Applied Mathematics and Theoretical Physics (DAMTP), University of Cambridge, Cambridge, United Kingdom. Correspondence: aspl2@cam.ac.uk

The beauty of SID is that its simple two-dimensional parameter space (Re, θ) harbours multiple flow regimes (figure 1b) containing the key physics of stratified turbulence. Beyond the laminar flow regime we find interfacial Holmboe waves, intermittent turbulence with periodic cycling between mixing and restratification mediated by shear instabilities, and fully developed turbulence and mixing (figure 1c) energised by continuous baroclinic shear production.

Second, we present high-resolution measurements of the three-dimensional velocity and density fields within the duct (see figure 2a) using simultaneous Particle Image Velocimetry (PIV) and Laser Induced Fluorescence (LIF). These data set a new standard in the field and enable us to delve into the finescale properties and energetics of stratified turbulence (Lefauve & Linden, 2022). We show that in the fully turbulent regime, the level of TKE dissipation in the turbulent shear layer is approximetely $\varepsilon \approx 2.2\, H^{1/2}\, (\Delta\rho/\rho!)^{3/2}\, \theta$ m^2 s^{-3} (where H is the duct height in m, and θ is the tilt in rad). Meanwhile, the mean buoyancy frequency is $N \approx 2.6 H^{-1/2}\, (\Delta\rho/\rho_0)^{1/2}$ rad s^{-1}, resulting in a buoyancy Reynolds number $Re_b \approx 3 \times 10^5\, H^{3/2}\, (\Delta\rho/\rho_0)^{1/2}\, \theta \approx 0.2\, Re\, \theta$. This scaling shows that large values $Re_b = O(10^2 - 10^3)$, i.e. well above the viscous limit of 20, can be accessed even at relatively low $Re = 10^3 - 10^4$ thanks to modest slopes of order $\theta \approx 0.1$ (i.e., 6 degrees). This explains the ability of SID to achieve in the laboratory the required separation of scales found in environmental stratified turbulence, and also enables us to extrapolate the ε, N and Re_b values in future, larger experiments (see figure 2b, and the yellow 'Practical SID region').

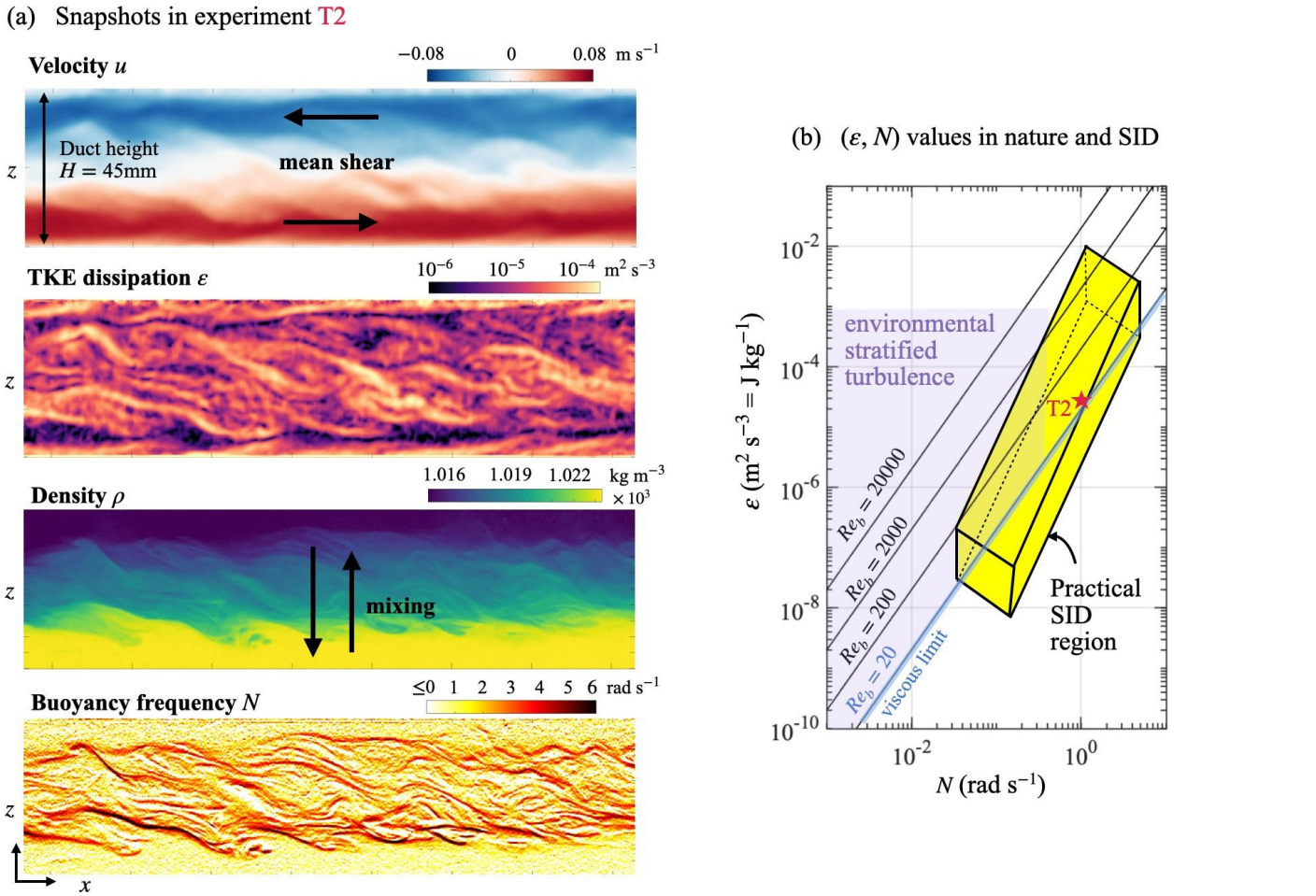

Figure 2: How to extrapolate laboratory turbulence to environmental turbulence? (a) Example of turbulent velocity and density measurements in a ~250 x 45 mm window. (b) Mean dissipation and stratification in SID vs environment (after Geyer et al. 2008).

References

Dauxois, T. et al. Confronting Grand Challenges in environmental fluid mechanics. *Phys. Rev. Fluids* **6**, 020501 (2021)

Geyer, W. R., Scully, M. E. & Ralston, D. K. Quantifying vertical mixing in estuaries. *Environ. Fluid Mech.* **8**, 495–509 (2008). Lefauve, A. & Linden, P. F. Experimental properties of continuously forced, shear-driven, stratified turbulence. Part 2. Energetics, anisotropy, parameterisation. *J. Fluid Mech.* **937**, A35 (2022)

Meyer, C. R. & Linden, P. F. Stratified shear flow: experiments in an inclined duct. *J. Fluid Mech.* 753, 242–253 (2014).

Classifications of underwater flow-transverse sedimentary bedforms

Lefebvre A. [1], Dalrymple R.W. [2], Cisneros J. [3], Scheiber L. [4], Hulscher S. [5], Slootman A. [6], Kleinhans M.G. [7], and Miramontes E. [1,8]

Keywords: dunes, sedimentary structures, estuaries, continental shelves, continental slope

Abstract

Despite the recommendations given in Ashley (1990) for the description and naming of "large-scale subaqueous bedforms", a plethora of terms continues to be used for flow-scale flow-transverse sedimentary bedforms, often without clear definition or distinction between the different nomenclatures. For example, (marine) dunes and sand waves are used interchangeably in many contexts, but they are also sometimes differentiated based on bedform size (dunes are smaller than sand waves), asymmetry (dunes are asymmetric and sand waves are symmetric) or environment / formation process (dunes form in rivers under the action of unidirectional currents and sand waves in tidal environments under the action of reversing currents). A survey of the literature showed that the names are used more or less depending on the environment (Figure 1). It is currently unclear if different terms are used due to intrinsic morphological or genetic differences, or to the traditions of different scientific communities. Ashley (1990) already noted that the "poor communication among scientists and engineers has perpetuated the multiplicity of terms". Researchers from fluvial, coastal or deep-marine environments, from industry or academia, from various disciplines, such as sedimentology, oceanography, coastal and offshore engineering or geomorphology may use a specific vocabulary. Furthermore, terminology may differ depending on the country or research group in which they work. All this makes communication difficult and may cause misinterpretations, hindering progress in understanding and cross-disciplinary collaborative pursuits.

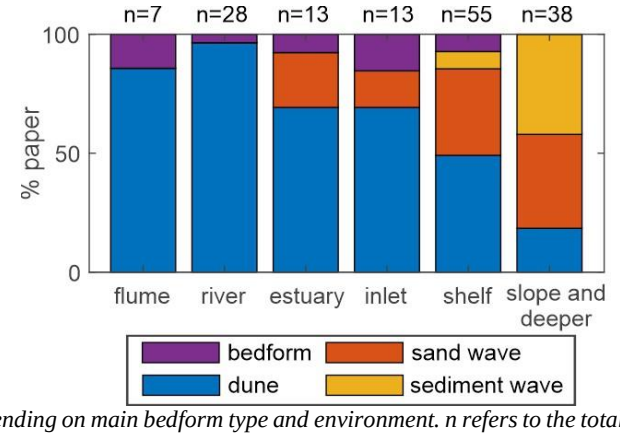

Figure 1. Percentage of papers depending on main bedform type and environment. n refers to the total number of papers for the specific environment.

The aim of the present contribution is to provide an updated classification of the different types of underwater flow-transverse sedimentary bedforms. The intent is to propose a common nomenclature to enable translation between classifications and to improve knowledge exchange, comparison and dialogue for researchers coming from different disciplines and working in varied environments.

As a starting point for this endeavour, users need to describe the bedforms in a standard, comprehensive manner in order to foster better understanding. For this, we first propose a standardised description table (Table 1), which can be used by scientists and practitioners to describe the sedimentary bedforms with which they are working. Importantly, each bedform characteristic is described and the way to calculate the quantitative descriptive parameters is detailed. The description table aims at providing a standard and consistent way to describe bedforms and their environmental setting prior to classifying them. The description table can be used independently of bedform type and further classification, which should minimise communication issues.

[1] MARUM, University of Bremen, Germany, alefebvre@marum.de
[2] Department of Geological Sciences and Geological Engineering, Queen's University, Canada
[3] Department of Geosciences, Virginia Tech, USA
[4] Ludwig-Franzius-Institute for Hydraulics, Estuarine and Coastal Engineering, Leibniz University Hannover, Germany
[5] Department of Civil Engineering, University of Twente, The Netherlands
[6] Department of Geology and Geological Engineering, Colorado School of Mines, USA
[7] Department of Physical Geography, Utrecht University, The Netherlands
[8] Faculty of Geosciences, University of Bremen, Germany

Two classification schemes are then proposed. The first is based on an understanding of the genetic processes. This should be used whenever possible because it informs about the underlying processes which formed the bedform. In order to complement the process-based classification, or in situations where the genetic processes are unknown, a second classification is introduced, based on geomorphological characteristics. Thus, we urge the different communities to consider using these descriptor and classification tools in order improve communication and research.

Table 1. Descriptive parameters of underwater flow-transverse sedimentary bedforms

Morphology	
Size	Height and length
Coverage	Number of bedforms; fraction of bed covered by bedforms
3D shape	Height and length 3D variability; crestline, brink line and/or troughline sinuosity; bifurcation index; presence of scour holes
2D shape	Asymmetry; stoss and lee slope lengths and mean angles; value and position of maximum angles; crest roundness
Hierarchy	Presence and possible superposition of several bedform scales
Bedform dynamics	Variations of morphological properties in time; migration history and rates
Orientation compared to the flow	Main orientation and variation in the orientation of the bedform (field) compared to the flow (from truly flow-transverse to oblique)
Sediment	
Sediment characteristics	Size; sorting; skewness; spatial variability
Sediment availability	Thickness (and continuity) of the mobile layer
Internal architecture	Thickness, angle, type and presence of cross bedding; angle of bounding surface between sets; grading and sorting pattern within strata
Hydrodynamics	
Main hydrodynamics	Presence of river, tidal, (internal) wave-related, wind-driven, storm-induced, geostrophic or general ocean circulation related currents, surface or internal waves
Flow structure	Velocity and turbulence characteristics of the hydrodynamics, with as much detail as possible (e.g. mean and max. tidal currents, directional variability). Also note the timing of the current measurements compared to bedform measurements.
Flow variation	Flow variation in time and/or space. In the case of tidal currents, relative strength of opposite flows degree of tidal ellipticality and the temporal variation in each relevant process
Non-dimensional numbers	Typical Froude; Reynolds and Particle Reynolds numbers
Environment	
Water depth	Total water depth; boundary-layer thickness if appropriate Flow/channel width if relevant; degree of confinement
Large-scale bed topography	Slope of the underlying bed, presence of bar, ridge, sandbank or other topographic elements, confinement in a channel
Anthropogenic context	Dredging activities, offshore infrastructure, bottom trawling, etc.
Biota	Distribution and dynamics of pelagic and benthic biota

References

Ashley, G. M. (1990) Classification of large-scale subaqueous bedforms: A new look at an old problem, Journal of Sedimentary Research, 60, 160-172, https://doi.org/10.2110/JSR.60.160

Anthropogenic forcings can prevail: the case of maintenance dredging in the Seine Estuary

Lemoine J.-P. [1], Grasso F. [2], and Le Hir P. [3]

Keywords: estuaries, global changes, dredging, sediment fluxes.

Abstract

Introduction

Large estuaries have historically undergone extensive artificialization to support urban and port development. Embankments and deepening of navigational fairways have significantly impacted morphology and subsequently hydrodynamics. These impacts manifest through different aspects such as tide propagation and Suspended Particulate Matter (SPM) dynamics (e.g., Grasso and Le Hir, 2019). Among these developments, the areas artificially deepened for navigation experience significant siltation rates as they act as sediment traps. These depositions often conduct port authorities to engage in nearly continuous dredging, displacing colossal quantities of sediment to maintain safety conditions. For instance, Liu & Zhang (2019) reported that in the Yangtze, 100 M.m3 per year can be dredged. In some cases, these sediment fluxes induced by MD are comparable to natural sediment fluxes (e.g., 159 M.tons per year of continental sediment supply in the Yangtze, as estimated by Xie et al., 2023), thus they are potentially strongly interfering with natural estuarine functioning.

The direct and short term implications of MD and associated sediment disposal have been extensively studied by many authors (e.g., Van Maren et al., 2015). However, the literature about the mid-term effects (i.e., over 10 years) of quasi-continuous dredging and dumping is limited, as it can only be assessed in-silica through the use of a validated model capable of reproducing dredging and disposal site dynamics at this timescale. Our research based on the use of a well validated model aimed to understand the implications of MD on the mid-term functioning and dynamics of estuarine systems to improve sediment management strategies.

Case study

The Seine Estuary, located in NW France, is a macrotidal sandy-muddy estuary that harbors both the ports of Rouen and Le Havre. Continuous dredging is essential to maintain its fairways, resulting in an annual displacement of around 7 M.m3 of sediment. In contrast, continental sediment inputs from watershed erosion were estimated at 1 M.m3/year. Dredging primarily occurs in three specific areas within the most downstream 20 km of the estuary, particularly in the Estuarine Turbidity Maximum (ETM) excursion zone. Sediment dumping is carried out at two distinct offshore sites (for more detailed information, see Lemoine et al., 2021).

Methods

The hydro-morpho-sediment model of the Seine Estuary, as described in Lemoine et al. (2021), was used to investigate the impact of MD on sediment dynamics over a decade (2009-2018). This morphodynamic model simulates the movement of both sand and mud in response to various environmental factors such as wind, waves, tides, and river inputs. Dredging operations are modeled as sedimentary processes triggered by sediment deposition in navigated areas. In addition to the validation described in previous research (e.g. Grasso et al., 2018), the simulated dynamics of dredging and dumping sites are in good agreement with in-situ data collected by port authorities, reproducing spatial and temporal variabilities in dredging effort, dredged sediment characteristics, and dumping site dynamics.

In this study, a comparative analysis is conducted between a reference simulation (including dredging and sediment dumping) and theoretical scenarios (without dumping and dredging) to investigate the indirect effects of dredging on: i) dynamics of suspended particulate matter, ii) composition of surface sediment, iii) morphological changes, iv) sediment fluxes, and v) quantities of sediment dredged during calculations. A numerical tracing protocol was implemented in the model to monitor the fate of dredged sediment and to evaluate their contribution and impact to the total SPM and surficial sediment cover (see also Lemoine et al., 2020).

Results

At the annual scale and at the estuary mouth scale, the dynamic of SPM is not affected by MD, despite a notable amount of previously dredged material returning to the system (Lemoine et al., 2020). Indeed, model results highlight that sediment exchanges between the water column and the sea-bed, driven by erosion/deposition processes, are approximately 10,000 times greater than the dredged quantities.

[1] GIP Seine-Aval, Espace des Marégraphes, Quai de Boisguilbert, F-76000 Rouen, France Ifremer – DYNECO/DHYSED, Centre de Bretagne, CS 10070, 29280 Plouzané, France, Now at Cerema REM, RHITME Research Team & UMR CNRS 6143, Continental and Coastal Morphodynamics "M2C", University of Rouen, jp.lemoine@cerema.fr

[2] &[3] Ifremer – DYNECO/DHYSED, Centre de Bretagne, CS 10070, 29280 Plouzané, France,

However, over a decadal timescale, it appears that dredging impacts morphodynamic evolutions, and generates either erosion or reduced deposition. It is noteworthy that MD influences the morphological changes of the entire system, even indirectly and at distance (~ 5km) from the dredging and dumping sites (Figure 1). Consequently, the distribution of currents is also affected by dredging at this timescale.

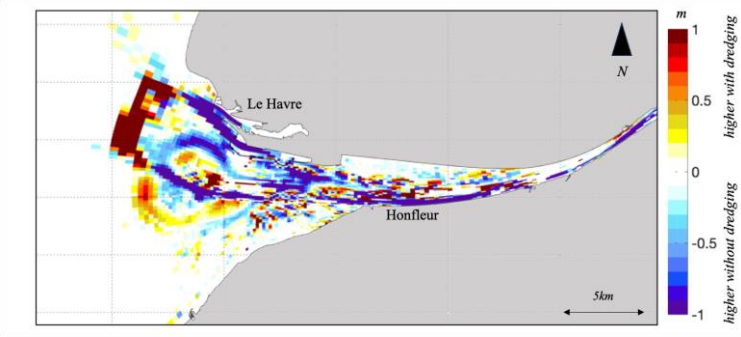

Figure 1. Differences in bathymetric changes simulated with and without dredging over the period July 2009 - July 2018 (bathymetric evolution with dredging minus without dredging) The dredging zones are located in the vicinity of Le Havre and along a narrow channel between Honfleur and the Bay (intense blue). The dumping zones of Le Havre are not depicted here; the dumping zone of Rouen corresponds to the intense "higher with dredging" area (red) in the north-western part of the outer estuary. For precise locations of dredging and dumping areas, please refer to Lemoine et al. (2021).

These numerical bathymetric observations can be linked to the sediment budget deficit induced by the port dredging strategy (disposal at sea). Flux computation also highlights that dredging alters sediment fluxes both in terms of spatial distribution and intensity. In particular, dredging amplifies sediment fluxes towards the estuary. Despite this amplification, simulations with dredging highlight an erosion of the inner estuary of approximately -2.5 M.m3/year, while simulations without dredging show the natural infilling tendency of estuaries at a rate of nearly +3 M.m3/year (Figure 2).

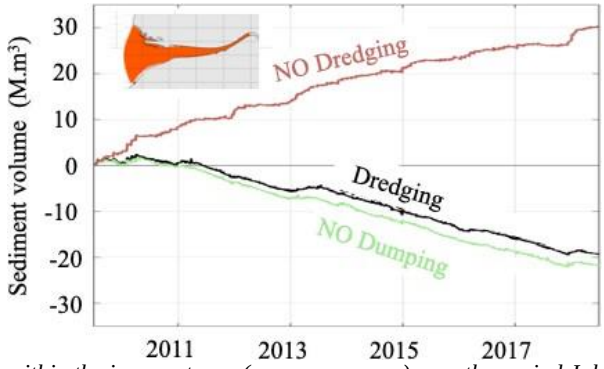

Figure 2. Changes in sediment volume within the inner estuary (see orange map) over the period July 2009 - July 2018

Conclusion

Our research confirms that the effect of maintenance dredging on sediment dynamics is negligible in the short term. However, over the mid-term or at hydro-morpho-sedimentary equilibria timescale, it reveals that sediment fluxes generated by maintenance dredging can significantly impact the sediment budget of estuaries. Thus, MD has the potential to influence the natural hydro-morpho-sedimentary dynamics of estuaries. Overall, we have shown that maintenance dredging is a potential primary driver of long-term estuarine dynamics, which need to be considered in prospective studies. Indeed, its implications on sediment budgets and associated morphological evolution trajectories are worth considering in prospective risk assessment and ecosystem service evaluations in response to global changes.

References

Grasso, F., Verney, R., Le Hir, P., Thouvenin, B., Schulz, E., Kervella, Y., Khojasteh Pour Fard, I., Lemoine, J.P., Dumas, F., Garnier, V. (2018). Suspended Sediment Dynamics in the Macrotidal Seine Estuary (France): 1. Numerical Modeling of Turbidity Maximum Dynamics. Journal of Geophysical Research: Oceans, 123(1), 558–577. https://doi.org/10.1002/2017JC013185

Grasso, F., Le Hir, P. (2019). Influence of morphological changes on suspended sediment dynamics in a macrotidal estuary: diachronic analysis in the Seine Estuary (France) from 1960 to 2010. Ocean Dynamics, 69(1), 83– 100. https://doi.org/10.1007/s10236-018-1233-x

Lemoine, J.P., Le Hir, P., Grasso, F. (2020). Numerical Study of Sediment Transport in the Seine Estuary: Contribution of Dredging. In K. D. Nguyen, S. Guillou, P. Gourbesville, & J. Thiébot (Eds.), Estuaries and Coastal Zones in Times of Global Change (pp. 241–255). Springer Singapore.

Lemoine, J. P., & Le Hir, P. (2021). Maintenance dredging in a macrotidal estuary: Modelling and assessment of its variability with hydro-meteorological forcing. Estuarine, Coastal and Shelf Science, 258, 107366. https://doi.org/https://doi.org/10.1016/j.ecss.2021.107366

Liu, M., Zhang, H.W. (2019). Correction of the Artificial Influence on Dredging Volume in the Yangtze Estuary Deep-water Channel. IOP Conference Series: Earth and Environmental Science, 304(2). https://doi.org/10.1088/1755-1315/304/2/022004

Van Maren, D.S., van Kessel, T., Cronin, K., Sittoni, L. (2015). The impact of channel deepening and dredging on estuarine sediment concentration. Continental Shelf Research, 95(October), 1–14. https://doi.org/10.1016/j.csr.2014.12.010

Xie, G., Zhang, Y., Liu, J., Xue, H., Ge, J., He, X., Ma, W., & Chai, F. (2023). Improvement of the sediment flux estimation in the Yangtze River Estuary with a GOCI data adjusted numerical model. Ocean Modelling, 186, 102284. https://doi.org/https://doi.org/10.1016/j.ocemod.2023.102284.

Impact of the reduction of Zostera meadows on sediment dynamics in a mesotidal coastal lagoon

Le Pevedic A. [1], Ganthy F. [2], and Sottolichio A. [3]

Keywords: seagrass meadows, sediment dynamics, mudflats, mesotidal lagoon

Abstract

Seagrass beds play a major role in coastal and estuarine sediment dynamics, due to their ability to promote particle deposition and limit bed erosion (Ward et al., 1984; Gacia et al., 1999; Neumeier and Amos, 2006; Kombiadou et al., 2014; Donatelli et al., 2018). However, the recent decline of seagrass meadows on a global scale has greatly reduced their function regulator of sediment fluxes. The Arcachon Basin (SW France) is an atlantic mesotidal lagoon hosting the largest Zostera noltei meadow in Europe, which have been particularly affected by decline. The reduction in the spatial footprint in the lagoon is estimated at 45% in 23 years, as proven several surveys made between 1989 and 2012 (Figure 1). Several observations indicate consequences on sediment coverage and water turbidity but they have barely been analyzed in detail. In this study, a hydro-bio-sedimentary numerical model is used in order to understand how the regression of seagrass beds has modified the sediments dynamics of this environment, where 75% of the total surface is occupied by intertidal mudflats.

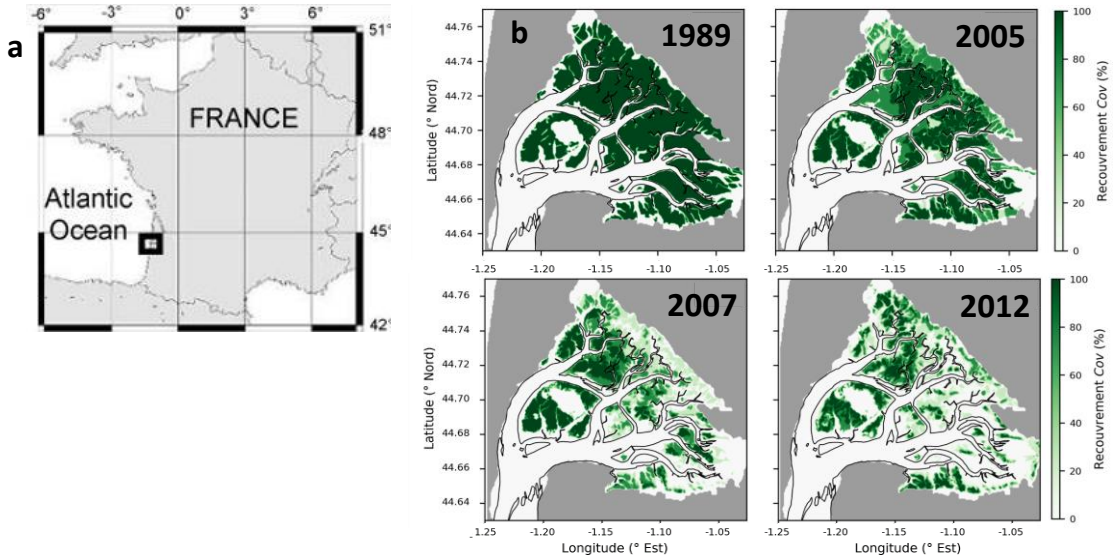

Figure 1: a) Location of the Arcachon lagoon. b) Maps of the lagoon showing the surface of meadows in 1989, 2005, 2007 and 2012 (data from Auby, 1991; Plus et al., 2010; Lafon et al., 2013)

The model used is based on the coupling of MARS3D model (Lazure and Dumas, 2008) for hydrodynamics and MUSTANG model (Mengual et al., 2017) for suspended sediment transport (mud and sand). It has the specificity of taking into account the influence of vegetation on hydrodynamics, but also on erosion and deposition fluxes, through the parameterization of effects of blocking or trapping by the foliage and the stabilization of the sediment bed by the roots. For the simulations, two scenarios are run with identical forcings, differing only in the map of vegetation coverage, to represent the pre- and post- decline configurations, before 1989 and after 2016 respectively.

Results revealed a significant increase of erosion fluxes with the regression of seagrass beds (Figure 2a and 2b). Between the pre- and post- decline scenarios, SSC increased by about 10 % in the channels and 30 % in the northern corner of the lagoon, but decreases by 30 % on the rest of the tidal flats. In summer, the increase in SSC is observed throughout the lagoon, with a percentage increase ranging between 50 % and 100 % in the western part of the lagoon and the inlet, and a 3- to 6-fold increase in the eastern part of the lagoon. The most significant changes in SSC occur at the landward end of the inner channels. These hotspots of SSC change (> 600 %) indicate the tendency for more sediments to reach the landward end of the channels and accumulate in these areas following seagrass decline.giving rise to suspended sediment concentration (SC) which on average doubled at the scale of the Basin and going so far as to be multiplied by 6 in certain internal channels of Basin bottom.

Seagrass loss not only modified tidal hydrodynamics by intensifying current velocities and altering tidal asymmetry, but also enhanced sediment erosion and limited deposition, due to the reduction of their capacity to stabilize the seabed and trap sediment.

The modification of these processes contributed jointly to the reorganization of sediment fluxes and the redistribution of the different sediment classes, consequently altering the seabed composition throughout the lagoon. A clear contrast emerged between the tidal flats in the center of the lagoon, which eroded and became sandier, and those located along the lagoon's coastline, which accreted and became siltier. The simulated changes in seabed level appeared very consistent with the observations made in the Arcachon lagoon,

[1] Ifremer, LITTORAL, Arcachon, France and University of Bordeaux, EPOC, Pessac, France, arnaud.le-pevedic@u-bordeaux.fr
[2] Ifremer, LITTORAL Arcachon, France, florian.ganthy@ifremer.fr
[3] University of Bordeaux, Laboratoire EPOC, Pessac, France, aldo.sottolichio@u-bordeaux.fr

suggesting that the decline of seagrasses may account for most of the bathymetric changes observed in this environment over the last three decades.

Although similar tendencies regarding the modification of sediment dynamics were observed in summer and winter, the intensity of the changes was much milder in the winter period, characterized by lower seagrass biomass. Only the seabed level exhibited larger variations during this season, due to the loss of below-ground biomass and subsequent reduction in seabed stabilization, associated with more energetic hydrodynamic conditions.

The significant remobilization of sediment and increase in suspended sediment concentration were shown to have deteriorated the environmental conditions by reducing light availability, which is expected to have induced additional seagrass loss. Future research should evaluate the impact of light condition deterioration on the decline of Zostera meadows in the Arcachon lagoon.

In addition, the regression of seagrasses implies a redistribution of the different sediment classes, leading to accretion and siltation of the basin bottom foreshores, as well as erosion and the increase in the sandy fraction of the foreshores in the areas more central (Figure 2c). Finally, the modification of the net erosion/deposition flows made it possible to explain the morphological evolutions observed in the lagoon over the past 30 years, suggesting that seagrass regression is the main contributor.

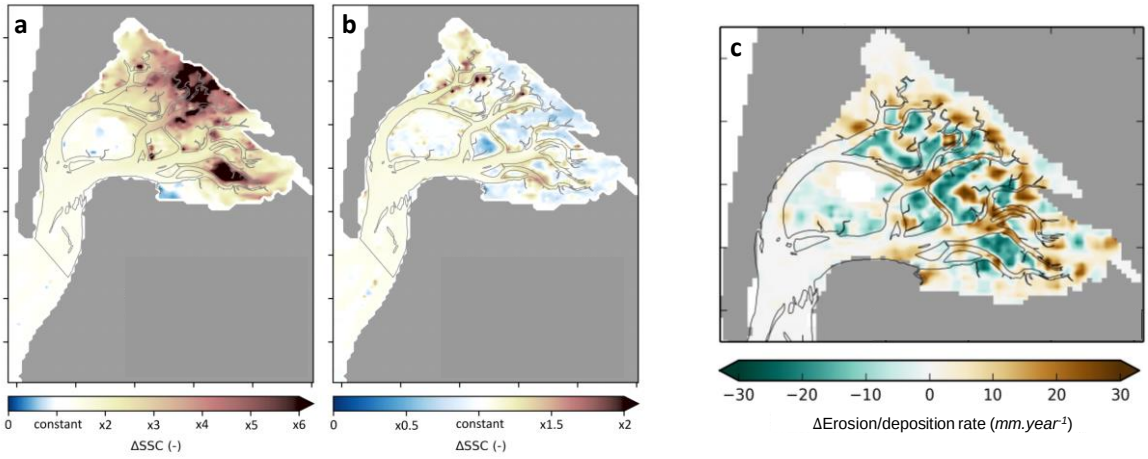

Figure 2: (a) and (b): Changes in time-averaged suspended sediment concentration (ΔSSC) due to seagrass decline in summer (a) and in winter (b). Positive values indicate increase in SSC. (c) Changes in the erosion rate due to seagrass decline. Positive/negative values denote more deposition/erosion.

References

Auby, I. (1991). Contribution à l'étude des herbiers de Zostera noltii dans le bassin d'Arcachon : Dynamique, production et dégradation, macrofaune associée. Thèse Doctorat d'Etat, Université Bordeaux 1, 162 pp

Donatelli, C., Ganju, N. K., Fagherazzi, S. and Leonardi, N. (2018). Seagrass Impact on Sediment Exchange Between Tidal Flats and Salt Marsh, and The Sediment Budget of Shallow Bays. Geophysical Research Letters, 45(10), 4933-4943

Gacia, E., Granata, T. C. and Duarte, C. M. (1999). An approach to measurement of particle flux and sediment retention within seagrass (Posidonia oceanica) meadows. Aquatic Botany, 65(1-4), 255-268

Kombiadou, K., Ganthy, F., Verney, R., Plus, M. and Sottolichio, A. (2014). Modelling the effects of Zostera noltei meadows on sediment dynamics : Application to the Arcachon lagoon. Ocean Dynamics, 64(10), 1499-1516.Lafon, V. (2013). Cartographie de l'herbier à Zostera noltii du Bassin d'Arcachon par télédétection spatiale. Rapport final

Lazure, P. and Dumas, F. (2008). An external–internal mode coupling for a 3D hydrodynamical model for applications at regional scale (MARS). Advances in Water Resources, 31(2), 233-250

Mengual, B., Hir, P., Cayocca, F. and Garlan, T. (2017). Modelling Fine Sediment Dynamics : Towards a Common Erosion Law for Fine Sand, Mud and Mixtures. Water, 9(8), 564

Neumeier, U. and Amos, C. L. (2006). The influence of vegetation on turbulence and flow velocities in European salt-marshes. Sedimentology, 53(2), 259-277

Plus M., Dalloyau S., Trut G., Auby I., de Montaudouin X., Emery E., Noël C. and Viala C. (2010). Long-term evolution (1988-2008) of Zostera spp. meadows in Arcachon Bay (Bay of Biscay). Estur Coast Shel Sci, 87:357-366

Ward, L. G., Michael Kemp, W. and Boynton, W. R. (1984). The influence of waves and seagrass communities on suspended particulates in an estuarine embayment. Marine Geology, 59(1-4), 85-103.

The local tidal response to bathymetry evolution and level rise in a channel-shoal environment

Lepper R. [1] and Kösters F. [1]

Keywords: sea level rise, bathymetry, tidal flats, tides, North Sea, Wadden Sea.

Abstract

Intertidal flats and salt marshes in channel-shoal environments are at severe risk from drowning under sea level rise (SLR) ultimately ceasing their function in coastal defense. Earlier studies indicated that these environments can be resilient against moderate SLR as their mean height is believed to correlate with tidal amplitude and mean sea level. Recent morphological analyses in the German Wadden Sea on the Northwestern European Continental shelf contradicted this assumption as mean tidal flat accretion surpassed relative SLR Shelf tenfold (Benninghoff and Winter, 2019; Lepper, 2023); indicating that nonlinear feedback between SLR, coastal morphodynamics, and tidal dynamics played a role. We explored this relationship in the German Wadden Sea's channel-shoal environment by revisiting the sensitivity of tidal dynamics to present-day SLR and coastal bathymetry evolution over one nodal cycle (1997 to 2015) with a numerical model (Lepper et al., 2024, in review). We found a proportional response of tidal high and low water to SLR when the bathymetry was kept constant. In contrast, coastal bathymetry evolution caused a spatially-varying hydrodynamic reaction with both increases and decreases of tidal characteristics within few kilometers (Figure 1). To our surprise, local and regional patterns differed significantly. In some places, we observed that the increase of tidal high and low water from sea level rise was nearly compensated by local bathymetry evolution (e.g., Figure 1, a, bottom left). As most observational data are obtained at the coast, this phenomenon has noteworthy implications on e.g., tidal gauge data or coarse resolution models.

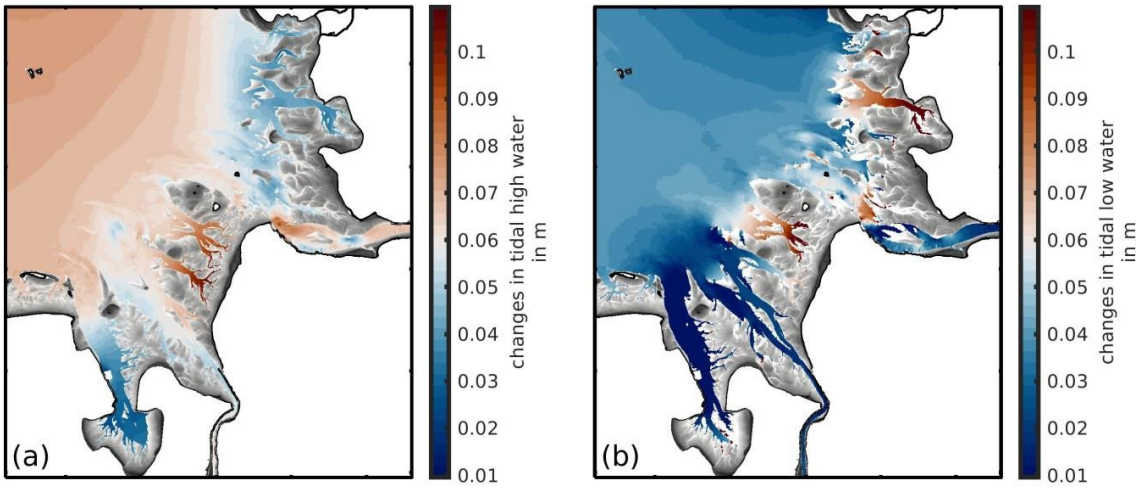

Figure 1. A detailed view at the changes in tidal high water (a) and low water (b). The displayed differences result from bathymetry evolution and SLR. Red and blue patches indicate an increase and a decrease of the respective tidal characteristic. White patches represent no-data values or land while gray patches indicate the intertidal zone at low water. Note that tidal high and tidal low water differences were illustrated with respect to the modeled SLR of 5.9 cm.

An explorative assessment of potential mechanisms gave some indication that energy dissipation declined near the coast which we related to decreasing tidal prism and declining tidal energy import. Results stress the fact that an accurate representation of coastal morphology in hind- and nowcasts and ensembles for bathymetry evolution to assess the impact of SLR are needed when using numerical models. However, it remains uncertain, why bathymetry evolution caused declining tidal prims although one may expect opposite under sea level rise.

References

Benninghoff, M., Winter, C. Recent morphologic evolution of the German Wadden Sea. Sci Rep 9, 9293 (2019). https://doi.org/10.1038/s41598-019-45683-1

Lepper, Robert. "A Contribution to Understanding the Recently Enhanced Coastal Siltation in the German Wadden Sea." Institut für Wasserbau (TU Hamburg), 2023. https://hdl.handle.net/11420/43675.

Lepper, R., Jänicke, L., Hache, I., Jordan, C., and Kösters, F.: Exploring the Tidal Response to Bathymetry Evolution and Present- Day Sea Level Rise in a Channel-Shoal Environment, EGUsphere [preprint], https://doi.org/10.5194/egusphere-2024-283, 2024.

[1] Federal Waterways Engineering and Research Institute, Hamburg (BAW), robert.lepper@baw.de

Modelling of current and sediment plumes around a coastal inlet

Li H. [1], Rucker C.A. [2], Lin L. [3], and Conner K.B. [4]

Keywords: Inlet, nearshore, hydrodynamics, sediment transport, sediment plume, numerical modelling.

Abstract

Nearshore transport and distribution of suspended sediment are greatly controlled by coastal waves and current. To study sediment fate and transport processes, the Eulerian and the Lagrangian modelling are two approaches that are often applied in numerical simulations of a water body. The Eulerian simulation of a current field focuses on fixed locations in a model domain and investigates flow variations over time, whereas the Lagrangian modelling focuses on individual water particle and the flow analysis is performed by following each particle within the model domain. While the Lagrangian modelling presents an individual particle's pathway by calculating its position over time, the Eulerian modelling describes the transport of water particles and dissolution by advection and diffusion in continuous flow field and demonstrates the concentration and distribution of water properties. Therefore, investigating migration of sediment plume, it is more appropriate to apply the Eulerian modelling approach, such as sediment transport modelling, sediment tracer simulations (see Elias et al., 2011).

Dredge and placement activities are required for maintaining a navigable depth for vessels traveling along a navigation channel and through an inlet. During these operations a great amount of sediment materials can be suspended and carried around by ocean current. The suspension and transport of sediments form a sediment plume surrounding dredge and placement sites. In nearshore coasts and estuaries, the sediment plume could travel a long distance, and suspended sediment concentrations in water column and sediment deposition in atypical locations could have a significant impact on aquatic species and ecosystems (see Suedel et al., 2015). In this study, the Eulerian modelling is performed at Beaufort Inlet, North Carolina. Sediment materials placed at designated nearshore and offshore sites are tracked as released sediment tracer and the sediment plume dynamics and fate are evaluated.

The Coastal Modelling System (CMS), consisting of a hydrodynamic and sediment transport model (CMS-Flow) and a spectral wave transformation model (CMS-Wave), is applied in the Beaufort Inlet system (Figure 1a). This model includes representation of relevant nearshore processes for practical applications of navigation channel performance and sediment management at coastal inlets and adjacent beaches (see Lin et al., 2011; Sanchez et al., 2011). To assess sediment migration from dredged material placement sites, the present study needs to trace sediment and demonstrate sediment plume spreading originated from those sites. This process can be specified and computed using the CMS feature of sediment tracer simulations (see Li et al., 2019).

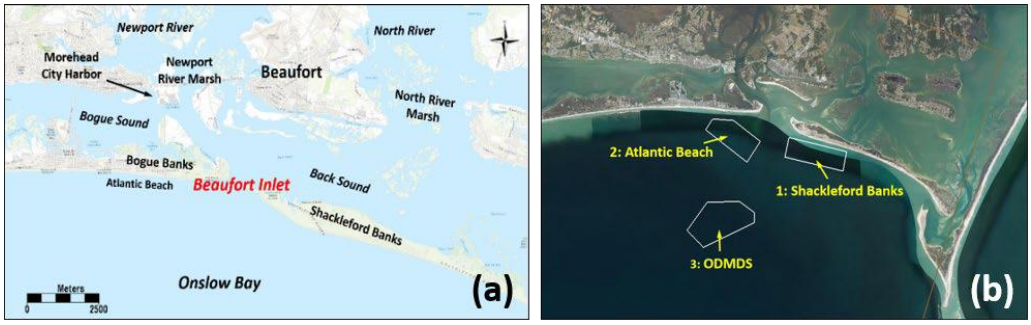

Figure 1. Beaufort Inlet, North Carolina: (a) Location map, (b) Designated material placement sites around the inlet system.

A telescoping variable-resolution CMS-Flow grid is developed for Beaufort Inlet and adjacent beaches. The telescoping grid system permits much finer local grid resolution to resolve hydrodynamic and sediment features in areas of high interest. The CMS-Wave grid with varying cell sizes is generated for wave modelling, covering the same domain and with similar spatial resolution as the CMS-Flow grid. Sediment materials from regular channel maintenance dredging are placed in designated areas as shown in Figure 1b.

A representative summer and a winter month are selected to model the spreading of sediment plume. The modelling scenarios are developed by specifying the placement sites as sediment sources, within which sediment materials in the top bed layer are tagged and tracked as sediment tracer. To conduct plume analysis, polygons are drawn as sediment traps to count sediment mass. The polygon areas include Inlet and navigation channel, open nearshore zone, and bay area.

[1] US Army Engineer Research Development Centre, Honghai.Li@usace.army.mil.
[2] US Army Engineer Wilmington District, Carter.A.Rucker@usace.army.mil.
[3] US Army Engineer Research Development Centre, Lihwa.Lin@usace.army.mil.
[4] US Army Engineer Wilmington District, Kevin.B.Conner@usace.army.mil.

Summer and winter month current patterns are demonstrated by the spatial distribution of monthly averaged current vectors in Figure 2a. The average current field illustrates net water transport from the ocean side to the bay side through the inlet. Averaged currents on the eastern side of the inlet channel have a relatively larger peak speed than on the western side. Flow split occurs into the bay behind Shackleford Banks and Bogue Banks.

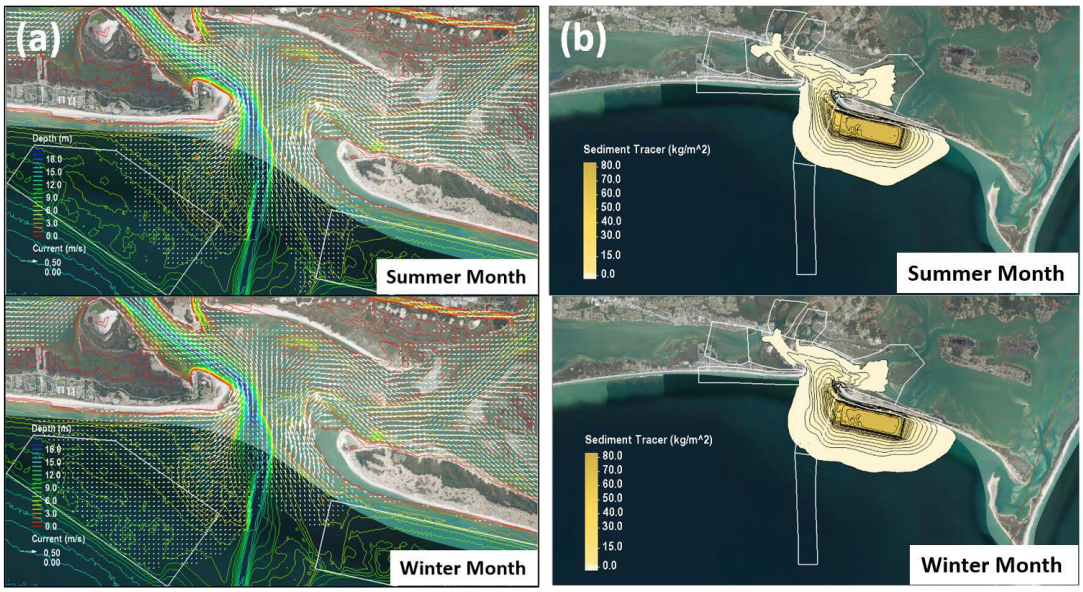

Figure 2. Calculated summer and winter results: (a) Monthly averaged currents, (b) Sediment plume distributions at the end of monthly simulations. Polygons indicate dredged material placement area, the Shackleford Banks site.

Corresponding to wave and current conditions, sediment plume distributions are illustrated by the material tracing from the Shackleford Banks site during the summer and winter month simulations (Figure 2b). The sediment plume is featured by spreading and dissipation surrounding the releasing site. At the end of the monthly simulations, there are longshore and offshore spreading in open nearshore area. Strong tidal flows on the eastern side of the inlet channel result in plume intrusion to the bay and the centre of the plume is moving northward through the eastern portion of the channel along Shackleford Banks. On the bay side, the plume moves in both directions towards Back Sound and Bogue Sound and it almost reaches the maximum coverage extending to North River Marsh on the east of and Newport River Marsh on the west of the inlet.

Quantitative movement of sediment is also estimated by counting total mass within sediment trap areas at the end of the simulations. The final results show that more than 95% of sediment mass placed stay within the Shackleford Banks site after the one-month simulation. Three percent of materials move to the inlet entrance channel and less than one percent of the sediment mass in the nearshore zone along Shackleford Banks (close to the placement site).

A coupled wave, hydrodynamic, sediment transport model, the Coastal Modelling System (CMS), is developed and applied to investigate transport and evolution of plumes for sand materials placed around the Beaufort Inlet estuarine system. The model calculations include tracking and delineating pathways of sand materials originated from different placement areas and surrogated as sediment tracer. From the model results, the major conclusions are: 1) tidal forcing is dominant in controlling the distribution and spreading of sediment plumes; 2) flow asymmetry and split through the inlet channel are confirmed in sediment tracer simulations; 3) nearshore material placement sites are under large influence of coastal processes (sediment movement in both cross shore and longshore directions); 4) sediments originated from the two nearshore sites follow different pathway leading to the bayside.

References

Elias, E, Gelfenbaum, G, Van Ormondt, M, Moritz, H.R. (2011) Predicting sediment transport patterns at the mouth of the Columbia River, Proc. Coastal Sediments, pp. 588–601.

Li, H, Beck, T.M, Moritz, H.R, Groth, K, Puckette, T, Marsh, J, Sanchez, A. (2019) Sediment tracer tracking and numerical modeling at Coos Bay Inlet, Oregon. Journal of Coastal Research, vol. 35(1), pp 4-25.

Lin, L, Demirbilek, Z, Mase, H. (2011) Recent capabilities of CMS-Wave: A coastal wave model for inlets and navigation projects. Journal of Coastal Research, Special Issue 59, pp. 7–14.

Sanchez, A, Wu, W, Beck, T.M, Li, H, Rosati III, J, Thomas, R, Rosati, J.D, Demirbilek, Z, Brown, M.E, Reed. C. (2011) Verification and validation of the Coastal Modeling System, report 3: hydrodynamics. ERDC/CHL TR-11-10. Vicksburg, MS: US Army Engineer Research and Development Center.

Suedel, B.C, Clarke, J.U, Wilkens, J.L, Lutz, C.H, Clarke, D.G. (2015) The effects of a simulated suspended sediment plume on eastern oyster (Crassostrea virginica) survival, growth, and condition. Estuaries and Coasts, vol. 38(2), pp. 578-589.

Coupled hydrological-hydrodynamic modeling of watershed, tidal rivers and estuaries: Assessing the impacts of drought, sea-level rise and human-accelerated chemical weathering on salt intrusion and freshwater salinization

Li M. [1], Chen Z. [2], Meija A. [3], Chant R. [4], Hadjimichael A. [3], Kaushal S. [5], Keitzer S. [2], Lassiter A. [6], Najjar R. [3], Puckett S. [7], Rohith A.N. [3], Spangler A. [3], Wang S. [8], and Wang X. [8]

Keywords: salt intrusion, sea level rise, drought, climate change, coupled hydrological, hydrodynamic modeling, freshwater supplies

Abstract

About two-thirds of the global drinking water supply come from surface waters, including tidal rivers, the tidal freshwater region of estuaries. Drought and sea level rise, which lead to saltwater intrusion from the ocean, and changes in land-use, which lead to freshwater salinization, are putting this precious water resource at risk. This risk extends to water uses for thermoelectric power, irrigation, and industrial production. Hydrodynamic models used to predict saltwater intrusion in estuaries employ a number of numerical schemes, varying grid resolutions, and different parameterizations for unresolved subgrid processes. Few con- sider salt inputs from watersheds. Watershed-scale hydrological models and hydrodynamic models of estuaries and coastal oceans are often run separately, making it hard to assess the combined impacts of drought and sea level rise on saltwater intrusion under climate change. Here we report the development of coupled hydrological-hydrodynamic models for predicting salt intrusion into estuaries and tidal rivers and artificial intelligence algorithms for designing management strategies to mitigate the impacts of salt contamination of water supplies. The hydrological model is based on the Soil and Water Assessment Tool (SWAT) and the hydrodynamic model is based on the unstructured-grid Finite Volume Coastal Ocean Model (FVCOM). As a pilot study, we have configured FVCOM for Chesapeake Bay and its major tributaries and SWAT for the watersheds of the Susquehanna River and the Potomac River. Hindcast simulations are conducted over a ten-year period (2001-2010) to investigate how river flows, tides and winds affect salt intrusion into the oligohaline and tidal fresh regions of the Susquehanna River, the Potomac River and the James River at daily to seasonal time scales. While tides in the James River features strong spring-neap cycles, tides in the Susquehanna River is a mixture of semi-diurnal and diurnal tides. A comparative analysis shows how tidal characteristics influences the salt intrusion into the three tidal rivers. Given their different geographic locations, the effects of local and remote winds are also different. To investigate how climate change affects salt intrusion at decadal and century time scales, climate downscaling projections are conducted for the mid-21st century (2041-2050) for two climate change scenarios and compared with the hindcasts in 2001-2010. The effects of sea-level rise and changing hydrological cycles on the salinity level in the tidal rivers are assessed and potential policy interventions such as reservoir releases are explored. Salt inputs from the watersheds due to human-accelerated chemical weathering and anthropogenic salt pollution are also considered and the effect of freshwater salinization is compared against that of oceanic salt intrusion.

[1]University of Maryland Center for Environmental Science – 2020 Horn Point Road, Cambridge, MD 21613, United States
[2]University of Maryland Center for Environmental Science – United States
[3]Pennsylvania State University – United States
[4]Rutgers University – United States
[5]University of Maryland, College Park – United States
[6]University of Pennsylvania – United States
[7]Izaak Walton League of America – United States
[8]Salisbury University – United States

Impact of islands on tidally dominated river plumes: a high-resolution modelling study

Li X. [1], Chrysagi E. [1], Klingbeil K. [1], and Burchard H. [1]

Keywords: river plumes, submesoscale island wakes, isohaline analysis, diahaline water exchange.

Abstract

When flow passes over topographic features such as headlands and islands, island wakes can arise at the lee side of the flow (Geyer et al., 1993; Dong et al., 2007). Island wakes are associated with enhanced biological productivity, increased mixing, and water mass transformation (Simpson & Tett, 1986; Hasegawa et al., 2004).

While previous studies have mainly focused on the dynamical and biological effects of island wakes in the open ocean, here we focus on a large tidally-dominated estuary with numerous islands, aiming to investigate the impact of such wakes on the offshore transport of river plumes. To this end, we use numerical simulations with unprecedented grid resolution in the plume region and around the islands. Our study area is the Pearl River Estuary, a region where satellite images indicate that oscillating wakes occur in the lee and far downstream of the islands.

We show that submesoscale island wakes are ubiquitous in the plume-influenced region and can affect a large area around the islands as the tidal flow reverses (Figure 1c). A high correlation is observed between these strong vorticity tails and the horizontal patterns of surface salinity mixing and salinity gradients. Sensitivity experiments show that the strong vorticity tails disappear with the hypothetical 'removal' of the islands (Figure 1d). The intense mixing associated with the tails will also vanish after the removal of the islands (Figure 1a, b). Analysis based on an isohaline coordinate framework shows that isohaline surface areas are reduced with the presence of islands. It is proven that this 'limiting' effect of islands on the plume extension is related to the salinity mixing and the associated diahaline water exchange. The evidence of island wakes in the PRE suggests that the effects of islands should be considered when interpreting observational data in this region (or other coastal ocean regions with the presence of islands), especially for surface dynamics close to the islands.

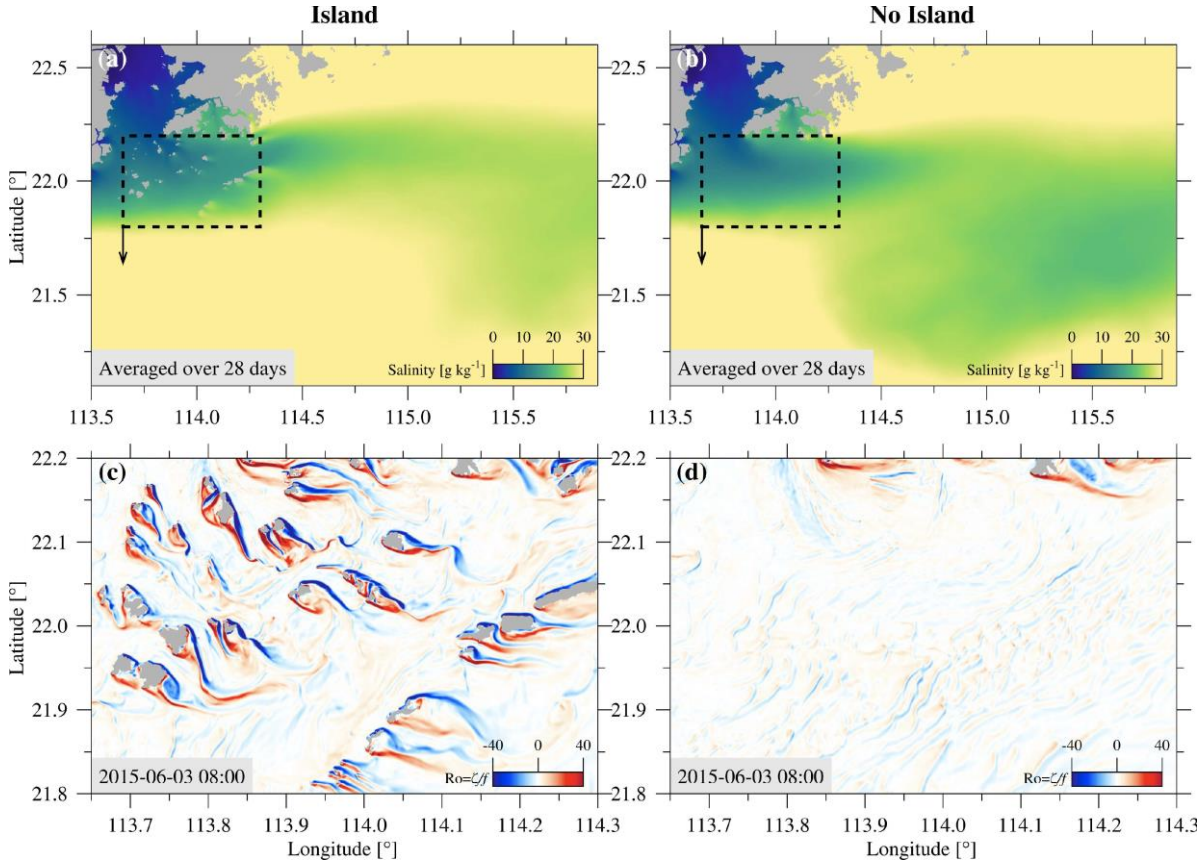

Figure 1. (a) Horizontal distribution of the spring-neap (28 days starting from 2015-06-03 00:00) averaged surface salinity in the "Island" experiment. The black box denotes the location of panel c. (b) Same as panel a, but for the "No Island" experiment. (c) Horizontal distribution of the instantaneous normalized surface vorticity Ro in the "Island" experiment. (d) Same as panel c, but for the "No Island" experiment.

[1] Leibniz Institute for Baltic Sea Research Warnemünde, Rostock, Germany, xiangyu.li@io-warnemuende.de.

References

Dong, C., McWilliams, J. C., & Shchepetkin, A. F. (2007). Island wakes in deep water. *Journal of Physical Oceanography*, 37(4), 962–981.

Geyer, W. R. (1993). Three-dimensional tidal flow around headlands. *Journal of Geophysical Research: Oceans*, 98(C1), 955– 966.

Hasegawa, D., Yamazaki, H., Lueck, R., & Seuront, L. (2004). How islands stir and fertilize the upper ocean. *Geophysical research letters*, 31(16).

Simpson, J., & Tett, P. (1986). Island stirring effects on phytoplankton growth. *Tidal mixing and plankton dynamics*, 41–76.

Noether's conservation laws for ocean boundary layers

Llorente V.J. [1,2], Padilla E.M. [3], Díez-Minguito M. [4], and Valle-Levinson A. [5]

Keywords: Ekman layer, eddy viscosity, symmetries, conserved quantity.

Abstract

This study presents conservation laws (and corresponding conserved quantities) in the ocean boundary layer that stablish theoretical relationships between surface wind-stress, eddy viscosity, and pressure gradients with the depth-dependent horizontal velocity field in finite-depth oceans.

Research work conducted by Ekman (1905) concerning wind-driven currents within the surface boundary layer is a fundamental theory to physical oceanography. It helps describe phenomena such as upwelling and downwelling, which significantly influence global circulation patterns and biological productivity. Ekman concluded that for steady horizontal currents in the water column, the equilibrium of momentum must be established between the Coriolis force and the vertical divergence of turbulent shear induced by the wind. For example, the analytical solution derived by Ekman means that the vertical profile of the horizontal currents features its maximum current at the surface, which is deflected 45º to the right (left) form the wind direction in the Northern (Southern) Hemisphere.

However, the Classical Ekman (1905)'s Theory cannot be expected to closely match actual observations of wind-driven circulation. One major drawback of the classical Ekman model was the assumption of eddy viscosity coefficient, named K, to be constant in the water column. It has long been recognized that wind-induced turbulent mixing is expected to be higher in the upper layers. Higher values of the eddy viscosity are expected within layers of uniform density and comparatively small within the transition layers and below mixed layers.

Therefore, understanding the Ekman layer is important to quantify deviations to observed magnitudes from the classical behaviour. For such propose, conservation laws are derived which allow to extract novel relevant theoretical relationships in the momentum equations, to the classical Ekman model and related models:

$$\begin{cases} f\mathbf{u}^{\perp} + \mathbf{b}(z) = \dfrac{\partial}{\partial z}\left(K(z)\dfrac{\partial \mathbf{u}}{\partial z}\right) & 0 < z < -H \\ \rho_0 K(0)\left.\dfrac{\partial \mathbf{u}}{\partial z}\right|_{z=0} = \boldsymbol{\tau}_w & z = 0 \\ \mathbf{u}(-H) = \mathbf{u}_\tau & z = -H \end{cases} \tag{1}$$

where $\mathbf{u} = (u, v)$ is the velocity field; $\mathbf{u}^{\perp} = (-v, u)$, the counterclockwise velocity field; K, the depth-dependent eddy viscosity; $\mathbf{b}$, the depth-dependent pressure gradients or any body force apply to the water column; $\rho 0$, a reference density (e.g., at surface level); $\boldsymbol{\tau}_w$, the surface wind stress; $\mathbf{u}_\tau$, the bottom shear velocity; and H, the depth of the water column. Both pressure gradients and eddy viscosity are separately prescribed. In the limit case of $H \to +\infty$, $\mathbf{b} = \mathbf{0}$, $\mathbf{u}_\tau = \mathbf{0}$, an $K = K0$ = const., the previous model reduced to the classical Ekman model.

To reach the aims of the work, we formulate the equations of the model (1) into a variational framework, therefore conservation laws ($\partial j_\star / \partial z = 0$ where $j_\star$ is the conserved quantity) can be obtained from the symmetry (continuous transformations) of Lagrangian, using Noether (1918)'s (first) Theorem. The Lagrangian functional of the model (1) accounts for: a viscous term that represents the vertical turbulent mixing, and a coupled Coriolis-pressure gradient term showing the rotation of the gradient of the velocity field and the mass transport. The invariance of the Lagrangian was studied for physical symmetries: translation in space,

$$\begin{cases} z' = z + \epsilon \\ \mathbf{u}' = \mathbf{u} \end{cases}, \tag{2}$$

scaling,

$$\begin{cases} z' = z \\ \mathbf{u}' = \mathbf{u} + \mathbf{u}\epsilon \end{cases}, \tag{3}$$

and rotation (or phase)

$$\begin{cases} z' = z \\ \psi' = \psi e^{if/|f|\epsilon} \\ \psi^{*\prime} = \psi^* e^{-if/|f|\epsilon} \end{cases}, \tag{4}$$

[1] University of Zaragoza (UNIZAR), Zaragoza, Spain, vjllorente@unizar.es
[2] Andalusian Institute for Earth System Research (IISTA), University of Granada (UGR), Granada, Spain, vjllorente@ugr.es
[3] Universitat Politècnica de Catalunya (UPC), Barcelona, Spain, enrique.padilla@upc.edu
[4] Andalusian Institute for Earth System Research (IISTA), University of Granada (UGR), Granada, Spain, mdiezm@ugr.es
[5] University of Florida (UFL), Gainesville, USA, arnoldo@ufl.edu.

of the solution for small real values of a parameter ϵ where $\psi = u + iv$ is the complex velocity field; $i^2 = -1$, the imaginary

unit; and ψ^*, the complex conjugate of ψ. Therefore, the boundary layer is studied in detail with the new conservation laws. The present research work is an extension of Llorente, Padilla, and Diez-Minguito (2023) where only the invariance of the Lagrangian was studied under the symmetry (2) and for the classical Ekman model.

For constant eddy viscosity (the classical Ekman model) those conservations laws relate:

1) production of enstrophy density ($\omega^2/2$) with cumulative helicity $\left(\int_z^0 \boldsymbol{\omega}\cdot\mathbf{u}\,\mathrm{d}z\right)$; density

2) kinetic energy density gradient ($\partial(\mathrm{u}^2/2)/\partial z$) with cummulative enstrophy $\left(\int_z^0 \omega^2/2\,\mathrm{d}z\right)$; and density

3) helicity density ($\boldsymbol{\omega}\cdot\mathbf{u}$) with production of kinetic $\left(\int_z^0 \mathrm{u}^2/2\,\mathrm{d}z\right)$. energy

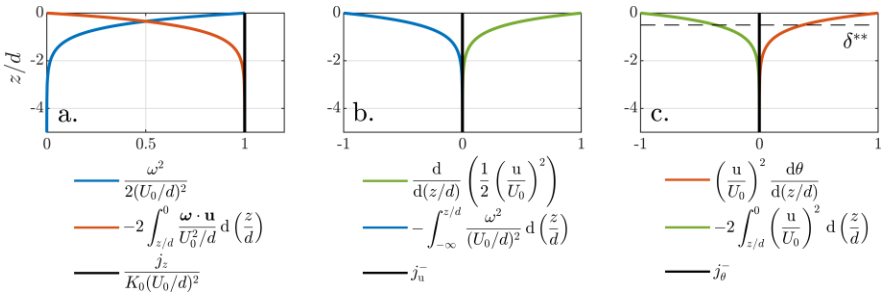

Figure 1. Balances in the Ekman layer. Conserved quantities $j_\star$ in black solid lines (panels a, b, and c). ω is the vorticity; θ, the veering angle; $\boldsymbol{u}$, the velocity field; $u^2 = \boldsymbol{u}\cdot\boldsymbol{u}$; K_0, eddy viscosity coefficient (assume constant); U_0 and d, reference velocity and Ekman depth from the Ekman' solution (Ekman, 1905); δ^{**}, the momentum thickness of the boundary layer.

The theoretical relationships evidence the balance (Figure 1) results in turbulent dissipation of kinetic energy and enstrophy inducing a rotation the velocity field, giving rise to the well-known Ekman spiral, distinguished by its helicity, $\mathcal{H} := \int_{-\infty}^0 \boldsymbol{\omega}\cdot\mathbf{u}\,\mathrm{d}z$

An interesting outcome are obtained when depth-integrate the conservation laws. For example, symmetry in scale leads to a direct relation of the surface deflection angle, ϕs, with the enstrophy, $\mathcal{E} := \int_{-\infty}^0 \omega^2/2\,\mathrm{d}z$, of the water column:

$$\cos\phi_s = \sqrt{2}\frac{d}{U_0^2}\mathcal{E}\,. \tag{5}$$

In the Classical Ekman (1905)'s Theory, the theoretical value of $\mathcal{E}$ yields $\cos\phi s = \sqrt{2}/2$, resulting in the well-known theoretical value of 45º. The direction of rotation is determined, e.g., by the sign of the helicity.

For depth-dependent eddy viscosity and extra body force, e.g., pressure gradients, the new balances as in Figure 1 are generalized. In such a case, the energy supply at the surface is not fully transmitted to the helicity. Stratification and body forces take energy away from the spiral. Indeed, the helicity of the spiral is bounded by the integral of a diffusive flux for the enstrophy density. After depth-integrate the conservation laws, a generalize formula for the surface deflection angle is obtained:

$$\cos\phi_s = \frac{\mathbf{u}_\tau\cdot\boldsymbol{\tau}_b}{\mathrm{u}_0\tau_w} + \frac{\rho_0}{\mathrm{u}_0\tau_w}\left[2\bar{K}\tilde{\mathcal{E}} + W_\mathbf{b}\right], \tag{6}$$

where $\boldsymbol{\tau}b$ is the bottom stress, $\bar{K}$ is the average of the eddy viscosity, $\tilde{\mathcal{E}}$ is the eddy-weighted-average enstrophy, and $W\mathbf{b}$ is the work on the water column by the body forces.

From a practical point of view, the relationships obtained (among others) could allow characterized better the oceanic boundary layer and to narrow down the values of K in the water column, which depend on the ratio between the shear at the bottom and at the surface. The key point is to be able to obtain a symmetry-preserving eddy viscosity from horizontal current profile observations. If the quantities $j_\star$ are conserved from the observational data, then try to infer an eddy viscosity from that.

References

Ekman, V.K. (1905) On the influence of the earth's rotation on ocean-currents. Arkiv för Matematik, Astronomi och Fysik 2 (11), 325, 1–52.

Llorente, V.J, Padilla, E.M., Díez-Minguito, M. (2023) Conserved quantities in the Ekman layer. EGU General Assembly 2023, Vienna, Austria, 24–28 Apr 2023, EGU23-8914.

Noether, A.E. (1918) Invariante variations probleme. Nachrichten von der Gesellschaft der Wissenschaften zu Göttingen, Mathematisch-Physikalische Klasse 2, 235–257.

T-UGOm unstructured grid hydrodynamic and data assimilation simulations of the Gironde Estuary for SWOT observations calibration/validation

Lyard F. [1], Jan G. [2], Caubet L. [3], Ayoub N. [4], and Bonnefond. P. [5]

Keywords: estuary hydrodynamics, data assimilation, satellite altimetry, Gironde

Abstract

T-UGOm is an unstructured grid 2D/3D hydrodynamic model, developed at LEGOS, that is intensively used for tidal and storm surges simulations over global Ocean down to estuarine/deltaic systems configurations. It is the underlying model for the FES tidal atlases and global storm surges simulations from which de-aliasing corrections for tides and DAC (dynamic atmospheric corrections, i.e. high frequency storm surge signal) are derived and provided to satellite altimetry operational services (CNES/JPL/ESA). Among several other estuaries and delta (Amazon, Cameroon, Seine, Elbe), it has been implemented for the Gironde estuary to support science investigations (tides, tides and river flow interactions, tracers and sediment transport, river plume, etc…) in the context of satellite observations, such as altimetry.

Recently the launch of the SWOT mission has triggered a renewed interest for satellite altimetry observations in the coastal seas and, more challengingly, the delta or estuaries systems. At the present, SWOT community is facing two issues, which are closely linked: first how do we calibrate and validate the SWOT data, whose technology is far more complex than usual altimetry, and how do we deal with the necessary de-aliasing corrections (i.e tides and storm surges) to overcome the satellite low time sampling (about 10 to 20 days re-visit period). The de-tiding issue is particularly crucial over systems where tides become substantially non-stationary because of their interactions with river discharge. In both cases, our approach consists in using high accuracy shallow-water simulations, based on a precisely tuned configuration and controlled by tide gauge data assimilation. Considering the calibration/validation issue, well monitored estuaries, such as the Gironde, can be considered as excellent candidates: their size allows for capturing an entire or half-side SWOT swath over the model extent; they are enclosed in terrestrial geoids (i.e. high resolution/accuracy geoids, at least compared to marine geoids); the tide gauge network is dense enough and accurately referenced on the vertical for precisely constraining the simulated water level at a quasi-centimeter level and formally linking it with SWOT observations.

In this study, we show that TUGO simulation with the assimilation or tide gauge data enables to extend usual calibration methodologies to the SWOT swath extent by providing an spatially extended tide gauge “sea level truth”.

We will present our investigations based on this approach applied to the first year of SWOT data (science orbit) and present our first assessment about SWOT data error budget. Additional assessments based on the Gironde 2018 pre-SWOT campaign water surface level in the lower and upper estuary) will be presented. This presentation is complementary to the one of Caubet et al. (this meeting) which focusses on another detiding approach, based on empirical rating curves to deal with the issue of non- stationary tides.

[1] LEGOS laboratory, CNRS/UPS/CNES/IRD, florent.lyard@univ-tlse3.fr.
[2] EODYN, gwenaele.jan@eodyn.com (Shom, now at eOdyn)
[3] LEGOS laboratory, CNRS/UPS/CNES/IRD, lucie.caubet@univ-tlse3.fr
[4] LEGOS laboratory, CNRS/UPS/CNES/IRD, nadia.ayoub@univ-tlse3.fr
[5] Observatoire de Paris – SYRTE, pascal.bonnefond@obspm.fr

Effects of sea level rise and tidal flat growth on tidal dynamics and geometry in the Elbe estuary

Mahavadi T.F. [1], Seiffert R. [2], Kelln J. [3], and Fröhle P. [4]

Keywords: sea level rise, estuaries, tidal dynamics, tidal range, tidal flats

Abstract

Introduction

In the German Bight (southeastern bight of the North Sea) and its estuaries future global mean sea level rise (SLR), as it is projected for this century (Fox-Kemper et al. 2021), will affect coastal protection as well as the ecosystem Wadden Sea and important waterways. In order to develop appropriate adaptation strategies, e.g. for navigation, port infrastructure as well as water management in the hinterland, investigations on the effects of SLR on tidal dynamics inside the estuaries of the German Bight are necessary.

Due to tidal flat morphodynamics (Friedrichs 2011) SLR will not only influence tidal dynamics, but also the bathymetry in the Wadden Sea. Studies show that most intertidal flats in the Wadden Sea were vertically growing in a rate higher than observed SLR in the recent past (1998-2016) (Benninghoff and Winter 2019). However, facing the future acceleration of SLR, it is difficult to quantify the extent to which tidal flat growth can keep pace with SLR. Nevertheless, potential tidal flat growth should be taken into account when studying SLR-scenarios, as it strongly affects tidal dynamics in the Wadden Sea (Wachler et al. 2020; Jordan et al. 2021).

Methods

Using a highly resolved hydrodynamic-numerical model, we analysed the influence of potential SLR and tidal flat elevation scenarios on tidal dynamics in the Elbe estuary. The study was conducted using the 3D-HN-model UnTRIM² (Casulli and Walters 2000). The model domain includes the German Bight with the estuaries Ems, Weser and Elbe. For this study the following scenarios were simulated: a reference scenario, a scenario with SLR of 110 cm added at the model boundary, several scenarios with SLR of 110 cm and different hypothetical simplified tidal flat elevation in the German Bight and the Elbe estuary (Figure 1). The tidal flat areas shown in Figure 1 were elevated uniformly by a certain amount in the entire model domain, which is a highly simplified assumption. For the Elbe estuary the scenarios with tidal flat growth are further differentiated firstly by elevating the tidal flats in the mouth section of the Elbe estuary (Scenario A) and secondly by elevating the tidal flats in the mouth section and also further upstream in the estuary (Scenario B).

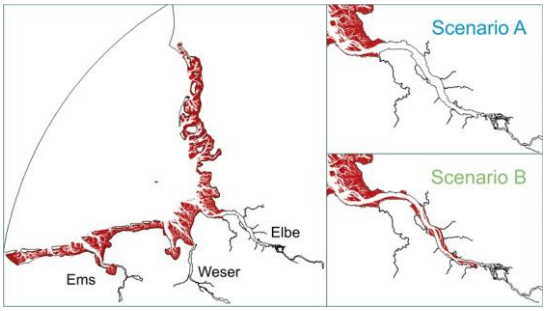

Figure 1 – Areas of tidal flat elevation in the entire model domain (left) and in the Elbe estuary (right) for two different Scenarios A and B

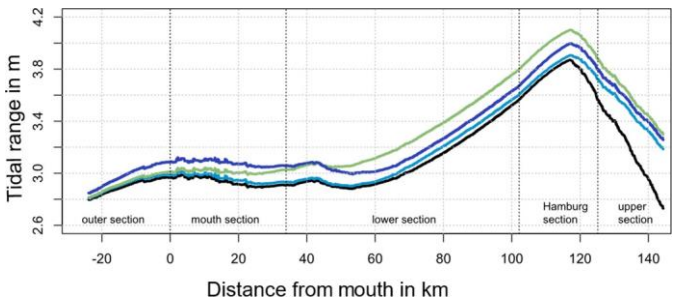

Figure 2 – Tidal range in m along the Elbe estuary profile for reference scenario (black), SLR of 110 cm (dark blue), SLR of 110 cm with 110 cm tidal flat elevation in Scenario A (light blue), SLR of 110 cm with 110 cm tidal flat elevation in scenario B (green)

Results

We analysed and visualised different mean tidal parameters along the profile of the estuaries. The results show an increase of tidal range in the Elbe estuary due to SLR and further reveal strongly varying changes with different tidal flat growth scenarios: while tidal flat elevation up to the mouth of the estuary can cause tidal range to decrease relative to SLR alone, tidal flat elevation in the entire estuary can lead to an increase in tidal range relative to SLR alone (Figure 2).

[1] Federal Waterways Engineering and Research Institute Hamburg (BAW), tara.mahavadi@baw.de
[2] Federal Waterways Engineering and Research Institute Hamburg (BAW), rita.seiffert@baw.de
[3] Federal Waterways Engineering and Research Institute Hamburg (BAW), jessica.kelln@baw.de
[4] Hamburg University of Technology (TUHH), froehle@tuhh.de

The tidal range in an estuary depends, among other things, on the estuary geometry. SLR and tidal flat elevation change the geometry of the estuary, which in turn affects tidal dynamics. To assess the changes in estuarine geometry, the following three parameters were analysed: mean water depth, convergence of cross-sectional-flow area and relative intertidal area. The results show changes in these three parameters of estuarine geometry due to SLR and tidal flat elevation, which can reveal explanatory approaches for the changes in tidal range. A detailed description of the methods, results and discussion of this study can be found in Mahavadi et al. (2023).

References

Benninghoff M, Winter C (2019) Recent morphologic evolution of the German Wadden Sea. Scientific reports 9(1):9293. doi:10.1038/s41598-019-45683-1

Casulli V, Walters RA (2000) An unstructured grid, three-dimensional model based on the shallow water equations. Int. J. Numer. Meth. Fluids(32):331–348. doi:10.1002/(SICI)1097-0363(20000215)32:3<331:AID-FLD941>3.0.CO;2-C

Fox-Kemper B, Hewitt HT, Xiao C, Aðalgeirsdóttir G, Drijfhout SS, Edwards TL, Golledge NR, Hemer M, Kopp RE, Krinner G, Mix A, Notz D, Nowicki S, Nurhati IS, Ruiz L, Sallée J-B, Slangen A, Yu Y (2021) Ocean, Cryosphere and Sea Level Change. In Climate Change 2021: The Physical Science Basis. Contribution of Working Group I to the Sixth Assessment Report of the Intergovernmental Panel on Climate Change 6:S.1211-1362. doi:10.1017/9781009157896.011.

Friedrichs CT (2011) Tidal Flat Morphodynamics: A Synthesis. Treatise on Estuarine and Coastal Science:137–170. doi:10.1016/B978-0-12-374711-2.00307-7

Jordan C, Visscher J, Schlurmann T (2021) Projected Responses of Tidal Dynamics in the North Sea to Sea-Level Rise and Morphological Changes in the Wadden Sea. Front. Mar. Sci. 8:40171. doi:10.3389/fmars.2021.685758

Mahavadi T, Seiffert R, Kelln J, Fröhle P (2023) Effects of Sea Level Rise and Tidal Flat Growth on Tidal Dynamics and Geometry of the Elbe Estuary. Preprint (accepted). doi:10.5194/egusphere-2023-1288

Wachler B, Seiffert R, Rasquin C, Kösters F (2020) Tidal response to sea level rise and bathymetric changes in the German Wadden Sea. Ocean Dynamics 70(8):1033–1052. doi:10.1007/s10236-020-01383-3

Puget Sound Dissolved Oxygen: Quantifying Changes and Identifying Mechanisms

Mascarenas D. [1], Leeson A. [2], Horner-Devine A. R. [3], MacCready P. [4], Roberts B. [5], and Brett M.T. [6]

Keywords: Puget Sound, oxygen, nutrients, urban estuaries, historical observational data

Abstract

What drives changes in dissolved oxygen concentration (DO) in Puget Sound? We investigate this question against a backdrop of significant public and political interest in the influence of human actions on local marine ecosystem health. Puget Sound is an urbanized, fjordal estuary comprising the southern portion of the Salish Sea. It is unique among North American estuaries in its depth (up to 260m), extreme bathymetric and hydrodynamic spatial variability, and large tides (MacCready, 2017). This inland sea has been home to Indigenous peoples for thousands of years, supporting human and non-human life via a rich marine ecosystem. Salmon in particular are keystone species for both marine and terrestrial environments; however, juvenile salmon growth may be hindered in low DO conditions (Del Rio et al., 2019).

Recent interest in the influence of wastewater treatment plant effluent on DO focuses on anthropogenic dissolved inorganic nitrogen (DIN; e.g., nitrate, ammonium) and its potential to drive increased primary productivity and subsequent deoxygenation as particulate organic matter sinks and is respired within the water column. Nearly 95% of Puget Sound nitrogen comes from oceanic sources (Mackas & Harrison 1997), but anthropogenic nutrients have been shown to be a driver of DO loss in other urban estuaries (e.g., Chesapeake Bay; ref. Clune et al., 2021).

To understand anthropogenic impacts on DO, we must first understand the role of natural and historical mechanisms in DO changes over various temporal and spatial scales. Current literature addresses variability in environmental factors such as DO in the nearby Strait of Georgia (e.g., Riche et al., 2014). In Puget Sound, Moore et al. (2008) correlated sea surface temperature and salinity in Puget Sound specifically to local weather and large-scale environmental indices such as Pacific Decadal Oscillation and El Niño-Southern Oscillation. We seek to add to this multi-faceted, regional conversation and focus on dissolved oxygen in Puget Sound via the following objectives.

Objective 1: Quantify trends and variability in DO and other state variables on varying spatial and temporal scales

We analyze historical and modern observational marine water quality data (e.g.; Ruffner, 2017; Alin et al., 2021; Collias, 1970) to first identify if, when, and where changes in DO have occurred in Puget Sound. Alongside DO, we evaluate changes in other physical and biogeochemical properties, such as salinity, temperature, and nutrient availability (e.g., nitrate) on decadal, interannual, seasonal, and episodic timescales. Given the inherent sparseness of observational data especially on longer timescales, sampling location and depth inconsistency requires careful spatial analyses. For example, Figure 1 shows decadal variability between recent observations (2010s) and earlier historical observations (1950s) using fall salinity, temperature, and DO data.

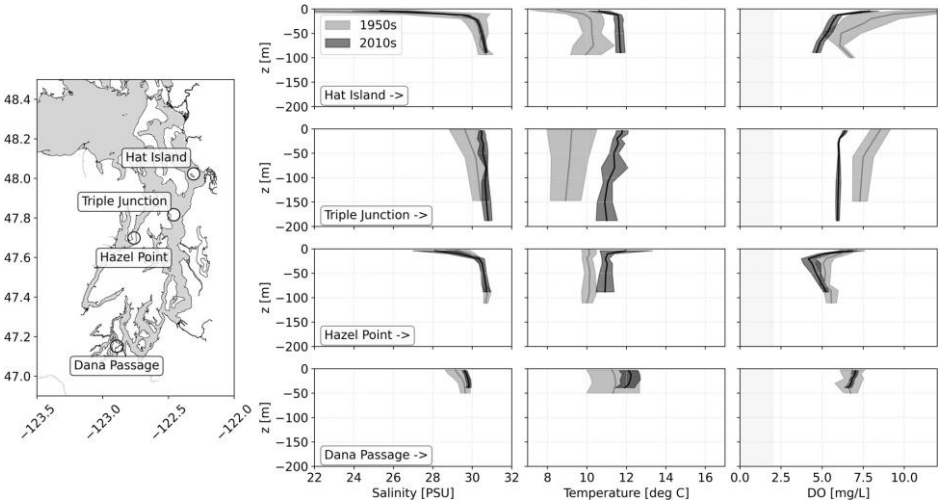

Figure 1. Selected decadal analysis locations in Puget Sound (left); fall decadal average profiles with 95% confidence intervals of salinity, temperature, and DO in the 1950s vs. 2010s (right).

[1] University of Washington, Dept. of Civil & Environmental Engineering, dakotamm@uw.edu
[2] University of Washington, Dept. of Civil & Environmental Engineering, auroral@uw.edu
[3] University of Washington, Dept. of Civil & Environmental Engineering, arhd@uw.edu
[4] University of Washington, School of Oceanography, pmacc@uw.edu
[5] University of Washington, Dept. of Civil & Environmental Engineering, bedaro@uw.edu
[6] University of Washington, Dept. of Civil & Environmental Engineering, mtbrett@uw.edu

95% confidence intervals show changes over time throughout the water column at specific sites in Figure 1. We observe that three of the four sites in Figure 1 show significantly higher temperatures in the 2010s. There is no significant difference in salinity at any of the sites, but DO is significantly lower at three of the four sites. Showing no temperature nor DO change, Dana Passage is spatially distinct from the sites with changes in both its distance from the entrance of Puget Sound and its complex topography. Expanding these analyses throughout Puget Sound and on different timescales, we will quantify trends and variability of DO and relevant state variables.

Objective 2: Identify mechanistic links between environmental changes and DO

After quantifying trends and variability of DO and other relevant state variables, we will use observational data records to identify mechanistic links between environmental changes within and around Puget Sound and measured DO. Similar regional studies have identified many different physical and biogeochemical factors that interplay, with timing being a crucial factor (Riche et al., 2014). The interactions of changes in oceanic and coastal processes may play a role in the renewal of bottom water in Puget Sound (e.g., upwelling cycles and changes). The timing and strength of storms may affect vertical mixing, which serves to reoxygenate previously stratified waters. Precipitation quantity and timing impact freshwater influx to the system. So too must we look at these factors (and more) with the context of climate change.

As an example of these analyses, we investigate whether freshwater influx may influence observed DO. Figure 2 shows Skagit River yearly and decadal mean discharge (USGS, 2024). and fall DO decadal average profiles from Hat Island (ref. Figure 1 for site location). The mouth of the Skagit River is located north of the Hat Island site in Puget Sound's Whidbey Basin; the Skagit is also the largest river in Puget Sound by volume.

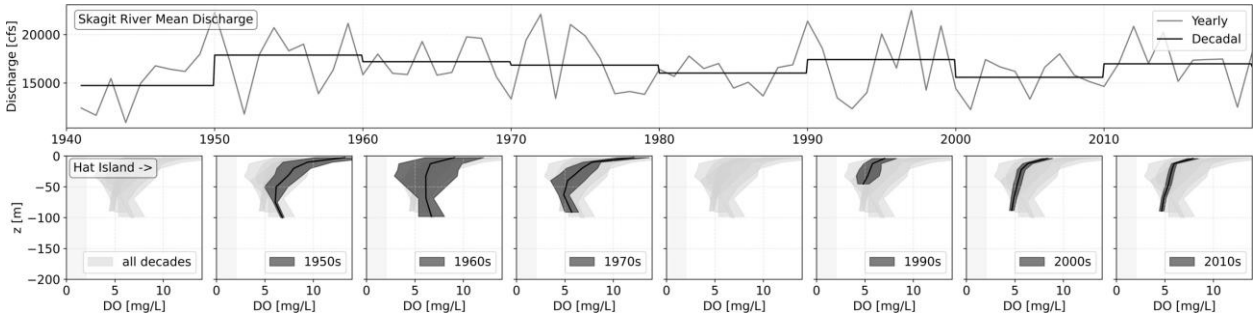

Figure 2. Skagit River yearly and decadal mean discharge (top); Hat Island fall DO average decadal profiles (ref. Figure 1), shading indicates 95% confidence intervals for all decades (grey) and specific decades (black), data unavailable for 1940s and 1980s.

This preliminary exploration indicates decadal variation in river flow alongside variation in DO: lower discharge decades tend to have marginally higher DO. However, further analyses are necessary to parse the local and system-wide impacts of freshwater variability: Does increased river flow impact DIN? Do changes in freshwater drive salinity and stratification change? How might this impact residence time and estuarine exchange? Do all of these changes influence deoxygenation? These questions must also be answered alongside concurrent variation in other environmental factors and their timing, including those outside of Puget Sound (e.g., the Fraser River, deep water renewal in the Strait of Juan de Fuca) and global changes (e.g., atmospheric CO2, rising temperatures).

By first using observational data to identify trends and variability in Puget Sound DO and other state variables in time and space, and then identifying mechanisms impacting these changes, we seek to enable understanding of anthropogenic influence in this complex system – and how to best protect and improve ecosystem health in Puget Sound.

References

MacCready, P. (2017). Puget Sound's physical environment. Encyclopedia of Puget Sound.

Del Rio, A. M; Davis, B. E.; Fangue, A. N.; Todgham, A. E. (2019). Combined effects of warming and hypoxia on early life stage Chinook salmon physiology and development, *Conservation Physiology*, Volume 7, Issue 1, 2019, coy078.

Mackas, D. L.; & Harrison, P. J. (1997). Nitrogenous nutrient sources and sinks in the Juan de Fuca Strait/Strait of Georgia/Puget Sound estuarine system: assessing the potential for eutrophication. *Estuarine, Coastal and Shelf Science*, 44(1), 1-21.

Clune, J. W.; Capel, P. D.; eds., (2021). Nitrogen in the Chesapeake Bay watershed—A century of change, 1950–2050 (ver. 1.2, 2024). *U.S. Geological Survey*, Circular 1486, 168 p.

Riche, O.; Johannessen, S. C.; Macdonald, R. W. (2014). Why timing matters in a coastal sea: Trends, variability and tipping points in the Strait of Georgia, Canada. *Journal of Marine Systems*, Volume 131, 2014, Pages 36-53, ISSN 0924-7963.

Moore, S. K.; Mantua, N. J.; Kellogg, J. P.; Newton, J. A. (2008). Local and large-scale climate forcing of Puget Sound oceanographic properties on seasonal to interdecadal timescales. *Limnology and Oceanography*, 53.

Ruffner, J. (2017). Long-term marine water column monitoring 1999-present. *WA Dept. of Ecology*.

Alin, S.; Newton, J.; eds., (2021). A compiled data product of profile, discrete biogeochemical measurements from 35

indi- vidual cruise data sets collected from a variety of ships in the southern Salish Sea and northern California Current System (Washington state marine waters) from 2008-02-04 to 2018-10-19 (NCEI Accession 0238424). *NOAA National Centers for Environmental Information*.

Collias, E. E. (1970). Physical and chemical oceanographic data of Puget Sound and its approaches, 1932-1966. *Washington Sea Grant*, Publication 70-4. U.S. Geological Survey (2024), USGS 12200500 Skagit River Near Mount Vernon, WA. National Water Information System data available on the World Wide Web (USGS Water Data for the Nation) at URL [http://waterdata.usgs.gov/nwis/].

Harmonic analysis of ill-posed inverse problems: application to short and sparse tidal records from SWOT

Matte P. [1] and Innocenti S. [2]

Keywords: coastal and estuarine tides, harmonic analysis, ill-posed inverse problems, software, SWOT.

Abstract

Incomplete (short and/or sparse) records pose a challenge for conventional tidal analysis methods, which fail to provide accurate tidal predictions due to overfitting or ill-conditioning. In coastal and estuarine regions, where multi-scale signals influence the water levels, the variability introduced by the complex interactions between tides, friction, basin geometry and other environmental factors requires adapting tidal analysis to the broadband nature of the tidal spectrum, characterized by temporally correlated noise.

Here, we present a software including Matlab and Python mirrored versions of a new harmonic analysis method that improves on existing techniques for tidal analysis of both stationary and non-stationary signals. Specifically, a new non-stationary formulation for the original NS_Tide model (Matte et al., 2013) is proposed to allow for a versatile definition of the external forcing variables influencing tidal components and stage levels. Moreover, the software incorporates new features and constraints allowing for the analysis of short or under-sampled water level records in a physically and statistically meaningful way. Among those new features:

- We define new criteria for constituent selection that account for constituent aliasing due to irregular or coarse sampling frequency, based on band-wise signal energy.
- We implement the moving-block bootstrap error computation proposed by Innocenti et al. (2022), well suited for signals with temporally correlated noise and adapted to irregular sampling. With these estimations we derive a series of post-fit statistics for constituent selection, including SNR and other linear and circular scores computed on tidal amplitude and phases.
- We formalize the regression problem into a feasible Generalized Least-Squares (GLS) framework that allows to include a non-trivial error variance-covariance matrix in the model optimization. Robust estimations (Leffler & Jay, 2009) as well as regularization options can be used in GLS when dealing with underdetermined systems (fewer observations than parameters).
- We redefine tidal inference using priors either on the tidal complex parameters, constituent amplitudes, or phases, along with adaptive constraints and penalties that can enforce a dynamical link between the model parameters.

To illustrate a few of these new capabilities, we analyse data from the new Surface Water and Ocean Topography (SWOT) satellite mission, launched on December 16th, 2022. Data from the mission's Calibration/Validation (Cal/Val) phase were collected over the St. Lawrence Estuary with a revisit time of 0.99349 days for a duration of ~90 days (April through July 2023). With this near-daily sampling period, K1 would require 262 days to be resolved, while O1 cannot be separated from M2 with records shorter than 262 days. In contrast, relevant semidiurnal and higher frequency constituents can be resolved with the 90-day SWOT Cal/Val record.

Here, a SWOT data sample at a location near Trois-Pistoles is analysed and used to reconstruct continuous water levels for comparison with a nearby tide gauge. We perform a harmonic analysis using a series of Rayleigh criterion corresponding to very permissive up to very conservative thresholds for fixing the minimum separation frequency allowed between aliased constituents. We define a new decision tree based on a nearby reference station, rather than tidal potential, and compare classical harmonic analysis (HA) with solutions from regularized least-squares (ridge regression, see Hoerl & Kennard (1970)) where the size of the model parameters is penalized.

Fig. 1a shows results of the resolved tidal energy, expressed as a summation of the constituents squared amplitudes, from either harmonic analysis or ridge regression, compared to the signal energy estimated from the data standard deviation. As expected with sparse records, HA cannot resolve more constituents than those allowed by the Rayleigh criterion with thresholds (Rmin) of about 1 or higher (~16 constituents in this example). In contrast, ridge regression effectively penalizes the size of the parameters, leading to usable solutions even with a considerable number of constituents (up to 68). However, with this method the total energy of the predicted tides is progressively underestimated as the number of constituents increases due to a higher penalization, which reflects in larger reconstruction errors (Fig. 1b). An optimum is therefore reached when the predicted energy approaches the signal energy. Hence, the latter can be used as an objective criterion for constituent selection.

[1] Meteorological Research Division, Environment and Climate Change Canada, pascal.matte@ec.gc.ca
[2] Meteorological Research Division, Environment and Climate Change Canada, silvia.innocenti@ec.gc.ca

We further test a definition of the Rayleigh criterion that allows different thresholds to be applied on each tidal band. Based on prior information at a nearby tide gauge (Trois-Pistoles), only 5% of the tidal energy is contained in the diurnal band, nearly 95% is in the semidiurnal band, and only 0.1% is in the quarter-diurnal band. When performing harmonic analysis of the SWOT sample using a fixed Rayleigh criterion threshold, Rmin = 1, a significant amount of the resolved tidal constituent energy is found at quarter-diurnal and higher frequencies (Fig. 1d). While the separation of these aliased frequencies is allowed by the Rayleigh criterion, an unrealistic amount of the total tidal energy is attributed to these bands, with the adverse effect of degrading the estimated semidiurnal amplitudes. Conversely, using band-specific Rayleigh criterion thresholds based on the expected relative energy in each band calculated from the reference station leads to a physically plausible estimation of the energy distribution between tidal bands (Fig. 1e). These also result in a more accurate reconstruction of the total water levels when compared to station data (Figs. 1b-c). Therefore, the new band-specific energy criterion can be considered a sound choice for constituent selection in tidal analysis, especially when dealing with sparse and/or short signals.

It is expected that similar criteria can be used to analyse other challenging tidal records, such as records of high and low waters. This will be further explored in this presentation, along with the new inference options and post-fit criteria. The two code implementations written in the Matlab and Python programming languages will be publicly available with accompanying documentation and unit tests at the publication of the official reference for the software.

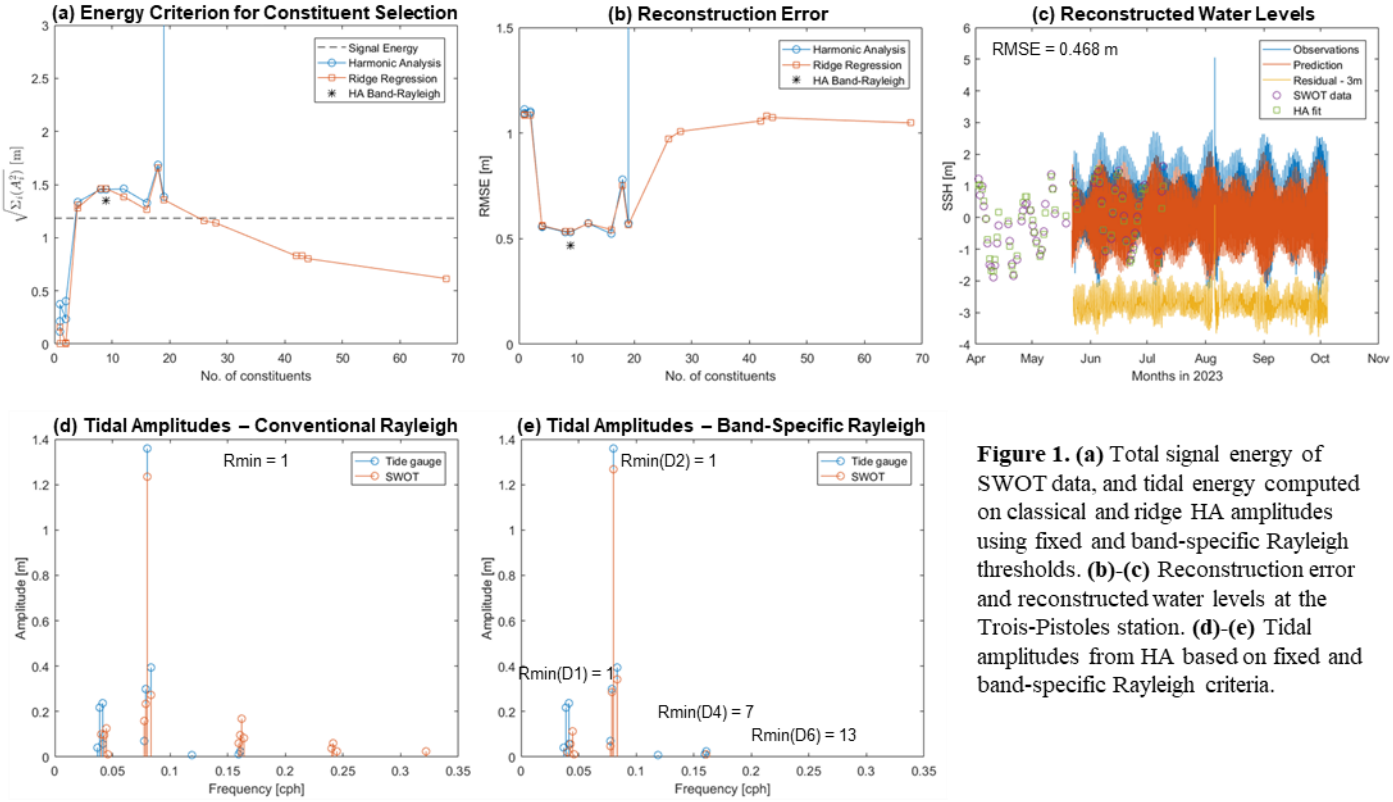

Figure 1. (a) Total signal energy of SWOT data, and tidal energy computed on classical and ridge HA amplitudes using fixed and band-specific Rayleigh thresholds. **(b)-(c)** Reconstruction error and reconstructed water levels at the Trois-Pistoles station. **(d)-(e)** Tidal amplitudes from HA based on fixed and band-specific Rayleigh criteria.

References

Hoerl, A. E., & Kennard, R. W. (1970). Ridge Regression: Biased Estimation for Nonorthogonal Problems. *Technometrics*, *12*(1), 55–67. https://doi.org/10.1080/00401706.1970.10488634

Innocenti, S., Matte, P., Fortin, V., & Bernier, N. (2022). Analytical and Residual Bootstrap Methods for Parameter Uncertainty Assessment in Tidal Analysis with Temporally Correlated Noise. *Journal of Atmospheric and Oceanic Technology*, *39*(10), 1457–1481. https://doi.org/10.1175/JTECH-D-21-0060.1

Leffler, K. E., & Jay, D. A. (2009). Enhancing tidal harmonic analysis: Robust (hybrid L1/L2) solutions. *Continental Shelf Research*, *29*(1), 78–88. Retrieved from http://www.sciencedirect.com/science/article/B6VBJ-4SGD4WG-5/2/656570adc05454b8abdae81e0a746be1

Matte, P., Jay, D. A., & Zaron, E. D. (2013). Adaptation of classical tidal harmonic analysis to nonstationary tides, with application to river tides. *Journal of Atmospheric and Oceanic Technology*, *30*(3), 569–589. https://doi.org/10.1175/jtech-d-12-00016.1

Internal Wave Driven Mixing on the New York Bight Inner Shelf

McSweeney J. [1], Jurisa J. [2], Suanda A. [3], Waterhouse A. [4], and MacKinnon J. [5]

Keywords: internal waves, turbulent dissipation, inner shelf

Abstract

Internal waves are ubiquitous in coastal regions, though there are many open questions related to their impact on coastal environments. On the inner shelf, as internal waves transit into shallowing water depths, the waves can evolve dramatically and nonlinearly over short distances (McSweeney et al 2020). There are relatively few in situ observational datasets of shoaling internal waves in inner shelf environments, and each has advanced our understanding of the dynamics in fundamental ways (MacKinnon and Gregg 2003, Tang et al. 2007, Kumar et al. 2021). Given the scarcity of observations, there remains much parameter space to be explored (Becherer et al. 2021) and questions related to the expected differences in the dynamics between narrow and broad shelves.

This analysis leverages new internal wave observations from New York Bight (NYB) to characterize the local internal wave field. Two moorings were deployed on the inner shelf NYB at 35 m and 50 m water depths over the summer-to-fall transition of 2023 and will be redeployed for the same period in 2024. These moorings include 1-2 m vertical resolution of temperature, salinity data, and current velocity data. The temperature data measured at 1-8 Hz. We use these data for an event-scale analysis, quantifying wave presence, amplitude, energy, and speed (as done in McSweeney et al. 2020). Turbulent kinetic energy dissipation (ε) will also be estimated from the thermistor strings using an Ellison length scale, following Cimatoribus (2014) and Jones (2020). Given the frequent presence of internal waves in the region (Figure 1), it is anticipated that internal waves play an important role in driving mixing and a goal of this analysis is to quantify their contribution to mixing and vertical heat flux.

This analysis has significant implications both regionally and more broadly. The NYB is a subregion of the Mid-Atlantic Bight, which is known for its strong seasonal stratification and the presence of a Cold Pool, a bottom-trapped volume of cold, nutrient-rich water. We hypothesize that internal waves are a significant contributor to the gradual warming of this Cold Pool from July to September, which can be seen in Figure 1. A better understanding of this process would advance understanding of this regional phenomenon, with downstream ecosystem impacts that are socio-economically important. More broadly, this data expands our currently observed parameter space to include relatively strong internal waves over a broad shelf. Efforts will be made to contextualize findings with previous studies.

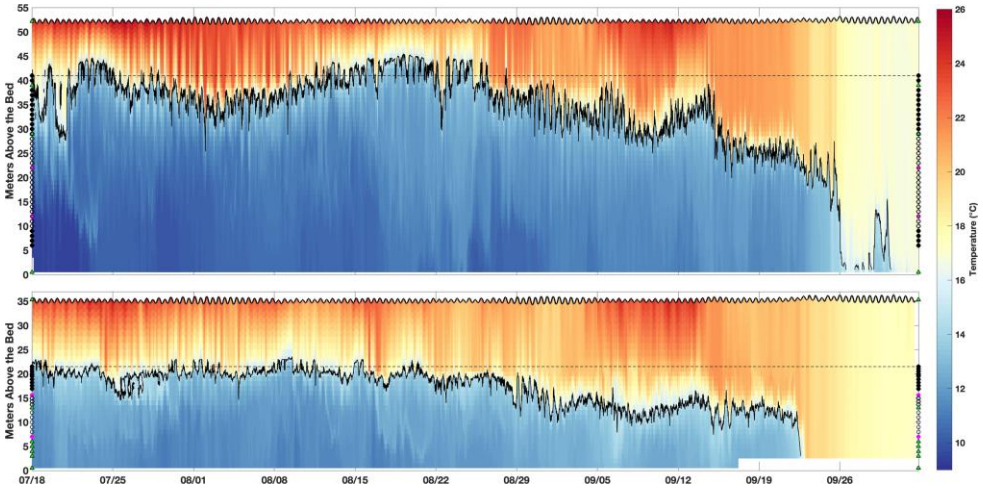

Figure 1. Timeseries of the 1-minute vertical temperature profile for the 50 m (top) and 35 m (bottom) moorings deployed 18 July – 3 October 2023. Vertical position of instruments is noted by the symbols on the left and right, with dashed lines indicating the subsurface location above which data is linearly interpolated to the surface measurement. Black circles indicate an 8 Hz fast response thermistor, which can be used to calculate TKE dissipation; open black circles indicate 2 Hz standard thermistors; green triangles indicate CTDs; and pink dots indicate 1 Hz pressure and temperature sensors. The 15°C isotherm is contoured.

[1] Stony Brook University, jack.mcsweeney@stonybrook.edu
[2] University of Maryland Center for Environmental Science – Horn Point Lab, jjurisa@umces.edu
[3] Department of Physics and Physical Oceanography at the University of North Carolina Wilmington, suandas@uncw.edu
[4] Scripps Institution of Oceanography, awaterhouse@ucsd.edu
[5] Scripps Institution of Oceanography, jmackinnon@ucsd.edu

References

Becherer, J., Moum, J. N., Calantoni, J., Colosi, J. A., Barth, J. A., Lerczak, J. A., ... & Waterhouse, A. F. (2021). Saturation Of the Internal Tide Over the Inner Continental Shelf. Part II: Parameterization. *Journal of Physical Oceanography*, 51(8), 2565-2582.

Cimatoribus, A. A., van Haren, H., & Gostiaux, L. (2014). Comparison of Ellison and Thorpe Scales from Eulerian Ocean Temperature Observations. *Journal of Geophysical Research: Oceans*, 119(10), 7047-7065.

Jones, N. L., Ivey, G. N., Rayson, M. D., & Kelly, S. M. (2020). Mixing Driven by Breaking Nonlinear Internal Waves. *Geophysical Research Letters*, *47*(19), e2020GL089591.

Kumar, N., Lerczak, J. A., Xu, T., Waterhouse, A. F., Thomson, J., Terrill, E. J., ... & Ahn, S. (2021). The Inner- Shelf Dynamics Experiment. *Bulletin of the American Meteorological Society*, 102(5), E1033-E1063.

MacKinnon, J. A., & Gregg, M. C. (2003). Mixing On The Late-Summer New England Shelf—Solibores, Shear, and Stratification. *Journal of Physical Oceanography*, 33(7), 1476-1492.

McSweeney, J. M., Lerczak, J. A., Barth, J. A., Becherer, J., Colosi, J. A., MacKinnon, J. A., ... & Waterhouse,
A. F. (2020). Observations of Shoaling Nonlinear Internal Bores Across the Central California Inner Shelf. *Journal of Physical Oceanography*, 50(1), 111-132.

Tang, D., Moum, J. N., Lynch, J. F., Abbot, P., Chapman, R., Dahl, P. H., ... & Newhall, A. (2007). Shallow Water '06: A Joint Acoustic Propagation/Nonlinear Internal Wave Physics Experiment. *Oceanography*, 20(4), 156-167.

Coral Reef Modelling of a Marine Protected Area near Cartagena, Colombia

Moreira D. [1], Tosic M. [2], and Martins F. [3]

Keywords: hydrodynamic models, downscaling, coastal seas, coral reefs, Caribbean.

Abstract

Coral reefs provide essential habitats, feeding grounds, and protection for marine species. However, these valuable ecosystems face threats from climate change and human activities, including ocean acidification and pollution. Recognizing corals as indicators of ocean health is crucial, particularly in vulnerable coastal regions like Cartagena. Therefore, it is vital to establish monitoring programs that employ mathematical models to track factors influencing water quality. Rising water temperatures due to climate change and sediment buildup prevents coral adaptation and sunlight penetration, affecting their reproductive capacity. Coastal regions like Cartagena Bay in the Colombia, Caribbean face significant threats due to water quality issues that inhibit marine ecosystem health (Tosic et al. 2018, 2019a, 2019b).

This study focuses on the marine protected area near Cartagena, specifically the coral reefs of the islands of Rosario and San Bernardo(Figure 1), and the primary objective is to expand the existing operational hydrodynamic model (Cartagena Bay Observatory) to include these offshore island areas, where is also included the pilot coral reef tool for the Varadero Coral Reefs located in the southest part of the bay, east of the mouth of the Canal del Dique. The Rosario and San Bernardo and National Marine Protected Area (MPA) also suffers from extensive exposure to sediments, which affect water turbidity of the surface layers, decreases sunlight penetration, and greatly affects coral survival rate, as demonstrated by Restrepo et al. (2016). Factors such as, nutrient influx from land-based sources like agriculture and sewage further aggravates the survival probabilities of the coral reef's communities To protect marine ecosystems and their biodiversity, environmental agencies and researchers often employ hydrodynamic models. These models use mathematical equations to simulate water behavior in marine systems. Input data, including reliable bathymetry, atmospheric and hydrodynamic information of the region, are essential for making sure the models can provide data as close to the reality as possible. Hydrodynamic models forecast the dynamic behavior of marine systems, offering insights into current velocities, temperature, salinity, pH levels, chlorophyll concentration, and sediment transport. As these models simplify complex oceanic processes through mathematical equations, ensuring their accuracy demands rigorous validation with real-world data, resulting in essential tools for preserving marine ecosystems and contributing to sustainable management practices.

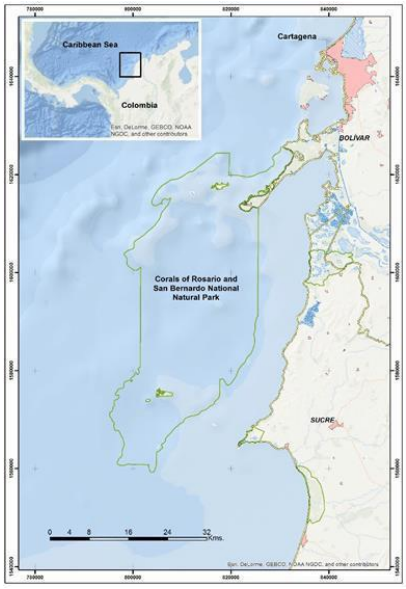

Figure 1 - Delimitation of the islands of Rosario and San Bernardo Marine Protected Area (source: Trujillo et al. 2017)

This work is part of the Basin Sea Interactions with Communities Project (BASIC) and aims to develop an oceanographic monitoring system to protect coral reefs in the Rosario and San Bernardo Natural Marine Park by extending the currently operational BASIC hydrodynamic model (Tosic et al. 2019a), which runs for Cartagena Bay. Focusing on monitoring water temperature and sediment transport, its domain will be extended to cover the desired area, which requires a larger mesh grid size and appropriate bathymetry. Expanding the model presents scientific challenges, particularly in terms of appropriate initialization and forcing for stable solutions in the coastal environment of Cartagena. Acquiring the appropriate bathymetry data for the new domain is crucial, along with tidal data sourced from a larger domain (Level 0) which will serve as the foundation for the extended model (Level 1). Consequently, two new grids must be created: one for Level 0, significantly larger to perform 2D tidal forecasts and to include the subsequent levels, and another for Level 1, designed for 3D simulations of hydrodynamics and water properties in the MPA. Later, these two levels will be integrated with the currently running version of the Cartagena Bay Observatory, that will be considered Level 2. The creation of these grids requires careful consideration of dimensions and coverage area, adjusting the number of cells to achieve the desired resolution for accurate results. Additionally, the new model requires inputs of hydrodynamic and atmospheric conditions in the region for the simulation, obtained from the external models CMEMS and NAM, respectively. Once this setup is complete, thorough testing and analysis of the model are necessary to refine and optimize it for the best possible results. This refinement process may entail parameter adjustments, improving grid resolution, and potentially iterative steps involving calibration, validation, and sensitivity analysis, incorporating in-situ measurements to compare with the model's results.

[1] Centre for Marine and Environmental Research, dmmoreira@ualg.pt
[2] Universidad EAFIT, mtosic@eafit.edu.co
[3] Instituto Superior de Engenharia, fmartins@ualg.pt

Once the setup and validation are done, the model will provide forecast data of water temperature, salinity, sediment transport, and current velocity on the designated area of the national parks, which will help identify and track important thresholds that exceed adequate coral reef conditions.

The forecast data provided by the new model for the Rosario and San Bernardo MPA is crucial for understanding the impact of temperature and sediment on coral resilience. This data will inform the development of preservation strategies and monitoring programs aimed at reducing pressures on corals and minimizing mortality within these protected areas. Furthermore, it will showcase the effectiveness and utility of hydrodynamical models in integrating monitoring programs. Additionally, the forecast data will be included in the interface of the Cartagena Bay Observatory for data visualization, which includes color maps illustrating temperature and sediment transport. A comparison will then be made between forecast data maps and historical data from the MPAs, alongside coral mortality records, to assess the impact of water temperature and sediment deposition on coral resilience. This analysis aims to identify ways in which the model can mitigate such impacts and aid in devising preservation strategies, where coral health indicators will be established based on the model results, utilizing established thresholds of environmental variables for corals. These indicators will be incorporated into the final operational model, generating forecasts for end users and stakeholders, and assisting in managing the coastal system. Hence, the new model can contribute to a Digital Twin of the Ocean (DTO), with a particular focus on monitoring coral reefs in vulnerable coastal regions like Cartagena. Through its precise simulation of oceanic processes, including water temperature, salinity, and sediment transport, it offers invaluable insights into coral reef health and aids in the development of effective preservation strategies.

References

Restrepo, J. D., Park, E., Aquino, S., Latrubesse, E. M. (2016). Science of the Total Environment, 553, 316–329. Coral reefs chronically exposed to river sediment plumes in the southwestern Caribbean: Rosario Islands, Colombia. DOI: https://doi.org/10.1016/j.scitotenv.2016.02.140.

Tosic, M., Restrepo, J. D., Izquierdo, A., Lonin, S., Martins, F., Escobar, R. (2018). Estuarine, Coastal and Shelf Science, 211, 217–226. An integrated approach for the assessment of land-based pollution loads in the coastal zone. DOI: https://doi.org/10.1016/j.ecss.2017.08.035.

Tosic, M., Martins, F., Lonin, S., Izquierdo, A., Restrepo, J. D. (2019a). Journal of Environmental Management, 236, 695–714. Hydrodynamic modeling of a polluted tropical bay: Assessment of anthropogenic impacts on freshwater runoff and estuarine water renewal. DOI: https://doi.org/10.1016/j.jenvman.2019.01.104.

Tosic, M., Restrepo, J. D., Lonin, S., Izquierdo, A., & Martins, F. (2019b). Estuarine, Coastal and Shelf Science, 216, 187–203. Water and sediment quality in Cartagena Bay, Colombia: Seasonal variability and potential impacts of pollution. DOI: https://doi.org/10.1016/j.ecss.2017.08.013.

Trujillo, J. C., Navas, E. J., Vargas, D. M. (2017). Cuadernos de Desarrollo Rural, 14(79). Valuing coral reef preservation in a caribbean marine protected area. Economic impact of scuba diving in corals of Rosario and San Bernardo national natural park, Colombia. DOI: https://doi.org/10.11144/Javeriana.cdr14-79.vcrp.

Flocculation in the Río de la Plata estuary

Mosquera R. [1,2], Pedocchi F. [1], Galletta F. [1], Morquio E. [1], and Bellón M. [1]

Keywords: estuaries, Río de la Plata, flocculation.

Abstract

The flocculation of cohesive sediments plays a significant role in the dynamics of sediment transport in estuaries. Turbulent mixing, along with salinity intrusion, creates conditions where the aggregation characteristics of fine sediments determine their settling and deposition in the water column. Suspended sediment dynamics in the Río de la Plata are primarily driven by erosion-deposition processes that regulate the exchange between the water and seabed (Fossati, 2014). Laboratory work was conducted using samples from the bottom of the Río de la Plata, where suspended sediment samples were monitored using the LISST 200X (Laser In Situ Scattering and Transmissometry instrument) for over a day (Pedocchi, 2006) during a settling experiment. The results indicate that the particle size distribution of suspended particulate matter and aggregate size groups can be categorized as follows: primary particles (mainly clay) with a diameter predominantly of 3 μm diameter; flocculi (aggregates of eroded soils consisting of primary particles) with a peak concentration at 10 μm in size; microflocs (composed of flocculi and primary particles) approximately 70 μm in size. Macroflocs (consisting of microflocs, flocculi and primary particles) were not captured in the lab. Besides the size of the different orders of aggregation, the fall velocity is also affected by density, which could also be estimated from these experiments as 2600 kg/m3 for primary particles, 1300 kg/m3 for flocculi (a very robust structure usually remaining unchanged under strong hydrodynamic conditions), and 1100 kg/m3 for microflocs (constituted by a looser structure easily broken when moderate to high turbulent shear stress is applied). Acoustic characterization of suspensions made in a mixing tank using an AQUAscatt 1000R (Acoustic Backscattering Sensor, ABS) with different salinity and floc densities, indicates that flocculi possess significant backscatter properties (Mosquera, 2021), while microflocs and higher orders of aggregation structures barely participate in the backscattered acoustic energy (Pedocchi, 2022).

Using remote sensing and numerical modeling to locate the turbidity front (Maciel, 2021), a survey conducted in late October of last year aimed to characterize changes in floc sizes in the stratified water column using the ABS, LISST, a SBE 19plus V2 (Conductivity, Temperature and Depth sensor, CTD) with an OBS 3+ (Optical Backscattering Sensor), an EXO2 sonde (Temperature, Conductivity, Pressure, pH, Dissolved Oxygen, Turbidity, Fluorescence of Chlorophyll-a, Phycocyanin and Dissolved Organic Matter). Hydrodynamic details were captured with vertical profiles using a Vector (Acoustic Doppler Velocimeter, ADV) and a downward-looking Sentinel V (Acoustic Doppler Current Profiler, ADCP) installed on a buoy. Hydrodynamic conditions during stratification show strong currents below 3 meters depth as indicated by Figure 1. With salinity ranging from 2 to 3 meters depth from 0 to 20 psu, changes not only in turbidity (reduced due to flocculation in high salinity), but also in the mean diameter (registered by the LISST) can be observed. Sediment concentration obtained with the ABS also shows a relative maximum near 2.50 meters depth indicating some acoustic backscatter increase due to salinity-induced acoustic impedance changes in the mixing zone. Estimates with the ADV measuring at 4 m depth indicate a Kolmogorov microscale of 300 μm, consistent with the size reported by the LISST. Figure 2 shows a detail of the particle size distributions in volume at three different depths away from the Schlieren effects induced by the transition in salinity, one in freshwater (1.50 m depth) and two in brackish water (4.50 and 6.15 m depth). At 1.50 m, primary particles, flocculi and microflocs sizes found in the laboratory can be observed. At 4.50 m depth, macroflocs of 270 μm can also be observed thanks to salinity and the mixing conditions. At 6.15 m depth, due to the high shear stresses induced by the bottom macroflocs are not present. Although flocculation was early identified as a significant process in the Río de la Plata (Urien, 1972), to our knowledge, these are the first direct measurements of flocculation in the Río de la Plata.

[1] Instituto de Mecánica de los Fluidos e Ingeniería Ambiental, Facultad de Ingeniería, Universidad de la República, Uruguay
[2] rmosquer@fing.edu.uy

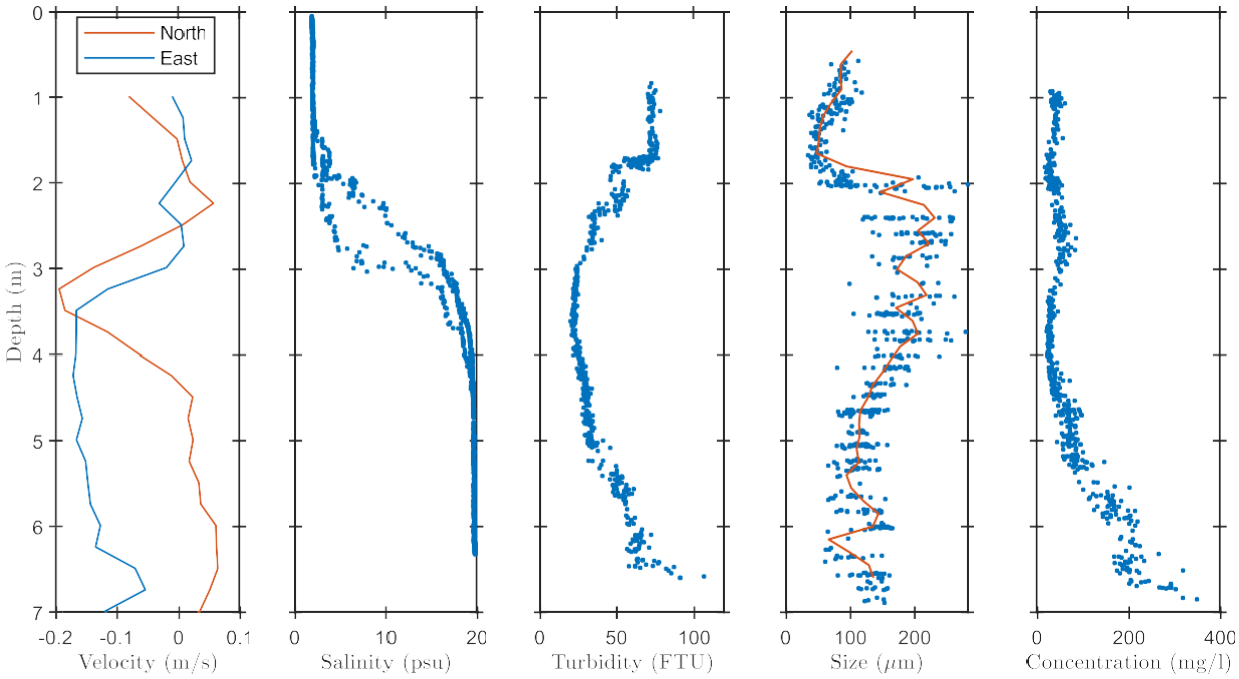

Figure 1 In the first panel east and north current velocity profiles with ADCP are shown; second panel indicates two profiles of salinity with CTD within than 15 minutes; third panel shows turbidity; forth panel indicates mean size with LISST in blue dots and its average every 15 cm; finally fifth panel shows suspended sediment concentration with ABS.

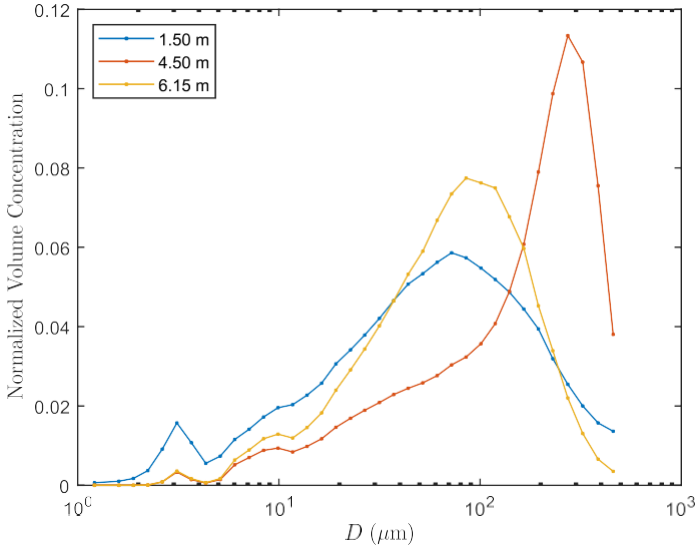

Figure 2 Particle size distributions in volume at 1.50, 4.50 and 6.15 meters depth.

References

Fossati, M, Cayocca, F, Piedra-Cueva, I, (2014) Fine sediment dynamics in the Río de la Plata. Adv. Geosci., 39, 75-80, doi:10.5194/adgeo-39-75-2014

Maciel, F.P, Santoro, P.E, Pedocchi, F (2021) Spatio-temporal dynamics of the Río de la Plata turbidity front; combining remote sensing with in-situ measurements and numerical modelling. Continental Shelf Research, 213, 104301, 1-19, doi:10.1016/j.csr.2020.104301

Mosquera, R (2021) Cohesive sediment dynamics in the Río de la Plata. [PhD dissertation, Universidad de la República], Universidad de la República Repository. https://www.colibri.udelar.edu.uy/jspui/handle/20.500.12008/26464

Pedocchi, F, Mosquera, R (2022) Acoustic backscatter and attenuation of a flocculated cohesive sediment suspension. Continental Shelf Research, 240, 104719, 13p, doi: 10.1016/j.csr.2022.104719

Pedocchi, F, García, M.H, (2006) Evaluation of the LISST-ST instrument for suspended particle size distribution and settling velocity measurements. Continental Shelf Research, 26, 943-958, doi:10.1016/j.csr.2006.03.006

Urien C. M. (1972) The Rio de la Plats estuary environments. Geological Society of America. Memoir, 133,2 13-234. doi:10.1130/MEM133-p213

Wind Influence on Mixing and Cross-Shore Transport in River Plumes

Muche Y. [1], Klingbeil K. [1], Lorenz M. [1], Yankovsky A. [2], and Burchard H. [1]

Keywords: river plumes, mixing, cross-shore transport

Abstract

Rivers play an essential role in the transport of terrestrially derived materials (like nutrients, sediments, pollutants, etc.) into the coastal ocean. Driven by the surface elevation gradient, wind, and earth's rotation, buoyant fresh water can spread across the shore as a 'river plume' (Horner-Devine et al., 2015). On its way across the shelf, the plume is subject to turbulent mixing which is mainly caused by tides and wind forcing (Spicer et al., 2021). Therefore, the plume layer loses buoyancy and eventually dissolves into the ambient ocean. An important physical quantity to describe the exchange of river water with the ocean is the cross-shore directed transport of fresh water (Izett, J. G. and Fennel, K., 2018a). A high cross-shore transport is hereby associated with a larger plume offshore extent. That way, also oceanic regions located further from the coast can be supplied with river-borne materials which can then contribute to marine biogeochemical cycles. Quantifying the cross-shore transport in river plumes could help to improve global ocean models which are usually too coarse to resolve individual rivers (Garvine, R. W. and Whitney, M. M., 2006). An important mechanism for transporting buoyant water across the shore is based on the balance of alongshore wind stress and the Coriolis force (Ekman balance). In the past, it has been observed, how upwelling favorable wind conditions can enhance the cross-shore propagation of a river plume significantly (Yankovsky et al., 2022; Yankovsky, A. E. and Voulgaris, G., 2019).

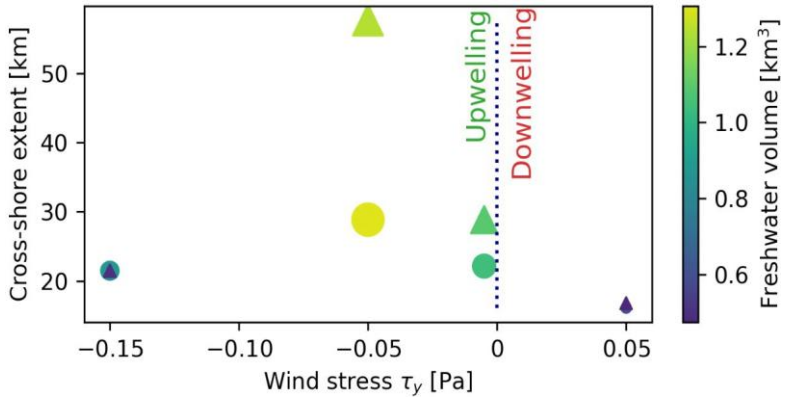

Figure 1: Relation between the plume cross-shore extent and alongshore wind strength under weak and strong tidal forcing. The circles represent scenarios with strong tides (2 m tidal amplitude) while the triangles represent scenarios with weak tides (1 m tidal amplitude). The cross-shore extent is determined from the decay of the alongshore integral of the equivalent freshwater thickness $\int(s_0\text{-}s)/s_0\,dz$ towards the sea. The markers are colored and sized according to the total fresh water volume contained in the open model domain. The freshwater volume is determined as an integral of the freshwater thickness $\int(s_0\text{-}s)/s_0\,dz$ over the x- and y-axes.

In this work, the influence of wind and tides on the plume mixing and cross-shore propagation is studied. A special focus is placed on how estuarine processes (like mixing or the estuarine exchange flow) influence the plume formation and cross-shore transport. Therefore, an innovative ocean model setup that resolves the whole plume-estuary continuum is created and run with semi-idealized forcing scenarios. This way, the pre-conditioning of plume water in the estuarine region can be studied and linked to the plume properties. State-of-the-art river plume models (E. Yankovsky and A.Yankovsky, 2024; Izett and Fennel, 2018a; Cole and Hetland, 2016) usually don't resolve these processes and are mainly focused on the coastal ocean region.

It is found, that the most effective cross-shore transports as well as largest plume extents are achieved under moderate upwelling favorable wind forcing (Fig. 1). Stronger wind as well as strong tides can suppress the wind-driven cross-shore transport due to the interaction of the surface and bottom boundary layers in shallow water. At the same time, a strong increase in estuarine mixing is observed when changing the wind forcing from moderately to strongly upwelling favorable (Fig. 2). The same happens when the wind direction is changed from upwelling to downwelling favorable. It is hypothesized, that (in agreement with the 'universal mixing law') the amount of estuarine pre-mixing determines the potential for further mixing of the plume until it finally dissolves in the ocean

[1] Leibniz Institute for Baltic Sea Research Warnemünde (IOW), Rostock, Germany. yannik.muche@io-warnemuende.de
[2] School of the Earth, Ocean and Environment, University of South Carolina, Columbia, SC, United States

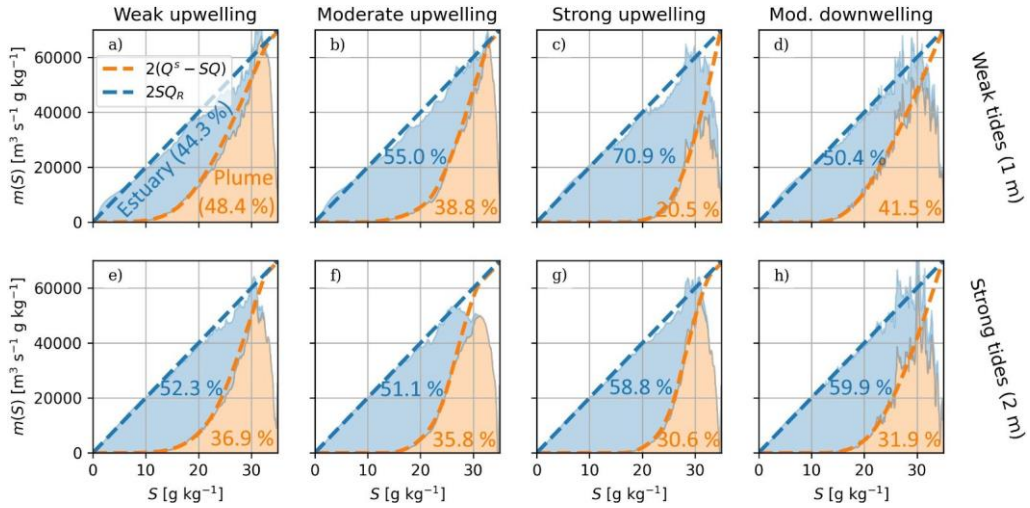

Figure 2: Salt mixing per salinity class for the same scenarios as in Fig. 1. Filled areas show the contributions of the plume (orange) and estuary (blue) to the salt mixing in the model at a certain salinity. Here, salt mixing is defined as the loss of salinity variance per salinity class S in the respective area (Burchard and Rennau, 2008). The blue dashed line shows the 'universal mixing law', a theoretical upper limit for the total mixing in salinity space (Burchard, 2020). It can be computed for an arbitrary salinity class S if the total runoff Q_R is known. The orange dashed line shows a theoretical mixing law for river plumes that was derived in this work. It is based on the exchange of volume (Q) and salt (Q^S) between the plume and estuary. The shown per cent values are the contributions of the modeled plume and estuary mixing to the total integrated mixing $\int m(S)\, dS$. The deviation of the modeled mixing from the theory at high salinities is due to the incomplete resolution of the respective isohaline areas in the model. All data is averaged over 20 tidal cycles.

Consequently, enhanced mixing in the estuary (e.g. due to wind or tides) leads to an early destruction of the plume layer as the river water leaves the estuary with a lower buoyancy. It is confirmed by the model results, that strong or downwelling favorable wind can shift the occurrence of salt mixing from the plume to the estuary and thus decrease the plume cross-shore transport.

References

Horner-Devine, A. R., Hetland, R. D., and MacDonald, D. G. (2015) Mixing and transport in coastal river plumes. Annual Review of Fluid Mechanics, 47, 569–594.

Spicer, P., Cole, K. L., Huguenard, K., MacDonald, D. G., and Whitney, M. M. (2021) The Effect of Bottom – Generated Tidal Mixing on Tidally Pulsed River Plumes. Journal of Physical Oceanography. https://doi.org/10.1175/jpo-d-20-0228.1

Izett, J. G. and Fennel, K. (2018a) Estimating the Cross-Shelf Export of Riverine Materials: Part 1. General Relationships From an Idealized Numerical Model. Global Biogeochemical Cycles, 32, 160–175, https://doi.org/10.1002/2017gb005667.

Garvine, R. W. and Whitney, M. M. (2006) An estuarine box model of freshwater delivery to the coastal ocean for use in climate models. Journal of Marine Research, 64, 173–194, https://doi.org/10.1357/002224006777606506.

Yankovsky, A. E. and Voulgaris, G. (2019) Response of a coastal plume formed by tidally modulated estuarine outflow to light upwelling-favorable wind. Journal of Physical Oceanography, 49, 691–703.

Yankovsky, A. E., Fribance, D. B., Cahl, D., and Voulgaris, G. (2022) Offshore Spreading of a Supercritical Plume Under Upwelling Wind Forcing: A Case Study of the Winyah Bay Outflow. Frontiers in Marine Science, 8, 2059.

Yankovsky, E. and Yankovsky, A. (2024) The cross-shelf regime of a wind-driven supercritical river plume. JOURNAL OF PHYSICAL OCEANOGRAPHY 54 (2), 537-556. doi: 10.1175/JPO-D-23-0012.

Burchard, H. (2020) A Universal Law of Estuarine Mixing. Journal of Physical Oceanography, 50, 81–93, https://doi.org/10.1175/jpo-d-19-0014.1.

Burchard, H. and Rennau, H. (2008) Comparative quantification of physically and numerically induced mixing in ocean models. Ocean Modelling, 20, 293–311, https://doi.org/10.1016/j.ocemod.2007.10.003.

Cole, K. L. and Hetland, R. D. (2016) The Effects of Rotation and River Discharge on Net Mixing in Small-Mouth Kelvin Number Plumes. Journal of Physical Oceanography, 46, 1421–1436, https://doi.org/10.1175/jpo-d-13-0271.1.

Dissipation within an estuarine frontal convergence zone

Nidzieko N.J. [1], Fisher A.W. [2], and Thomson J. [3]

Keywords: coastal fronts, submesoscale turbulence.

Abstract

We present observations of mixing and turbulent kinetic energy dissipation at a tidally-formed front in the Salish Sea. A REMUS 600 autonomous underwater vehicle conducted repeat transects perpendicular to the tidal front that forms in the vicinity of Waldron Island, one of the northernmost San Juan Islands. The vehicle carried microstructure instruments and acoustic current profilers for the calculation of terms in the turbulent kinetic energy budget. The goal of these measurements was to resolve fine-scale dynamics that lead to the enhancement of mixing and vertical exchange in the vicinity of coastal fronts. The interaction between surface wave breaking, bubble-entrainment, and downwelling convergence were of particular focus, with a primary goal being to investigate the specific nature and transiency of turbulent exchange at these locations.

We present detailed measurements of turbulent energetics and Reynolds stresses to elucidate exchange processes at this episodic and transient frontal feature. These observations are linked to the dynamics driving frontogenesis through control volume analyses and estimates of topographic form drag such that the role(s) of surface fronts in ventilating and mixing coastal and estuarine waters can be quantitatively characterized. These results are discussed in the context of other vertical motions in estuarine mixing.

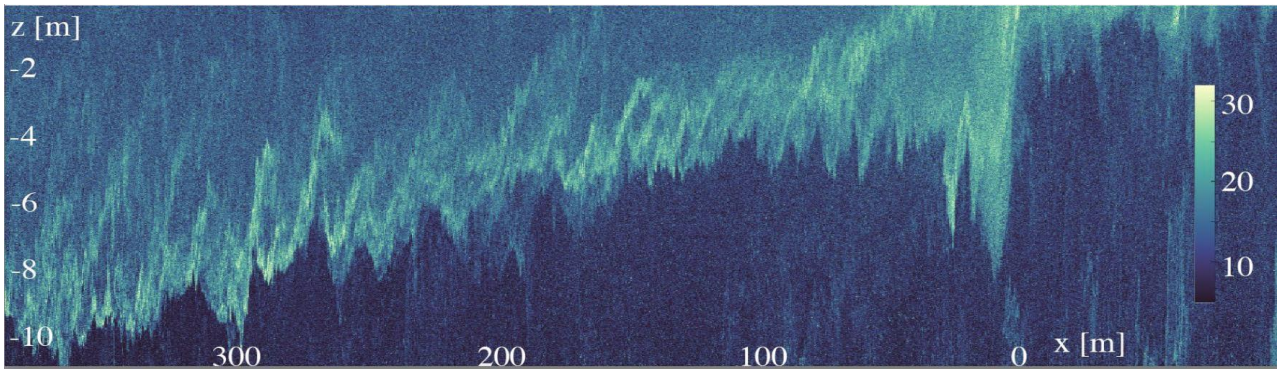

Figure 1. Acoustic backscatter (collected with a Nortek Signature 1000) observed across a density front in the Salish Sea.

[1] University of California Santa Barbara
[2] Washington State Department of Ecology
[3] Applied Physics Lab/University of Washington

The Role of Marsh Area and Volume in Coastal Flood Protection

O'Donnell J. [1,2], Cifuentes-Lorenzen A. [1,2], and Whitney M.M. [1]

Keywords: Coastal, Flooding, Marsh, Models, Climate, Adaptation.

Abstract

Flooding in coastal communities is mainly caused by the movement of water from the ocean on to the land. In areas of highly developed and complex coastal geomorphology the flow of water over and around the topography, roads, and flood control structures (tide gates, berms etc.) causes the increase in flood elevation to substantially lag that in the adjacent ocean and to have a lower peak value. Sparse observations of water level fluctuations have often obscured recognition of these effects, and coarse-scale models generally misrepresent the risk. Further, "sea level rise viewers" that simply add projected increase in mean sea level to the 100-year flood level and project it over the adjacent land, or those that use large domain models with no local validation (e.g. https://coast.noaa.gov/slr/; https://maps.coastalresilience.org/connecticut/) may be valuable for planning an project screening, but are likely to be prone to significant errors in the estimates of the pattern and extent of future flood risk at the property and neighborhood scale. Sanders et al. (2020) describe two examples in which coarse resolution risk maps diluted the awareness of flood risk by the residents because patterns did not align with their knowledge of the area. We present a case study in which the complications of geomorphology and coastal development make the assessment of present and future flood risk and the development of effective adaptation strategies difficult.

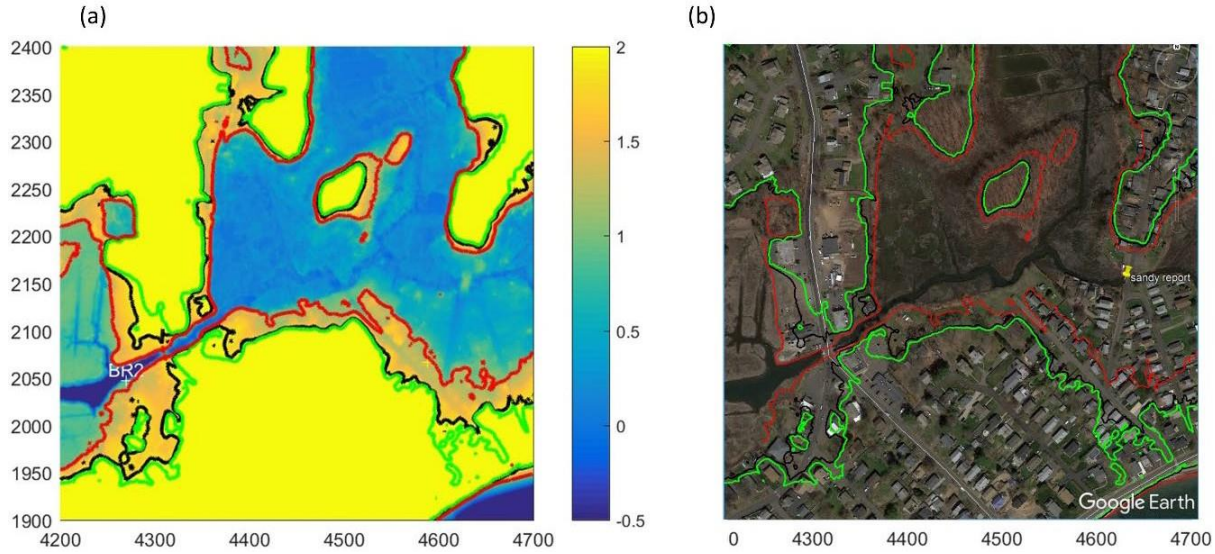

Figure 1 (a) Topography of the study area shown by the colors using the key on the right. North is up, and distances and elevations are in m relative to NAVD88. The black line shows the 1.9 m contour and the green line shows the 2.15 m contour. (b) GoogleEarth display of the 1.9 m (black) and 2.15 m (green) contours in the study area overlaid on aerial photography. The red line shows the 1.1 m contour which was the maximum level reported during super storm Sandy in the marsh at the location shown by the yellow pin.

Figure 1 shows an area of Branford, Connecticut, that surrounds a large marsh (Sybil Creek) that is separated from the ocean (Long Island Sound, LIS) by a sandy spit that has been highly developed and supports an important local road. The area was significantly impacted by super-storm Sandy in 2012. Water from LIS was initially restricted from entering the Creek by a large tide gate (near BR2 in Figure 1). However, this was overtopped when the water in the Sound exceeded 1.9 m in LIS. In the southeast corner of the map a major coastal road (Limewood Ave, or CT146) runs along the coastline. During Sandy, the waves that impacted the shoreline from LIS overtopped the road. The water on Limewood Avenue then flowed through the neighborhood and into the marsh surrounding Sybil Creek. Despite the overtopping of both the tide gate and the coastal road, the water level in Sybil Creek (estimated by our model and confirmed by high water marks recorded by the USGS) reached only 1.1 m NAVD. Consequently, the elevation of the tide gate, RT 146, and the volume of the marsh provided valuable flood protection to the properties between the 1.1 m contour and the 2.5 m contour. This study addresses how the anticipated increase in mean sea level will impact these protective services, and what measures could reduce the risk.

[1] Department of Marine Sciences, University of Connecticut, Groton, CT 06340

[2] Connecticut Institute for Resilience and Climate Adaptation, University. of Connecticut, Groton, CT 06340

We made measurements of water level at the tide gate (BR2 in Figure 1) to assess the link between water level fluctuations there and at the closest long-term NOAA gage at New Haven, CT. We also maintained a wave sensor offshore of RT146 to assess the performance of a model (Ilia et al., 2023) of wind generated waves. We then developed a simple model of the water level in the creek and marsh complex, following that of Roman et al. (1995) that was forced by water level fluctuations in LIS and the flow over the tide gate, and the wave-driven splash-over flux estimated using the EurOtop II formula (Van der Meer et al., 2016). Without an estimate of the joint probability of wave heights and sea level it is not possible to estimate the risk of future flooding adequately. This should be addressed in the future.

However, the model allows us to assess what conditions would likely lead to flooding. At normal high tide levels, significant wave heights in the range of 1.4 to 1.6 m will lead to significant flooding at the coastal road. During severe storms, the water level at high tide increases to 1.6 m NAVD and significant wave heights in the range 1.0 to 1.5 m will lead to substantial road flooding.

The models we developed also allow us to estimate the effects of sea level rise on the change in the risk of flooding in the area surrounding the Sybil Creek Marsh. It is clear that the land and properties are protected from high water by the tide gate and bridge, and by the berm that carries the road along the coast. When the water level in LIS was 2.5 m NAVD during super storm Sandy, the water level in the marsh was only 1.1 m. Our model results show that an increase in sea level of 0.25 m allows flooding to 1.9 m, an increase of 0.8 m, and shrinks the vertical extent of the flood protection zone from 1.4 m to 0.6 m. This rapid loss of flood risk protection is a robust characteristic of the model, especially at low sea level change values where the model is most reliable. The same analysis has the more positive result that small increases in the elevation of Limewood Avenue would reduce the flood risk considerably. In addition, the lack of development in the marsh, together with the operation of the tide gate provided sufficient volume to store the flux of water into the marsh so that the level did not rise as quickly as it did in LIS. Since the amplitude of the principle tidal constituent (M2) is comparable to the magnitude of large surges, the duration of the peaks in total water level last only a few hours. Consequently, the buffering capacity of the marsh storage has a significant role in flood protection.

This analysis of the causes of coastal flooding and the impact of sea level rise on future flood risk demonstrates that it is critical to appreciate the effects of the geometry of the coast, and the presence of roads and flow control structures. Addressing these complications may not always be necessary for general policy development, however, they are critical when decisions about priorities and options for implementation of adaptation strategies are being considered. Some important structures are at scales that are smaller than those generally resolved in coastal flood models (e.g. tide gates), and others involve processes that are not well represented (e.g. wave run-up and overtopping). Models that include these effects are needed, as are in-situ measurements to evaluate their effectiveness.

References

Ilia, A., Cifuentes-Lorenzen, A., McCardell, G., O'Donnell, J. (2023). Wind Wave Growth and Dissipation in a Narrow, Fetch- Limited Estuary: Long Island Sound. J. Mar. Sci. Eng. 11, 1579. https://doi.org/10.3390/jmse11081579

Roman, C.T., Garvine, R.W. and Portnoy, J.W. (1995). Hydrologic modeling as a predictive basis for ecological restoration of salt marshes. Environ. Mgmt., 19: 559–566.

Sanders, B. F., Schubert, J. E.,Goodrich, K. A., Houston, D., Feldman, D. L., Basolo, V., et al. (2020). Collaborative modeling with fine-resolution data enhances flood awareness, minimizes differences in flood perception, and produces actionable flood maps. Earth's Future, 7, e2019EF001391. https://doi.org/10.1029/2019EF001391

Van der Meer, J.W., N.W.H. Allsop, T. Bruce, J. De Rouck, A. Kortenhaus, T. Pullen, H. Schüttrumpf, P. Troch, and B. Zanuttigh. (2016). EurOtop II Manual on wave overtopping of sea defences and related structures: An overtopping manual largely based on European research, but for worldwide application (2nd Edt). http://www.overtopping-manual.com/assets/downloads/EurOtop_II_2018_Final_version.pdf

Parametrisation of SPM modelling contaminant transport in estuarine waters

Ortiz V. [1], Weilbeer H. [2], Fricke B. [3], Hoppe P. [4], and Pröfrock D. [5]

Keywords: estuaries, sediment transport, particle-bound contaminants.

Abstract

The Elbe estuary is a valuable natural area protected by European environmental laws but also the most important shipping route for international maritime traffic in Germany since it provides maritime access to the port of Hamburg. The tidal river Elbe is a federal waterway that requires regularly maintenance to guarantee sufficient water depths for navigation. Here, dredged fine material compromises often fluvial sediments that can carry legacy pollutants collected along the entire Elbe catchment. The management of fine sediments is challenging in estuaries and coastal natural waters that are affected by legacy as well as new emerging pollutants since they mix with marine sediments, accumulate after particle settling, and their potential accumulation for various chemicals can pose a risk of enhancing harmful pollution in vulnerable areas. This constrains the possible uses and relocation alternatives of the mixed sediments, for example, for the development of new sediment relocation alternatives that aim to protect ecological valuable areas in the Wadden Sea. Numerical modelling assessments about sediment transport and fate of particle-bound pollutants become essential to assess the ecological risk of remobilizing polluted sediments by natural or man-induced conditions. For instances, to investigate the remobilisation of legacy pollutants through storm surge events, or climate change induced strong rain events and long-standing droughts, but also to design sustainable future sediment management strategies.

In practice, the transport of particle-reactive pollutants bound to sediments in estuaries might be approximated from measurement projections, sediment transport models or more complex biogeochemical models. However, those methods either simplified the involved chemical or hydrodynamic processes, and often lack on reliability for forecasting the particulate pollutant transport and distribution at estuary-scales. Therefore, a coupled sediment and contaminant transport model could be convenient. The challenge here is to represent robustly the physical and chemical processes controlling dissolved and particle-bound phases (Fig. 1). Pollutants like heavy metals and persistent organic pollutants are transported through water (dissolved) or through suspended particulate matter (SPM) and bedload (particle-bound) and their distribution in water and solid phases depends not only on the chemistry of the pollutant but also on the physicochemical conditions of the estuarine waters as well as the SPM properties. The salinity gradient, changes in pH value or seasonal suspended matter composition can alter the ions composition in water and on the surfaces of SPM, which influence sorption and desorption of pollutants (Turner, A. 1996). Free available SPM-surfaces and free ions in water can alter dissolved and particle-bound concentrations in dependency to the pollutant chemical kinetic and affinity to organic and inorganic grain-coatings (Mosley and Liss 2020). These influencing factors on the partitioning of heavy metals are known (Fitzsimons et al. 2011), but little is known about their relevance at estuary-wide scales.

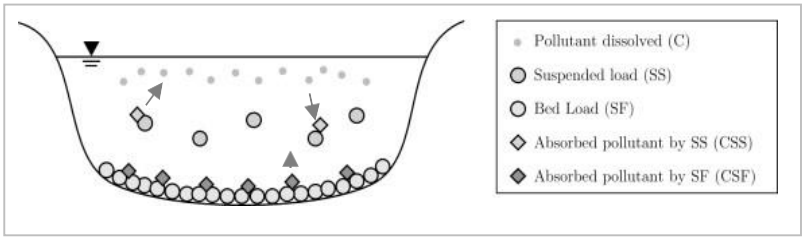

Figure 1. Simplified adsorption and desorption of pollutants in SPM and sediments from BAW, 2023

To investigate the influence of variable estuarine conditions on the transport of particle-reactive pollutants at estuary-scales, numerical and laboratory experiments have started within the interdisciplinary project Contaminant Transport Modelling at the Elbe estuary (CTM-Elbe). A fractionated transport approach of suspended particle matter is investigated with the 3D-hydrodynamic modelling system UnTRIM-Sedimorph (Casulli et al. 2000; Malcherek et al. 2005), focusing on the hydrodynamic behaviour of sediments and particles that carry particle-bound heavy metals and organic pollutants. Here, the parametrization of an organic fraction in the sediment transport model is at first addressed since organic matter acts as the main carrier of organic pollutants found in the Elbe estuary like for instances hexachlorobenzene (HCB), polychlorinated biphenyls (PCBs), and dichlorodiphenyltrichloromethane (DDT) and its metabolites.

[1] Federal Waterways Engineering and Research Institute, Dept Hydraulic Engineering in Coastal Areas (BAW); Universität Hamburg, Department of Chemistry, Inorganic and Applied Chemistry, victoria.ortiz@baw.de.
[2] Federal Waterways Engineering and Research Institute, Dept Hydraulic Engineering in Coastal Areas(BAW).
[3] Federal Waterways Engineering and Research Institute, Dept Hydraulic Engineering in Coastal Areas (BAW).
[4] Helmholtz-Zentrum Hereon, Institute of Coastal Environmental Chemistry, Department Inorganic Environmetal Chemistry; Universität Hamburg, Department of Chemistry, Inorganic and Applied Chemistry.
[5] Helmholtz-Zentrum Hereon, Institute of Coastal Environmental Chemistry, Department Inorganic Environmental Chemistry.

On the other hand, organic coatings in SPM induce electrochemical charges that influence the reactivity of the grain surfaces and sorption of inorganic pollutants (Mosley and Liss 2020). The integration of an organic fraction into a fractionated sediment transport model is tested against measurements at the Elbe: 1) without tidal influence with a calibrated model in a section of approx. 60 km of the Elbe river between Hitzacker (Elbe-km523) and the weir Geesthacht (Elbe-km-585), and 2) with tidal influence in the Elbe estuary from the weir Geesthacht until the mouth of the Elbe in the North Sea (Fig. 2).

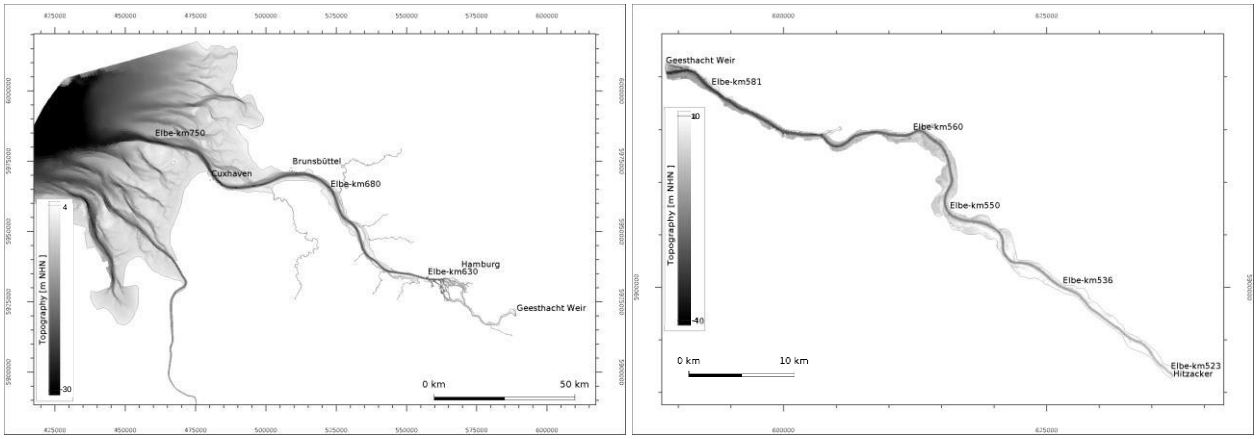

Figure 2. Study area: model area with tidal influence in the Elbe estuary (left) and model area without tidal influence upstream-estuary in the river Elbe (right).

References

Casulli, Vincenzo and Roy A. Walters (2000), An unstructured, three-dimensional model based on the shallow water equations, International Journal for Numerical Methods in Fluids 2000, 32: 331 – 348. BAW (2023) About the Transport and Distribution of Organic and Inorganic Sediment-bound Pollutants in Estuaries and Coastal Waters. Report for the EU-Interreg project IMMERSE (Task 3.12). Available online at https://northsearegion.eu/immerse/deliverables/wp3-deliverables/

Fitzsimons, M. F.; Lohan, M. C.; Tappin, A. D.; Millward, G. E. (2011): 4.04 - The Role of Suspended Particles in Estuarine and Coastal Biogeochemistry. In Eric Wolanski, Donald McLusky (Eds.): Treatise on Estuarine and Coastal Science. Waltham: Academic Press, pp. 71–114. Available online at https://www.sciencedirect.com/science/article/pii/B9780123747112004046.

Malcherek, A.; Piechotta, F.; Knoch, D. (2005): Mathematical Module Sedimorph – Validation Document. Technischer Bericht.Bundesanstalt für Wasserbau: Karlsruhe, Hamburg. Available online at https://wiki.baw.de/en/index.php/Mathematical_Model_SEDIMORPH

Mosley, Luke M.; Liss, Peter S. (2020): Particle aggregation, pH changes and metal behaviour during estuarine mixing: review and integration. In *Mar. Freshwater Res.* 71 (3), p. 300. DOI: 10.1071/MF19195.

Turner, A. (1996): Trace-metal partitioning in estuaries: importance of salinity and particle concentration. In *Marine Chemistry* 54 (1-2), pp. 27–39. DOI: 10.1016/0304-4203(96)00025-4.

Strategies and dynamics facilitating coastal flood mitigation without reflection

Orton P. [1], Talke S. [2], and Dykstra S. [3]

Keywords: storm surge, flooding, dissipation, reflection, nature-based solutions, storm surge barriers.

Abstract

A challenge with estuarine and riverine flood mitigation measures is that the water kept out of one floodplain could induce flooding elsewhere. Seawalls and storm surge barriers have been shown to raise offshore water levels and, in some cases, induce flooding. Even marsh island restoration may induce flooding at some locations if it reduces estuary surface area and, as a result, increase tidal range. Back-barrier estuaries are a useful location to study these topics because they line about 10% of the global coastline and they often have developed floodplains subject to increasingly frequent flooding due to sea level rise. Jamaica Bay, New York City, is an example of an urbanized back-barrier estuary characterized by a deep dredged inlet, dredged channels, and historical landfill that replaced perimeter wetlands with neighbourhoods fronted by seawalls. Our prior work has demonstrated how these changes have increased tidal ranges and storm tides due to increased reflection within the bay and reduced dissipation and choking at the inlet (Orton et al. 2020; Pareja-Roman et al. 2023). These changes have contributed significantly to recent widespread chronic and extreme event flooding.

In this study, we use hydrodynamic modelling of several proposed Jamaica Bay flood mitigation scenarios for a varied set of 100-year storm tide events to quantify flood reductions and induced flooding. Scenarios include perimeter marsh restoration (requiring managed retreat in this urbanized system), sedimentary restoration (shallowing and narrowing of dredged channels), and a combined surge barrier/levee system proposed by the US Army Corps of Engineers (the "Tentatively Selected Plan"). The surge barrier system successfully stops flooding for events up to the design level but induces flood-wave reflection. The resulting higher peak water levels outside the protected area require higher external flood defences (see left panel below).

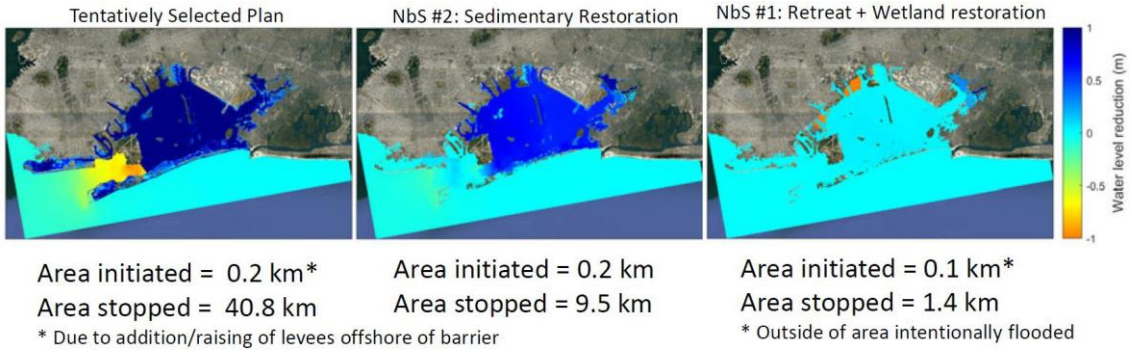

Figure: Maps of the water level reductions (control - scenario) resulting from the three flood mitigation scenarios.

Sedimentary restoration results in a large reduction and minimal reflection in a storm tide (middle panel) as it enters the bay due to a large increase in dissipation. This approach sharply reduces but does not eliminate flooding in the bay and induces a small amount of flooding of unprotected areas outside the bay. Perimeter wetland restoration slightly reduces storm tide amplitudes in the bay through increased storage. As a result, it has remote effects, reducing flooding at the eastern end of the bay. The dynamics of dissipation and storage are well-represented for a back-barrier system through the concept of choking (Stigebrandt, 1980; Orton et al. 2020), which captures the direct relationship between long wave damping and bay area, inlet length, and wave amplitude and the inverse relationship with wave period, water depth and inlet width. Due to the dependence of choking on wave period, different 100-year storms lead to very different reductions and induced flooding in this system, with the storm highlighted above being a fast-moving storm and short-duration storm tide. A longer-duration storm tide results in less choking and less induced flooding. We will conclude by discussing lessons for improving future flood mitigation efforts.

[1] Stevens Institute of Technology, philip.orton@stevens.edu
[2] California Polytechnic State University, stalke@calpoly.edu
[3] University of Alaska Fairbanks, sdykstra@alaska.edu

References

Orton, P. M., Sanderson, E. W., Talke, S. A., Giampieri, M., MacManus, K. (2020) Storm tide amplification and habitat changes due to urbanization of a lagoonal estuary. Nat. Haz. Earth Syst. Sci., 20, 2415-2432.

Pareja-Roman, L. F., Orton, P.M., Talke, S. A. (2023) Effect of Estuary Urbanization on Tidal Dynamics and High Tide Flooding in a Coastal Lagoon. J. Geophy. Res., 128, e2022JC018777.

Stigebrandt, A. (1980) Some aspects of tidal interaction with fjord constrictions. Estuar., Coast. Mar. Sci., 11, 151-166.

Coastal dynamics and saltwater intrusion in the Po Delta: the summer 2022 drought

Paladio Hernandez A. [1], Germano B.L.,[2], Unguendoli S. [3], Valentini A., Bellafiore D. [5], and Ferrarin C. [6]

Keywords: river-sea modelling, saltwater intrusion, Po Delta, 2022 drought

Abstract

Understanding the water transport and circulation in estuaries and deltas is among the key topics of oceanographic and climate research. In this research, a comprehensive modelling study aimed at evaluating the variability of coastal dynamics and saltwater intrusion (SWI) in the Po Delta region is presented. This region spans approximately 87,000 km² with unique dynamics along the Po River branches and the delta lagoons, representing one of the most climatically diverse areas in Italy. The Po Delta region is of particular interest due to the rising importance of SWI, which poses threats to both ecological systems and water supply, especially in agriculture (Bellafiore et al., 2019).

From 2000 to 2022, seven years have recorded a negative hydroclimatic balance, characterized by increased intensity in individual rainfall events but an overall reduction in the total number of events. The decrease in precipitation, particularly between March and September, coupled with rising average temperatures, has significantly elevated water demand, most notably in the agricultural sector (Maicu et al., 2018). The Po Delta has recently faced a severe ecological crisis due to drought (Bonaldo et al., 2023). Productive activities, particularly agriculture, suffered the consequences of water shortage, and the coastal regions of the Po Delta underwent extensive SWI.

In this study, the SHYFEM model was applied over an unstructured domain covering the whole Po Delta (all river branches and lagoons) and its adjacent coastal areas. In addition to the model vertical z layer discretization scheme, two novel techniques were tested: z* layer and hybrid-z* layer (Arpaia et al., 2023), this implementation will aim to enhance the current SWI forecast model's predictive capabilities. The results from our study were then compared with measured data to evaluate which method best represents saltwater intrusion. Additionally, the default vertical discretization (z layer), which has already been validated for its reliability (Bellafiore et al., 2021), serves as a benchmark for comparison against the newly introduced methods.

The long-term model simulations were used to characterize the variability of the coastal dynamics as well as of the intrusion of marine waters along the river branches. The numerical study allowed to evaluate the relative role of the hydrodynamic processes in such complex systems at the land-sea transition. Particular attention was dedicated to the 2022 Summer drought which determined the intrusion of marine waters up to 40 km upstream.

References

Arpaia, L., Ferrarin, C., Bajo, M., & Umgiesser, G. (2023). A flexible z-layers approach for the accurate representation of free surface flows in a coastal ocean model (SHYFEM v. 7-5-71). Geoscientific Model Development, 16. https://doi.org/10.5194/gmd-16- 6899-2023

Bellafiore, D., Ferrarin, C., Braga, F., Zaggia, L., Maicu, F., Lorenzetti, G., Manfè, G., Brando, V., & De Pascalis, F. (2019). Coastal mixing in multiple-mouth deltas: A case study in the Po delta, Italy. Estuarine, Coastal and Shelf Science, 226. https://doi.org/10.1016/j.ecss.2019.106254

Bellafiore, D., Ferrarin, C., Maicu, F., Manfè, G., Lorenzetti, G., Umgiesser, G., Zaggia, L., & Levinson, A. V. (2021). Saltwater Intrusion in a Mediterranean Delta Under a Changing Climate. Journal of Geophysical Research: Oceans, 126. https://doi.org/10.1029/2020JC016437

Bonaldo, D., Bellafiore, D., Ferrarin, C. et al. The summer 2022 drought: a taste of future climate for the Po valley (Italy)? Reg Environ Change 23, 1 (2023). https://doi.org/10.1007/s10113-022-02004-z

Maicu, F., De Pascalis, F., Ferrarin, C., & Umgiesser, G. (2018). Hydrodynamics of the Po River-Delta-Sea System. Journal of Geophysical Research: Oceans, 123. https://doi.org/10.1029/2017JC013601

[1] CNR-ISMAR, Institute of Marine Sciences, National Research Council, Venice, Italy; alejandropaladiohernandez@cnr.it

[2] Hydro-Meteo-Climate Service of the Regional Agency for Prevention, Environment and Energy of Emilia-Romagna, Arpae-SIMC, Italy, lgbiolchi@arpae.it

[3] Hydro-Meteo-Climate Service of the Regional Agency for Prevention, Environment and Energy of Emilia-Romagna, Arpae-SIMC, Italy, sunguendoli@arpae.it

[4] Andrea Valentini, Hydro-Meteo-Climate Service of the Regional Agency for Prevention, Environment and Energy of Emilia-Romagna, Arpae-SIMC, Italy, avalentini@arpae.it

[5]CNR-ISMAR, Institute of Marine Sciences, National Research Council, Venice, Italy, debora.bellafiore@cnr.it

[6] CNR-ISMAR, Institute of Marine Sciences, National Research Council, Venice, Italy, christian.ferrarin@cnr.it

South Atlantic Central Water intrusions and pathways on Southeast Brazilian Bight

Passos E. [1], Sancho L. [2], Espíndola R. [2], Fernandes A. [1], and Calil P. [3]

Keywords: Cross, Shelf Exchange, Coastal Upwelling, Ekman Transport.

Abstract

Continental shelves, constituting only 8% of the ocean's surface, serve as vital transitional zones between the ocean and the continents, boosting a rich trophic web. However, these ecosystems are increasingly vulnerable to anthropogenic impacts, as highlighted by various studies (CASTRO et al., 2006; LALLI and PARSONS, 1997; MANN and LAZIER, 2013). The hydrodynamics of continental shelves, intricately linked with their morphological features, undergo significant seasonal variations. Various factors, including wind-driven circulation, tidal forces, and the presence of coastal waves, contribute to the complex hydro- dynamic processes shaping these regions (DAUHAJRE et al., 2017; HUTHNANCE, 1992; CASTRO, 1997).

The exchange of energy and mass within continental shelves, influenced by well-defined lateral gradients and shallow depths, is characterized by a delicate balance of forces where friction plays a pivotal role (HUTHNANCE, 1975). Despite being less pronounced than along-isobath flows, cross-shelf exchanges significantly impact shelf gradients, posing contemporary challenges in coastal oceanographic physics (BRINK, 2016). This intricate inter- play between various forces underscores the dynamic nature of continental shelves and their importance in understanding broader oceanic processes.

The Southeast Brazilian Bight (SBB), situated between Cabo de São Tomé and São Sebastião in Brazil, exhibits the essence of a mid-latitude continental shelf. Its hydrodynamics, influenced by the Brazil Current (BC), wind patterns, and tides, exhibit a spectrum of scales, from supra- and subinertial to seasonal. Notably, the SBB features a coastal upwelling near Cabo Frio city, fostering increased productivity and ecological effects through a localized rise in chlorophyll levels. This phenomenon is intrinsically tied to the presence of the South Atlantic Central Water (SACW), originating from the Brazil-Malvinas Confluence, further emphasizing the interconnectedness of regional oceanic dynamics (EMILSSON, 1961; RODRIGUES and LORENZZETTI, 2001; CERDA and CASTRO, 2014).

For this study, a numerical simulation of the South Atlantic Ocean near Brazil was conducted using the Coastal and Regional Ocean Community model (CROCO). The model domain ex- tended from 21°30'S to 25°30'S and 46°W to 40°W, where the bathymetry ranges from a few meters near the surface to over 4 km. The simulation was carried out with a horizontal resolution of 500 m and using 50 layers in S-coordinates. The model simulation was initiated on January 1.

*Speaker
[1] Universidade do Estado do Rio de Janeiro [Brasil] = Rio de Janeiro State University [Brazil] = Université d'Etat de Rio de Janeiro [Brésil] (UERJ) – UERJ, Av. Sao Francisco Xavier, 524, Maracana, 20550-900, Rio de Janeiro, Brazil
[2] Universidade Federal do Rio de Janeiro [Brasil] = Federal University of Rio de Janeiro [Brazil] = Université fédérale de Rio de Janeiro [Brésil] (UFRJ) – Av. Pedro Calmon, 550 - Cidade Universit´aria, Rio de Janeiro - RJ, 21941-901, Brazil
[3] Institute of Carbon Cycles - Helmholtz-Zentrum Hereon (Hereon) – 1 Max–Planck Straße, Geesthacht, 21502, Germany,

Vertical and horizontal mixing in river plumes Australia

Pattiaratchi C. [1], Janekovic I. [2], and Stanley D. [3]

Keywords: river plumes, vertical mixing, fronts, ocean gliders.

Abstract

Australia is the driest living continent and therefore is marked by the absence of large river inputs to the ocean. Many rivers are often dry and flow during periods of intense rainfall linked to climate modes (e.g. La Niña and/or Indian ocean dipole) or storm systems (tropical cyclones, atmopsheric rivers). Therefore, observations of river plumes on Australian coastal are rare and fortuitously the recent extended La Niña event resulted in extreme rainfall events across southern states of Australia. This allowed for the sampling of river plumes across 3 States using ocean gliders.

Oceanographic observations has been traditionally undertaken using ships but the emergence of autonomous ocean gliders have provided an alternative measurement platform to acquire high spatial and temporal resolution data even during periods of extreme weather conditions. These data sets enable researchers to discover physical processes as well as document the natural variability of the ocean and coastal ecosystems. The Australian Integrated Marine Observation System (IMOS) ocean glider facility has been in operation since 2006 and have completed more than 370 glider missions around Australia. The recent extended La Niña events resulted in major rainfall events, some generated through atmospheric rivers (north-west cloud bands). These rainfall events resulted in major river plumes through terrestrial rivers that were sampled using ocean gliders in Western Australia (Swan River), South Australia (Murray River) and New South Wales (Hawkesbury River). Dynamics of river plumes have not sampled prior to these events. Each of the river plumes exhibited contrasting dynamics with vertically well mixed fronts to typical river plumes. The roll-rate of the ocean glider was used to define the different mixing processes in these plumes.

Ocean gliders are autonomous underwater vehicles that use a buoyancy engine together with wings for forward propulsion. They travel in a saw-tooth pattern at a speed of ~25 km/day to a maximum water depth of 200m. The gliders acquire data from the surface to ~5 m above the seabed at 4Hz yielding a vertical resolution of ~7cm. Each glider was equipped with a Seabird-CTD, WETLabs BBFL2SLO3 optical sensor (measuring Chlorophyll-a fluorescence, CDOM & 660nm Backscatter) and an Aanderaa Oxygen optode.

Swan River, Western Australia

In 2021, the region recorded a total rainfall of 892 mm, more than 150 mm above the annual average. Highest rainfall occurred in July and a satellite image taken on 4 August show the Swan river plume in the ocean containing high chlorophyll (Figure 1). Glider observations in September/October 2021 (Figures 1b,c) indicated a distinct frontal system separating the vertically mixed cooler, lower salinity, higher chlorophyll water inshore.

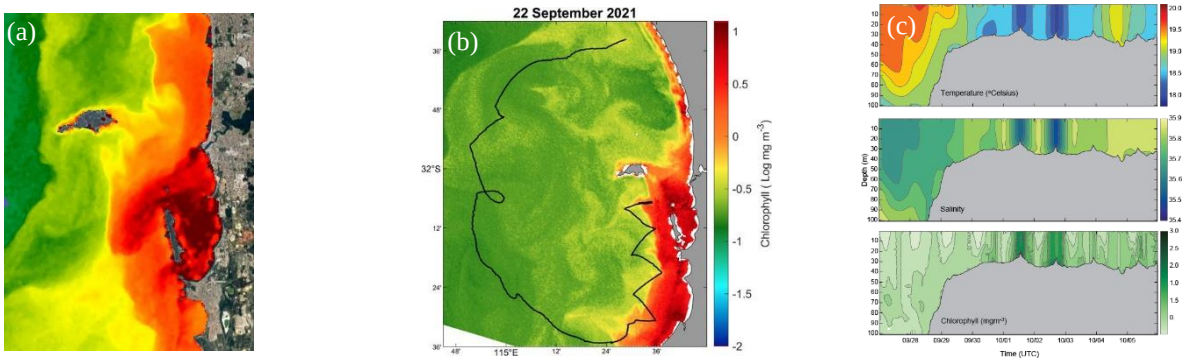

Figure 1 – (a) Sentinel-3 image of surface chlorophyll concentrations obtained in 4/5 August 2021 showing the river plumes; (b) Sentinel-3 image of surface chlorophyll concentrations overlain by the ocean glider track; (c) Ocean glider data showing the horizontal and vertical structure of the fronts associated with the river plumes.

[1] chari.pattiaratchi@uwa.edu.au, School of Civil, Environmental and Mining Engineering and the UWA Oceans Institute, The University of Western Australia
[2] ivica.janekovic@uwa.edu.au, School of Civil, Environmental and Mining Engineering and the UWA Oceans Institute, The University of Western Australia
[3] Dennis.stanley@uwa.edu.au, School of Civil, Environmental and Mining Engineering and the UWA Oceans Institute, The University of Western Australia

Hawkesbury River, New South Wales

The Sydney catchment received significant rainfall in April 2022 resulting in large freshwater flows into the ocean that were sampled by a glider (Figure 2). The data indicated a typical lower salinity plume extending offshore with higher chlorophyll in depths 20-40m with higher values at the end of the plume (Figure 2).

Figure 2 – (a) Sentinel-3 image of surface chlorophyll concentrations including the ocean glider track; and, (b) Ocean glider data showing the horizontal and vertical structure of the river plume.

Murray River, South Australia

The Murray river has the largest river catchment in Australia. In 2022-23, a flood event occurred in the Murray River between November 2022 and February 2023, from heavy rain in the interior catchment. This flood event was the largest since 1956, and the third highest flood ever recorded in South Australia. Glider observations in March 2023 Indicated a thin layer of salinity (< 5m) at the surface which was higher in chlorophyll and backscatter (Figure 3). There were also higher subsurface chlorophyll concentrations associated with the thermocline and higher backscatter along the seabed.

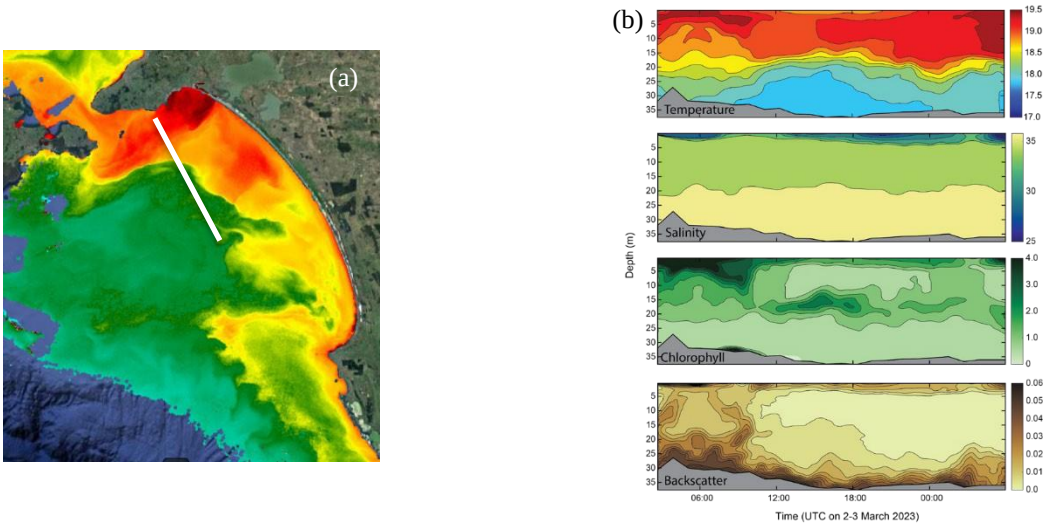

Figure 3 – (a) Sentinel-3 image of surface chlorophyll concentrations including the ocean glider track (white line); and, (b) Ocean glider data showing the horizontal and vertical structure of the river plume.

The three examples of presented above are representative transects that allow us to analyse the major mixing processes in the far field of the plumes. In particular, the different aspects of tides, wind and interfacial mixing will be examined through the use of Thorpe scale to estimate dissipation and the glider roll-rate to define the mixing through the water column.

Circulation, hypoxia and deep water renewal in a multi-inlet tropical estuary

Pawlak G. [1, 2], Adelson A. [2], Collin R. [3], Davis K. [4], Giddings S. [2], and Kastner S. [5]

Keywords: tropical estuaries, hypoxia, deep water renewal, multiple inlets.

Abstract

Hypoxia is one of the most widespread deleterious anthropogenic influences on estuarine and coastal waters, but has been primarily reported and studied in temperate coastal waters and estuaries. Relatively little work has been done in shallow tropical waters, despite the important implications for tropical ecosystems which sustain important fisheries habitats and coastal biodiversity. To address this knowledge gap we carried out an intensive observational study of Bahía Almirante, a shallow, multiple-inlet tropical estuary, in the Bocas del Toro region on the Caribbean coast of Panama, which has experienced documented hypoxia and warming events resulting in coral bleaching and die offs.

The observational campaign carried out between 2019 and 2021, together with analyses of historical data and numerical model output, revealed a strongly salt-stratified system with recurrent, seasonal hypoxia at depth, particularly in the inner bay (Adelson et al 2022). Barotropic flow between multiple inlets in Bahia Almirante is associated with alongshore pressure gradients that are modulated at timescales of weeks to months by larger scale processes. Baroclinic exchange is generally weaker than the barotropic transport and is damped during periods of strong mean flow. Tidal forcing is minimal in the system and exchange with the inner bay is weak so that this part of the bay is often isolated, particularly at depth.

Figure 1 shows a schematic of the shallow tropical estuary system dynamics as derived from the analysis. High oxygen demand, associated with decay of organic sediments, leads to relatively rapid oxygen drawdown so that the system tends toward hypoxia. Reoxygenation of bottom waters is shown to be consistent with lateral advection, occurring when (1) there is inflow at depth in the channels and (2) inflow density exceeds the bottom layer density in the inner bay. This is mechanistically similar to deep water renewal commonly observed in fjords, where refreshment can occur when diapycnal mixing drives density reduction of the stagnant water mass. In this tropical estuary, warming of the isolated bottom water mass via radiative heating is the dominant contribution to density reduction, a novel mechanism in deep water renewal dynamics.

Seasonality in hypoxia is primarily determined by inflow density which is, in turn, related to seasonal variability in coastal salinity stratification. Refreshment timescales based on offshore density variability and density reduction rates (Stigebrandt et al. 1996) yield estimates that are consistent with observed refreshment intervals and also explain the seasonality in hypoxia in the bottom of Bahia Almirante. Modulation by low frequency barotropic flow variations may account for interannual variability. The observed deep water renewal dynamics also account for seasonally occurring shallow hypoxic events that occur when dense inflow drives upward displacement of deep hypoxic water in the inner bay.

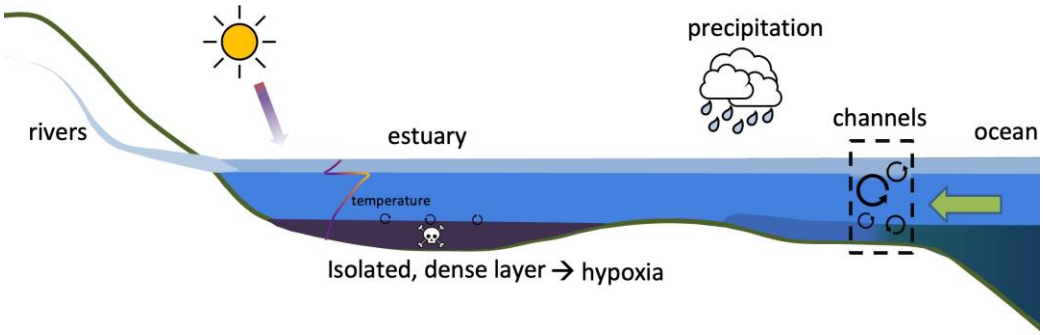

Figure 1: Schematic of estuary system dynamics for Bahia Almirante.

[1] Mechanical and Aerospace Engineering, University of California San Diego, pawlak@ucsd.edu
[2] Scripps Institution of Oceanography, University of California San Diego, pawlak@ucsd.edu, aeadelso@ucsd.edu, sarahgid@ucsd.edu.
[3] Smithsonian Tropical Research Institute, collinr@si.edu.
[4] Civil and Environmental Engineering, University of California Irvine, davis@uci.com.
[5] Western Washington University, kastnes@wwu.edu.

References

Adelson, A.E., Altieri, A.H., Boza, X., Collin, R., Davis, K.A., Gaul, A., Giddings, S.N., Reed, V. and Pawlak, G., 2022. Seasonal hypoxia and temperature inversions in a tropical bay. Limnology and Oceanography, 67(10), pp.2174-2189.

Stigebrandt, A., Aure, J. and Molvjer, J., 1996. Oxygen budget methods to determine the vertical flux of particulate organic matter with application to the coastal waters off western Scandinavia. Deep Sea Research Part II: Topical Studies in Oceanography, 43(1), pp.7-21.

Sediment transport in a tropical estuary of the Red River Delta (Vietnam)

Pénicaud J. [1], Toublanc F.[1], Marsaleix P.[1], Herrmann M. [1,2], and Ouillon S. [1,2]

Keywords: physics, estuaries, fine sediment, sediment transport, modelling

Abstract

Rivers are responsible for 95% of the sediment flux to the ocean (Syvitsky et al. 2003), and Southeast Asia is one of the main contributors (67%) to this supply (Milliman and Farnsworth 2013). The Red River-Thai Binh system in northern Vietnam is the major source of water and sediment input to the Gulf of Tonkin. Previous macro-studies have estimated the current sediment load to be around 40 - 10^6 t/yr (Le et al. 2007, Vinh et al. 2014). However, these results are based on the watershed stations data (upstream of the mouths) and therefore do not translate the real input to the ocean, as they do not take into account the complex estuarine dynamics.

The Red River delta is the most densely populated area in Vietnam and plays a crucial role in food supply and the economy, with intense economic exchanges through the Hai Phong harbor. The Van Uc River is the 3rd of the 9 distributaries of the Red River delta in terms of water discharge, accounting for 14% of this discharge (Vinh et al 2014). The Van Uc river mouth is planned to host a new 20,000 ha harbor project, which will completely alter the configuration and therefore the dynamics of the estuary, potentially affecting sediment transport. Sediment transport can have significant impacts on coastal erosion and deposition and thus on costs in coastal management (changes in land use, dredging, …Vu et al., 2018). Understanding the dynamics and evolution of sediment transport at the river/ocean interface is therefore of paramount importance.

Our purpose is to analyze the variability of the sediment transport at different timescales: tidal cycle, spring-neap tides and seasonal variations. For this, we use the hydrodynamic numerical model SYMPHONIE (Marsaleix et al., 2006, 2008) coupled with the sediment transport model MUSTANG (Le Hir et al., 2011; Grasso et al., 2015; and Mengual et al., 2017).

The Gulf of Tonkin configuration of Piton et al. (2021) and Nguyen-Duy et al. (2021) has been upgraded to obtain a 3D high-resolution grid in the Van Uc estuary. After calibration and validation against in situ measurements (Piton et al. (2020)), yearly simulations were conducted in order to examine the hydro-sedimentary variability at different time scales. The validated simulation will be presented, as well as the results on the hydrodynamics and sediment transport within the Van Uc estuary.

References

Grasso, Florent, Pierre Le Hir, and Philippe Bassoullet. 2015. "Numerical Modelling of Mixed-Sediment Consolidation." *Ocean Dynamics* 65 (4): 607–16. https://doi.org/10.1007/s10236-015-0818-x.

Le Hir, Pierre, Florence Cayocca, and Benoît Waeles. 2011. "Dynamics of Sand and Mud Mixtures: A Multiprocess-Based Modelling Strategy." *Continental Shelf Research* 31 (10): S135–49. https://doi.org/10.1016/j.csr.2010.12.009.

Le, Thi Phuong Quynh, Josette Garnier, Billen Gilles, Théry Sylvain, and Chau Van Minh. 2007. "The Changing Flow Regime and Sediment Load of the Red River, Viet Nam." *Journal of Hydrology* 334 (1–2): 199–214. https://doi.org/10.1016/j.jhydrol.2006.10.020.

Marsaleix, P., F. Auclair, and C. Estournel. 2006. "Considerations on Open Boundary Conditions for Regional and Coastal Ocean Models." *Journal of Atmospheric and Oceanic Technology* 23 (11): 1604–13. https://doi.org/10.1175/JTECH1930.1.

Marsaleix, Patrick, Francis Auclair, Jochem Willem Floor, Marine Julie Herrmann, Claude Estournel, Ivane Pairaud, and Caroline Ulses. 2008. "Energy Conservation Issues in Sigma-Coordinate Free-Surface Ocean Models." *Ocean Modelling* 20 (1): 61– 89. https://doi.org/10.1016/j.ocemod.2007.07.005.

Mengual, Baptiste, Pierre Le Hir, Florence Cayocca, and Thierry Garlan. 2017. "Modelling Fine Sediment Dynamics: Towards a Common Erosion Law for Fine Sand, Mud and Mixtures." *Water* 9 (8): 564. https://doi.org/10.3390/w9080564.

Milliman, John D., and Katherine L. Farnsworth. 2013. *River Discharge to the Coastal Ocean: A Global Synthesis*. Cambridge University Press. https://books.google.com/books?hl=fr&lr=&id=GWymw0PtH1MC&oi=fnd&pg=PR5&dq=milliman+and+farnsworth+2011&ots=5 Ukfi2tzd2&sig=M7MgGRoj7PpzoX4FIMfoKi8YfQ8.

[1] UMR 5566 LEGOS, Université de Toulouse, IRD, CNES, CNRS, UPS, 14 avenue Edouard Belin, Toulouse 31400, France

[2] Department of Water – Environment - Oceanography, University of Science and Technology of Hanoi, Vietnam Academy of Science and Technology, No 18 Hoang Quoc Viet Str, Hanoi 10000, Vietnam

Nguyen-Duy, Tung, Nadia K. Ayoub, Patrick Marsaleix, Florence Toublanc, Pierre De Mey-Frémaux, Violaine Piton, Marine Herrmann, Thomas Duhaut, Manh Cuong Tran, and Thanh Ngo-Duc. 2021. "Variability of the Red River Plume in the Gulf of Tonkin as Revealed by Numerical Modeling and Clustering Analysis." *Frontiers in Marine Science* 8 (November): 772139. https://doi.org/10.3389/fmars.2021.772139.

Piton, Violaine, Marine Herrmann, Patrick Marsaleix, Thomas Duhaut, Trinh Bich Ngoc, Manh Cuong Tran, Kipp Shearman, and Sylvain Ouillon. 2021. "Influence of Winds, Geostrophy and Typhoons on the Seasonal Variability of the Circulation in the Gulf of Tonkin: A High-Resolution 3D Regional Modeling Study." *Regional Studies in Marine Science* 45: 101849.

Piton, Violaine, Sylvain Ouillon, Vu Duy Vinh, Gaël Many, Marine Herrmann, and Patrick Marsaleix. 2020. "Seasonal and Tidal Variability of the Hydrology and Suspended Particulate Matter in the Van Uc Estuary, Red River, Vietnam." *Journal of Marine Systems* 211 (November): 103403. https://doi.org/10.1016/j.jmarsys.2020.103403.

Syvitski, James P. M, Scott D Peckham, Rachael Hilberman, and Thierry Mulder. 2003. "Predicting the Terrestrial Flux of Sediment to the Global Ocean: A Planetary Perspective." *Sedimentary Geology*, Climate Impact on Sedimentary Systems, 162 (1): 5– 24. https://doi.org/10.1016/S0037-0738(03)00232-X.

Vinh, V. D., S. Ouillon, T. D. Thanh, and L. V. Chu. 2014. "Impact of the Hoa Binh Dam (Vietnam) on Water and Sediment Budgets in the Red River Basin and Delta." *Hydrology and Earth System Sciences* 18 (10): 3987–4005. https://doi.org/10.5194/hess-18-3987-2014.

Vu, D. T., T. Yamada, and H. Ishidaira. 2018. "Assessing the Impact of Sea Level Rise Due to Climate Change on Seawater Intrusion in Mekong Delta, Vietnam." *Water Science and Technology* 77 (6): 1632–39. https://doi.org/10.2166/wst.2018.038.

Dissipation Rate of Turbulent Kinetic Energy Contributes to Positive fluxes of Dissolved oxygen in Fjords

Pérez-Santos I. [1,2,3], Linford P. [2], Rozas L. [4], Ross L. [5], Saldías G. [2,6,7], and Rojas M. [8]

Keywords: turbulence, gas fluxes, oxygen, fjords, Patagonia.

Abstract

Fjord ecosystems are considered an aquatic critical zone (Bianchi et al., 2020); therefore requiring investigation to determine the natural and anthropogenic physical, biological, and chemical inter-related processes that affect ecosystem functioning. One recently discovered process affecting Patagonian fjords is the deoxygenation of deep water (Linford et al., 2023), due mainly to the advection of the poor oxygen water from the Equatorial region. Additionally, hypoxic conditions were reported (Silva and Vargas 2014; Schneider et al., 2014; Pérez-Santos et al., 2018; Linford et al., 2024) but in such areas as the Puyuhuapi Fjord, anoxia was never recorded, owing to the occurrence of deep water ventilation (Pinilla et al., 2020). The changes in ocean ventilation are one of the leading causes attributed to global oxygen loss (2%) in the last 50 years (Schmidtko et al., 2017; Breitburg et al., 2018). Therefore, the main goal of this work is to quantify the contribution of the dissipation rate of turbulent kinetic energy ( ) in aiding water ventilation due to the occurrence of positive dissolved oxygen (DO) fluxes in the northern Patagonian fjords. Holtermann et al. (2022) recently quantified DO fluxes in the Baltic Sea using a turbulence microprofiler coupled with a fast-response DO sensor. This work reported a seasonal variability of turbulence and DO fluxes, with the lowest values recorded in the summer. Additionally, mixing processes that occurred at the study area's edges were higher than mixing observed at intermediate and deep zones.

In the present study, a VMP250 RDL microprofiler was used to measure with a high vertical resolution (512 Hz) the dissipation rate of turbulent kinetic energy and the physical (temperature and conductivity) and chemical (DO) characteristics of water at approximately 60 stations in the northern Patagonian fjords during seasonal campaigns from 2022–2023 (Figure 1a). To calculate the DO fluxes, we apply the methodology proposed by Valle-Levinson (2010) and Lefort et al., (2012) to quantify processes involved in the DO variability using the equation , were in which the mixing coefficient (K_{shear}) can be calculated in terms of the diapycnal eddy diffusivity (K_ρ) and the vertical gradient of DO () will be measured with a DO fast sensor installed in the VMP250. Finally, K_{shear} will be computed fallowing equationε proposed by Cuypers et al., (2011).

The results showed a range of ε between 10^{-9} and 10^{-4} W kg^{-1} and values of K_{shear} ranging from 10^{-5} to 10^{-2} m^2s^{-1} (Figure 1b and 1c). The highest values ε and K_{shear} were recorded in the Chiloé Inner Sea where previously intense mixing has been reported due to barotropic tide energy (Ruiz et al., 2021). In terms of DO fluxes records, higher values were reported at the surface layer (10^{-5} and 10^{-3} $\mu molL^{-1}s^{-1}$) (Figure 1d), but significant events were recorded at the subsurface and deep layers as evidenced by one of the stations carried out in the Puyuhuapi Fjord were hypoxia (Schneider et al., 2014, Pérez-Santos et al., 2018; Linford et al., 2024) but also ventilation processes (Pinilla et al., 2020) occurred. As the case study of Figure 1d showed, the intense turbulence contributes to positive DO fluxes at different layers outside the surface layer, where atmospheric-fjord interactions, in addition to primary production, promotes the interchange and increase of DO. Moreover, internal waves originating from the fjord's irregular topography could contribute to subsurface and deep positive DO fluxes favoring deep-water ventilation, but more research is needed to investigate how this mechanism is involved in the generation of intense turbulence and positive DO fluxes at the subpycnocline fjords-layer.

References

Bianchi, T.S., DiMarco, S.F., Cowan, J.H., Hetland, R.D., Chapman, P., Day, and Allison, J.W.: The science of hypoxia in the Northern Gulf of Mexico: A review, Science of The Total Environment, 408, 7, 1471–1484, https://doi.org/10.1016/j.scitotenv.2009.11.047, 2010.

Breitburg, D. et al. 2018. Declining oxygen in the global ocean and coastal waters. Science 359, 1-11, 2018.

[1] Centro i~mar, Universidad de Los Lagos, Puerto Montt, Chile. ivan.perez@ulagos.cl.

[2] Centro de Investigación Oceanográfica COPAS Sur-Austral, Universidad de Concepción, Concepción, Chile.

[3] Centro de Investigaciones en Ecosistemas de la Patagonia (CIEP), Coyhaique, Chile

[4] Departamento de Ciencias de la Ingeniería, Universidad de Los Lagos, Chile.

[5] Department of Civil and Environmental Engineering, University of Maine, Orono, ME, USA.

[6] Departamento de Física, Facultad de Ciencias, Universidad del Bío-Bío, Concepción 4051381, Chile.

[7] Centro FONDAP de Investigación en Dinámica de Ecosistemas Marinos de Altas Latitudes (IDEAL), Valdivia 5090000, Chile.

[8] Programa de Magíster en Oceanografía, Universidad de Valparaiso y Pontificia Universidad Católica, Chile.

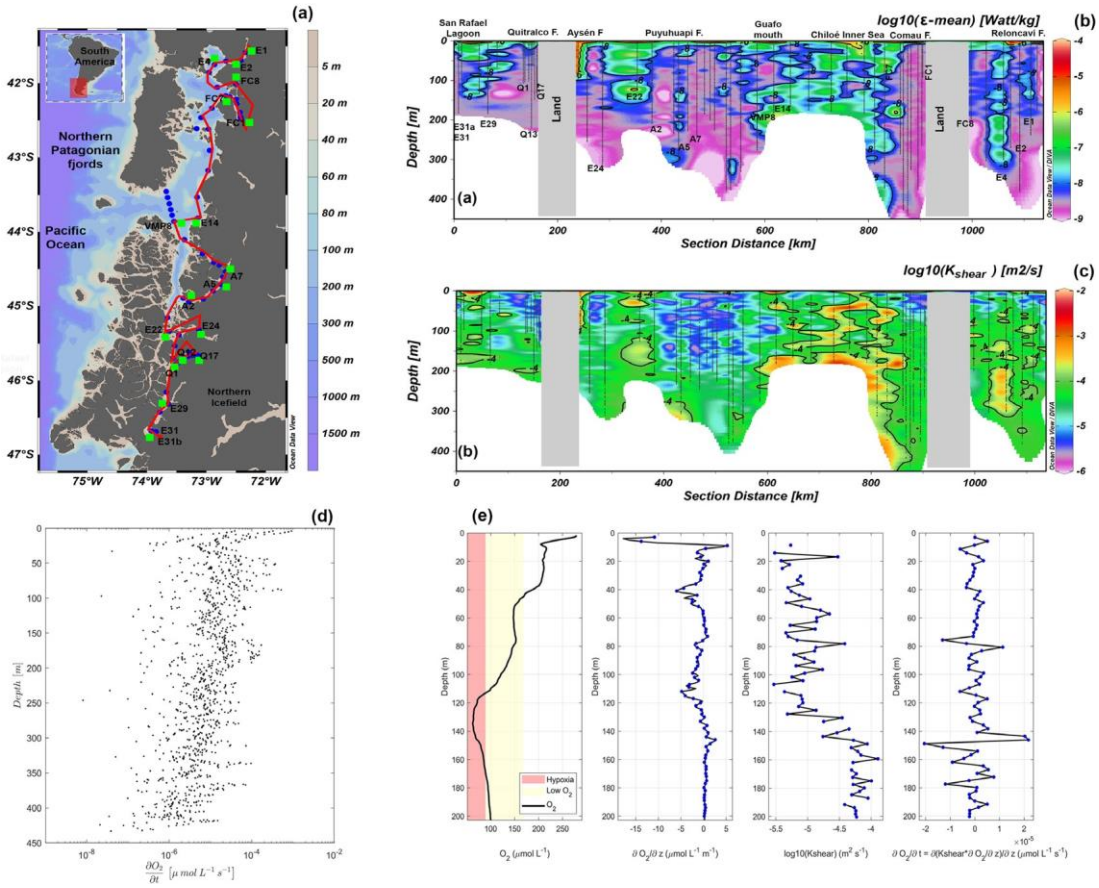

Figure 1. (a) Study area with sampling stations. (b) Dissipation rate of turbulence kinetic energy, (c) the diapycnal eddy diffusivity coefficient (k_{shear}), and (d) DO fluxes obtained in a vertical section along the northern Patagonian fjords during August 2023. (e) Shows an example of the DO flux calculation in Puyuhuapi Fjord in March 2023.

Cuypers, Y., Bouruet-Aubertot, P., Marec, C. Fuda, J.-L. (2011). Characterization of turbulence and validation of fine-scale parametrization in the Mediterranean Sea during BOUM experiment, Biogeosciences Discuss., 8, 8961–8998, doi:10.5194/bgd-8-8961-2011.

Holtermann, P., Pinner, O., Schwefel, R., & Umlauf, L. (2022). The role of boundary mixing for diapycnal oxygen fluxes in a stratified marine system. Geophysical Research Letters, 49, e2022GL098917. https://doi. org/10.1029/2022GL098917.

Lefort, S., Y. Gratton, A. Mucci, I. Dadou, and D. Gilbert (2012). Hypoxia in the Lower St. Lawrence Estuary: How physics controls spatial patterns, J. Geophys. Res., 117, C07018, doi:10.1029/2011JC007751.

Linford, P., Pérez-Santos, I., Montes, I., Dewitte, B., Buchan, S., Narváez, D., et al. (2023). Recent deoxygenation of Patagonian fjord subsurface waters connected to the Peru–Chile undercurrent and equatorial subsurface water variability. Global Biogeochemical Cycles, 37, e2022GB007688. https://doi. org/10.1029/2022GB007688.

Linford, P., Pérez-Santos, I., Montero, P., Díaz, P. A., Aracena, C., Pinilla, E., Barrera, F., Castillo, M., Alvera-Azcárate, A., Alvarado, M., Soto, G., Pujol, C., Schwerter, C., Arenas-Uribe, S., Navarro, P., Mancilla-Gutiérrez, G., Altamirano, R., San Martín, J., and Soto-Riquelme, C.: Oceanographic processes driving low-oxygen conditions inside Patagonian fjords, Biogeosciences, 21, 1433–1459, https://doi.org/10.5194/bg-21-1433-2024, 2024.

Pérez-Santos, I., Castro, L., Ross, L., Niklitschek, E., Mayorga, N., Cubillos, L., ... and Daneri, G.: Turbulence and hypoxia contribute to dense biological scattering layers in a Patagonian fjord system, Ocean Science, 14, 5, 1185-1206, doi:10.5194/os-14-1185-2018, 2018.

Pinilla, E., Castillo, M. I., Pérez-Santos, I., Venegas, O., and Valle-Levinson, A.: Water age variability in a Patagonian fjord, Journal of Marine Systems, 210, 103376, doi:10.1016/j.jmarsys.2020.103376, 2020.

Schneider, W., Pérez-Santos, I., Ross, L., Bravo, L., Seguel, R., and Hernández, F.: On the hydrography of Puyuhuapi Channel, Chilean Patagonia, Progress in Oceanography, 129, 8-18, doi:10.1016/j.pocean.2014.03.007, 2014.

Silva, N., and Vargas, C. A.: Hypoxia in Chilean patagonian fjords, Progress in Oceanography, 129, 62-74, doi:10.1016/j.pocean.2014.05.016, 2014.

Schmidtko, S., Stramma, L., & Visbeck, M. 2017. Decline in global oceanic oxygen content during the past five decades. Nature,542, 335-339. https://doi.org/10.1038/nature21399.

Valle-Levinson, A. (2010). Contemporary issues in estuarine physics. Cambridge University press, 327pp.

Ruiz, C., Artal, O., Pinilla, E., and Sepúlveda, H. H.: Stratification and mixing in the Chilean Inland Sea using an operational model, Ocean Modelling, 158, 101750, doi:10.1016/j.ocemod.2020.101750, 2021.

Generation, propagation and mixing of tidal plume fronts in the near to mid-field Rhine River Plume

Pietrzak J. [1], Rijnsburger S. [1], Lamb K. [2], Jones N. [3], Flores Audibert R. [4], Horner-Devine A. [5], and Souza A. [6]

Keywords: river plumes, tidal plume fronts, turbulence, mixing, coastal seas.

Abstract

The Rhine River Plume forms one of the largest Regions of Freshwater Influence (ROFI) in Europe. It dominates the transport of freshwater along the low-lying Dutch coast, Fig. 1. We present observations of the formation and evolution of the tidal plume fronts on every ebb tide recorded by the STRAINS-II (STRAtification Impacts Near-shore Sediment) field campaign off the Dutch coast in 2014.

Tidal plume fronts have been described in many systems worldwide, (e.g. Horner-Devine et al., 2009, 2015; Kilcher and Nash, 2010). More recently Rijnsburger et al (2018) showed their presence in this shallow tidal river plume subjected to tidal straining. They also measured the generation of internal waves on the ebb tide, ahead of a newly released tidal plume front, recorded at two mooring sites in 12 and 18 m of water.

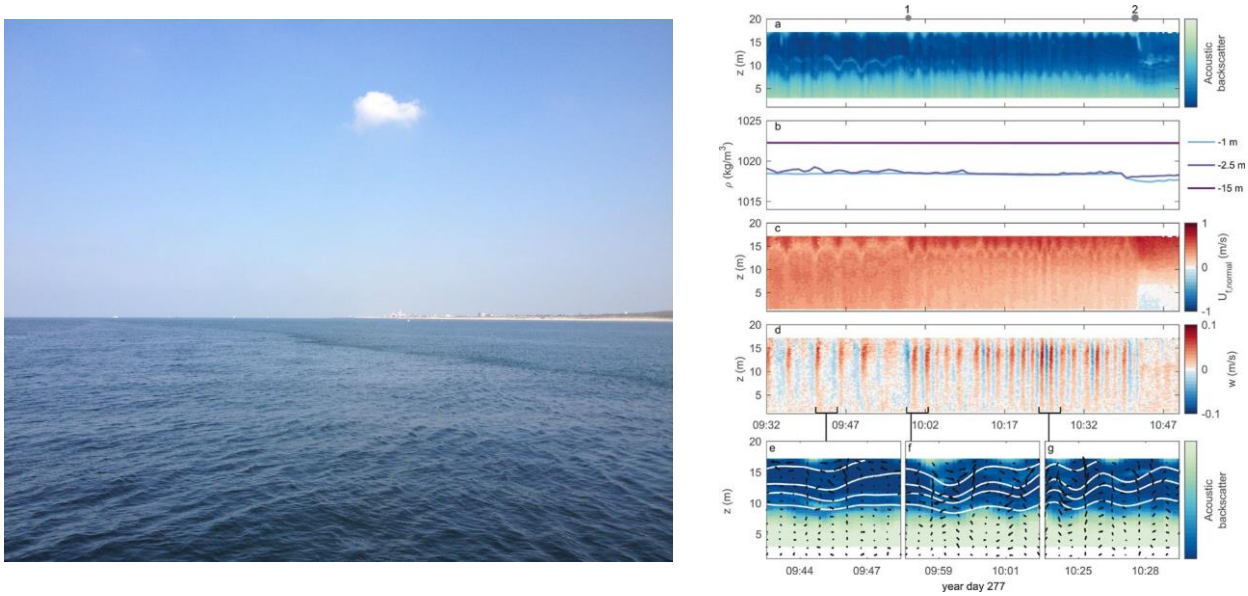

Figure 1: Left Photograph of the Rhine River Plume off the coast of the Netherlands in the near to mid-field Rhine River Plume. Note the presence of tidal plume fronts. Photograph taken by J. Pietrzak. Right: data from field campaigns in 2014. 'Internal solitary waves example on day 277 (October 4, 2014). (a) Acoustic backscatter signal from the acoustic Doppler current profiler at the mooring site (b) Density at three different heights in the water column, −1 m, −2.5 m, and −15 m. (c) Front normal velocity (m/s), where positive values indicate flow in the direction of frontal propagation. (d) Vertical velocity w (m/s), where upward is positive. (e)–(g) represent three internal wave events of 5 min, where color represents acoustic backscatter. White lines are reconstructed isopycnals, velocity vectors represent the wave-induced currents. The gray dots represent (1) 10:00 and (2) 10:43 arrival of the tidal plume front.' Figure and caption reproduced from Rijnsburger et al. (2021).

[1] Delft University of Technology
[2] University of Waterloo
[3] University of Western Australia
[2,4] Universidad Técnica Federico Santa María
[5] University of Washington
[6] CINVESTAV Mérida

Here, we present remote sensing data and radar data that show the propagation of tidal plume fronts towards the coast. We also show observations from near-shore salinity sensors that tracked their propagation into shallow water. Moreover, a boat survey, carried out offshore of the Sand Engine, further revealed tidal plume fronts propagating all the way to the coast. Here we further explore internal waves in the data, and their generation by multiple tidal plume fronts. We also explore their trapping in the mid-field of the Rhine River Plume, and their propagation towards the coast.

Using both a 2D non-hydrostatic model, together with a 3D hydrostatic model and the field data, we explore the interaction of the tidal plume fronts, and relic tidal plume fronts in the near to mid-field plume and their influence on vertical mixing and dissipation. The tidal plume fronts are thickest and fastest under downwelling winds and thinner and slower under upwelling winds. We use simple energy and mixing arguments to highlight their control the evolution of the stratification in the near to mid-field river plume.

As the tidal plume fronts propagate onshore they shoal, break and increase cross-shelf mixing. They also increase sediment resuspension and transport algae from the Rhine River towards the coast. Using an idealised 2D non-hydrostatic model we explore mixing internal solitary waves can produce as they shoal and break.

We describe a cross-shore frontal pumping mechanism and show how this impacts near shore mixing, sediment resuspension and offshore transport. We consider how this changes during periods of extreme drought and floods. We consider similarities and differences to other river plumes, and how we can apply our knowledge from highly sampled river plumes, to remote river plume systems.

References

Kilcher, L. F., & Nash, J. D. (2010). Structure and dynamics of the Columbia River tidal plume front. Journal of Geophysical Research: Oceans, 115(C5). https://doi.org/10.1029/2009jc006066

Horner-Devine, A.R, D. A. Jay, P. M. Orton and E.Y. Spahn. (2009). A conceptual model of the strongly tidal Columbia River plume, Journal of Marine Systems 78, 460–475 doi:10.1016/j.jmarsys.2008.11.025

Horner-Devine, A. R., Hetland, R. D., & MacDonald, D. G. (2015). Mixing and transport in coastal river plumes. Annual Review of Fluid Mech., 47, 569–594. https://doi.org/10.1146/annurev-fluid-010313-141408

Rijnsburger, S., Flores, R. P., Pietrzak, J. D., Horner-Devine, A. R., & Souza, A. J. (2018). The influence of tide and wind on the propagation of fronts in a shallow river plume. Journal of Geophysical Research: Oceans, 123, 1–17

Rijnsburger, S., Flores, R. P., Pietrzak, J. D., Horner-Devine, A. R., Souza, A. J., & Zijl, F. (2021). The evolution of plume fronts in the Rhine region of freshwater influence. Journal of Geophysical Research: Oceans, 126.

Rijnsburger, S., R.P. Flores, J. D. Pietrzak, K. G. Lamb, N. L. Jones, A. R. Horner-Devine, A. J. Souza (2021) Observations of Multiple Internal Wave Packets in a Tidal River Plume

Exchange Flow and Mixing in Patagonian Fjords Under Climatic Variability Modes

Pinilla E. [1], Ross L. [1], and Pérez-Santos I. [2]

Keywords: Total Exchange Flow (TEF), Salinity Variance, Patagonian Fjords, Estuarine Dynamics, Stratification, Drought Impact, Freshwater Inputs, Wind Influence on Estuaries, Tidal Forces, Harmful Algal Blooms (HABs).

Abstract

Fjords, characteristic estuarine systems of high latitudes, provide unique insights into the complexities of estuarine dynamics influenced by climate variability and anthropogenic pressures. Marked by significant freshwater inputs as well as complex coastlines and bathymetries, fjord systems can exhibit a range of stratification conditions that play a crucial role in their estuarine circulation. This stratification can be altered by the interplay of wind, tides, and remote forcing, resulting in varied patterns of exchange, and mixing processes. The 2016 drought in Chilean Patagonia, resulting in reduced river discharge and subsequent environmental disturbances such as significant harmful algal blooms (HABs), highlights the vulnerability of these ecosystems to climatic anomalies. Moreover, projections indicating an increase in the frequency and intensity of such droughts due to climate change emphasize the urgency of understanding and mitigating these impacts. The intricate dynamics of fjords and the profound impact of climate fluctuations on their hydrological balance necessitate a comprehensive understanding of their water exchange and mixing processes.

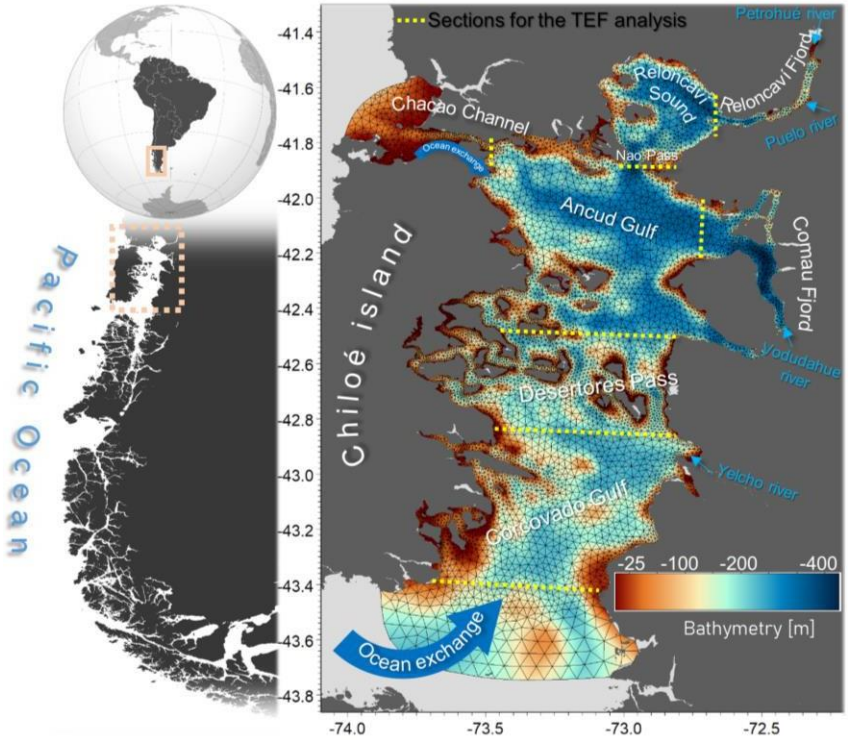

Figure 1. Overview of the Chiloe Inland Sea (CIS) study area. This map displays the six basins under analysis, with yellow lines marking the divisions of the area into smaller volume segments for detailed study. The size of triangular elements denotes the spatial resolution of the hydrodynamic model, while the color represents the depth of each basin.

The objective of this study is to assess how extreme drought conditions impact the exchange flow and mixing within a complex fjord system. The Total Exchange Flow framework (TEF) (MacCready, 2011) and salinity variance budget (MacCready et al., 2018) will be used, as they offer a robust methodology for quantifying time-averaged net transport of volume and mass between the ocean and estuaries, segmented by salinity classes, thereby capturing both tidal and subtidal dynamics. Using these methodologies to achieve our objective, we aim to answer three specific research questions: 1) How does the Total Exchange Flow (TEF) vary at different locations throughout a year marked by extreme drought conditions (2016) compared to a typical year (2018), 2) what is the relative contribution of tide, wind and river input for each of these scenarios and locations, and 3) how does the reduced river input during the drought year affect fjord mixing processes?

[1] Department of Civil and Environmental Engineering, University of Maine, Orono, ME, USA. elias.pinilla@maine.edu; lauren.ross1@maine.edu.
[2] Centro i-mar de la Universidad de los Lagos, Puerto Montt, Chile, ivan.perez@ulagos.cl

To address these questions, we will run numerical simulations of the entirety of the Chiloé Inland Sea (CIS) in Northern Patagonia (Figure 1) to quantify the TEF during both the drought and typical years. We use a 3-dimensional hydrodynamic model (MIKE-3 FM) with an unstructured mesh that is forced by a hydrological model (FLOW-IFOP) to provide freshwater sources and an atmospheric model (WRF) that supplies wind and heat fluxes.

Our initial results of the Total Exchange Flow (TEF) within the Reloncaví Fjord examined for the years 2016 and 2018, revealed that the TEF is sensitive to variations in freshwater inputs, tidal forcing, and wind. River flow stands out as the principal factor influencing the TEF, particularly noticeable during the austral winter and spring months (July-Dec). The year 2016 marked a shift, with the influence of river flow diminishing and giving precedence to wind and tidal forces, especially in the austral summer and fall. The annual average Total Exchange Flow (TEF) for both years indicates a decrease in the average TEF value by approximately 15% in 2016 compared to 2018. In 2016, the TEF spanned a higher salinity class (>33), suggesting a more pronounced saltwater intrusion from the ocean at the fjord's mouth. This contrasts with 2018, where higher salinity classes ranges decreased (<32.8), reflecting changes in estuarine mixing and the intensity of saline intrusion.

While river discharge is the primary driver of estuarine dynamics in the Reloncaví Fjord, wind significantly influences daily temporal scales (3-10 days). Our results have shown that during periods of low discharge, even weak wind events can cause a substantial uplift of subsurface waters. This dynamic is particularly critical during drought conditions, which may elevate chemical tracers such as low oxygen concentrations or oceanic nutrients to the surface, potentially altering the fjord's ecological balance. Additionally, our findings highlight river flow as a critical driver of estuarine mixing in Reloncaví Fjord, revealing a strong correlation between river discharge and mixing intensity. This suggests that higher river flows increase salinity variance, enhancing the mixing. These outcomes align with findings by Broatch and MacCready (2022) in the Salish Sea and contrast to previous studies such as Wang et al. (2017), Li et al. (2018), MacCready et al. (2018), and Wang and Geyer (2018), where a pronounced spring–neap effect was observed. However, we expect that in shallower areas with greater tidal influence, like Desertores Pass and Chacao Channel, mixing could be more relevant due to this process.

Our study not only sheds light on the complex interplay between freshwater inputs, tidal and wind forces, and their impact on estuarine mixing and circulation but also illustrates the possible ecological ramifications of these physical processes. By utilizing a comprehensive database on river flow (FLOW Model), we were able to estimate ΔS, defined as the difference between the representative incoming (Sin) and outgoing (Sout) salinity, and reconstruct stratification patterns spanning from 1979 to 2021. This analysis uncovered a connection between destratification events and the emergence of HAB species like Pseudochattonella sp. and Heterosigma akashiwo, which severely impacted aquaculture through substantial fish mortalities in 1988 and 2021 associated with Heterosigma akashiwo, and in 2009, 2016, and 2019 with Pseudochattonella sp. The 2016 HAB of Pseudochattonella sp. stands out as the most devastating event to date, highlighting the critical need for the development of prediction and mitigation strategies. The linkage between hydrodynamic changes and HABs event is a first step to providing these valuable insights into the dynamic responses of fjord systems to environmental changes, paving the way for future studies aimed at enhancing resilience and sustainability in these critical habitats.

References

Li, X., W. R. Geyer, J. Zhu, and H. Wu, 2018: The transformation of salinity variance: A new approach to quantifying the influence of straining and mixing on estuarine stratification. J. Phys. Oceanogr., 48, 607–623, https://doi.org/10.1175/JPOD-17- 0189.1

MacCready, P., (2011) Calculating estuarine exchange flow using isohaline coordinates. J. Phys. Oceanogr., 41, 1116–1124, https://doi.org/10.1175/2011JPO4517.1

MacCready, P., W. R. Geyer, and H. Burchard, (2018) Estuarine exchange flow is related to mixing through the salinity variance budget. J. Phys. Oceanogr., 48, 1375–1384, https://doi.org/10.1175/ JPO-D-17-0266.1.

Broatch, E. M., & MacCready, P. (2022). Mixing in a salinity variance budget of the Salish Sea is controlled by river flow. *Journal of Physical Oceanography*, *52*(10), 2305–2323. https://doi.org/10.1175/jpo-d-21-0227.1

Wang, T., W. R. Geyer, and P. MacCready, 2017: Total exchange flow, entrainment, and diffusive salt flux in estuaries. J. Phys. Oceanogr., 47, 1205–1220, https://doi.org/10.1175/JPO-D-16-0258.1:

Wang, T., and W. R. Geyer, 2018: The balance of salinity variance in a partially stratified estuary: Implications for exchange flow, mixing, and stratification. J. Phys. Oceanogr., 48, 2887– 2899, https://doi.org/10.1175/JPO-D-18-0032.1.

Tidal and Subtidal Dynamics at the Toe of a Salt Wedge

Pinilla E. [4], Valle-Levinson A. [5], Sottolichio A. [6], Rojas C. [1], Perez-Santos I. [7], Barros D. [5], and Ross L. [1]

Keywords: salt wedge, mixing, tidal flows, subtidal flows, estuary.

Abstract

The Penobscot River Estuary is located on the northeast coast of Maine in the United States. This estuary features a mobile pool of contaminated sediments that are resuspended and transported downstream during high river flows and trapped by salinity fronts (Geyer and Ralston, 2018), which we will refer to here as a salt wedge. This study aims to determine the mechanisms driving tidal and subtidal circulation and mixing at the toe of the salt wedge in the Penobscot River Estuary during high river discharge conditions and to link these mechanisms to sediment erosion, suspension, and deposition. To reach this goal, we use in-situ collected measurements of current velocity, salinity, temperature, turbulent kinetic energy dissipation (proxy for mixing), and turbidity. The measurements were collected over one full semi-diurnal tidal cycle (~12h) at two cross-channel transects (~500 m apart) on June 29th, 2023, and in an along-channel transect conducted at the end of ebb tide the day before (June 28th) to determine the along-channel location of the salt wedge. Results showed that despite the close distance of the transects, the tidal and subtidal current velocity patterns showed different strength and structure (Figure 1, columns 1 and 2). An analysis of the subtidal along-channel momentum balance indicates that advection balances the effects of the baroclinic pressure gradient and centrifugal accelerations caused by channel curvature. Frictional effects were negligible in comparison. Quantification of the vertical eddy viscosity showed maximum values where the water column was homogenous, indicating that frictional effects near bottom were elevated either before or after the toe of the salt wedge was advected past the study area.

The transect that was most upstream indicated that during ebb tide sediments were advected into the study site, with a clear indication of the tail of the turbidity maximum. After the turbidity maximum was downstream, the turbidity decreased starkly despite the maintenance of strong out-estuary currents (>1 m/s). Turbidity values remained low until the start of flood tide, allowing for resuspension, and the toe of the salt wedge again reached the upstream transect, indicating that the salinity front indeed traps the suspended sediment. The downstream transect (500 m downstream of the upstream transect) shows a similar pattern with turbidity, but with little or no resuspension and rather advection dominating the changes in turbidity.

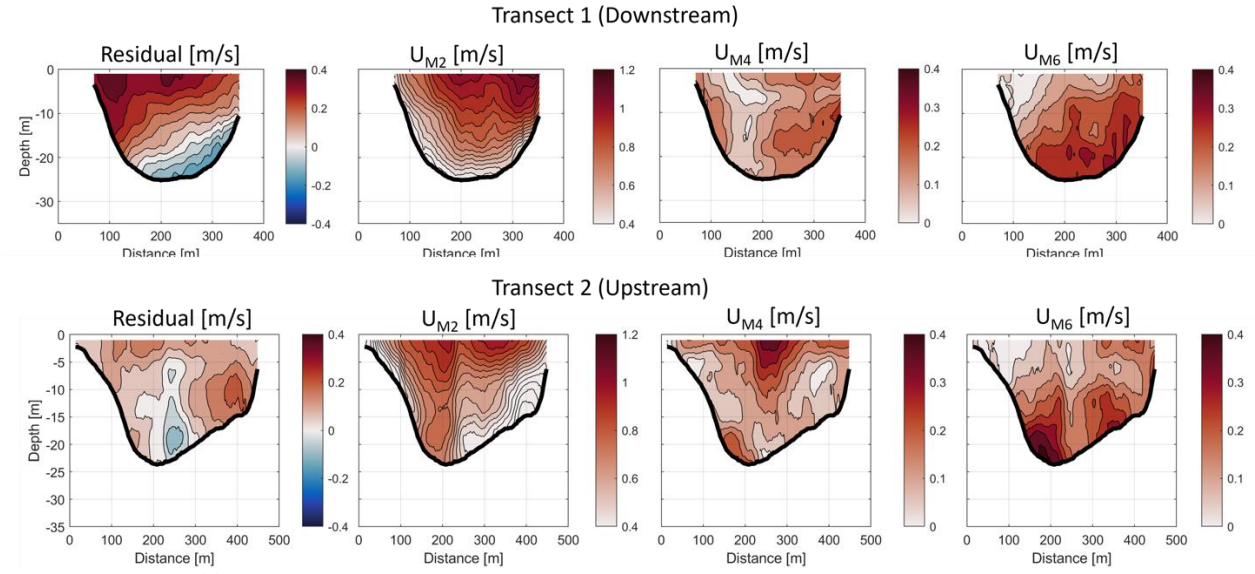

Figure 1. (Column 1) The residual (subtial flow) at the downstream and upstream transects, (Column 2) the semi-diurnal along-channel velocity amplitude, (Column 3) the quarter-diurnal along-channel velocity amplitude and (Column 4) the sixth-diurnal along-channel velocity amplitude.

References

Geyer, W.R., Ralston, D.K. (2018) A mobile pool of contaminated sediment in the Penobscot Estuary, Maine, USA. Science of the Total Environment, 612, 694-707.

[4] University of Maine, Maine, USA. Corresponding Author: lauren.ross1@maine.edu
[5] University of Florida, USA
[6] University of Bordeaux, France
[7] Centro i~Mar, University of Los Lagos, Chile
[5] Federal University of Rio Grande, Brazil

Idealised modelling of the influence of cohesive sediment on sand wave dynamics

Ploeg W. [1], Roos P.C. [2], Borsje, B.W. [3], and Hulscher S.J.M.H. [4]

Keywords: sand waves, cohesive sediment, process-based morphodynamic modelling, linear stability analysis.

Abstract

Bed form dynamics have long been studied due to their relevance for coastal management. For instance, bed form growth and migration may lead to the filling of navigation channels, re-exposure of cables and pipelines, and endanger the integrity of foundations of off-shore installations (Németh et al., 2003). This study focuses on the dynamics of tidal sand waves (also known as tidal sand dunes), i.e. rhythmic bed features with a typical height of several meters, a wavelength of hundreds of meters and an annual migration of multiple meters. They are commonly found in shallow shelf seas, for instance in the North Sea, the Baltic Sea and the Irish Sea (Van der Meijden et al., 2023).

Sand waves have been explained as free instabilities of the sea bed, implying they will inherently form on the (unstable) flat sea bed due to residual flow cells resulting from tide-topography interactions (Hulscher, 1996). However, all studies so far consider non-cohesive (sandy) sediments, whereas the impact of cohesive sediment on sand wave dynamics is suggested to be profound. Although sand waves are found in areas with a muddy sediment fraction (Van Dijk et al., 2012), no bedforms are found if the cohesive sediment fraction exceeds 10-15% (Baas et al., 2016; Schindler et al., 2015). Some authors put this threshold even lower, suggesting small amounts of cohesive sediment may already inhibit sand wave formation (Borsje et al., 2009). Therefore, this study aims to address how cohesive sediment impacts sand wave dynamics.

To achieve this objective, we systematically develop an idealized, process-based morphodynamic model accounting for different sediment fractions, both non-cohesive and cohesive. The hydrodynamics are described by the shallow water equations. Sediment transport per sediment fraction is governed by bedload transport, for which a simple transport predictor is applied, and suspended load per fraction, described by the advection-diffusion equation. The Hirano (1971) approach is employed to describe the bed composition, and the Exner equation is employed to describe the evolution of the bed level. In future results, the effect of the cohesive sediment on the sediment transport shall be included as described in Van Ledden (2001).

To analyse the model results, a linear stability analysis is performed (see e.g. Hulscher, 1996; Roos et al., 2007). In this approach, we consider the flat bed configuration (the basic state). Linear stability analysis allows to study the stability of this basic state for features of different wavelengths (“modes”). For each of these modes, the stability analysis reveals whether the amplitude of the mode will increase or decrease (the growth rate γ) as well the migration rate of the bed feature. The mode with the largest growth rate is termed the fastest growing mode (FGM) and is presumed to dominate the dynamics; this allows to also quantify the wavelength of the bed features. In this study, this method is expanded to also allow for analysis of multiple sediment fractions. This is done in a similar way as Damveld et al. (2019), allowing to also explore the sorting pattern of the sediment over the sand wave.

In Figure 1, first results of this analysis are shown for a bi-modal sediment mixture. The first fraction represents a coarse (D = 0.35 mm) fraction that is solely transported by bedload transport, whilst the other represents a fine (D = 0.15 mm) fraction solely transported as suspended load. In these first results, both fractions are modelled as non-cohesive, but the transport and erosion parameters of the finer fraction are chosen to represent a muddier fraction. The multi-modal sediment transport is explicitly solved for. However, the interaction between the fractions is, in these first results, included by correcting the input parameters for hiding-exposure in the basic state. Already without a cohesive interaction with the other fraction, profound effects can be observed. In the left panel, it can clearly be observed that the addition of even a small fraction of fine sediment (ffine) leads to large changes in the growth rate. This is further explored in the right panel, showing that a small fine sediment fraction (ffine = 0.05) already reduces the growth rate by roughly 20%. Conversely, the topographic wavenumber k* of the FGM (inversely related to the wavelength) barely changes with the addition of fine sediments. Additional results (not shown here) indicate a clear sediment sorting pattern, with the fine sediment accumulating in the troughs of the sand waves, and the coarse sediment accumulating on the crests. An impact on sand wave migration is not observed due to the symmetric tidal forcing.

[1] Water Engineering and Management, University of Twente, Enschede, The Netherlands, w.ploeg@utwente.nl (corresponding author)
[2] Water Engineering and Management, University of Twente, Enschede, The Netherlands, p.c.roos@utwente.nl
[3] Water Engineering and Management, University of Twente, Enschede, The Netherlands, b.w.borsje@utwente.nl
[4] Water Engineering and Management, University of Twente, Enschede, The Netherlands, s.j.m.h.hulscher@utwente.nl

The decreased growth rates when increasing the fine sediment fraction can be directly explained as a consequence of the sediment sorting. After all, the fine sediment accumulates in the troughs; hence, if more fine sediment is present in the mixture, more sediment will accumulate in the troughs, and troughs will become shallower. As such, the growth rate of the bed form amplitudes decreases. Based on literature, we would also anticipate a strong impact of fine sediment fraction on the wavelength, but our first results (see Figure 1) do not display this strong relation. We attribute this to the way that hiding exposure is currently implemented in our model, where disturbances of the sediment composition beyond the initial composition do not yield changes in the hiding exposure effect. Furthermore, the first results exemplify the large effect of a fine sediment, behaving like a muddy sediment, even when not considering the cohesive interactions. At the conference, we will present further model results including this cohesive interaction.

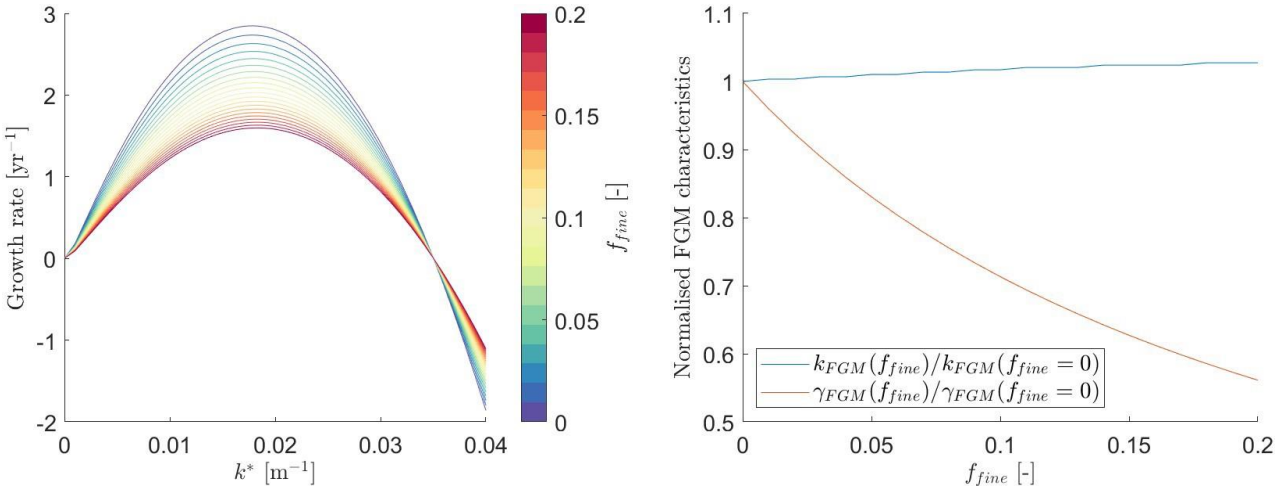

Figure 1: The effect of the fraction of fine sediment (f_{fine}) on sand wave dynamics without cohesive interaction between the fractions. Left panel: impact of f_{fine} on the growth rate of the bedform as a function of the topographic wavenumber k^* (inversely proportional to the wavelength). Right panel: impact of f_{fine} on the growth rate and wavelength of the fastest growing mode of the bedform.

Acknowledgements

This project is taking place as part of the project 'OR ELSE: Operational Recommendations for Ecosystem-based Large-scale Sand Extraction', funded by the Dutch Research Council (NWO) under project number NWA.1389.20.097.

References

Baas, J. H., Best, J. L., & Peakall, J. (2016). Predicting bedforms and primary current stratification in cohesive mixtures of mud and sand. *Journal of the Geological Society*, *173*(1), 12–45. https://doi.org/10.1144/jgs2015-024

Borsje, B. W., de Vries, M. B., Bouma, T. J., Besio, G., Hulscher, S. J. M. H., & Herman, P. M. J. (2009). Modeling bio-geomorphological influences for offshore sandwaves. *Continental Shelf Research*, *29*(9), 1289–1301. https://doi.org/10.1016/j.csr.2009.02.008

Damveld, J. H., Roos, P. C., Borsje, B. W., & Hulscher, S. J. M. H. (2019). Modelling the two-way coupling of tidal sand waves and benthic organisms: A linear stability approach. *Environmental Fluid Mechanics*, *19*(5), 1073–1103. https://doi.org/10.1007/s10652-019-09673-1

Hirano, M. (1971). River bed degradation with armouring. *Japan Society of Civil Engineers*, *3*, 194–195.

Hulscher, S. J. M. H. (1996). Tidal-induced large-scale regular bed form patterns in a three-dimensional shallow water model. *Journal of Geophysical Research: Oceans*, *101*(C9), 20727–20744. https://doi.org/10.1029/96JC01662

Németh, A. A., Hulscher, S. J. M. H., & De Vriend, H. J. (2003). Offshore sand wave dynamics, engineering problems and future solutions. *Pipeline & Gas Journal*, *230*(4), 67–69.

Roos, P. C., Hulscher, S. J. M. H., van der Meer, F. M., Dijk, T., Wientjes, I., & van den Berg, J. (2007). Grain size sorting over offshore sandwaves. In C. M. Dohmen-Janssen & S. J. M. H. Hulscher (Eds.), *River, Coastal and Estuarine Morphodynamics: RCEM 2007* (Vol. 1, pp. 649–656). CRC Press. https://doi.org/10.1201/noe0415453639-c84

Schindler, R. J., Parsons, D. R., Ye, L., Hope, J. A., Baas, J. H., Peakall, J., Manning, A. J., Aspden, R. J., Malarkey, J., Simmons, S., Paterson, D. M., Lichtman, I. D., Davies, A. G., Thorne, P. D., & Bass, S. J. (2015). Sticky stuff: Redefining bedform prediction in modern and ancient environments. *Geology*, *43*(5), 399–402. https://doi.org/10.1130/G36262.1

Van der Meijden, R., Damveld, J. H., Ecclestone, D. W., Van der Werf, J. J., & Roos, P. C. (2023). Shelf-wide analyses of sand wave migration using GIS: A case study on the Netherlands Continental Shelf. *Geomorphology*, *424*, 108559, 1–17. https://doi.org/10.1016/j.geomorph.2022.108559

Van Dijk, T. A. G. P., Van Dalfsen, J. A., Van Lancker, V., Van Overmeeren, R. A., Van Heteren, S., & Doornenbal, P. J. (2012). Benthic Habitat Variations Over Tidal Ridges, North Sea, The Netherlands. In *Seafloor Geomorphology as Benthic Habitat* (pp. 241–249). Elsevier Inc. https://doi.org/10.1016/B978-0-12-385140-6.00013-X

Van Ledden, M. (2001). *Modelling of sand-mud mixtures Part II: A process-based sand-mud model* (pp. 1–75). WL | Delft Hydraulics.

Mixing at fronts in a microtidal estuary and plume

Ralston D.K. [1] and Geyer W.R. [1]

Keywords: mixing, stratification, freshwater discharge, scalar variance, Mobile Bay

Abstract

Salinity fronts in estuaries are often regions of locally intensified mixing. Horizontal velocity convergence at surface or bottom fronts can lead to accumulation near the front of positively or negatively buoyant material, respectively. Fronts can be generated by tidal flows interacting with bathymetric features, and are often associated with high discharge, strongly stratified conditions as in salt wedge estuaries or tidal intrusions fronts. Here we examine the role of fronts in mixing of salt and fresh water in Mobile Bay. Mobile Bay is located on the Gulf of Mexico and has the fourth largest coastal river discharge in the U.S. The mean river outflow is 1900 m3/s, but seasonally discharge ranges from 100 m3/s during the summer and early fall to more than 15,000 m3/s during major events. Mobile Bay is microtidal and with dominantly diurnal tides ranging in amplitude from 0.1 to 0.8 m. The embayment is large (50 km long, 15-35 km wide) and shallow (mostly < 4 m) except for a narrow navigational channel (15 m deep) that extends from the mouth to the head of the bay. The navigational channel cuts through an otherwise shallow ebb tide delta that connects Mobile Bay to the Gulf of Mexico.

The highly modified bathymetry, weak tides, and large and variable river discharge make Mobile Bay a distinctive case study for examining mixing processes. We use a high-resolution numerical model to quantify freshwater transport and salinity mixing in the estuary over a range of realistic forcing conditions. Model results are compared with observations using in-situ and remote sensing data, including moored time series, shipboard survey transects, and satellite synthetic aperture radar (SAR) images to identify front locations. The period of observations and model results is from April to June 2021, spanning multiple spring-neap cycles and several large river discharge events. Mixing is quantified based on the vertical salinity variance budget and includes both resolved turbulent and numerical mixing.

The freshwater content of the estuary and adjacent shelf varies depending primarily on the river inputs and the mixing in the estuary. The spring-neap cycle affects the position of the salinity intrusion, and thus the mixing, with more landward extent of the salinity during neap tides. Bottom fronts form at the edges of the navigational channel and create localized regions of intensified mixing. Lateral baroclinic exchange from the channel onto the adjacent shoals enhances the stratification, and tidal shear causes increased mixing, particularly during the transition from neap to spring tides. Surface salinity fronts form at multiple headlands and constrictions. During flood tides, tidal intrusion fronts cause intensified mixing inside the mouth of the estuary, whereas during the ebb, surface fronts created at headlands result in multiple plume fronts that propagate into the coastal ocean. The plume fronts are also influenced by the bathymetry of the ebb delta, where lateral shear from flow through deeper gaps in the shallow sill create multiple lobes to the plume fronts. The lateral shear induced by the bathymetry enhances the internal shear layer-mixing from the baroclinic plume. An additional factor influencing the overall mixing is the wind. Surface wind stress increases the mixing rate at shallow pycnoclines in both the estuary and plume. Wind also enhances the near-surface shear in the ambient currents, increasing the convergence at surface fronts and the associated mixing. Overall, localized mixing at fronts accounts for a disproportionate amount of the total mixing during both flood and ebb tides.

[1] Woods Hole Oceanographic Institution, Woods Hole, MA, USA

Lateral circulation and salt fronts determine mixing in a mesotidal estuary with tidal flats

Reese L. [1], Gräwe U. [1], Klingbeil K. [1], Li X. [1,2], Lorenz M. [1], and Burchard H. [1]

Keywords: physics, estuaries, mixing, lateral circulation

Abstract

Estuaries are locations where terrestrial freshwater, such as discharge from a river, is mixed with salty ocean water. This mixing process is effectively a transformation of water masses, which can best be traced in salinity space. In a novel approach to identify key mechanisms driving this water mass transformation, we have thus applied a combination of analyses in salinity space and Euclidean space. To this end, we used results from a realistic, three-dimensional hindcast study of the tidal Elbe, a mesotidal estuary located in northwest Germany adjacent to the North Sea. In a preceding study by Reese et al. (2024), the spatial distribution of the exchange of water masses between estuary and ocean was mapped using the diahaline water transport, which can be understood as entrainment across isohaline surfaces, as well as the local mixing per salinity class. It was found that mixing and water mass transformation in the estuary are localised along steep topography gradients such as the shoals of the navigational channel, see Fig. 1. In detail, ocean water is entrained into the estuary in the upstream, near-bottom region of isohaline surfaces, while estuarine waters are exported towards the ocean in the downstream, near-surface region of an isohaline. Building on these findings, we present our newest results from a subsequent, in-depth analysis of the mechanisms triggering the formation of the modelled mixing hotspots. This analysis reveals a dominant mixing signal of the M2 tidal cycle, for which two main drivers were identified: First, the formation of a salt front due to differential advection between the navigational channel and surrounding tidal flats leads to intense mixing directly at the intersection of the front with the shoal topography, especially during ebb tide, as previously described by Warner et al. (2020) for the Hudson estuary. Second, a single-cell lateral circulation drives mixing hotspots at the turning points of the circulation near the shoals of the navigational channel, where a strong vertical shear coincides with vertical stratification due to freshwater discharge. Lastly, a weaker spring-neap signal of strongest mixing during the transition from neap to spring tides, when stratification is strongest, is found to be masked during a high discharge event.

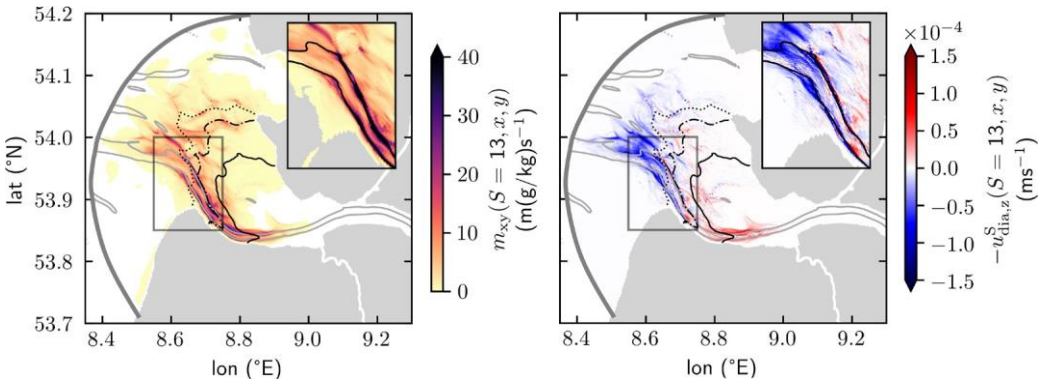

Fig. 1: Horizontal distribution of local mixing mxy(S, x, y) (left) and negative effective vertical diahaline velocity uSdia,z (right) for the isohaline S = 13 g kg^{-1} , averaged over two spring-neap cycles during a high-discharge event in June 2013. Outflow from the estuary toward the North Sea is shown in blue, inflow is shown in red. The bold gray line represents the open boundary of the numerical setup, thin gray lines represent the 12-m isobath, and the black lines show the relative height of the S = 13 g kg^{-1} isohaline above ground at intervals of 0.2 (bold), 0.5 (dash-dot), and 0.8 (dotted). The inset figures in each panel show details from the location of the the black rectangles, with the 12-m isobath as a bold black line. Figure and description modified from Reese et al. (2024).

References

Reese, L., Gräwe, U., Klingbeil, K., Li, X., Lorenz, M., and Burchard, H. (2024): Local Mixing Determines Spatial Structure of Diahaline Exchange Flow in a Mesotidal Estuary: A Study of Extreme Runoff Conditions. J. Phys. Oceanogr., 54, 3–27, https://doi.org/10.1175/JPO-D-23-0052.1.

Warner, J. C., Geyer, W. R., Ralston, D. K., and Kalra, T. (2020): Using tracer variance decay to quantify variability of salinity mixing in the Hudson River estuary. J. Geophys. Res. Oceans, 125, e2020JC016096, https://doi.org/10.1029/2020JC016096.

[1] Institute for Baltic Sea Research Warnemünde, Rostock, D-18119, Germany. Corresponding author: Lloyd Reese, reese@io-warnemuende.de

[2] Southern Marine Science and Engineering Guangdong Laboratory (Zhuhai), Zhuhai, 511458, China

Trajectories, magnitude, and fate of continental microplastic loads to the inner shelf: a case study of the world's largest choked coastal lagoon plume export

Rodriguez C. [1], Silva P. [1], Moreira L. [1], Zacher L. [2], Fernandes A. [2], Bouyssou R. [3], Jalón-Rojas I. [4], Moller O. [1], Garcia-Rodriguez F. [1,5], Pinho G.L.L. [1], and Fernandes E. [1]

Keywords: Coastal Plume, South Atlantic, Numerical Modelling, Plastic Fiber Transport, Accumulation Hotspots.

Abstract

Estuarine environments have a transitional importance on the presence and behaviour of plastic pollutants acting as source and sink of these anthropogenic particles, by both buffering and exporting continental discharges to the adjacent coastal environment (Pazos et al., 2021). Continental plastic loads, together with direct plastic inputs from fisheries, offshore industries, and other maritime activities (Boucher and Friot, 2017; Boucher et al., 2020), undergo various physical, chemical, and biological degradation processes driven by external environmental factors, such as mechanical action from wind and waves, solar radiation, oxygen availability and interaction with organisms. These processes lead to the formation of smaller size categories and dynamic changes in particle properties over time (Verma et al., 2016; Chamas et al., 2020). Consequently, estuaries are key compartments for both dispersion and fragmentation of macroplastics (>25 mm) into mesoplastics (5 mm – 25 mm) and microplastics (1 µm - 5 mm), experiencing changes in dimensions and densities and altering their buoyancy properties (Jalón-Rojas et al., 2019).

In the southern cost of Brazil, Patos Lagoon, the world's largest choked lagoon, is considered the sixth hotspot of plastic leakage to the ocean in South America, only after La Plata River, Guanabara Bay, Amazon, São Francisco, and Tocantins Rivers (Alencar et al., 2023). The Patos Lagoon Estuary is a highly significant ecosystem where freshwater from a vast and densely populated area continuously flows into the Atlantic Ocean, exporting not only freshwater but also suspended sediment, nutrients, plastics, and other contaminants (Jung et al., 2020, Bortolin et al, 2022). The estuary´s hydrodynamics is mainly modulated by the wind regime and the discharges over the drainage basins, with interannual variability related to climatic modes of oscillation such as El Niño Southern Oscillation (ENSO) (Távora et al., 2020). These factors force and control the formation, intensity, and behavior of hypopycnal coastal plumes (Calliari et al., 2009, Marques et al. 2009), which modulate different patterns of plastic debris export towards the coast. In this context, Patos Lagoon is potentially crucial as both a source and sink of anthropogenic waste, and ulterior export to the coastal region by the coastal plume formation and dynamics, making the estuary a "hotspot" of marine pollution (Pinheiro et al., 2021).

In this context, numerical modelling tools together with field data were used to assess for the first time the capacity of the Patos Lagoon coastal plume to export MPs to the inner shelf under different hydrodynamic conditions (Fig. 1a). The TELEMAC-3D hydrodynamic model (www.opentelemac.org) coupled with the TrackMPD model (Jalón-Rojas et al., 2019) were applied to simulate MPs dispersion and export through the Patos Lagoon coastal plume under different intensities of ENSO. The behaviour of MPs was analysed for nine plume events during the period of 2014 and 2016, being three of them classified as neutral, three as weak and three as very strong ENSO events, presenting different discharge intensities, coastal plume structure and duration. Also, two field surveys were conducted during plume events to validate the model approach and quantify MPs concentrations and loads applying a bottom-up approach. This approach was employed to estimate the potential MPs export from the estuary´s towards the inner shelf (Fig. 1a).

MPs concentration in surface plume waters ranged from 0.22 items.m^{-3} to 1.53 items.m^{-3} and were confirmed by FTIR as synthetic polymers in a 90%, being Polypropylene (PP) and Polyethylene (PE) the most abundant in a 73% (Fig. 1b). The accumulation pattern was observed on the plume´s frontal system, consistent with simulation results (Fig. 1c). The estimated average MPs potential export rate attained 9.6 million items.day^{-1} during moderate plume events and 53.5 million items.day^{-1} during high discharge plume events.

[1] Instituto de Oceanografia, Universidade Federal do Rio Grande (FURG), Rio Grande, RS, 96203-900, Brazil. carolinarp@furg.br
[2] Instituto de Química, Universidade Federal do Rio Grande do Sul (UFRGS), Porto Alegre 91501-970, Brazil.
[3] INRAE, 50 avenue de Verdun, 33612 CESTAS, cedex, France.
[4] Univ. Bordeaux, CNRS, Bordeaux INP, EPOC, UMR 5805, F-33600 Pessac, France.
[5] Centro Universitario Regional del Este (CURE), Ruta 9 intersección Ruta 15, Rocha, Uruguay.

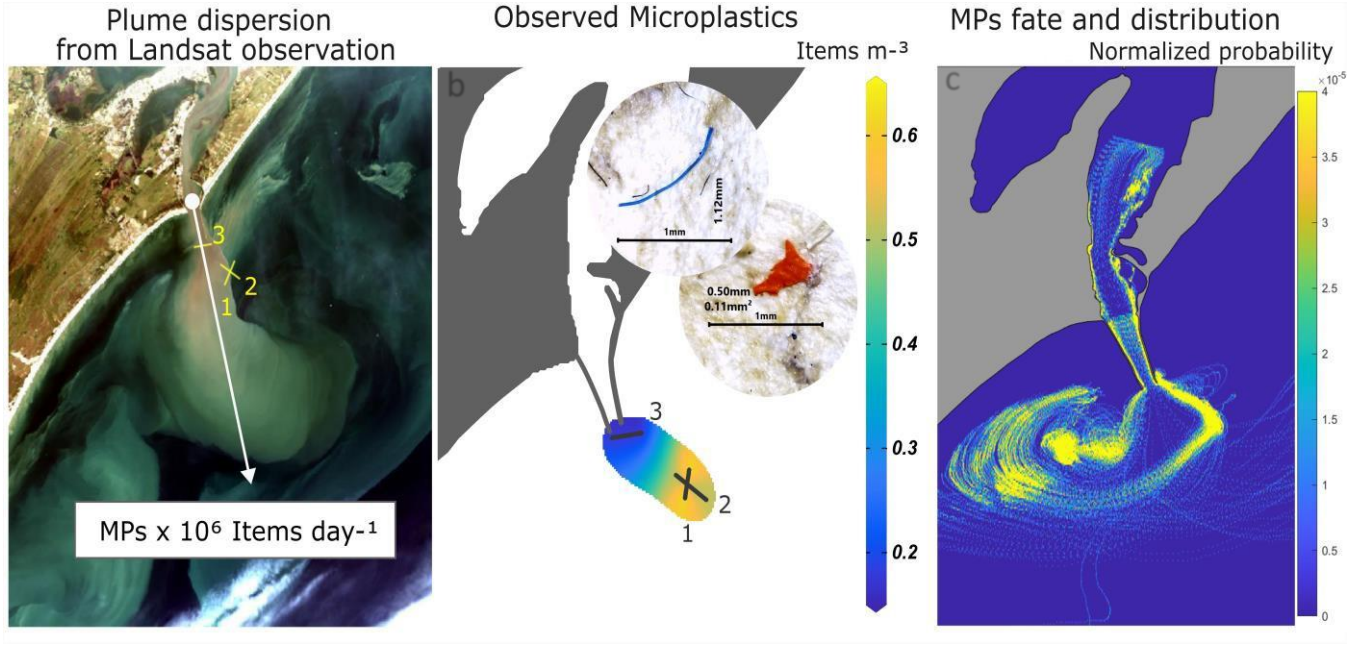

Figure 1. Landsat observation for the Patos Lagoon coastal plume behavior (a) and position of the sampling transects during the first field sampling on June,2022. The magnitud of the average plastic export, calculated through a bottom-up approach, is indicated in the white box in the order of millions items.day^{-1}. The observed microplastics density (b) indicate an acumulation pattern on the plume front (transects 1 and 2), similar pattern as observed in the TrackMPD simulation results (c). TrackMPD results also demonstrated the southwest transport of plastic particles, in response of NE predominant wind direction, and the presence of an accumulation hotspot in the gyre between the jetties and Cassino's beach.

Different trends of horizontal and vertical dispersion and accumulation of MPs were observed. Strong discharge events, coupled with intense northeast winds, facilitated rapid south-westward export of MPs. Conversely, moderate to weak discharge events retained MPs closer to the estuary's mouth, enabling either longer trajectories or earlier deposition. Significant MPs accumulation hotspots were identified in the gyre between the jetties and Cassino's beach, as well as in the saline front within the plume boundaries (Fig. 1c). These accumulation zones may function as reservoirs for MPs particles, potentially posing threats to local ecosystems. Understanding these dynamics is crucial for ongoing monitoring efforts to assess potential harmful interactions over time.

References

Alencar, M. V., Gimenez, B. G., Sasahara, C., Elliff, C. I., Velis, C. A., Rodrigues, L. S., Conti, L. A., Gonçalves-Dias, S. L. F., Cetrulo, T. B., Scrich, V. M., & Turra, A. (2023). Advancing plastic pollution hotspotting at the subnational level: Brazil as a case study in the Global South. Marine Pollution Bulletin, 194(March). https://doi.org/10.1016/j.marpolbul.2023.115382

Bortolin, E. C., Távora, J., & Fernandes, E. H. L., 2022. Long-term variability on suspended particulate matter loads from the tributaries of the world's Largest Choked Lagoon. Frontiers in Marine Science, 9(March), 1–17. https://doi.org/10.3389/fmars.2022.836739

Boucher, J., and Friot, D. (2017). Primary Microplastics in the Oceans: a Global Evaluation of Sources. Gland: IUCN. https://doi.org/10.2305/IUCN.CH.2017.01.en

Boucher, J., Billard, G., Simeone, E., & Sousa, J. (2020). The marine plastic footprint. In The marine plastic footprint. https://doi.org/10.2305/iucn.ch.2020.01.en

Calliari, L. J., Winterwerp, J. C., Fernandes, E., Cuchiara, D., Vinzon, S. B., Sperle, M., & Holland, K. T. (2009). Fine grain sediment transport and deposition in the Patos Lagoon-Cassino beach sedimentary system. Continental Shelf Research, 29(3), 515– 529. https://doi.org/10.1016/j.csr.2008.09.019

Chamas, A., Moon, H., Zheng, J., Qiu, Y., Tabassum, T., Jang, J. H., Abu-Omar, M., Scott, S. L., & Suh, S. (2020). Degradation Rates of Plastics in the Environment. ACS Sustainable Chemistry and Engineering, 8(9), 3494–3511. https://doi.org/10.1021/acssuschemeng.9b06635

Jalón-Rojas, I., Wang, X. H., & Fredj, E. (2019). A 3D numerical model to Track Marine Plastic Debris (TrackMPD): Sensitivity of microplastic trajectories and fates to particle dynamical properties and physical processes. Marine Pollution Bulletin, 141(February), 256–272. https://doi.org/10.1016/j.marpolbul.2019.02.052

Jung, B. M., Fernandes, E. H., Möller, O. O., & García-Rodríguez, F. (2020). Estimating suspended sediment concentrations from river discharge data for reconstructing gaps of information of long-term variability studies. Water (Switzerland), 12(9), 1–14. https://doi.org/10.3390/W12092382

Marques, W. C., Fernandes, E. H., Monteiro, I. O., & Möller, O. O. (2009). Numerical modeling of the Patos Lagoon coastal plume, Brazil. Continental Shelf Research, 29(3), 556–571. https://doi.org/10.1016/j.csr.2008.09.022

Pazos, R. S., Amalvy, J., Cochero, J., Pecile, A., & Gómez, N. (2021). Temporal patterns in the abundance, type and composition of microplastics on the coast of the Río de la Plata estuary. Marine Pollution Bulletin, 168. https://doi.org/10.1016/j.marpolbul.2021.112382

Pinheiro, L. M., Agostini, V. O., Lima, A. R. A., Ward, R. D., & Pinho, G. L. L. (2021). The fate of plastic litter within estuarine compartments: An overview of current knowledge for the transboundary issue to guide future. Environmental Pollution, 279, 116908. https://doi.org/10.1016/j.envpol.2021.116908

Tavora, J., Fernandes, E. H. L., Thomas, A. C., Weatherbee, R., & Schettini, C. A. F. (2019). The influence of river discharge and wind on Patos Lagoon, Brazil, Suspended Particulate Matter. International Journal of Remote Sensing, 40(12), 4506–4525. https://doi.org/10.1080/01431161.2019.1569279

Verma, R., Vinoda, K. S., Papireddy, M., & Gowda, A. N. S. (2016). Toxic Pollutants from Plastic Waste- A Review. Procedia Environmental Sciences, 35, 701–708. https://doi.org/10.1016/j.proenv.2016.07.069

Spatial-temporal variability of TEF, salt flux, and mixing in a well-mixed estuary

Rojas C. [1], Ross L. [2], Sottolichio A. [3], Lorenz M. [4], and Burchard H. [5]

Keywords: estuarine dynamics, total exchange flow, mixing, macrotidal estuary

Abstract

Estuaries, with a large percentage of the world's populations living on or near their shorelines, are of great socioeconomic importance. Thus, it is critical to understand the physical mechanisms that impact their health, such as their circulation and exchange flow. In particular, the exchange between coastal and estuarine waters determines residence times, which affect water quality conditions and thus biogeochemical processes such as hypoxia, nutrient fluxes, and the transport of contaminants (MacCready & Geyer, 2010).

The influence of density gradients on the estuarine hydrodynamics is well understood. Similarly, mechanisms such as tidal asymmetry or lateral dynamics have also been found to be important in the generation of exchange flow. However, recent studies have shown that these processes could yield exchange flows with the same structure and orientation, making it difficult to differentiate their importance. In the case of well-mixed systems, buoyancy gradients may not be dominant due to large tidal effects (Burchard & Hetland, 2010). One important tidal process is the difference in the volume of water within an estuary between high and low tides, or the tidal prism. This volume alters the salinity intrusion length which affects the stratification and mixing. Further, because of fortnightly tidal variability these effects are expected to vary between the spring-neap cycle. Despite this, systems where tidal effects are of main importance, such as macrotidal estuaries, have been scarcely studied and thus the importance of tidal effects in these systems is only partially understood.

On the other hand, a key aspect of the estuarine residual circulation is that it can be understood as a mechanism governed by advective processes at the boundaries (tidal and river flows) and modulated by diffusive processes within the estuary volume (mixing). While several definitions of mixing have been proposed, the definition proposed by MacCready et al. (2018) as the destruction of the salinity variance within an estuarine volume, has proven to be a suitable measure. Even though their work provided a connection between mixing and the exchange flow using a salinity budget, they did not address the mechanisms responsible for its variability. Expanding on this work, Wang & Geyer (2018) studied the mixing-exchange flow relationship along with mechanisms that vary with spring-neap tides and river conditions based on the turbulence production and turbulent buoyancy flux and how these are related to the integrated volume salinity variance dissipation. Using a model of the Hudson estuary, they found that mixing varies by more than one order of magnitude between spring and neap tides, which considerably alters the salinity variance in the estuary. Among their results, they found that river conditions play an important role in determining the magnitude of the exchange flow, mixing, and the salinity intrusion length whereas the tides mostly affect mixing with different mechanisms during the spring-neap cycle.

Although the estuarine parameter space is broad and several estuarine conditions have been studied, only scarce studies have been carried out on macrotidal estuaries. Since these systems are characterized by having a considerable tidal range, they provide a natural laboratory to study the variability and drivers of exchange flow and mixing over the spring-neap cycle. Therefore, this study aims to answer: (1) What is the spatial and temporal variability of the exchange flow of a funnel-shaped and tidally-driven estuary? (2) How is mixing related to the exchange flow variability under different river regimes during spring-neap tides? To answer these questions we consider the macrotidal Gironde estuary (Figure 1) using numerical simulations from the TELEMAC-3D finite-element open-source model. The model was configured to use the k-ϵ turbulence model in both vertical and horizontal axes and has 20 equidistant terrain-following layers that expand and contract following the tides. The model includes the Garonne and the Dordogne rivers whose combined river discharge (monthly averaged) varies between 150 and 2000 m³/s with flood events reaching peak values of 5000 m³/s. Three different river regimes were considered to force the model: 300, 700, and 1100 m³/s, as low, mid, and high regimes, respectively with identical tidal conditions.

The Total Exchange flow (TEF) methodology was used to calculate the exchange flow (MacCready, 2011). To quantify mixing (M), we use the result from MacCready et al. (2018) according to which, under steady state:

$$M \sim S_{in} S_{out} Q_R$$

where S_{in} and S_{out} are the inflow and outflow layers and Q_R is the river volume flux. To quantify the temporal variability of advection and diffusion in the Gironde, we use the salinity budget equation (MacCready et al., 2018).

[1] University of Maine, Department of Civil and Environmental Engineering, Orono, US, cristian.rojas@maine.edu
[2] University of Maine, Department of Civil and Environmental Engineering, Orono, US, lauren.ross1@maine.edu
[3] University of Bordeaux, Laboratoire EPOC, Bordeaux, France, aldo.sottolichio@u-bordeaux.fr
[4] Leibniz Institute for Baltic Sea Research Warnemünde, Rostock, Germany, marvin.lorenz@io-warnemuende.de
[5] Leibniz Institute for Baltic Sea Research Warnemünde, Rostock, Germany, hans.burchard@io-warnemuende.de

We analyze TEF and mixing in 20 sections along the thalweg of the Gironde. Results show that the exchange flow along the Gironde decreases upstream with similar variability for the inflow and outflow layers (Figure 2A). At the mouth, TEF inflow transport shows a smaller increase between the low and high river regimes while a larger variability was observed on TEF outflow, similar to the results in the Hudson estuary of Wang & Geyer (2018). TEF outflow variability qualitatively follows the along-channel variability in bathymetry and estuary width (Figure 2A,D). The tidally averaged volume conservation indicates that morphological changes seem to be a key factor in driving the spatial variability of TEF in the downstream region of the estuary where tidal flats are substantial. Little variability was observed in the upstream part of the estuary for the three river regimes (Figure 2B). A region of storage in the downstream part of the estuary was observed only for the low river regime model. With higher river conditions, the regions characterized by having flats (0 - 15 km) showed a deficit. The flux-weighted salinities decrease steadily from mouth to head and the stratification ΔS increased with the river regime. Using a salinity threshold of 2 g/kg at the bottom, the salinity intrusion length was found to be ~ 36 and ~ 31 km from the mouth under the mid and high river regimes, respectively. In the case of the low regime, this threshold was not observed on the transects considered, indicating that the intrusion length was greater than 47 km.

The relationship between TEF and mixing indicates different spatial and temporal variability. In the case of the low river regime, the maximum stratification at the mouth occurred during late neap tide whereas at the head occurred centered on neap tides. In the case of the high river regime, the maximum stratification occurred close to the spring tide. The river regime affects the stratification greatly, showing larger stratification with increasing riverine outflows (not shown). Further, the quantification of the advection and diffusion terms in the salinity budget equation indicate an unsteadiness in the salt balance. This situation has been observed in other systems and indicates different importance of the dispersive and advective salt fluxes over the system.

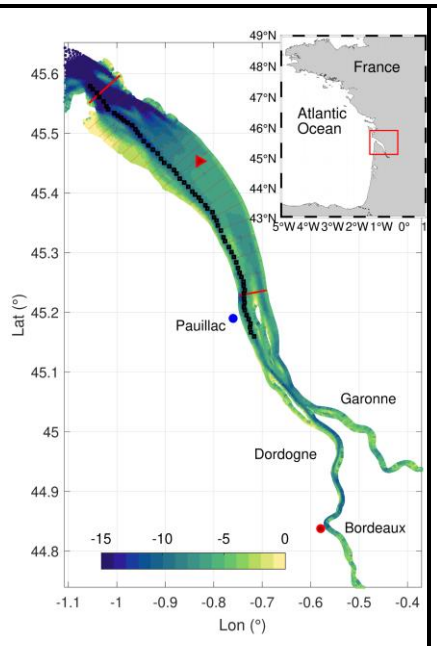

Figure 1. The Gironde, France. Red lines depict the 20 transects considered in the study. The color is depth (m). The inset figure represents the location of the Gironde (red box) in Europe.

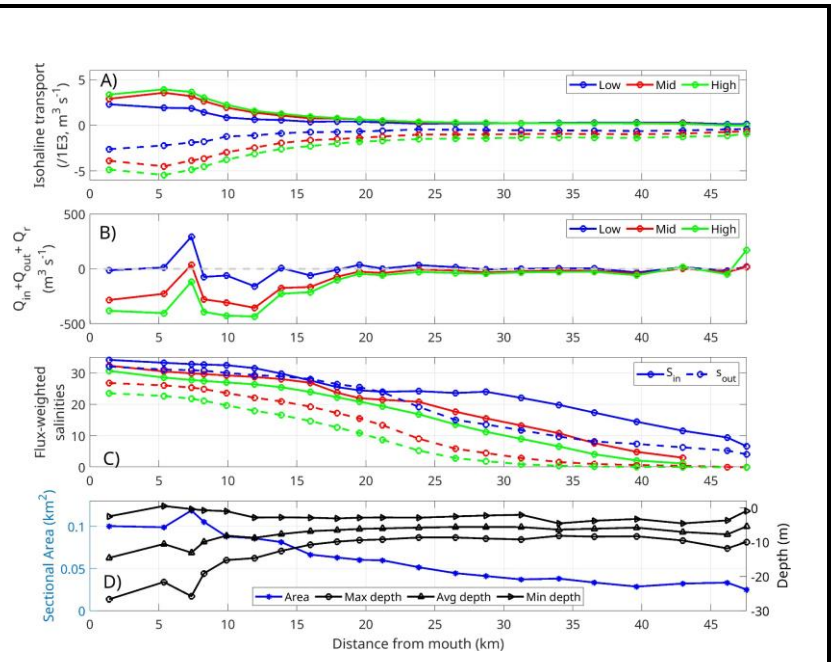

Figure 2. Along-channel variability of (A) the isohaline transport (TEF), (B) the tidally averaged volume conservation, (C) the salinity inflow and outflow values (continuous and dash-lines, respectively), and (D) the along-channel variability of the area and depth. The color code in the first three panels represents the low, mid, and high regimes.

References

Burchard, H., & Hetland, R. D. (2010). Quantifying the contributions of tidal straining and gravitational circulation to residual circulation in periodically stratified tidal estuaries. Journal of Physical Oceanography, 40(6), 1243-1262.

MacCready, P. (2011). Calculating estuarine exchange flow using isohaline coordinates. Journal of Physical Oceanography, 41(6), 1116-1124

MacCready, P., & Geyer, W. R. (2010). Advances in estuarine physics. Annual Review of Marine Science, 2, 35-58.

MacCready, P., Geyer, W. R., & Burchard, H. (2018). Estuarine exchange flow is related to mixing through the salinity variance budget. Journal of Physical Oceanography, 48(6), 1375-1384.

Wang, T., & Geyer, W. R. (2018). The balance of salinity variance in a partially stratified estuary: Implications for exchange flow, mixing, and stratification. Journal of Physical Oceanography, 48(12), 2887-2899.

Understanding Tidal Sandbank Dynamics and Impacts of Sand Extraction in Sediment-Scarce Environments

Roos P.C. [1], Van Lancker V. [2], Van den Eynde D. [2], van Veelen T.J. [1], and Hulscher S.J.M.H. [1]

Keywords: tidal sandbanks, sediment scarcity, marine sand extraction, morphodynamic modelling, morphosedimentary system response, data analysis, Belgian Continental Shelf, sand extraction toolbox.

Abstract

Marine sand extraction is rapidly accelerating, with increasing amounts of sand needed for coastal nourishments, land reclamations, and the construction industry. The impact of depleting sand resources is already felt on the Belgian Continental Shelf (BCS) and is an emerging challenge on the Netherlands Continental Shelf (NCS); see Figure 1. This has severe repercussions on the ecosystem services sandbanks provide and threatens our access to sand supplies in the future.

Here we present the BANX-project, funded by the Netherlands Science Organisation (NWO) and carried out at the University of Twente (UT, The Netherlands) and the Institute of Natural Sciences (RBINS)/Ghent University (UGent) (Belgium). Starting in September 2024, BANX aims to provide knowledge and tools to support the long-term management (years to decades) and sustainable exploitation of tidal sandbanks in environments with sediment scarcity.

To this end, a novel process-based morphodynamic model will be developed to understand sandbank evolution under sediment-scarce conditions, both autonomously and in response to sand extraction (PhD A in Figure 2). A pilot study has already been carried out (Van Veelen et al., 2022). Simultaneously, indicators will be identified that help detect potentially irreversible morphosedimentary system responses based on data from the BCS (including geological substrate, PhD B). Finally, the above will be combined to create an extraction toolbox that supports the spatiotemporal design of extraction strategies (Postdoc C). BANX thus benefits from the modelling expertise of UT and the geological and morphosedimentary expertise at RBINS/UGent. See Figure 2 on the next page for an outline of the project structure.

Utilisation is enhanced by the active involvement of eleven key users, representing government agencies, marine consultancies, dredging industry, knowledge institutes and environmental organisations (from Belgium, The Netherlands and UN). Because sand scarcity, as currently experienced on the BCS and locally on the NCS, has been recognized as a major concern by the United Nations Environment Program (UNEP, 2022), the significance of BANX extends far beyond the BCS and NCS.

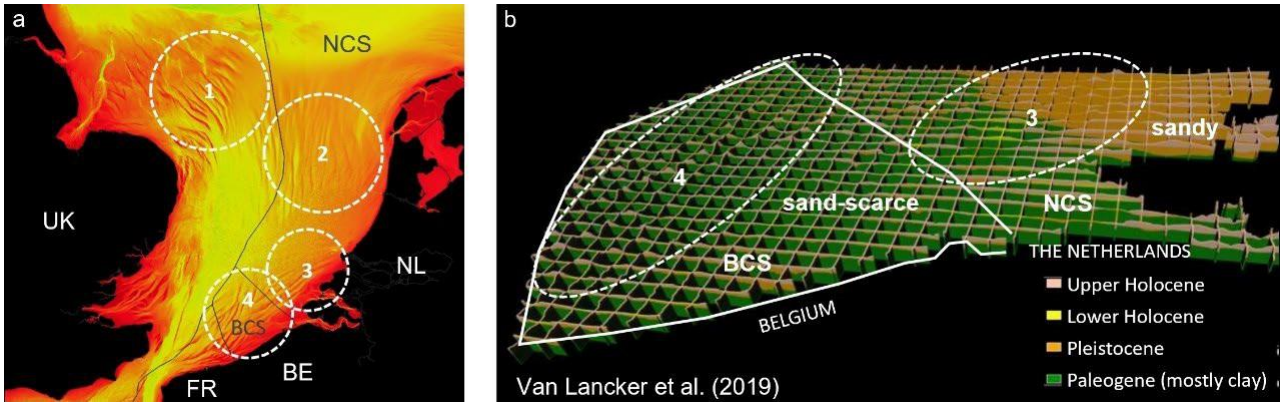

Figure 1: (a) Bathymetric chart of southern North Sea showing four tidal sandbank systems: 1. Norfolk Banks, 2. Dutch Banks, 3. Zeeland Banks, 4. Flemish Banks. (b) Seabed geology of BCS and part of NCS, showing sand scarcity (Van Lancker et al., 2019).

[1] Water Engineering & Management, University of Twente, Enschede, The Netherlands. p.c.roos@utwente.nl, t.j.vanveelen@utwente.nl, s.j.m.h.hulscher@utwente.nl
[2] Institute of Natural Sciences (RBINS), Brussels, Belgium. vvanlancker@naturalsciences.be, dvandeneynde@naturalsciences.be

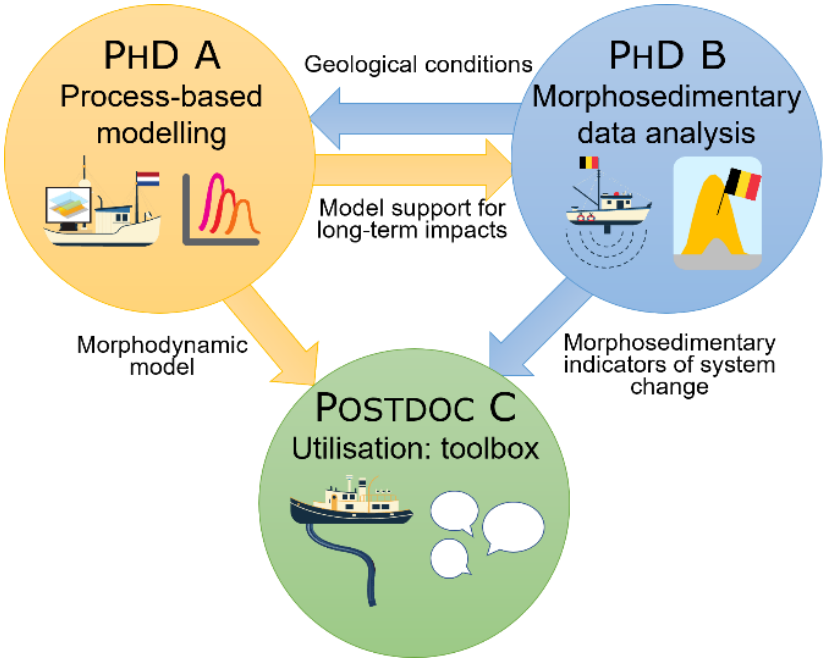

Figure 2: Project structure of BANX, including links among the three subprojects: PhD A (at UT), PhD B (at RBINS/UGent) and Postdoc C (at UT).

References

UNEP (2022). Sand and sustainability: 10 strategic recommendations to avert a crisis. GRID-Geneva, United Nations Environment Programme, Geneva, Switzerland.

Van Lancker, V.R.M., Francken, F., Kapel, M., Kint, L., Terseleer, N., Van den Eynde, D., Hademenos, V., Missiaen, T., De Mol, R., De Tré, G., Appleton, R., van Heteren, S., van Maanen, P.P., Stafleu, J., Stam, J., Degrendele, K., & Roche, M. (2019). Transnational and Integrated Long-term Marine Exploitation Strategies (TILES). Final Report. Brussels: Belgian Science Policy 2019 – 82 p. (BRAIN-be - Belgian Research Action through Interdisciplinary Networks). http://www.belspo.be/belspo/brain- be/projects/FinalReports/TILES_FinRep_AD.pdf

Van Veelen, T.J., Roos, P.C., & Hulscher, S.J.M.H. (2022). Sediment scarcity: modelling the morphodynamics of sandbanks when sand is limited. Proceedings of the 39th IAHR World Congress, 4.

Galilean Tidal Bores

Rousseaux G. [1], Beaudoin A. [2], Fourdrinoy J. [3], Braud P. [1], and James N. [4]

Keywords: tidal bore, estuaries, river current, PIV measurements, SPH methods.

Abstract

A tidal bore is a non-linear wave propagating upstream of estuaries with an important tidal range (Figure 1).

Figure 1: An in-situ tidal bore of the undular type with lateral turbid jets on the banks observed at Saint-Pardon near Bordeaux on the Dordogne river, France (Picture taken by Germain Rousseaux, 10-19-2013).

The tidal bore is also a cultural heritage and an attraction for tourists.

Several types of tidal bores have been reported in the literature so far: dispersive with a decaying undulation (Figure 2) or partially breaking or totally breaking with or without local and or global flow reversal of the river current at the passage of the tidal front [Rousseaux et al. 2016, Berchet et al. 2018, Satria Putra 2019 et al., Thomas & David 2021].

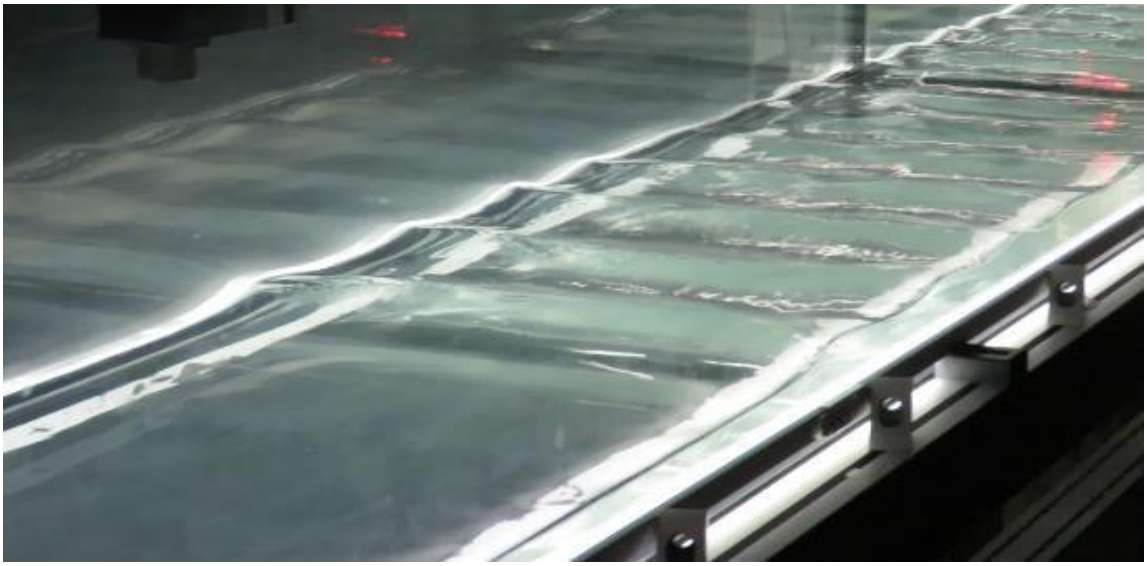

Figure 2: An experimental tidal bore with its undulation generated in the Pprime laboratory by a volume inversion method [Rousseaux et al. 2016] in an open water channel of rectangular geometry with a global flow reversal. The LED lit the secondary waves downstream of the tidal bore front from the channel sides through the glass windows.

[1] CNRS, Institut Pprime, Poitiers (France), germain.rousseaux@cnrs.fr
[2] University of Poitiers, Institut Pprime, Poitiers (France)
[3] EDF, Chatou, (France)
[4] University of Poitiers, LMA, Poitiers (France)

Here, we show for the first time thanks to a combination of Particle Image Velocimetry measurements with the Davis software and numerical simulations using DualSPHysics that the classification of tidal bores has to take into account the Galilean frame of reference of observation. Indeed, the tidal bore is usually viewed "from the banks" by an external observer, says the fisherman. We will argue in this work that a better point of view is the one "from the fish" frame of reference namely of the river current (Figure 3). Then, what seems to be different tidal bores are, in practice, tidal bores seen from different Galilean perspectives. We will distinguish weak and strong bore depending on the balance with the effect of the current. A theoretical discussion on the good dimensionless Galilean parameters taking into account the geometry of the estuary will follow. In the case of partially or totally breaking tidal bores, the numerical modelling of flows with a complex free surface is a very useful benchmark for testing the SPH methods implemented in DualSPHysics, in particular to choose the kernel function (Cottet et al., 2014).

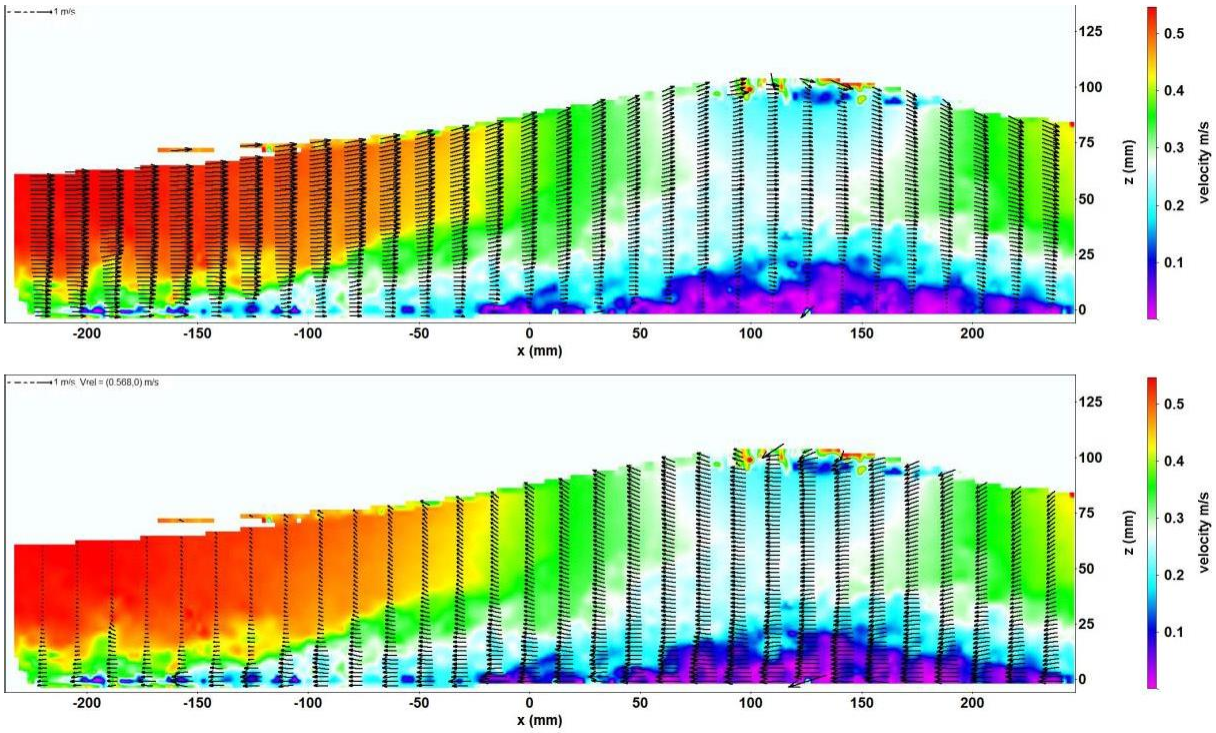

Figure 3: An experimental tidal bore generated in the Pprime laboratory by a partially closing gate in an open water channel of rectangular geometry without global flow reversal. (Top) superposition of the velocity field (dark arrows) of the river current (upstream parameters U=0.57m/s, h=0.07cm) to the tidal bore seen laterally: one notices no local flow reversal ; (Bottom) velocity field of the tidal bore without the contribution of the river current: one notices the local flow reversals. The background color is the modulus of the speed. This type of tidal bore is dominated by the river current without global flow reversal: it is thus a so-called weak bore of an undular type.

References

Rousseaux G., Mougenot J.-M., Chatellier L., David L. and Calluaud D. (2016) A novel method to generate tidal-like bores in the laboratory. European Journal of Mechanics/B, Volume 55, Part 1, p. 31-38.

Berchet A., Simon B., Beaudoin A., Lubin P., Rousseaux G. and Huberson S. (2018) Flow fields and particle trajectories beneath a tidal bore: a numerical study. International Journal of Sediment Research, Volume 33, Issue 3, p. 351-370.

Satria Putria Y., Beaudoin A., Rousseaux G., Thomas L. and Huberson S. (2019) 2D numerical contributions for the study of non-cohesive sediment transport beneath tidal bores. Comptes Rendus Mécanique, Volume 347, Issue 2, p. 166-180.

Thomas L. & David L. (2022) Eulerian and Lagrangian coherent structures in a positive surge. Experiments in Fluids, 63(2), 43. Cottet G. H., Etancelin J.M., Perignon F. and Picard C. (2014). High order semi-lagrangian particles for transport equations:numerical analysis and implementation issues, ESAIM: Mathematical Modelling and Numerical Analysis 48: 1029–1064.

Analysis of salt intrusion in a tidal estuary under changing conditions with a cross-estuary saltflux decomposition

Rummel K. [1], Kolb P. [2], Li X. [1], Gräwe U. [1], Klingbeil K. [1], Reese L. [1], and Burchard H. [1]

Keywords: tidal estuary, salt intrusion, saltflux decomposition.

Abstract

The brackish water zones of estuarine systems between coastal zones and rivers provide a unique ecosystem. Changes in salt intrusion do not only influence these ecosystems, but can have social and economical implications. For example, an increase in salt intrusion may affect freshwater abstraction for drinking water or agricultural use. Hence, changes in the salt dynamics of an estuary can have severe consequences.

Salt intrusions in estuaries are influenced by several environmental factors including the tides and the river discharge. As droughts are expected to become more likely with climate change, periods of reduced river discharge and thus increased salt intrusion into the estuary will likely occur more frequently (e.g. Lee et al., 2024). The correlation between river discharge and salt intrusion can be seen, e.g., in Figure 1 for the Weser estuary. The mesotidal Weser estuary, located in North-West Germany, will be the primary focus of this study.

However, natural changes of environmental conditions are not the only aspect that has to be considered for estimating the development of salt intrusions. Often, estuaries are of a high social relevance as connections between the sea and landward located ports. To maintain the accessibility of such ports for larger ships, dredging of the navigational channel is a common practice in many estuaries. Kolb et al. (2022) have shown that historic dredging of the Weser estuary has had an influence on the salt dynamics in the Weser estuary. To be able to estimate the consequences of natural variability and anthropogenic measures on the salt intrusion, a deepened understanding of the mechanisms of salt transport and their response to changing conditions is essential.

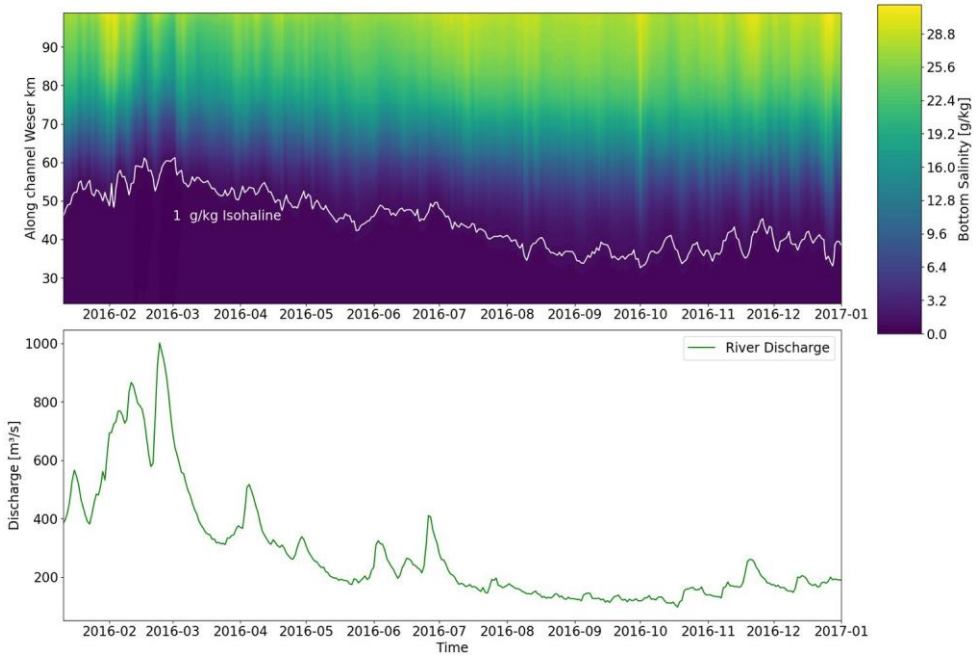

Figure 1: Simulated daily mean values of the bottom salinity in the navigational channel of the Weser estuary for the year 2016 (upper panel). The position of the 1 g/kg isohaline is given in white. The observed Weser river discharge of the year 2016 is shown in the lower panel.

To analyse the different salt transport mechanisms, we transfer a decomposition of suspended matter transport based on a study by Burchard et al. (2018) to the saltflux through cross-sections of the Weser estuary. Within this decomposition, the down-estuary transport of salt due to the river runoff is balanced by four factors, which are typically leading to an upstream salt transport. These include tidal pumping, the estuarine circulation, tidal straining and Stokes transport.

[1] Leibniz-Institute for Baltic Sea Research Warnemünde, Germany, karoline.rummel@io-warnemuende.de
[2] Federal Waterways Engineering and Research Institute, Hamburg, Germany

The saltflux decomposition is applied to results of a high-resolution 3D model simulation of the Weser estuary. Our numerical setup uses a curvilinear grid in which one grid line always follows the thalweg of the navigational channel. This permits a focus on the dominating processes in the channel and simplifies cross-channel analysis (Reese et al., 2024). A continuous analysis of several cross-sections along the estuary allows a comparison of the salt dynamics in different parts of the estuary. With the high-resolution model we are able to focus on areas of low salinity where the transport mechanisms are not yet entirely understood.

Here, we present first results about the development of the above mentioned salt transport mechanisms under different scenarios like changing river discharge and anthropogenic measures based on a saltflux decomposition analysis.

References

Burchard, H., Schuttelaars, H.M., Ralston D.K. (2018): Sediment Trapping in Estuaries. Annual Review of Marine Science, 10, 371-395.

Kolb, P., Zorndt, A., Burchard, H., Gräwe, U., Kösters, F. (2022): Modelling the impact of anthropogenic measures on saltwater intrusion in the Weser estuary. Ocean Science, 18 (6), 1725–1739.

Lee, J., Biemond, B., de Swart, H., Dijkstra, H.A. (2024): Increasing risks of extreme salt intrusion events across european estuaries in a warming climate. Communications Earth & Environment, 5 (1), 60.

Reese, L., Gräwe, U., Klingbeil, K., Li, X., Lorenz, M., Burchard, H. (2024): Local mixing determines spatial structure of diahaline exchange flow in a mesotidal estuary– a study of extreme runoff conditions. Journal of Physical Oceanography, 54(1), 3- 27.

Circulation and sediment fluxes over shore-oblique sand deposits at a wave energetic shelf

Safak I. [1], Ayhan B.U. [1], Parlak M.S. [1], Warner J.C. [2], and Kalra T.S. [3]

Keywords: coastal sea, continental shelf, wave, subtidal, momentum, vortex force, skewness, ridge, sediment flux.

Abstract

The forecast of water exchange between the continental shelf and the coastline is required in a variety of coastal and ocean applications such as sediment budget and coastal morphodynamic evolution. This exchange is controlled by physical processes including hydrodynamics, human interventions, and resulting bathymetric evolution. To improve the understanding of this exchange, field observations and process-based modeling of ocean circulation and sediment processes over the entire shelf and nearshore need to be conducted under varying forcing conditions. Accordingly, circulation and sediment transport over the shore-oblique sand deposits at the shelf offshore of Fire Island, New York, USA (Warner et al., 2014) have been investigated. Field measurements of atmospheric parameters, flows, waves, and sediment fluxes were collected during a wave energetic season. The observations were analyzed where the flow was decomposed into tidal and subtidal parts. A hydrodynamic model that couples atmospheric processes, ocean circulation, waves, and sediment transport (Warner et al., 2010) was set up and validated using the experimental data of the vertical structures of the stratified hydrodynamics, waves, suspended load, and bedload.

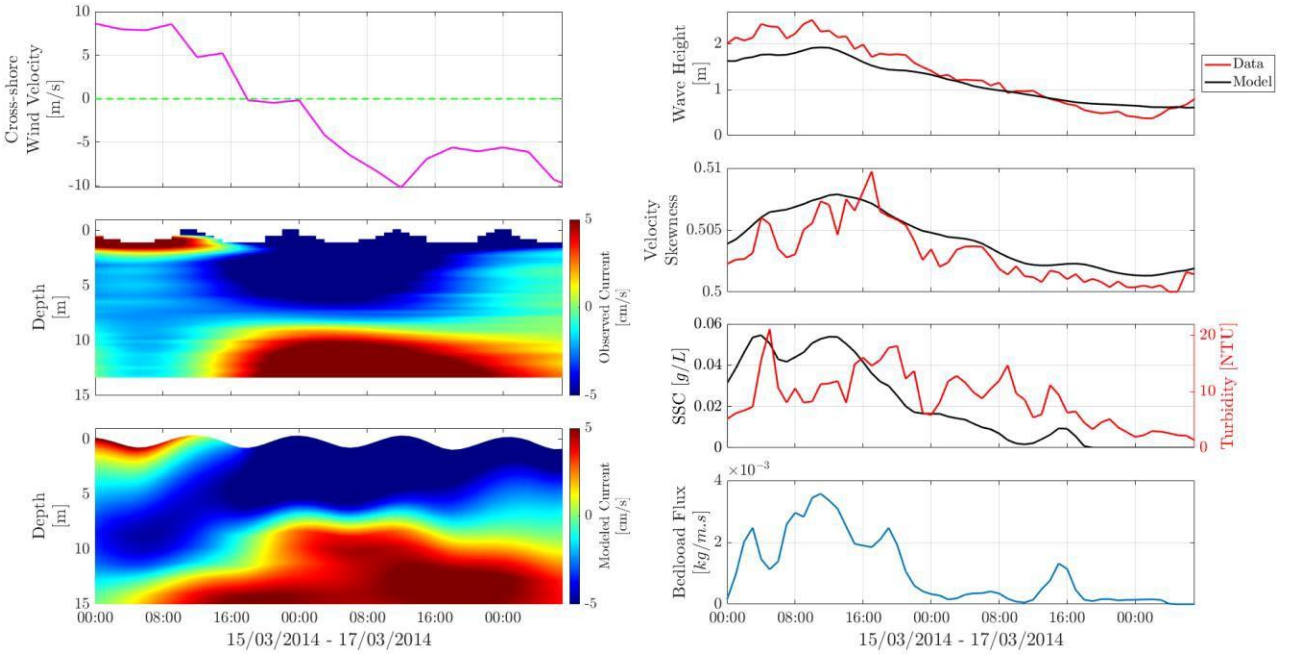

Figure 1 – Two-day-long time-series of cross-shore wind, observed and modeled subtidal cross-shore currents (left panels); wave height, wave skewness, sediment resuspension, and cross-shore bedload flux (right panels). In the color code of the vertical structures of the cross-shore subtidal flows on the left panels, red and blue correspond to onshore-directed and offshore-directed currents, respectively. The red and black curves on the right panels correspond to the observed and modeled parameters, respectively.

The physical processes that control the flows over the shelf and the nearshore were diagnosed. The analysis indicated that the surface momentum induced by the winds impose a major control on the magnitude and direction of the observed and modeled subtidal shelf currents. The along-shelf current velocities were significantly correlated to the along-shelf wind energy and, throughout the water column, in the same direction as the along-shelf winds. The along-shelf momentum near the sea surface was largely governed by a balance between vertical mixing (due to wind stress) and an opposing pressure gradient; near the bed, bottom streaming also became significant in addition to this pressure gradient and the vertical mixing there (due to bottom friction).

[1] Istanbul Bilgi University, Istanbul, Türkiye. ilgar.safak@bilgi.edu.tr ; umut.ayhan@bilgi.edu.tr ; said.parlak@bilgi.edu.tr
[2] United States Geological Survey, Woods Hole, Massachusetts, USA. jcwarner@usgs.gov
[3] Woods Hole Group, Bourne, Massachusetts, USA. tkalra@woodsholegroup.com

For the cross-shelf subtidal flows, the observations and the model results had a two-layer vertical structure: dominantly, the surface flows and the near-bed flows were directed towards offshore and onshore, respectively (Fig.1, left panels). The relatively high alongshore velocities, compared to cross-shore velocities, make Coriolis a significant process in the cross-shelf subtidal momentum balance, in addition to the vertical mixing, pressure gradient, and bottom streaming.

In the nearshore, in addition to these processes, wave-induced impacts such as wave breaking and vortex force, the second of which is due to the interaction of the Stokes drift with the spatial gradients of the horizontal currents, also became significant. The magnitudes, horizontal and vertical extents of these wave impacts and their relative significances in the alongshore and cross-shore directions were shown to depend on the energy and the direction of the incoming waves. The observed and modeled sediment resuspension and bedload transport (Fig.1, right panels) were correlated to the wave-current bottom stress and wave skewness (Parlak et al., 2023), which are critical for not only the maintenance of the sand deposits at the shelf but also the evolution of the coastline (Safak et al., 2017). Future work will include the evaluation of these observed and modeled sediment processes over the entire shelf and the nearshore under varying forcing conditions in order to achieve a better understanding of the sediment exchange between the continental shelf and the coastline.

Acknowledgments

This study was supported by the U.S. Department of the Interior, United States Geological Survey Grant No. G21AC10799-00. Computing resources used in this work were provided by the National Center for High Performance Computing of Turkey (UHeM) under grant number 1011242021.

References

Parlak, M.S., Ayhan, B.U., Warner, J.C., Kalra, T.S., Safak, I. (2023) Wave asymmetry impacts on sediment processes at the nearshore of Fire Island, New York. Coastal Sediments 2023, New Orleans, USA. https://doi.org/10.1142/9789811275135_0173

Safak, I., List, J.H., Warner, J.C., Schwab, W.C. (2017) Persistent shoreline shape induced from offshore geologic framework: effects of shoreface connected ridges, Journal of Geophysical Research-Oceans, 122. https://doi.org/10.1002/2017JC012808

Warner, J.C., Armstrong, B., He, R., Zambon, J.B. (2010) Development of a coupled ocean-atmosphere-wave-sediment transport (COAWST) modeling system. Ocean Modelling, 35. https://doi.org/10.1016/j.ocemod.2010.07.010

Warner, J.C., List, J.H., Schwab, W.C., Voulgaris, G., Armstrong, B., Marshall, N. (2014) Inner-shelf circulation and sediment dynamics on shoreface-connected ridges offshore of Fire Island, NY. Ocean Dyn., 64. https://doi.org/10.1007/s10236-014-0781-y

Resilience to climate change and demographic pressure in wetlands and swamps of the northern coast of Yucatán, Mexico

Salles P. [1] and Pacheco R. [2]

Keywords: wetlands, salinity variability, confined coastal aquifer, environmental health.

Abstract

The northern coast of the Yucatán Peninsula is composed of barriers islands, shallow lagoons, wetlands and swamps, which harbor diverse ecosystem services and communicate with the Gulf of Mexico through natural inlets and shelter ports. These connections allow the water exchange with variable efficiency, and the inland water body can be regarded as many quasi-independent ecosystems separated by watersheds and with negligible flow exchange between them. Besides, significant volumes of freshwater (10-15% of tidal prism) from the confined coastal aquifer enter these systems through hundreds of springs of various sizes and flow rates.

Climate change (sea level rise and increased variability in seasonal and yearly precipitation) and demographic pressure (increased freshwater abstraction from the aquifer for human use) are stressors that hinder the equilibrium and resilience of these coastal systems, whose environmental health depends, to a great extent, on the hydroperiod and salinity levels, which in turn depend on (a) the efficiency and intensity of the water exchange with the ocean and (b) the seasonal and long-term variable aquifer freshwater input. This ongoing study (2010-2024) presents some results from different systems in the region, with emphasis on the Carbonera shallow lagoon and the Sisal wetland (see Figure 1), aimed to increase our understanding of such coastal systems and to evaluate its resilience.

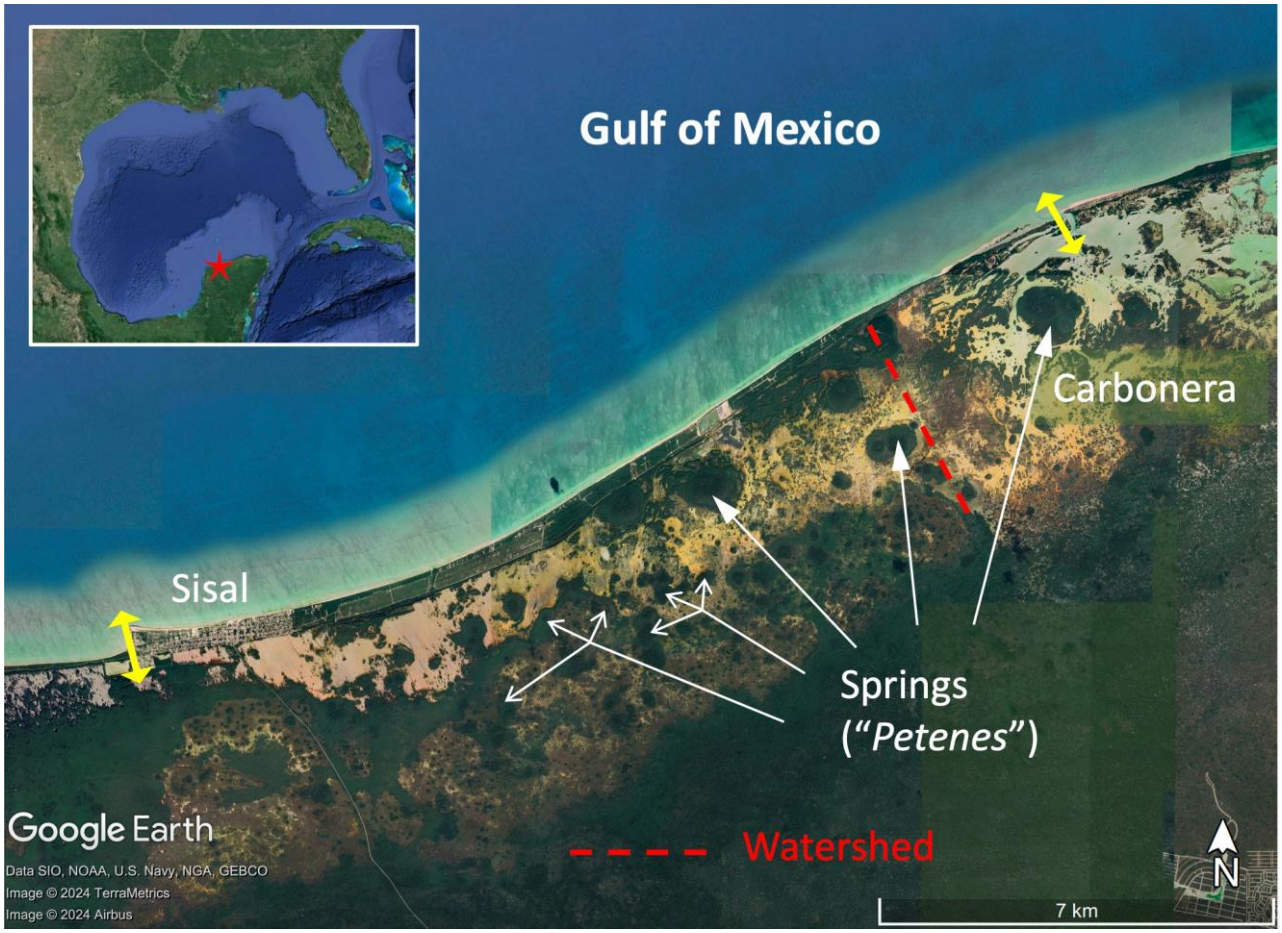

Figure 1. Study area

[1] National University of Mexico (Engineering Institute) and National Coastal Resilience Laboratory; psallesa@iingen.unam.mx.
[2] National University of Mexico (Engineering Institute) and National Coastal Resilience Laboratory; rpachecoc@iingen.unam.mx.

Exchange Flow and Stratification Variability across the Freshwater Froude Number and Mixing Number Parameter Space

Sanchez R. [1], Giddings S.N. [2], Chen J.-L., Chou Y.-J., Lemagie E., MacCready P., Ralston D., Seaton C., Sutherland D., and Wu X.

Keywords: Freshwater Froude, Mixing Number, ocean-driven exchange flow, TEF.

Abstract

Motivation:

The estuarine exchange flow, or tidally-averaged circulation, sets the exchange of salt, heat, nutrients, and other passive tracers between the estuarine and oceanic environment. Ocean-estuary exchange impacts the distribution of tracers within an estuary, as well as tracer residence time. Therefore, understanding the drivers of estuarine circulation is essential to coastal management. Traditionally, the exchange flow has been described as a balance between mixing from tides and buoyancy input from rivers. The relative strength of these two forcing mechanisms determines estuary stratification and the magnitude of circulation. The classical solution describing estuarine circulation (e.g., Hansen and Rattray, 1965) can be shown to produce a relationship between the exchange velocity (U_E) and inflowing river discharge (U_r) as $U_E \propto$ with no mixing dependence. However, for tidally dominated systems, diffusive solutions are more appropriate, and the exchange flow increases with tidal velocity amplitude with $U_E \propto U_{Tide}$ (Chen et al., 2012). These theories work well in describing the exchange flow within estuaries that can clearly be defined as tidally dominated or density dominated, typically short and long estuaries relative to the tidal intrusion, respectively (Chen et al., 2012). However, predicting the exchange flow in systems with intermediate length scales, realistic forcing and varying geometry is more difficult. This challenge arises because realistic estuaries tend to be a complex blend of friction, advection, and pressure gradients (Hetland, 2010), and mixing can be tidally asymmetric and drive its own residual circulation (Burchard and Hetland 2010). Additionally, estuaries can experience non-local forcing such as dense water intrusions during upwelling or sea level setup during storms which can impact the exchange flow. We revisit the question of how the exchange flow varies as a function of river discharge and tides while also keeping in mind the effects of remote forcing and local factors. Specifically, we make use of the Freshwater Froude number (Fr_f) and Mixing number (M) estuary classification scheme (Geyer and MacCready, 2014) to identify broad patterns in exchange flow variability under realistic conditions.

Methods:

For our analysis, we utilized model output from a suite of realistic model runs and placed them in the Fr_f-M parameter space (Fig. 1). M describes the effectiveness of tidal mixing and is proportional to U_{tide}, while Fr_f is proportional to U_r. Our models range from the weakly stratified, large Strait of Juan de Fuca (Salish Sea), which has both a low Fr_f and low M, to the strongly stratified, Columbia River which has a large Fr_f and large M. Using realistic models adds additional complexity but improves the robustness of observed relationships. For each model, we calculate bulk quantities including inflowing/outflowing volume transport (Q_{in}, Q_{out}), inflowing/outflowing salinity (S_{in}, S_{out}), and stratification (S_{in}-S_{out}). We calculate these quantities at the mouth of each estuary using the Total Exchange Flow (TEF) framework which makes use of isohaline coordinates to ensure the bulk quantities are consistent with the Knudsen relation (MacCready 2011, Lorenz et al., 2019).

Results:

We find that the time average of the exchange flow and stratification (ΔS) are roughly proportional to U_r and Fr_f (Fig. 2), consistent with theory. However, the classical relation does a poor job at describing the *variability* of the exchange flow. Instead, predicting exchange flow variability depends on the estuary's location in the Fr_f-M space. For an estuary with both large Fr_f and M, a theory which considers the Richardson number produces a more accurate prediction. Although the appropriateness of this theory is still under consideration. While for estuaries with low Fr_f and high M, the exchange flow is proportional to tidal amplitude. For estuaries with overall weak forcing, such as the Salish Sea, ocean-driven external forcing of the exchange flow can become more important than the traditional forcing parameters U_r and U_{Tide}.

The second component of our analysis evaluates the effects of oceanic variability on the exchange flow across the Fr_f-M parameter space. We evaluate model output from different estuaries along the Pacific Northwest coast which experience similar upwelling and downwelling regimes. The estuaries can experience both the baroclinic and barotropic effects of remote wind forcing. Our analysis suggests estuarine circulation response to external forcing depends on the relative strength of river discharge to coastal sea surface setup, and that stratification is more sensitive than the exchange flow to remote forcing.

[1] Scripps Institution of Oceanography, UC San Diego, rmsanche@ucsd.edu
[2] Scripps Institution of Oceanography, UC San Diego, sgiddings@ucsd.edu Other co-authors are not corresponding.

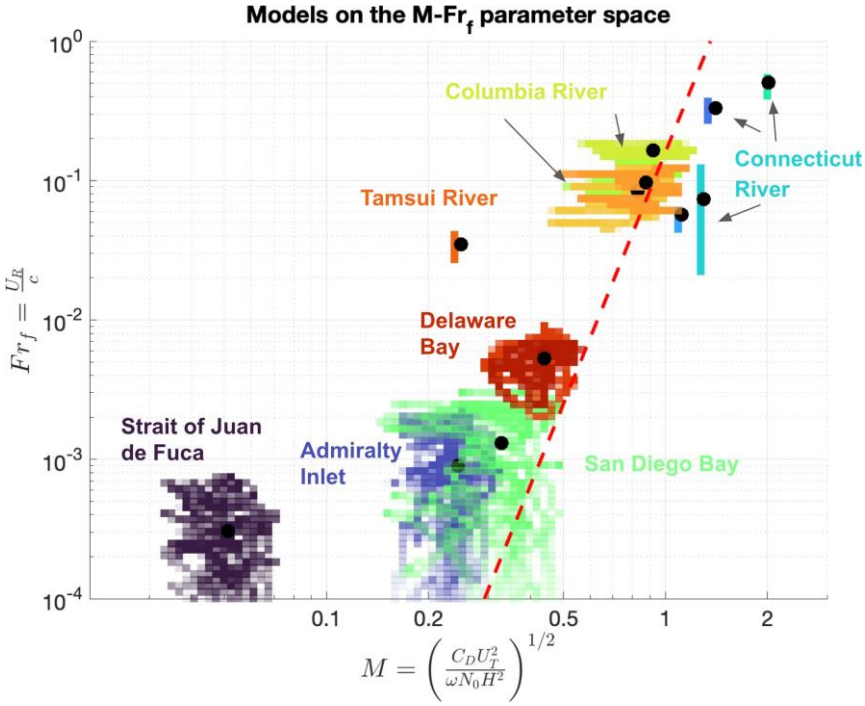

Figure 1: The locations of realistic models analyzed on the Fr_f and M parameter space. The red dashed line separates estuaries which should remain fully stratified during the tidal cycle.

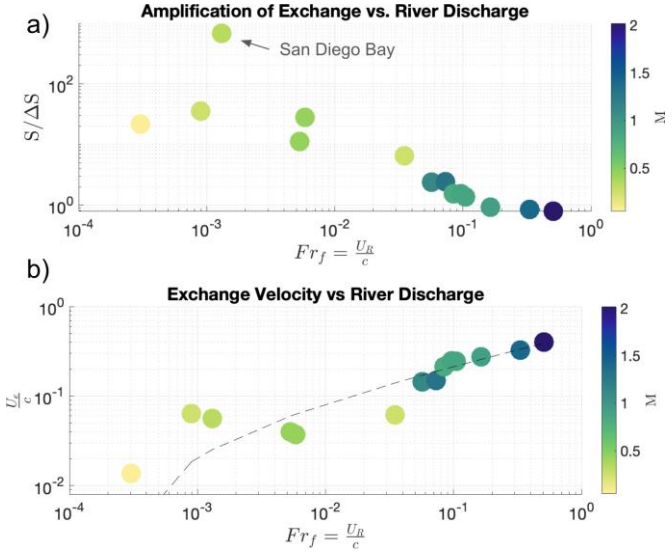

Figure 2: a) Freshwater Froude number (Fr_f) versus $S_{in}/(S_{in}-S_{out})$, the amplification factor. b) Fr_f versus the exchange velocity normalized by, the internal wave speed. The dashed line is a 1/3 fit. The color of all dots is the Mixing number (M) and all variables were calculated using TEF.

References

Hansen, D.V., Rattray, M. (1965). Gravitational circulation in straits and estuaries. Journal of Marine Research, 23:104–22

Chen, S., Geyer, W.R., Ralston, D.K., Lerczack, J.A. (2012). Estuarine Exchange Flow Quantified with Isohaline Coordinates:

Contrasting Long and Short Estuaries. Journal of Physical Oceanography, 42:748-763, DOI: 10.1175/JPO-D-11-086.1 Hetland, R. (2010). Estuarine Overmixing. Journal of Physical Oceanography, 40:199-211, DOI: 10.1175/2009JPO4247.1

Burchard and Hetland (2010). Calculating the Contributions of Tidal Straining and Gravitational Circulation to Residual Circulation in Periodically Stratified Estuaries. Journal of Physical Oceanography, 40:1243:1262, DOI: 10.1175/2010JPO4270.1 MacCready, P. (2011). Calculating Estuarine Exchange Flow using Isohaline Coordinates. Journal of Physical Oceanography,41:1116-1124, DOI: 10.1175/2011JPO4517.1

Lorenz, M., Klingbeil, K., MacCready, P., Burchard, H., (2019). Numerical issues for the Total Exchange Flow (TEF) analysis framework for quantifying estuarine circulation. Ocean Science, 15, 601-614, DOI: 10.5194/os-15-601-2019

Geyer, W.R., MacCready, P. (2014) The Estuarine Circulation. Annual Review of Fluid Mechanics. 46:175–97

Patos Lagoon estuary-shelf exchange processes

Schettini C.A.F., Bordin L.H., Santa-Rosa P.R.A., Fernandes E.H.L., and Moller Jr O.O.

Keywords: circulation, salinity, suspended sediment.

Abstract

The Patos Lagoon is one of the largest coastal lagoons in the world, covering an area of 10,000 km^2, and is connected to the Atlantic Ocean through the Rio Grande Channel at its southern end. This channel is approximately 70 km long and widens progressively from its mouth inland, with the mouth being the narrowest section (~500 m). The lagoon itself is approximately 200 km long and 40 km wide, receiving freshwater input from an area of approximately 200,000 km^2, with an average flow rate of about 2,500 m^3/s. Despite considering losses due to direct evaporation from the lagoon's free surface (~1,000 m^3/s), there is a residual long-term flow from the continent to the ocean. However, on shorter time scales (days/weeks), the lagoon-to-ocean flow becomes much more complex. The processes governing lagoon-to-ocean exchange essentially depend on local and remote winds, and astronomical tides (micro-tidal regime) are not significant. The lagoon is oriented parallel to the coast, coinciding with the direction of prevailing winds. The wind regime has a cyclical pattern that can be summarized as varying between southwest (prevalent conditions) and north-northeast (cold front conditions).

The action of the wind directly on the lagoon causes tilting of the water level, increasing the level at the downwind end, which creates a pressure gradient between the lagoon and the ocean. When the wind blows from the north-northeast, the gradient is towards the lagoon, resulting in flood flow. Conversely, it results in ebb flow. However, on a larger scale, the wind also produces coastal level fluctuations (meteorological tides), which are much more pronounced than astronomical variations. Cold front passages can generate coastal level elevations of around 1 m. This, synergistically with local effects, intensifies the pressure gradient towards the lagoon.

With the aim of investigating and quantifying lagoon-ocean exchanges associated with transient wind states, a field experiment was conducted to record hydrodynamic and water quality data. Over thirty consecutive days, between February 22nd and March 22nd, 2021, during the period from 7:00 to 9:00 am, measurements of flow rate, salinity, temperature, and turbidity were taken at a cross-section located 7 km from the mouth. This section has the narrowest width (~800 m) between the mouth and the lagoon. Flow rate measurements were carried out using a 1200 kHz RDI Workhorse acoustic Doppler current profiler (ADCP) while navigating through the section. Between two and three consecutive ADCP surveys were conducted each day. During the second survey, a JFE-Advantech Rinko Profiler CTD probe was used in yoyo mode. This CTD records data at 10 kHz, and during navigation, it was lowered and raised consecutively through the section, obtaining between 14 and 16 vertical profiles. This CTD also recorded turbidity, chlorophyll, and dissolved oxygen data. Turbidity data were converted to suspended particulate matter (SPM) concentration values through calibration with water samples collected in the central part of the section.

On the west bank of the section lies the Rio Grande Bar pilots' station, where a meteorological station and tide gauge are operational, as well as a Sontek Argonaut ADCP anchored approximately 200 m from the shore. In the central portion of the section, there is an environmental monitoring buoy from the SimCosta Project (https://simcosta.furg.br/home), which also has a downward-looking ADCP (Nortek Signature model) and sensors for water quality parameters (salinity, temperature, turbidity, among others), as well as a meteorological station. Both systems (pilots and SimCosta) operate regularly and have long time series. River discharge data for the main tributaries were obtained from the Hidroweb database (ANA/SNRH), which consists of daily data. Flow data between Lagoa Mirim and Lagoa dos Patos were provided by the Lagoa Mirim Development Agency (ALM/UFPEL). Meteorological data on precipitation and evaporation were obtained for the meteorological stations of Pelotas and Porto Alegre, in daily values.

The data obtained in this experiment were explored to assess the lateral variability of flow, salinity, and SPM concentration, as well as to perform an evaluation of water and SPM balance. Fortuitously, the experiment period coincided with an extreme condition of low river discharge, representing a 1% probability event. During the period, three events of moderate intensity frontal systems occurred, which produced the inversion of coastal wind direction (from southward to northward) and a rise in sea level at sub-tidal frequency of about 0.8 m, inducing flood flow. The volume exchange rates through the estuary were around 10,000 m3/s, both during flood and ebb, with an average flow through the estuary of about 1,000 m3/s. Using a box model to perform the hydrological balance, computing the fluvial input from major tributary rivers, from Lagoa Mirim, and from precipitation, and the loss to the atmosphere through evaporation, the balance value was 850 m3/s. Considering the limitations of the database used in the box model, this result is considered quite satisfactory and supports the sampling strategy (1 sample per day) in capturing the flow variability reasonably well.

Institute of Oceanography – Federal University of Rio Grande, Brazil

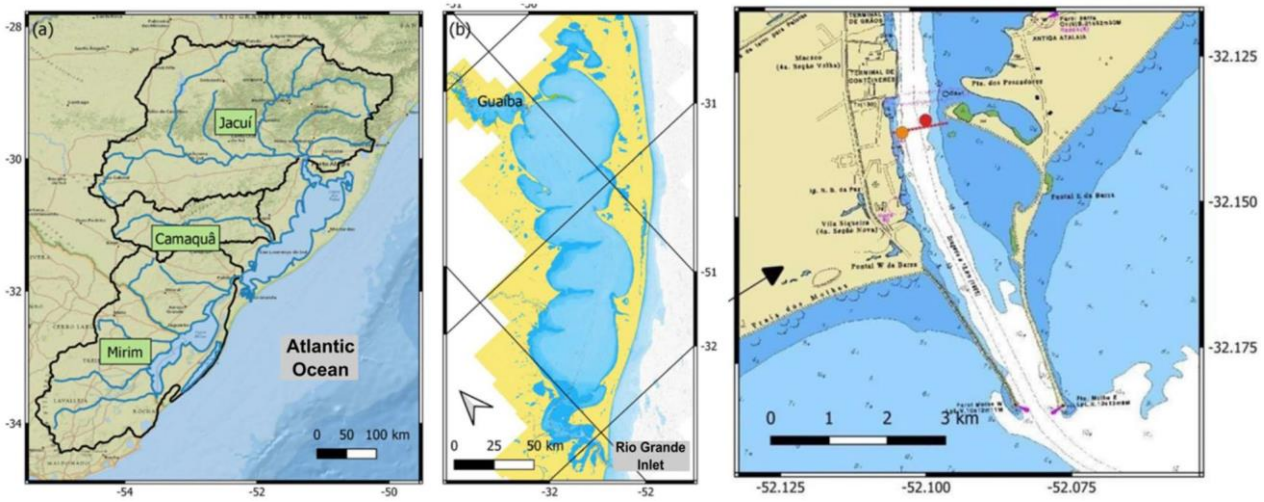

Figure 1: (a) the Patos Lagoon and its drainage basin with main rivers; (b) zoomed view of the Patos Lagoon with indication of the bathymetry; and (c) the lower part of the Rio Grande Channel with the indication of the experimental cross-section.

During flood conditions, the salinity distribution was relatively homogeneous, with salinity around 33 g/kg, which is the regional coastal salinity. During ebb conditions, the water column showed varied degrees of stratification, and even a situation where the column appeared relatively homogeneous but with salinity around 6 g/kg. These results indicate that during the flood, there is advection of coastal water into the system. However, during ebb periods, the water column structure will depend on the duration of the ebb. If this is long enough, there will be a portion that has been advected from the lagoon body along the channel. The highest SPM concentrations were always recorded during flood conditions and generally relatively well distributed in the water column. During ebb events, the highest concentrations occurred in a stratified manner and near the bottom. During the experiment period, there was a balance of SPM import into the system.

Importance of the Vertical Eddy Viscosity Profile on the Subtidal Salt Intrusion and Stratification in Well-Mixed and Partially Stratified Estuaries

Schuttelaars H. [1], Basdurak B. [2], Jongbloed H. [3], and Dijkstra Y. [1]

Keywords: subtidal salt dynamics, wind stress,

Abstract

The influence of wind stress on subtidal salt intrusion and stratification in well-mixed and partially stratified estuaries is discussed in this paper. In a recent paper by Jongbloed et al. (2022), it was shown that even in mild conditions, wind forcing can influence the estuarine salinity structure in a substantial way. By studying the role of wind forcing on dominant salt transport balances and associated salt transport regimes, four different regimes were identified. Of these regimes, the dispersive regime and the Chatwin regime were extensively studied before. By adding wind forcing, two new regimes were identified, namely a downwind and upwind regime. In Fig 1. an example is given of such a regime plot for a fixed estuarine Froude number Fr = 0.0025, varying estuarine Rayleigh number Ra and wind straining number Fw. The gray area in this figure indicated parameter values for which no physically and mathematically sound solution exists.

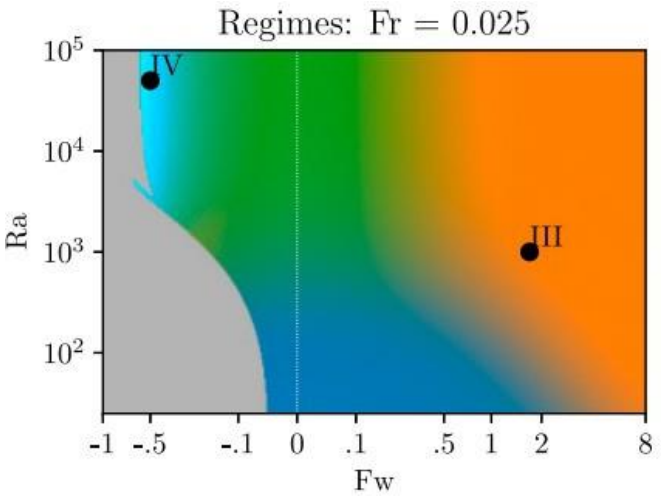

Figure 1: The different subtidal salt regimes for Fr = 0.0025. Blue denotes the dispersive regime, green the Chatwin regime, orange (indicated by III) the downwind regime, and cyan (IV) the upwind regime. In the gray region, no solution is found that id both physically and mathematically sound.

The model employed in Jongbloed et al. (2022) assumed that the vertical eddy viscosity and diffusivity is constant in space (both in the horizontal and vertical direction), not considering the importance of wind straining and vertical stratification on the vertical mixing. In this contribution, an advanced parameterization of the vertical eddy viscosity and diffusivity will be included. This parameterization was developed in Basdurak et al. (2023) and includes the effects of wind straining and stratification in a physically sound and mathematically consistent way. In this contribution, their influence on the salt intrusion, vertical stratification and the dominant salt transport mechanisms will be systematically studied. Furthermore, because of this more advanced formulation, also for parameter combinations where no solutions could be found with a spatially constant eddy viscosity and diffusivity (indicated as a gray region in Fig. 1) physically consistent subtidal salt profiles can be found using the new eddy viscosity formulation, thus completing the regime plots presented in Jongbloed et al. (2022).

References

Jongbloed, H., Schuttelaars, H.M., Dijkstra, Y.M., Donkers, P.B. Hoitink, A.J.F. Influence of Wind on Subtidal Salt Intrusion and Stratification in Well-Mixed and Partially Stratified Estuaries (2022). Journal of Physical Oceanography, 52(12), pp. 3139–3158

Basdurak, N.B., Burchard, H. and Schuttelaars, H.M. A local eddy viscosity parameterization for wind-driven estuarine exchange flow, Part II: Entrainment (2023). Progress in Oceanography, 219, art. no. 103166, DOI: 10.1016/j.pocean.2023.103166.

[1] Delft Institute of Applied Mathematics, EEMCS, Delft University of Technology, Delft, The Netherlands, email: h.m.schuttelaars@tudelft.nl

[2] Institute of Marine Sciences, Middle East Technical University, Erdemli, 33731, Turkey

[3] Hydrology and Quantitative Water Management, Wageningen University and Research, Wageningen, The Netherlands

Spatial and Temporal Variations in Atmospheric Gas Flux from the Hudson River: The Estuarine Gas Exchange Maximum

Scully M. [1]

Keywords: estuarine circulation, stratification, gas exchange

Abstract

A unique combination of data collected from fixed instruments, spatial surveys and a long-term observing network in the Hudson River demonstrate the importance of spatial and temporal variations in atmospheric gas flux. The atmospheric exchanges of oxygen (O2) and carbon dioxide (CO2) exhibit variability at a range of time scales including pro- nounced modulation driven by spring-neap variations in stratification and mixing. During weak neap tides, bottom waters become enriched in pCO2 and depleted in dissolved oxygen because strong stratification limits vertical mixing and isolates sub- pycnocline water from atmospheric exchange. Estuarine circulation also is enhanced during neap tides so that bot- tom waters, and their associated dissolved gases, are transported up-estuary. Strong mixing during spring tides effectively ventilates bottom waters resulting in enhanced CO2 evasion and O2 invasion. The spring-neap modulation in the estuarine portion of the Hudson River is enhanced because fortnightly variations in mixing have a strong influence on phytoplank- ton dynamics, allowing strong blooms to occur during weak neap tides. During blooms, periods of CO2 invasion and O2 evasion occur over much of the lower stratified estuary. The along-estuary distribution of stratification, which decreases up-estuary, favors enhanced gas exchange near the limit of salt, where vertical stratification is absent. This region, which we call the estuarine gas exchange maximum (EGM), results from the convergence in bottom transport and is analogous to the estuarine turbidity maximum (ETM). Much like the ETM, the EGM is likely to be a common feature in many partially mixed and stratified estuarine systems.

[1] Woods Hole Oceanographic Institution (WHOI) – 266 Woods Hole Rd Woods Hole, MA 02543, United States

Interaction of Tides with Recurring Polynya in an Arctic Fjord: SWOT Measurements During the Cal/Val 1-Day-Repeat Orbit Phase

Shan S. [1], Hannah C. [2], and Valle-Levinson A. [3]

Keywords: tide, polynya, fjord, Arctic, SWOT.

Abstract

Polynyas (nonlinearly shaped openings enclosed in sea ice) are vital components of both physical and biological systems in ice-covered seas. Little is known about polynya-tide interactions in fjords, particularly in the Pangnirtung Fjord, a seasonally ice-covered fjord located on the southern Baffin Island, Nunavut, Canada. The Fjord is home to an indigenous community of about 1500 people, and it connects to Cumberland Sound via a shallow sill (~20 m). A small (4km x 2km) recurring polynya has been observed near the sill location. The large tidal range in the Fjord (up to 6.7 m) suggests a need to test the tidally forced polynya hypothesis in which tidal flows over the sill inject heat to the surface waters. However, the lack of observations in this remote location has so far prevented a quantitative investigation of the polynya-tide interaction. In this study, we demonstrate the new technological capacity of the SWOT (Surface Water and Ocean Topography) mission for high-resolution mapping of small recurring polynya in an Arctic fjord. We achieve this using daily data during the 1-day-repeat (calibration/validation) orbit phase from the KaRIn instrument (Ka-band wide-swath synthetic aperture Radar Interferometer) on board the SWOT satellite. We compare and validate the SWOT's daily sea surface heights and ice conditions with tide-gauge derived water levels and SAR sea ice images, respectively. Our analysis seems to support the tidally forced polynya hypothesis in the Pangnirtung Fjord.

[1] Department of Physics and Space Science, Royal Military College of Canada, Shiliang.Shan@rmc.ca
[2] Ocean Sciences Division, Fisheries and Oceans Canada, Institute of Ocean Sciences, Charles.Hannah@dfo-mpo.gc.ca
[3] Department of Civil and Coastal Engineering, University of Florida, arnoldo@ufl.edu

Marine Heatwaves in Chesapeake Bay: Effects on Subsurface Temperatures and Dissolved Oxygen

Shunk N.P. [1], Mazzini P.L.F. [2], and Walter R.K. [3]

Keywords: marine heatwaves, estuary, subsurface, heat budget, Chesapeake Bay, dissolved oxygen

Abstract

Marine Heatwaves (MHW), extreme temperature events akin to atmospheric heatwaves, have only recently received attention by the estuarine scientific community. Thus far, studies have focused solely on surface events due to scarcity of long-term subsurface data, and subsequently subsurface impacts associated with MHWs in estuaries are not well understood. This study investigates, for the first time, the subsurface temperature and dissolved oxygen (DO) anomalies associated with surface MHW events in a large, temperate, partially mixed estuary: the Chesapeake Bay (CB). Using over three decades (1986-2021) of in-situ data from several long-term monitoring programs in the CB (including sub-daily moored measurements and monthly/bimonthly cruises along the main stem) and a global atmospheric reanalysis product (ERA5), we were able to 1) characterize the spatiotemporal structure of subsurface temperature and DO anomalies during surface MHW events on seasonal time scales, 2) identify the vertical extent of warming before and after events, and 3) examine the relative role of atmospheric heat flux in driving temperature changes during the onset and decline of events. Subsurface temperature anomalies during surface MHW events followed a one-dimensional response to surface heating (caused primarily by air-sea heat flux); vertical transport and diffusion of heat was controlled by seasonal density stratification and mixing. We found two distinct temperature regimes: a thermally stratified spring-summer regime, when positive temperature anomalies were confined to the surface mixed layer; and a vertically homogeneous fall-winter regime, when temperature anomalies extended throughout the water column. A simple 1-D surface mixed layer heat budget identified air-estuary heat flux changes as the leading driver of MHW onsets and declines, with latent heat flux being the dominant term. Additionally, we observed that subsurface temperature anomalies were elevated days to weeks before and after MHW events, while surface temperature anomalies were elevated for months before and after events. This indicates that the timescales of elevated temperatures are typically much longer than the duration of individual MHW events, and therefore should be carefully taken into consideration when assessing the impact of these extreme events in the estuarine ecosystem. Meanwhile, DO anomaly patterns had a more complex spatiotemporal structure, with considerable along-channel gradients. During MHWs, notable DO decreases (1–4 mg L-1) primarily occurred in the winter/spring below the SML, with the greatest DO decreases (~5 mg L-1) occurring in the upper region of CB below the mixed layer depth. Additionally, the hypoxic zone expanded from spring through fall during events. Yet only a small fraction of these DO anomalies could be attributed to MHW temperature-induced solubility changes, demonstrating that other physical and/or biogeochemical processes dominate changes in DO during these events. In the CB, concurrent low DO during MHW events and persistent high temperatures before, during, and after events can compound the impacts of MHWs on habitat, which will be further exacerbated by climate change, severely impacting this valuable estuarine ecosystem.

[1] Virginia Institute of Marine Science, William & Mary, npshunk@vims.edu
[2] Virginia Institute of Marine Science, William & Mary, pmazzini@vims.edu
[3] California Polytechnic State University, rkwalter@calpoly.edu

3D modelling of salt intrusion and sediment trapping in an engineered estuary affected by human interventions

Siemes R. [1], Duong T.M. [2], Borsje B. [3], and Hulscher S. [4]

Keywords: estuaries, salt intrusion, sediment dynamics, human interventions, 3D modelling

Abstract

In estuaries, fresh- and saltwater meet resulting in salt intrusion (SI) processes that affect various estuarine functions. During extreme events, such as low river flows or storm surges, saltwater intrudes further inland, which limits freshwater availability. In addition, the stratification (i.e. the vertical variation in salinity) affects estuarine ecosystem functioning and species diversity (see Attrill, 2002). The stratification creates a vertical density gradient, causing freshwater to flow towards the sea near the surface while the denser saltwater flows landward near the bed. This flow pattern, called estuarine circulation, promotes trapping of marine and fluvial sediments near the limit of salt intrusion limit. Consequently, a region can develop with suspended sediment concentrations (SSCs) up to 100 times larger than the SSC flowing into the estuarine region, called the estuarine turbidity maxima (ETM; see Burchard et al., 2018). The ETM is accompanied by a 'bottom pool' of settled sediments which may necessitate frequent dredging to ensure port navigability.

Globally, estuarine intertidal wetlands are often reclaimed for human activities. Nevertheless, there is a growing acknowledgment of their diverse ecosystem services, leading to initiatives for wetland restoration. This has prompted questions into the influence of intertidal wetlands on salt intrusion (SI) processes and sediment trapping in estuaries. Modelling studies hint at an ambiguous relation between wetland area and SI-lengths (Yang & Wang, 2015; Lyu & Zhu, 2018. Hendrickx et al., 2023), but understanding of this ambiguous relationship is lacking. Additionally, various European estuaries experienced significant increases in SSC concentrations in recent decades. Winterwerp et al. (2013) proposed a conceptual model to explain how human interventions can create estuaries in which almost all sediments are trapped within the ETM. However, to what extend such ETMs are created by human interventions, and how changing hydrodynamic conditions affect sediment trapping in the ETM, is not well understood (Burchard et al., 2018).

This work aims to improve our understanding of how changes in estuarine geometry, related to two human interventions that frequently occur globally, affect SI-processes and sediment trapping in estuaries: 1) changing channel depth ($ddcc$), as channels are deepened worldwide to improve port navigability and 2) reclaiming or restoring intertidal wetland area (wi; hereby the inlet area is not affected). A schematised 3D model is developed using the Delft3D-FM software (DFM). Model conditions reflect the Rotterdam Waterway ($wwii \approx$ 0km and $ddcc \approx$ 16.5m), the Netherlands, a micro- tidal environment which ranges from a partially mixed to a salt-wedge estuarine regime. High sedimentation can be observed 15km inland (Figure 1), presumably due to a local ETM which has been observed previously (de Nijs et al., 2012).

The model's hydrodynamics are validated and sediment characteristics are calibrated for present-day conditions, after which geometric scenarios are considered for various river discharges, starting with an annual average discharge followed by a low or high discharge curve. For each scenario, a constant tidal signal is used consisting of the M2, M4 and M6 tidal constituents. SSC at the off-shore boundaries are set at 10mg/L; the fluvial SSC increases with the fluvial discharge, following the linear equation for the Rhine of Cox et al (2021).

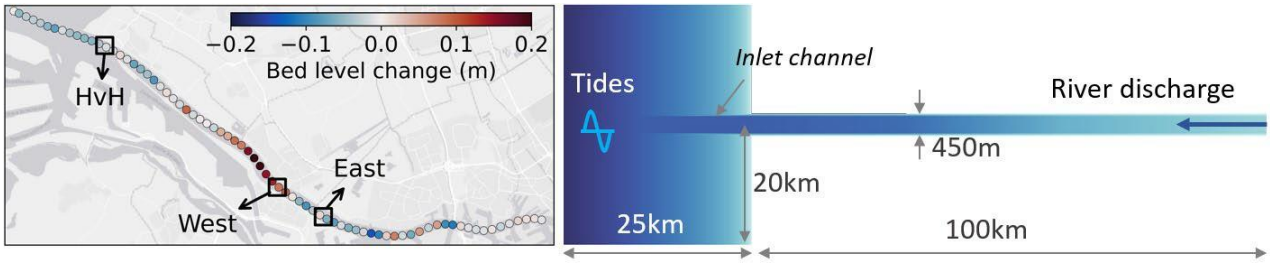

Figure 1: Left) The Rotterdam Waterway, showing the average bed-level change over two months, from the inlet till 30km inland, and the locations used for validation (HvH) and calibration (West and East). Right) Top view of the schematised model domain without human interventions.

[1] University of Twente, the Netherlands, r.w.a.siemes@utwente.nl
[2] University of Twente, IHE Delft Institute for Water Education, Deltares, the Netherlands, t.m.duong@utwente.nl
[3] University of Twente, the Netherlands, b.w.borsje@utwente.nl
[4] University of Twente, the Netherlands, s.j.m.h.hulscher@utwente.nl

To improve process-based understanding, the modelled advective transports F (for salinity: F_s, for SSC: F_c) are decomposed into 3 main components: 1) the subtidal depth-averaged component, representing the flux related to the residual flow (F_{res}), 2) the subtidal depth-varying component, representing the flux related to the estuarine circulation (F_{circ}) and 3) the depth-averaged tide-varying component, representing the tidal oscillation (F_{tide}).

When considering salt transport, transport into the estuary comes from $F_{s,circ}$ and $F_{s,tide}$ which is transported out by $F_{s,res}$. An increase in intertidal wetland width increases the tidal prism of estuaries, thereby enhancing the tidal flow. This suppressed the stratification in the estuary, weakening the estuarine circulation flow. Hence, wetland widening consistently reduces $F_{s,circ}$ and increases $F_{s,tide}$. When the estuary is strongly stratified, which is the case with larger discharges or with deeper channels, the reduction in $F_{s,circ}$ outweighs the increase in $F_{s,tide}$, resulting in a decrease in salt transport into the estuary and subsequently a slight reduction in the SI-length (order of 0.1-1km for wetlands of up to 3km in total width). When the estuary is more mixed, i.e. with lower discharges and shallower channels, the contribution of $F_{s,circ}$ becomes negligible and the increase in $F_{s,tide}$ is dominant. In this case, the increase in tidal prism due to wetland widening enhances salt import into the estuary, increasing the SI-length (order of 0.5-5km).

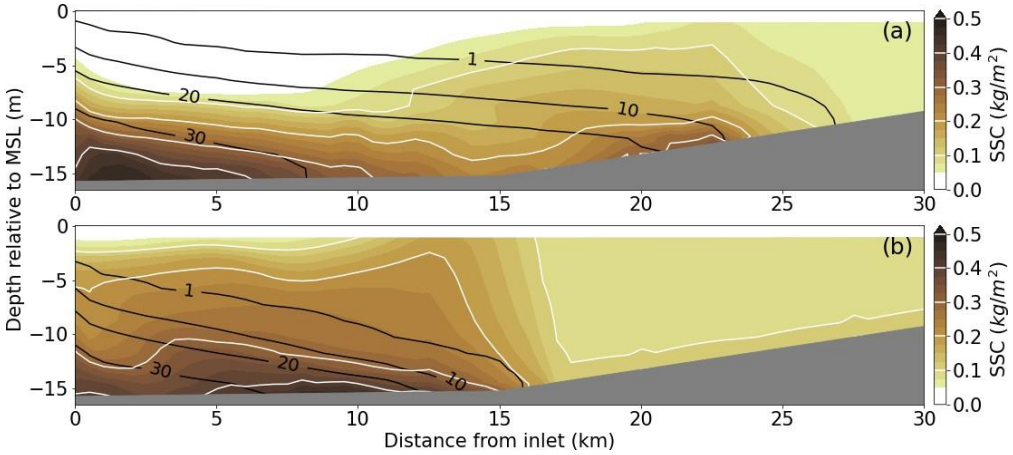

Figure 2: Modelled SSC during an average discharge (a; 1760mm^3/ss) and a high discharge (b; 3750mm^3/ss) for the geometric scenario most closely resembling the present-day Rotterdam Waterway. Black lines indicate the salinity isohalines (in psu).

Next, sediment transport is considered. Measured bed level changes indicate that a bottom pool may exist in the Rotterdam Waterway, roughly 20km inland (Figure 1). In Figure 2, modelled SSC are shown for two discharges in the geometric scenario most closely resembling the present-day Rotterdam Waterway ($wwii$ = 0km, $ddcc$ = 16.5m). With an average discharge, an ETM with accompanying bottom pool is identified near the salt intrusion limit, 20-25km inland (Figure 2a). With an average discharge, both coastal and fluvial sediments are imported and trapped in the estuary, ratio ~ 2:5. Import of marine sediments is dominated by Fc,circ. When the river discharge gradually increases, the ETM and bottom pool move downstream (Figure 2b). Sediment export by Fc,res increases non-linearly with the river discharge. Import of marine sediments by Fc,circ and Fc,circ increase up to a discharge of ~3000$mm3/ss$, above that, both terms also export sediments to the coast. Export of sediments is dominated by Fc,res.

Results highlight how intertidal wetlands can both increase or decrease the SI-length depending on the degree of stratification of the estuary. When adding intertidal area, the strongly stratified estuary experienced a decrease in salt intrusion length. The more mixed estuary experienced an increase in salt intrusion length. For sediment transport, results indicate that a threshold may exist above which trapped sediments can be flushed out of the estuary. Currently, the impact of the geometric scenario's (changing channel depth and intertidal wetland width) on sediment trapping in estuaries will be considered.

References

Attrill, M. J. (2002). A testable linear model for diversity trends in estuaries. Journal of Animal Ecology, 71 (2), 262-269. doi: https://doi.org/10.1046/j.1365-2656.2002.00593

Burchard, H., Schuttelaars, H. M., & Ralston, D. K. (2018). Sediment trapping in estuaries. Annual Review of Marine Science, 10 (1), 371-395. doi: 10.1146/annurev-marine-010816-060535

Yang, Z., & Wang, T. (2015). Responses of estuarine circulation and salinity to the loss of intertidal flats – a modeling study. Continental Shelf Research, 111, 159-173. https://doi.org/10.1016/j.csr.2015.08.011

Lyu, H., & Zhu, J. (2018). Impacts of Tidal Flat Reclamation on Saltwater Intrusion and Freshwater Resources in the Changjiang Estuary. Journal of Coastal Research, 35 (2), 314-321. doi: 10.2112/JCOASTRES-D-18-00077.1

Hendrickx, G. G., Kranenburg, W. M., Antol´ınez, J. A., Huismans, Y., Aarninkhof, S. G., & Herman, P. M. (2023). Sensitivity of salt intrusion to estuary-scale changes: A systematic modelling study towards nature-based mitigation measures. Estuarine, Coastal and Shelf Science, 295 , 108564. doi:https://doi.org/10.1016/j.ecss.2023.108564

Winterwerp, J.C., Wang, Z.B. Man-induced regime shifts in small estuaries—I: theory. Ocean Dynamics 63, 1279–1292 (2013). https://doi.org/10.1007/s10236-013-0662-9

Michel A.J. de Nijs and Julie D. Pietrzak. Saltwater intrusion and ETM dynamics in a tidally-energetic stratified estuary. Ocean Modelling, 49-50:60–85, 2012. ISSN 1463-5003. doi: https://doi.org/10.1016/j.ocemod.2012.03.004.

Sediment Entrainment Vulnerability at the Confluence of Nontidal Streams and Tidal Estuaries

Smith S. [1,2], Libby D. [3], and Van Dam B. [1]

Keywords: Sediment Entrainment, Confluence, Land Sea Connections

Abstract

The research summarized in this poster focuses on the alignment of conditions conducive to sediment entrainment at the confluence of non-tidal streams with tidal estuaries with im- plications to aquatic habitat, water quality, and human health in shellfish harvesting areas. Previous research indicates bacteria can be absorbed to sediment particles, potentially contributing to water contamination beyond acceptable limits for shellfish harvesting enforced by coastal resource managers. Accordingly, this research supports the closure of information gaps related to land-sea connections, coastal sediment dynamics, and a mechanism of bacte- ria contamination dependent on both watershed and estuary conditions. The prediction of sediment entrainment at the confluence of freshwater streams and estuary mud flats is chal- lenging because of the dependence on precipitation events, stream flow, tidal fluctuations, and sedimentary environments that vary spatially and temporally. This research targets improvement in the capacity to predict locations and conditions where and when sediment entrainment is likely to occur. The study location is the confluence of Crippen's Brook with the Jordan River estuary in Trenton, Maine (USA). We describe and evaluate conditions coincident with relatively high vulnerability to sediment entrainment in intertidal confluence areas based on time series of stream flow and tide conditions. Streamflow and tide data are combined with topographic measurements in the intertidal confluence area to estimate hydraulic conditions over time. Hydraulic predictions are compared to critical conditions for sediment mobilization based on confluence grain size measurements and mapping. The analyses, performed at hourly time steps, are designed to identify and describe vulnerability to sediment mobilization, including the frequency that conditions for mobilization become established in confluence settings.

[1] School of Earth and Climate Sciences (ECS) – University of Maine Orono, ME 04469, United States
[2] Center for Sustainability Solutions – University of Maine Orono, ME 04469, United States
[3] School of Earth and Climate Sciences (ECS) – University of Maine Orono, ME 04469, United States

Partial Reflection in Tidal Estuaries

Talke S.A. [1], Dykstra S. [2], Orton P. [3], and Jay D.A. [4]

Keywords: tides, reflection, secular change.

Abstract

Partial reflections in waves occur anytime there is a change in the phase speed (celerity). Thus, tides and other long waves in estuaries undergo a partial reflection when the depth changes, as can be noted using the inviscid phase speed of $\sqrt{gh}$. ~~Les~~s remarked causes of partial reflections include changes to width, drag coefficient (or effective

friction), tidal velocity, and river flow. In this presentation, we use an analytical model of tides based on Jay (1991) and Dronkers (1964) to investigate the influence of different types of partial reflections on tidal dynamics. In particular, we investigate how changes to geometry, tidal velocity, river velocity, salinity stratification, and drag coefficient alter the effective friction and phase speed, inducing a partial reflection. We show that alteration in the damping and phase shifts of partial reflections have altered tidal properties in Jamaica Bay, the Columbia River Estuary and in the Cooper River, South Carolina over secular time scales. A curious artifact of partial tide wave reflections, also observed in electrical power transmission, is that a non-0° phase shift in the reflected wave is induced. This contrasts a full reflection with a 0° phase shift. We elucidate the causes and consequences of the non- zero phase shift in the reflected wave on tidal amplitudes and velocities, particularly with regard to changing dynamics caused by anthropogenic or natural changes.

[1] California Polytechnic State University, San Luis Obispo stalke@calpoly.edu
[2] University of Alaska Fairbanks, sdykstra@alaska.edu
[3] Stevens Institute of Technology, porton@stevens.edu
[4] Portland State University, djay@pdx.edu

A 3D model of Lorient Bay to study turbidity dynamics and sediment fluxes between inner estuaries and marine coastal waters

Tessier C. [1], Saremi S. [2], Chiron T. [3], Sedrati M. [4], and Grosdemange D. [5]

Keywords: Lorient Bay; turbidity dynamics; sediment fluxes; river-coast interaction.

Abstract

Lorient Agglomeration launched in 2022 the Dour Glaz Project, a global hydro-sediment study of estuarine and coastal waters, based on observations and numerical modelling. The objective is to develop a decision support tool with shared understanding, for the integrated management of dredging and dumping operations of harbor's sediments.

The study area includes the Lorient Bay, two small inner estuaries and the marine coastal area up to Groix island. The MIKE 3D hydrodynamic model was implemented to reproduce tidal dynamics, rivers runoff and wind forcing over one year. Coupling a mud transport module, we simulated the turbidity dynamics with several fine fractions to track river sources and marine inflows. The model was validated with satellite observations and with a set of turbidity buoys from the Lorient Agglomeration monitoring plan 2022-2023.

Turbidity variability over sensitive habitats and sediment fluxes into the Bay were analyzed depending on tidal conditions, rivers inputs and waves resuspensions. The model brought a better knowledge of the Bay dynamics and on exchanges with coastal waters. Additionally, it allowed to evaluate the impact on dumping operations, in comparison to natural turbidity climate.

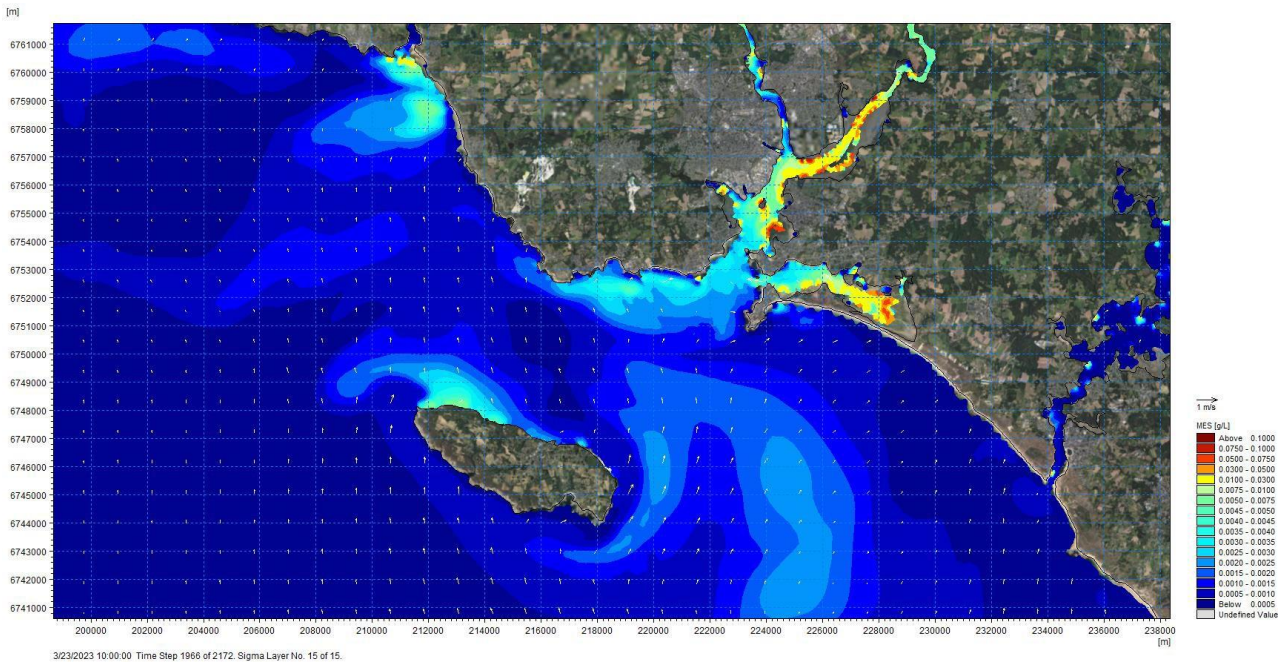

[1] DHI France, 4 rue Edouard Nignon, 44300 Nantes, cte@dhigroup.com
[2] DHI Espana, Avenida de la Libertad, 17 2nd , 20004, San Sebastián, Spain
[3] Lorient Agglomeration, Pôle Attractivité et Rayonnement, BP 20001, 56314 LORIENT Cedex, France
[4] GEO-OCEAN, Univ Bretagne Sud, Univ Brest, CNRS, IFREMER, UMR6538, F- 56000, Vannes, France
[5] GAIA Terre-Bleue, Criée Ouest, Bureau n°6, 29900 Concarneau, France

Effects of river discharge on exchange flows at the entrance to a subtropical river

Torres J. [1], Laurel A. [1], and Valle-Levinson A. [1]

Keywords: exchange flows, wind forcing, baroclinic forcing

Abstract

Current velocity profiles and near-bottom water densities were measured to investigate the spatial structure of exchange flows at the entrance to a subtropical river, Peace River in South Florida, USA. Data were collected over nearly 11 months at three sites: one in the deepest part of the channel, and two over the channel's flanking shoals. Also studied were the temporal variations of the exchange flow's spatial structure and linked to the forcing from river, tides, and winds. Empirical orthogonal function analysis identified that relative contributions from each one of the forcing agents was consistent with the spatial structure expected from theoretical results. The background exchange flow structure at the lower river involved inflow in the channel and outflow over shoals, consistent with river-induced density- driven flows. Wind forcing modified this structure, in a way that it reinforced or opposed the river-induced flow depending on the wind direction. Tidal forcing seemed to be irrelevant in modulating the exchange flows. The comparison among forcings was corroborated with the Wedderburn, densimetric tidal Froude number and the Stress numbers.

[1] University of Florida – United States. torresjuan@ufl.edu

Liftoff and spreading dynamics of a rip current plume in stratification

Torres W.I. [1], Moulton M. [1,2], and Chickadel C.C. [1]

Keywords: Wave Dynamics and Beaches, Estuarine and Coastal Dynamics

Abstract

Rip currents are dominant mechanisms for cross-shelf transport in the nearshore ocean. Recent field observations demonstrate that buoyancy differences between rip currents and the ambient coastal ocean affect their lateral spreading and cross-shore extent. Wave-circulation modeling using COAWST (coupling ROMS and SWAN), of an idealized bathymetric rip plume was used here to examine the effect of ambient vertical thermal stratification on rip current spreading. Due to strong vertical mixing in the nearshore, a rip plume's density is homogenous. Therefore, upon entering stratification, the rip experiences buoyancy gradients in the upper and lower layers. These buoyancy gradients drive a transverse circulation, resulting the eventual bottom detachment (liftoff) of the plume in the bottom layer. Whether the plume narrows or widens in the upper layer depends on the relative importance of boundary layer mixing and wave-current interaction spreading versus baroclinicity. For strong coastal stratification (dT/dz > 0.16°C/m), the rip plume subducts and no longer has a surface expression. This is qualitatively consistent with airborne infrared observations of rip plumes (Moulton et al. 2021).

A novel diagnostic equation for flow diffluence was derived and used to characterize the effects of waves, bottom drag, and buoyancy on the plume. The transverse plume circulation is attributed to modified gravity current type mechanics, wherein the axial advection of transverse momentum balances the baroclinic pressure gradient, wave-induced vortex forces, and vertical mixing. A simplified model for rip plume evolution, based upon these physics, was developed. The simple model accurately estimates the COAWST-simulated cross-shore liftoff and spreading/narrowing, even for weak stratification (dT/dz = 0.01°C/m). These findings suggest that even subtle differences in ambient stratification can affect the behavior of rip plumes, which has implications for cross-shore exchange, ecological connectivity, and human safety.

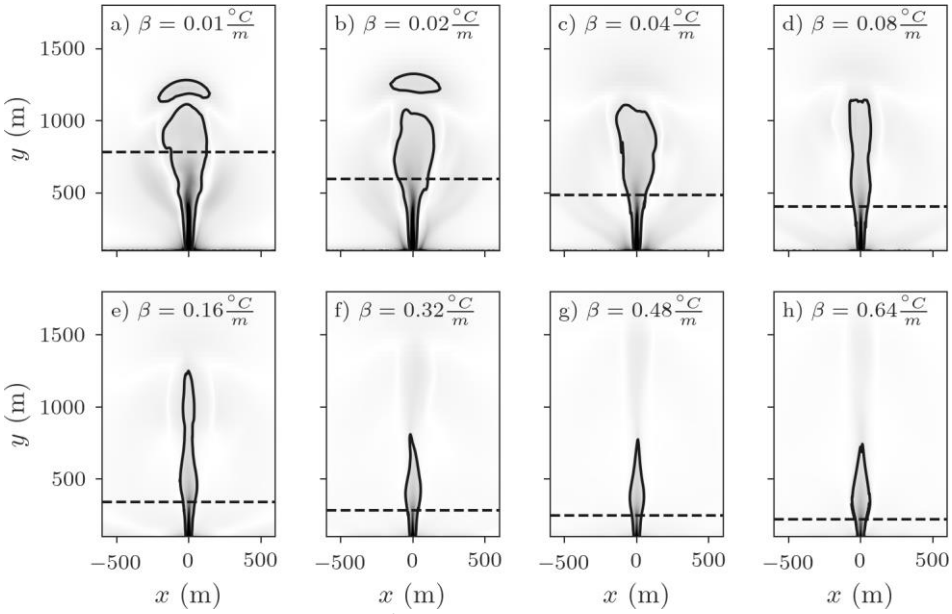

Figure 1. Contours of unity Froude number ($Fr = V/(gh)^{1/2}$) at the surface in COAWST simulations of an idealized rip current over a range of vertical stratification conditions (β). Fr = 1 corresponds with the edge of the jet. This illustrates that buoyancy gradients can determine whether jet will spread or narrow in the surface layer.

References

Moulton, M., Chickadel, C. C., & Thomson, J. (2021). Warm and cool nearshore plumes connecting the surf zone to the inner shelf. *Geophysical Research Letters*, 48, e2020GL091675. https://doi.org/10.1029/2020GL091675

[1] Department of Air-Sea Interaction and Remote Sensing, Applied Physics Laboratory, University of Washington, Seattle, WA, USA
[2] National Center for Atmospheric Research, Boulder, Colorado, USA

Modelling salinity and stratification in the GBM (Ganges-Brahmaputra-Meghna) delta

Toublanc F. [1], Durand F. [1], Khan J. [1], Krien Y. [1], Sherin V.R. [2], Bertin X. [3], Islam A.S. [4], and Suneel V. [5]

Keywords: delta, 3D modelling, salinity intrusion, stratification, tides

Abstract

The Ganges-Brahmaputra-Meghna system is the largest delta in the world, located in the Northern Bay of Bengal. It is very densely populated and characterized by low topography (typically less than 3m above mean sea level) (Krien et al. 2016). Many processes influence its dynamics, from high-frequency tides to sea level rise, as well as seasonal variations of the river flow (wet/dry season) and extreme events (cyclones) (Krien et al., 2017; Elahi et al., 2020). It consistently presents a sharp salinity front, separating the freshwater of riverine origin in the Northern part of the delta from the Bay of Bengal saline water to the South (Sherin et al., 2020). The position of this front oscillates landward and ocean-ward over a broad range of timescales, under the influence of the various physical processes mentioned above (Bricheno et al., 2021). It turns out that this variability has profound impacts on the socio-economic conditions and migrations of the riparian population (Chen et al., 2018, 2022). For all these reasons, the GBM delta is a particularly vulnerable area, where it is crucial to understand the processes involved in the water level variability and the salinity dynamics associated to it.

In this study, we use a cross-scale ocean circulation model, SCHISM (Semi-implicit Cross-scale Hydroscience Integrated System Model, Zhang et al., 2016), in a 3D baroclinic high-resolution configuration encompassing the Bay of Bengal and the whole GBM delta. This configuration is an evolution of a previous 2D configuration implemented and used in various studies over the past few years (Krien et al., 2016, 2017; Tazkia et al., 2017; Khan et al., 2020, 2021, 2022). Several in situ salinity timeseries (Sherin et al., 2020), as well as tide gauge data, including tidal harmonics and time series, are used to validate the model.

The aim of this study is to better understand the interactions between salinity and the tidal dynamics. The GBM delta and associated plume are highly stratified (Sinha et al., 1999; Alam et al., 2020) with a large difference in salinity intrusion between the dry and the wet season (Figure). Strong stratification tends to stabilize the water column and alter the tidal dissipation within the plume. Through different sensitivity tests, we explore in the model the impact of this stratification on the tidal amplitude along the coast and on its seasonal modulation.

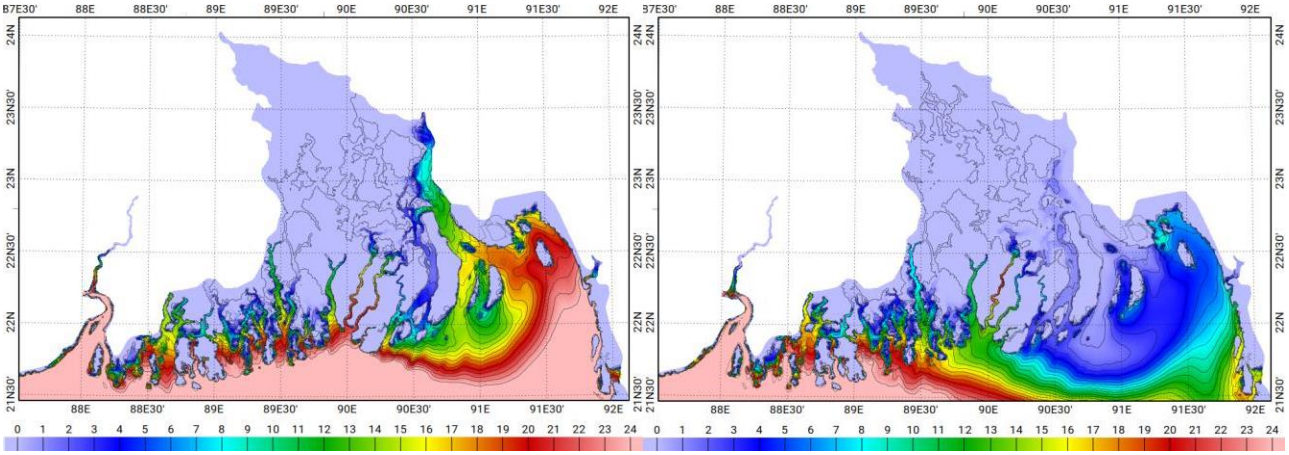

Figure: Mean monthly Sea Surface Salinity (SSS) in the GBM delta during the dry season (March, left) and the wet season (September, right)

[1] LEGOS, Université Toulouse, IRD, CNRS, CNES, UPS, Toulouse, France, florence.toublanc@univ-tlse3.fr, fabien.durand@univ-tlse3.fr, jamal.khan@univ-tlse3.fr, yann.krien@univ-tle3.fr
[2] Indian National Centre for Ocean Information Services, Ministry of Earth Sciences, Hyderabad, India, sherinsvr@gmail.com
[3] LIENSs, CNRS-La Rochelle Université, La Rochelle, France, xbertin@univ-lr.fr
[4] Institute of Water and Flood Management, Bangladesh University of Engineering and Technology, Dhaka, Bangladesh, akmsaifulislam@iwfm.buet.ac.bd
[5] National Institute of Oceanography, Dona Paula, Goa, India, suneel@nio.org

References

Alam, M. M. U., A. I. Khan, S. K. Sunny, A. Rahman, M. S. Rahman, B. Mahmud, A. R. Shaheen (2020). An exclusive in-situ dataset on physicochemical parameters in the gappy northern Bay of Bengal, Data in Brief, 31, 2020, 106024, doi.org/10.1016/j.dib.2020.106024.

Bricheno, L. M., Wolf, J., & Sun, Y. (2021). Saline intrusion in the Ganges-Brahmaputra-Meghna megadelta. Estuarine, Coastal and Shelf Science, 252, 107246. https://doi.org/10.1016/j.ecss.2021.107246

Chen, J., V. Mueller (2018). Coastal climate change, soil salinity and human migration in Bangladesh. Nat. Clim. Change 8, 981–985. https://doi.org/10.1038/s41558-018- 0313-8.

Chen, J., V. Mueller, F. Durand, E. Liscoa, Q. Zhongg, V. R. Sherin, AKM S. Islam (2022), Salinization of the Bangladesh Delta Worsens Economic Precarity. Population and Environment, https://doi.org/10.1007/s11111-022-00411-2, 2022

Elahi, M. W. E., Jalón-Rojas, I., Wang, X. H., & Ritchie, E. A. (2020). Influence of seasonal river discharge on tidal propagation in the Ganges-Brahmaputra-Meghna Delta, Bangladesh. Journal of Geophysical Research: Oceans, 125, e2020JC016417. https://doi.org/10.1029/2020JC016417

Khan, M. J. U., Durand, F., Testut, L., Krien, Y., & Islam, A. S. (2020). Sea level rise inducing tidal modulation along the coasts of Bengal delta. Continental Shelf Research, 211, 104289, doi: 10.1016/j.csr.2020.104289

Khan, M. J. U., Durand, F., Bertin, X., Testut, L., Krien, Y., Islam, A. K. M., ... & Hossain, S. (2021). Towards an efficient storm surge and inundation forecasting system over the Bengal delta: chasing the Supercyclone Amphan. Natural Hazards and Earth System Sciences, 21(8), 2523-2541, doi.org/10.5194/nhess-21-2523-2021.

Khan, M. J. U., Durand, F., Emanuel, K., Krien, Y., Testut, L., & Islam, A. K. M. (2022). Storm surge hazard over Bengal delta: a probabilistic–deterministic modelling approach. Natural Hazards and Earth System Sciences, 22(7), 2359-2379, doi.org/10.5194/nhess-22-2359-2022

Krien, Y., Mayet, C., Testut, L., Durand, F., Tazkia, A. R., Islam, A. K. M. S., ... & Ballu, V. (2016). Improved bathymetric dataset and tidal model for the northern Bay of Bengal. Marine Geodesy, 39(6), 422-438, doi: 10.1080/01490419.2016.1227405.

Krien, Y., Testut, L., Islam, A. K. M. S., Bertin, X., Durand, F., Mayet, C., ... & Khan, Z. H. (2017). Towards improved storm surge models in the northern Bay of Bengal. Continental Shelf Research, 135, 58-73, doi 10.1016/j.csr.2017.01.014.

Sherin, V. R., Durand, F., Papa, F., Islam, A. S., Gopalakrishna, V. V., Khaki, M., & Suneel, V. (2020). Recent salinity intrusion in the Bengal delta: Observations and possible causes. Continental shelf research, 202, 104142, doi: 10.1016/j.csr.2020.104142.

Sinha, P.C., Rao, Y.R., Dube, S.K., Murthy, C.R., Chatterjee, A.K. (1999). Application of two turbulence closure schemes in the modelling of tidal currents and salinity in the Hooghly estuary. Estuar. Coast Shelf Sci. 48, 649–663. https://doi.org/10.1006/ ecss.1999.0478.

Tazkia, A. R., Krien, Y., Durand, F., Testut, L., Islam, A. S., Papa, F., & Bertin, X. (2017). Seasonal modulation of M2 tide in the Northern Bay of Bengal. Continental Shelf Research, 137, 154-162, doi 10.1016/j.csr.2016.12.008.

Ye, F., Zhang, Y. J., Friedrichs, M. A., Wang, H. V., Irby, I. D., Shen, J., & Wang, Z. (2016). A 3D, cross-scale, baroclinic model with implicit vertical transport for the Upper Chesapeake Bay and its tributaries. Ocean Modelling, 107, 82-96. https://doi.org/10.1016/j.ocemod.2016.10.004

New insights into near-bed SPM concentration and sand/mud fraction in the use of Sediment Composition Index

Tran D. [1], Verney R. [2], and Fettweis M. [1]

Keywords: Sediment composition index, OBS, ADV, sand/mud fraction.

Abstract

Introduction

Optical turbidity and acoustic sensors have been widely used in laboratory experiments and field studies to investigate suspended particulate matter concentration over the last four decades. Both methods face a serious challenge as laboratory and in-situ calibrations are usually required. Furthermore, in coastal and estuarine environments, the coexistence of mud and sand often results in multimodal particle size distributions, amplifying erroneous measurements. This paper proposes a new approach of combining a pair of optical turbidity-acoustic sensors to estimate the total concentration and sediment composition of a sand/mud mixture in an efficient way without an extensive calibration. More specifically, we defined a Sediment Composition Index, such that

$$SCI = 10\log_{10}(OBS) - SNR \quad (1)$$

where OBS is the signal measured by an Optical Backscatter Sensor (in NTU) and SNR is the signal measured by an ADV, Acoustic Doppler Velocimetry, sensor (in dB) (Pearson et al, 2021, Tran et al 2023). In this study, we empirically derived the SCI functions from laboratory experiments. Such SCI functions (Eq. 2 and 3), were then, applied to in-situ hydro-sedimentary dynamics data at the monitoring station MOW1 (Belgium) to investigate the impact of sand mining and beach nourishment activities in the region.

Approach

Based on Eq. 1 and a series of 60 experiments we were able to derive SCI functions for a pair of OBS and ADV which allows us to infer the sand/mud fraction, f_{sand}, and total concentration C, (Tran et al, 2023).

$$f_{sand} = -0.089*SCI - 0.098 \quad (2)$$

$$C = 10\text{^}(f_{sand} + Amp)/10) \quad (3)$$

The lab-derived SCI functions (Fig. 1 and Eqs. 2, 3) were applied to field data with one more step of calibrating the coefficients with "pure mud" conditions. Pure mud conditions are calm periods, i.e., small waves and low current periods in a tidal cycle. During pure mud conditions, the measured concentrations should be equal to the SCI-predicted-concentrations (Fig. 2 the grey, vertical lines). The SCI functions with new coefficients were then applied to in-situ data at station MOW1, situated about 3 km offshore of Zeebrugge, Belgium. Data at MOW1 consists of hourly water samples, particle size distributions, turbidity, and hydrodynamic conditions for the year 2013 during 125 tidal cycles, providing one of the most comprehensive field data sets in the North Sea.

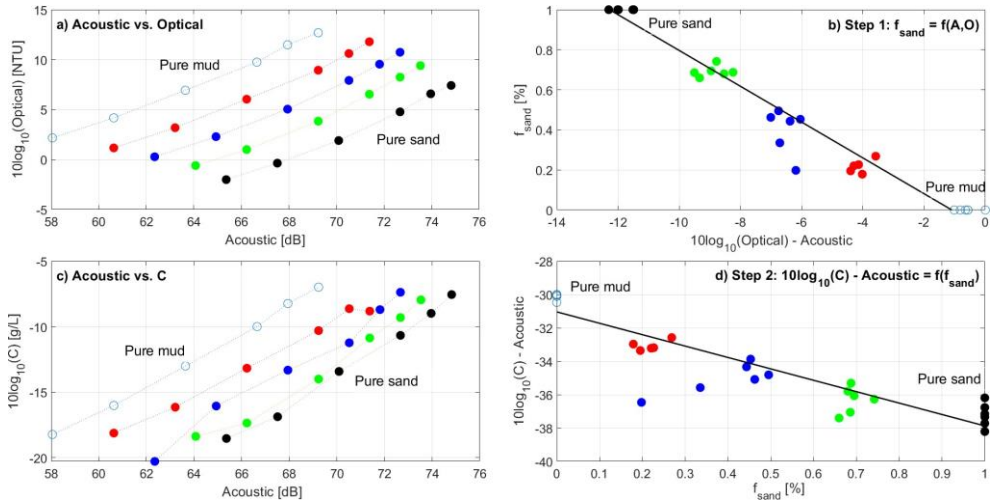

Figure 1. SCI functions obtained from laboratory experiments (b, d). Relationships between raw, uncalibrated optical and acoustic signals and total concentration (a, c). Pure sand: $f_{sand} = 1$ (or $f_{mud} = 0$) and vice versa. Reprinted from Tran et al (2023).

[1] Royal Belgian Institute of Natural Sciences, OD Nature, Brussels, Belgium, dtran@naturalsciences.be
[2] IFREMER, Laboratoire DHYSED, Plouzané, France

Results and conclusions

Overall, the application of the SCI method allows one to investigate near-bed sand/mud dynamics and SPM concentration directly from raw, uncalibrated OBS and ADV signals without the need for intensive gravimetric measurements of filtered water samples. Figure 2 shows that during spring tide the suspended sediment composition changed from muddy to sandy environment. The altitude data revealed that instead of local resuspension of sand, there was some deposition at the time, suggesting a possibility of advection transport of sand from adjacent areas. This observation was confirmed by comparing with the dredging and beach nourishment activities in the area (Kint et al, 2023). Application of SCI functions to other deployments in 2013 also showed a strong correlation between the fraction of sand/mud and total concentration with coastal engineering activities.

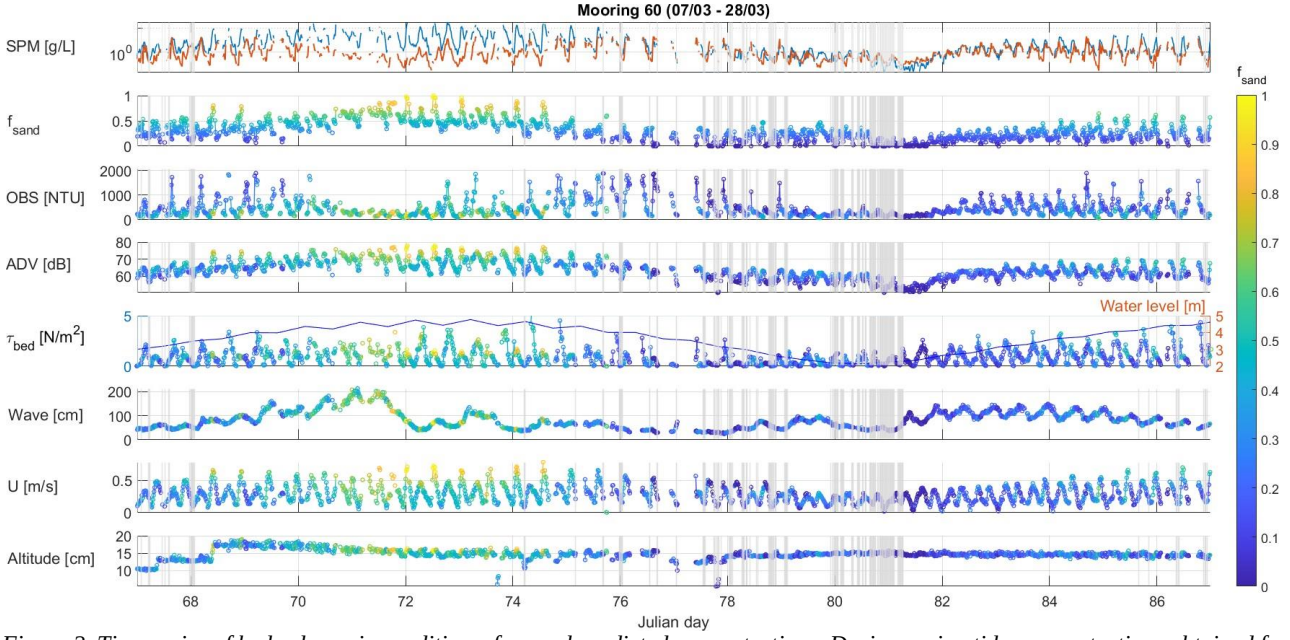

Figure 2. Time series of hydrodynamic conditions, f_{sand} and predicted concentrations. During spring tide, concentrations obtained from OBS measurements were significantly lower than concentrations computed from SCI functions. During neap tide, both concentrations from OBS and SCI method were similar. SCI method also provided information on sand/mud fraction.

In conclusion, results show that the application of SCI method to field data provides a deeper understanding of the sand/mud dynamics and/or concentration variations under different conditions. The results also suggest that the use of OBS alone leaves out important information and underestimates the near-bed concentration due to failure to capture the presence of sand. The SCI method is also applicable to different pairs of optical turbidity and acoustics sensors, providing flexibility and efficiency in either revisiting historical field data or for current/future long-term, high-frequency measurements. In the future, we will apply this method for acoustic profiler sensors to obtain more comprehensive information on the ratio of sand/mud and SPM concentrations in a water column.

Acknowledgments

This work is part of the research program “PiNS: Particle in the North Sea” funded by Federal Public Planning Service Science Policy and “EU_Sed” Marie Sklodowska-Curie Postdoctoral Fellowship (No 101067047).

References

Kint, L., Barette, F., Degrendele, K., Roche, M., Van Lancker, V., (2023). Sediment variability in intermittently extracted sandbanks in the Belgian part of the North Sea. Frontiers in Earth Science, 11:1154564, DOI: 10.3389/feart.2023.1154564.

Pearson, S., Verney, R., Prooijen, B., Tran, D., Hendriks, E., Jacquet, M., Wang, Z., (2021). Characterizing the composition of sand and mud suspensions in coastal and estuarine environments using combined optical and acoustic measurements. JGR: Ocean, 126(7), e2021JC017354.

Tran, D., Desmit, X., Verney, R., Fettweis, M., (2023). Application of sediment composition index to predict suspended particulate matter concentration in the North Sea. INTECOH 2023, South Korea.

Storm-driven continental shelf seiches – mechanisms, dynamics and recent floods

Trinh T.T. [1], Orton P. [1], Ayyad M. [1], and Talke S.A. [2]

Keywords: storm surge, coastal flooding, continental shelf seiche, edge wave, estuary, tropical cyclone.

Abstract

Coastal flooding is driven by tides, wind setup, pressure loading, wave setup, and can be compounded by rainfall and river inputs. These dynamic processes commonly cause a primary storm surge that typically peaks with peak onshore winds, though peak flooding may occur near high-tide. After the onshore winds have subsided, water level oscillations called "resurgence" by Munk et al. (1956), can arise. Munk identified the resurgences in New York Bight (NYB) that occurred during and after the 1944 hurricane as coastal edge waves, which are super-inertial waves trapped by refraction. To better understand the mechanism of resurgence, we analyse water level resurgences in the New York Harbour (NYH) for all tropical cyclones from 1860 to present, using a nearly continuous hourly tidal record. We apply wavelet transforms and spectral analysis to the non-tidal anomaly to detect significant resurgences and quantify their amplitude, period, and decay timescale. We applied linear regression of resurgence characteristics (magnitude, period and decay timescale) with tropical cyclone parameters (e.g., maximum sustained wind speed, storm translation speed) and storm surge magnitude. We found that resurgences' magnitude is positively correlated with storm surge, intensity and speed, and to track angle. Historical data also show that the magnitude of the NYB shelf seiche can attain an amplitude of one meter or more and has caused flooding four times since 2017 during both tropical and extratropical cyclones.

We next developed a numerical model simulation with idealized onshore shelf-wide wind forcing to study the intrinsic natural frequency and dynamical characteristics of the resurgences. The results show that the resonant period is approximately seven hours, which matches the period observed in historical events. The resurgence was identified to be a cross-shelf propagating standing wave that achieve maximum magnitude in the coastal zone and are almost zero on the continental shelf break and deep ocean. The predominant mechanism of resurgences is thus shelf seiches whose energy is trapped and amplified by the convergent NYB coastline. At the continental shelf break (transition to deep water), a ~180 degrees reflection is observed; thus, consistent with observations, the modelled wave oscillates back and forth on the continental shelf as a decaying free-wave, with some energy radiated up and down the coast. Because of its potential influence on flooding, the effect of resurgences should be considered in evaluations of flood hazard under sea-level rise.

References

Munk, W., Snodgrass, F., Carrier, G. (1956). Edge Waves on the Continental Shelf. Science, 123(3187), 127-132. http://www.jstor.org/stable/1750948

[1] Stevens Institute of Technology, ttrinh2@stevens.edu
[2] California Polytechnic State University, stalke@calpoly.edu

Three-layered exchange flows in a weakly-frictional tropical estuary

Valle-Levinson A. [1], Cardona Y. [2], Toro V. [3], and Paniagua-Arroyave J. [4]

Keywords: exchange flows, tidal, residual flows, ADCP measurements, tropical estuary, three layer circulation

Abstract

Underway current velocity profiles were collected in conjunction with water density pro- files at eight stations in a cross-estuary transect that spanned 7 km in a tropical estuary of the southern Colombian Caribbean, the Gulfo of Uraba. The purpose of the measurements as to determine whether having the main river discharge on one of the sides, instead of at the head of the estuary, would modify the paradigmatic estuarine circulation. This circulation consists of a tidally averaged buoyant outflow at the surface, combined with dense inflow underneath. The Gulf of Uraba is oriented in a NNW direction, is ˜80 km long, 25 km wide at its entrance and 7 km wide at its narrowest section. This constricting section is determined by on mouth of the delta of the Atrato River, which spans along-estuary distances from 11 to 25 km from the head. The river discharges, on average, between 2000 and 4000 m^3/s throughout its delta. The depth along the thalweg ranges from ˜60 m at the mouth to 20 m at the constriction. Tides are mixed with semidiurnal dominance and a maximum range is 0.7 m at the estuary's entrance in spring tides. Tides amplify by 16% toward the head. Frictional effects are characterized by Ekman numbers (ratio of frictional to Croiolis accelerations) lower than 0.1.

Observations illustrate the signature of the Atrato River discharge restricted to depths < 3m. This buoyant layer seems decoupled from the rest of the water column. Tidally averaged current velocity profiles exhibit a seaward flowing buoyant layer. Underneath, an inflowing layer occupies roughly one half of the water column. Unexpectedly, a third layer appears outflowing further below, over nearly 40% of the water column. Because this flow structure cannot be attributed to the paradigmatic flow driven by a horizontal density gradient under frictional conditions, it is hypothesized that the resulting three-layered residual flow structure is driven by tides. This hypothesis is anchored in Ianniello's (1977) and Winant's (2008) theoretical results of tidally driven residual flow in semi enclosed basins affected by weak frictional conditions, as suggested by the low Ekman numbers observed. Beyond the three-layered flow hypothesis, a key question remains: how persistent is this three-layered residual flow structure, both spatially (along the estuary) and in time? This question will be addressed with numerical model results.

References

Ianniello J (1977) Tidally induced residual currents in estuaries of constant breadth and depth. J Mar Res 35(4):755–786

Winant CD (2008) Three-dimensional residual tidal circulation in an elongated, rotating basin. J Phys Oceanogr 38:1278–1295

[1] Civil and Coastal Engineering Department, University of Florida, Gainesville, USA – United States

[2] National University – Colombia

[3] University of Antioquia – Colombia

[4] Eafit University – Colombia

Diagnostic Tool Development for Assessments of Coastal Pollution Vulnerability

Van Dam B. [1] and Smith S. [1,2]

Keywords: land, sea connections, setting identification, machine learning, proxy metrics

Abstract

Assessment of estuary susceptibility to water quality problems requires knowledge of how land-sea connections governing pollution vulnerability vary across coastal settings. Approaches for systematic evaluations of land-sea connections are particularly important for the identification of pollution culprits across geographic domains.

This poster describes an interactive setting identification tool originally designed for the complicated conditions along coastal Maine (USA), referred to as the "Estuary Builder." The tool combines spatial data and machine learning to classify estuarine areas into several archetypical setting types called "coastal pollution response units" (CPRUs) that share physiographic, land cover, and infrastructure characteristics relevant to water pollution problems. The tool has been designed with runoff flow paths derived from LiDAR elevation data to route excess precipitation on the landscape to user-defined embayment outlets, aggregates proxy spatial data metrics related to pollution sources, delivery, and residence time (SDR) culprits, and associates delineated estuary units with a corresponding CPRU based on SDR metrics. Outcomes from the platform provide support for coastal research investigations and management decision-making by identifying the setting type and drivers of pollution vulnerability in specified locations, and by providing a basis for organized comparisons of coastal locations based on land sea connections.

"Margin" watershed areas bordering estuaries included in the Estuary Builder framework constitute the land-sea connection interface. The locations are particularly susceptible to climate change dynamics that can influence the transport of pollutants from land areas into estuarine waters through elevated runoff and tide conditions. The current version of the Estuary Builder is customized for bacteria pollution culprits and contemporary conditions. However, the flexible framework of the tool can be adapted to accommodate diagnosis of multiple axes of vulnerability related to land-sea connections and coastal morphometry in varied coastal settings and climate change scenarios. Future work will focus on refinement of proxy spatial data metrics to improve capture of SDR processes, particularly physical estuary dynamics driving temporal and spatial patterns of pollution.

[1] School of Earth and Climate Sciences – University of Maine, Orono, Maine 04469, United States. bea.vandam@maine.edu
[2] Senator George J. Mitchell Center for Sustainability Solutions – University of Maine, Orono, Maine 04469, United States. sean.m.smith@maine.edu

Understanding estuarine sand dunes through linear and nonlinear modeling

van der Sande W.M. [1], Roos P.C. [1], Gerkema T. [2], and Hulscher S.J.M.H. [1]

Keywords: Estuarine sand dunes, morphodynamic modeling, linear stability analysis, nonlinear modeling

Abstract

Estuarine sand dunes are large-scale bed patterns with wavelengths of the order of tens to hundreds of meters, and heights on the order of meters. They cover (large) parts of the beds of estuaries worldwide, and have a significant influence on flow dynamics at the bedform scale (Kostaschuk, 2000; Kwoll et al., 2017). On the estuarine scale, sand dunes affect tidal dynamics and sediment transport (Herrling et al., 2021) and mitigate salt intrusion (Geerts et al., 2024). Hence, understanding the dynamics of these bedforms is important to understand processes at the estuarine scale.

Process-based morphodynamic models are a helpful tool to help understand how different processes influence bedforms (e.g., Campmans et al., 2017; Damveld et al., 2020). We distinguish between linear and nonlinear models. Linear models (e.g, Damveld et al., 2019) assume a infinitesimally small bed amplitude, enabling simplification of the morphodynamic problem. Although computationally cheap, the output is limited to a preferred wavelength and growth and migration rates. Nonlinear models (e.g., Paarlberg et al., 2009) drop the assumption of a small bed amplitude, and thus can yield geometrical properties of dunes in or near equilibrium – at the cost of computation time.

Here, we present two linear stability models and one nonlinear model, each incorporating an estuarine-specific effect on sand dunes. The two linear stability models focus on two types of estuarine circulation, which is the residual circulation with a seaward velocity component near the surface and a landward component near the bed. The first is the gravitational circulation stemming from a longitudinal salinity gradient, the second is the strain-induced circulation stemming from tidal variations in stratification (i.e., SIPS). Alternatively, in the nonlinear model we first ignore salinity gradients, and instead focus on nonhydrostatic effects. These are flow effects that can be caused by strong bed level gradients, for instance at the steeper lee side of bedforms. The lee side of bedforms results in increased turbulent kinetic energy, and can, if steep enough, ultimately give rise to flow separation in the trough of dunes. Field observations of flow over estuarine dunes have demonstrated the relevance of this process for estuarine sand dunes. In summary, the three modeling tools discussed here are: (1) a linear stability model to investigate the influence of gravitational circulation on estuarine sand dunes (Van der Sande et al., 2021), (2) a linear stability model to investigate the effect of strain-induced circulation (Van der Sande et al., 2023), and (3) a nonlinear model which includes nonhydrostatic effects such as flow separation (Van der Sande et al., submitted).

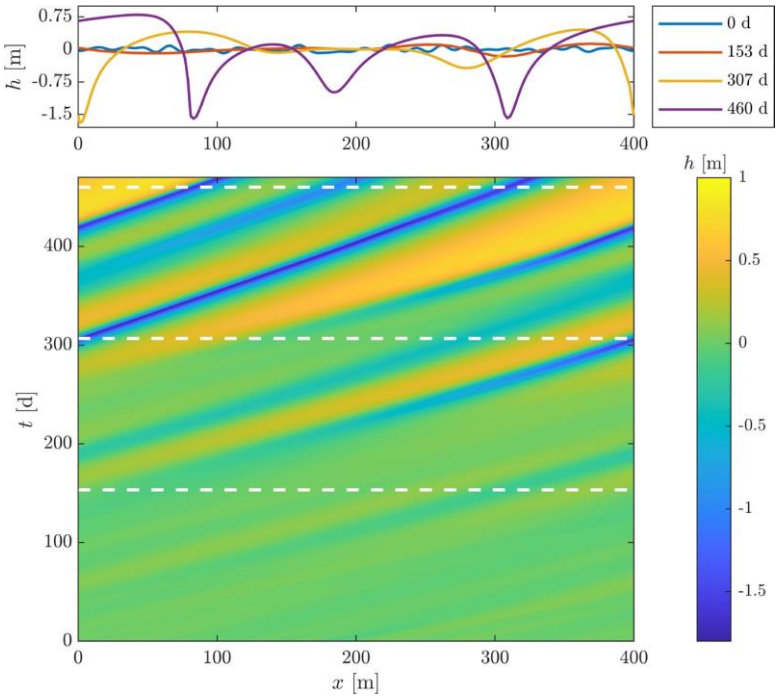

Figure 1: Example of morphodynamic evolution as obtained with our nonlinear model shown by a timestack of the topography. Yellow and blue shades indicate dune crests and troughs, respectively.

[1] Department of Water Engineering and Management, University of Twente, Enschede, The Netherlands,.
[2] Department of Estuarine and Delta Systems, NIOZ Royal Netherlands Institute for Sea Research, Yerseke, The Netherlands.

Results show the following: (1) gravitational circulation can cause upstream migration of sand dunes. That is, upstream-directed near-bed flow induces upstream-directed bed load sediment transport, as such causing an upstream component of migration which can be stronger than the downstream-directed migration induced by river flow. These findings confirm earlier observations from the Gironde estuary, France, which showed seasonal reversal of asymmetry (Berné et al., 1993), caused by the salinity gradient being pushed seaward during higher river discharge. Similarly, the model results explain later observations from the Weser estuary, Germany (Lefebvre et al., 2022). Other dune characteristics (growth rate and preferred wavelength) were not significantly affected by a longitudinal salinity gradient.

Strain-induced circulation has a similar effect on sand dunes as gravitational circulation: they drive upstream migration through upstream-directed near-bed flow. Besides, results show that reduced turbulent mixing due to (time- varying) stratification gives rise to shorter wavelengths. This effect is qualitatively verified by observation data from the Elbe, Germany (Muurman, 2021; Zorndt et al., 2011).

The nonlinear model shows evolution of sand dunes from an almost flat bed (Figure 1). The initial growth of topographic modes is exponential, conform outcomes of linear stability analyses (such as in Hulscher, 1996). In the spatial spectrum, dunes seem to grow by amalgamation of smaller-scale bedforms (Fourrière et al., 2010). This leads us to conclude that these two mechanisms are not mutually exclusive. Furthermore, we investigate the morphodynamic evolution for three cases, each representing a position in a prototype estuary: upstream (strong residual flow, small depth and tidal velocity amplitude), middle, and downstream (small residual flow, large depth and tidal velocity amplitude). Dunes in the upstream case are short, migrate fast and have relatively small height, whereas towards downstream dunes become longer, higher, and migrate slowly. Furthermore, dunes downstream are less steep than upstream. These findings align with the idea of estuarine sand dunes as a transient bedform between river dunes and tidal sand waves, and qualitatively agree with observations (Lefebvre et al., 2022).

To conclude, we outline three morphodynamic models of estuarine sand dunes, each focusing on one process relevant in estuaries. Gravitational circulation and strain-induced circulation both are drivers of upstream migration of sand dunes. Furthermore, results show that strain-induced circulation also reduces the wavelength of estuarine sand dunes. Lastly, a new nonhydrostatic and nonlinear model of estuarine sand dunes shows the evolution of dunes from an almost flat bed to quasi-equilibrium.

References

Berné, S., Castaing, P., le Drezen, E., & Lericolais, G. (1993). Morphology, internal structure, and reversal of asymmetry of large subtidal dunes in the entrance to Gironde Estuary (France). Journal of Sedimentary Petrology, 63(5), 780–793. https://doi.org/10.1306/d4267c03-2b26-11d7-8648000102c1865d

Campmans, G. H. P., Roos, P. C., de Vriend, H. J., & Hulscher, S. J. M. H. (2017). Modeling the influence of storms on sand wave formation: A linear stability approach. Continental Shelf Research, 137, 103–116. https://doi.org/10.1016/j.csr.2017.02.002

Damveld, J. H., Borsje, B. W., Roos, P. C., & Hulscher, S. J. M. H. (2020). Horizontal and Vertical Sediment Sorting in Tidal Sand Waves: Modeling the Finite-Amplitude Stage. Journal of Geophysical Research: Earth Surface, 125(10). https://doi.org/10.1029/2019JF005430

Damveld, J. H., Roos, P. C., Borsje, B. W., & Hulscher, S. J. M. H. (2019). Modelling the two-way coupling of tidal sand waves and benthic organisms: a linear stability approach. Environmental Fluid Mechanics, 19, 1073–1103. https://doi.org/10.1007/s10652- 019-09673-1

Fourrière, A., Claudin, P., & Andreotti, B. (2010). Bedforms in a turbulent stream: Formation of ripples by primary linear instability and of dunes by nonlinear pattern coarsening. Journal of Fluid Mechanics, 649, 287–328. https://doi.org/10.1017/S0022112009993466 Geerts, S. J., van der Sande, W. M., Hulscher, S. J. M. H., Geurts, B. J., & Roos, P. C. (2024). Estuarine sand dunes as a nature-based solution against salt intrusion. In NCR days 2024.

Herrling, G., Becker, M., Lefebvre, A., Zorndt, A., Krämer, K., & Winter, C. (2021). The effect of asymmetric dune roughness on tidal asymmetry in the Weser estuary. Earth Surface Processes and Landforms, 46(11), 2211–2228. https://doi.org/10.1002/esp.5170

Hulscher, S. J. M. H. (1996). Tidal-induced large-scale regular bed form patterns in a three-dimensional shallow water model. Journal of Geophysical Research, 101(C9), 20727–20744. https://doi.org/10.1029/96JC01662

Kostaschuk, R. (2000). A field study of turbulence and sediment dynamics over subaqueous dunes with flow separation. Sedimentology, 47(3), 519–531. https://doi.org/10.1046/j.1365-3091.2000.00303.x

Kwoll, E., Venditti, J. G., Bradley, R. W., & Winter, C. (2017). Observations of Coherent Flow Structures Over Subaqueous High- and Low- Angle Dunes. Journal of Geophysical Research: Earth Surface, 122(11), 2244–2268. https://doi.org/10.1002/2017JF004356 Lefebvre, A., Herrling, G., Becker, M., Zorndt, A., Krämer, K., & Winter, C. (2022). Morphology of estuarine bedforms, Weser Estuary, Germany. Earth Surface Processes and Landforms, 47(1), 242–256. https://doi.org/10.1002/esp.5243

Paarlberg, A. J., Dohmen-Janssen, C. M., Hulscher, S. J. M. H., & Termes, P. (2009). Modeling river dune evolution using a parameterization of flow separation. Journal of Geophysical Research: Earth Surface, 114(F1). https://doi.org/10.1029/2007JF000910 Muurman, S. D. (2021). Data analysis of estuarine dunes: Linking estuarine sand dune characteristics to environmental parameters (MSc thesis). Enschede: Civil Engineering and Management, University of Twente.

Van der Sande, W. M., Roos, P. C., Gerkema, T., & Hulscher, S. J. M. H. Nonlinear modeling of river dunes: insights in long-term evolution of dune dimensions and form roughness. Under Review.

Van der Sande, W. M., Roos, P. C., Gerkema, T., & Hulscher, S. J. M. H. (2021). Gravitational Circulation as Driver of Upstream Migration of Estuarine Sand Dunes. Geophysical Research Letters, 48(14). https://doi.org/10.1029/2021GL093337

Van der Sande, W. M., Roos, P. C., Gerkema, T., & Hulscher, S. J. M. H. (2023). Shorter estuarine dunes and upstream migration due to intratidal variations in stratification. Estuarine, Coastal and Shelf Science, 281. https://doi.org/10.1016/j.ecss.2023.108216

Zorndt, A. C., Wurpts, A., & Schlurmann, T. (2011). The influence of hydrodynamic boundary conditions on characteristics, migration, and associated sand transport of sand dunes in a tidal environment: A long-term study of the Elbe Estuary. Ocean Dynamics, 61, 1629–1644. https://doi.org/10.1007/s10236-011-0452-1

Morphodynamics of channel networks in tide-influenced deltas

van der Vegt M. [1] and Kleinhans M.G. [2]

Keywords: deltas, channel networks, river discharge, tides, morphodynamics.

Abstract

Deltas often have channel networks with multiple bifurcations and confluences. Tides and river flow can take different pathways, causing the different channels to influence each other. The bifurcations and confluences are the locations where water, salt and sediment are distributed over the delta channel network, thereby impacting the hydrodynamics, salinity distribution and morphological evolution of the entire delta. Some examples of channel networks in deltas are shown in Figure 1. For example, in the Yangtze delta several smaller channels connect the main branches. The construction of training dams, by which one of the connecting channel was effectively closed off, resulted in strong deposition of sediment in other channels. Similar delta-wide effects have been reported for other deltas. We do not yet understand how the different channels in a delta interact in terms of hydrodynamics and morphological change and how changes in one channel may influence that of the others. Therefore, the main om this study is to improve our understanding of the morphodynamics of channel networks in deltas as a function of channel network properties (width, length and number of channels) and external forcing (river discharge and tides).

We adopted a modeling approach and used the same model as described in Iwantoro et al. (2021;2022). This model solves the 1D width- and depth-averaged Shallow Water Equations, uses a Van Rijn or Engelund-Hansen sediment transport predictor, a nodal point relation based on Bolla Pitaluga et al. (2003) for sediment division at channel bifurcations and solves the Exner equation to calculate morphological changes. We used a channel configuration as shown in Figure 1c and systematically varied river discharge, tidal amplitude and width and length of the channels, with a special attention to the role of the connecting channel.

In a first set of simulations we excluded tides and only studied a channel network forced by river discharge. Without connecting channel, hence we have a three-channel network with only two downstream channels, the delta evolves into an asymmetric system in which one of the downstream channels is deeper and receives most discharge, while the other is shallower and receives hardly any water. Adding the connecting channel has large effects on the morphology. For weak and high river discharge, the connecting channel causes the channels to develop a smaller asymmetry. For intermediate discharge conditions, the delta can evolve into a system with periodic asymmetry, in which the two main branches that are connected via the connecting channel periodically switch between being the major and minor branch. This periodic behavior is caused by the nonlinear friction, which depends on the channel depth and flow velocity. While one of the branches is deepening and other shallowing, the water level difference between the two main branches decreases. As a result, the connecting channel periodically switches its flow direction, because the water level gradient between the main branches changes sign. Thereby a confluence changes into a bifurcation and vice versa. This also causes a change in the morphodynamic evolution, in which the shallow channel starts eroding and the deep channel silting up. The time scale of periodic behavior depends on the lengths of the channels and ranges between decades and centuries.

Tides have a strong influence as well. For a system without connecting channel, it was already shown by Iwantoro et al. (2022) that tides can make the depth of a three-channel system less asymmetric by either enlarging the range of conditions for which the symmetric channel configuration is stable to bed perturbations, or by making the depth-asymmetry of the final equilibrium smaller once the symmetric system is unstable to bed perturbations. For most configurations studied, the connecting channel causes the final depth asymmetry of the downstream channels to be less asymmetric compared to the three channel system. As found for the river-only case, also for systems with tides the bed levels of channels can become periodic. Tides reduce the amplitude of the periodic behavior and shorten the time scale. Furthermore, the model results show that multiple morphodynamic equilibria exist and that the depth of each branch in equilibrium depends on the initial conditions.

We will present a systematic analysis of the results and expand the parameter space that was studied. Whereas the lengths and widths of the channel network presented here were still symmetric, we will expand our analysis to study how asymmetries in channel length and width, as found in many deltas, influence the morphology. However, the first results shown here already highlight the important role of connecting channels for the morphological evolution of channel networks and give clues on why these connecting channels exist, how their closure can have drastic effects on the morphology of the delta and how they influence the morphodynamics of the entire network.

[1] Department of Physical Geography, Utrecht University, the Netherlands, m.vandervegt@uu.nl .
[2] Department of Physical Geography, Utrecht University, the Netherlands

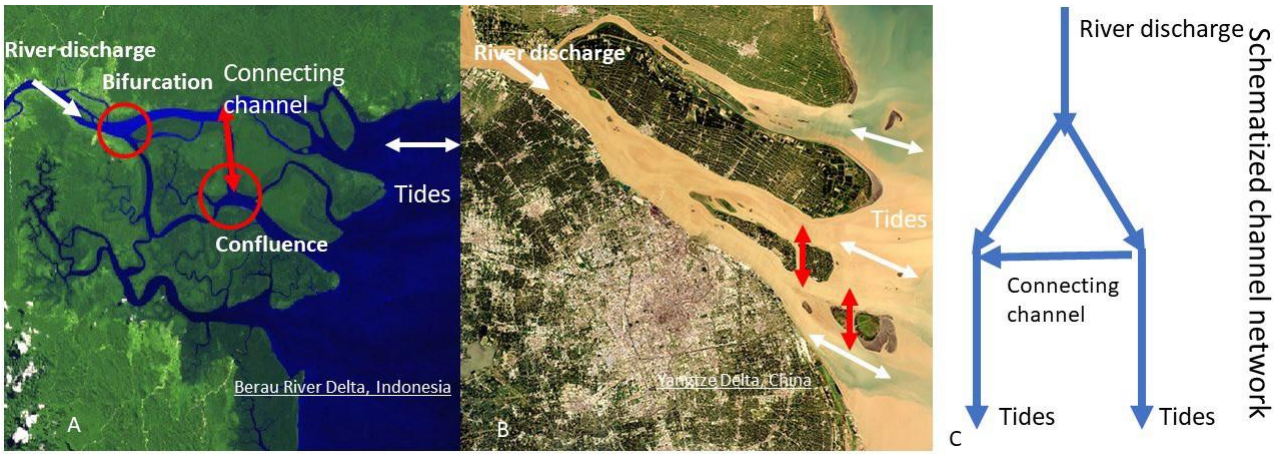

Figure 1: a) Map of the Berau Delta, Indonesia, showing the channel network and the presence of bifurcations, confluences and connecting channels. B) Same as a), but now for the Yangtze delta. C) Network of six channels as used in the morphodynamic model simulations. In some sets of simulation the connecting channel was absent, making this a three channel network.

References

M. Bolla Pittaluga, R. Repetto, and M. Tubino. Channel bifurcation in braided rivers: Equilibrium configurations and stability. *Water Resources Research*, 39(3):ESG11–ESG113, 2003.

A. Iwantoro, M. van der Vegt M., and M. Kleinhans. Effects of sediment grain size and channel slope on the stability of river bifurcation. *Earth Surface Processes and Landforms*, 46 (10), 2021

A. Iwantoro, M. van der Vegt, and M. Kleinhans. Stability and asymmetry of tide-influenced river bifurcations. *Journal of Geophysical Research: Earth Surface*, 127(6), 2022.

Morphodynamic evolution of estuarine intertidal flats under sea level rise

van der Wegen M. [1], Naidoo J.J. [2], El Milady H. [3], Aguilera Chaves M. [4], Roebke B. [5], Alonso A.C. [6], and Dastgheib A. [7]

Keywords: estuaries, morphodynamics, intertidal flats, sea level rise.

Abstract

Introduction

The estuarine intertidal zone forms an important ecosystem that plays a vital role as habitat, but also serves as a natural coastal protection against flooding by wave attenuation and as a morphodynamic basis for vegetated zones like salt marshes and mangroves, see Figure 1.

For the development of coastal management strategies and policies and to ensure the system's sustainability as sea level rises it is essential to understand the long-term morphodynamic evolution of intertidal systems. Climate change and human activities like dike construction or reduction in sediment supply put pressure on intertidal area where accelerating sea level rise (SLR) has the potential of drowning estuaries.

Figure 2. Intertidal flats in the Western Scheldt estuary, Netherlands. Source: Rijkswaterstaat Beeldbank

Sea level rise is historically unprecedented so that detailed data on impavct on estuarine morphodynamic development is lacking. Thus, modeling efforts plays an import role in assessment studies, where different types of models may strengthen each other and lead to more robust conclusions. Aggregated modeling efforts show potential morphodynamic impact of sea level rise on estuarine systems, e.g. Lodder et al. (2019), Huismans et al. (2022). More high-resolution models like Delft3D allow for more detailed physical processes and output heterogeneity, but require extensive computation time, e.g. Elmilady et al., (2019), Robke et al., (2022), Zheng et al., (2021).

Aim

This study aims to assess the morphodynamic evolution of intertidal flats under SLR using high-resolution modeling (Delft3D) for different case studies and to parametrize SLR impact to the benefit of more aggregated, faster modeling efforts.

Method

Our work is based on various published and validated morphodynamic Delft3D models, to which different SLR scenarios are added. The models include schematized tidal basins comparable to the Waddensea basins (Colina Alonso et al., 2020, Elmilady et al., 2022) and a Western Scheldt case study (Robke et al., 2020, see Figure 3). The current research then investigates in more detail the spatial behavior of the tidal flats under different SLR scenarios and the impact of different sediment classes and their interaction (i.e. sand /mud).

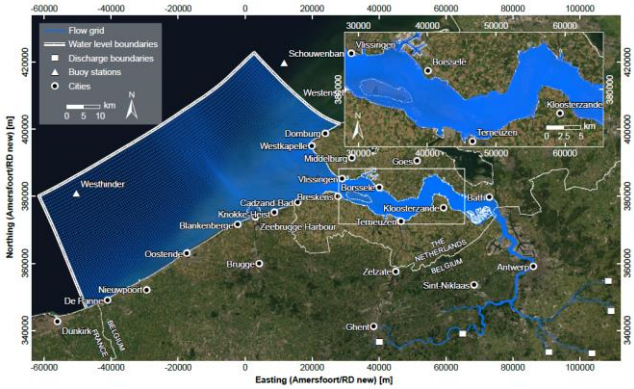

Figure 3 High-resolution Delft3D Western Scheldt estuary model, Netherlands Robke et al (2020)

[1] IHE Delft and Deltares
[2] Transnet National Ports Authority
[3] IHE and TUD
[4] Deltares
[5] Deltares
[6] Deltares and Delft UT
[7] IHE Delft and IMDC

Results

For all case studies the intertidal area accretes and reduces in area under SLR (Figure 3.). The morphodynamic behaviour of the intertidal area lags behind SLR while area closer to the sediment source adapts faster to SLR. Partial drowning of intertidal area occurs, when the intertidal area can no longer keep up with SLR. More drowning occurs for larger (extremer) SLR. The model results also show that with sand-mud interaction, less intertidal area is lost as compared to excluding interaction. Mud pressence changes under SLR (see Figure 4) while the spatial distribution of mud varies between runs including or excluding sand-mud interaction. In general, tidal flats become more muddy with and without SLR. SLR results in tidal flats becoming muddier at certain locations in the basin/estuary, while other locations become less muddy. Intertidal area becomes flatter due to SLR for a wide tidal basin, whereas for an elongated basin and the Western Scheldt estuary, the tidal flats remain steep.

The current high-resolution model analysis reveals relationships between SLR rates and adaptation timescales, sediment properties, and intertidal area and hypsometry. These relationships can be parametrized to be used in more aggregated and low computation effort modeling efforts like by Lodder et al. (2019), Huismans et al. (2022).

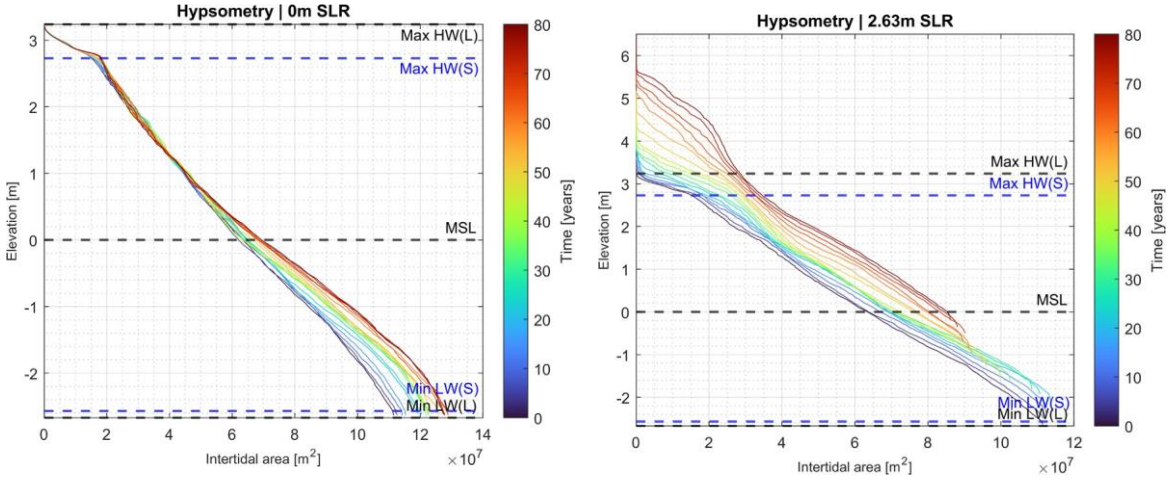

Figure 3 Hypsometric evolution of intertidal area over 80 years without sea level rise (left panel) and with 2.63m sea level rise (right panel) in the Western Scheldt

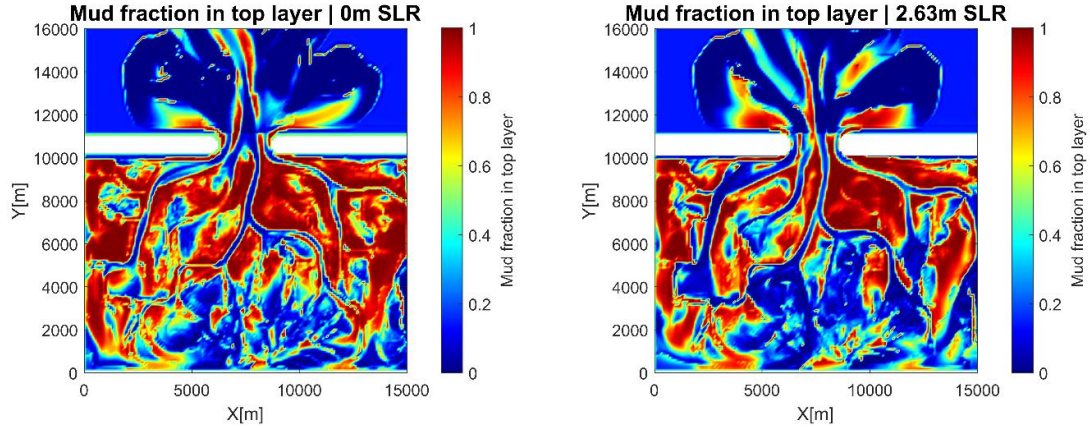

Figure 4Modeled 100-year top layer mud fraction without sea level rise (left panel) and with 2.63m sea level rise for schematized Waddensea basin

References

Colina Alonso Weerdenburg Maren, Huismans (2020) Modelling sand-mud interaction in Delft3D.Investigation of sand-mud modules in Delft3D and Delft3D-FM Deltares, Delft, The Netherlands, pp. 66.

Elmilady, Van der Wegen, Roelvink, & Jaffe. (2019). Intertidal area disappears under sea level rise: 250 years of morphodynamic modeling in San Pablo Bay, California. *Journal of Geophysical Research: Earth Surface*, *124*(1), 38-59.

Elmilady van der Wegen Roelvink van der Spek (2022) Modeling the Morphodynamic Response of Estuarine Intertidal Shoals to Sea-Level Rise. Journal of Geophysical Research: Earth Surface 127: e2021JF006152, https://doi.org/10.1029/2021JF006152

Huismans van der Spek Lodder Zijlstra Elias Wang (2022) Development of intertidal flats in the Dutch Wadden Sea in response to a rising sea level: Spatial differentiation and sensitivity to the rate of sea level rise. Ocean & Coastal Management 216: 105969

Lodder, Wang, Elias, Van der Spek, Looff, Townend (2019) Future Response of the Wadden Sea Tidal Basins to Relative Sea- Level rise—An Aggregated Modelling Approach. Water 11: 2198 DOI 10.3390/w11102198

Röbke, Elmilady, Van der Wegen, Taal (2020) The long-term morphological response to sea level rise and different sediment strategies in the Western Scheldt estuary (The Netherlands). Deltares, Delft, The Netherlands, pp. 98.

Zheng, Elmilady, Röbke, Taal, Wang, van Prooijen, ... & Van der Wegen. (2021). The impact of wind-waves and sea level rise on the morphodynamics of a sandy estuarine shoal. *Earth Surface Processes and Landforms*, *46*(15), 3045-3062.

A new harmonic regression approach to predict estuarine salinity variation subject to storm surge effects

van Keulen D. [1], Kranenburg W. [2], and Hoitink T. [3]

Keywords: physics, estuaries, salt intrusion.

Abstract

Obtaining rapid and accurate predictions of estuarine salinity is key to operational water management, but challenging. To allow short-to-medium term predictions, a new physics-inspired harmonic regression model has been developed to forecast salinity time-series at a monitoring station. This model is best applicable to short and well-mixed systems. It extends an existing approach of hybrid harmonic regression models used for tidal surface level elevation predictions. The subtidal salinity variations are captured in a simplified, analytical, steady-state salt intrusion model that requires the tidal elevation and salinity at sea, and the river discharge and salinity at an upstream station. For well- mixed systems, variations around the steady-state are largely related to the advective displacement of the salinity curve by the tidal motion and storm-surges. Displacement by the tidal excursion is accounted for with a harmonic extension of the model. Storms-surge effects are incorporated with a linear relation. To cope with times-series containing prolonged periods with low salt levels, corresponding to the river salinity, and only occasional periods where the salt front reaches the station, a truncation procedure is implemented in the model. The new method is tested in the Ems Estuary and the Scheldt Estuary. Application to 2-year and 4-year datasets show that the model explains between 97.2 and 86.5% of the observed salinity variance. Without use of observed salinity at the downstream boundary, the explained variance reduced to values between 77.7 and 81.6%. By utilizing the regression method with minimal data input, fast salinity predictions can be obtained with minimal data input that offer insights in the effects of the dominant physical processes.

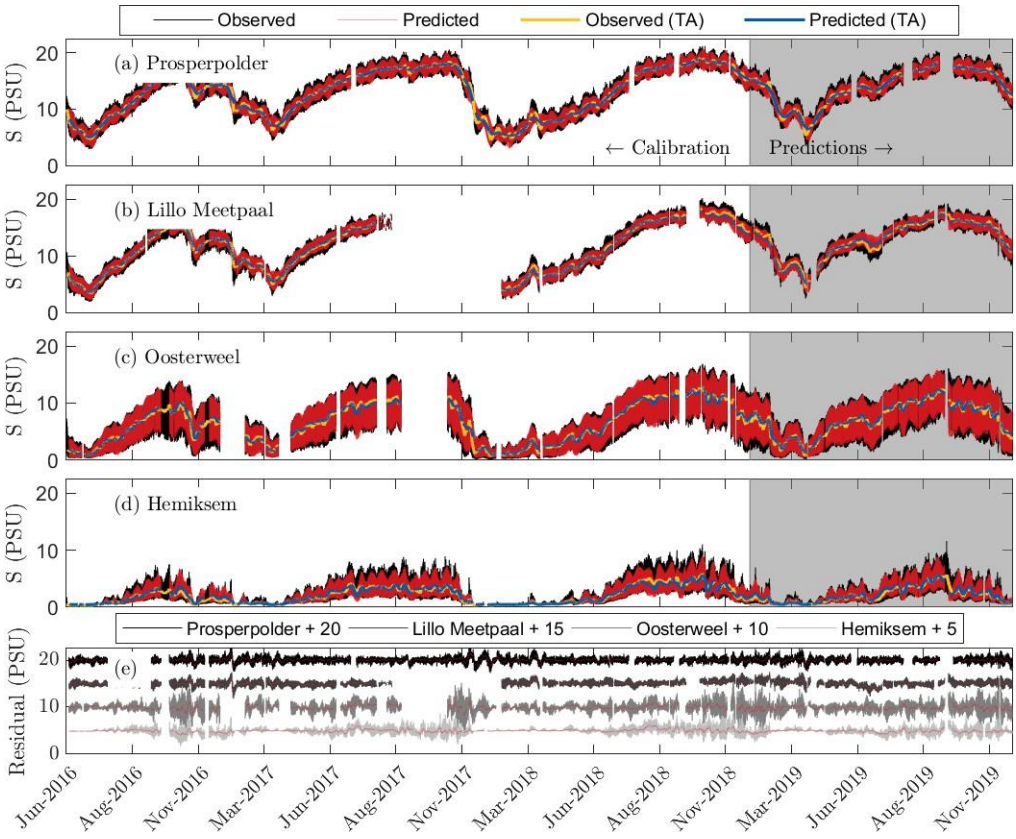

[1] Hydrology and Environmental Hydraulics Group, Department of Environmental Sciences, Wageningen University & Research, Wageningen, The Netherlands; Unit Marine and Coastal Systems, Deltares, Delft, The Netherlands; Daan.vanKeulen@wur.nl
[2] Unit Marine and Coastal Systems, Deltares, Delft, The Netherlands; Department of Hydraulic Engineering, Delft University of Technology, Delft, The Netherlands; Wouter.Kranenburg@deltares.nl
[3] Hydrology and Environmental Hydraulics Group, Department of Environmental Sciences, Wageningen University & Research, Wageningen, The Netherlands; Ton.Hoitink@wur.nl

Modelling resuspension including spatio-temporal variability in sediment stability

van Kessel T. [1] and Bi Q. [2]

Keywords: mud flats, salt marshes, consolidation, drying, stability

Abstract

A classical approach for modelling resuspension of cohesive sediments is to specify fixed values for the critical shear stress τ_c and resuspension parameter *M*. Variations in resuspension do still occur by variations of hydrodynamics forcings (specifically the current- and wave-induced bed shear stress) and sediment availability (as resuspension may be reduced by bed depletion).

However, in practice bed properties are not constant, but vary in time and space. Just after slack water, the bed may be covered with a thin layer of fresh deposits with very little resistance to resuspension ($\tau_c < 0.1$ Pa). Just after a storm period, the top layer may have been eroded, exposing a base layer with strong resistance to erosion ($\tau_c > 1$ Pa). There is a feedback loop between hydrodynamic forcing and cohesive bed strength, resulting in typically soft deposits in low- energy environments and strong beds in high-energy environments. Also, bed strength may increase in time by consolidation and, if exposed for sufficient time at intertidal areas or salt marshes, drying.

Prescribing maps of τ_c and *M* is unfeasible as this would require many in-situ observations and would still ignore most temporal dynamics, notably those at short time scales. A more feasible approach is not to prescribe τ_c and M, but to compute these parameters from deposition, consolidation, and resuspension history of the bed, i.e. from the resulting bed density.

A methodology for this was proposed in Van Rees et al. (2024), adopting a two-layer approach. In each layer, porosity and resulting bed density may change because of pore water flow induced by self-weight consolidation and/or suction. Instead of τ_c and M, material functions are prescribed for the relationships between permeability and porosity, and porosity and effective stress. Subsequently, τ_c and M are prescribed as functions of effective stress and permeability, respectively. The present work is an extension of this work, moving from a highly schematized 1D implementation towards a full 3D model implementation in D3D-WAQ, including generalization to accommodate multiple sediment fractions, and application for the Scheldt estuary. Figure 1 shows a generic flow chart for this implementation.

Herein we compare the classical and extended model behaviour, demonstrating the effects of the spatio-temporal dynamics of bed properties on gross and residual sediment transport, on resuspension and deposition and on bed level and bed density. We discuss the importance of these dynamics relative to the 'classical' hydrodynamic forcing. We also discuss the consequences for the modelled accretion rate of intertidal mud flats and supra-tidal salt marshes, which are often underestimated in 'classical' models, and the implications for SPM dynamics and contaminant transport. Figure 2 illustrates the difference with and without variable sediment stability for a 1D example on mudflat accretion. This example includes sediment characteristics and a tide- and wave-induced bed shear stress representative for the Scheldt estuary. Whether or not consolidation and evaporation effects are included makes a large difference: without consolidation, no accretion occurs as fresh deposits are all quickly resuspended. With (subtidal) consolidation about 2 cm net accretion is computed over a year, and with (intertidal) consolidation and drying about 10 cm net accretion is computed.

References

Van Rees F., J. Hanssen, S. Gamberoni, A. Talmon and T. van Kessel (2024) Effect of air exposure time on erodibility of intertidal mud flats. Submitted to Frontiers

[1] Deltares, thijs.vankessel@deltares.nl
[2] Deltares, qilong.bi@deltares.nl

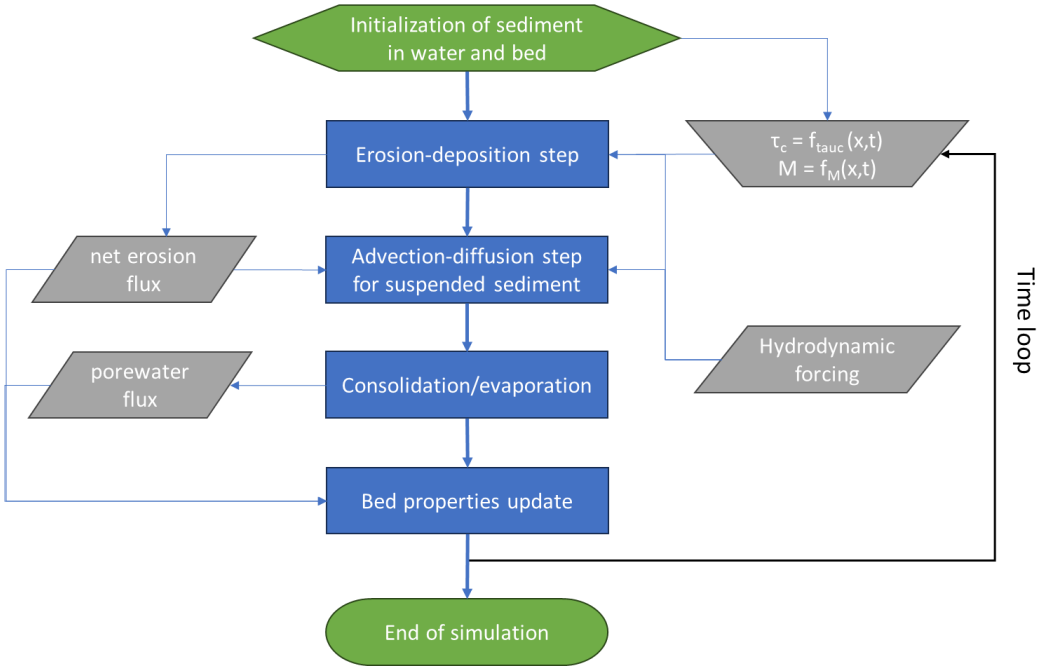

Figure 1. Flow chart for computation of resuspension for variable sediment stability properties

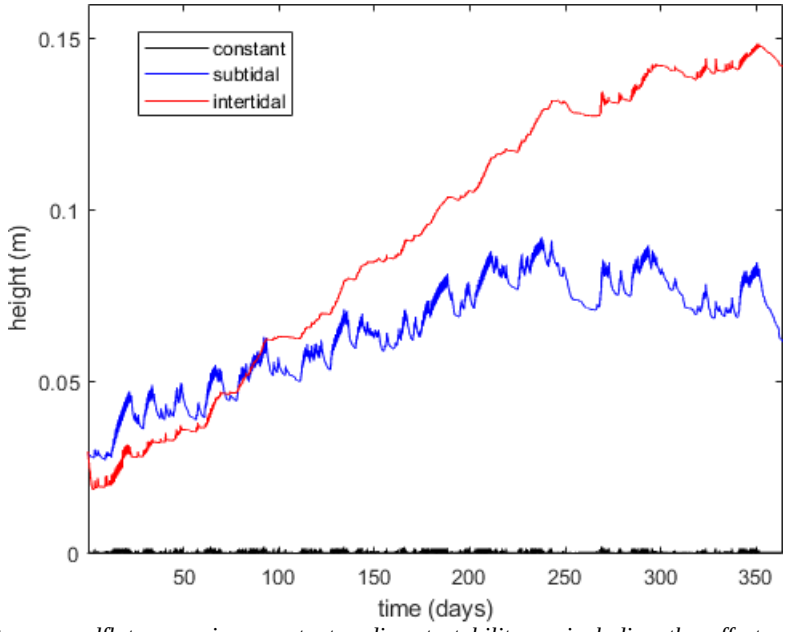

Figure 2. Accretion rate on mudflat, assuming constant sediment stability or including the effect of consolidation (subtidal) and consolidation + drying (intertidal) hereon.

Adaptation timescales of estuaries and tidal basins to human interventions

Van Maren B. [1]

Keywords: estuarine dynamics, tidal amplification, human interventions

Abstract

Many estuaries and tidal basins are strongly influenced by various human interventions (land reclamations, infrastructure development, channel deepening, dredging and disposal of sediments). Such interventions lead to a range of hydrodynamic and morphological responses (a changing channel depth, tidal amplitude and/or suspended sediment concentration). The response time of a system to interventions is determined by the processes driving this change, the size of the system, and the magnitude of the intervention. A quantitative understanding of the response time to an intervention therefore provides important insight into the processes driving the response.

We have developed a methodology to estimate the response timescales of human interventions using available morphological and hydraulic data by fitting exponential decay functions to this data. The exponential decay functions describe the historic changes remarkably well and provide valuable insight into the response of physical systems to human interventions. The method has been applied to investigate the response of the Ems and Scheldt estuaries to deepening using historic water level observations, and to investigate the response of the Wadden Sea to closure of tidal basins using morphological data.

The tidal range of the Sea Scheldt is especially increasing because of deepening in the 1970's. The tidal range of the Ems estuary was more strongly influenced by a series of deepening efforts. For both the Ems and the Scheldt the adaptation times are shortest at the landward limit of deepening. Closure of the South Sea (part of the Dutch Wadden Sea) initially triggered sediment import, but net sediment import into the Wadden Sea was largely completed around 60 years after closure. The mud-dominated tidal flats respond much more slowly, however, with associated timescales of several centuries.

[1]Deltares [The Netherlands] – Boussinesqweg 1, Delft, the Netherlands, Netherlands

Importance of the Vertical Eddy Viscosity Profile on the Subtidal Salt Intrusion and Stratification in Well-Mixed and Partially Stratified Estuaries

Van Ooijen C. [1], Dijkstra Y. [1], Rozendaal M. [1], and Schuttelaars H. [1]

Keywords: estuaries, hydrodynamics, idealised model, lateral bathymetries, momentum advection, residual flow

Abstract

Lateral bathymetries, that is, bathymetries that vary in the cross-channel direction exclusively, have significant effects on the hydrodynamics in estuaries. For example, these lateral bathymetries cause lateral tidal motion, but they also affect along-channel residual flow through lateral momentum advection. Such effects are magnified if the bathymetry is steep, meaning that bathymetry gradients and the depth difference between the shallower and deeper parts of the estuary are large. Examples of estuaries with steep bathymetries are the Scheldt estuary in the Netherlands and Belgium, and the Hudson estuary in the United States, both containing deep channels that are much deeper than shallower parts of the estuary.

While many studies have investigated estuarine hydrodynamics in the presence of general bathymetries (for example Li and Valle-Levinson, 1999), not much is known about the sensitivity of the hydrodynamics to the bathymetric steepness, especially in fully three-dimensional contexts. Furthermore, because of its non-linear nature, not much is known about the role of momentum advection in generating residual flows in estuaries with steep bathymetries. To shed light on this, we have systematically studied the effect of bathymetric steepness on estuarine hydrodynamics, focusing on advection-driven residual flow in particular.

The dynamics are modelled using the three-dimensional Reynolds-averaged shallow water equations with constant vertical eddy viscosity. At the seaward boundary, the model is forced by the tidal water level, which oscillates uniformly at the semidiurnal tidal frequency. Furthermore, to focus on advection-driven residual flow, other mechanisms such as river discharge, baroclinic flow, and Stokes drift are neglected. In order to guarantee convergence of the numerical method, the advective terms are multiplied by 0.1.

We consider a continuous range of Gaussian bathymetries with equal cross-sectional area, controlled by a bathymetric steepness parameter. The model is applied to a rectangular estuary of 3 km wide and 10 km long. To solve the model, a truncation method was employed, in which the model equations and boundary conditions are projected on a harmonic temporal basis and a vertical basis consisting of eigenfunctions of the vertical mixing operator. The resulting equations are subsequently discretised using a spectral element method and solved by means of the Newton-Raphson method.

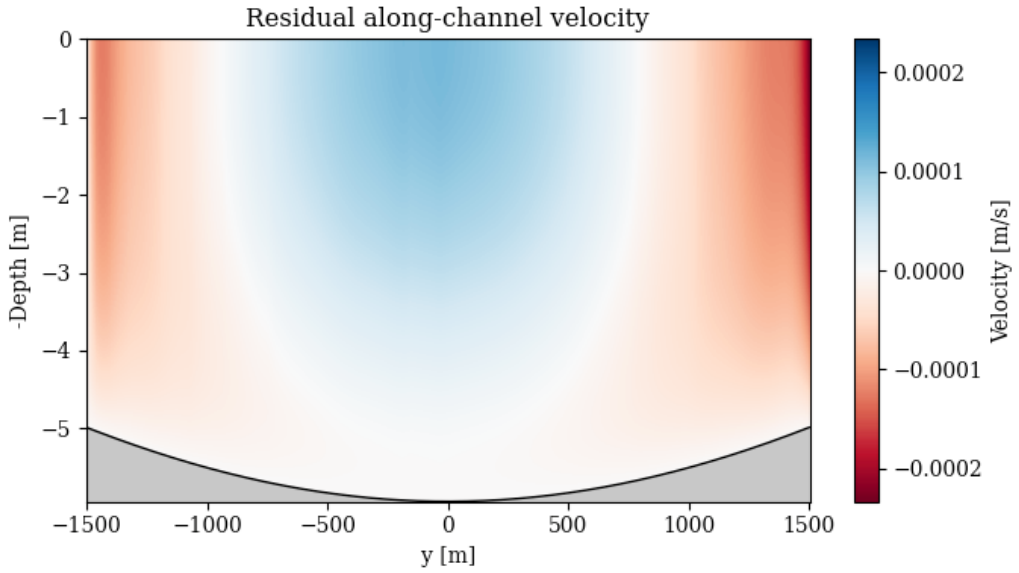

Figure 1: Residual along-channel velocity [m/s] in the central cross-section (x = 5 km) of an estuary with gentle bathymetry. Positive (blue) values indicate flow towards the landward boundary, and negative (red) values indicate flow towards the seaward boundary.

[1] Delft Institute of Applied Mathematics (DIAM), Delft University of Technology, c.r.vanooijen@tudelft.nl

The results indicate that steeper bathymetries are associated with large differences in the strength of the tidal along-channel flow between deep and shallow parts of the estuary. As a result, strong lateral tidal flows are generated that become dominant in the shallower parts of the domain. Steeper bathymetries also result in stronger and notably more asymmetric advection-driven residual flow fields (see Figures 1 and 2). This asymmetry is indirectly caused by the Coriolis effect: Coriolis deflection leads to asymmetry in the lateral tidal velocity field, which in turn leads to asymmetric lateral momentum advection, which causes the asymmetry in the residual flow field.

This research is the first step in a larger project about idealised non-linear three-dimensional hydrodynamics and sediment dynamics in estuaries. In the near future, we aim to apply the model to longer estuaries as well, and include advection in its full power instead of multiplying the advective terms by 0.1.

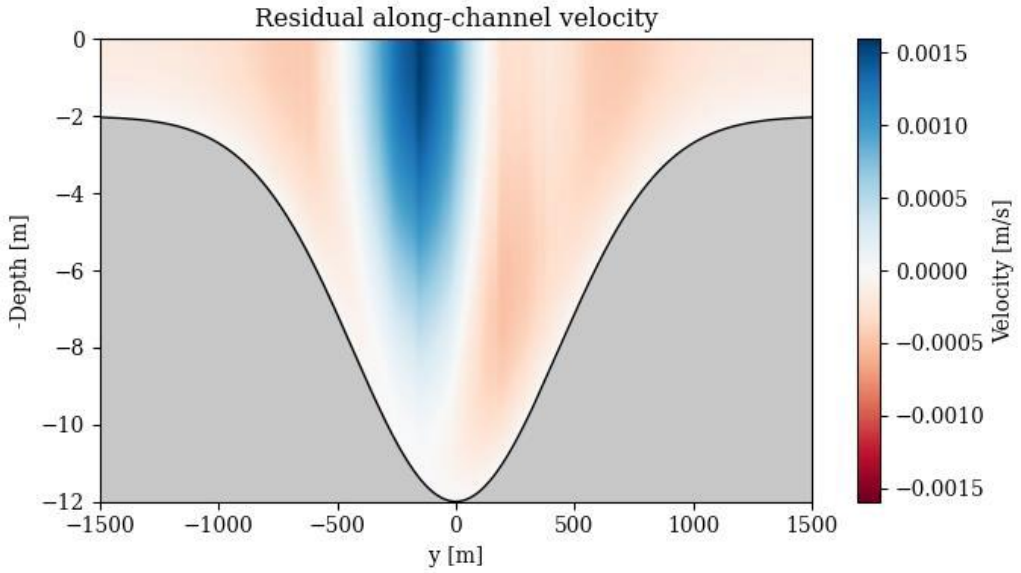

Figure 2: Residual along-channel velocity [m/s] in the central cross-section (x = 5 km) of an estuary with steep bathymetry. Positive (blue) values indicate flow towards the landward boundary, and negative (red) values indicate flow towards the seaward boundary.

References

Li. C, Valle-Levinson, A. (1999) A two-dimensional analytic tidal model for a narrow estuary of arbitrary lateral depth variation: The intratidal motion. Journal of Geophysical Research: Oceans, 104(C10), 23525-23543. DOI: 10.1029/1999JC900172.

Field measurements of the erosion and transport of sand-mud mixtures in intertidal areas in the Dutch Wadden Sea

van Weerdenburg R. [1], van Maren B. [2], Colosimo I. [3], and van Prooijen B. [4]

Keywords: sediment dynamics, sand, mud, erosion, mudflats, intertidal shoals, field measurements.

Abstract

The sediment bed in estuaries and tidal basins often consists of mixtures of sand and mud. Quantitative analysis of the sediment dynamics in these systems, for example to evaluate sediment management strategies, requires thorough understanding of not only the dynamics of the individual fractions, but also their complex interactions. The composition and properties of the bed sediment mixture determine the resistance against erosion and the erosion rate. The mixture is non-cohesive for small mud fractions (i.e. < 20-30%) and cohesive for larger mud fractions. The small amounts of mud in non-cohesive mixtures may already largely limit the erodibility of the sediment mixture compared to the erodibility of pure sand. For large mud fractions, (self-weight) consolidation (i.e. compaction by expelling pore water) and its effects on the erodibility of the mixture becomes important.

In this presentation, we present field measurements on the erodibility and transport of both cohesive and non-cohesive sediment mixtures in intertidal areas in the Dutch Wadden Sea, and we aim to quantify the erodibility of the sediment bed based on the characteristics of the sediment mixture.

We use field measurements collected at fringing tidal flats by Colosimo et al. (2020; 2023) and in a recent field campaign at one of the tidal divides in the Dutch Wadden Sea in November 2023 until January 2024 (see measurement locations in Figure 1a). The fringing tidal flats are relatively muddy, with a fraction of fines (particle diameter (D) < 63 µm) in the top layer around 50-60%. The tidal divide is relatively sandy, with a fraction of fines up to 20-30%. Although all measurement locations are located at intertidal areas, the bed elevation at the locations varies between –1.10 m and +0.10 m NAP (≈ MSL), such that the duration of aerial exposure varies widely.

The field measurements include continuous measurements of velocity profiles (ADCP), waves (ADV), suspended sediment concentrations (OBS and ADV backscatter) and changes in bed elevation (ADV and EchoSounder, see Figure 1b) for periods of around two months. A wide range of environmental conditions was captured in the field campaigns, with severe winter storms with winds from different directions during the winter 2023-2024 measurement campaign at the tidal divide: The (significant) wave heights at the tidal divide exceeded 1.0 m during three storms (see Figure 2a).

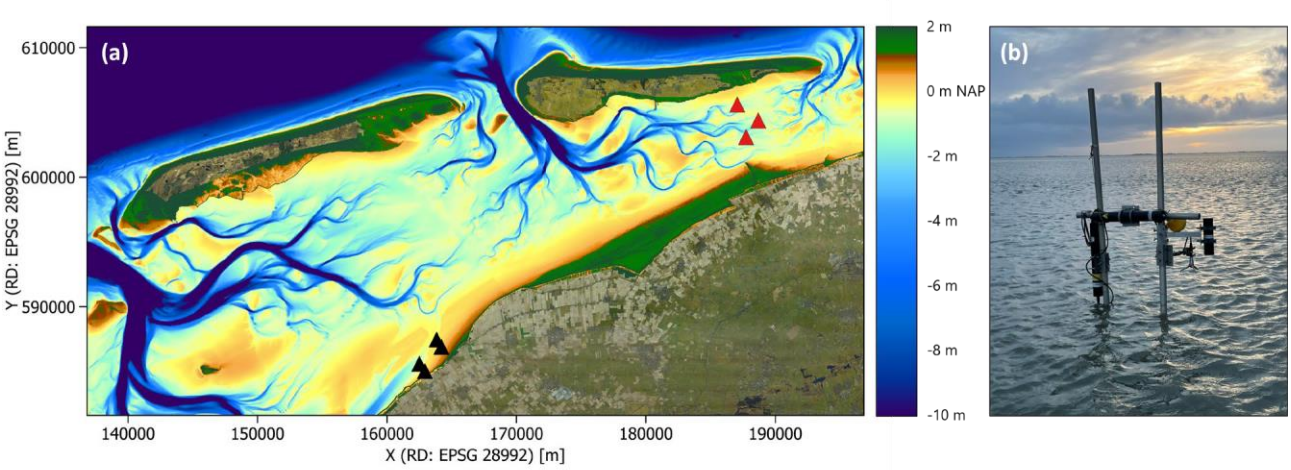

Figure 1: (a) Measurement locations at fringing tidal flats (black triangles) and at a tidal divide (red triangles) in the Dutch Wadden Sea, with the colormap showing the measured bathymetry relative to NAP (≈ MSL). (b) Measurement frame with ADV and EchoSounder instruments at the tidal divide during low water.

[1] Delft University of Technology & Deltares, r.j.a.vanweerdenburg@tudelft.nl
[2] Delft University of Technology & Deltares, bas.vanmaren@deltares.nl
[3] Delft University of Technology, irene.colosimo.24@gmail.com
[4] Delft University of Technology, b.c.vanprooijen@tudelft.nl

Measurements of the hydrodynamic conditions (i.e. currents and waves) are used to determine the bed shear stresses at each of the locations. The OBS data and the ADV backscatter in the measurement volume (green box in Figure 2b) are used as measures for the sediment concentration. The reflection of the ADV signal onto the seabed (blue box in Figure 2b) is used to determine the bed elevation dynamics. The reflection of the acoustic signal onto multiple layers in the sediment bed suggests the presence of low-density deposits on top of a dense underlayer, which is yet to be investigated further by analysing the bed sediment samples that were collected during the field measurements.

Using the records of both the sediment concentrations and the bed elevation dynamics allows us to unravel the advective sediment transport and local water-bed exchange. The bed shear stresses and observed erosion rates are subsequently used to evaluate the erodibility of the mixed sediment bed at each of the locations.

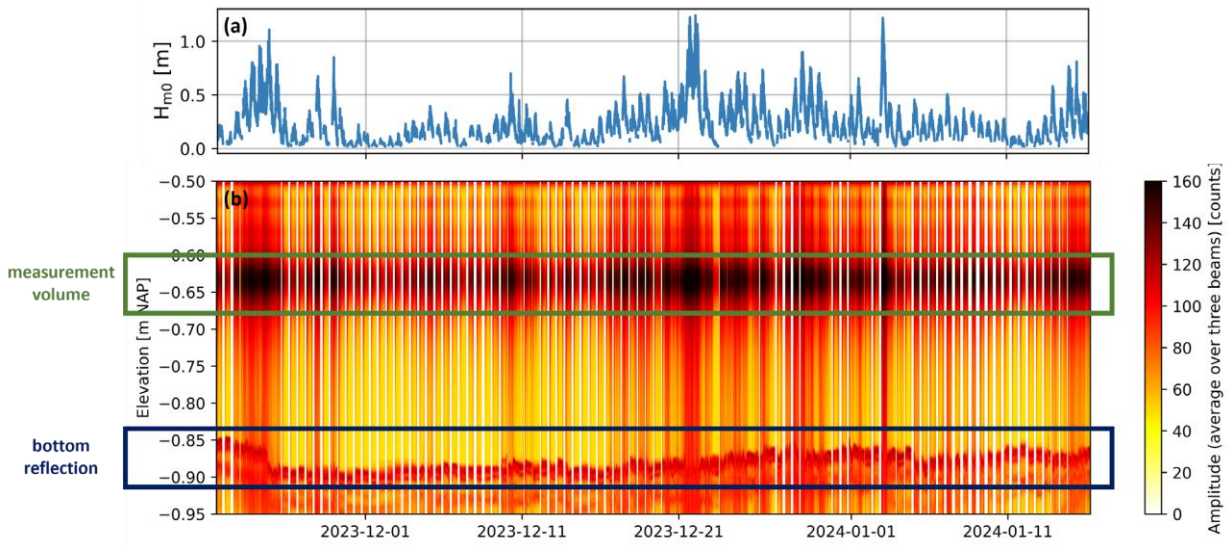

Figure 2: Timeseries of (a) significant wave height from ADV pressure measurements and (b) vertical profiles of the ADV backscatter (i.e. probe check data) at one of the measurement locations at the tidal divide. The amount of backscatter in the measurement volume (indicated by the green box) is used as a measure for the sediment concentration. The reflection of the acoustic signal onto the seabed (indicated by the blue box) reveals the bed elevation dynamics. Gaps in the H_{m0} timeseries and vertical white bars in the backscatter profiles indicate periods of low water, during which the ADV instrument emerged.

The field measurements at the fringing tidal flats reveal that the resistance against erosion increases significantly during periods of aerial exposure during low water. The development of strength of the bed is positively related to the duration at which the flats remain dry. The exposure time of the fringing tidal flats is strongly related to wind conditions (e.g. extended exposure during persistent winds from the landward direction), resulting in a strong correlation between the wind conditions and the ability of a deposit to withstand the next inundation period.

The field measurements at the tidal divide reveal erosion rates up to several centimeters during heavy winter storms with (significant) wave heights over 1.0 m (see Figure 2a) and orbital velocities near the bed of around 0.5-0.6 m/s. The bed elevation fluctuates within a range of roughly 5-10 cm during the 2 months of measurements. Although the hydrodynamic conditions were similar at the three measurement locations, the changes in bed elevation where relatively small at the location with the largest amount of fines in the sediment bed (i.e. the location for which the ADV signal is illustrated in Figure 2). We expect the mud fraction to not only increase the erosion threshold (the critical condition at which erosion starts), but also to limit the erosion rate as soon as the erosion threshold is exceeded.

We further explore the water-bed exchange at the two contrasting sites (i.e. in terms of sediment composition and aerial exposure duration) using a 1DV numerical model, from which we conclude that the strength development under aerated conditions is a very important aspect of sediment dynamics in muddy intertidal areas. At sandy intertidal areas, a small mud fraction in the bed already limits the erodibility of the sediment bed compared to a pure sandy bed.

Acknowledgement

This research is part of the WadSED project (Wadden Sea and Estuaries: system Dynamics and sediment management under climate change), which is (partly) financed by the Dutch Research Council (NWO). We gratefully acknowledge Rijkswaterstaat-CIV and Pieter van der Gaag and Arie van der Vlies of Delft University of Technology for their support during the field measurements in the Dutch Wadden Sea.

References

Colosimo, I., de Vet, P.L., van Maren, D.S., Reniers, A.J., Winterwerp, J.C. & van Prooijen, B.C. (2020). The impact of wind on flow and sediment transport over intertidal flats. Journal of Marine Science and Engineering, vol. 8 (11), 910.

Colosimo, I., van Maren, D.S., de Vet, P.L.M., Winterwerp, J.C. & van Prooijen, B.C. (2023). Winds of opportunity: The

effects of wind on intertidal flat accretion. Geomorphology, vol. 439, 108840.

Tracking extreme events and their impact on sediment dynamics at the interface between estuary and coastal sea

Verney R. [1], Poppeschi C. [2], and Charria G. [3]

Keywords: extreme events, waves, river flow, suspended sediment concentration, long-termtrend.

Abstract

The latest Intergovernmental Panel on Climate Change report of 2023 alerts about an increase in the occurrence and intensity of extreme hydro-meteorological events such as storms and extreme river flows, i.e. drought and floods. Investigating the occurrence of these extreme events in the past 15 years and their impacts on sediment dynamics will provide crucial knowledge for anticipating future trajectories of coastal ecosystems.

In this study, we investigate the occurrence of extreme wave and river flow events (from 2006 to 2022) and their impact on suspended sediment concentration at the mouth of the Seine Estuary. Daily river flow data are available from hydro.eaufrance.fr and interpolated at each high tide (Q), while hourly wave orbital velocity data are extracted close to the SCENES station from WW3 model hindcast data (marc.ifremer.fr). Wave orbital velocity data are reduced at the tidal scale by calculating the percentile 90 per tide (HsP90). Suspended particulate matter concentration (SPMC) are available every 30min at the surface and close to the bed from 2015 to 2022 at the SCENES station, located at the mouth of the Seine Estuary (Verney et al., 2024a; Verney et al., 2024b). The raw high frequency signal is detrended from the tidal dynamics by removing a climatologic tidal signal per tidal range classes in absence of wave, as described in Verney et al (2024b) and providing SPMC anomalies. This allows to better examine the influence of wave and river flow events.

In this study, an extreme event is identified using the peak over threshold method. An inter-annual climatology for Q and HsP90 is calculated over the period 2006-2021, and smoothed using a percentile 90 over a 30-day rolling window. Hence extreme wave or river flow events correspond to HsP90 or Q values exceeding the smoothed climatology threshold. This method not only considers the highest peaks in signal, mainly in winter, but allows to track extreme events all over the year, accounting for the seasonal variability in forcings. The same method is applied to the SPMC anomaly time series to detect extreme event in surface and bottom SPM signals.

From 2006 to 2022, 211 extreme wave events and 20 extreme river flow events are detected (Figure 1). Extreme river flow events show a marked seasonality, with the most intense events in winter (Q>1100m3/s) and moderate events in summer (Q>800m3/s). In general, the stronger the river flow event, the longer, even if short but high intensity extreme river flow events are observed. An exceptional intense extreme river flow event was recorded in June 2016, reaching 2000m3/s while the average river flow discharge for this period is lower than 400m3/s. Similarly to river flow, wave extreme events are featured by a strong seasonality, with stronger peaks in winter. Most of the events are short (from 2 to 4 tides). These extreme events, especially wave events, are associated with a peak in SPMC anomaly (both surface and bottom), but only 60% correspond to an extreme SPM value. These mismatches are observed in winter, during high intensity wave events, that could be explained by less fine sediment on the seabed, washed out by preceding events.

The response of SPMC anomaly to extreme events is stronger (on average) in winter but the impact on the estuarine system must be examined in comparison of the monthly average SPMC anomaly (Figure 2). In winter, wave events induce bottom SPMC anomalies that range from 0.025 to 0.15g/l while the monthly interannual percentile 90 of SPMC anomaly reaches 0.08g/l, i.e. only 2 times larger. In summer, SPMC anomalies associated with extreme wave events reach 0.02 to g/l while the interannual percentile 90 over this period reaches 0.015g/l, corresponding up to 4 times the interannual value. We can then conclude that extreme events in atypical, summer periods, are relatively more impacting than in winter.

Finally, we examined the long-term evolution of extreme river flow event over the last 60years. Recalculating the interannual percentile 90 threshold over this period, we observed a significant increase in both extreme event occurrences and intensity between 1962-1981 (22 events) and 2001-2021(40 events). Also the number of short extreme event (<20days) increased when comparing the two periods. Investigating further the seasonality of these extreme river flow events, we observed similar patterns of extreme records in winter and summer. Interestingly, significant differences are reported in spring for high intensity events (Q>900m3/s) : no extreme events were detected in 1962-1981, while 7 were observed in April/early May in 1982-2001 and 5 in May/June in 2002-2021. This time shift during the spring period is highly impacting as occurring in periods of lower river flow, hence generating potentially higher gradients in SPMC at the estuary/sea interface with possible stronger impacts on the ecosystem.

[1] Ifremer, DYNECO/DHYSED, CS10070, 29280 Plouzané, France, romaric.verney@ifremer.fr.
[2] LOPS, Ifremer, Univ. Brest, CNRS, IRD, CS10070, 29280 Plouzané, France, coline.poppeschi@ifremer.fr
[3] LOPS, Ifremer, Univ. Brest, CNRS, IRD, CS10070, 29280 Plouzané, France, guillaume.charria@ifremer.fr

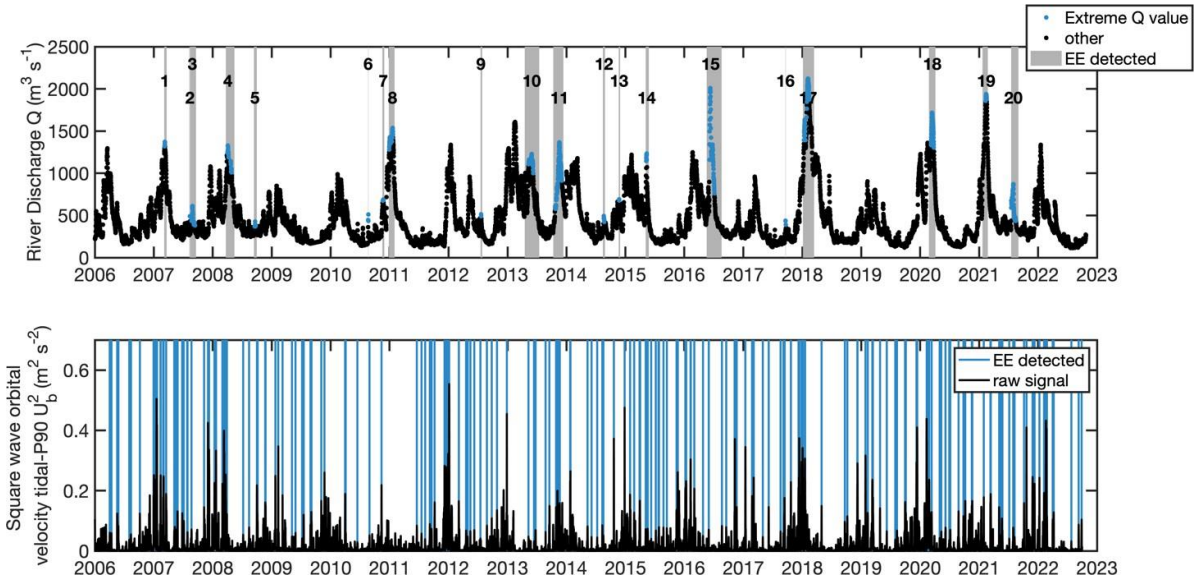

Figure 1: Extreme forcing events from river flow (extreme values in blue points, extended extreme period in grey on top figure) and square wave orbital velocity (blue lines on bottom figure).

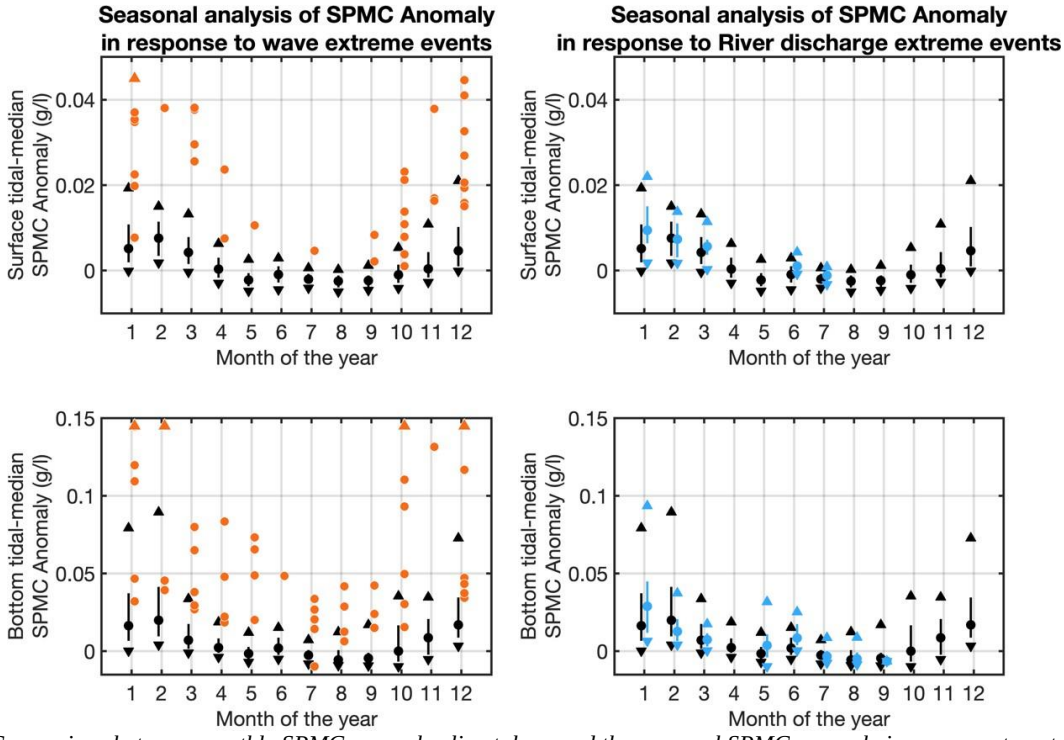

Figure 2: Comparison between monthly SPMC anomaly climatology and the seasonal SPMC anomaly in response to extreme events. Left: wave events, Right: river flow events. Top panel: surface, Bottom panel: bottom. Climatology anomalies are represented by black markers and lines: circles show the monthly median anomaly, lines indicate the percentile 25 and 75, up and down triangles the percentile 90 and percentile 10 respectively. Orange circles represent event-average tidal-median SPMC anomalies. Up orange triangles indicate high SPMC anomalies above 0.05 and 0.15g L^{-1} for surface and bottom data respectively. Blue markers and lines indicate the monthly distribution of SPMC anomalies during extreme river flow events (similarly to SPMC anomalies)

References

Verney R., Le Berre D., Repecaud M. (2024a). COAST-HF - SCENES station dataset from 2015 to 2022 - environmental parameter, SEANOE https://doi.org/10.17882/99434

Verney R., Le Berre D., Repecaud M., Bocher A., Bescond T., Poppeschi C., Grasso F. (2024b) Suspended particulate matter dynamics at the interface between an estuary and its adjacent coastal sea: Unravelling the impact of tides, waves and river discharge from 2015 to 2022 in situ high-frequency observations, Marine Geology,107281,ISSN 0025-3227, https://doi.org/10.1016/j.margeo.2024.107281.

Annual tracking of the sediment dumped following harbour dredging activities in the internal and external estuary of the Loire

Walther R. [1], Isserty G. [2], and Bertrand O. [3]

Keywords: estuaries, dredging activities, Loire

Abstract

Supervised by the Loire Estuary Public Interest Group (GIPLE), several 3D models were built and calibrated to provide answers at the scale of the estuary, for several physical processes: hydrodynamics conditions, dynamics of mud, water quality, dumping and dredging operations. These models take full advantage of the TELEMAC system modules and demonstrates their ability to provide good results at a large scale despite complex processes. This paper presents in the first part the building and calibration steps for two of the models developed: the hydrosedimentary model with dredging processes, and the local dumping model before these two models are unified. The second part focuses on the operating strategy and exploitation of the model for the harbour of Nantes Saint-Nazaire, to estimate the hydrosedimentary impact of sediment discharges from harbour dredging activities over a year.

The Loire estuary is one of the three major French estuaries. It is a macro-tidal estuary with a mean spring tidal range of about 5 m allowing the tide to propagate up to Ancenis, 90 km upstream from the mouth (Saint-Nazaire). The water quality of the estuary is considered as relatively bad with a large maximum turbidity due to significant developments over the two last centuries including a deep-water port development downstream in the Saint-Nazaire area with an outer navigation channel down to -12.5m Chart Datum and the creation of a unique inner navigation channel at -5m CD up to the city of Nantes located 55 km upstream from Saint-Nazaire. Large scale hydrosedimentary modelling can be a great decision-making tool for any stakeholder in such estuary, whether it is to properly manage the cities drinking water supply, to assess the filling rate of navigation channels… The global model was calibrated for each of the main processes that occur in the estuary (water level, waves, salinity, suspended sediment concentration SSC)

First part: building and calibration

The graph on the left of the Figure 1 shows the annual dynamic of SSC inside the inner estuary. The maximum turbidity signal corresponds well to the one observed in situ. When the flowrate of the river Loire is important, the maximum of turbidity and the fluid mud are contained below the kilometric point 25, and when it is very low, it can reach up to Mauves (kilometric point 70). Model results are also compared to several SYVEL (continuous measurement network) gauge stations measurements of the SSC. The three stations presented in the right of the Figure 1 show different modelled and measured SSC dynamic depending on longitudinal locations.

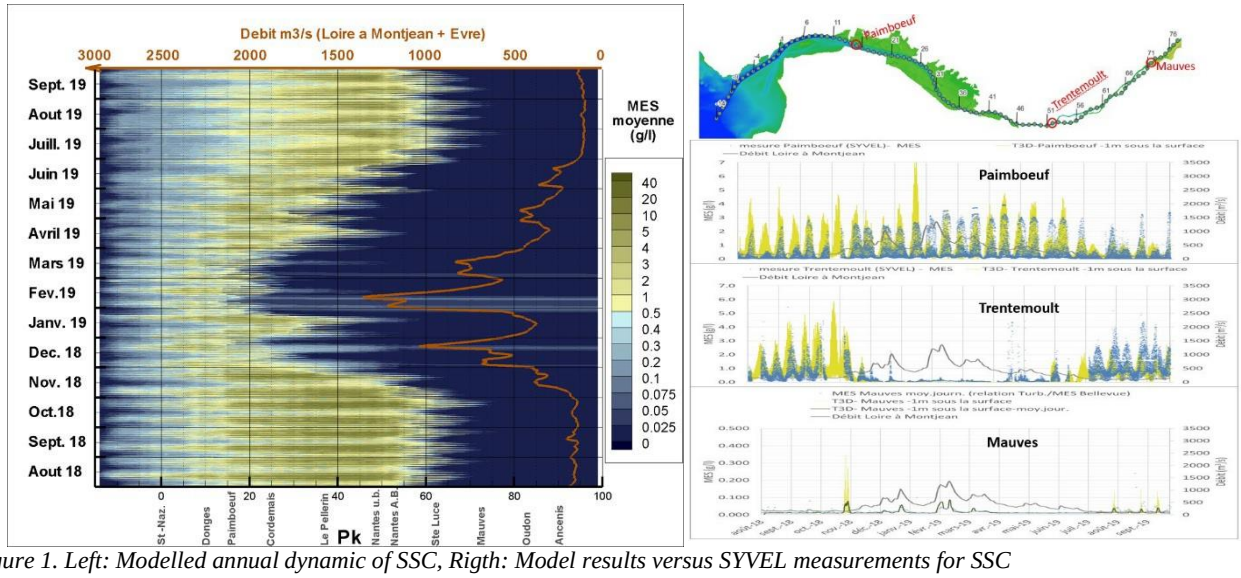

Figure 1. Left: Modelled annual dynamic of SSC, Rigth: Model results versus SYVEL measurements for SSC

[1] Artelia, regis.walther@arteliagroup.com
[2] Artelia, guillaume.isserty@arteliagroup.com
[3] Artelia, olivier.bertrand@arteliagroup.com

The local model of the Lambarde dumping site is calibrated over around 10 years, from September 2011 to October 2021. The main objective of this local model is to reproduce the global evolution of the site, with good correlation between model and measurements as far as volume is concerned. The model properly reproduces both the temporal evolution of the global volume of the mud deposition on the area (Figure 2 on the left), and the temporal evolution of the mean elevations for every sub-zone (Figure 2 on the right). As far as elevations are concerned, a good calibration shows the capability of the model to reproduce the spreading of the deposit, and the erosion flux during period where no dumping is done.

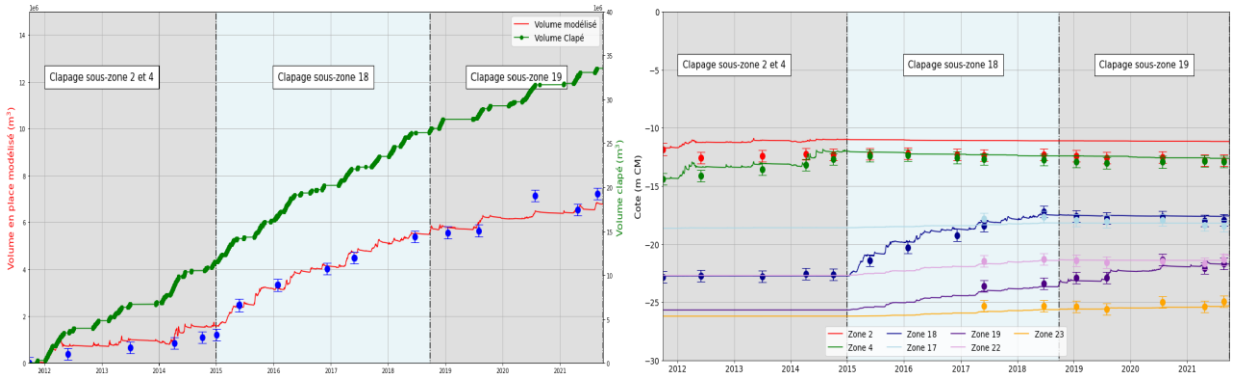

Figure 2. Left: Calibration result for in-place volume – Model in red line, dumped volume in green line and in-place volume data in blue dots; Right: Calibration results for mean elevations. Model in plain lines and data in dots.

<u>Second part: Annual tracking of the sediment dumped following harbour dredging activities in the internal and external estuary of the Loire</u>

A dredged navigation channel supplies Saint-Nazaire Harbor at the mouth of the estuary and Nantes Harbor 55 km upstream. Over one year on average:

- 3.64 million m^3 are dredged and dumped in the disposal area of The Lambarde in the external estuary,
- 0,3 million m^3 are dredged with a stationary dredge and discharges in the navigation channel.
- 1,5 million m^3 are dredged with water injection.

The harbour wishes to upgrade its dredging facilities, which would change the volume distribution between them. To estimate the current impact of its dredging practices and to establish a baseline to study other practices, the model is exploited to calculate the annual mass balance of the estuary of what is currently dredged. Unlike previous versions of the TELEMAC hydrosedimentary module, GAIA makes it possible to differentiate the sediment of the Lambarde from those in the natural estuary. It is therefore possible to quantify suspended concentrations and deposits according to their origin, at any time and in any place. The storage of all the results over one year allowed many analyses and in particular a mapping of the percentiles of SSC resulting from the dispersion of sediments from the Lambarde.

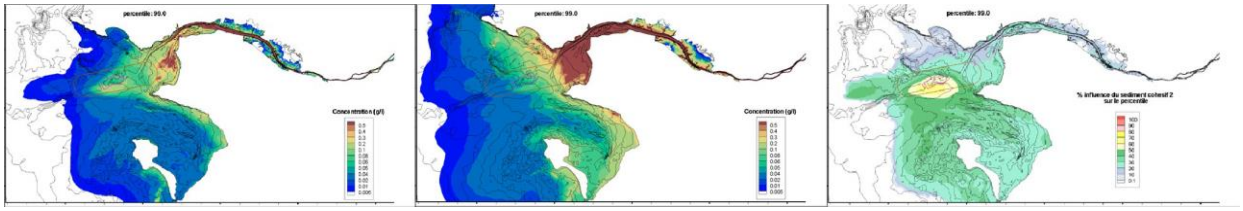

Figure 3. Percentile 99 of the SSC at each point (left: sediment from the Lambarde; middle: sediment from the estuary and right: percentage of influence of sediment from the Lambarde on percentile 99 of the SSC

Despite all these technical advances, it remained difficult to establish a clear impact in a simple way. Is the notion of impact always realistic over a long period of time? Part of the dumped sediment replaces (by tidal pumping) estuarine sediment in the maximum turbidity and then follows a natural estuarine dynamic. An additional calculation without dredging would certainly be necessary in order to fully answer the questions.

Mass balance calculation at the estuary scale have been made, but the results are very sensitive to the start and end dates of the analysis and the location of the downstream boundary. These balances therefore depend in particular on a hydrosedimentary history, a hydro-meteorological forcing and a geographical position of downstream boundary and can be discussed.

What drives salt intrusion in a low-lying river delta during an exceptional drought?

Wegman T.M. [1], Pietrzak J.D. [2], Horner-Devine A.R. [3], Dijkstra H.A. [4], and Ralston D.K. [5]

Keywords: estuaries, salt intrusion, droughts.

Abstract

Estuaries face aggravated susceptibility to salt intrusion during times of reduced river flow. Climate change will aggravate the frequency and intensity of salt intrusion events due to the increase in drought frequency and sea level rise. This poses a growing challenge for low-lying delta regions, typically densely inhabited and reliant on freshwater resources.

This study aims to investigate the response of a low-lying river delta, which behaves as a salt wedge estuary to river discharge, coastal set-up, and tidal range during a prolonged drought. We analysed an extensive dataset, collected in the Rhine-Meuse Delta, spanning a period of 17 weeks during the drought of 2022 in the Netherlands (Figure 1).

During the field campaign, the Rhine discharge remained below the seasonal 2nd percentile for 53 consecutive days, classifying as an exceptional drought (see Figure 2). One defining feature of this delta is its numerous branches and a complicated, human-controlled discharge network.

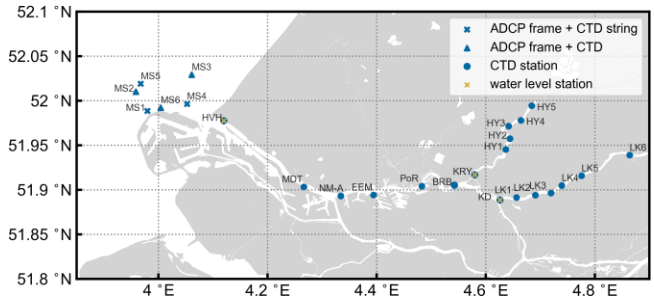

Figure 1 Overview of the measurement locations in the Rhine-Meuse Delta.

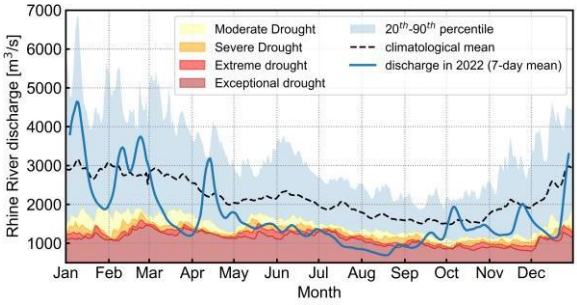

Figure 2 The Rhine River discharge in 2022, showing the mean and 20-90 percentile range for the climatological period (1992-2021), as well as different drought indications.

Observations in a period of low river flow show that the Rhine River discharge is a good overall indicator for salt intrusion length (Figure 3). Coastal set-up is an important secondary effect, moving the tidally averaged salinity limit upstream and downstream during surge events on timescales of 1.5 to 6 days (Figure 4). The combined effect of river discharge and coastal set-up is evident in the relation between the subtidal barotropic pressure gradient between the mouth and an upstream water level station. The salinity intrusion speed of $L2$ is closely related to the rate of change of subtidal water levels at the mouth. Within one event $L2$ can move up to 6.2 km upstream and up to 12.5 km downstream. This is of order magnitude of the tidal excursion length which is estimated to be 8.5 km. During these events $L2$ reaches a maximum 'event-average' speed of 7.4 km/day, and tidally averaged speeds reach up to 4.25 km/day.

[1] Delft University of Technology, t.m.wegman@tudelft.nl
[2] Delft University of Technology, j.d.pietrzak@tudelft.nl
[3] University of Washington, arhd@u.washington.edu
[4] Utrecht University, h.a.dijkstra@uu.nl
[5] Woods Hole Oceanographic Institution, dralston@whoi.edu

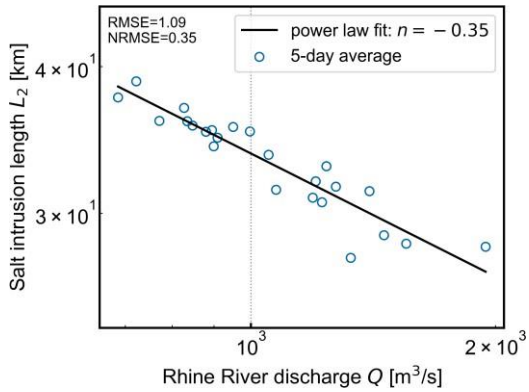

Figure 3 Discharge dependence of salt intrusion, the black lines indicate the best power law fit. The Rhine River discharge versus salt intrusion length for a 5-day average.

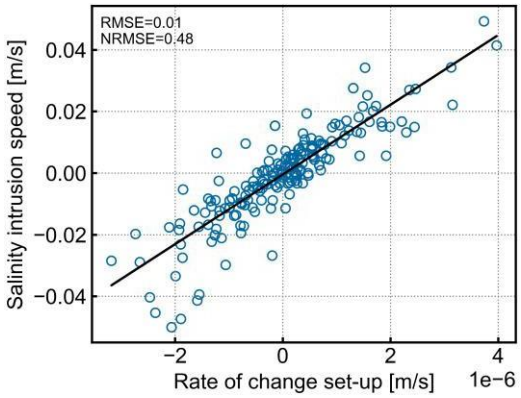

Figure 4 Coastal set-up dependence of salt intrusion length the tidally averaged rate of change of subtidal water level at Hoek van Holland versus salinity intrusion speed.

The salt intrusion length in the upstream side branches is best predicted by salinity at the mouth of the branches, rather than discharge through those branches (see Figure 5). In contrast to the overall system, there is no power law applicable between salt intrusion length and discharge through those branches. This can be explained by the fact that the discharge through those branches Q_{branch} is determined by human controls along the river branch and these total discharges are one to two order magnitude(s) smaller than the Rhine River discharge. However, the salinity intrusion speed of the very low salinity limit ($L_{0.3}$), also referred to as the salinity intrusion speed , is affected by the discharge, and can be described by , see Figure 6.

$$\Delta t \qquad A$$

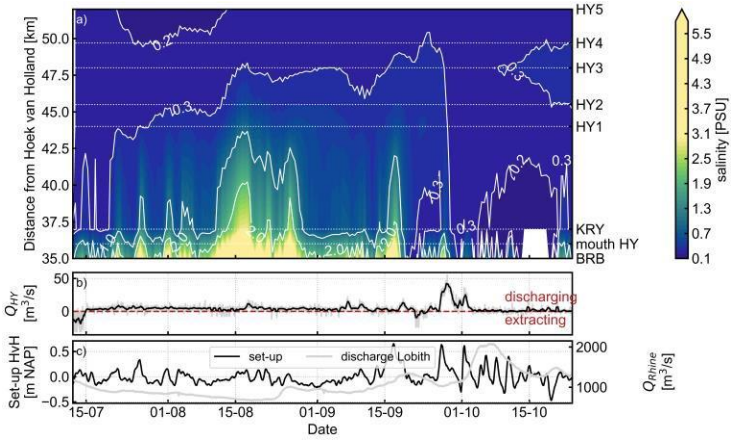

Figure 5 Salinity contours in de Nieuwe Maas and Hollandsche IJssel, between salinity stations BRB and HY5. including a) salinity contours, b) discharge through the Hollandsche IJssel, where positive values represent a net freshwater discharge on the branch, and negative values net extractions from the branch c) set-up in metres NAP (Normaal Amsterdams Peil) at Hoek van Holland and Rhine River discharge.

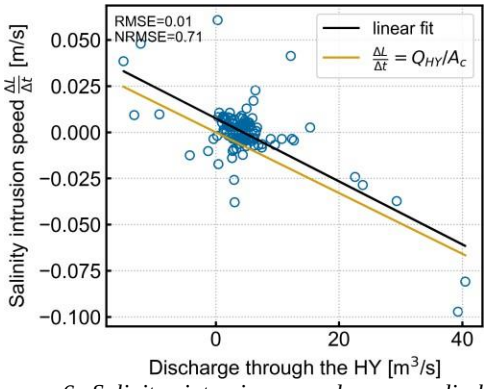

Figure 6 Salinity intrusion speed versus discharge through the mouth of the river branch.

On long timescales, the discharge is the main driver for salt intrusion length in the stratified Rhine-Meuse estuary. Nonetheless, significant intrusion events occur on shorter timescales, spanning from a day to a week, driven by subtidal fluctuations of water level at the river mouth. Upstream side-branches show different response to the main system, as the discharge is highly influenced by managed freshwater pulses and extractions. Here, the role of the discharge is seen in flushing and sucking saline waters downstream and upstream the branches. The future outlook is to examine the influence of the Rhine River plume dynamics on salt intrusion, where also baroclinic effects of wind-forcing will be taken into account.

Impact of climate change on compound-flooding in UK estuaries

Wei X. [1], Payo A. [2], Xu Y. [3], and Amoudry L. [4]

Keywords: flood risk, climate change, UK estuaries, semi-analytical modelling.

Abstract

Estuarine flooding is at the forefront of coastal management concerns and climate mitigation strategies. Estuarine flooding often stems from compound events with inundation resulting from a combination of fluvial/terrestrial and marine sources. Coastal management and climate mitigation strategies are implemented at both estuary-specific scales and national/regional scales. While scientific evidence for individual estuaries can be derived from climate projections downscaled to the estuary scale, comprehensive evidence at the national/regional scale for groups of estuaries is limited. This scarcity is partly caused by the prohibitive cost associated with downscaled projections at this broader scale.

Our research explores the potential effects of climate change on compound flood hazard in UK estuaries. We have categorized UK estuaries into distinct typologies based on marine and terrestrial forcings (e.g., tides, storms, river flow, sea level rise), and estuarine characteristics such as geographical locations, coastline features, catchment size, and estuary shape. This categorization is achieved through a cluster analysis of data gathered from published/gray literature, satellite imagery, and completed numerical simulations, including climate projections of riverine (eFLaG, see Hannaford et al., 2023) and marine forcing conditions (e.g., UKCP18, see Lowe et al., 2022). For each estuary type, we have identified and categorized the patterns of future changes in dominant physical forcings. We then used a simplified, idealized semi-analytical models to investigate how these changes in forcings could potentially modify flood risks in the various estuary types. This model, which is an extension of the work of Wei et al. (2016), incorporates changes in water motion induced by storms and river discharge. The model is computationally efficient and can qualitatively simulate complex hydrodynamic processes such as tidal propagation and storm surge dynamics, therefore ideal for exploring sensitivity of flood risks to changes in forcing and estuarine characteristics representative for each of the estuary types. The results of this study provide valuable insights into the potential impacts of climate change on compound flooding hazards in UK estuaries. They emphasize the importance of incorporating climate projections into flood risk assessments and demonstrate the effectiveness of simplified numerical models in understanding climate risks to estuaries at a national scale. This research contributes to ongoing efforts to comprehend the vulnerability of UK estuaries to compound flood hazards and aids in the development of holistic strategies for managing estuarine flood risks in a changing climate.

References

Hannaford, J., Mackay, J. D., Ascott, M., Bell, V. A., Chitson, T., Cole, S., Counsell, C., Durant, M., Jackson, C.R., Kay, A.L. and Lane, R.A. (2023). The enhanced future Flows and Groundwater dataset: development and evaluation of nationally consistent hydrological projections based on UKCP18. Earth System Science Data, 15(6), 2391-2415.

Lowe, J.A., Bernie, D., Bett, P., Bricheno, L., Brown, S., Calvert, D., Clark, R., Eagle, K., Edwards, T., Fosser, G. and Fung, F. (2018). UKCP18 science overview report. Met Office Hadley Centre: Exeter, UK, pp.1-73.

Wei, X., Schramkowski, G. P., & Schuttelaars, H. M. (2016). Salt dynamics in well-mixed estuaries: Importance of advection by tides. Journal of Physical Oceanography, 46(5), 1457-1475.

[1] National Oceanography Centre, Liverpool, United Kingdom, xwei@noc.ac.uk
[2] British Geological Survey, Keyworth, United Kingdom, agarcia@bgs.ac.uk
[3] The National Key Laboratory of Water Disaster Prevention, Hohai University, Nanjing, China, yanwenxu@hhu.edu.cn
[4] National Oceanography Centre, Liverpool, United Kingdom, laou@noc.ac.uk

Turbulent Dissipation Inside the Wave Boundary Layer

Wheeler D.C. [1,2], Giddings S.N. [1], Merrifield M. [1], and Pawlak G. [1,3]

Keywords: estuaries, IG waves, turbulence.

Abstract

Recently, researchers have shown that infragravity (IG) frequency oscillations (periods of about 25 s to 250 s) are important in sediment transport and closure processes for shallow estuarine mouths located in the surfzone (for example, see Mendes et al. 2020). Other studies have also shown that shallow estuarine mouths can act as low-pass frequency filters, leading to oscillations within estuaries dominated by IG frequencies with velocity amplitudes as large as tidal velocities (for example, see Williams and Stacey 2016). Such large velocity amplitudes suggest that IG oscillations likely play an important dynamical role. However, few studies to date have examined the effects of IG waves within shallow estuaries outside of sediment transport, nor have they discussed dynamical mechanisms for their contribution to sediment transport.

This study focuses on how IG waves affect bottom boundary layer generated turbulence in shallow estuaries. Turbulence is the primary mechanism through which IG waves can increase mixing. Turbulence parameters can also be directly related to the bottom stress, which plays an important role in sediment suspension and transport. Therefore, by understanding how IG waves interact with tides and other processes to increase turbulence, we can determine when IG waves are likely to be dynamically important. Specifically, we use turbulent dissipation measurements obtained from recent work (Wheeler and Giddings 2023) to examine how and when IG waves significantly increase turbulence levels in Los Peñasquitos Lagoon. Los Peñasquitos Lagoon is a low-inflow, bar-built estuary in Southern California with a mouth that has been heavily modified due to the presence of a road. The shallow sill at the mouth is typically above sea level at low tide, while most of the estuary interior is around 2-m deep or less. When submerged, the shallow sill acts as a low pass frequency filter where larger sea and swell waves dissipate in the surfzone while IG waves propagate into the estuary, often with large orbital velocities relative to the tidal velocities (Harvey et al. 2023).

Using our turbulent dissipation observations, we show that these IG oscillations lead to wave boundary layers up to the order of 1m that can occupy significant portions of the water column in shallow estuaries. To understand observations of bottom generated turbulence in this situation, we outline 3 distinct frequency regimes. The low frequency (LF) regime describes when velocities are quasi-steady, as is typically true for tidal currents where a fully developed boundary layer extending throughout the water column exists. The high frequency (HF) regime describes when observations are far above the wave boundary layer, as is typically true for measurements of sea/swell waves where the wave boundary layers are very small, on the order of mm to cm. The intermediate frequency regime (IF) describes measurements that are within the wave boundary layer and wave velocities cannot be treated as pseudo- steady. A sketch of these regimes under different wave conditions is shown in Figure 1 along with a boundary layer length scale (l_w) and the boundary layer height ($z_w=4*l_w$).

We then evaluate the behavior of turbulence in the IF regime using an idealized, numerical, 1-dimensional, eddy viscosity turbulence model. We show that the average turbulent dissipation over a wave period in the IF regime can be approximated as an exponential decay between the LF regime at the bottom of the water column and the HF regime at the top of the wave boundary layer. The numerical model shows a scaling for the wave boundary layer height that matches prior work and extends to cases where wave velocities are greater than the mean current.

To apply this approximation to observations, we extend the Grant and Madsen (1979) solution to calculate the time dependent bottom stress, which is necessary for calculating the bottom boundary condition for the IF regime. We then apply the IF region approximation to our observations in Los Peñasquitos Lagoon to show that it accurately explains our turbulent dissipation measurements 30cm above the bottom. Our data then suggests that waves significantly increase turbulent dissipation inside the wave boundary layer when $\bar{u}/\sigma_u < 3/2$, where $\bar{u}$ is the mean current and σ_u is the standard deviation of the velocity.

[1] Scripps Institution of Oceanography, University of California, San Diego, 92093, USA

[2] dcwheele@ucsd.edu

[3] Department of Mechanical and Aerospace Engineering, University of California, San Diego, 92093, USA

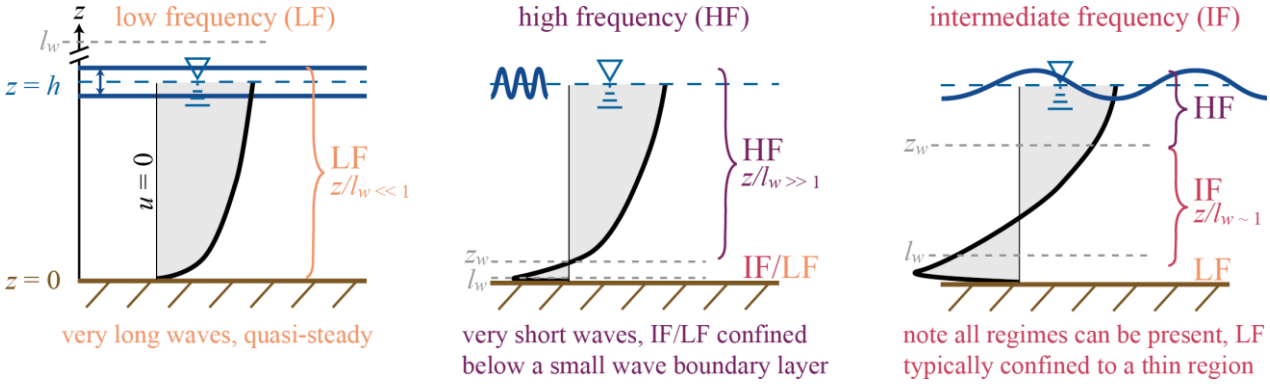

Figure 1. Diagram of velocity profiles and the depth regions of the 3 frequency regimes under tidal (left, low frequency), sea (middle, high frequency), and infragravity (right, intermediate frequency) waves. The lower and upper dashed grey lines represent the boundary layer length scale (l_w) and boundary layer height (z_w) respectively.

References

Grant, W.D., Madsen, O.S. (1979) Combined wave and current interaction with a rough bottom. Journal of Geophysical Research: Oceans, 84(C4), 1797-1808. https://doi.org/10.1029/JC084iC04p01797

Harvey, M.E., Giddings, S.N., Pawlak, G., Crooks, J. (2023) Hydrodynamic variability of an intermittently closed estuary over interannual, seasonal, fortnightly and tidal timescales. Estuaries and Coasts, 46, 84-108. http://doi.org/10.1007/s12237-021- 01014-0

Mendes, D., Fortunato, A.B., Bertin, X., Martins, K., Lavaud, L., Silva, A.N., Pires-Silva, A.A., Coulombier, T., Pinto, J.P. (2020) Importance of Infragravity waves in a wave-dominated inlet under storm conditions. Continental Shelf Research, 192, https://doi.org/10.1016/j.csr.2019.104026Wheeler, D.C., Giddings, S.N. (2023) Measuring turbulent dissipation with acoustic doppler velocimeters in the presence of large, intermittent, infragravity frequency bores. Journal of Atmospheric and Oceanic Technology, 40, 285-304. https://doi.org/10.1175/JTECH-D-21-0144.1

Williams, M.E., Stacey, M.T. (2016) Tidally discontinuous ocean forcing in bar-built estuaries: The interaction of tides, Infragravity motions, and frictional control. Journal of Geophysical Research: Oceans, 121(1), 571-585. https://doi.org/10.1002/2015JC011166

Simulating algal species competition in the Sacramento-San Joaquin Delta using an idealized one-dimensional model

White S. [1], Bouma-Gregson K. [2], and Stacey M. [3]

Keywords: physics, ecology, turbulence, numerical modelling, phytoplankton

Abstract

Maximizing time in the photic zone is a critical component dictating the success of an algal species. However, access to the photic zone is complicated by factors like stratification and turbulent mixing. Some algal species (diatoms) have compensated for their limited time in the photic zone by maximizing growth rate, such that when they are in the photic zone they can synthesize carbon as quickly as possible. However, diatoms cannot swim—instead, they sink downward with a slight negative buoyancy. Other species of algae (cyanobacteria) have developed vacuoles that allow for positive buoyancy, but these species tend to have lower growth rates, and their vertical velocities are easily overpowered by vertical mixing.

There is a strong interest from both scientific and management perspectives in understanding what factors dictate the dominance of cyanobacteria, a harmful algal species, over diatoms, which are often beneficial to estuarine ecosystems. This question is especially at play in the Sacramento-San Joaquin Delta, a highly engineered estuary in Northern California. The Delta receives large inputs of anthropogenic nutrients from wastewater treatment plants which result in elevated dissolved inorganic nitrogen levels (Novick et al., 2015), placing the estuary at a high risk for algal blooms (Paerl, 2012; Dahm et al., 2016) including risk for bloom events with toxic algal species (commonly referred to as harmful algal blooms (HABs)). Historically, despite elevated nutrient levels, the Delta has experienced limited bloom activity compared to other estuaries. Low algal concentrations are commonly attributed to high turbidity levels and/or top-down control from invasive filter feeders. In recent years, these strong defenses have begun to wane, resulting in increased harmful algal bloom events (Lehman et al., 2017). Lehman et al. (2008) used statistical methods to derive correlations between these harmful algal events and factors like warm surface water temperature and high residence times; however, questions remain on the mechanisms through which these factors enable cyanobacteria to dominate over diatoms.

For our work, we explored the physical mechanisms dictating competition between diatoms and harmful cyanobacteria by simulating the two species in an idealized one-dimensional water column model. Specifically, we investigated the hypothesis set forth by Huisman et al. (2004) that the magnitude of turbulent dissipation determines regimes shifts between sinking and floating species of algae. We based our idealized model on the Stockton Shipping Channel in the Sacramento-San Joaquin Delta, a 10-meter deep regularly dredged channel that has routinely experienced harmful algal blooms throughout the past decade.

We simulated a three-day period and sampled growth, loss, and swimming rates from empirical estimates from literature to parametrize population dynamics. Our results focus on how the final biomass of an algal species varies as a function of turbulent dissipation, stratification, and initial concentration. We also investigated how the phasing of temporal forcings, such as simulated tides and diurnal wind, affected a species' dominance by determining access to the photic zone. In our discussion, we review future steps, including how this work will be validated by planned fieldwork and methods to integrate our modeling approach into a large-scale three-dimensional model of the Sacramento-San Joaquin Delta with hopes to enable forecasting of future harmful algal bloom events.

References

Dahm, C. N., A. E. Parker, A. E. Adelson, M. A. Christman, and B. A. Bergamaschi. "Nutrient Dynamics of the Delta: Effects on Primary Producers." *San Francisco Estuary and Watershed Science* 14, no. 4, 1-36 (2016). https://doi.org/10.15447/sfews.2016v14iss4art4.

Huisman, J., J. Sharples, J. M. Stroom, P. M. Visser, W. E. A. Kardinaal, J. M. H. Verspagen, and B/ Sommeijer. "Changes in Turbulent Mixing Shift Competition for Light Between Phytoplankton Species." *Ecology* 85, no. 11 (2004): 2960–70. https://doi.org/10.1890/03-0763.

Lehman, P. W., G. Boyer, M. Satchwell, and S. Waller. "The Influence of Environmental Conditions on the Seasonal Variation of Microcystis Cell Density and Microcystins Concentration in San Francisco Estuary." *Hydrobiologia* 600, no. 1 (March 1, 2008): 187–204. https://doi.org/10.1007/s10750-007-9231-x.

Lehman, P. W., T. Kurobe, S. Lesmeister, D. Baxa, A. Tung, and S. J. Teh. "Impacts of the 2014 Severe Drought on the Microcystis Bloom in San Francisco Estuary." *Harmful Algae* 63 (March 1, 2017): 94–108. https://doi.org/10.1016/j.hal.2017.01.011.

[1] University of California, Berkeley; siennaw@berkeley.edu
[2] United States Geological Survey
[3] University of California, Berkeley; mstacey@berkeley.edu

Novick, E., Holleman, R., Jabusch, T., Sun, J., Trowbridge, P., Senn, D., Guerin, M., Kendall, C., Young, M. and Peek, S. “Characterizing and quantifying nutrient sources, sinks and transformations in the Delta: synthesis, modeling, and recommendations for monitoring.” *San Francisco Estuary Institute, Technical Report*. (December 2015).

Paerl, H. W., and V. J. Paul. “Climate Change: Links to Global Expansion of Harmful Cyanobacteria.” *Water Research*, Cyanobacteria: Impacts of climate change on occurrence, toxicity and water quality management, 46, no. 5 (April 1, 2012): 1349–63. https://doi.org/10.1016/j.watres.2011.08.002.

River plume and internal wave dynamics in a Patagonian fjord

Williams M.E. [1], Escauriaza C. [2], Fringer O. [3], WinklerPrins L. [4], Monasterio M. [5], and Gomez R. [6]

Keywords: fjord, river plume, internal waves.

Abstract

The Patagonia region in southern Chile, characterized by its complex geography with mountains, fjords, and glaciers, is also home to diverse ecosystems and coastal wildlife. Rivers fed predominantly by glaciers in summer and cold storms in winter transport sediments, freshwater, and nutrients to the fjords. Internal waves are ubiquitous in stratified fjord environments, and surface signatures of internal waves are observed on a range of spatial scales (e.g. Figure 1). In large river plumes, internal waves are generated at the plume front when velocity of propagation of the front falls below the internal wave phase speed (Nash and Moum, 2005). Here we aim to extend our knowledge of plume and internal wave dynamics in smaller glacial river plumes in steep watersheds through in situ measurements, remote sensing, and numerical modeling.

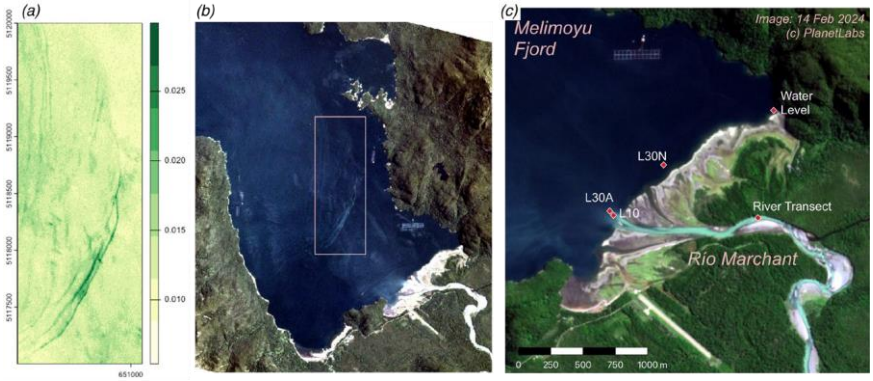

Figure 1. (a) Green reflectance values from satellite image. (b) Satellite image showing surface signatures of internal waves. Rectangle corresponds to area showin in (a). (c) Mooring locations for January – February 2024 field study. Image shows low tide on 14 February 2024. Measurements in Figure 2 below are at location L30A.

In this work, we are using the Melimoyu fjord in southern Chile (44º05'S, 73º06'W) as a representative system. A field campaign during January and February 2024 measured river, fjord, and plume dynamics with in situ measurements of velocity, temperature, salinity, water level (Figure 1c) complemented with drone imagery. Numerical simulations on an idealized boundary condition and domain with dimensions based on the field site can represent the basic river-fjord interactions and internal wave motions. We perform simulations in SUNTANS (Fringer et al., 2006), solving the 3D nonhydrostatic Reynolds-averaged Navier-Stokes equations, using the Boussinesq approximation. Here we present detailed measurements of plume and internal wave dynamics with high frequency measurements (Figure 2), as well as explore the fate of internal waves in fjords with idealized simulations.

References

Fringer, O. B., Gerritsen, M., & Street, R. L. (2006). An unstructured-grid, finite-volume, nonhydrostatic, parallel coastal ocean simulator. *Ocean Modelling*, 14(3-4), 139-173.

Nash, J. D., & Moum, J. N. (2005). River plumes as a source of large-amplitude internal waves in the coastal ocean. *Nature*, 437(7057), 400-403.

[1] Departamento de Ingeniería Hidráulica y Ambiental & Facultad de Ciencias Biológicas, Pontificia Universidad Católica de Chile, Santiago, Chile, megan.williams@uc.cl
[2] Departamento de Ingeniería Hidráulica, Pontificia Universidad Católica de Chile, Santiago, Chile, cescauri@uc.cl
[3] Civil & Environmental Engineering, Stanford University, Stanford, California
[4] Civil & Environmental Engineering, University of California, Berkeley, California
[5] Pontificia Universidad Católica de Chile, Santiago, Chile

[6] Pontificia Universidad Católica de Chile, Santiago, Chile

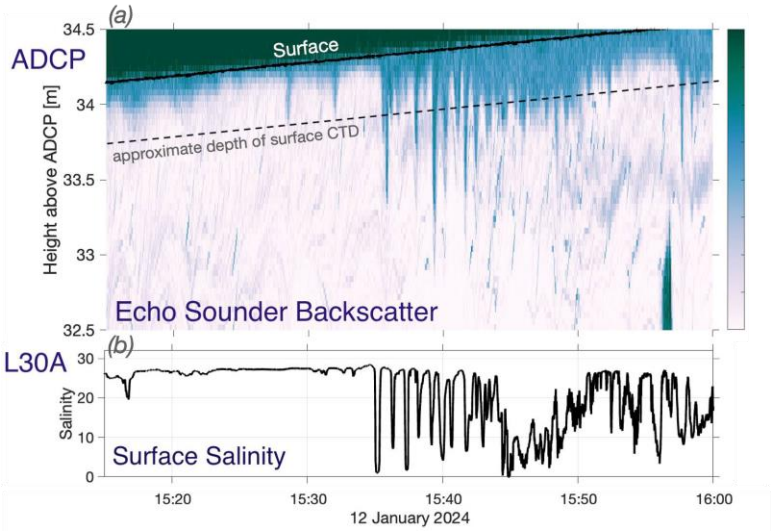

Figure 2. (a) ADCP Echosounder Backscatter showing the upper 2 m of the water column. High backscatter shows presence of the thin fresh surface layer (and corresponding higher suspended material concentration). (b) Surface salinity from the mooring near the ADCP. The depth of the surface CTD was approximately 50 cm. The arrival of an internal wave train alters the thickness of the surface layer starting between 15:30 and 15:40. Salinity measurements show the surface CTD measuring fresh or salty water as the interface moves above and below the instrument.

Seasonal and Spatial Patterns in Sediment Transport in an Erosional Marsh System

WinklerPrins L. [1], Lacy J. [2], Stacey M. [3], and Thorne K. [4]

Keywords: salt marsh, erosion, geomorphology, sediment transport, sediment budget

Abstract

Salt marshes provide expansive ecosystem services to coastal regions, including serving as bird and fish habitat, providing flood protection, and sequestering carbon and toxins (Barbier et al. 2011). While marshes are naturally dynamic, they are undergoing net loss in the 21st century largely due to lateral erosion (Camp- bell et al. 2022). In regions where marsh migration is constrained by built infrastructure, or where sediment resources may be insufficient for vertical or lateral expansion, approaches to prevent net marsh loss against lateral erosion are limited. To better understand and strategize around these conditions, detailed studies of marsh-edge loss mechanisms and their connections to sediment transport dynamics are necessary (Smith et al. 2021).

Most work on lateral marsh-edge change has focused on the impacts of storms or on annual-scale dynamics, and rarely have entire marsh units—including bay-edge interfaces and tidal creeks—been instrumented simultaneously to understand patterns in sediment transport throughout the entire marsh system. To address this gap, we performed a calendar year of intensive study at Whale's Tail Marsh South (Fig.1A), an 0.75 km2 high marsh in the Mediterranean climate of South San Francisco Bay. The marsh is constrained on its landward boundaries by levees, its bay-side edge (orange curve) is open to San Francisco Bay, and it has one main tidal channel (blue curve). At this edge, the fronting kilometers of mudflats are separated from the high marsh platform by a ~1 m tall scarp (Fig.1B), which is eroding. In this work, we asked the following interlinked questions: how do seasonal wind/wave regimes affect marsh-edge erosion rates? Does sediment loss at the marsh edge lead to deposition within the marsh interior, even if sediment travels via tidal channel? What are the variability and controls of erosion and marsh platform deposition?

To answer these questions, we performed in-situ sensor and sediment pad deployment during a study year alongside aerial photogrammetry of the marsh. We performed two seasons of study, June-Aug. and Dec-Feb.; in each, we installed co-located pressure and turbidity sensors at 5 locations along a bay-side 32 m-long transect (Fig.1A T1) and 4 locations along a channel-side 24 m-long transect (Fig.1A T2) on the marsh platform surface to quantify turbidity conditions and flood/ebb sediment fluxes. In the same periods, we installed sediment deposition pads staggered between the sensor stations along the transects (with additional stations up to 72 m into the marsh and a third transect, T3) to directly measure deposition on the marsh surface. Tile-based observations were used to develop distance-from-channel models of deposition rates, which were then interpolated over the entire marsh-top platform, using the assumption that deposition can be attributed by proximity. In both seasons, we also installed velocimeters and turbidity sensors on the mudflats offshore of the southwestern marsh-edge boundary to quantify nearshore and forcing wave conditions. Wave properties of the entire study year were modeled using Delft 3D-WAVE (n.b. Any use of trade, firm, or product names is for descriptive purposes only and does not imply endorsement by the U.S. Government.) over all four seasons. We produced high-resolution (5 cm pixel) digital surface models (DSMs) in May 2021, September 2021, November 2021, February 2022, and May 2022 of Whale's Tail Marsh South (Logan et al. 2023), allowing us to quantify lateral and volumetric marsh-edge retreat across the system. (Note, the marsh-edge was virtually unvegetated, so we made no adjustment.)

We found pronounced seasonal differences in lateral retreat rates of the marsh. There was rapid land- ward movement of the bay boundary (i.e. > 0.5 m of erosion over a season) during the summer and spring seasons, and virtually zero change in the fall and winter seasons. From the wind and wave records, we at- tributed this to the strong seasonal differences in wave-forcing conditions. When rates of lateral retreat were the largest (the warm seasons), conditions were marked by a sea breeze pattern, with daily morning calm but afternoon sustained 6+ m/s winds from the west. In contrast, during the fall and winter study periods, the conditions were typically calm with only five storm events with sustained 6+ m/s winds, generally from the south-southwest.

[1] University of California, Berkeley & California Polytechnic State University, San Luis Obispo. lukas_wp@berkeley.edu
[2] U.S. Geological Survey, Pacific Coastal & Marine Science Center, jlacy@usgs.gov
[3] University of California, Berkeley, mstacey@berkeley.edu
[4] U.S. Geological Survey, Western Ecological Research Center, kthorne@usgs.gov

These differences in wind and thus wave regimes led to spring and summer sea- sons having much higher mean and cumulative incident wave power metrics at the marsh edge versus fall and winter. Comparison to wind records from the prior 18 years suggested that our study year was fairly representative of the long-term averages for the region, despite a highly variable winter storm climate in California. We also noticed 2-5 cm of erosion/deepening in the mudflats during spring a summer periods, and similar amounts of accretion in the fall period (none in winter), although these measurements of eleva- tion change were within uncertainty bounds of vertical DSM position. Still, this may suggest that the marsh-mudflat system undergoes a "relaxation" period in autumn, after the high retreat rates of spring and summer, where eroded material settles on adjacent mudflats.

From both our tile-based deposition model and marsh-top sensors, the marsh as a whole was found to be importing sediment in the summer and more slowly in the winter, the product of much higher nearshore and marsh platform turbidity in the summer season, which we attributed to the more energetic wave conditions driving resuspension and edge erosion. This seasonal difference was true for both sediment imported to the marsh from the bay edge and along the tidal channel. Rates of import from the interpolation model, in Fig.1C for summer/winter, demonstrated that in both seasons, the loss of sediment from the erosional edge was not quite balanced with marsh platform import. Following our assumption of attributing sediment deposited to proximity of bay-edge or tidal channel, much more of the whole-marsh import was driven by tidal channel flows than bay-edge flows, although they had similar rates of import once scaled by length (of edge or channel) . While the exact direction of flow over the marsh surface during inundation periods re- mains uncertain as marsh platform sensor data showed evidence of lateral flow (i.e. not perpendicular to the marsh-edge boundaries) that was not captured by the study design, sediment deposition was structured with distance from bay-edge or channel. Deposition generally exponentially decayed from a near-edge peak to an asymptote with distance. At the bay-edge, the zone of maximum deposition was shifted inland up to 6 meters, likely due to wave action. Marsh interior deposition values were similar across sites and seasons, but the deposition rates were much higher adjacent to the tidal creek than along the bayside. We posit that this was because the marsh-edge region acted as a zone of tidal through-flow with less vegetative cover and thus fewer opportunities for deposition. The variability of sediment fluxes over the marsh platform was complex, often affected by immediate wave conditions and occasionally exporting.

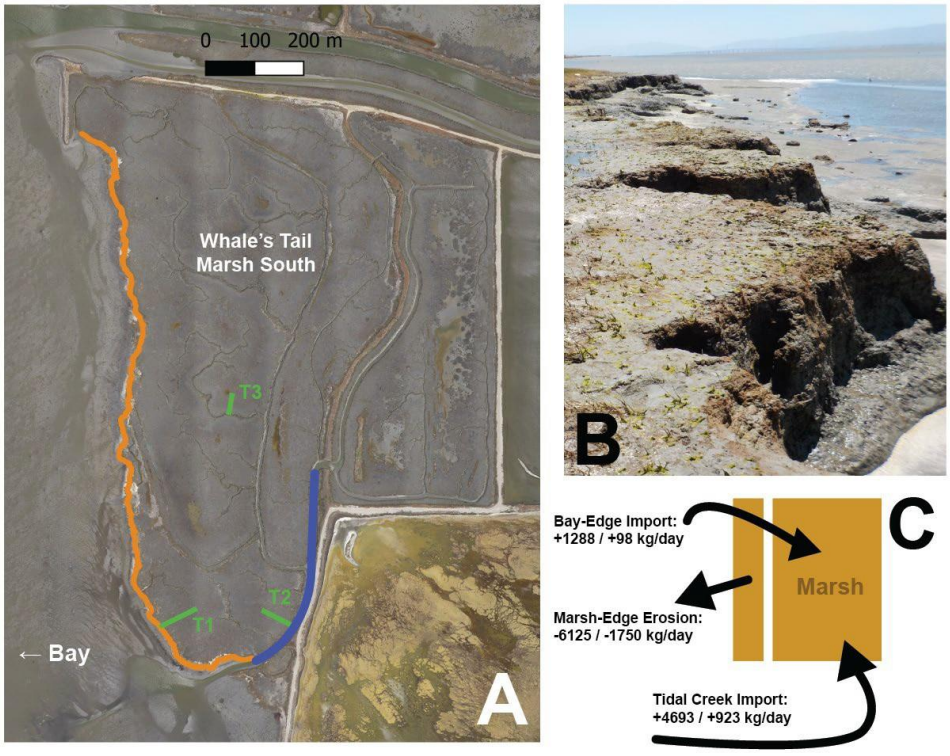

Figure 1: A) Image of Whale's Tail Marsh South with eroding lateral edge (orange), primary tidal channel (blue), and our study transects (green). B) Photo of scarped edge. C) Schematic and rates of sediment fluxes [summer] / [winter].

As a whole, Whale's Tail Marsh South is undergoing fairly rapid loss of area but slower loss of sediment. Seasons with high wave activity driven by spring and summer sea breezes—caused the most lateral erosion but also elevated nearshore turbidity levels which contributed to marsh platform sediment import via the bay-edge and tidal channels, supporting the argument of marsh-edge sediment "recycling" from Hopkinson et al. (2018). Following Donatelli et al. (2020) and Bouma et al. (2016), our study encourages considering the mudflat and marsh as parts of a coupled sedimentary system, but we found strong seasonal signals in San Francisco Bay that merit different considerations versus hurricane-dominated marshes of the east and gulf coasts.

References

Barbier, E. B., Hacker, S. D., Kennedy, C., Koch, E. W., Stier, A. C., & Silliman, B. R. (2011). The value of estua- rine and coastal ecosystem services. Ecological Monographs, 81(2), 169–193. https://doi.org/10.1890/10-1510.1

Bouma, T. J., Van Belzen, J., Balke, T., Van Dalen, J., Klaassen, P., Hartog, A. M., Callaghan, D. P., Hu, Z., Stive,
M. J. F., Temmerman, S., & Herman, P. M. J. (2016). Short-term mudflat dynamics drive long-term cyclic salt marsh dynamics: Lateral Salt Marsh Dynamics. Limnology and Oceanography, 61(6), 2261–2275. https://doi.org/10.1002/lno.10374

Campbell, A. D., Fatoyinbo, L., Goldberg, L., & Lagomasino, D. (2022). Global hotspots of salt marsh change and carbon emissions. Nature, 612(7941), 701–706. https://doi.org/10.1038/s41586-022-05355-z

Donatelli, C., Zhang, X., Ganju, N. K., Aretxabaleta, A. L., Fagherazzi, S., & Leonardi, N. (2020). A nonlinear re- lationship between marsh size and sediment trapping capacity compromises salt marshes' stability. Geology, 48(10), 966–970. https://doi.org/10.1130/G47131.1

Hopkinson, C. S., Morris, J. T., Fagherazzi, S., Wollheim, W. M., & Raymond, P. A. (2018). Lateral Marsh Edge Erosion as a Source of Sediments for Vertical Marsh Accretion. Journal of Geophysical Research: Biogeosciences, 123(8), 2444–2465. https://doi.org/10.1029/2017JG004358

Logan, J., Winklerprins, L. T., & Lacy, J. R. (2023). Structure-from-motion derived orthomosaic imagery and digi- tal surface models (DSMs) from the intertidal region at Whale's Tail Marsh, South San Francisco Bay, CA [dataset].
U.S. Geological Survey. https://doi.org/10.5066/P9L9R2VS

Tidal asymmetry and salt intrusion in the Ems estuary, North Sea

Wünsche A. [1], Becker M. [2], Fritzsch R. [1], Kelln J. [1], and Winter C. [2]

Keywords: tidal asymmetry, estuaries, Ems estuary, temporal variability, salinity, measurements

Abstract

Tidal asymmetry in estuaries and other tidal regimes of coastal systems is commonly evaluated to assess (changes in) system states. It classifies local states as either flood or ebb dominant. The method for deriving the tidal asymmetry is often determined by the available data basis. As such, it can be estimated based on hydrodynamic parameters, sediment properties, or the geometry of the estuary. Due to the wide availability of monitoring data of water level, the derivation from these is one of the most common methods. In recent years the number of descriptors deriving tidal asymmetry increased noticeably. In this study, we compare and discuss their sensitivity to the quality of the input data.

Our study area is the Ems estuary, located southwest of the North Sea between the Netherlands and Germany. The estuary stretches about 100 km from the island Borkum landward until the tidal weir, which marks the inland boundary of the tidally influenced area. The shape of the estuary can be described by three features: the outer part adjacent to the North Sea is funnel-shaped and borders the central area, characterised by the Dollard, a tidal flat, and north of it, the main shipping channel. Further inland, the cross-section narrows into a channel-like course. Tides in the estuary are predominant semi-diurnal and described as asymmetric. The Ems estuary has been repeatedly studied (e.g. Talke et al. 2009, van Maren et al. 2015) to understand the mechanism that led to the observed increase of suspended sediment concentrations, coupled with the occurrence of fluid mud. The transition to its hyperturbid state is linked to a drastic change in the estuarine geometry (Winterwerp und Wang 2013), both vertically and horizontally. Repetitive interventions have amplified and deformed the tides, resulting in changes in current phases of M2 and M4, as well as in shifting tidal asymmetry to a stronger flood dominant state that favours sediment import (e.g. Dijkstra et al. 2019). Several studies, which vary in terms of analysis period, data set and type (e.g. field measurements in van Maren et al. 2023 or simulation results in Chernetsky et al. 2010), have occasionally revealed opposing directions of tidal asymmetry for similar sections of the Ems estuary. This provides another reason to investigate the extent to which the data basis can influence the outcome of tidal asymmetry.

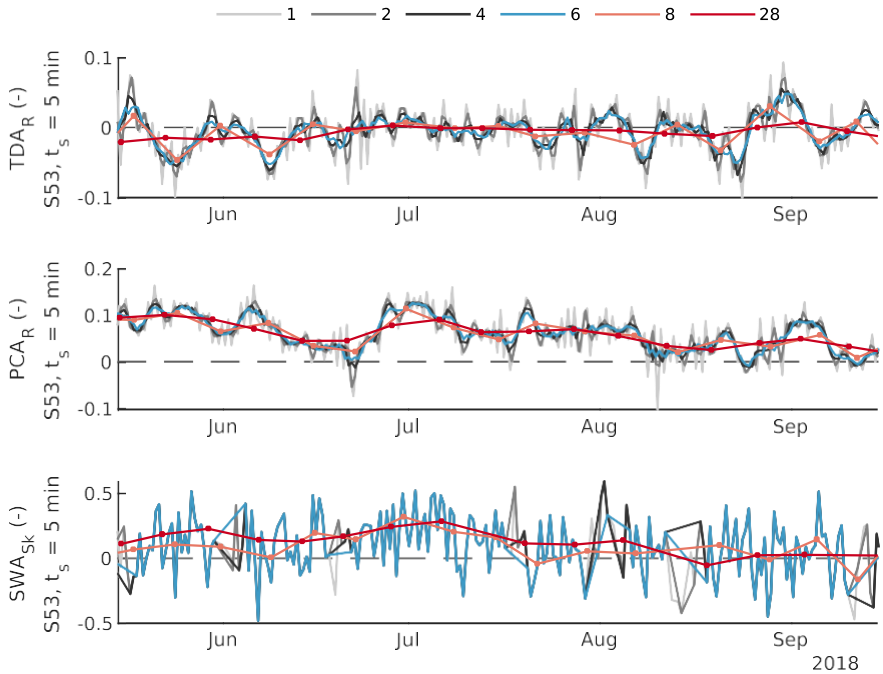

*Figure 1: Time series of scaled **a** tidal duration asymmetry (TDA) at km 53, **b** peak current asymmetry (PCA) at km 53 and **c** slack water asymmetry (SWA) at km 53 from May 15 to September 15, 2018. TDA and PCA are derived by using the ratio method (R) and SWA is derived by derivative skewness (Sk). Window length (tides) are displayed in different colors: 1 to 4 tides in grey tones, 6 tides in blue, 8 tides in orange and 28 tides in red. A dashed grey line represents zero. Positive values represent flood dominance, negative values represent ebb dominance. The sampling interval of the input data is 5 minutes*

[1] Federal Waterways Engineering and Research Institute, Hamburg, Germany, anna.wuensche@baw.de
[2] Institute of Geosciences, Coastal Geology and Sedimentology, Christian-Albrechts-Universität zu Kiel, Kiel, Germany

Based on one-year measurements of water level and near-surface current velocity along the Ems estuary, we computed tidal asymmetry from different descriptors: phase lag, tidal duration asymmetry, peak current asymmetry and slack water asymmetry. The descriptors are deduced from harmonic, ratio, and skewness methods. These methods yield values of tidal asymmetry in different ranges for the same interpretation of the dominant asymmetry direction. To compare the different methods, we scaled the descriptors to a new value range using conformal maps. We investigated the sensitivity of the descriptors by varying the sampling intervals of the input time series and the length of the computation window.

The sensitivity of the descriptors is strongly site-specific, particularly in response to variations in sampling intervals. That variability may lead to changes in the asymmetry direction in tidal duration asymmetry and phase lag. This sensitivity is most pronounced at locations where the initial difference between flood and ebb duration is minimal. The highest sensitivity is encountered calculating slack water asymmetry, which is likely related to the short duration of slack water compared to the duration of a full tide. Increasing the window length acts as a low-pass filter, reducing the variability of the tidal asymmetry, especially when computed over a small number of tides (Figure 1). Moreover, the relevance of the window length and the analysis period becomes apparent in the differences in the direction of tidal asymmetry resulting from spring or neap tides.

Overall, we find that data quality and analysis period play a crucial role in the assessment of tidal asymmetry in the Ems estuary. Consistent with other studies (e.g. Gong et al. 2016), the river discharge has a pronounced and downstream decreasing impact on the tidal asymmetry. This influence is particularly prominent in descriptors derived from current data during (high) discharge events. Wünsche et al. (under review) discuss the critical nature of interpreting (residual) sediment transport based solely on tidal asymmetry and point to the need for more comprehensive datasets.

Outlook

In addition to our sensitivity study (Wünsche et al., under review), we present preliminary findings regarding the long-term development of tidal asymmetry in the Ems estuary by extending the analysis period to 20 years. We are interested in the connection between spatially variations of tidal asymmetry, observed shifts in dominant asymmetry directions combined with the long-term alterations in near-surface salinity. Furthermore, the transformation of seasonal patterns in tidal asymmetry and salinity. That includes to investigate the extent to which possible long-term changes can be attributed to the recent progression in river discharge, leading to an increasing number of years with low discharge conditions. Moreover, we illustrate the impact of high and low discharge seasons on the research parameters of tidal asymmetry and salinity.

References

Chernetsky, A. S.; Schuttelaars, H. M.; Talke, S. A. (2010): The Effect of Tidal Asymmetry and Temporal Settling Lag on Sediment Trapping in Tidal Estuaries. In: Ocean Dynamics 60 (5), S. 1219–1241. DOI: 10.1007/s10236-010-0329-8.

Dijkstra, Yoeri M.; Schuttelaars, Henk M.; Schramkowski, George P.; Brouwer, Ronald L. (2019): Modeling the transition to high sediment concentrations as a response to channel deepening in the Ems River Estuary. In: Journal of Geophysical Research: Oceans (124:1-17). DOI: 10.1029/2018JC014367.

Gong, Wenping; Schuttelaars, Henk; Zhang, Heng (2016): Tidal asymmetry in a funnel-shaped estuary with mixed semidiurnal tides. In: Ocean Dynamics 66 (5), S. 637–658. DOI: 10.1007/s10236-016-0943-1

Talke, S. A.; Swart, H. E. de; Schuttelaars, H. M. (2009): Feedback between residual circulations and sediment distribution in highly turbid estuaries: An analytical model. In: Continental Shelf Research 29 (1), S. 119–135. DOI: 10.1016/j.csr.2007.09.002.

van Maren, D. S.; Colina Alonso, A.; Engels, A.; Vandenbruwaene, W.; Vet, P. L. M. de; Vroom, J.; Wang, Z. B. (2023): Adaptation timescales of estuarine systems to human interventions. In: Front. Earth Sci. 11, Artikel 1111530. DOI: 10.3389/feart.2023.1111530.

van Maren, Dirk S.; Winterwerp, Johan C.; Vroom, Julia (2015): Fine sediment transport into the hyper-turbid lower Ems River: the role of channel deepening and sediment-induced drag reduction. In: Ocean Dynamics 65 (4), S. 589–605. DOI: 10.1007/s10236- 015-0821-2.

Winterwerp, Johan C.; Wang, Zheng Bing (2013): Man-induced regime shifts in small estuaries—I. Theory. In: Ocean Dynamics 63 (11-12), S. 1279–1292. DOI: 10.1007/s10236-013-0662-9.

Wünsche, Anna; Becker, Marius; Fritzsch, Ralf; Kelln, Jessica; Winter, Christian: The sensitivity of tidal asymmetry descriptors in the Ems estuary. [under review]. In: Ocean Dynamics.

Impact of estuarine exchange flow on multi-tracer budgets in the Salish Sea

Xiong J. [1], MacCready P. [2], and Leeson A. [3]

Keywords: estuarine circulation, fjord circulation, biogeochemical budgets.

Abstract

Estuarine exchange flow, which is often many times greater in magnitude than the volume transport of river discharge, regulates all aspects of estuarine biogeochemical processes. It is common to evaluate the residence time in estuaries, and many studies have done this using a variety of methods. However the motivation for residence time studies is biogeochemistry, and this can be influenced by much more than the exchange flow, depending on the tracer in question. In the study, we analyzed realistic simulations from a coupled physical-biological model to quantify the volume-integrated budgets of heat, total nitrogen (TN), and dissolved oxygen (DO) in the Salish Sea and its inner basins due to net exchange flow (influx - outflux) and other processes influencing each tracer. The Salish Sea is a large, fjordal estuary in the US and Canadian Pacific Northwest. Total Nitrogen is the sum of the nitrogen concentration of all the NPZD tracers. The model, LiveOcean (MacCready et al., 2021), was validated with extensive hydrographic and moored observations for 2017. Budgets for all three tracers are shown in Fig. 1. Episodically, marked heat/DO influx and TN outflux occurred during strong downwelling. The seasonal variations in net budgets are primarily regulated by air-sea heat flux (for heat), exchange flow (for TN), and combined air-sea flux, photosynthesis, respiration and exchange flow (for DO). The exchange flow exports heat and DO all year round except for occasions when intrusions of surface warm and oxygen-rich water from the coast bring in heat and DO. The amount of heat/DO export by the exchange flow approximates heat/DO import from the atmosphere/photosynthesis/respiration. Exchange flow dominates TN import in the summertime and TN export in the wintertime. Vertical tracer gradients, greatly impacted by shifts in coastal wind direction and strength, determines the seasonal trend of exchange flow budget terms.

[1] University of Washington, jxiong7@uw.edu
[2] University of Washington, p.maccready@gmail.com
[3] University of Washington, auroral@uw.edu

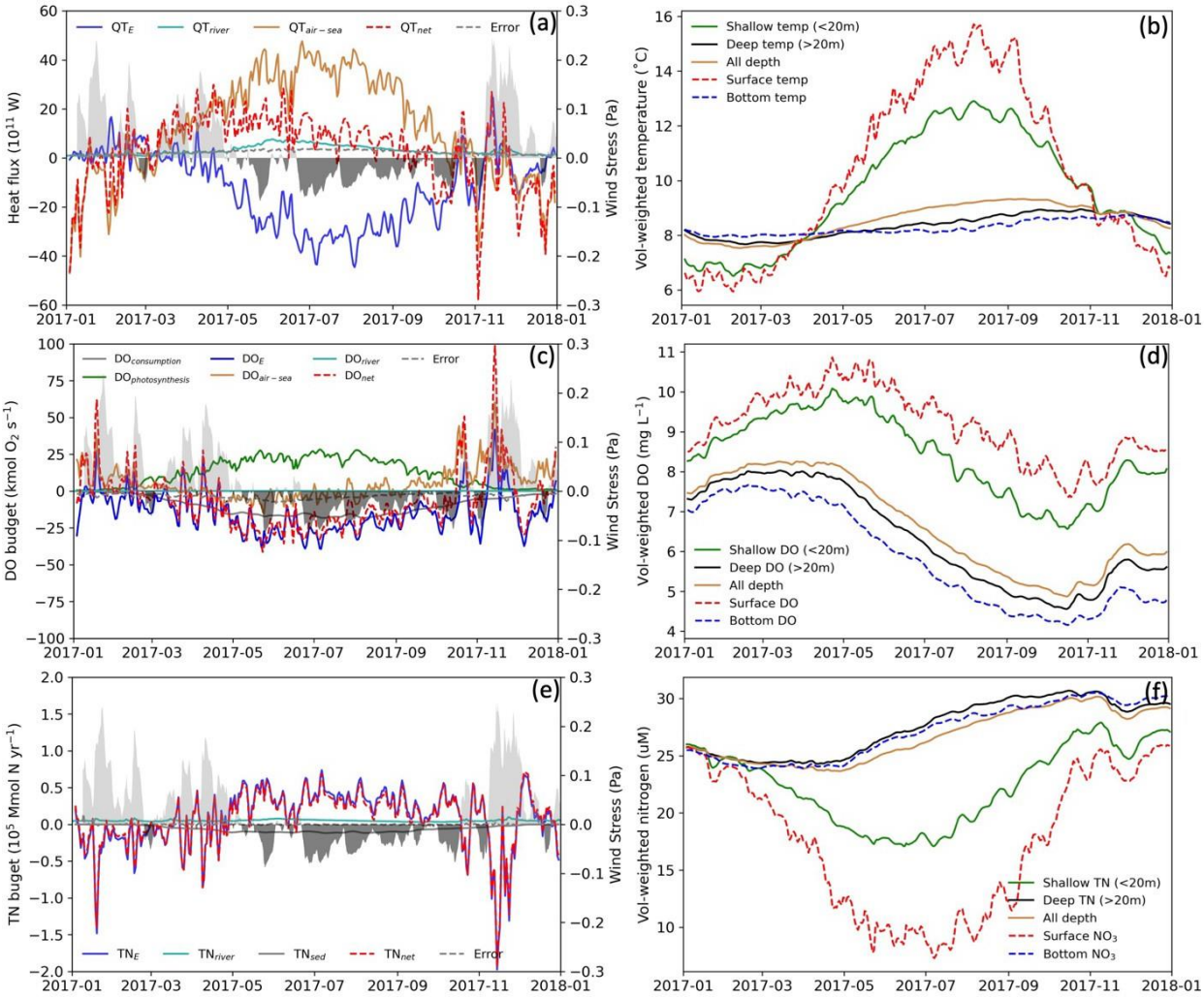

Figure 1. (a, c, e) time series of each term that contributes to heat (upper panel), DO (middle panel), and TN (lower panel) budgets in the Salish Sea. The gray dashed lines represent budget error and the shaded gray-ish regions indicate wind stress related to downwelling (positive value) and upwelling (negative value). The north-south wind stress from the model was extracted at (125°W, 47.5°N) and smoothed with a weighted 8-day filter as a proxy for the shelf Ekman response (Austin & Barth, 2002). (b, d, f) volume-weighted tracer concentrations at different depths.

References

MacCready, P., McCabe, R. M., Siedlecki, S. A., Lorenz, M., Giddings, S. N., Bos, J., Albertson, S., Banas, N. S., & Garnier, S. (2021). Estuarine Circulation, Mixing, and Residence Times in the Salish Sea. *Journal of Geophysical Research: Oceans*, *126*(2). doi:10.1029/2020jc016738

Austin, J. A., & Barth, J. A. (2002). Variation in the position of the upwelling front on the Oregon shelf. *Journal of Geophysical Research: Oceans*, *107*(C11), 3180. doi:10.1029/2001jc000858

Effects of Extreme Events on Transport Processes in Delaware River Estuary, USA

Yang Z. [1] , Liu J. [2], Huang Y. [3], Hetland R. [4], Sun N. [5], Wang T. [6], and Deb M. [7]

Keywords: Estuarine circulation, saltwater intrusion, microplastic transport, storm surge, sea level rise.

Abstract

Estuarine circulation and transport processes are controlled by bathymetry, atmospheric, hydrological, and oceanic forcing. Extreme events, such as droughts and compound flooding induced by hurricanes, play an important role in estuarine transport processes. This study utilizes a high-resolution coastal model based on the Finite Volume Community Ocean Model (FVCOM) to simulate the saltwater intrusion and microplastic transport under normal and extreme conditions in the Delaware River Estuary in mid-Atlantic coast of United States. The Delaware River Estuarine model is integrated with the Distributed Hydrology Soil Vegetation Model (DHSVM) for the Delaware River Basin to provide river boundary condition. Both DHSVM and FVCOM for the Delaware River Basin and Estuary have been validated with stream flow, water level, and velocity data, especially for the period of Hurricane Irene, which caused compound flooding in the estuary as a result of river flood and coastal storm surge. The validated model was used to simulate saltwater intrusion under long-term drought condition in the Delaware River Basin. Sensitivity analysis of saltwater intrusion in response to future sea level rise indicated that the salt front moved further upstream as sea level rises. Model results showed that the adjustment timescale of saltwater intrusion varies nonlinearly with sea level rise. A microplastic model was developed in the framework of FVCOM to simulate microplastic transport with characteristics of plastic size, shape and density. The microplastic model was validated against experimental data and analytical solution in an idealized model setting. Model validation showed that the model effectively replicates microplastic profiles in different transport modes, including bedload, surface-load, suspended-load, and mixed-load. Subsequently, the microplastic model was applied to simulate microplastic fate and transport in the Delaware River Estuary, employing the physical configuration of the saltwater intrusion model. This application also involved assessing the impacts of different microplastic sources, such as airborne and point sources, on the microplastics' distribution within the estuary.

[1] Pacific Northwest National Laboratory, zhaoqing.yang@pnnl.gov
[2] Stanford University, jinliang.liu@stanford.edu
[3] Pacific Northwest National Laboratory, Yicheng.huang@pnl.gov
[4] Pacific Northwest National Laboratory, robert.hetland@pnnl.gov
[5] Pacific Northwest National Laboratory, ning.sun@pnnl.gov
[6] Pacific Northwest National Laboratory, taiping.wang@pnnl.gov
[7] Pacific Northwest National Laboratory, mithun.deb@pnnl.gov

Role of internal waves in the Winyah Bay plume response to upwelling-favourable winds

Yankovsky A. [1], Voulgaris G. [2], Papageorgiou C. [3], and Fribance D. [4]

Keywords: estuarine outflow, buoyant plume, front, internal waves, mixing, upwelling.

Abstract

Under the influence of upwelling-favorable winds, the freshwater outflow from Winyah Bay, SC, USA can spread offshore as a narrow tongue of buoyant water, on some occasions reaching the shelfbreak, which lies ~100 km off the coast. According to recent observational and modeling studies (Yankovsky et al., 2022; Yankovsky and Yankovsky, 2024; Dykstra et al., 2024), several ingredients are required for this crossing: (i) the outflow should be decoupled from the bottom boundary layer near the mouth either through strong buoyancy forcing or due to relatively light tidal- and wind-induced mixing; (ii) the plume is advected by the combined action of the offshore Ekman and alongshore geostrophic transport; (iii) the plume remains supercritical (in terms of the internal Froude number) over long distance from the mouth; (iv) there is continuous radiation of internal waves within the plume in the upwind direction, which prevents the transverse spreading of the plume. A dedicated observational campaign reported here delineates these dynamics.

We present shipboard observations of the Winyah Bay plume sampled on June 6-7, 2023, which was forced by southeasterly, upwelling-favorable winds of 5-10 m/s during the survey. The measurements utilized a self-propelled catamaran RoboCat with GPS used as a platform for the 5-beam Nortek Signature 1000 AD2CP, which yields both velocity and turbulent kinetic energy (TKE) dissipation profiles. At each station along two transects reported here, RoboCat collected data for at least 20 min within a 50-m circle of the prescribed station location. The water column was also sampled with an uprising microstructure profiler deployed from a small boat in close proximity to RoboCat. These data were complemented with standard ADCP and CTD measurements from the R/V Savannah. Figure 1 shows the sampling trajectory. Transect A ran offshore from jetties along the longitudonal axis of the plume till the ambient shelf water was encountered. It comprised 12 stations; 9 were sampled with microCTD, which provides superior accuracy compared to shipboard CTD. The plume extended offshore for more than 25 km after approximately one day of the sustained upwelling favorable wind. A shallow, ~2 m deep tidal plume extended ~10 km offshore; farther offshore the buoyant layer deepened to 5 m and another interior front containing buoyant water of two tidal pulses lay 17 km offshore (Fig. 2). Past the interior front energetic submesoscale processes were present resulting in overturnings with the O(1) m vertical scale. At the offshore stations, maximum TKE dissipation was observed in the middle of the water column (Fig. 2); the same feature was observed precviously, see Yankovsky et al. (2022) for details. Transect B was sampled twice across the plume axis with shipboard CTD. Buoyant water concentrated on the upwind (southern) edge of the plume, where the horizontal salinity gradients were also higher, and the transverse dimension of the plume was less than 10 km. Undulations of the pycnocline in plume's transverse dimension and elevated TKE values at the base of the plume suggest a possibility of the upwind radiation of internal waves previously found in numerical experiments.

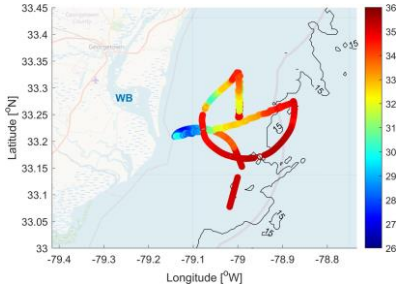

Figure 1. Study area: color dots are underway salinity measurements, black contour is the 15-m isobath, WB is Winyah Bay.

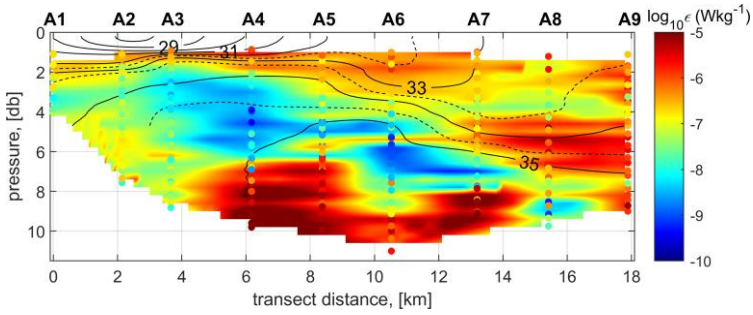

Figure 2. Transect A, microCTD stations only: salinity (black contours) and the TKE dissipation (color shading). Typically, three microCTD casts were conducted at each station.

[1] University of South Carolina, Columbia, SC, USA, ayankovsky@geol.sc.edu
[2] University of South Carolina, Columbia, SC, USA and U.S. National Science Foundation, USA, gvoulgaris@geol.sc.edu
[3] University of South Carolina, Columbia, SC, USA, cpapageorgiou@seoe.sc.edu
[4] Coastal Carolina University, Conway, SC, USA, dfribance@coastal.edu

Internal wave properties are estimated by numerically solving the eigenvalue problem below as in Yankovsky et al. (2022):

$$\frac{d^2w}{dz^2} + \lambda w = k^2 w, \text{ where } \lambda = \frac{N^2}{(U-C)^2} - \frac{1}{U-C}\frac{d^2U}{dz^2} \text{ with boundary conditions } w = 0 \ (z = 0, -H) \quad (1)$$

Here w is the vertical velocity component, U=$U(z)$ is the mean current, k is the wave number, N is the buoyancy frequency, C is the wave phase speed, and H is the water depth. Wave problem is solved for stratification and the mean current velocity profile observed at station A9 (Fig. 3). The problem is solved with and without the second term in the λ coefficient, which describes the effect of the vertical vorticity gradient. All but one mode are eliminated by the mean current shear, and waves cannot propagate in the positive direction (offshore) (Fig. 4). Maximum in d^2U/dz^2 below the pycnocline acts as a restoring force, reducing the internal wave phase speed and causing strong vertical shear in the internal wave velocity field at mid-depth (compare Fig. 2 and 5). These features can explain the observed maximum of the TKE dissipation at 4-8 m depth at stations A8-A9.

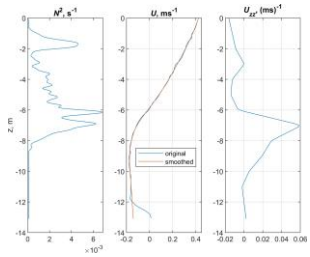

Figure 3. Vertical profiles from A9 station used for solving (1).

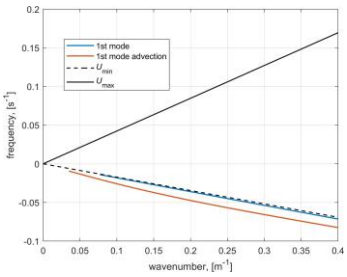

Figure 4. Dispersion curves corresponding to the full solution of (1), and the solution with d^2U/dz^2 set to zero.

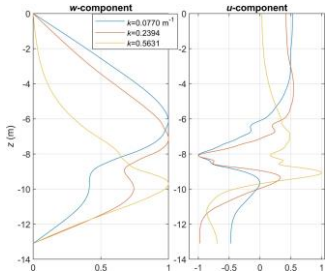

Figure 5. Vertical profiles of vertical w and horizontal u velocity components for various wavenumbers.

The presented observations conform to the idealized modeling results by Yankovsky and Yankovsky (2024) and the wave property analysis deduced from (1): internal waves are generated in the offshore segment of the plume due to the advection of the plume momentum by wind-induced currents. Initially, their crests are aligned with the direction of the near-surface wind-induced drift and the wave propagation is only weakly affected by the mean cross-shelf velocity structure. As waves propagate upwind, the wave fronts also turn inshore since the offshore propagating modes are eliminated by strong near-surface velocity shear. This wave refraction continues until the critical layer is approached, which is seen both in the dispersion diagram (Fig. 4) and in the localized horizontal velocity maxima at mid-depth (Fig. 5). These layers result in a strong mid-depth vertical shear causing the internal wave breaking. Thus, vertical shear associated with the two-layer cross-shelf upwelling circulation has a strong impact on both the propagation and the vertical structure of internal waves, whereas the vorticity gradient term acts as a restoring force along with the density gradient (buoyancy force). Vigorous mixing and overturning in the offshore part of the plume resolved by our innovative sampling techniques can be attributed to the internal wave dynamics. The plume remains transversely constrained, likely due to the upwind radiation of internal waves. Overall, the cross-shelf plume emerges as a distinctive regime of coastal plumes affected by upwelling winds.

References

Dykstra, S.L., Ricche, G., Marmorino, G., Yankovsky, A.E. (2024) Forcing conditions of cross-shelf plumes on a wide continental shelf, Winyah Bay, South Atlantic Bight. Submitted to Remote Sensing of Environment.

Yankovsky, A.E., Fribance, D.B., Cahl, D., Voulgaris, G. (2022) Offshore spreading of a supercritical plume under upwelling wind forcing: a case study of the Winyah Bay outflow. Frontiers in Marine Science, 8:785967. doi: 10.3389/fmars.2021.785967

Yankovsky, E., Yankovsky, A. (2024) The cross-shelf regime of a wind-driven supercritical river plume. Journal of Physical Oceanography, 54, 537-556. DOI: 10.1175/JPO-D-23-0012.1

Coastal Trapped Wave Effects on Subinertial Current Variability in the Southern California Bight

Zhang H.J. [1], Merrifield M. [2], Send U. [3], Giddings S.N. [4], and Kurapov A.

Keywords: nearshore circulation, remote forcing, coastally trapped waves, alongshore transport

Abstract

The alongshore transport of plankton, river runoff, and other tracers is a key concern in the heavily populated Southern California Bight (SCB), which stretches from Point Conception in the north to Punta Colonet, Baja California in the south. In the outer shelf (60 -100m), much of the flow variability resides in the weather band (see Lentz and Winant, 1986). While the California Current System (CCS) at large is mostly wind driven, wind forcing has a secondary effect on alongshore velocity in the SCB due to comparatively weaker winds (see Hickey et al., 2003). As a result, the variability of the alongshore current has a strong dependency on remote wind forcing, the effects of which are communicated into the region as subinertial disturbances in adjusted sea level (ASL). Some of these disturbances have been shown to originate as far as the equator, propagating polewards as Kelvin Waves with the coastline on the right all the way to British Columbia (see Amaya et al., 2021). High frequency radar observations along the US west coast corroborates the existence of these fast propagating disturbances (O(100-300) km/day) in the current field, and also reveal a higher mode, slower wave (O(10) km/day) that is confined to the Southern California Bight due to bathymetric scattering and a sharp curvature change in the coastline at Point Conception (see Kim et al., 2011).

In the past, ASL at San Diego has been successfully used as a boundary condition to force coastally trapped wave models to replicate the variability of alongshore velocity in the Northern and Central CCS, although these models were not applied within the SCB (see Chapman, 1987; Connolly et al., 2014). However, the alongshore current inside the bight is observed to be strongly influenced by sea level equatorward and outside of the region (see Hickey, 2003). Pringle and Riser (2003) used lagged wind stress between San Diego and the tip of Baja California to reconstruct the measured surface temperature at Point Loma and demonstrate the control of remote winds on nearshore circulation, though they did not directly consider the effects on alongshore currents due to lack of observations.

Using a combination of models and observations spanning multiple years, we analyze the coastally trapped wave (CTW) signal in the SCB with a particular emphasis on the San Diego region. CTWs were examined and characterized in two different ROMS models: The West Coast Operational Forecast system (WCOFS), and a Coupled Ocean Atmosphere Waves Sediment Transport (COAWST) model developed for the San Diego region. Both model grids have overlapping domains and a spatial resolution of 2 km, though the southern boundary of WCOFS is located about 1000 km further south than that of COAWST. In particular, the WCOFS domain includes Sabastián Vizcaíno Bay, a large hook shaped feature about 500 km south of San Diego that is a known source of CTW generation (see Ramos-Musalem et al., 2023). When the modeled alongshore currents are compared to moored ADCP observations at the Del Mar mooring, we find that the observed alongshore current variability agrees better with WCOFS ($r = 0.4$) than COAWST ($r = 0.2$). However, neither model fully captures the observed variability due to the complex bathymetry of the shelf and shelf eddies. In addition, the Del Mar mooring is located inside the bend of a submarine canyon, a complex bathymetric feature which also induces current variability when a CTW passes over (see Saldías et al., 2021). The Hovmöller diagram below shows the northward propagating sea level anomalies present in both models. Using a lagged correlation analysis, we find that the ASL anomalies in WCOFS propagate northwards at a speed of 2.3 m/s, consistent with previous estimates of the propagation speed of Kelvin Waves in this region (see Hickey et al., 2003).

We hypothesize that the increased agreement in WCOFS is due to the inclusion of wind stress along Baja California, and that this is necessary to capture the variability of the alongshore current in the San Diego region.

By characterizing the respective representations of CTWs in each model, we investigate the alongshore current variability induced by the inclusion of the Baja coast into the model domain. We calculated the linear regression coefficient between the alongshore current at the location of the Del Mar mooring with every other grid cell to create a map of the region in the flow field that shares variability and common forcing mechanisms with the San Diego nearshore circulation. This revealed a narrow band of elevated regression coefficients that adhere to the coastline.

Furthermore, the introduction of lagged alongshore velocity into this regression analysis demonstrates that this coherent coastal band propagates poleward consistent with the behavior of a CTW. This propagating signal is decomposed with a complex EOF analysis to isolate the CTW driven circulation, which we then use to quantify the direct contribution of the CTW field on alongshore transport.

[1] Scripps Institution of Oceanography, jiz053@ucsd.edu
[2] Scripps Institution of Oceanography, mamerrifield @ucsd.edu
[3] Scripps Institution of Oceanography, usend @ucsd.edu
[4] Scripps Institution of Oceanography, sgiddings @ucsd.edu
[5] National Oceanic and Atmospheric Administration, alexander.kurapov@noaa.gov

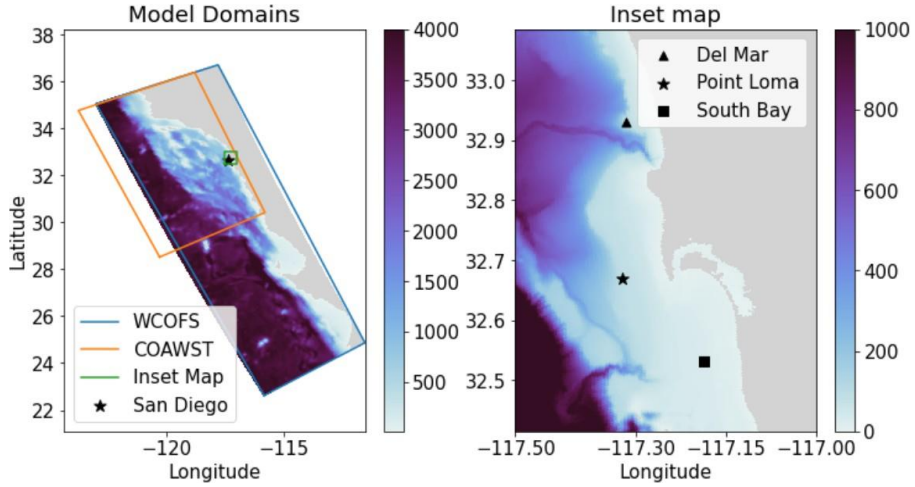

Figure 1. A regional map. (Left) The model domains of WCOFS and COAWST are shown on top of the WCOFS bathymetry. San Diego is indicated on the map by the star. (Right). Close up view of San Diego with the location of each mooring.

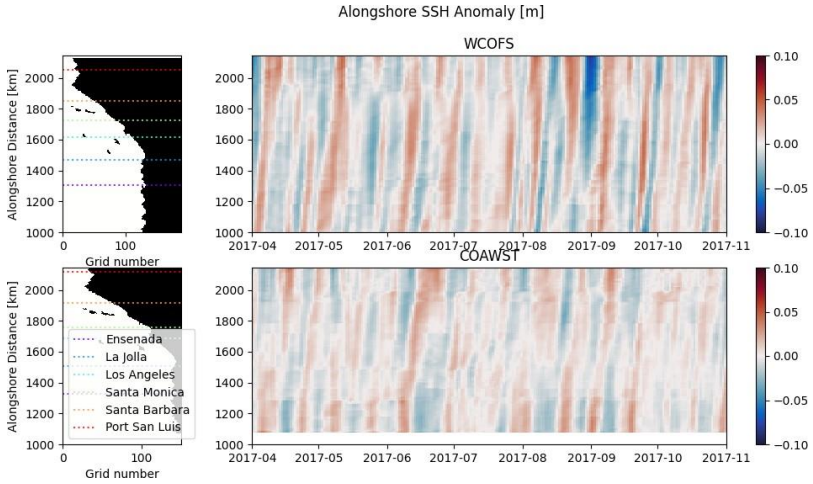

Figure 2. (Right) A Hovmöller diagram of sea level anomalies along the coast of the SCB in each model gridded onto alongshore distance. Distance is measured starting from the southernmost coastal point in the WCOFS domain.

References

Lentz, S. J., & Winant, C. D. (1986). Subinertial currents on the southern California shelf. Journal of Physical Oceanography, 16(11), 1737-1750.

Hickey, B. M., Dobbins, E. L., & Allen, S. E. (2003). Local and remote forcing of currents and temperature in the central Southern California Bight. Journal of Geophysical Research: Oceans, 108(C3).

Amaya, D. J., Jacox, M. G., Dias, J., Alexander, M. A., Karnauskas, K. B., Scott, J. D., & Gehne, M. (2022). Subseasonal-to-seasonal forecast skill in the California Current System and its connection to coastal Kelvin waves. Journal of Geophysical Research: Oceans, 127(1), e2021JC017892.

Kim, S. Y., Terrill, E. J., Cornuelle, B. D., Jones, B., Washburn, L., Moline, M. A., & Kosro, P. M. (2011). Mapping the US West Coast surface circulation: A multiyear analysis of high-frequency radar observations. Journal of Geophysical Research: Oceans, 116(C3).

Chapman, D. C. (1987). Application of wind-forced, long, coastal-trapped wave theory along the California coast. Journal of Geophysical Research: Oceans, 92(C2), 1798-1816.

Connolly, T. P., Hickey, B. M., Shulman, I., & Thomson, R. E. (2014). Coastal trapped waves, alongshore pressure gradients, and the California Undercurrent. Journal of Physical Oceanography, 44(1), 319-342.

Pringle, J. M., & Riser, K. (2003). Remotely forced nearshore upwelling in Southern California. Journal of Geophysical Research: Oceans, 108(C4).

Ramos-Musalem, K., Gille, S. T., Cornuelle, B. D., & Mazloff, M. R. (2023). High-Frequency Variability Induced in the Southern California Bight by a Wind Event in Sebastián Vizcaíno Bay, Baja California. Journal of Geophysical Research: Oceans, 128(6), e2022JC019547.

Saldías, G. S., Ramos-Musalem, K., & Allen, S. E. (2021). Circulation and upwelling induced by coastal trapped waves over a submarine canyon in an idealized eastern boundary margin. Geophysical Resesarch Letters, 48(11), e2021GL093548.

From natural dynamics to anthropogenic impacts: A near-century of geomorphological change in a medium macrotidal estuary

Zheng J. [1,2,4], Xia X. [1,2,3], Sun H. [3], Chen Y. [1,3], Sottolichio A. [4], Jalón-Rojas I. [4], Liu Y. [1,3], Cai T. [1,3], Wang X. [1,3], and He Z. [2]

Keywords: Geomorphological changes, multidecadal shifts, tide evolution, medium-size estuary, human activities.

Abstract

Since the 1970s, human interventions like navigation projects, land reclamation, sand mining, and dam construction have notably altered the geomorphology of the Oujiang River Estuary (ORE) in Zhejiang Province, China (Fig. 1a). The ORE, a medium-sized, funnel-shaped, macrotidal estuary with a mean tidal range exceeding 4m during normal semidiurnal tides, exemplifies the impact of combined anthropogenic activities on coastal environments. While extensive research has predominantly focused on the geomorphological evolution of large-sized estuaries, globally common small to medium-sized estuaries, like ORE, remain understudied despite their critical role in global coastal and seabed dynamics (Milliman and Syvitski, 1992).

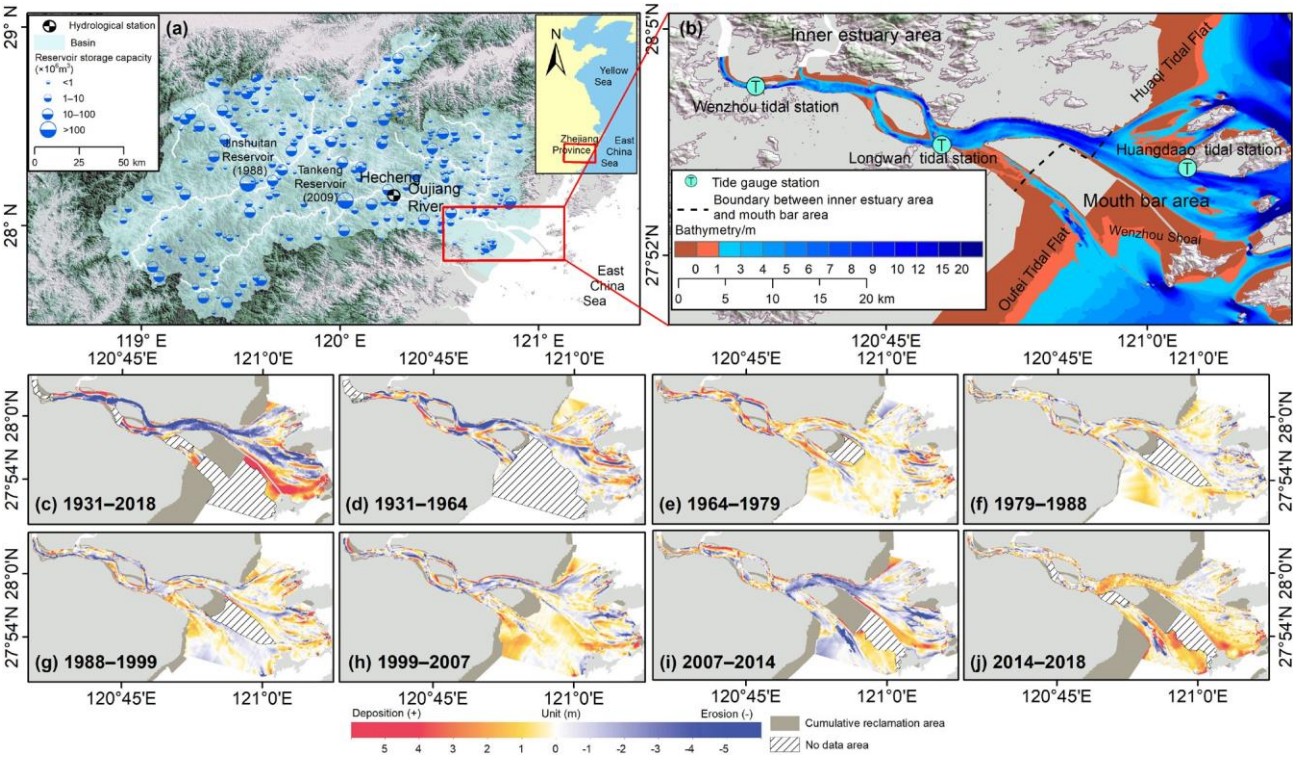

Figure 1. Maps of the study area (a) and (b), as well as patterns of erosion and deposition in the Oujiang River Estuary (ORE) from 1931 to 2018 (c–j).

In this study, we investigated the geomorphological changes in the ORE over 88 years, spanning from 1931 to 2018, while examining their relationships with shifts in hydrodynamic and sediment transport patterns. Our analysis was based on a comprehensive dataset including bathymetric surveys, river discharge records, tide data, and historical satellite imagery. All bathymetric data were standardized to WGS84 and adjusted to the theoretical lowest water level datum. 50 m resolution Digital Elevation Models were subsequently created through TIN interpolation using depth values from marine charts. Tidal records (1960–2018) from three stations were analyzed for annual average high and low tide levels, tidal range, and multiyear averages of flood and ebb duration. Satellite imagery from the USGS was radiometrically and atmospherically corrected in ENVI and georeferenced to WGS84. Shorelines were manually delineated in ArcGIS.

[1] Second Institute of Oceanography, Ministry of Natural Resources, China, xiaxm@sio.org.cn.
[2] Ocean College, Zhejiang University, China.
[3] Key Laboratory of Ocean Space Resource Management Technology, Ministry of Natural Resources, China.
[4] EPOC, University of Bordeaux, France.

The study identifies a five-phase morphological evolution of the ORE (Fig. 1c–j): marked erosion (1931–1964), extensive accretion (1964–1979), minor erosion/deposition oscillations (1979–2007), fast erosion (2007–2014), and rapid back-siltation (2014–2018). Before the 1970s (Fig. 1d–e), the ORE exhibited a natural state with morphodynamics, featuring wandering, braided, and meandering channels interspersed with shoals. Erosion and deposition patterns maintained a dynamic equilibrium: erosion occurred during periods of high river discharge, while net upstream sediment transport and deposition took place during low river discharge, influenced by the dominant flood tides. However, post-1970s human interventions disrupted this dynamic equilibrium, leading to varied geomorphological responses (Fig. 1f–j). Navigational projects stabilized channels and shoals, influencing local sedimentation, while dams reduced both the frequency and magnitude of floods, further reducing the possibility of intense scouring and erosion that natural state occurred. Land reclamation reduced intertidal areas, narrowed channels, and advanced coastlines towards the water, while dredging for reclamation infill and sand extraction intensified erosion. Human activities have altered hydrodynamics and sediment transport, leading to increased high tidal levels and reduced low tidal levels, thus amplifying the tidal range (up to 25.6% increase between 1960 and 2018 at Wenzhou station in the upper reach of the inner estuary). Moreover, the duration of flood tides has been lengthened (e.g. from 4.8 to 5.5 between 1960 and 2018 at Wenzhaou station), whereas the ebb tide duration has been shortened (from 7.6 to 7 h between 1960 and 2019 at Wenzhao station). These tidal variations are particularly pronounced in the upper estuary. These changes are attributable to two main causes: reduced tidal damping from lessened friction after intertidal area loss due to channel deepening and narrowing (Dronkers, 2017; Jalón-Rojas et al., 2018), and increased tidal convergence from the narrowing of the upstream channel (Talke et al., 2021). Given the flood-dominant nature of the ORE and the fact that sediment deposition within the ORE predominantly originates from the outer sea via tidal currents transport, the aforementioned alterations in tidal range and asymmetry are likely to enhance tidal pumping, thereby increasing sediment importation.

References

Milliman, J.D., Syvitski, J.P.M., 1992. Geomorphic/tectonic control of sediment discharge to the ocean: the importance of small mountainous rivers. J. Geol. 100, 525–544.

Dronkers, J., 2017. Convergence of estuarine channels. Cont. Shelf Res. 144, 120–133.

Jalón-Rojas, I., Sottolichio, A., Hanquiez, V., Fort, A., Schmidt, S., 2018. To what extent multidecadal changes in morphology and fluvial discharge impact tide in a convergent (turbid) tidal River. J. Geophys. Res. Oceans 123 (5), 3241–3258.

Talke, S.A., Familkhalili, R., Jay, D.A., 2021. The influence of channel deepening on tides, river discharge effects, and storm surge. J. Geophys. Res. Oceans 126 (5), e2020JC016328.

Impact of intertidal habitats on tidal propagation in estuaries

Zhu R. [1], Zhang W. [2], and Wei X. [3]

Keywords: estuaries, intertidal habitats, tidal propagation, tidal wavenumber, nature-based solution

Abstract

Intertidal habitats, such as mudflats, sandflats, salt marshes, and mangroves, are vital ecosystems in estuaries. These habitats serve crucial functions such as providing breeding and nursing grounds for marine species, aiding the mitigation of global warming through carbon capture and storage, improving estuarine water quality by filtering pollutants and excess nutrients, and safeguarding against flooding and erosion hazards by dissipating wave energy. Due to coastal development and climate change, intertidal habitats have been lost worldwide at rapid rates, triggering significant changes in estuarine tidal propagation and posing challenges for sustainable estuarine management. To mitigate the accelerating flooding, erosion, and biodiversity risks posed by climate change (e.g., sea-level rise, extreme weather) and human activities (e.g., damming, dredging, and reclamation), estuarine intertidal habitats are increasingly conserved, restored, and created around the world as nature-based solutions.

Given the critical roles of tides in estuarine flooding, bed erosion, and waterborne material transport (e.g., sediment, salt, nutrients, pollutants), it is crucial to understand the controlling mechanisms behind the influence of intertidal habitats on tidal propagation in estuaries and their responses to climate change and human activities. Analytical modeling has been effectively used to systematically understand the physics of tidal wave propagation in estuaries with intertidal habitats. However, the existing analytical studies have focused on estuaries with narrow intertidal areas (e.g., Speer and Aubrey, 1985; Jay, 1991; Friedrichs and Madsen, 1992; Winterwerp and Wang, 2013; Hepkema et al., 2018). In these studies, the intertidal water velocities were assumed to vanish, hence the longitudinal momentum transfer over the intertidal zone was dismissed. Also, tidal dynamics were solved by cross-sectionally averaged models, therefore the effects of vertical and lateral processes on tidal wave propagation remain poorly understood. To overcome these limitations, in this study, we developed an analytical model that not only accounts for water storage and momentum transfer over the intertidal zone but also explicitly resolves interactions between intertidal and subtidal water motions.

This research systematically investigates the underlying mechanisms governing tidal movement in estuaries characterized by extensive intertidal habitats. It examines how these habitats influence tidal dynamics, considering various estuarine features, through the utilization of an analytical width-averaged model within idealized estuaries. The model dynamically connects water movements within intertidal and subtidal zones (see Fig. 1), incorporating lateral water exchange driven by i) intertidal water storage and ii) intertidal momentum transfer. Our solution indicates that the influence of intertidal habitats on tidal propagation in estuaries is determined by the product of a complex wavenumber

(k) and estuary length (L), and the wavenumber k is affected by the ratio of total estuary width to subtidal channel width (through i) and intertidal-subtidal flux ratio (through ii). Sensitivity analysis reveals that intertidal habitats tend to amplify tides in estuaries with small kL (e.g., weak friction, short length, deep water, low-frequency waves, small vertical eddy viscosity, or narrow habitat), but lead to tidal damping under conditions with large kL. Our results also show that the intertidal momentum transfer reduces the water exchange between intertidal and subtidal areas, hence counterbalancing the above-mentioned intertidal effects. This study has been submitted to the Journal of Fluid Mechanics (Zhu et al., 2024).

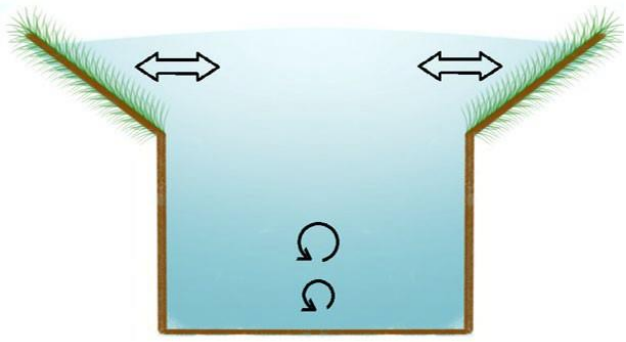

Figure 1. Model sketch with the cross-sectional view of an idealized estuary. The arrows represent water exchange processes between the intertidal and subtidal waters.

[1]Key Laboratory of Ministry of Education for Coastal Disaster and Protection, Hohai University, Nanjing, China, r.j.zhu@hhu.edu.cn
[2]The National Key Laboratory of Water Disaster Prevention, Hohai University, Nanjing, China, w.zhang@hhu.edu.cn
[3]National Oceanography Centre, Liverpool, United Kingdom, xwei@noc.ac.uk

References

Speer, P.E, Aubrey D.G. (1985) A study of non-linear tidal propagation in shallow inlet/estuarine systems Part II: Theory. Estuarine, Coastal and Shelf Science, 21, 207-224, https://doi.org/10.1016/0272-7714(85)90097-6.

Jay, D.A. (1991) Green's law revisited: Tidal long-wave propagation in channels with strong topography. Journal of Geophysical Research, 96, 20585, https://doi.org/10.1029/91JC01633.

Friedrichs, C.T, Madsen O.S. (1992) Nonlinear diffusion of the tidal signal in frictionally dominated embayments. Journal of Geophysical Research, 97, 5637, https://doi.org/10.1029/92JC00354.

Winterwerp, J.C, Wang Z.B. (2013) Man-induced regime shifts in small estuaries—I: theory. Ocean Dynamics, 63, 1279-1292, https://doi.org/10.1007/s10236-013-0662-9.

Hepkema, T.M, de Swart H.E, Zagaris A, Duran Matute M. (2018) Sensitivity of tidal characteristics in double inlet systems to momentum dissipation on tidal flats: a perturbation analysis. Ocean Dynamics, 68, 439-455, https://doi.org/10.1007/s10236-018- 1142-z.

Renjie Zhu, Wei Zhang, Xiaoyan Wei. (2024) Impact of intertidal habitats on tidal propagation in estuaries. Journal of Fluid Mechanics, under review.

Processes controlling sediment plumes of dumping activities in a mesotidal setting

Zorndt A. [1] and Kösters F. [2]

Keywords: dredging and dumping, sediment plumes, sediment transport, modelling, Weser estuary

Abstract

In the Weser estuary, Germany, a large dredging campaign is planned to deepen the estuary's navigation channel. The sediment disposals of the dredging material have to be evaluated regarding their impact on the suspended sediment concentrations and the resulting sediment distribution patterns. Based on this, an ecological impact assessment follows.

The Weser estuary is located in the south-east of the North Sea (see Fig. 1). The outer estuary is wide and funnel-shaped with a tidal range of 2.8 m at the outmost station ALW. In the more channelized inner estuary, the tidal range increases and amounts to 4.3 m at the tidal weir (mean values 2013-2022). The estuary's turbidity maximum is associated with the brackish water zone and located in the northern part of the inner estuary (Kösters et al., 2014). Highest suspended sediment concentrations are measured at station NUF with a tidal average of 300 mg/l and a tidal maximum of 740 mg/l. Up- and downstream, values decrease. 30 km north at station DWG, average and maximum tidal values amount to 80 mg/l and 200 mg/l (mean values for the hydrological year 2016, measuring height 1 m below mean tidal low water).

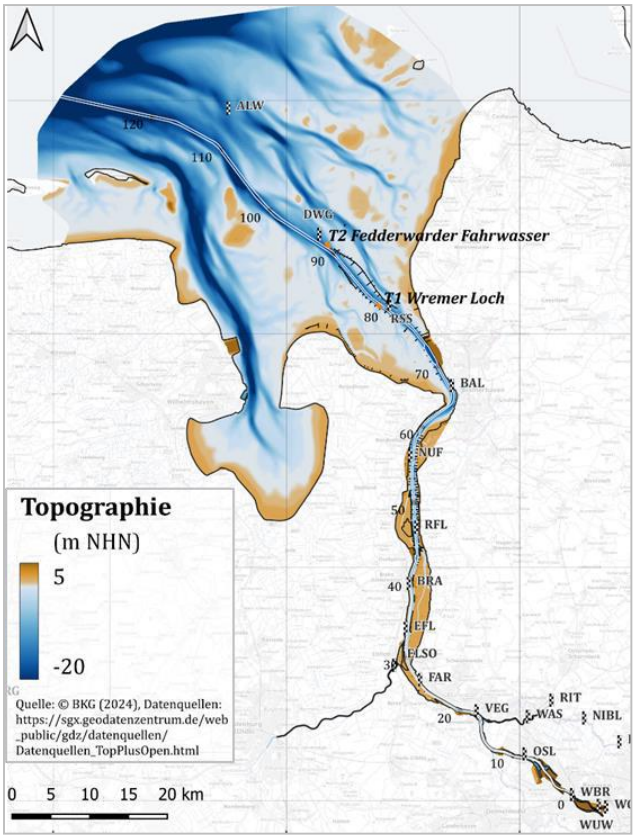

Figure 1: Model domain and bathymetry of the Weser estuary.

Sedimentation in the estuary's navigation channel requires maintenance dredging of 2.5 Mio. m³ of mud and 4.5 Mio. m³ of sand a year. Now, to make way for bigger ships, a channel deepening with capital dredging of another 8.9 Mio. m³ sediments is in planning, including 1.5 Mio. m^3 mud and 7.4 Mio. m^3 sand (wet volume). The material will be dumped at different sites in the outer estuary which are already in use for maintenance dredging today. According to regulations, mud can only be disposed at the sites T1 and T2 located in the southern part of the outer estuary (see Fig. 1).

We investigate the sediment disposals with a hydrodynamic and sediment transport model. From the simulation results, we can estimate the suspended sediment concentrations and sediment distribution caused by the sediment disposals.

Here, we will focus on the mud fraction of the dredging material, i. e. fine sediments < 63 µm.

The model which is used has been validated for 3d baroclinic circulation and suspended sediment dynamics for the hydrological year 2016. The natural transport of sediments already present is described with eight sediment fractions, including two fractions covering fine sediments < 63 µm. Additionally, five fractions are used to describe the distribution of the dredged material, also including two fine sediment fractions.

Describing qualitatively the impacts of the disposals as shown by the model, each disposal is followed by a peak in sediment concentrations. Part of the sediment settles on the disposal site, the rest is advected further by the tidal currents. The more frequent the disposals, the higher the availability of disposed fine sediments in the area becomes. Hence, there is ongoing resuspension of this material by tidal currents or waves and as a result, the average sediment concentration increases. The results show that the fine sediments have a wider distribution in the estuary than previously assumed. Only a small part remains in the vicinity of the disposal sites. A big portion settles on mud-flats in the southern outer estuary. More than 50 % of the dredged fine sediment returns to the estuarine turbidity maximum, where it has originally been dredged, due to the baroclinic circulation.

[1] Federal Waterways Engineering and Research Institute (BAW), anna.zorndt@baw.de
[2] Federal Waterways Engineering and Research Institute (BAW), frank.koesters@baw.de

However, the processes that influence the sediment plumes of the disposed material are manifold. As an example, the disposal process itself plays a role. The conditions during the disposal as well as the grain distribution and water content of the dredging material determine how much of the material settles at the disposal site, to be resuspended later on, and how much is going into suspension directly after dumping. In a regional scale model such as ours, the dumping process is parameterized (Gundlach et al., 2021). To study the sensitivity of such parameterizations, we investigated how the portion of the sediment released directly into the water column effects average sediment concentrations. Our analyses show that increasing this portion from 50 % to 100 % causes an increase of average sediment concentrations by 20 %.

Other processes influencing the sediment plumes are flocculation and connected to this different settling velocities as well as the erodibility of the deposited sediments in contrast to that of naturally present sediments of the region.

In a poster contribution, we would like to present our approach to capture the above-described processes and how we model them. Moreover, we will discuss the measurements we have based our model approaches on, and the sensitivity of the model results on the choices we made.

References

Gundlach, J., Zorndt, A., Visscher, J., Schlurmann, T. (2021) Modelling dynamic plume behaviour. Central Dredging Association (Ed.): CEDA Dredging Days2021, Virtual Conference – Proceedings, https://hdl.handle.net/20.500.11970/108931.

Kösters, F., Grabemann, I., Schubert, R. (2014), On SPM Dynamics in the Turbidity Maximum Zone of the Weser Estuary. In: Die Küste 81. Karlsruhe: Bundesanstalt für Wasserbau, https://hdl.handle.net/20.500.11970/101702.